VOLUME 76 DECEMBER 7, 1972 NUMBER 25

JPCHAx

THE JOURNAL OF PHYSICAL CHEMISTRY

PUBLISHED BIWEEKLY BY THE AMERICAN CHEMICAL SOCIETY

Here is the ideal way to obtain the ***most reliable reference data available today!*** *All you need is a subscription to the new*

JOURNAL OF PHYSICAL AND CHEMICAL REFERENCE DATA

published by the American Chemical Society and the American Institute of Physics for the National Bureau of Standards.

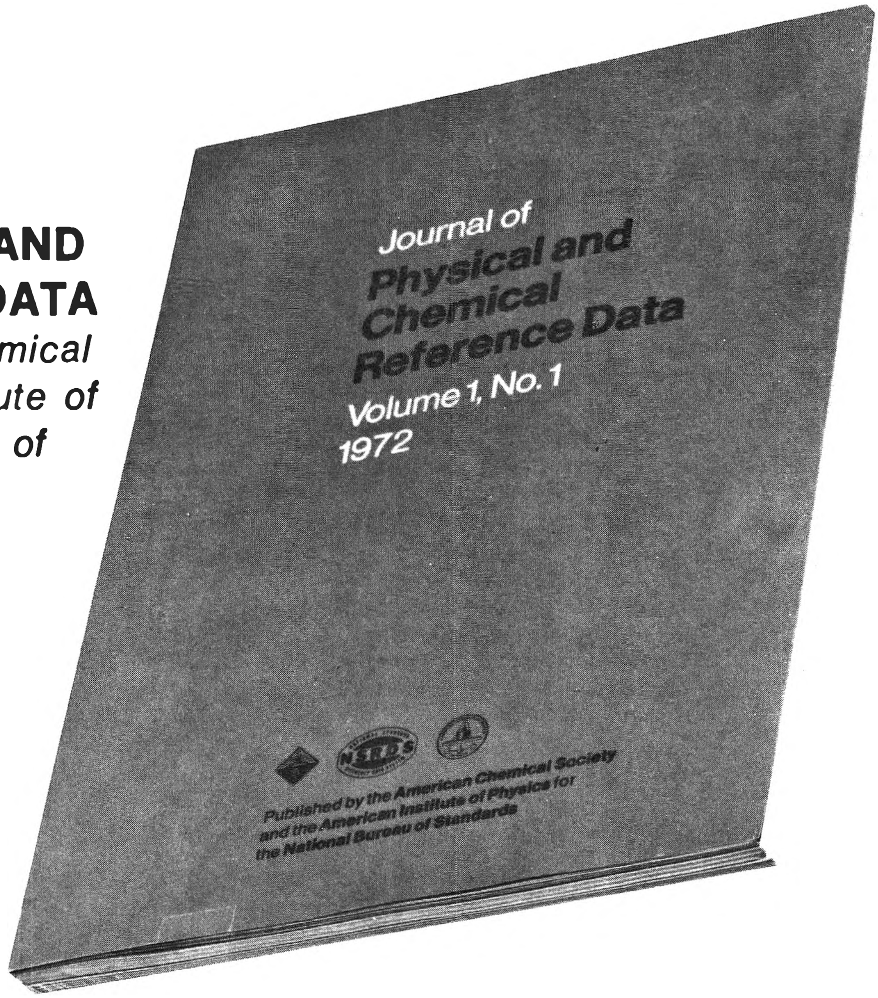

The *Journal of Physical and Chemical Reference Data* fills an important gap in the literature of the physical sciences. Its subject matter is the quantitative numerical data of physics and chemistry. As the new publication vehicle of the National Standard Reference Data System, the *Journal* will contain carefully evaluated data, with recommended values and uncertainty limits chosen by experts in each field. Critical commentary on methods of measurement and sources of error, as well as full references to the original literature, will be an integral part of each compilation.

Examples of some of the critical compilations scheduled for publication in the four issues of Volume I (1972) include:

- Tables of Molecular Vibrational Frequencies, Part 5, T. Shimanouchi
- Gaseous Diffusion Coefficients, by T. R. Marrero and E. A. Mason
- The Spectrum of Molecular Oxygen, by P. Krupenie
- Thermal Conductivity of the Elements, by C. Y. Ho, R. W. Powell and P. E. Liley
- Selected Values of Critical Supersaturation for Nucleation of Liquids from the Vapor, by G. M. Pound
- Gas Phase Reaction Kinetics of the Hydroxyl Radical, by W. E. Wilson, Jr.
- Selected Values of Heats of Combustion and Heats of Formation of Organic Compounds Containing the Elements CHNOPS, by E. S. Domalski
- Microwave Spectra of Molecules of Astrophysical Interest: Formaldehyde, Formamide, Thio-Formaldehyde, by D. R. Johnson, F. J. Lovas and W. H. Kirchhoff

Future compilations are expected to cover areas such as the following:

Band gaps in semiconductors
Nuclear moments
Atomic energy levels and transition probabilities
Diffusion in metals
Electron swarm data
Elastic constants of metals
Surface tension of liquids
Properties of molten salts
Activity coefficients of electrolytes
Equation of state of atmospheric gases
Ionization and appearance potentials

The *Journal of Physical and Chemical Reference Data* is intended to be a definitive source of reliable data on physical and chemical properties. Just fill in the order form at the bottom of this page to receive this invaluable reference source.

JOURNAL OF PHYSICAL AND CHEMICAL REFERENCE DATA
AMERICAN CHEMICAL SOCIETY
1155 Sixteenth Street, N.W.
Washington, D.C. 20036

Yes, I would like to receive the JOURNAL OF PHYSICAL AND CHEMICAL REFERENCE DATA at the one-year rate checked below:

	U.S.	Canada	PUAS	Other Countries
AIP and ACS members	$20.00	$20.00	$23.00	$23.00
Nonmembers	$60.00	$60.00	$63.00	$63.00

Bill me ☐ Bill company ☐ Payment enclosed ☐

Name ____________________

Street ____________________ Home ☐ Business ☐

City ____________ State ________ Zip ________

JP 72

THE JOURNAL OF

PHYSICAL CHEMISTRY

AMERICAN CHEMICAL SOCIETY, *1155 Sixteenth St., N.W., Washington, D. C. 20036*

Books and Journals Division
JOHN K CRUM, *Director*
JOSEPH H. KUNEY, *Head, Business Operations Department*
RUTH REYNARD, *Assistant to the Director*

All manuscripts should be sent to *The Journal of Physical Chemistry*, Department of Chemistry, University of Minnesota, Minneapolis, Minn. 55455.

Additions and Corrections are published once yearly in the final issue. See Volume 75, Number 26 for the proper form.

Extensive or unusual alterations in an article after it has been set in type are made at the author's expense, and it is understood that by requesting such alterations the author agrees to defray the cost thereof.

The American Chemical Society and the Editor of *The Journal of Physical Chemistry* assume no responsibility for the statements and opinions advanced by contributors.

Correspondence regarding accepted copy, proofs, and reprints should be directed to Editorial Production Office, American Chemical Society, 20th and Northampton Sts., Easton, Pa. 18042. Manager: CHARLES R. BERTSCH. Assistant Editor: EDWARD A. BORGER. Editorial Assistant: JOSEPH E. YURVATI.

Advertising Office: Centcom, Ltd. (formerly Century Communications Corporation), 142 East Avenue, Norwalk, Conn. 06851.

Business and Subscription Information

Remittances and orders for subscriptions and for single copies, notices of changes of address and new professional connections, and claims for missing numbers should be sent to the Subscription Service Department, American Chemical Society, 1155 Sixteenth St., N.W., Washington, D. C. 20036. Allow 4 weeks for changes of address. Please include an old address label with the notification.

Claims for missing numbers will not be allowed (1) if received more than sixty days from date of issue, (2) if loss was due to failure of notice of change of address to be received before the date specified in the preceding paragraph, or (3) if the reason for the claim is "missing from files."

Subscription rates (1972): members of the American Chemical Society, \$20.00 for 1 year; to nonmembers, \$60.00 for 1 year. Those interested in becoming members should write to the Admissions Department, American Chemical Society, 1155 Sixteenth St., N.W., Washington, D. C. 20036. Postage to Canada and countries in the Pan-American Union, \$5.00; all other countries, \$6.00. Single copies for current year: \$3.00. Rates for back issues from Volume 56 to date are available from the Special Issues Sales Department, 1155 Sixteenth St., N.W., Washington, D. C. 20036.

This publication and the other ACS periodical publications are now available on microfilm. For information write to: MICROFILM, Special Issues Sales Department, 1155 Sixteenth St., N.W., Washington, D. C. 20036.

Notice to Authors last printed in the issue of November 23, 1972

The Editors join with the international community of radiation chemists in dedicating this issue of The Journal of Physical Chemistry to

a celebration of 25 years of radiation research at Notre Dame and in honor of

Milton Burton

on the occasion of his 70th birthday

"An institution is the lengthened shadow of one man."

Ralph Waldo Emerson, *Self Reliance*

MILTON BURTON

In a very real sense the Radiation Laboratory of the University of Notre Dame is the lengthened shadow of Milton Burton. Indeed, a great deal of the evolution of radiation chemistry into an interdisciplinary science of international scope has occurred under his impetus.

Burton has personally spread the gospel of radiation chemistry throughout the world. He has been a tireless traveler always anxious to lecture, to organize and to participate in conferences. He opened the doors of the Radiation Laboratory for people around the world to study and to work as research assistants and associates so that they might return home to pursue careers in radiation research. In much of the world "Milton Burton" is synonymous with "radiation chemistry." At a banquet in Moscow in 1965, Michel Magat suggested that Burton be called the godfather of radiation chemistry because it is generally recognized that he gave the field its name. Most of his professional life has indeed been devoted to that field, but he was not always a radiation chemist.

Milton Burton's formal education was received at New York University with a B.S. in 1922, M.S. in 1923, and Ph.D. in physical chemistry under F. O. Rice in 1925. After 10 years in industry, he realized that his interest and ability lay in academic work and he returned to his alma mater where he taught and conducted research in photochemistry and kinetics. Those were the exciting times which followed the realization that all of chemistry would have to be explained in terms of the new quantum mechanics. Burton had finished his graduate work just at the birth of the quantum theory and shortly thereafter Dirac proclaimed that "all of chemistry was understood in principle." Working out the details was a challenge taken up by the chemists but support for research in those days was meager and progress was slow. Burton started at NYU with his characteristic vigor and launched an impressive amount of research with his collaborators, H. A. Taylor, T. W. Davis, J. E. Ricci, and others, turning out research publications at the rate of about five a year. He became widely known for his imaginative work in the use of potential energy functions of molecules for the interpretation of photochemical and kinetic mechanisms. A year spent in Berkeley in collaboration with G. K. Rollefson culminated in the book "Photochemistry and the Mechanism of Chemical Reactions," which was found to be most useful and stimulating by a whole generation of physical chemists. It incorporated the new quantum mechanics as an integral part of the treatment and was perhaps the first truly modern book on photochemistry.

World War II came and Burton was called upon to lead a project on the chemical effects of high-energy radiation at the Met Lab in Chicago. The field did not have a name when he went to Chicago, but Burton soon realized that a specific designation was needed and hit upon "radiation chemistry," the name now universally recognized. One of the first things that Burton did in his new job was to make arrangements to use the Van de Graaff generator of the Notre Dame Department of Physics as a radiation source, and work in radiation chemistry at Notre Dame was initiated in 1942. Therefore it is perhaps more accurate in the year 1972 to say that there have been 30 years of radiation research at Notre Dame instead of the 25 which are more visibly in the record.

Excellent beginnings in the radiation chemistry of water and of organic compounds and in the study of effects of radiation on solid materials were made during the war years by Burton and his Met Lab group and reported in the classified literature. After the war, when the same work was continued without classification, it was often by people who knew of the earlier work. Unclassified publications grew, yet most of the earlier work was never declassified. There is perhaps little overall loss to science because of this situation, but it has made it difficult to assign credit for those early accomplishments and Burton's group has not had the recognition that it deserves. Prominent members of the Met Lab group of radiation chemists were: W. A. Garrison (Berkeley), A. O. Allen (Brookhaven), R. L. Platzman (Chicago), A. R. Van Dyken (AEC), T. W. Davis (New York University), Sheffield Gordon (Argonne), T. J. Neubert (Illinois Tech), C. J. Hochanadel, J. C. Ghormley, and John Boyle (all now of Oak Ridge), Aaron Novick (Oregon State), J. G. Burr (University of Oklahoma), and Philip Yuster (Argonne). W. H. Hamill was associated with the work done at Notre Dame. The profound influence of James Franck upon this program was widely acknowledged by all.

In 1945, Burton accepted appointment as Professor of Chemistry at the University of Notre Dame and in the fall of 1946 he began a career of teaching and research which would last for 25 years. Except for one year spent as a visiting professor at Göttingen, he has been in residence at Notre Dame all of this time. Of course, as Emeritus Professor in 1972, he continues to work.

The Radiation Laboratory came into existence on February 1, 1947, at which time it was supported under the name of "Radiation Project" by the Office of Naval Research. W. H. Hamill and the late R. R. Williams were original members and J. L. Magee, the present Director of the Radiation Laboratory, joined the Chemistry Department and the "Project" in September 1948. The first Ph.D. in radiation chemistry was R. H. Schuler, now Professor of Chemistry at Carnegie Mellon University and Director of their Radiation Laboratory. Other members of the first wave of graduate students who have remained in radiation chemistry are R. R. Hentz, S. Gordon (ANL), H. A. Schwarz (BNL), and T. J. Sworski (ORNL). Altogether there have been over 250 graduate students and postdoctorals who have been affiliated with the Radiation Laboratory. They are to be found in almost all of the laboratories around the world involved in radiation research.

It was inevitable that activities of the "Project" should grow rapidly under the guidance of a principal investigator who had the properties of both an infinite energy source and a most effective catalyst. For support of the growth, a direct contractual relationship between the newly created Atomic Energy Commission and Notre Dame was established on February 1, 1949. By 1957 it had become evident that nothing short of a substantial building could contain the explosive propensities of the "Radiation Project." The AEC received Burton's request for support of the construction of a building with enthusiasm, but there was a question concerning use of federal funds for construction on private university campuses. This problem was resolved by a statement of presidential policy early in 1960 which resulted in the Authorization Act of June 1960. The total sum eventually budgeted for the building by the AEC was $2.2 million. On September

22, 1960 the "Radiation Project" was rechristened "Radiation Laboratory" and construction of the building began in December 1961.

The Radiation Research Building was dedicated at a special Convocation on September 1, 1963 with an address by Glenn Seaborg, Chairman of the AEC. Among the honored guests were James Franck (Nobel Laureate and revered mentor of Professor Burton) and S. C. Lind (a founding father of radiation chemistry and close friend).

Burton added the Radiation Chemistry Data Center (with initial support from the National Bureau of Standards and present support from both the NBS and AEC) to the activities of the Radiation Laboratory on July 1, 1965. In September 1966, the Radiation Laboratory received its present status as a "University Institute." The interdisciplinary character of the Radiation Laboratory is exemplified by its staff, research associates, and research assistants who are drawn from the disciplines and Departments of Chemistry, Biology, Physics, Chemical Engineering, Metallurgy and Materials Science, Electrical Engineering, and Engineering Science.

When Burton went to Notre Dame, he undertook a program to consolidate the position of radiation chemistry in the unclassified literature through a series of papers published in the *Journal of Physical and Colloid Chemistry* which were widely influential. About this time, many of us who thought of ourselves as primarily radiation chemists considered the radiation chemistry of water as the most important field. It was believed that soon after energy absorption H and OH radicals were formed in the water and that their action could account for all of the chemical effects of radiation. Of course, we all admitted that there were many details remaining to be worked out, but we were sure that the framework was correct. There was, however, a troublesome problem regarding the yield of the ferrous sulfate dosimeter. This dosimeter, introduced by Hugo Fricke in 1927, had a central position in the radiation chemistry of the early 1950's; to understand it was of very great theoretical and practical importance. Unfortunately, different groups of experimenters had reported yields of ferrous oxidation different by more than 20% and for a while no one was able to resolve the discrepancies. Burton decided that a calorimetric measurement of the high-energy radiation absorption would provide an unambiguous answer, and so with R. M. Lazo and Harold Dewhurst he set up the appropriate experiment; their yield determination has since that time become the accepted value.

Burton was vigorous in attempting to stimulate activity which would lead to better understanding not only of water but of all other materials as well. His own research at the time was principally on organic compounds, effects of resonance in aromatics, energy transfer, and the relations between radiation chemistry and photochemistry. We were members of the group at that time and remember the feeling of excitement which pervaded all. We talked about elementary processes, about the time scale of events, and about the role of tracks. One of us (J. L. M.) started a series on elementary processes in collaboration with Burton and a more specific study of track effects. The other (R. R. H.) worked on the study of radiation and photochemistry of organic compounds.

Burton had been fascinated with the role of excited states in chemistry for a long time and initiated a series of studies, which had great influence, to determine their roles in radiation chemistry. He was the first to use mixtures in a systematic way to study energy transfer. Studies of luminescence of irradiated systems demonstrated that excited states which emitted the observed light had not been directly created by the radiation but had precursors. S. Lipsky, now at the University of Minnesota, was prominent in this program. Later, in pursuing the role of excited states, Burton hit upon a repetitive time-sampling technique which he developed with Dreeskamp for the study of luminescence decay. The method has been used very effectively, particularly in connection with comparison of ultraviolet and high-energy radiation stimulation in various systems.

Burton continued investigations of processes in gases excited by glow discharges for many years. This activity was complementary to his research in radiation chemistry just as his activity in photochemistry was. Low energy electrons produce the chemical effects in these systems by creation of excited states and production of radicals by direct dissociation. Burton predicted the latter process from intuitive considerations. It is now recognized as an important mechanism in discharges and plasmas. Although Kuppermann's early work in track effects is better known, his graduate research was in the glow discharge program.

Soon after the Radiation Laboratory building was dedicated, a professional research staff was added to introduce more continuity in a research organization which was largely composed of postdoctorals and graduate students. Hentz, Funabashi, Mozumder, Ludwig, and Helman were appointed in the new category. The work of Senior Staff members was independent but there was a loose informal collaboration at all times. In particular, Burton's influence was ubiquitous. For example, work on the pressure dependence of the radiolysis of water was undertaken at Burton's suggestion by Hentz. It had been known for a long time that the ammoniated electron absorbs largely in the infrared and has a large (75 ml/mol) partial molal volume. Discovery by Hart and Boag of the hydrated electron absorption, largely in the visible, suggested comparisons between the two types of excess electrons. The studies of radiolysis of water at high pressures have shown that the partial molal volume of the hydrated electron is small ($\sim$7 ml/mol) and this puts strong limits on theoretical models which can be used.

The use of organic glasses composed principally of the aliphatic hydrocarbons was initiated in the Radiation Laboratory. Hamill showed it to be a versatile technique for studying properties of ions, radicals, and other intermediates in irradiated systems.

The recurrent theme in Burton's research work, lectures, and writings has been a concern with "Elementary Processes in Radiation Chemistry." Such a concern is illustrated by a recent statement of the scope of research at the Radiation Laboratory: "The objective of research in radiation chemistry is development of a complete picture of the sequence of events from deposition of high-energy radiation in a system to production of ultimate chemical effects. Between the initial act of energy deposition and the ultimate effect in systems exposed to high-energy radiation, a complicated array of elementary reactions occurs. Such elementary reactions involve a variety of transient species (ions, electrons, excited states, free radicals) of lifetimes that usually range from milliseconds to fractions of a picosecond or less. Thus, a major preoccupation of research in radiation chemistry is the development and application of methods for study of the formation and behavior of transient species resulting from the effect of high-energy radiation on matter in all states of aggregation." The research of Burton and his associates has contributed greatly towards the attainment of such an objective.

A prominent aspect of Burton's career has been his interest in stimulation of activity in others. He has always been active in promotion of conferences. The first international symposium on Radiation Chemistry and Photochemistry was organized by Burton and held at Notre Dame in June 1947. In 1950 an interdisciplinary conference involving biologists, chemists, physicists, and radiologists was held at Oberlin, Ohio. Burton was prominent in the organization of this conference and participated in the subsequent formation of a scientific society, the Radiation Research Society, which grew out of it, serving as its president in 1958–59. In October 1952, Burton invited a small group of radiation chemists with a special interest and expertise in the radiation chemistry of water to Notre Dame for the first Informal Conference on the Radiation Chemistry of Water. There have now been five such conferences held at Notre Dame, the last in October 1966; published proceedings of the informal discussions have, in each case, been made available promptly after the Conference to the radiation chemistry community. Professor Burton played a leading role in organization of the Gordon Research Conference on Radiation Chemistry and was Chairman of the first conference in 1953. These conferences have been held annually since that time and have been the single most stimulating and fruitful forum for exchange of results and ideas among members of the international community of radiation chemists. Other conferences organized subsequently, such as the Miller Conference, have adopted similar patterns.

A conference on Comparative Effects of Radiation was called under the auspices of the Committee on Photobiology, Division of Biology and Agriculture, of the National Academy of Sciences–National Research Council, and was held in Puerto Rico in February 1960. Needless to say, the Conference was organized and operated under the chairmanship of Milton Burton who also was coeditor of the resulting book of the same name. The first Faraday Society General Discussion to be held in the United States was managed through the efforts of Professor Burton, in connection with the dedication of the Radiation Research Building at Notre Dame in September 1963. Most recently, Professor Burton organized the International Meeting on Primary Radiation Effects in Chemistry and Biology which was held in Buenos Aires, Argentina in March 1970.

The idea of a conference to celebrate 25 years of radiation research at Notre Dame and to honor Milton Burton on his 70th birthday occurred to a number of people at about the same time. The more widely the idea was discussed the more enthusiasm was generated. An organizing committee of W. H. Hamill, R. R. Hentz, J. K. Thomas, and J. L. Magee, Chairman, was formed; the conference was planned, set for April 4–7, 1972, and held at the Center for Continuing Education at Notre Dame. There were about 200 scientists in attendance at the meeting. The format was patterned after the Gordon Conference with most of the time devoted to open discussion. The papers of this issue contain but a fraction of the exciting material discussed at the meeting.

John L. Magee
Robert R. Hentz

THE JOURNAL OF

PHYSICAL CHEMISTRY

Volume 76, Number 25 December 7, 1972

JPCHAx 76(25) 3677–3910 (1972)

COMMUNICATIONS TO THE EDITOR

AUTHOR INDEX

In papers with more than one author the name of the author to whom inquiries about the paper should be addressed is marked with an asterisk in the by-line.

THE JOURNAL OF

PHYSICAL CHEMISTRY

VOLUME 76, NUMBER 25 DECEMBER 7, 1972

Concentration Effects on Primary Processes in the Radiation Chemistry of Aqueous Solutions

E. Peled, D. Meisel, and G. Czapski*

Department of Physical Chemistry, The Hebrew University, Jerusalem, Israel *(Received February 18, 1972)*

The effect of halides on $G(e_{aq}^-)$ and $G(OH)$ was studied by pulse radiolysis. Nearly no increase was found, neither in $G(e_{aq}^-)$ nor in $G(OH)$, on increasing the halide concentration (up to 2 M chloride). Concentrations of either 1 M Cl^-, Br^-, or I^- had negligible effect on $G(H) + G(H_2)$. $G(H_2)$ was slightly increased at the expense of $G(H)$. The results are discussed in the light of the spur diffusion model and other recent models. It was concluded that chemical competition between the scavengers used here and the annihilation processes cannot play a significant role in the radiation chemistry of aqueous solutions.

Introduction

The spur diffusion model has been most successfully applied when explaining the radiation chemistry of aqueous solutions. Even so, and though this model does quite clearly explain most of the experimental results of irradiated aqueous solutions (up to 0.1 M or even 1 M solute's concentration), it was claimed that certain observations do not agree with this model.[1] However, it has recently been shown that most of these observations can be indeed interpreted in the light of the spur diffusion model.[2-4] Sworski[5] suggested that H_3O and/or H_2O^*, which are homogeneously distributed, may play a leading role in the radiation chemistry of aqueous solutions, but his model is shown to be in contradiction with other results.[3,4] Hamill[6-10] suggests that certain solutes may react with oxidizing species, *i.e.*, "holes," or with reducing species such as "dry" electrons, in times shorter than 10^{-11} sec, before the latter have become solvated or even before their complete thermalization occurs. Hamill[10] suggests, moreover, that certain experimental results belie the existence of spurs. Hamill[6-10] also proposes that several anions, halides for instance, are efficient "hole" scavengers, while several solutes, such as acetone, nitrate, Cd^{2+}, and others, are unhydrated electron (e_{dry}^-) scavengers and therefore increase $G(e_{aq}^-)$ and/or $G(OH)$.

We have studied the effect of halides on $G(OH)$, $G(e_{aq}^-)$, and $G(H)$ and have tested the experimental results in the light of the spurs diffusion model and also of Hamill's model.

Experimental Section

Materials. Triple-distilled water was used for all solutions. All reagents were of analytical grade and were used without further purification.

Dosimetry and Irradiation Source for $G(H_2)$ Measurements. Irradiations for these measurements were carried out in a ^{137}Cs γ source. The dose rate was about 2000 rads min^{-1} and total doses amounted to 20,000-80,000 rads. A Fricke dosimeter served for dose rate determinations, taking $G(Fe^{3+}) = 15.6$.

$G(H_2)$ Determination. All solutions were argon saturated and irradiated in 10-cc syringes. Gas products were determined by gas chromatography, the detailed method of which has been described previously.[11] All the $G(H_2)$ values were found to be linear with dose, and are the average of 5 measurements. All $G(H_2)$ values were corrected for the increase in the electron density of the solutions.

Determination of Radical Yields. The initial yields of all the radicals were determined by pulse radiolysis. A Varian-7715 linear accelerator gave 5-MeV electron pulses, with 200-mA current. Pulse lengths varied between 0.1 and 0.3 μsec, yielding 3×10^{-6} M of e_{aq}^- at most. A Spectrosil irradiation cell, 4 cm long, with an optical path of 12.3 cm, was used. The analyzing light source was a 150-W xenon arc lamp. A 1P28 photomultiplier was used for ranges between 270 and 675 nm, and a R196 one for ranges between 520 and 950 nm, when measuring the e_{aq}^- spectrum. All yields were corrected for the change in the electron density of the solutions.

(1) M. Anbar, "Fundamental Processes in Radiation Chemistry," P. Ausloos, Ed., Interscience, New York, N. Y., 1968.
(2) H. A. Schwarz, *J. Phys. Chem.*, **73**, 1928 (1969).
(3) E. Peled and G. Czapski, *J. Phys. Chem.*, **74**, 2903 (1970).
(4) E. Peled, U. Mirski, and G. Czapski, *J. Phys. Chem.*, **75**, 31 (1971).
(5) T. J. Sworski, *Advan. Chem. Ser.*, **No. 50** (1965).
(6) W. H. Hamill, *J. Phys. Chem.*, **73**, 1341 (1969).
(7) T. Sawai and W. H. Hamill, *J. Phys. Chem.*, **74**, 3914 (1970).
(8) T. Sawai and W. H. Hamill, *J. Chem. Phys.*, **52**, 3843 (1970).
(9) P. L. T. Bevan and W. H. Hamill, *Trans. Faraday Soc.*, **66**, 2533 (1970).
(10) S. Khorana and W. H. Hamill, *J. Phys. Chem.*, **75**, 3081 (1971).
(11) G. Czapski and E. Peled, *Isr. J. Chem.*, **6**, 421 (1968).

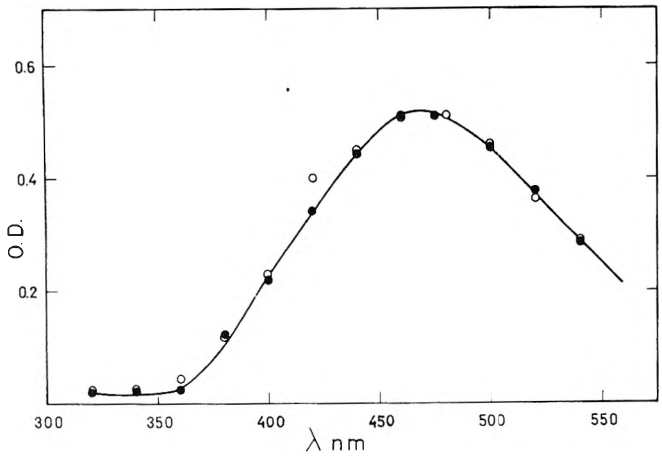

Figure 1. Effect of 2 *M* NaCl on $(SCN)_2^-$ spectrum in 2 × 10^{-2} *M* KSCN, N_2O saturated solutions: ●, no chloride, O, 2 *M* NaCl.

Results

a. Effect of OH Scavengers on G(OH). Thiocyanate is quite an efficient OH scavenger, yielding the radical ion $(SCN)_2^-$ through the reactions

$$OH + SCN^- \rightleftarrows SCN + OH^- \text{ (or } SCNOH^{-}\text{ [12])} \quad (1)$$

$$SCNOH^- \text{ or } SCN + SCN^- \rightleftarrows (SCN)_2^- \quad (2)$$

In 2 × 10^{-2} *M* KSCN all OH radicals react with SCN^- and equilibria 1 and 2 are shifted toward $(SCN)_2^-$, yet at such low concentrations it is very unlikely that the thiocyanate ion would react with the suggested holes whose lifetime is very short, if they exist at all. Since e_{aq}^- has quite an appreciable absorption in the region of the $(SCN)_2^-$ absorption, solutions were saturated with N_2O, thus converting all e_{aq}^- to OH radicals

$$N_2O + e_{aq}^- \rightarrow N_2 + OH + OH^-$$

Since the possibility of a shift in $(SCN)_2^-$ spectrum due to the addition of high NaCl concentrations was suspected, the entire spectrum was taken and is shown in Figure 1. Addition of 2 *M* NaCl to N_2O saturated solution of 2 × 10^{-2} *M* KSCN gave exactly the same spectrum and the same yield of $(SCN)_2^-$. $\tau_{1/2}$ of the $(SCN)_2^-$ decay was greater than 30 μsec and was unaffected by the addition of Cl^-. The electronic set-up rise time was less than 0.3 μsec, thus correction by extrapolation to the beginning of the pulse amounted to less than 4% of the yield, and the accuracy of the initial yield determination is thought to be of that same accuracy in these experiments. No absorption due to Cl_2^- could be observed and no absorption other than that of $(SCN)_2^-$ could be detected in the range 270–700 nm. Addition of 2 *M* NaCl to oxygenated solution of SCN^- caused no change in the spectrum of $(SCN)_2^-$ and hardly any change in its yield. The equilibrium constant $K_3 = 3 \times 10^{-5}$ [13]

$$Cl^- + [SCN]_2^- \overset{K_3}{\rightleftarrows} ClSCN^- + SCN^- \quad (3)$$

therefore at 2 *M* NaCl and 2 × 10^{-2} *M* SCN^- only less than 0.3% of the $[(SCN)_2^-]$ is expected to be converted to $ClSCN^-$. Thus, practically all chlorine atoms are converted into $(SCN)_2^-$ radicals *via* reactions 3 and 4

$$Cl + SCN^- \rightarrow ClSCN^- \quad (4)$$

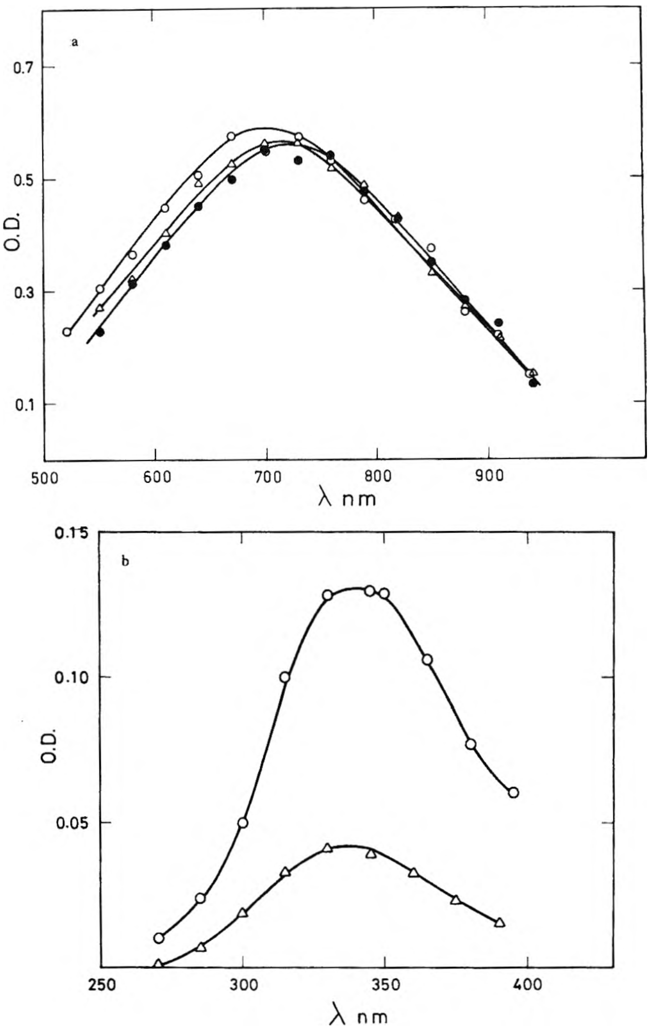

Figure 2. (a) Effect of Cl^- on e_{aq}^- yield and spectrum and (b) effect of Cl^- on Cl_2^- yield and spectrum in argon saturated, 0.1 *M* methanol at pH ~9 solutions. Corrected for e_{aq}^- absorption in that region: ●, no chloride; Δ, 0.5 *M* NaCl; O, 2 *M* NaCl.

b. Effect of OH Scavengers on $G(e_{aq}^-)$ and $G(Cl_2^-)$. The effect of increasing $[Cl^-]$ on $G(e_{aq}^-)$ and on $G(Cl_2^-)$ in deaerated solutions containing 0.1 *M* methanol at pH ~9 was studied simultaneously. The analyzing light beam was split into two, where the e_{aq}^- absorption was recorded in the range 520–950 nm, and the Cl_2^- absorption in the range 270–395 nm. Methanol was added to these solutions since it was found to increase the half-life of e_{aq}^-, probably by scavenging H and OH radicals in the bulk of the solution. In this set of experiments $\tau_{1/2}$ of e_{aq}^- decay was greater than 25 μsec and the electronic rise time was about 1 μsec. Extrapolation to the beginning of the pulse introduced a correction of 7% at most, thus $G(e_{aq}^-)$ could be measured quite accurately. The results are given in Figure 2 and Table I. Two features are to be stressed in this figure. (i) The e_{aq}^- spectrum was shifted toward shorter wavelengths on increasing NaCl concentration, while no shift of this kind was observed in the Cl_2^- spectrum. The effect of electrolytes on the e_{aq}^- spectrum was observed previously[14] yet little attention has been paid to that effect. Such a negligence would cause an appreciable error in $G(e_{aq}^-)$ deter-

(12) D. Behar, unpublished results.
(13) M. Schoneshofer, *Int. J. Radiat. Phys. Chem.*, **1**, 505 (1969).
(14) (a) M. Anbar and E. J. Hart, *J. Phys. Chem.*, **69**, 1244 (1965); (b) S. Arai, A. Kora, and Imamura, *J. Phys. Chem.*, **74**, 2102 (1970).

TABLE I: Effect of [X^-] and Other Solutes on $G(e_{aq}^-)$ and $G(Cl_2^-)$[a]

Halide	Other solutes	$G(e_{aq}^-)$	$G(Cl_2^-)$
	pH ~9	2.80[c,f]	
0.5 *M* NaCl	pH ~9	2.80[g]	0.32[b]
2 *M* NaCl	pH ~9	2.74[h]	0.93[b]
	0.2 *M* NaOH	3.31[f]	
2 *M* NaCl	0.2 *M* NaOH	3.25[h]	0.0
	0.5 *M* Na_2SO_4 pH ~9	2.81[f]	
2 *M* NaCl	0.5 *M* Na_2SO_4 pH ~9	2.67[h]	0.87[b]
2 *M* NaCl	0.4 *M* Na_2HPO_4 pH ~9	d	0.88[b]
1 *M* NaCl[e]	pH ~9	2.75 (λ 625, 650, 675)[i]	
1 *M* NaBr[e]	pH ~9	2.60 (λ 625, 650, 675)[i]	
1 *M* NaI[e]	pH ~9	2.60 (λ 625, 650, 675)[i]	

[a] All solutions were Ar saturated containing 0.1 *M* methanol unless otherwise stated. All *G* values corrected for the electron density of the solutions. [b] ϵ_{340} for Cl_2^- was taken as 12,500.[15] $G(Cl_2^-)$ was corrected for e_{aq}^- absorption in that region. [c] All $G(e_{aq}^-)$ values are related to this value which itself was estimated by comparison with the e_{aq}^- yield at 10^{-2} *M* methanol (see Table II) assuming $G(e_{aq}^-)$ = 2.6 at 10^{-2} *M* methanol. [d] e_{aq}^- decays too fast and $G(e_{aq}^-)$ could not be measured accurately. [e] This series was 10^{-2} *M* in methanol. [f] λ_{max} 720. [g] λ_{max} 715. [h] λ_{max} 700. [i] The only wavelengths studied.

mination. In the study of $G(e_{sol}^-)$ in alcoholic solutions[14b] an increase of $G(e_{sol}^-)$ was reported as a result of Cl^- addition. All, or part of this increase may be caused by a spectral shift of the spectrum of e_{sol}^- due to the chloride. (ii) Only a minor effect on $G(e_{aq}^-)$ could be detected by increasing [Cl^-] up to 2 *M*, assuming that at λ_{max} $\epsilon(e_{aq}^-)$ = 15,800 M^{-1} sec^{-1} [15] remains constant in spite of the change in λ_{max}. The initial absorption of the e_{aq}^- was also measured at 625, 650, and 675 nm in deaerated solutions of bromide and iodide containing 0.1 *M* methanol at pH ~9. The same $G(e_{aq}^-)$ values were obtained for the three wavelengths mentioned above. No change in $G(e_{aq}^-)$ was detected in any of these solutions.

In solutions containing 0.2 *M* NaOH and 0.1 *M* methanol we found an increase of about 20% in the yield of e_{aq}^- as compared to the yield in neutral solution, as expected due to the conversion of H atoms to e_{aq}^- by OH^- ions. The inclusion of 2 *M* NaCl caused negligible increase in $G(e_{aq}^-)$

TABLE II: Effect of [Methanol] on $G(e_{aq}^-)$ and $G(Cl_2)$

Solute	$G(e_{aq}^-)$[g]	$G(Cl_2^-)$[g]
a	2.6[b]	
10^{-2} *M* MeOH[a]	2.6[b] (assumed)	
0.1 *M* MeOH[a]	2.8[b]	
1.0 *M* MeOH[a]	2.9[b]	
0.1 *M* MeOH + 2 *M* NaCl[a]	2.74[c]	0.93[d]
1.0 *M* MeOH + 2 *M* NaCl[a]	2.72[c]	0.92[d]
10^{-2} *M* MeOH + 0.5 *M* NaCl[e]		0.32
10^{-2} *M* MeOH + 0.5 *M* NaCl[f]		0.32
0.5 *M* MeOH + 0.5 *M* NaCl[f]		0.21
1.0 *M* MeOH + 0.5 *M* NaCl[f]		0.19
2.0 *M* MeOH + 0.5 *M* NaCl[f]		0.15

[a] Argon saturated. [b] λ_{max} 720. [c] λ_{max} 700. [d] λ_{max} 340, corrected for e_{aq}^- absorption in that region. [e] O_2 saturated. [f] N_2O saturated. [g] All *G* values are corrected for the electron density of the solutions.

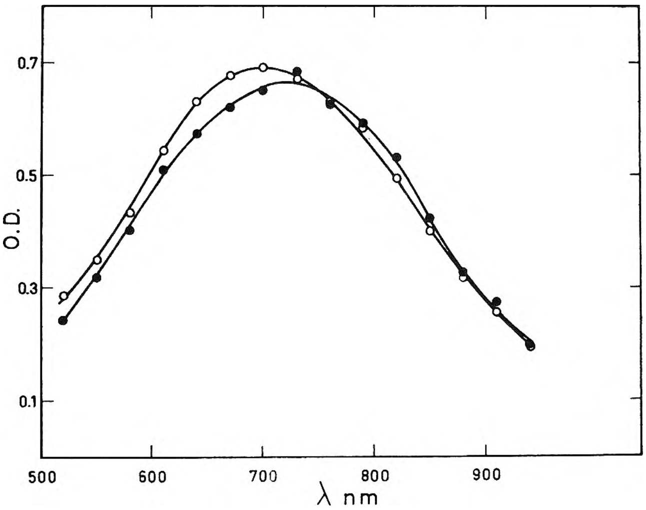

Figure 3. Effect of Cl^- on e_{aq}^- yield and spectrum in 0.2 *M* NaOH, deaerated solutions containing 0.1 *M* methanol: ●, no chloride; O, 2 *M* NaCl.

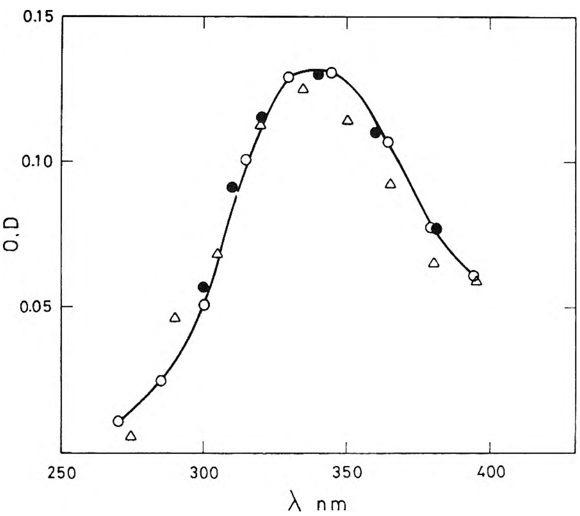

Figure 4. Effect of 0.5 *M* sulfate and 0.4 *M* phosphate on $G(Cl_2^-)$ in argon saturated, 0.1 *M* methanol, 2 *M* NaCl solutions: ●, no additive; O, 0.5 *M* Na_2SO_4; Δ, 0.4 *M* Na_2HPO_4.

while the same shift in the spectrum is clearly observed (Figure 3). No Cl_2^- was found at that high pH. In solutions containing 2 *M* NaCl at pH ~9 $G(Cl_2^-)$ remained unchanged by addition of 0.4 *M* Na_2HPO_4 or 0.5 *M* Na_2SO_4 (Figure 4). All these results are summarized in Table I.

Methanol was added to our solutions and its effect on $G(e_{aq}^-)$ and $G(Cl_2^-)$ was checked; the results are presented in Table II. Methanol has an observable effect on $G(e_{aq}^-)$: from 10^{-2} to 1 *M* methanol, $G(e_{aq}^-)$ increased from 2.6 to 2.9. In the presence of 2 *M* NaCl no effect of methanol on $G(Cl_2^-)$ and $G(e_{aq}^-)$ was observed. At lower [Cl^-], methanol competes with chloride on OH radicals.

Since acetate was suggested as a "hole" scavenger,[10] we studied its effect, and the effect of formate and citrate, on $G(e_{aq}^-)$. In deaerated 10^{-2} *M* methanol solutions, $G(e_{aq}^-)$ = 2.70, 2.55, and 2.65 for 1 *M* acetate (pH 9), 1 *M* formate (pH 8), and 0.5 *M* citrate (pH 9), respectively, which nearly equals $G(e_{aq}^-)$ = 2.6 in the absence of these anions.

(15) M. S. Matheson and L. M. Dorfman, "Pulse Radiolysis," M.I.T. Press, Cambridge, Mass., 1969.

TABLE III: Effect of Cl^-, Br^-, I^- on $G(H)$ and $G(H_2)$[a]

Halide[b]	$G(H_2) + G(H)$[c]	$G(H_2)$[d]	$G(H)$
	1.10	0.45[e]	0.65
Cl^-	1.01		
Br^-	0.94	0.54[f]	0.40
I^-	0.97	0.61	0.36

[a] All G values are corrected for the electron density of the solutions. [b] Concentration, 1 M of the sodium salt. [c] Measured in deaerated neutral 10^{-3} M acetone and 0.1 M 2-propanol. [d] The same solutions as in b, excluding 2-propanol. [e] J. W. T. Spinks and R. J. Woods, "An Introduction to Radiation Chemistry," Wiley, New York, N. Y., 1964. [f] Reference 18.

The effect of Cl^- on G_{red} in acid solutions was studied by irradiating deaerated 0.1 M 2-propanol solutions, either in 1 M $HClO_4$ or in 1 M HCl with a ^{137}Cs γ source. We found $G(H_2) = 3.95$ in HCl and $G(H_2) = 3.94$ in 1 M $HClO_4$ solutions.

c. Effect of e_{aq}^- Scavengers on $G(Cl_2^-)$. Acetone being suggested as an efficient dry electron scavenger was used to examine its effect on $G(Cl_2^-)$. Deaerated solutions at natural pH containing either 10^{-3} M acetone or 1 M acetone and 1 M NaCl were irradiated. We found $G(Cl_2^-) = 0.50$ at 10^{-3} M acetone and 0.53 at 1 M acetone. Thus no real effect of acetone on $G(Cl_2^-)$ is observed.

d. Effect of Halides on G(H) and G(H₂). The effect of Cl^-, Br^-, and I^- on $G(H_2)$ and $G(H)$ was studied using a ^{137}Cs γ source. Deaerated solutions at neutral pH contained 0.1 M 2-propanol, thus converting H atoms to molecular hydrogen, and 10^{-3} M acetone as e_{aq}^- scavenger. Results in Table III show no increase in $G(H) + G(H_2)$, on addition of 1 M of any of the halides, on the contrary a slight decrease may be observed.

Discussion

First we will summarize our experimental results and then analyze them in view of the various models.

(1) Chloride (2 M) has no real effect either on $G((CNS)_2^-)$ or on its spectrum in O_2 or N_2O saturated solutions (Figure 1), *i.e.*, $G(OH)$ and $G(e_{aq}^-)$ are practically the same in 10^{-2} M CNS^- in the presence or absence of 2 M Cl^-.

(2) Cl^- (2 M), Br^- (1 M), I^- (1 M), and acetate (1 M) have a negligible effect on $G(e_{aq}^-)$. (Figure 2a and Table I).

(3) $G(H_2) \sim 1$ in the presence or absence of 1 M Cl^-, 1 M Br^-, and 1 M I^- in solutions containing 0.1 M 2-propanol and 10^{-3} M acetone. Since $G(H_2)$ slightly increases in these solutions these halides do not increase $G(H)$, but rather decrease it slightly (Table III).

(4) $G(Cl_2^-)$ increases from 0.31 to about 0.93 going from 0.5 to 2 M Cl^- in solutions containing 0.1 M MeOH (Table I and Figure 2b). The increase of [MeOH] from 10^{-2} to 1.0 M does not affect $G(Cl_2^-)$ in solutions of 2 M Cl^-. N_2O (10^{-2} M) does not affect $G(Cl_2^-)$ in the presence of 10^{-2} M methanol (Table II).

(5) NaOH prevents the formation of Cl_2^- (Table I).

(6) Phosphate (0.4 M) and Na_2SO_4 (0.5 M) have nearly no effect on $G(Cl_2^-)$ in solutions containing 10^{-1} M methanol (Table I and Figure 4).

a. The Chloride System. We found that $G(Cl_2^-) = 0.32$ in deaerated N_2O and O_2 saturated solutions of 10^{-2} M methanol with 0.5 M Cl^-. These results indicate that Cl_2^- is not formed in the bulk of the solution. When the concentration of methanol is increased from 10^{-2} to 1 M in 2 M Cl^- solutions, no effect on $G(Cl_2^-)$ is observed and its value remains about 0.9. Since the half-life of OH radicals in 1 M methanol solutions is about 10^{-9} sec ($k_{OH+MeOH} = 5 \times 10^8$ [16] M^{-1} sec^{-1}) and as no competition between Cl^- and methanol is detected in 1 M methanol plus 2 M Cl^-, it can be concluded that in these solutions Cl_2^- is formed at times shorter than 10^{-9} sec, *i.e.*, Cl_2^- is formed in the spur or by H_2O^+. However, when $[Cl^-]$ is decreased to 0.5 M, methanol begins to decrease $G(Cl_2^-)$. The reduction in $G(Cl_2^-)$ does not follow simple kinetic competition and the efficiency of the reduction of $G(Cl_2^-)$ by methanol is higher at lower Cl^- concentrations. This observation cannot be explained by equilibria 5 and 6, as N_2O has no effect on $G(Cl_2^-)$ in the solutions.

$$OH + Cl^- \rightleftharpoons ClOH^- \tag{5}$$

$$ClOH^- + Cl^- \rightleftharpoons Cl_2^- + OH^- \tag{6}$$

We will add reactions 7 and 8 in order to account for the formation of Cl_2^- in the spurs, where $[H^+]$ is high

$$ClOH^- + H^+ \rightleftharpoons Cl + H_2O \tag{7}$$

$$Cl + Cl^- \rightleftharpoons Cl_2^- \tag{8}$$

A mechanism consisting of reactions 5–8 (assuming that $k_5 \sim k_7 \sim k_8 \sim 10^9$–$10^{10}$ M^{-1} sec^{-1}) appears to be consistent with the fact that N_2O has no effect on $G(Cl_2^-)$, as in the bulk, where the pH $\sim$9, reaction 7 is slow and equilibrium 7 is shifted to the left. Therefore the formation of Cl_2^- through reaction 8 is too slow and $ClOH^-$ will decay directly or through dissociation into OH. This mechanism implies that reaction 6 is shifted at pH 9 to the right.

At higher $[Cl^-]$ equilibria 5–8 are strongly shifted to the right, reducing the OH concentration available for scavenging by methanol (the reduction in [OH] is expected to be inversely proportional to $[Cl^-]^2$).

The effect of $[CH_3OH]$ on $G(Cl_2^-)$ can also be explained by scavenging of the OH precursor by Cl^-, and the inefficient reaction of CH_3OH with it.

It was found that scavengers of H^+, such as 0.5 M SO_4^{2-} and 0.4 M HPO_4^{2-}, at pH 9, have no effect on $G(Cl_2^-)$. This behavior contradicts the mechanism proposed and the role of reaction 7 in the spur, as $[H^+]$ in the spur should be lowered substantially by these solutes (with SO_4^{2-}, the HSO_4^- formed in the spur may dissociate as the pK of HSO_4^- is lowered sufficiently by the high ionic strength; such an effect would not occur with $H_2PO_4^-$). The reaction of HPO_4^{2-} with H^+ will raise the spur's pH, slow down reaction 7, and form in the spur $H_2PO_4^-$. If $H_2PO_4^-$ will react in a similar way with $ClOH^-$ in reaction 7a as H^+ does in reaction 7, the results will still be consistent, including the lack of an effect of N_2O.

$$ClOH^- + H_2PO_4^- \rightarrow Cl + H_2O + HPO_4^{2-} \tag{7a}$$

We found the occurrence of reaction 7a but it seems that k_{7a} is 10-fold slower than k_7, which is somewhat too slow to account for the results with this mechanism.

From the above mentioned arguments it can be concluded that the mechanism of reactions 5, 6, 7, 7a, and 8 does not explain satisfactorily $G(Cl_2^-)$. This may be either due to the complexity of the reaction $2Cl^- + OH \rightarrow OH^- + Cl_2^-$ or reaction of H_2O^+ with Cl^-, as suggested by Hamill.[6-10] The suggestion that H_2O^+ is the precursor of Cl_2^- is in some conflict with Hamill's picture, as 1 M acetone does not increase $G(Cl_2^-)$ although acetone is supposed to react with e_{dry}^-. This could indicate that if H_2O^+ is a precursor of

(16) M. Anbar and P. Neta, *Int. J. Appl. Radiat. Isotopes*, **18**, 493 (1967).

Cl_2^-, no annihilation of e_{dry}^- with H_2O^+ occurs. Equilibria 5-8 may also explain Anbar and Thomas' results[17] predicting a linear dependence of $1/G(Cl_2^-)$ on $1/[Cl^-]^2$. As the radiation chemistry of the Cl^- system, *per se*, is far from being well understood, it is a pitfall for misinterpretations.

b. Irradiation of Halides Solutions in View of the Spur Diffusion Model. All our experimental results are in full agreement with the spur diffusion model. The fact that Cl^-, Br^-, and I^- do not affect $G(e_{aq}^-)$ is to be expected if the rates of the spur reactions e_{aq}^- + OH, H + OH, and OH + OH are similar to those of e_{aq}^- + M, H + M, and M + M, where M stands for the halide atom. From the above discussion it is expected that G(OH) will not change in 2 M Cl^- as in the spurs OH radicals are converted to Cl atoms. The increase of $G(e_{aq}^-)$ from 2.6 in water to 2.9 in 1.0 M MeOH can be expected as the OH radicals in the spurs are partially converted to methanol radicals and the "back" reaction e_{aq}^- + $\dot{C}H_2OH$ is slower than the reaction e_{aq}^- + OH. ($\tau_{1/2}$ of e_{aq}^- is markedly increased when 10^{-2} M MeOH is added to neutral water.) The increase of $G(e_{aq}^-)$ from 2.8 to 3.3, when $[OH^-]$ increases from 10^{-5} to 0.2 M in 2 M Cl^- solutions can be explained by the partial conversion of H atoms to e_{aq}^- within the rise time of the electronic equipment. (The half-life of the reaction H + $OH^- \rightarrow e_{aq}^-$ is less than 0.2 μsec in our conditions while the electronic rise time is about 0.3 μsec.)

The decrease of G(H) from 0.65 in water to about 0.4 in 1 M I^- may result from the high reactivity of I_2 and I_3^- toward H atoms. The rate of the spur back reaction H + H_2O_2 is much slower than the rate of the reaction H + I_2 (or I_3^-) as $k_{H+H_2O_2} = 2 \times 10^7\ M^{-1}\ sec^{-1}$ while $K_{H+I_2} = 4 \times 10^{10}\ M^{-1}\ sec^{-1}$.[16]

The fact that $G(H_2)$ = 0.6 in 1 M I^- is more difficult to explain (similar results were recently obtained on the Br^- system[18]). It seems that this increase in $G(H_2)$ may result from a direct effect or from reactions of subexcited electrons with I^-. The energy of subexcited electrons is below 6 eV[19] while the electron detachment energy of I^- is about 5 eV. Therefore when a subexcited electron ionizes I^- two electrons with energy of 0-1 eV are obtained in addition to an I atom. The range of these electrons in water is only a few ångströms. This process would occur in or not far from the center of the spurs where a relatively high local concentration of e_{aq}^-, H, and OH is present. These two electrons, formed by the subexcited electron, will be very close to the I atom, thus they will have a greater probability to recombine with the I atom, but if not, these electrons may recombine to yield H_2 or will react with other radicals in the spur. It should be stressed that while the average distance between electrons in the spurs is a few tens of ångströms, the distances between the above discussed electrons and I atoms will be only a few ångströms. This process increases markedly the probability for radical recombination, and consequently $G(H_2)$ and $G(I_3^-)$ increase.

c. Discussion on Hamill's Results. Hamill discussed in several places the role of dry electrons and holes and the effect of scavengers on the various G values of radical and molecular products.[6-10] He assumed, for example, that ions like the halides may react with holes (or alternatively, excited water molecules). His observations show that in concentrated solutions of "hole scavengers" an increase in $G(e_{aq}^-)$ and G(OH) is found. The basic assumptions in this interpretation are the following:

(a) At times less than 10^{-11} sec after the deposition of the radiation in aqueous systems an entity (e_{dry}^--hole) is formed. The hole may be dry H_2O^+ or H_3O^+. Alternatively the species may be some kind of excited H_2O.

(b) These entities can annihilate partially or yield radicals or molecular products.

(c) Dry electron or hole scavengers react partially with these species prior to the formation of the solvated radicals and partial annihilation.

The reactions of "hole scavengers" may be the following

$$(e^- + H_2O^+) \xrightarrow{M^-} M + OH + H + e_{aq}^- \qquad (I)$$

In this mechanism the hole trapping of one (H_2O^+ + e^-) pair would result in a total of two oxidizing (M and OH) and two reducing (e_{aq}^- and H) radicals.

$$(e^- + H_3O^+ + OH) \xrightarrow{M^-} M + OH + H + e_{aq}^- \qquad (II)$$

The same total radicals per scavenged pair is expected from mechanisms I and II, the only difference between these two mechanisms is that $H_3O_{dry}^+$ is trapped by M^- instead of H_2O^+.

$$(H_2O^+ + e^-) \xrightarrow{M^-} M + H_2O + e_{aq}^- \qquad (III)$$

In mechanism III, each pair yields on hole scavenging only one e_{aq}^- and one M radical.

$$H_2O^* \xrightarrow{M^-} M + e_{aq}^- \qquad (IV)$$

In this mechanism, the dry pair is replaced by an excited water molecule.

If I^- is used as the hole scavenger one should get, according to mechanisms I and II, $G(-H_2O)^{20} < G(e_{aq}^-) + G(H) + 2G(H_2) = G(\Sigma I) \le 2G(-H_2O)^{20}$ and moreover G(H) should approach $G(e_{aq}^-)$. If mechanisms I-IV play a significant role in the radiation chemistry of aqueous solutions then both $G(e_{aq}^-)$ and G(OH) should increase markedly because the prompt recombination of e^- with H_2O^+ or H_3O^+ or the deexcitation of H_2O^* would be prevented by these scavengers.[6-10] Our results show no increase in G(H) in the halide systems, an observation which is in apparent disagreement with mechanisms I and II. The constancy of $G(e_{aq}^-)$ and G(OH) in all the systems which we studied is in contradiction with all four mechanisms. Hamill's results are in disagreement with our work. He[8,10] found that Cl^- increases $G(e_{aq}^-)$ by 30-40%, that the halides markedly increase G(oxidation) and that acetate scavenges "holes" and thus increases $G(Cd^+)$ ($=G(e_{aq}^-)$). We believe that our results have the advantage as we measured $G(e_{aq}^-)$ directly and corrected for ionic strength effect on the spectrum of e_{aq}^-. In our systems no complications due to complexation or to secondary reactions of new species were detected in both our measurements of $G(e_{aq}^-)$ and G(OH).

Hamill[10] suggested that the results from the halide systems "bear upon the nature of the spur, and even raise questions concerning its existence." We think that I^- and Br^- systems provide strong evidence for the existence of spurs. Hamill[10] measured $G(I_3^-)$ and $G(Br_3^-)$ at the end of 0.5-μsec pulse, thus no bulk contribution to I_3^- and Br_3^- is expected in these experiments. The formation of I_3^-, which was attributed by Hamill to oxidation of several I^- ions by one excited H_2O^+ should yield two reducing species. Therefore, $G(e_{aq}^-)$ and G(H) in 1 M I^- and 1 M Br^- should increase markedly, in contradiction to the present results.

(17) M. Anbar and J. K. Thomas, *J. Phys. Chem.*, **68**, 3829 (1964).
(18) T. Sawai, *Bull. Chem. Soc. Jap.*, **44**, 1977 (1971).
(19) R. L. Plazman, "Radiation Research," G. Slini, Ed., North-Holland Publishing Co., Amsterdam, 1967, p 20.
(20) $G(-H_2O)$ = 4.2 is the yield of water decomposition at low scavenger concentration.

Hence we are forced to conclude that the source of I_3^- and Br_3^- with $G \sim 1.5$ is not the excited H_2O^+ but simply the spur recombination reactions I + I and I + I_2^- and Br + Br and Br + Br_2^-. We found that in 1 M I^- $G(e_{aq}^-) = 2.6$, $G(H) = 0.36$, and $G(H_2) = 0.61$, thus $G(-H_2O) = 2.6 + 0.36 + 2 \times 0.61 = 4.18$. Hamill's values are much higher than this value $G(\Sigma I) = 5.32$ for 1 M I^- and $G(\Sigma Br) = 5.71$ for 1 M Br^-, and after correction for the electron density of these solutions, the values are $G(\Sigma I) = 4.95$ and $G(\Sigma Br) = 5.37$. We believe that these high yields should be interpreted from the point of view of the specific radiation chemistry of I^- and Br^- concentrated solutions and not from the point of view of basic processes in radiation chemistry of aqueous solutions. Very recently[21] it was shown that, in addition to the equilibria corresponding to equilibria 5 and 6, the Br^- system involves some more equilibria and an additional species Br_3^{2-} was suggested to exist in such concentrated bromide solutions. It is reported[22] that Br_3^{2-}, for example, has a higher absorption than Br_2^- at the peak of Br_2^-. Thus, the Br^- system, and presumably the I^- system, are much more complicated than previously considered and general conclusions from these systems to the radiation chemistry of aqueous solutions are not straightforward forthcoming.

Hamill[10] found that in 2 M acetate and 0.05 M I^-, $G(I_2^-) = 0.97$ while in 0.4 M acetate and 0.01 M I^-, $G(I_2^-) = 1.86$ although the ratio [acetate]/[I^-] is the same. It means that at high concentrations, acetate is much more reactive toward the oxidizing radical (OH or its precursor) than I^-. Hamill suggested that acetate is a hole scavenger and thus prevents the reaction of the OH radical with I^-. Since we have found that acetate had negligible effect on $G(e_{aq}^-)$, hole trapping by acetate before prompt recombination, as suggested by Hamill, contradicts our results.

Although our results contradict Hamill's model, this does not necessarily rule out the existence and chemical reactions of dry electrons and dry H_3O, H_2O^+, and OH. If these species are capable of reacting with solutes in aqueous solutions, our results lead us to either of the following features of these species.

(1) The dry species do not annihilate but can either get thermalized and solvated or react as such with solutes.

(2) The partial annihilation is a much too fast reaction with which even high concentration of solutes cannot compete. The dry species which escape this fast recombination can react with solutes as dry species or after solvation.

With these features of dry species we do not expect any effect of solutes on the yields. Nevertheless, competition of two scavengers for these species may be concentration dependent, as at low concentration they compete only for the solvated species while at high concentration they compete also on the dry entities.

Conclusions

(1) In the systems studied here, no disagreement with the spur diffusion model was observed. On the contrary, most of our results can be explained only on the ground of such a model.

(2) Our results contradict any mechanism which assumes the chemical reaction of scavengers with dry entities (e_{dry}^-, $H_2O_{dry}^+$, $H_3O_{dry}^+$) or H_2O^* in competition with their annihilation. However, our results do not rule out chemical reactions of dry entities as long as they do not compete with the annihilation processes.

(21) D. Zehavi and J. Rabani, *J. Phys. Chem.*, **76**, 312 (1972).
(22) B. Cercek, *Int. J. Radiat. Phys. Chem.*, **4**, 23 (1972).

Electronic Absorption Spectra of Excess Electrons in Molecular Aggregates. I. Trapped Electrons in γ-Irradiated Amorphous Solids at 77°K

Tadamasa Shida,* Suehiro Iwata,

The Institute of Physical and Chemical Research, Wako-shi, Saitama, Japan

and Tsutomu Watanabe

Department of Applied Physics, The University of Tokyo, Tokyo, Japan *(Received March 10, 1972)*

Publication costs assisted by The Institute of Physical and Chemical Research

Absorption spectra of trapped electron have been recorded for the low-temperature matrices of over 40 different molecules and compared with the theoretical spectra derived from a hydrogenic model for the electron. Remarkable agreement between experiment and theory was obtained for almost all the cases. The analysis of the line shape of the observed spectra in terms of the theory provided information concerning the nature of absorption, the binding energy, and the Bohr radius of the electron in the ground state. Some experimental data of interest appearing in the recent literature were also analyzed by the present theory to obtain successful explanations of the observed spectral features.

Introduction

It is a striking thing that such an elementary entity as an electron renders itself sensuous blue color when it is in ammonia or water. It is natural, therefore, that the previous workers attempted to reproduce theoretically the observed transition energy.[1-4] However, due to the complexity of the system the theoretical treatments were confined within the realm of the assumption that a single 1s- to 2p-type transition was mainly responsible for the absorption. Owing to the prominence of the character of the 1s-2p-type transition for water and ammonia (*vide infra*) semiquantitative agreements were achieved by the previous theories for the transition energy. However, the characteristically broad and asymmetric absorption line shape has not been fully accounted for. There has been a long-standing speculation that the broadness and asymmetry are due to the contribution of higher transitions,[1,2] but this has not been rigorously tested because of the difficulty of realistic delineation of the excited electron. Thus, even though one may say that "the higher energy levels are only slightly influenced by the form of the potential well at small distances and can be adequately represented by hydrogen-like states,"[1] one can not easily estimate, for example, the effective "nuclear charge" felt by the optical electron from the theoretical calculation.

In this paper we propose a compromising semiempirical approach based on a hydrogenic model for the excess electron in condensed matter. It is found that the proposed theory is applicable to the trapped electron in γ-irradiated frozen matrices of a variety of substances and that pertinent information of the electronic state is obtained from the comparison between the experimental and the theoretical spectra constructed on the basis of the model.

Preliminary Discussion

An excess electron in the condensed medium is stabilized by the total polarization of the medium which consists of the orientational polarization of molecules having a permanent dipole moment and the electronic polarization of the medium molecule. Only the former component of the polarization provides a persisting potential for the excess electron and the latter follows the motion of the electron self-consistently. This correlation between the excess and the medium electrons prevents derivation of a simple potential energy curve for the excess electron and a segmental description of the energy of the system (excess electron plus medium) is required.[1-4]

However, since the optical transition energy between the ground (eq 1) and the nth states is related to the total energy of the system relative to a reference energy state as[1-4,5]

$$h\nu_n = E_n - E_1 \tag{1}$$

one may conceive an imaginary effective one-electron potential whose eigenenergies are equal to E_n's. Obviously, the explicit delineation of such an effective potential is prohibitive. However, if the potential was known, the optical excitation of the excess electron could be treated as a usual potential problem. Schematically, such a potential may be drawn as in solid curves of Figure 1.

A reasonable assumption for further steps will be as follows: the ground-state electron confined in a small region may be characterized mainly by the potential at small distances. Conversely, for the excited states the local potential at small distances may not be so influential as quoted above. Then, one may be able to replace the potential curve with a set of approximate potentials as indicated by broken and dotted curves in Figure 1.

In this work we employ Coulombic potentials for the approximation. Thus, for the potentials in Figure 1 the approximate curves are represented as $-Z_1/r$ and $-Z_2/r$ and so on. Such a truncation of the realistic potential may

(1) J. Jortner, *J. Chem. Phys.*, **30**, 839 (1959).
(2) D. A. Copeland, N. R. Kestner, and J. Jortner, *J. Chem. Phys.*, **53**, 1189 (1970).
(3) K. Fueki, D. F. Feng, and L. Kevan, *J. Phys. Chem.*, **74**, 1976 (1970).
(4) K. Fueki, D. F. Feng, L. Kevan, and R. E. Christoffersen, *J. Phys. Chem.*, **75**, 2297 (1971).
(5) T. Shida, S. Iwata, and T. Watanabe, to be submitted for publication.

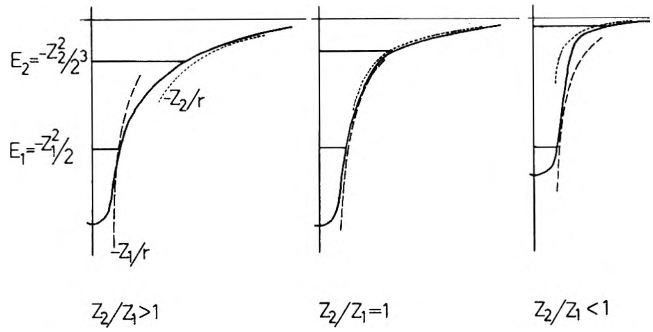

Figure 1. Schematic representation of the effective potential for the excess electron. The left (A) and the right (C) indicate respectively a potential of a longer and a shorter range than the Coulombic potential at the middle (B). The bottom of the conduction state of the excess electron is taken as the reference energy state.

seem to be too drastic but its justification will be discussed elsewhere.[5] Let us assume that the effective charge Z_n is related to the actual total energy of the nth electronic state of the system relative to the conduction state[4] as

$$E_n = -Z_n^2/2n^2 \tag{2}$$

In other words, we regard that the electron in the nth bound state is energetically equivalent to a hydrogenic electron which is in the Coulomb potential of $-Z_n/r$. For the continuum state also we consider a hydrogenic potential $-Z_c/r$ and, for convenience, call the ratio $A_n \equiv Z_n/Z_1$ and $A_c \equiv Z_c/Z_1$ the attenuation coefficient. From Figure 1 it is seen that A exceeding unity means that the effective potential in solid curves is of a longer range type than the Coulomb potential and *vice versa*. Physically speaking, the medium of polar molecules having a permanent dipole moment will provide a long-range potential whereas in nonpolar molecules the effective potential will quickly tend to zero as indicated by Figure 1C.

The main advantage of this hydrogenic model is that one can calculate the transition moment analytically. Assuming, for simplicity, that the coefficient A_n and A_c for all the excited states can be represented by a single value of A, we obtain the following theoretical spectral distribution of the oscillator strength over the whole energy region including the continuum state[5]

$$f(E_{1n}) = 2^8 3^{-1} n^5 (n^2 - 1) A^5 (2 - A)^2 (n - A)^{2n-5} (n + A)^{-2n-5} \delta(E - E_{1n}) \equiv f_n \delta(E - E_{1n}) \tag{3}$$

$$\mathrm{d}f(E_{1k})/\mathrm{d}E = 2^8 3^{-1} Z^6 A (2 - A)^2 (k^2 + A^2 Z^2)(Z^2 + k^2)^{-5} \exp\{(-4AZ/k) \operatorname{arccot}(Z/k)\}\{1 - \exp(-2\pi AZ/k)\}^{-1} \tag{4}$$

which are quite analogous to those for the hydrogenic atom.[6] In eq 3 and 4 E is the photon energy and E_{1n} and E_{1k} are the transition energies to the nth bound excited state and to the continuum state where the ionized electron has the momentum of k.

$$E_{1n} = E_n - E_1 = (Z^2/2)(1 - A^2/n^2) \tag{5}$$

$$E_{1k} = E_k - E_1 = Z^2/2 + k^2/2 \tag{6}$$

Note that we have dropped the suffix 1 from Z_1.

The oscillator strength is further modified by the line-broadening procedure to take into account the statistical fluctuation of the environment of the electron in the condensed medium.[5] The fluctuation is assumed to obey the Gaussian distribution as

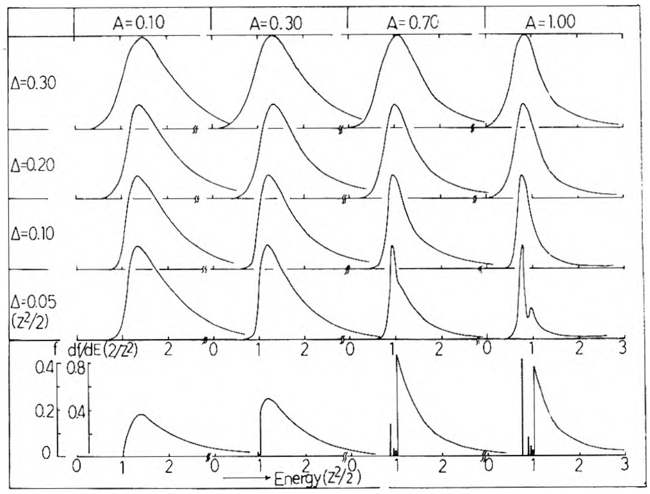

Figure 2. Some examples of the theoretical simulation spectrum. The spectral oscillator strength distribution given by eq 3 and 4 is shown at the bottom of the figure for various values of A. Note that f is dimensionless while $\mathrm{d}f/\mathrm{d}E$ is given in units of $(Z^2/2)^{-1}$. The distribution is further line broadened as specified by the value of $\Delta_{1/2}$ to obtain the simulation of the absorption spectrum. For the continuum state the product of $\mathrm{d}f/\mathrm{d}E$ times ΔE (in units of $Z^2/2$) is regarded as a "line." All the simulation spectra shown in the body of the figure are normalized to the absorption maximum and the energy is given in units of $Z^2/2$.

$$\mathrm{d}f(E)/\mathrm{d}E = \sqrt{\alpha/\pi}\Sigma f_n \exp\{-\alpha(E - E_{1n,1k})^2\} \tag{7}$$

where f_n is identical with that in eq 3 for the discrete transitions ($E < Z^2/2$) and is equal to $\{\mathrm{d}f(E_{1k})/\mathrm{d}E\}\Delta E$ for the ionization ($E > Z^2/2$) where ΔE stands for a small energy interval in the continuum state. α is related to the half-height width $2\Delta_{1/2}$ of the Gaussian distribution as

$$\tfrac{1}{2} = \exp(-\alpha\Delta_{1/2}^2) \tag{8}$$

Then, the absorption line shape of the theoretical spectrum (eq 7) can be fixed if the values of A, $\Delta_{1/2}$, and Z are known. Instead of assessing these quantities from the physical consideration we determine them semiempirically; we first construct a set of simulation spectra for a wide range of A and $\Delta_{1/2}$ using the "ionization potential," $Z^2/2$, as the unit of energy. From the set of the simulation spectra a best-fit one is searched in comparison with the experimental spectrum. By identifying the observed absorption maximum M_{obsd} (in eV) with the peak of the theoretical spectrum at an energy of $m(Z^2/2)$ we obtain the value of $Z^2/2$ in eV as M_{obsd}/m. Once the values of A, $\Delta_{1/2}$, and Z are fixed, one can obtain the transition energy for the discrete levels by eq 5, the effective charges Z and AZ, and the Bohr radius of the ground state by $r_B = 1/Z$ (in atomic units).

Some examples of the simulation spectrum are shown in Figure 2 which includes also the spectra before the line broadening. It is seen that as the value of $\Delta_{1/2}$ increases the structure due to the discrete transitions is smeared out and the band becomes broad and symmetric. For a fixed value of $\Delta_{1/2}$, the spectrum becomes sharp and symmetric (at the half-heights) as the value of A increases from zero toward unity which is due to the diminution of the contribution from the bound-free transition. It is

(6) E. U. Condon and G. H. Shortley, "The Theory of Atomic Spectra," Cambridge University Press, New York, N. Y., 1935, p 133; H. A. Bethe and E. E. Salpeter, "Quantum Mechanics of One- and Two-Electron Atoms," Springer-Verlag, West Berlin, 1957, p 304.

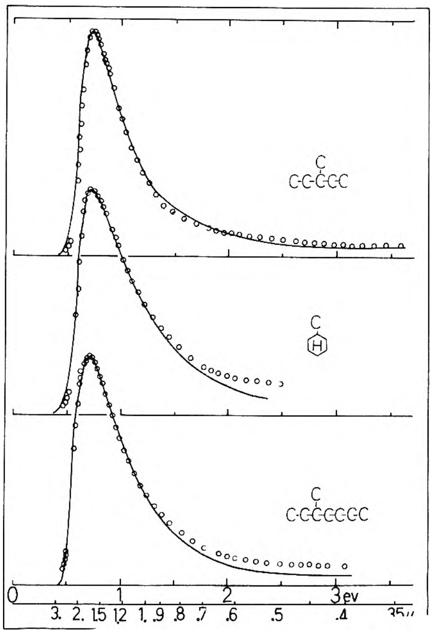

Figure 3. Absorption spectra of e_t^- in paraffins: circles, observed; solid curves, theoretical (*cf.* entry no. 1-3 in Table I). To avoid complexity in the figures an obvious abbreviation is made for the chemical formula of the matrix molecule.

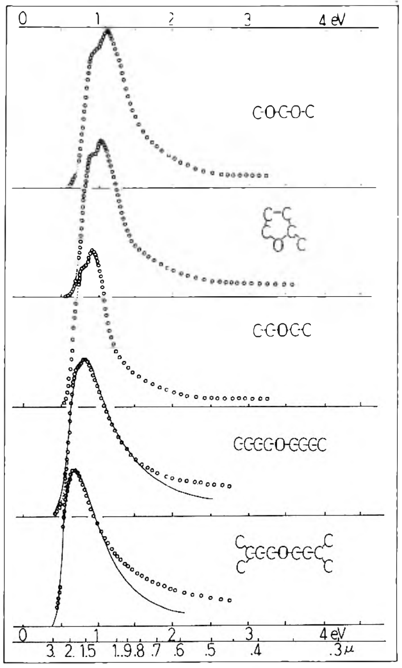

Figure 4. Absorption spectra of e_t^- in ethers. See caption for Figure 3 (*cf.* entry no. 4-8 in Table I).

noted that although the absorption maximum is roughly at the ionization threshold $Z^2/2$ for all the values of A, the major component of the absorption changes gradually from the bound-free to the 1s-2p-type discrete transition as A increases from zero to unity.

In the following sections the spectral data of trapped electrons in various matrices will be compared with the theoretical spectrum outlined above. In General Discussion we also compare some experimental data in the literature with the theory.

Experimental Section

All the samples formed transparent glassy solids at 77°K. Ethers and amines contaminated with stabilizers or decomposed products were purified by contacting them with potassium-sodium alloy under vacuum. Aromatic impurities in paraffins were removed by passing through an activated alumina column. The liquid samples were placed in a silica cell of $0.5 \sim 2$ mm thickness, degassed, frozen at 77°K, and subjected to γ irradiation at 77°K to doses of 5×10^{18} to 5×10^{19} eV/g. After the irradiation the sample exhibited an intense absorption due to the trapped electron (abbreviated as e_t^-) in the near-infrared and visible regions which was measured by a Cary 14 RI spectrophotometer. The sample was photobleached partially or totally with light of selected wavelengths (given in the figure caption. The total bleaching left a small residual absorption in the near uv due to unspecified radicals concomitantly produced with the electron. The difference between the absorption immediately after irradiation and the residual absorption was plotted to obtain the net absorption due to e_t^- (open circles in the figures). Similarly, the absorption of partially bleached samples was obtained by subtracting the residual absorption remaining after the subsequent total bleaching. All the observed spectra shown in the figures were normalized to the maximum absorbance.

Experimental Results and Individual Discussion

Paraffins. The spectrum of e_t^- in paraffinic glasses has been reported previously.[7,8] However, the absorption at $\lambda > 2\ \mu$ was not precisely measured because of the background vibrational absorption. We have extended the measurement to the threshold of absorption by using properly thin cells (Figure 3). The curves are drawn by assigning the values of A and $\Delta_{1/2}$ in Table I to the theoretical spectrum given by eq 7. (In all the figures below open circles represent the observed absorption while the solid curves are theoretical. All the spectral data are compiled in Table I and not all the experimental results will be presented in the figure).

With the assigned value of $A = 0.2$ the observed spectrum should be associated mostly with the bound-free transition (see Figure 2). Hamill proposed that the absorption of e_t^- in 3-methylpentane glasses may consist of the components of a discrete and a bound-free transition of a comparative order of magnitude.[9] His argument is based on the anomalous spectral behavior observed for the pulse-radiolyzed 3-methylpentane at low temperatures[10] and on the quantum yield of selective photobleaching.[11] However, we consider that the apparent quantum yield may not necessarily be relevant to the discussion on the nature of electronic state of electrons in condensed media because of the possible wavelength-dependent competition between the bleaching (detrapping) and the stabilization (retrapping). As for the cited result of the low-temperature pulse radiolysis, it is not necessarily convincing in view of more recent reports.[12]

Ethers. Figure 4 shows the spectra for a series of ali-

(7) J. B. Gallivan and W. H. Hamill, *J. Chem. Phys.*, **44**, 2378 (1966).
(8) J. Lin, K. Tsuji, and F. Williams, *J. Amer. Chem. Soc.*, **90**, 2766 (1968).
(9) W. H. Hamill, *J. Chem. Phys.*, **53**, 473 (1970).
(10) J. T. Richards and J. K. Thomas, *J. Chem. Phys.*, **53**, 218 (1970).
(11) D. W. Skelly and W. H. Hamill, *J. Chem. Phys.*, **44**, 2891 (1966).
(12) N. V. Klassen, H. A. Gillis, and D. C. Walker, *J. Chem. Phys.*, **55**, 1979 (1971).

TABLE I: Observed and Theoretical Spectral Data[a]

Entry no.		Ia	Ib	IIa	IIb	IIc	IIIa	IIIb	IIIc
1	3-Methylpentane	0.700	0.672	0.20	0.10	1.300	0.537	0.198	2.66
2	Methylcyclohexane	0.760	0.845	0.20	0.225	1.375	0.552	0.201	2.63
3	3-Methylheptane	0.708	0.795	0.20	0.15	1.325	0.534	0.198	2.67
4	Methyltetrahydrofuran	1.030	0.520						
5	Ethyl ether	0.918	0.511						
6	Methylal	1.100	0.624						
7	*n*-Butyl ether	0.825	0.796	0.275	0.2375	1.325	0.623	0.214	2.47
8	Isoamyl ether	0.689	0.930	0.25	0.175	1.300	0.530	0.197	2.68
9	Diethylenetriamine	1.283	0.842	0.525	0.2875	1.175	1.092	0.283	1.86
10	Isobutylamine	1.290	0.786	0.725	0.2625	1.025	1.258	0.304	1.74
11	*n*- + Isoamylamine	1.150	0.801	0.40	0.25	1.250	0.920	0.259	2.03
12	*sec*-Butylamine	1.055	0.583	0.725	0.1375	0.950	1.110	0.285	1.85
13	Diisopropylamine	0.825	0.654	0.625	0.1375	1.000	0.825	0.246	2.15
14	Triethylamine	0.729	0.809	0.30	0.225	1.300	0.560	0.203	2.60
15	*N,N*-Dimethylaminopropylamine	0.868	1.048	0.425	0.2875	1.250	0.694	0.271	1.95
16	Methanol	2.390	0.428	0.95	0.115	0.800	2.987	0.469	1.14
17	Methanol[b]	2.485	0.373	0.96	0.105	0.800	3.106	0.477	1.10
18	Ethanol	2.320	0.607	0.75	0.15	0.950	2.442	0.423	1.25
19	Ethanol[b]	2.360	0.559	0.75	0.125	0.925	2.551	0.433	1.22
20	1-Propanol[b]	2.360	0.644	0.65	0.15	1.000	2.360	0.416	1.27
21	1-Butanol[b]	2.250	0.666	0.60	0.15	1.050	2.143	0.397	1.33
22	2-Butanol[b]	2.290	0.733	0.60	0.20	1.075	2.130	0.396	1.34
23	1-Pentanol[b]	2.250	0.724	0.55	0.20	1.125	2.000	0.383	1.38
24	Isoamyl alcohol[b]	2.360	0.775	0.55	0.225	1.125	2.098	0.393	1.34
25	2-Propanol[b]	1.930	0.782	0.40	0.225	1.225	1.575	0.340	1.55
26	Glycerin	2.524	0.753	0.45	0.20	1.175	2.148	0.397	1.33
27	Ethylene glycol	2.389	0.590	0.725	0.1375	0.950	2.514	0.429	1.23
28	Propylene glycol	2.290	0.873	0.425	0.2875	1.250	1.832	0.366	1.44
29	1,4-Butanediol	2.250	0.760	0.65	0.225	1.050	2.251	0.406	1.30
30	1,3-Butanediol	2.210	0.841	0.60	0.25	1.100	2.009	0.384	1.37
31	2,3-Butanediol	2.213	1.102	0.45	0.275	1.225	1.806	0.364	1.45
32	Hexylene glycol	1.420	1.100	0.40	0.40	1.325	1.071	0.280	1.88
33	Diethylene glycol	2.250	0.795	0.50	0.25	1.175	1.915	0.375	1.41
34	Methyl Cellosolve[b]	2.160	0.726	0.55	0.20	1.125	1.920	0.375	1.40
35	Ethyl Cellosolve[b]	2.160	0.773	0.475	0.2375	1.200	1.800	0.363	1.45
36	Tetrahydrofurfuryl alcohol[b]	2.060	0.898	0.40	0.30	1.275	1.615	0.344	1.53
37	*n*-Propyl Cellosolve[b]	2.160	0.833	0.425	0.2875	1.250	1.728	0.356	1.48
38	*n*-Butyl Cellosolve[b]	2.180	0.816	0.375	0.2625	1.275	1.710	0.354	1.49
39	2-Aminoethanol	1.750	0.777	0.425	0.2375	1.225	1.428	0.324	1.63
40	3-Amino-1-propanol	1.600	0.875	0.40	0.30	1.275	1.255	0.303	1.74
41	1-Amino-2-propanol	1.460	1.010	0.35	0.40	1.375	1.062	0.279	1.89
42	2-(2-Amino-1-ethylaminoethanol	1.460	1.075	0.45	0.425	1.300	1.123	0.287	1.84
43	*N*-β-Hydroxypropylethylenediamine	1.240	1.112	0.35	0.45	1.425	0.870	0.252	2.09
44	Diisopropylamine + ethanol (1:1)	1.991	0.919	0.40	0.35	1.300	1.531	0.335	1.57
45	10 *M* aqueous KOH	2.140	0.434	1.08	0.125	0.700	3.057	0.473	1.11
46	10 *M* aqueous KOH[b]	2.300	0.356	1.08	0.105	0.700	3.285	0.491	1.08
47	Single crystal of ice[c]	1.937	0.317	0.85	0.070	0.825	2.348	0.415	1.27
48	Methanol 4°K[d]	2.021	0.721	0.825	0.2125	0.925	2.184	0.400	1.32
49	Methanol 25°K[d]	2.157	0.592	0.83	0.145	0.875	2.465	0.425	1.24
50	Methanol 51°K[d]	2.262	0.504	0.83	0.120	0.875	2.585	0.435	1.21
51	Methanol 77°K[d]	2.355	0.455	0.83	0.105	0.850	2.771	0.451	1.17
52	Ethanol 4°K[d,e]	0.818	0.646	0.675	0.1625	1.000	0.818	0.245	2.15
53	Ethanol 4°K[d,f]	1.586	1.077	0.60	0.25	1.100	1.442	0.325	1.62

[a] I (experimental): a, observed absorption maximum in eV (M_{obsd}); b, relative band width (half-height width *vs.* M_{obsd}). II (assigned theoretical spectrum): a, attenuation coefficient (A); b, line-broadening parameter in units of $Z^2/2$ ($\Delta_{1/2}$); c, theoretical absorption maximum in units of $Z^2/2$ (m). III (derived information): a, ground-state energy in eV ($M_{obsd}/m \equiv Z_{obsd}^2/2$); c, Bohr radius in Å ($0.529/Z_{obsd}$). [b] The sample is partially photobleached. [c] Reference 25. [d] Reference 27. [e] Curve b of Figure 14. [f] Curve of Figure 14.

phatic ethers. The structure which gradually fades away with the increase of the paraffinic character of the molecules is extraordinary compared with the featureless spectra commonly observed for e_t^- in other matrices. From the set of simulation spectra which covered the range of $A = 0.1{\sim}1.1$ and $\Delta_{1/2} = 0.01{\sim}0.4$ (in units of $Z^2/2$) we could not find a superposable spectrum except for the *n*-butyl and isoamyl ethers.

The failure of correspondence between the experimental and theoretical spectra could be attributed to one of the two possible reasons below. (1) In the construction of the simulation spectrum we assigned, for simplicity, a single value of A for all the excited states. This may be an oversimplification for some matrices and if we differentiate A according to each electronic state, a better simulation spectrum will be obtained. (2) One of the primary assumptions in the theory is that the electron in the ground state can be approximated by the 1s-type wave function. If the electron interacts with a specific ether bond, the wave function may be distorted from the assumed spherical form and the line shape may be altered accordingly.

The proximity of A values for n-butyl and isoamyl ethers to those for the paraffins suggests that the general environment of the electron in these higher ethers is similar to that in the paraffins.

Amines. The spectra in Figure 5 indicate a rather subtle correlation between the spectral features and the molecular character. The energy at the absorption maximum and the band width for the first three primary amines are large compared with the polysubstituted diisopropylamine and triethylamine. *sec*-Butylamine is the intermediate between the two groups. Also, the spectrum for N,N-dimethylamino-n-propylamine seems to be a hybrid of those of triethylamine and the primary amines. Such a correlation has been pointed out previously.[13] From the above result as well as that for alcoholic matrices discussed below it may be said that the difference in the functional group of matrix molecule results in the spectral difference and a possible speculation will be made in the next subsection.

Monohydroxy Alcohols. Although the spectra of e_t^- in this class of matrix have been observed by many authors,[14] the absorption in the near-infrared region has not been carefully measured. As shown in Figure 6, higher alcohols exhibit bumps in this region in addition to the major absorption in the visible. This structure is not of the same nature as that of the spectra for the ethers because the partial bleaching with longer wavelengths ($\lambda > 0.7\ \mu$) removed the structure as shown in Figure 7. Qualitative observations indicate that the infrared band is more easily photobleached than the visible band and that the former is more sensitively removed by electron-scavenging impurities. The dose dependence of the absorption is also different between the infrared and the visible bands, the former being more easily saturated. Because of this complexity we compared the theoretical spectrum only for methanol and ethanol which gave no infrared absorption. The comparison was made, however, for all the photobleached samples (Figure 7).

The observed difference between the near-infrared and visible bands indicates that there are two types of trap and the shallower ones increase as the alkyl branch becomes larger. It may be speculated that the electrons giving rise to the infrared and the visible absorptions are trapped respectively in the regions where the paraffinic and the hydroxyl groups are locally concentrated.

Since in such a higher alcohol as 1-pentanol the bulky alkyl group would prevent the formation of extensive hydrogen network, the electron surviving the partial photobleaching will see only dimeric or at most a few associated hydroxyl groups in its vicinity and yet the spectra for the photobleached primary alcohols are more or less similar, the λ_{max} being in a narrow range of 2.2~2.5 eV (Table I). On the other hand, the λ_{max} of the secondary alcohol (2-propanol) shifts remarkably to red as has been observed for the solvated electron in liquid 2-propanol.[15] A recent result of pulse radiolysis of 2-propanol at 77°K indicates

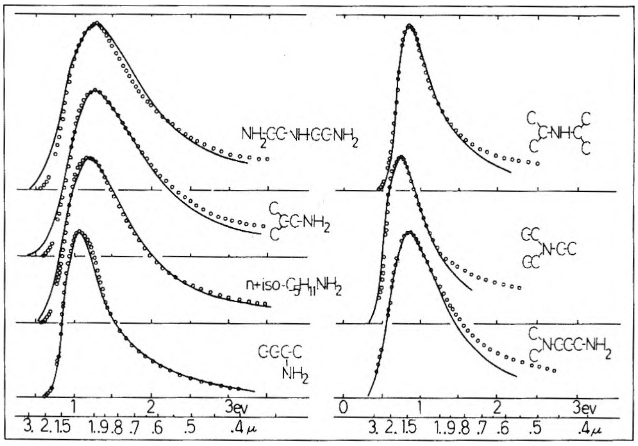

Figure 5. Absorption spectra of e_t^- in amines. See caption for Figure 3 (*cf.* entry no. 9–15 in Table I).

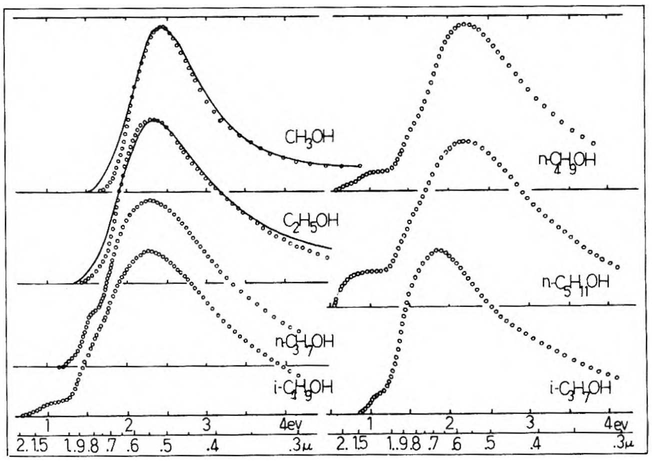

Figure 6. Absorption spectra of e_t^- in monohydroxy alcohols. See caption for Figure 3 (*cf.* entry no. 16 and 18 in Table I). Comparison with the theoretical spectrum is made only for methanol and ethanol for the reason stated in the text.

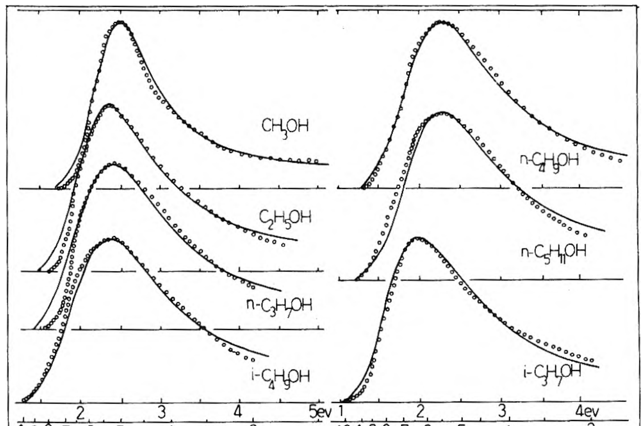

Figure 7. Absorption spectra of e_t^- in monohydroxy alcohols after partial photobleaching of the irradiated samples. See caption for Figure 3 (*cf.* entry no. 17–25). $\lambda > 0.7\ \mu$ was used for methanol and ethanol and $\lambda > 1\ \mu$ for the rest.

(13) S. Noda, K. Fueki, and Z. Kuri, *Chem. Phys. Lett.*, **8**, 407 (1971).
(14) For example, A. Habersbergerova, L. Josimovic, and J. Teply, *Trans. Faraday Soc.*, **66**, 669 (1970).
(15) M. C. Sauer, Jr., S. Arai, and L. M. Dorfman, *J. Chem. Phys.*, **42**, 708 (1965).

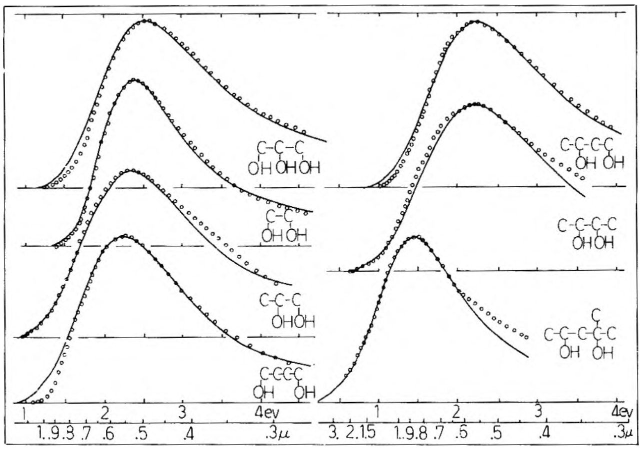

Figure 8. Absorption spectra of e_t^- in polyhydroxy alcohols. See caption for Figure 3 (*cf.* entry no. 26–32 in Table I).

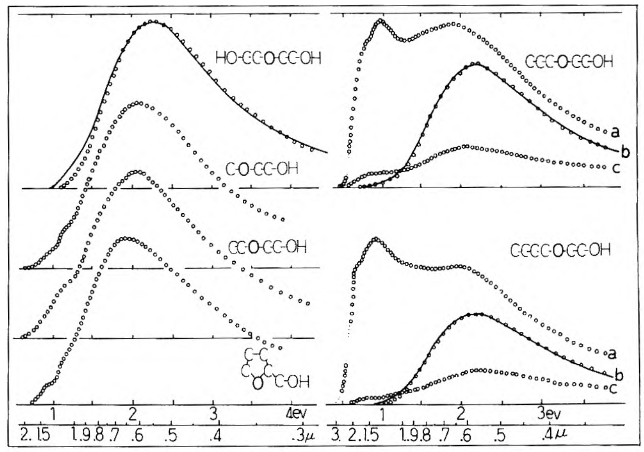

Figure 9. Absorption spectra of e_t^- in ether alcohols. See caption for Figure 3 (*cf.* entry no. 33–38 in Table I). Only for diethylene glycol the spectrum immediately after irradiation was compared with the theoretical spectrum. For all the samples the bleaching with $\lambda > 1\ \mu$ was carried out but the result of the comparison with the theoretical spectrum is illustrated only for *n*-propyl and *n*-butyl Cellosolves (solid curves for the spectra b which are obtained after bleaching with $\lambda > 1\ \mu$. Spectra c are obtained after subsequent bleaching with $0.6\ \mu > \lambda > 0.4\ \mu$). The data for the others are listed in Table I.

that the polar groups are reoriented toward the electron even in the low-temperature glass.[16] Referring to these results, it may be conceived that the degree of reorientation is different between the primary and the secondary alcohols owing to the blocking two methyl groups in the latter and that this difference makes the distance between the electron and the polar group of 2-propanol slightly longer which, in turn, causes the spectral red shift. The correlation between the spectrum and the type of the functional group of the amines mentioned above may be similarly explicable.

Although the apparent λ_{max} for the primary alcohols are similar as mentioned above, the coefficients A in Table I show a gradual decrease with increasing the size of the alkyl group which implies more contribution of the bound–free transition according to the theory. This is reasonable because the dilution of the matrix with the alkyl group will provide an environment resemblant to the paraffinic matrices where the electron is concluded to suffer mainly the bound–free transition. Table I also shows that the ground-state energy becomes larger (in absolute magnitude) as the primary alcohol becomes smaller which is understandable because for smaller alcohols the stabilization due to the interaction between the electron and the permanent dipole moment should increase through the increase of the number of the dipole in the unit volume and through the easier rotation of dipole toward the electron. It is not inconsistent that the λ_{max} remains relatively constant while the ground-state energy increases with the decrease of the molecular size because the reoriented permanent dipole moments remain "frozen" during the optical transition of the electron.

Polyhydroxy Alcohols. As shown in Figure 8, e_t^- in the polyhydroxy alcohols did not show the infrared absorption but only a single visible band similar to that observed for the partially bleached monohydroxy alcohols. The result suggests that the phase of the polyhydroxy alcohols is not segregated into the nonpolar and polar regions owing to the abundance of the hydrogen bridges. All the alcohols in Figure 8 except 2,3-butanediol and hexylene glycol have the primary alcoholic group, CH_2OH. This may be the reason for the spectral similarity between the primary mono- and polyhydroxy alcohols. As for the secondary diols, the remarkable red shift for hexylene glycol is similar to that for 2-propanol. However, the shift is not so conspicuous for 2,3-butanediol, and it might be that the vicinal hydroxyl groups accidentally provide a similar environment to the electron as in the primary alcohols.

Compared with the monohydroxy alcohols the attenuation coefficients shown in Table I are not so regular. It seems that the presence of the secondary alcohol group in the molecule suppresses the value of A to $0.4 \sim 0.45$ while the pure primary diols (ethylene glycol and 1,4-butanediol) maintain similar features as the monohydroxy primary alcohols. At present we can only speculate that the inter- and intramolecular hydrogen bridges involving the secondary alcohol group might be responsible for the lower A values.

Ether Alcohols. For the partial esters of polyhydroxy alcohols the infrared absorption becomes prominent again as in the cases of higher monohydroxy alcohols (see, *e.g.*, *n*-butyl Cellosolve in Figure 9). The infrared absorption manifests a slight structure similarity to the ethers in Figure 4. Thus, it is apparent that in the Cellosolves as in the higher alcohols the hydrogen bridge between the hydroxyl groups separates the phase into the ethereal and the alcoholic regions to give rise to two types of e_t^-. The absence of the infrared absorption for diethylene glycol in Figure 9 is analogous to the absence of the corresponding absorption in polyhydroxy alcohols. The partial photobleaching with $\lambda > 1\ \mu$ eliminated the infrared absorption as shown representatively for *n*-propyl and *n*-butyl Cellosolves (curves a to b). Successive bleaching with shorter wavelengths ($0.4\ \mu < \lambda < 0.6\ \mu$) recovered slightly the infrared absorption (curves b to c). Therefore, the electrons trapped in the two different regions seem to go forth and back upon bleaching. Part of the electrons trapped in alcoholic region, however, seems to suffer the photoinduced decomposition[17]

$$ROH + e_t^- \xrightarrow{h\nu} RO^- + H$$

because the recovery of the infrared absorption shown in

(16) L. Kevan, *Chem. Phys. Lett.*, **11**, 140 (1971).
(17) T. Shida and W. H. Hamill, *J. Amer. Chem. Soc.*, **88**, 3689 (1966).

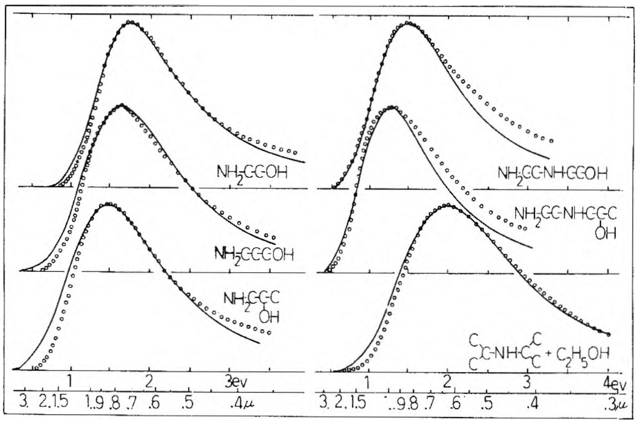

Figure 10. Absorption spectra of e_t^- in amino alcohols. See caption for Figure 3 (*cf.* entry no. 39–44 in Table I). The mixture is 1:1 by volume at room temperature.

curve c is disproportionately small. The values of A and $\Delta_{1/2}$ assigned to the spectrum after the first bleaching are close to those for the mono- and polyhydroxy alcohols which indicates that the electrons after the first bleaching are mainly localized in the alcoholic region.

The present results of the ether alcohols are consistent with the results of the previous work on the mixtures of methyltetrahydrofuran plus ethanol[18] or methanol[19] at 77°K which upon irradiation produce two absorption bands characteristic of each component. If the ethereal oxygen was as strong a hydrogen acceptor as the hydroxyl oxygen, the mixtures of the previous work as well as the ether alcohols studied in this work would not be microscopically segregated, so that one would have a single kind of e_t^- as in the polyhydroxy alcohols.

Amino Alcohols. Contrary to the ether alcohols, the amino alcohols give rise to a single band as shown in Figure 10. Also, a mixture of diisopropylamine and ethanol exhibits only a single band which is an intermediate of the absorption bands of e_t^- in the constituent matrices. In these matrices one can expect four different combinations for the hydrogen bridges, OH→OH, OH→NH, NH→OH, and NH→NH. If the first pair predominated, the phase of the medium would be segregated into two regions and one might have two distinct absorption bands as in the case of higher alcohols and ether alcohols. The appearance of an intermediate single band suggests that all the combinations participate in the hydrogen network formation so that the electron may see a relatively homogeneous medium compared with the higher alcohols.

The pairs of 3-amino-1-propanol *vs.* 1-amino-2-propanol and 2-(2-aminoethylamino)ethanol *vs.* *N*-β-hydroxypropylethylenediamine in Figure 10 provide additional examples of the red shift in the matrix having the secondary alcohol group.

Aqueous Solution. Figure 11 (upper two spectra) shows the familiar spectrum of e_t^- in the alkaline ice.[20] The partial photobleaching makes the spectrum a little sharper and shifts the λ_{max} slightly as has been observed previously.[21,22] The sharpening has been taken as an indication of the dispersion of the nature of trap site. In accordance with this interpretation the value of $\Delta_{1/2}$, a measure of the randomness of trap, decreases slightly upon the bleaching (Table I).

With the assigned value of A = 1.08 the first excited level should locate near the 2p level of a hydrogenic atom,

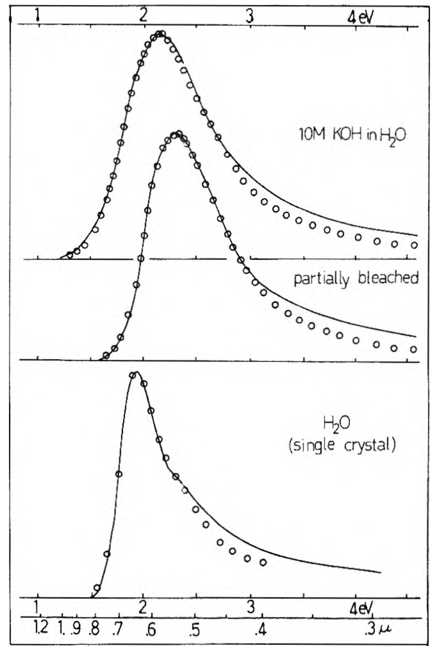

Figure 11. Absorption spectra of e_t^- in aqueous systems: upper two, alkaline glassy solid immediately after irradiation and after the subsequent partial photobleaching with λ >0.7 μ; bottom, single crystal of ice.[25] See caption for Figure 3 (*cf.* entry no. 45–47 in Table I).

i.e., about $\frac{1}{4} \times Z^2/2$ below the ionization threshold of $Z^2/2$ (see eq 5). Also, most of the oscillator strength should reside in the first transition, and the contribution of the bound-free transition should be small as has been briefly pointed out by Copeland, *et al.*,[2] (*cf.* the spectra at the bottom of Figure 2). This conclusion is in apparent contradiction to the experimental result that the activation spectrum of photoconduction superposes on the optical absorption spectrum over the measured region of 1.9~3.4 eV.[23]

However, in a preliminary experiment on the photobleaching of trapped electron in aqueous alcoholic glasses containing various amounts of potassium hydroxide we found that the efficiency of bleaching increased with the concentration of the salt although the spectral pattern was not much affected by the presence of the additive.[24] Since the light used for bleaching corresponded to the absorption due to the 1s-2p type transition, it seems that the 2p electron whether in ice or water–alcohol glasses is released from the trap by some influence of the ionic solute. It is interesting in this context that the result of the study on the single crystal of ice is consistent with the theoretical conclusion above (see below).[25] Also, it is interesting that the hydrated electron in water without the excessive alkaline hydroxide is not apparently photobleachable by the intense laser light.[26]

(18) L. Shields, *J. Phys. Chem.*, **69**, 3186 (1965).
(19) K. Sawai and W. H. Hamill, *J. Phys. Chem.*, **73**, 3452 (1969).
(20) D. Schulte-Frohlinde and K. Eiben, *Z. Naturforsch. A*, **17**, 445 (1962).
(21) B. G. Ershov and A. K. Pikaev, *Advan. Chem. Ser.*, **No. 81**, 1 (1968).
(22) G. V. Buxton, F. S. Daintcn, T. E. Lantz, and F. P. Sargent, *Trans. Faraday Soc.*, **66**, 2962 (1970).
(23) I. Eisele and L. Kevan, *J. Chem. Phys.*, **53**, 1867 (1970).
(24) T. Shida and M. Imamura, unpublished results.
(25) K. Kawabata, *J. Chem. Phys.*, **55**, 3672 (1971).
(26) G. Kenney-Wallace and D. C. Walker, *J. Chem. Phys.*, **55**, 447 (1971).

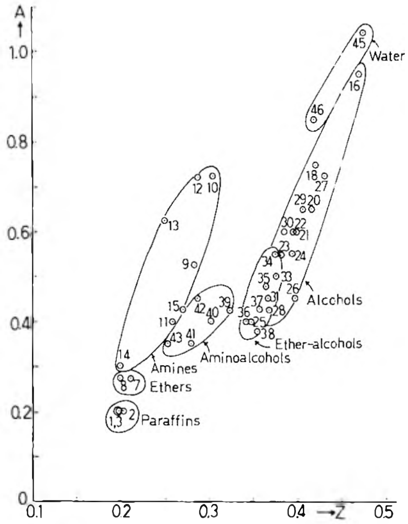

Figure 12. Plot of the attenuation coefficient A *vs.* the effective charge for the ground state Z. The numbers refer to the entry in Table I.

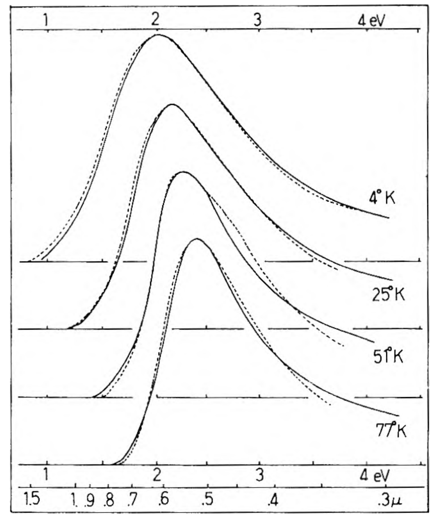

Figure 13. Absorption spectra of e_t^- in methanol at various low temperatures.[27] See caption for Figure 3 (*cf.* entry no. 48–51 in Table I).

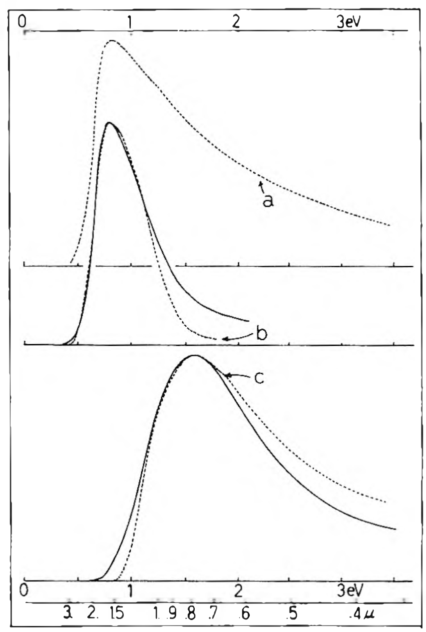

Figure 14. Absorption spectra of e_t^- in ethanol at 4°K:[27] a, immediately after irradiation; b, the component of a photobleached by light of λ 1.2 μ; c, same as a after the bleaching. Dotted curves are experimental.[27] Solid curves are theoretical (*cf.* entry no. 52 and 53 in Table I).

General Discussion

Except for the case of ether, the agreement between theory and experiment is satisfactory. One might claim that with two parameters any theory could give as good a result as the present approach. However, the quantities A and $\Delta_{1/2}$ are not completely arbitrary and should be subject to some restriction imposed by the physical meaning attached to them: as mentioned above, the attenuation coefficient should tend to zero for the nonpolar matrix such as paraffin and should become larger with the polarity of the matrix molecule. As for $\Delta_{1/2}$, we expect a higher value for a larger molecule having an irregular molecular shape. Although we searched a best-fit set of A and $\Delta_{1/2}$ purely from the graphical matching between the observed and the simulated spectra, the selected values showed some regularity indicative of physical significance. For example, the plot of A against Z shown in Figure 12 demonstrates a relatively smooth sequence of the polarity of the matrix molecule. As will be discussed elsewhere,[5] Z also should be subject to a physical restriction of $Z \geq 5/16(1 - 1/\epsilon_s)$ where ϵ_s is the static dielectric constant of the matrix which may be in the range of $2 \sim 3$ at 77°K. The values of Z in Figure 12 are in conformity with this restriction.

Recently two interesting papers concerning the spectrum of e_t^- in frozen solids have been published.[25,27] Hase, *et al.*, found that the absorption spectrum of e_t^- in alcohols and ice shows a temperature-dependent change between 4 and 77°K.[27] Some of their results are reproduced in Figures 13 and 14 (dotted curves). The spectrum for methanolic glasses becomes gradually sharper and asymmetric as the glass is warmed from 4°K to progressively higher temperatures (Figure 13). The values of $\Delta_{1/2}$ assigned to the observed spectra indicate that the statistical fluctuation of the environment of the electron is *higher* for lower temperatures. We conjecture that the enhanced rigidity at lower temperatures prevents the reorientation of the functional group to the electron and that the electron will see a more disordered environment than in the softer matrix. The components of absorption, the dotted curves b and c of Figure 14, have been associated with "unrelaxed" and "relaxed" traps in the ethanol matrix.[27] We applied our theory to each component and obtained the theoretical spectra in solid curves which are in fair agreement with the experimental spectra. Since $\Delta_{1/2}$ assigned to the relaxed trap is still much larger than that for e_t^- in ethanol at 77°K, the component c is expected to suffer a similar sharpening as shown in Figure 13 when the temperature is raised toward 77°K.

The second paper of interest concerns the spectrum of e_t^- in single crystals of pure ice (open circles shown at the bottom of Figure 11).[25] The simulation curve drawn with $A = 0.85$ and $\Delta_{1/2} = 0.07$ (in units of $Z^2/2$) apparently explains the sharp and partly structured experimental spectrum. The significantly smaller value of $\Delta_{1/2}$, of course,

(27) H. Hase, M. Noda, and T. Higashimura, *J. Chem. Phys.*, **54**, 2975 (1971).

implies that the environment of the electron is much more regular in the crystal than in the amorphous glass. The smaller value of A than that for the alkaline ice (A = 1.08) means less polarity in the crystal which is reasonable because the excessive alkaline hydroxide in the glassy solid would enhance the dielectric constant and lower the rigidity to permit more rotation of water molecule toward the electron. It should be emphasized that Kawabata has found that e_t^- in the crystal is hardly photobleached by the light corresponding to the absorption on the low-energy side of the spectrum. This result is consistent with our assignment of A = 0.85 which guarantees that the absorption on the low-energy side is mainly due to the 1s–2p-type bound transition.

Acknowledgment. The authors wish to acknowledge the discussions of Dr. M. Imamura and Mr. M. Tachiya.

Electronic Absorption Spectra of Excess Electrons in Molecular Aggregates. II. Solvated Electrons

Tadamasa Shida,* Suehiro Iwata,

The Institute of Physical and Chemical Research, Wako-shi, Saitama, Japan

and Tsutomu Watanabe

Department of Applied Physics, The University of Tokyo, Tokyo, Japan *(Received March 10, 1972)*

Publication costs assisted by The Institute of Physical and Chemical Research

Spectra of solvated electrons from various sources have been compiled for analysis in terms of the theory proposed in the preceding paper. The observed absorption line shape has been well reproduced by the theoretical simulation spectrum. In particular, the temperature and the pressure effects on the spectrum of hydrated electron are reasonably accounted for.

Introduction

Recent developments in the pulse radiolysis technique have broadened our scope of the solvated electron in liquids.[1] However, the newly observed spectra have not always been fully discussed from the theoretical viewpoint. Since the theory proposed in the preceding paper proved to be successful for the explanation of the optical spectrum of trapped electron in γ-irradiated frozen solids,[2] we have applied it to the solvated electron in liquids whose spectral data are now abundantly available in the literature. Although the phenomenological agreement with experiments does not prove the uniqueness of the theory, the results in this as well as in the preceding papers should add to the credence of the proposed theory.

Discussion on the Individual Spectrum

According to the hydrogenic model in the preceding paper, the nature of the medium for the excess electron can be characterized by the attenuation coefficient A and the degree of randomness of the trap site $\Delta_{1/2}$. The values of these quantities are determined semiempirically by superposing the experimental spectrum on the theoretical spectrum which is an envelope of the oscillator strengths for a hydrogenic atom. The effective charge Z' for the upper states of the atom is supposed to be properly attenuated as $Z' = AZ$ where Z is the effective charge assigned to the ground state. By this comparison between the theory and experiment one can deduce the following information on the electronic states: the ground-state energy $-Z^2/2$ relative to a reference energy state, the effective charge for the ground Z as well as for the excited states AZ, and the Bohr radius of the ground-state $1/Z$.

In the following we apply the above theoretical analysis to the individual spectrum reported in the literature. Both the theoretical and experimental information will be summarized in Table I.

Paraffins. Gillis, *et al.*, found for the first time the absorption spectrum of the solvated electron in low-viscosity liquid paraffins.[3] The spectrum observed for liquid propane at $-185°$ is reproduced in open circles of Figure 1. A similar pulse-radiolytic experiment by Klassen, *et al.*, also revealed a similar spectrum for a more rigid paraffinic glass[4] (the dotted curve in Figure 1. The original spectrum shown in ref 4 is not corrected for the absorption in the silica cell. The author wishes to thank Dr. Klassen for sending him the corrected spectrum in Figure 1.) The solid curves in Figure 1 are obtained by assigning the values of A and $\Delta_{1/2}$ in Table I to the theoretical spectrum discussed in the preceding paper.[2] Compared with the trapped electron in frozen paraffins[2] the values of $\Delta_{1/2}$ for the solvated electron in viscous liquids are a little larger which may be attributed to the enhanced thermal fluctuation of the solvents. As in the case of the trapped electron the electronic absorption is mostly associated

(1) *Ber. Bunsenges. Phys. Chem.*, **75**, 608–714 (1971) (special issue for the excess electron in condensed media.)
(2) T. Shida, S. Iwata, and T. Watanabe, *J. Phys. Chem.*, **76**, 3683 (1972).
(3) H. A. Gillis, N. V. Klassen, G. G. Teather, and K. H. Logan, *Chem. Phys. Lett.*, **10**, 481 (1971)
(4) N. V. Klassen, H. A. Gillis, and D. C. Walker, *J. Chem. Phys.*, **55**, 1979 (1971)

TABLE I: Experimental and Theoretical Spectral Data[a]

Entry no.		I	IIa	IIb	IIc	IIIa	IIIb	IIIc
1	Propane[b]	0.606	0.20	0.275	1.400	0.433	0.178	2.97
2	3-Methylhexane[c]	0.627	0.20	0.350	1.450	0.432	0.178	2.97
3	Tetrahydrofuran[d]	0.596	0.55	0.060	0.975	0.611	0.212	2.49
4	Ethylenediamine[e]	0.948	0.45	0.275	1.225	0.774	0.238	2.21
5	Methanol, rt[f]	1.980	0.87	0.170	0.875	2.263	0.407	1.29
6	Methanol, −78°[f]	2.180	0.84	0.150	0.875	2.491	0.427	1.23
7	Ethanol, rt[f]	1.750	0.60	0.300	1.125	1.555	0.338	1.56
8	Ethanol, −78°[f]	2.125	0.65	0.175	1.025	2.073	0.390	1.35
9	2-Propanol, rt[f]	1.530	0.40	0.175	1.200	1.275	0.306	1.73
10	2-Propanol, −78°[f]	1.870	0.40	0.100	1.150	1.626	0.345	1.53
11	Glycerin[f]	2.360	0.83	0.170	0.900	2.622	0.438	1.20
12	Glycerin, 32[f]	2.000	0.99	0.130	0.775	2.580	0.435	1.21
13	Glycerin, 8[f]	1.880	1.06	0.135	0.750	2.506	0.429	1.23
14	Ammonia, −15°[e]	0.768	1.08	0.145	0.725	1.060	0.279	1.89
15	Deuterioammonia, 78[g]	0.870	1.05	0.145	0.750	1.160	0.292	1.81
16	Ammonia, 13.8[e]	1.593	1.08	0.145	0.725	2.197	0.401	1.31
17	Water, 1 bar[h]	1.710	1.08	0.125	0.700	2.442	0.423	1.24
18	Water, 1.10 kbar[h]	1.770	1.08	0.135	0.725	2.441	0.423	1.24
19	Water, 2.13 kbar[h]	1.840	1.08	0.135	0.725	2.537	0.431	1.22
20	Water, 3.53 kbar[h]	1.910	1.05	0.145	0.750	2.546	0.432	1.22
21	Water, 4.88 kbar[h]	1.940	1.00	0.140	0.775	2.503	0.428	1.23
22	Water, 6.26 kbar[h]	2.000	0.99	0.135	0.775	2.580	0.435	1.21
23	Water, −4°[i]	1.842	1.08	0.135	0.725	2.540	0.431	1.22
24	Water, 90°[i]	1.550	0.98	0.160	0.800	1.937	0.377	1.40
25	Water, 203°[i]	1.234	0.95	0.200	0.850	1.451	0.326	1.62
26	Water, 300°[i]	1.050	0.425	0.2375	1.225	0.857	0.250	2.10
27	Water, 361°[i]	0.970	0.225	0.1875	1.325	0.732	0.232	2.28
28	Water, 390°[i]	0.960	0.15	0.325	1.475	0.650	0.218	2.42

[a] Key to the columns. I (experimental): observed absorption maximum in eV (M_{obsd}). II (assigned theoretical spectrum): a, attenuation coefficient (A); b, line-broadening parameter in units of $Z^2/2$ ($\Delta_{1/2}$); c, theoretical absorption maximum units of $Z^2/2$ (m). III (derived information): a, ground-state energy in eV ($M_{obsd}/m \equiv Z^2{}_{obsd}/2$); b, effective charge for the ground state (Z_{obsd}); c, Bohr radius of the ground-state electron in Å ($0.529/Z_{obsd}$). [b] Reference 3. [c] Reference 4. [d] Reference 5. [e] Reference 6. [f] Reference 7, rt denotes room temperature. [g] Reference 8. [h] Reference 11. [i] Reference 13.

with the bound-free transition with $A = 0.2$. Since the absorption of the solvated electron appears not to have been detectable above −118°,[3] the electron is considered to be easily delocalized both optically and thermally.

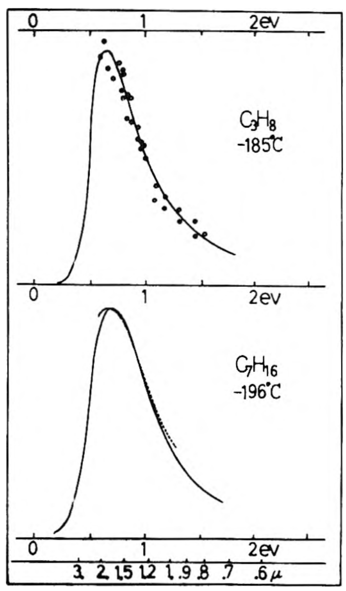

Figure 1. Absorption spectra of solvated electron in low-temperature paraffins. Open circles and the dotted curve are experimental.[3,4] Solid curves are theoretical (*cf.* entry no. 1 and 2 in Table I).

Polar Liquids. Figure 2 shows the spectra observed by Dorfman[5,6] and by Arai[7] for several polar liquids (circles and dotted curves). It is noted that the relatively sharp absorption band of the ether and the noticeable difference between the primary and secondary alcohols are quite analogous to the results of the trapped electrons.[2] The narrower band width for the cooled alcohols is reflected to a smaller value of $\Delta_{1/2}$ in Table I which indicates the suppressed thermal fluctuation of the solvents.

Figure 3 is a collection of spectra for some binary solutions reported by Schindewolf,[8] Dorfman,[6] and Arai.[7] For the ammonia–water system the attenuation coefficient is roughly unity and is relatively insensitive to the composition of the solution. Since both ammonia and water are small rotatable molecules having comparative permanent dipole moments, the effective one-electron potential for the solvated electron may be approximated by such a curve as that in Figure 1B of the preceding paper for all the compositions of the solution. As for the ground-state energy $-Z^2/2$, it decreases with the concentration of ammonia as shown in Table I. The ground-state energy may be compared with the following expression obtained for a molecular model of the solvating medium[9,10]

(5) L. M. Dorfman, F. Y. Jou, and R. Wageman, ref 1, p 681.
(6) J. L. Dye, M. G. DeBacker, and L. M. Dorfman, *J. Chem. Phys.*, **52**, 6251 (1970).
(7) S. Arai and M. C. Sauer, Jr., *J. Chem. Phys.*, **44**, 2297 (1966).
(8) R. Olinger and U. Schindewolf, ref 1, p 693.
(9) K. Fueki, D. F. Feng, and L. Kevan, *J. Phys. Chem.*, **74**, 1976 (1970).
(10) T. Shida, S. Iwata, and T. Watanabe, to be submitted for publication.

$$E_1^0 = \int\psi^*(-\tfrac{1}{2}\Delta)\psi d\tau + \{-N\mu\langle\cos\theta\rangle_{av}/\epsilon_{op}R^2 - N\alpha/2\epsilon_{op}^2R^4 + \tfrac{1}{2}(1 - 1/\epsilon_s)f(R)\}\int_{r<R}\psi^2 d\tau + \tfrac{1}{2}(1 - 1/\epsilon_s)\int_{r>R}f(r)\psi^2 d\tau \quad (1)$$

where the symbols other than the self-explanatory ones are as follows: N, the number of solvating molecules in the first solvation layer; μ, dipole moment; $\langle\cos\rangle$, net projection of the moment toward the electron; $\epsilon_s, \epsilon_{op}$, dielectric constants; R, cavity radius; $f(r)$, a self-consistent electric potential. The decrease of the ground state with the addition of ammonia, therefore, may be mainly attributed to the expansion of the cavity which decreases the stabilization due to the electron-dipole interactions given by the first two terms in the curly brackets.

In contrast to the ammoniacal solution, the attenuation coefficient of the aqueous alcohol solutions shows a systematic increase with the water content indicating the increase of the polarity for the solvated electron (Table I).

Water. The very original solvated electron in water is now being studied under various conditions. The results obtained by Hentz, *et al.*,[11] as well as by Robinson, *et al.*,[12] show that the spectrum shifts to blue with the pressure (Figure 4, circles). The assigned value of A decreases slightly with the pressure while $\Delta_{1/2}$ changes little (Table I). Accordingly, the theoretical spectrum becomes more symmetrical with the pressure in agreement with the experiment. The constancy of $\Delta_{1/2}$ in Table I is consistent with Hentz's view that the immediate vicinity of the elec-

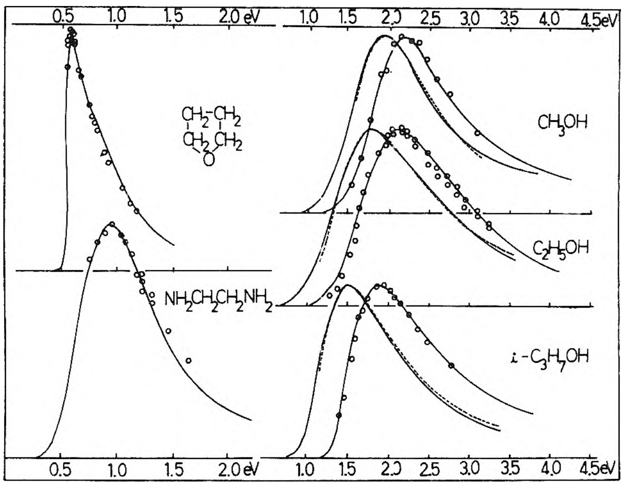

Figure 2. Absorption spectra of solvated electron in polar liquids. Open circles and dotted curves are experimental observed for the liquids at room temperature and at −78°, respectively.[5−7] Solid curves are theoretical (*cf.* entry no. 3–10 in Table I).

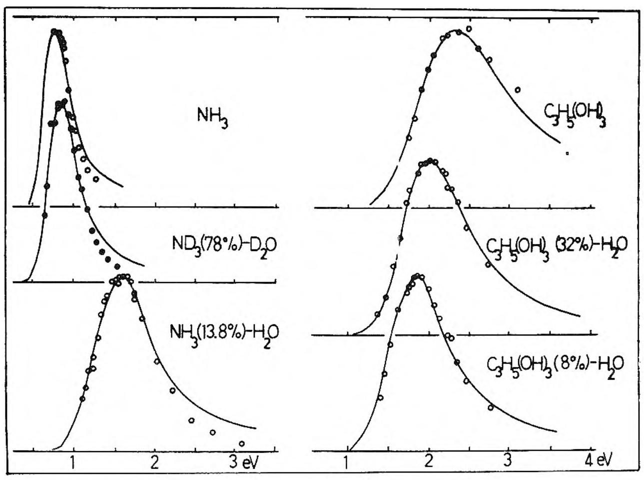

Figure 3. Absorption spectra of solvated electron in aqueous solutions. Circles are experimental.[5,7,3] Solid curves are theoretical (*cf.* entry no. 11–16 in Table I).

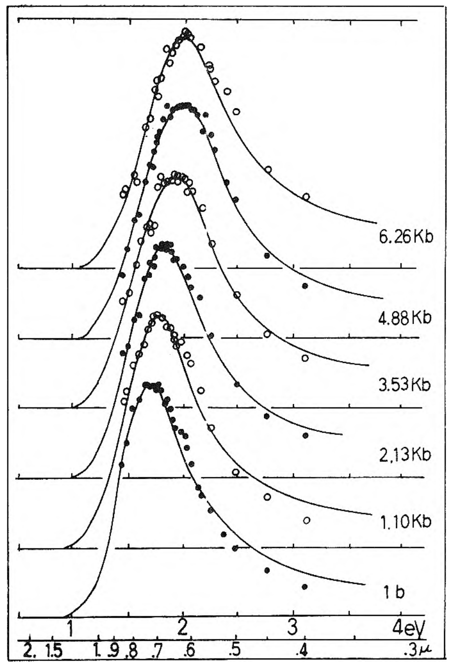

Figure 4. Absorption spectra of hydrated electron in pressurized water. Circles are experimental.[11] Solid curves are theoretical (*cf.* entry no. 17–22). The symbol Kb stands for kilobar.

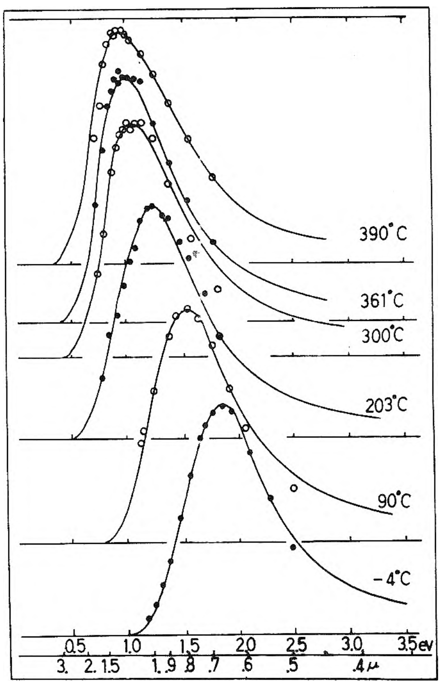

Figure 5. Absorption spectra of hydrated electron at various temperatures. Circles are experimental.[13] Solid curves are theoretical (*cf.* entry no. 23–28 in Table I).

(11) R. R. Hentz, Farhataziz, and E. M. Hansen, *J. Chem. Phys.*, **55**, 4974 (1971).

(12) M. G. Robinson, K. N. Jha, and G. R. Freeman, *J. Chem. Phys.*, **55**, 4933 (1971).

tron is little influenced by the pressure whereas the slight decrease of A might be accounted for by the increased hindrance of the rotation of dipoles in the bulk which suppresses the polarity of the solvent.

The temperature effect on the spectrum is much more conspicuous as shown in circles of Figure 5.[13] The coefficient A decreases rapidly with temperature and at the extreme temperature of 390° it becomes as low as 0.15. Since at this supercritical temperature most of the water molecule may be in the monomeric form and be vigorously agitated,[14] the effective potential for the optical electron would not be of a long-range type as shown by Figure 1A or B in the preceding paper and the situation for the electron may be similar to that in paraffins. The decrease of the ground-state energy at higher temperatures is explicable by the temperature dependence of the terms in eq 1; above all, the decrease in $\langle \cos \theta \rangle_{av}$ ($\simeq \mu/3kTR^2$) and N and the increase in R will be effective for the destabilization. It is emphasized that the change of the absorption line shape from symmetric to asymmetric upon the temperature rise is automatically explained by the present theory in terms of the decrease in the value of A which means the gradual change of the major component of the absorption from the 1s–2p bound–bound to the bound–free transitions.

Concluding Remark

Considering that the hydrogenic model is coarse graining in the sense that it ignores the microscopic structure of the solvent, it is gratifying that the model can account for the difference of the solvent molecule to a considerable extent and extract some information proper to the electron in the solvent.

(13) B. D. Michael, E. J. Hart, and K. H. Schmidt, *J. Phys. Chem.*, **75**, 2798 (1971).
(14) W. A. P. Luck, *Ber. Bunsenges. Phys. Chem.*, **69**, 626 (1965); *J. Phys. Chem.*, **74**, 4006 (1970).

γ-Ray Irradiated Sodium Chloride as a Source of Hydrated Electrons[1]

C. Gopinathan, P. S. Damle, and Edwin J. Hart*

Chemistry Division, Argonne National Laboratory, Argonne, Illinois 60439 *(Received March 15, 1972)*

Publication costs assisted by Argonne National Laboratory

Hydrated electrons form when γ-ray irradiated sodium chloride dissolves in water. By dissolving the salt in aqueous solutions with different N_2O and O_2 concentrations, N_2 evolves in amounts expected for e_{aq}^-. Below 0.0004 M O_2 the ratio of rate constants, $k[e_{aq}^- + O_2]/k[e_{aq}^- + N_2O]$, of 2.3 ± 0.1 is found for dissolving irradiated NaCl compound with a ratio of 2.4 ± 0.1 in electron or γ-ray irradiated solutions. At higher O_2 concentrations, O_2 is a more effective scavenger of the precursor of e_{aq}^- and the rate constant ratio for this species reaches 14.8. In O_2-free solutions, the N_2 yield is independent of the N_2O concentration in the range 0.0003–0.010 M N_2O and approximates the F center yield. The mechanism of e_{aq}^- formation in dissolving irradiated NaCl is briefly discussed.

Introduction

For nearly 2 decades it has been known that irradiated sodium chloride induces chemical effects when it dissolves in water.[2-5] Hydrogen and iodine form when solution takes place in aqueous iodide.[4] Light emission[6,7] and the oxidation of ferrous ion[8] were discovered a little later. Since then, other studies[9-11] reveal that fluorescent solutes intensify the emission, whereas other solutes such as O_2, NO_3^-, and reducing agents quench this emission. While the possibility of direct excitation of water has been considered, these phenomena have generally been attributed to the release and reaction of hydrated electrons.

There has been a revival of interest in this field. A new explanation has been published,[12] postulating the release of triplet excitons when irradiated sodium chloride dissolves in water. If this is indeed the case, then the applications to aqueous radiation chemistry are obvious since evidence for exciton reactions in the radiation chemistry of frozen aqueous systems has been reported recently.[13] A

(1) Work performed under the auspices of the U. S. Atomic Energy Commission.
(2) M. Hacskaylo and D. Otterson, *J. Chem. Phys.*, **21**, 552 (1953).
(3) M. Hacskaylo and D. Otterson, *J. Chem. Phys.*, **21**, 1434 (1953).
(4) W. G. Burns and T. F. Williams, *Nature (London)*, **175**, 1043 (1955).
(5) J. G. Rabe, B. Rabe, and A. O. Allen, *J. Phys. Chem.*, **70**, 1098 (1966).
(6) T. Westermark and B. Grapengiesser, *Nature (London)*, **188**, 395 (1960).
(7) T. Westermark and B. Grapengiesser, *Ark. Kemi*, **17**, 139 (1961).
(8) T. Westermark, B. Grapengiesser, and N. Biesert, *Ark. Kemi*, **17**, 151 (1961).
(9) G. Ahnström, *Acta Chem. Scand.*, **19**, 300 (1965).
(10) L. E. Eriksson, *Acta Chem. Scand.*, **16**, 2113 (1962).
(11) B. Lelierere and J. P. Adloff, *J. Phys. (Paris)*, **25**, 789 (1964).
(12) J. P. Mittal, *Nature (London)*, **A230**, 160 (1971).
(13) P. N. Moorthy, C. Gopinathan, and K. N. Rao, *Radiat. Eff.*, **2**, 175 (1970).

model of aqueous radiolysis involving excitons has also been proposed.[14,15] However, a later group of workers[16] support the earlier suggestion that hydrated electrons are involved in the light emission process. We attempt to establish beyond controversy the nature of the chemical reducing species released into water when irradiated salt dissolves, as this may have important consequences for the radiation chemistry of water and of the structure of the hydrated electron.

Experimental Section

For all experiments where salt was irradiated, Merck Reagent Grade NaCl (Batch 7407) was used without further modification. Where aqueous solutions of salt were irradiated, analytical reagent grade NaCl or the above batch of NaCl was used. The water used was triple distilled in the normal way. All other chemicals used were of analytical reagent grade. The gases used were Matheson Research Grade.

The hydrogen yields were measured by taking a known weight ($\sim$3 g) of irradiated NaCl in a syringe, flushing it for 15 min with a stream of argon gas, and then pushing a sufficient amount of argon-purged 0.4 M H_2SO_4 into the syringe until the salt dissolved. The resultant solution was drawn into a Van Slyke apparatus, and the hydrogen gas equilibrated by stirring and analyzed on an attached gas chromatograph.

A more elaborate procedure was followed for determining N_2 yields from N_2O solutions. Water adjusted to pH 11 with CO_3^{2-}-free NaOH was carefully degassed on a vacuum line and saturated with N_2O that had been purified by freezing and pumping. O_2-saturated pH 11 solutions were similarly made. Mixing these two solutions in the proper ratios in syringes gave solutions containing the desired amounts of N_2O and O_2. A known amount (6.14 g) of irradiated NaCl was taken in a Pyrex cell provided with a fritted glass disk and a three-way stopcock. This dissolver unit was attached to a vacuum line and pumped for about 15 min until the residual pressure was less than 10^{-4} mm. Helium was then introduced and allowed to flow throughout the salt at atmospheric pressure. With helium flowing, the cell was removed from the vacuum line and fitted into the 5/20 cone of the Van Slyke apparatus containing 20 ml of the solution to be used for dissolving the salt. This solution was forced up through the salt, effecting complete solution. The resultant solution and evolved gas were replaced by Hg and moved into a syringe that was then detached from the dissolving unit. This solution and gas mixture was next drawn back into the Van Slyke apparatus and equilibrated and the evolved N_2 was measured on the molecular sieve column used for the H_2 analysis. All unirradiated NaCl controls gave a small amount of N_2. We have subtracted this amount from the N_2 yields shown in Table I and in the figures. Whereas this correction was insignificant at the higher N_2 measurements, it amounted to about 30% for the lower N_2 yields. For this reason experimental fluctuations become greater in solutions containing the higher concentrations of N_2O and O_2.

The light emission was measured with a 1P28 photomultiplier. A Pyrex tube containing water or the required aqueous solution was clamped directly onto the window of the tube. The irradiated sodium chloride was dropped in through a funnel-shaped tube. The photomultiplier output was fed into an oscilloscope through a resistor–capacitor (RC) coupling and the trace was photographed. Any distortion produced by the RC coupling is unimportant for the present work as only relative emissions for various solutions have been given.

^{60}Co γ rays were used for all irradiations except those described below in which emission from Linac-irradiated NaCl was sought. The dose delivered to the NaCl was calculated from the dose measured in the Fricke dosimeter ($G(Fe^{3+})$ = 15.6) multiplied by the ratio of densities of NaCl to 0.8 N H_2SO_4 (2.165/1.024).

Results

1. Light Emission. In agreement with earlier workers, we find that when irradiated salt dissolves in water, light emission takes place. We also find that the addition of potassium nitrate efficiently quenches this emission. With 0.0001 M NO_3^- the emission falls to about 50% compared with the emission from a similar sample added to helium-purged, solute-free water. The presence of 0.001 M NO_3^- reduces the emission by 90 ± 10%. The intensity of the initial light pulse obtained in the absence of solute was used to calculate the percentage decrease in emission. A similar quenching by NO_3^- of irradiated NaCl fluorescence in fluorescein solutions has already been reported[9] so we did not continue our emission measurements.

2. A Search for Fluorescence by Pulse Radiolysis Technique.[17] A saturated chlorine water solution (pH 1.1), a dilute chlorine water solution (pH 3.3), and sodium bromide solutions in the concentration range 10^{-4}–1 M (neutral pH) were irradiated with 3-μsec electron pulses (6.0 MeV) from a linear accelerator.[18] Under the same conditions no emission could be detected after the end of the electron pulse in the wavelength region 400–600 nm apart from the fluorescence emitted from a similar water filled cell.

3. Hydrogen Yields. Dissolving the irradiated salt in 0.4 M H_2SO_4 (argon-purged) produces hydrogen, in agreement with earlier work.[4,5] The hydrogen yield is given as a function of the time of irradiation of NaCl in Figure 1. The reason for the bad scatter of points at higher doses is not known, but the actual yields are not of much significance since small and irreproducible amounts of oxygen remain or are adsorbed on the surface of the salt even after argon purging. Not only is O_2 a quencher of light emission but it also lowers the H_2 yields by forming HO_2 from the H atoms liberated by the reaction of the e_{aq}^- with H^+. However, the yields are significant inasmuch as they show that the amount of H_2 increases with dose establishing that the H_2 yield arises from the defect centers in the irradiated salt as was earlier concluded.[5] The small yield of H_2 occasionally found in our unirradiated salt is difficult to explain. This may come from impurities or from a small concentration of defects already present in the salt.

4. N_2 Yields from N_2O. Dissolution of irradiated NaCl in alkaline N_2O solutions releases nitrogen with a yield that increases with dose. The effect of N_2O concen-

(14) C. Gopinathan, *Proc. Dept. Atomic Energy Symp. Chem., Chandigarh, India*, **2**, 196 (1960).
(15) C. Gopinathan, *Proc. Symp. Radiat. Chem., Trombay, India, Bhabha Atomic Research Center Report 489*, 28 (1970).
(16) H. J. Arnikar, P. S. Damle, and B. D. Chaure, *Radiochem. Radioanal. Lett.*, **5**, 25 (1970); *J. Chem. Phys.*, **55**, 3668 (1971).
(17) These experiments were suggested by Professor H. J. Arnikar of the University of Poona, Poona, India.
(18) C. Gopinathan, P. S. Damle, and E. J. Hart, unpublished work.

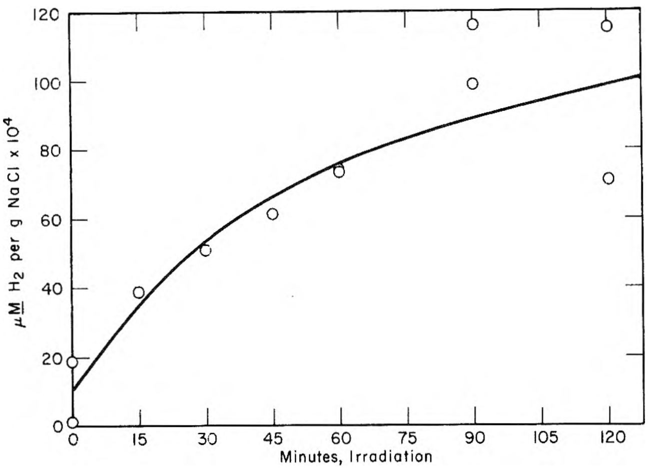

Figure 1. Hydrogen evolution from dissolved γ-ray irradiated crystalline NaCl : dose rate = 49.7 ± 0.6 krads/*min*.

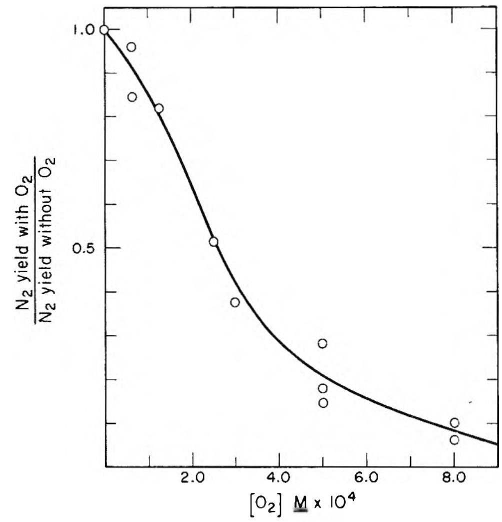

Figure 2. Effect of oxygen concentration on nitrogen evolution during dissolution of γ-ray irradiated NaCl in 0.001 M N_2O solutions: γ-ray dose = 4.5 Mrads.

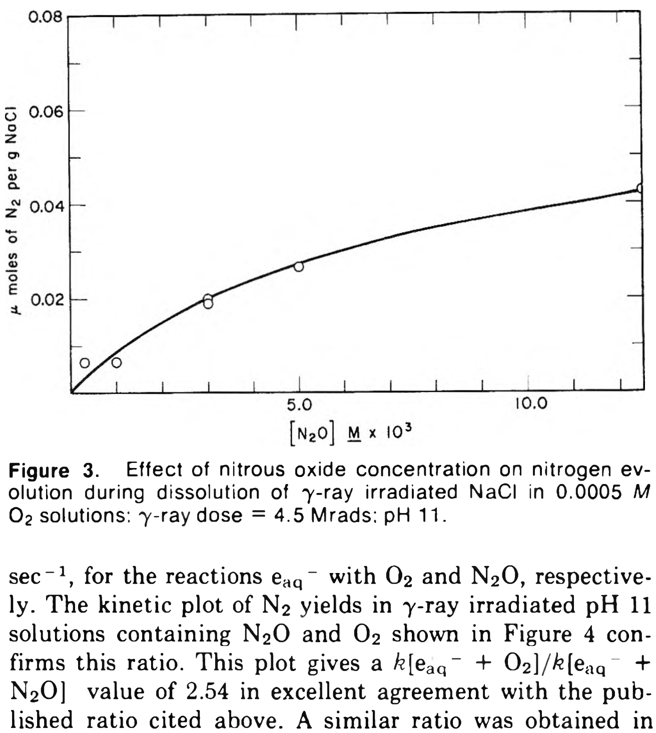

Figure 3. Effect of nitrous oxide concentration on nitrogen evolution during dissolution of γ-ray irradiated NaCl in 0.0005 M O_2 solutions: γ-ray dose = 4.5 Mrads; pH 11.

tration on N_2 yield is shown in Table I for NaCl irradiated to a dose of 4.5 Mrads. These data reveal that the N_2 produced by the irradiated salt is independent of the N_2O concentration in the range 0.0001–0.003 M N_2O. Furthermore, if we assume that the dose given in the present work saturates the NaCl with F centers, then at least 70% of the F centers reported by Ahnström[9] for coarse NaCl produces N_2 according to the reactions

$$\text{F centers} \xrightarrow{H_2O} e_{aq}^-$$

$$e_{aq}^- + N_2O \longrightarrow N_2 + O^-$$

At a concentration of 3×10^{-4} M, the mean separation of N_2O molecules is 821 Å and the species produced from F centers must travel about half this distance on the average to react with N_2O. Since there is no increase in the N_2 yields over a 30-fold increase in N_2O concentration we conclude that there is close to a 1:1 conversion of F centers into e_{aq}^- and that short-range neutralization of e_{aq}^- by the "hole species" does not occur in these N_2O solutions.

The quenching of a major fraction of the light emission by 0.0001-0.001 M NO_3^- also suggests that this process, too, involves e_{aq}^-.

TABLE I: Effect of N_2O Concentration on N_2 Formation from Dissolved NaCl Irradiated to a γ-Ray Dose of 4.5 × 10^6 Rads

$[N_2O]$, M	μmol of N_2/g of NaCl	$[N_2O]$, M	μmol of N_2/g of NaCl
1.0×10^{-4}	0.058	1.0×10^{-3}	0.057
3.0×10^{-4}	0.071	3.0×10^{-3}	0.067

5. *N_2O-O_2 Competition.* In order to establish the nature of the species reacting with N_2O, we investigated the effect of added O_2. The NaCl in all cases was irradiated to a dose of 4.5 Mrads. The results are shown in Figures 2 and 3. Figure 2 shows the effect of changing oxygen concentration in a 10^{-3} M N_2O solution at pH 11. Figure 3 shows the effect of changing N_2O concentration in a pH 11 solution containing 5×10^{-4} M O_2. It is clear from these figures that O_2 at higher concentrations reacts much faster with the "hydrated electron" in these systems than the $k[e_{aq}^- + O_2]/k[e_{aq}^- + N_2O]$ ratio of 2.30 obtained from the rate constants,[19] 2.0×10^{10} and 8.7×10^9 M^{-1} sec^{-1}, for the reactions e_{aq}^- with O_2 and N_2O, respectively. The kinetic plot of N_2 yields in γ-ray irradiated pH 11 solutions containing N_2O and O_2 shown in Figure 4 confirms this ratio. This plot gives a $k[e_{aq}^- + O_2]/k[e_{aq}^- + N_2O]$ value of 2.54 in excellent agreement with the published ratio cited above. A similar ratio was obtained in γ-ray irradiated 5 M NaCl solutions containing 0.0001 M O_2 with variable N_2O.

Discussion

As its concentration increases O_2 becomes increasingly more effective than N_2O in scavenging e_{aq}^- generated upon the dissolution of irradiated NaCl crystals. This unexpected result is clearly brought out in the kinetic plots of Figure 5. The lower curve of this figure is for the 0.001 M N_2O, variable O_2 data of Figure 2. Instead of the normal linear relationship, with a $k(e_{aq}^- + O_2)/k(e_{aq}^- + N_2O)$ ratio of 2.3 the slope of this plot increases as the $[O_2]/[N_2O]$ ratio increases. From the initial slope of this curve we calculate a rate constant ratio, $k(e_{aq}^- + O_2)/$

(19) E. J. Hart and M. Anbar, "The Hydrated Electron," Wiley-Interscience, New York N. Y., 1970.

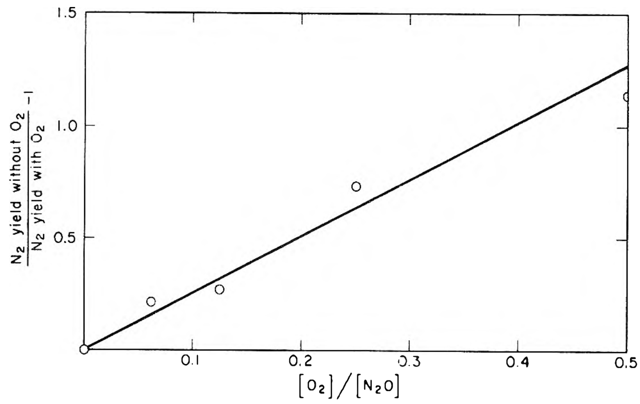

Figure 4. Kinetic plot of nitrogen yield in γ-ray irradiated solutions containing O_2 and 0.001 *M* N_2O: γ-ray dose = 4.5 Mrads; pH 11.

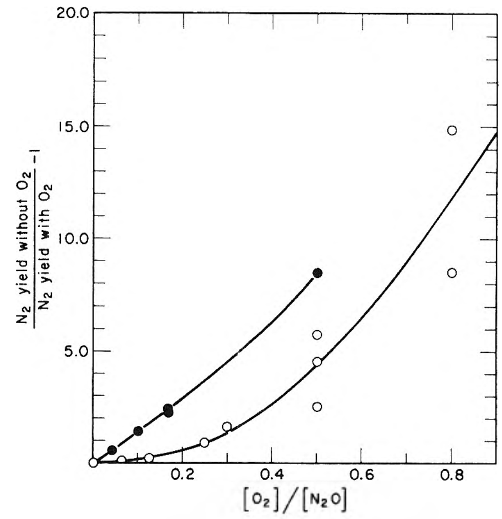

Figure 5. Kinetic plots of nitrogen yield as a function of $[O_2]/[N_2O]$ ratio in solutions prepared from irradiated NaCl (data from Figures 2 (○) and 3 (●).

$k(e_{aq}^- + N_2O)$, of 2.3 ± 0.2. On the other hand a rate constant ratio of 14.8 is calculated from the upper curve of Figure 5 obtained from a kinetic plot of the high O_2 concentration data of Figure 3.

This ratio is about six times the normal value of 2.30. Note too that the slope of the lower curve approaches that of the upper curve at high $[O_2]/[N_2O]$ ratios thereby supporting our conclusion that the effectiveness of O_2 in scavenging e_{aq}^- (or its precursor) increases with increasing concentration.

The solubilities of N_2O and O_2 were determined in a saturated NaCl solution at room temperature in order to prove that the changing solubility of the gases as the NaCl dissolves does not affect the rate constant ratios. They were, respectively, 5.8×10^{-3} and 2.1×10^{-4} *M*. Comparing these values with the known solubilities of N_2O and O_2, 2.5×10^{-2} and 1.25×10^{-3} *M*, respectively, in water it is seen that the O_2 concentration is, in fact, diminished more than that of N_2O. Therefore, the lowered solubility of these gases cannot be the cause of the higher rate constant ratio for irradiated salt. In actual practice, of course, it is likely that the reactions take place under supersaturated conditions without sufficient time being available for the release of gases. Since O_2 and N_2O are neutral molecules kinetic salt effects may be ruled out as was experimentally demonstrated above by carrying out N_2O and O_2 competition measurements in γ-ray irradiated 5 *M* NaCl.

Both as shown in the present work as well as in earlier work, hydrated electron scavengers are able to quench light emission at very low concentrations as has been shown above as well as in earlier work.[9-11,16] This result together with the fact that F centers are converted into e_{aq}^- very efficiently suggests that the F center release is essentially a bulk process. That the variation of N_2O concentration has no effect on the yield confirms this view, and also suggests the unimportance of any "short-range" neutralization process. Our N_2O-O_2 competition data confirm e_{aq}^- formation but also support the existence of a second species which reacts much faster with O_2 than with N_2O. According to Figure 5 it seems that the reaction with this second species becomes more important at higher O_2 concentrations. However, it is difficult to say whether the rate constant ratio at low O_2 concentrations is identical with the normal ratio of 2.30 or not. At the moment, therefore, it is possible only to speculate about the nature of this second species of unusually high O_2 reactivity. Among the possibilities to be considered are an exciton and a "hydrated electron" ("e_{aq}^-") still under the electrostatic influence at the "hole," which must be released into the solution, along with "e_{aq}^-."

While the exciton alternative looks very attractive, since it is easy to imagine trapped energy being directly transferred to water, there are certain drawbacks. A Frenkel exciton is defined as a quantum of delocalized excitation in an ordered matrix.[20,21] The structure in water, being essentially short range, will therefore not allow the movement of the excitons to the extent required. It is interesting to imagine this new species as a different form of e_{aq}^-. When the NaCl structure breaks up, the trapped electron is probably directly transferred from its defect site in the NaCl lattice to a corresponding site in the water structure, assuring instantaneous hydration. At the moment we can only speculate why there is a different "primordial" form of e_{aq}^- which reacts very much faster with O_2. The trapped positive holes in the NaCl lattice, whatever form they are in, must also be released into the water along with the electron. If "e_{aq}^-" comes under the electrostatic influence of a hole during release into water, it will form a species which is strongly paramagnetic, thereby explaining our fast reaction with oxygen. The form in which the hole is released does not matter. Only a certain amount of mobility of the hole-e_{aq}^- pair is required. Disappearance of the hole will liberate e_{aq}^-. This hole-e_{aq}^- pair is similar to the excitonic species ($H_2O^+ \cdots e^-$) already postulated.[22]

On the basis of the oxidation of tetramethyl-*p*-phenylenediamine (TMPD) to Wursters blue by dissolving irradiated NaCl, a positive charge, presumably H_2O^+, has recently[22,23] been suggested as the oxidant. The reducing species is unquestionably e_{aq}^- as has been demonstrated by our work and by the reduction of tetranitromethane[22] and by other e_{aq}^- scavengers.[23]

These studies may contribute little to an understanding of the radiolysis of pure water or dilute aqueous solutions.

(20) D. L. Dexter and R. S. Knox, "Excitons," Interscience, New York, N. Y., 1965.
(21) J. Frenkel, *Phys. Rev.*, 1276 (1931).
(22) J. P. Mittal and J. Shankar, *Radiochem. Radioanal. Lett.*, **6**, 115 (1971).
(23) J. P. Mittal to C. Gopinathan, private communication.

However, irradiated salt may be looked upon as a source of low-energy electrons and when dissolving in water as a source of e_{aq}^-.[24] But whether the hole-e_{aq}^- pair postulated as responsible for our "oxygen" effect forms in pure water remains an unresolved question. Predictions that oxygen at 0.001 M would lower the e_{aq}^- yield in subnanosecond time periods could not be confirmed by our preliminary experiments with Argonne's 50-psec electron pulse.

Acknowledgment. C. G. wishes to thank Dr. J. Shankar for helpful discussions and encouragement and Dr. J. P. Mittal for discussions on recent unpublished data.

(24) H. J. Arnikar to E. J. Hart, private communication.

Fluorescence of the Uranyl Ion in Electron-Irradiated Sulfuric Acid Solutions[1]

C. Gopinathan, G. Stevens, and Edwin J. Hart*

Chemistry Division, Argonne National Laboratory, Argonne, Illinois 60439 *(Received March 15, 1972)*

Publication costs assisted by Argonne National Laboratory

The characteristic fluorescence of the UO_2^{2+} ion is obtained in sulfuric acid solutions by irradiation with 6.3 MeV electrons and by tritium β rays from ^3HOH. The effect of UO_2^{2+} concentration in the range from 0.007 to 0.50 M UO_2SO_4 in 0.9 M sulfuric acid is reported. Although Čerenkov light emission may contribute to the fluorescence, it is not the primary source of excitation. Energy transfer from water to the UO_2^{2+} ion and excitation by water subexcitation electrons are briefly discussed as possible mechanisms.

Introduction

Although the phenomenon of excitation energy transfer is well established in organic systems consisting of complex molecules, direct energy transfer in aqueous systems remains an open question. We have studied the fluorescence of the aqueous UO_2^{2+} ion in an attempt to elucidate the role of excitation energy transfer as a primary process in the irradiation of liquid water. The UO_2^{2+} ion fluoresces by direct photoactivation in aqueous solution.[2] Its emission spectrum centered at 515 nm is assigned to a partly forbidden transition. A number of studies[3-8] of the light emission produced when water or ice is irradiated with ionizing radiation have appeared. In most of these studies the light emission is attributed to causes other than the fluorescence of H_2O and since water is a simple low molecular weight molecule, it is not an ideally fluorescent material. Therefore, studying the light emission process in aqueous solutions containing well-known fluorescent ions seems to be a good way of establishing possible energy transfer processes in water.

Our work was carried out with solutions of 0.90 M or higher in H_2SO_4 in order to intensify the fluorescent spectrum and to eliminate reactions of e_{aq}^- with UO_2^{2+}

Experimental Section

Purified uranyl sulfate (recrystallized reagent grade) was dried in a vacuum desiccator before dissolving in H_2SO_4. The other chemicals (to be listed) were of analytical reagent grade, and were used without further purification. Pure tritiated water of 3000 Ci/ml activity was obtained by the oxidation of tritium gas by O_2 at the surface of a palladium thimble using a procedure already described.[9] This water was diluted with deaerated triply distilled water to an activity of about 10 Ci/ml. From this water we prepared solutions of the desired radioactivity.

The faint emission from the tritiated water solutions was measured by an integrating device consisting of a light chopper, a monochromator, a phototube, a picoammeter, and a 400 channel analyzer. The light chopper disk had 6 equidistant symmetrical slots and rotated at exactly 1 rpm. The tritiated solutions, approximately 1 ml in volume, were contained in sealed Pyrex tubes. The emitted light was focussed by a quartz lens onto the slits of the monochromator with the light chopper between the monochromator and the lens. The light emerging from the monochromator was collected by a phototube whose output was read on a picoammeter and its signal stored in the 400 channel analyzer and displayed on a cathode ray oscilloscope. The sweep time was adjusted so that the 400 channels were covered in exactly the same time that one light and one opaque portion of the chopper moved across the slit. By this arrangement it was possible to add the

(1) Work performed under the auspices of the U. S. Atomic Energy Commission.

(2) C. A. Parker, "Photoluminescence of Solutions," Elsevier, New York, N. Y., 1968, p 472.
(3) L. I. Grossweiner and M. S. Matheson, *J. Chem. Phys.*, **20**, 1654 (1952).
(4) L. I. Grossweiner and M. S. Matheson, *J. Chem. Phys.*, **22**, 1514 (1954).
(5) W. M. Jones, *J. Chem. Phys.*, **20**, 1974 (1952).
(6) J. A. Ghormley and A. O. Allen, Oak Ridge National Laboratory Report ORNL-128 (1958).
(7) D. N. Sittratamarao and D. F. Duncan, *J. Phys. Chem.*, **67**, 2126 (1963).
(8) G. Czapski and K. Katakis, *J. Phys. Chem.*, **70**, 637 (1966).
(9) E. J. Hart, *J. Phys. Chem.*, **56**, 594 (1952).

results of many sweeps, display the results on the oscilloscope, and record them. The results appeared as a plateau and a base line with the plateau representing the light passing through the slits, and the base line representing the background when the rotating disk intercepts the light from the tritiated solution. The difference between the two was a measure of the fluorescence at that particular wavelength. In cases of weak signals or no emission, the base line and plateau were indistinguishable. In the later phase of the present work, another apparatus, consisting of a monochromator and a chopper as before, but with a lock-in amplifier replacing the oscilloscope and the 400 channel analyzer, was used. In this method it was possible to record directly the spectra by feeding the output of the amplifier to an X-Y recorder. The UO_2^{2+} spectra obtained with both units were identical.

In the electron pulse radiolysis experiments a conventional layout was used. This consisted of a linear accelerator with electron energy adjusted to 6.3 ± 0.2 MeV and the pulse length to 3 μsec. The sample was contained in a cylindrical quartz cell 4 cm long and 2 cm in diameter with flat optical windows. The cell was irradiated perpendicular to its long axis. The light emitted was collected by a concave mirror placed on the longitudinal axis of the cell. This mirror reflected the light to a second mirror which then reflected the beam out of the accelerator pit onto a concave mirror, reflecting prism, monochromator, and then into a 1P28 photomultiplier. The output from the photomultiplier was fed into an oscilloscope and the trace photographed. The rise time of the system (about 20 nsec) was fast enough to measure the emission decay curves without significant distortion.

During the pulse of 3 μsec, the intense Čerenkov emission, when displayed on the oscilloscope, appeared as a rough square wave with a small spike at the leading edge. The difference between the base line and the flat portion of the square wave obtained for irradiated pure water was taken as the intensity of the Čerenkov emission. Under these conditions, a fluorescing solution with sufficiently long emission lifetime had a signal that appeared as a tail on the trailing edge of the Čerenkov emission pulse. In order to measure the fluorescence accurately the sensitivity of the oscilloscope was increased by a factor of 10 or more thereby expanding the scale. Under these conditions the fluorescence could be accurately measured since there was negligible scattered light and the photomultiplier was operated under conditions of linear response in the spectral range 250–500 nm.

Results and Discussion

The relative fluorescence decay of a typical sample is shown in Figure 1. The results on the upper curve were obtained on 0.50 M UO_2^{2+} in 0.90 M H_2SO_4 irradiated by a 3-μsec pulse of 6.0-MeV electrons. The relative emission from the same cell filled with water or with 0.9 M H_2SO_4 is given for comparison. The UO_2^{2+} fluorescence decays with a half-life of about 3 μsec and is fairly long lived compared to the emission from the water control.

The fluorescence spectrum of the radiolytically excited UO_2^{2+} emission is identical with that of the photoexcited UO_2^{2+} emission. Figure 2 shows the emission spectrum taken on a 0.23 M UO_2^{2+} solution in 0.90 M H_2SO_4. The emission was measured 0.4 μsec after the end of the 3-μsec electron pulse and has been corrected for the wavelength dependence of photomultiplier response. Although the resolution in Figure 2 is poor, there is no question but that it agrees with the known optically induced fluorescence spectrum of UO_2^{2+}.[2]

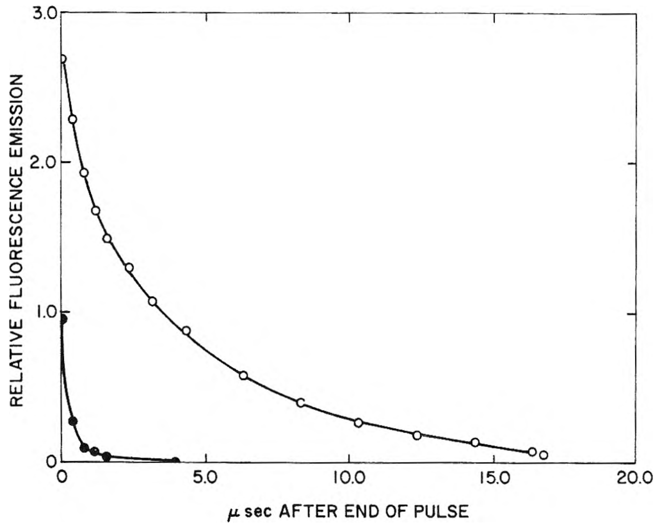

Figure 1. Emission at 513 nm after the end of a 3.0-μsec, 6.0-MeV electron pulse: O, cell containing 0.50 M UO_2SO_4; ● same cell containing H_2O or 0.9 M H_2SO_4 only.

The fluorescence intensity measured at 513 nm increases with increasing concentration of UO_2^{2+}. Figure 3 shows the relative fluorescence intensity measured 1 μsec after the pulse as a function of UO_2^{2+} concentration. In these experiments a correction was made for the blank fluorescence from a water-filled cell. Although the dose was reproducible to within ±3% on a particular day the fluorescence response varied from day to day because of differences in cell orientation and optical alignment. On Figure 3 each set of points taken at different times has been multiplied by a constant factor calculated on the assumption that identical UO_2^{2+} concentrations produced the same amount of fluorescence independent of the day it was measured.

Because of the efficient photoexcitation process in the UO_2^{2+} optical absorption band it was important to estab-

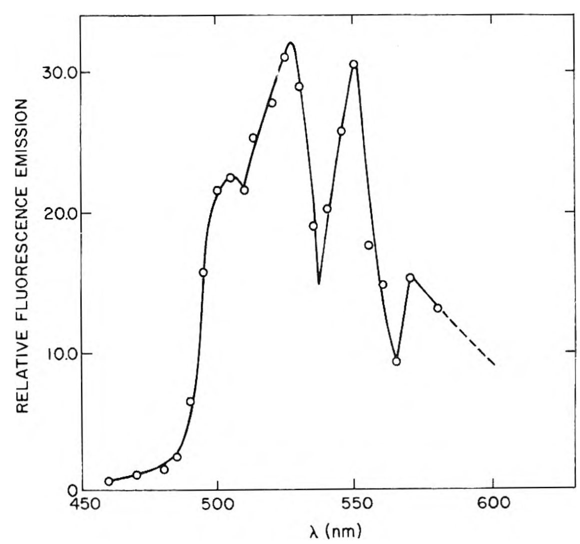

Figure 2. Emission spectrum from 0.23 M UO_2SO_4 in 0.9 M H_2SO_4 0.4 μsec after the end of the electron pulse (correction has been made for photomultiplier response).

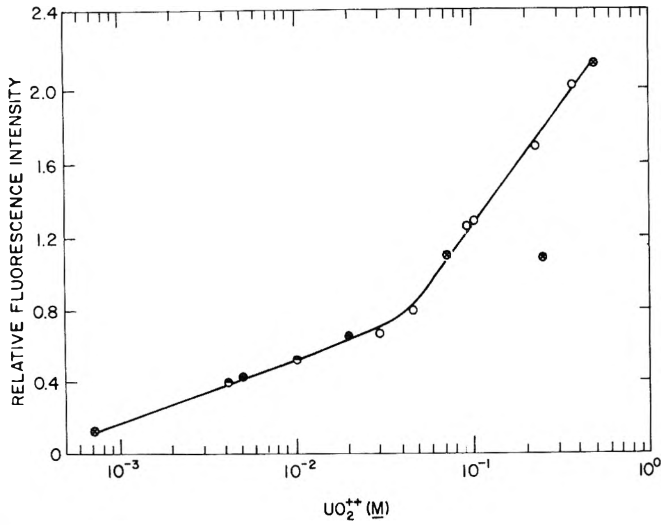

Figure 3. Variation of the emission intensity at 513 nm (1.0 μsec after the end of the electron pulse) as a function of UO_2SO_4 concentration in 0.9 *M* H_2SO_4. Different symbols indicate independent measurements taken on different days (see text).

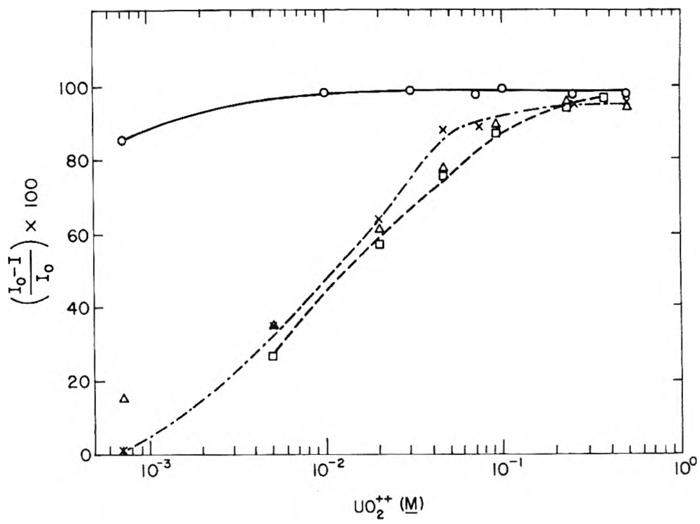

Figure 5. Effect of UO_2SO_4 concentration on the amount of self-absorbed Čerenkov emission (as percentage of original emission without UO_2SO_4). All solutions are 0.9 *M* in H_2SO_4: O, 250 nm; ×, 350 nm; Δ, 435 nm; □, 420 nm.

lish the extent to which Čerenkov emission is responsible for the radiolytically induced UO_2^{2+} fluorescence. We have answered this question in two ways, first, by estimating the amount of internal absorption by a linear emitter for the electron pulse excited emission and then in a second way by using 18-keV tritium β rays where the Čerenkov emission is absent. The Dixon formula[10,11] for calculating the internal absorption and thereby the amount of Čerenkov radiation absorbed during irradiation is

$$\frac{I}{I_0} = \frac{1 - 10^{-\mathrm{OD}}}{2.303\,\mathrm{OD}} \tag{I}$$

where OD = *kcd*. In this equation, I/I_0 represents the fraction of the emission internally absorbed and OD is the optical density, the product of the molar extinction coefficient, *k*, the concentration, *c*, and cell length, *d*. In our case, since the emissions from the cell were observed along the longitudinal axis of the cell, *d* = 4.0 cm, the length of the emitter.

The optical densities of the solutions of different concentrations of UO_2^{2+} in 0.9 *M* H_2SO_4 were measured in 1.0-mm cells at 420 nm in the concentration region 0.028–0.5 *M*. Beers law held over this concentration range. From these results the OD for a 4-cm path length and the percentage of self absorption, $[1 - (I/I_0)]100$, were calculated using eq I. The results are shown in Figure 4. Note that over 80% of the Čerenkov emission is already self-absorbed in 0.05 *M* UO_2^{2+}. Therefore, if the observed emission comes mainly through absorption of Čerenkov light, there should be no more than a 20% increase in the emission at concentrations greater than 0.05 *M* UO_2^{2+}. This conclusion is contrary to the experimental results of Figure 3 where it is shown that the emission increases by more than a factor of 2 in the concentration range from 0.05 to 0.50 *M* UO_2^{2+}. This result supports our conclusion that most of the emission does not arise through excitation by Čerenkov radiation.

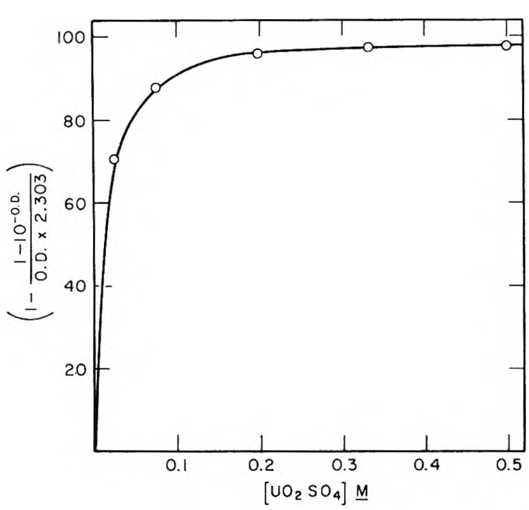

Figure 4. Plot of the percentage of self-absorption at 420 nm calculated from the measured optical densities of UO_2SO_4 solutions of different concentrations in 0.9 *M* H_2SO_4. Percentage of self-absorption = $100\{1 - [(1 - 10^{-\mathrm{OD}})/2.303\mathrm{OD}]\}$.

Further support that Čerenkov radiation is not necessary to excite UO_2^{2+} emission was obtained by measurements of the relative Čerenkov intensity as a function of uranyl concentration at various wavelengths. The results appear in Figure 5. Here the variation in the percentage of Čerenkov radiation absorbed, $[(I_0 - I)/I_0]100$, by solutions containing UO_2^{2+} is compared with the emission in the absence of UO_2^{2+} (I_0). A comparison of this figure with that of Figure 3 clearly shows that there is no relation between the percentage of Čerenkov radiation self-absorbed at 250, 350, 420, and 435 nm and actual UO_2^{2+} emission intensity at 513 nm. At 250 nm about 85% of the Čerenkov radiation is absorbed at a UO_2^{2+} concentration of 7.2×10^{-4} *M*. Thus, if fluorescent emission originates from the absorption of Čerenkov radiation at this wavelength then there should be only a 15% increase in emission intensity as the concentration increases above 10^{-3} *M*. This is definitely not the case. This same reasoning applies to the shorter wavelengths also since the absorp-

(10) W. R. Dixon, *Nucleonics*, **8(4)**, 68 (1951).
(11) Z. P. Zagorski and Z. Zimek, *Nucleonika*, **15**, 337 (1970).

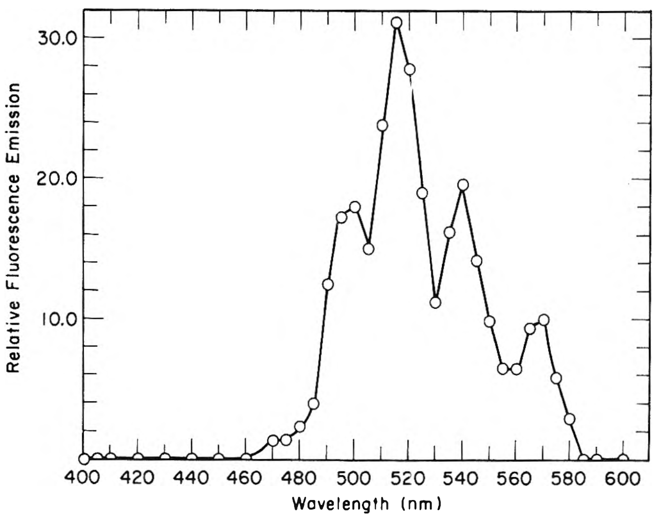

Figure 6. Spectrum of light emission from a 2.5 M H_2SO_4 solution containing 0.2 M UO_2SO_4 and 2.5 Ci of ^3HOH/ml corrected for photomultiplier response.

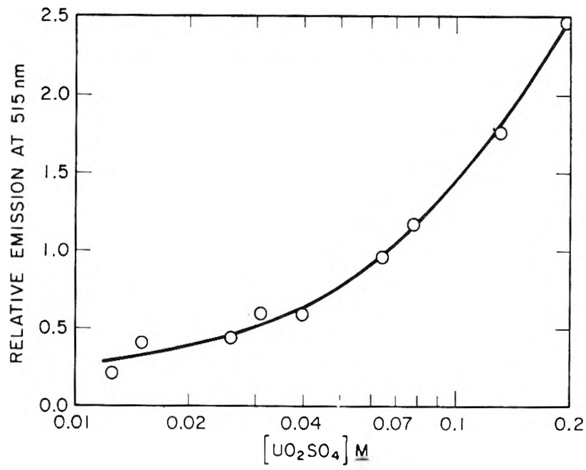

Figure 7. Variation of emission intensity at 515 nm as a function of UO_2SO_4 concentration in 2.5 M H_2SO_4 and 2.5 Ci of ^3HOH/ml.

tion intensity of UO_2^{2+} solutions increases rapidly at the shorter wavelengths.

A comparison of the amount of Čerenkov emission absorbed at 350, 420, and 435 nm also does not bear any relation to the observed change in emission intensity at 513 nm. In the concentration range from 0.1 to 0.5 M less than a 15% increase in fluorescent emission is expected. However, the actual emission increases by a factor of 2 in this concentration range. At the lower concentration, 0.03–0.10 M UO_2^{2+}, Čerenkov absorption increases from 70 to 90% whereas in this same concentration range the fluorescence emission increases by a factor of about 2. These results support the conclusion that the main cause of the emission is not by optical excitation induced by the self-absorbed Čerenkov radiation.

The conclusive proof that UO_2^{2+} fluorescence may be radiolytically induced through a mechanism not involving Čerenkov radiation is provided by our tritiated water experiments. This is because tritium β particles cannot give rise to Čerenkov emission in water because the maximum β-ray energy is only 18 KeV. Figure 6 shows the emission spectrum from a 0.2 M UO_2SO_4 solution in 2.5 M H_2SO_4 containing 2.5 Ci/ml of tritium. This spectrum agrees with the one in Figure 2 as well as with the optically induced fluorescence spectrum. In the absence of UO_2SO_4 no emission could be detected from tritiated water alone containing the same activity. This result does not contradict earlier reports of light emission[6,8] from tritiated water. Because of the use of a monochromator, our sensitivity was too low to detect emission from tritiated water alone.

Both the above studies, pulse radiolysis, as well as tritiated water, show that explanations other than Čerenkov absorption have to be sought to explain the UO_2^{2+} fluorescence. The next possibility to be considered is the direct excitation of UO_2^{2+}. Figure 3 shows that when the uranyl concentration changes from 0.01 to 0.5 M, *i.e.*, by a factor of 50, the emission intensity increases by a factor of about 3. If direct absorption of radiation was the cause of emission, then the emission would be expected to increase proportionately with increasing electron fraction of UO_2^{2+} (44.3-fold).

In order to avoid the complications of Čerenkov radiation, we studied the intensity of emission at 515 nm of UO_2SO_4 solutions in 2.5 M H_2SO_4 containing 2.5 Ci of tritium/ml as a function of UO_2SO_4 concentration. The results are shown in Figure 7. The variation with UO_2SO_4 concentration follows the general shape and is in the correct concentration range for the theoretical yield *vs.* concentration effects predicted for subexcitation electrons.[12] Unfortunately our concentration range does not extend up to the 1.0–2.0 mol % required for the limiting value of the yield. Subexcitation electrons have been suggested as participating in the radiation induced "photo" dissociation of concentrated formic acid solutions by ^{60}Co γ rays[13] and it is expected that they may excite either allowed or forbidden optical transitions in UO_2^{2+} solutions.

The emission of these tritiated water-UO_2^{2+} solutions is greatly intensified upon cooling to the glassy state, an effect well documented for photoexcitation of UO_2^{2+} solutions.[14] A 5.7 M sulfuric acid solution containing 0.075 M UO_2SO_4 and 1 Ci of tritium/ml, when frozen to −196°, gave a glow easily visible in the dark. The spectrum is similar to the room temperature spectrum, with three main peaks at 500, 518, and 545 nm. Quantitative studies show that the emission intensity at 515 nm increases by a factor of 16 when the temperature is decreased from 25 to −196°. It has been known for some time that energy transfer may take place in low-temperature sulfuric acid glasses. From a study of Cl^- yields in γ-ray irradiated 5.3 M H_2SO_4 glasses containing $ClCH_2COOH$ it has been suggested[15] that part of the chloride yield may arise from mobile energy in the form of excitons reacting with $ClCH_2COOH$ molecules. This may occur through the following type of reaction

$$H_2O^* + ClCH_2COOH \rightarrow Cl^- + H^+ + CH_2COOH + OH \quad \text{(II)}$$

Similarly, in aqueous alcohol solutions frozen to −196°, it has been suggested that even hydrogen abstractions can

(12) R. L. Platzman, *Radiat. Res.*, **2**, 1 (1955).
(13) E. J. Hart, *J. Amer. Chem. Soc.*, **81**, 6085 (1959).
(14) E. Rabinowitch and R. L. Belford, "Spectroscopy and Photochemistry of Uranyl Compounds," Macmillan, New York, N. Y., 1964, p 81.
(15) F. S. Dainton and C. Gopinathan, *Trans. Faraday Soc.*, **65**, 143 (1969).

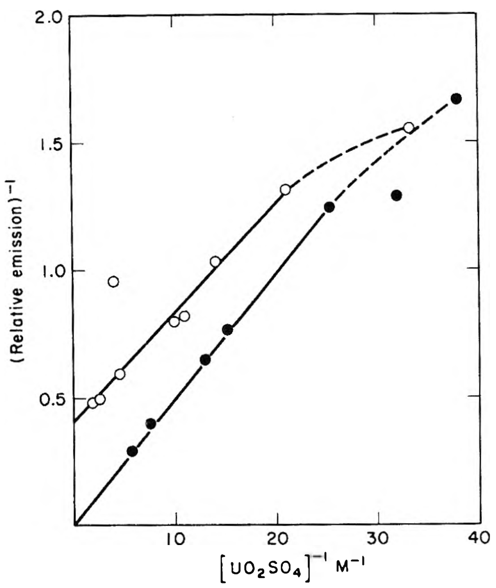

Figure 8. Plot of the inverse of light emission intensity as a function of inverse of UO_2SO_4 concentration: O, pulse radiolysis results in 0.9 *M* H_2SO_4; ●, ^3HOH results in 2.5 *M* H_2SO_4.

arise through mobile excitons.[16,17] A similar process may occur in our glassy system.

We next consider an energy transfer process occurring through water. A possible mechanism is by exciton interaction moving through the structural part of water. A similar mechanism has been proposed to explain the production of molecular products in irradiated water through the interaction of two excitons.[18] Although the present work does not provide direct support for this model it suggests the possible importance of energy transfer in liquid irradiated water and aqueous solutions. Possible mechanisms involving exciton interaction are

$$H_2O^*(\text{excitons}) + UO_2^{2+} \xrightarrow{k_1} (UO_2^{2+})^* \longrightarrow UO_2^{2+} + h\nu \quad (1)$$

$$H_2O^* \xrightarrow{k_2} \text{products} \quad (2)$$

Quenching process 2 involves the effect of impurities and the conversion of excitation energy into vibrational and rotational excitation energies. According to this mechanism the fluorescence intensity should be proportional to

$$k_1[UO_2^{2+}]/(k_1[UO_2]^{2+} + k_2C)$$

where C is a constant. This relationship suggests that the reciprocal of the fluorescence intensity varies linearly with the reciprocal of the UO_2^{2+} concentration. Figure 8 displays plots of this function for the pulse radiolysis and tritiated water experiments. The striking similarity between these curves at high UO_2^{2+} concentrations is evident from this figure and suggests that a similar process takes place in both these systems. This, together with the linearity of the plots in the concentration region shown, provides support for the mechanism outlined above.

Recently a thorough study of fluorescence of aqueous salicylate solutions under X irradiation and optical excitation has been published.[19,20] The results have been quantitatively interpreted in terms of direct energy absorption by the salicylate ion followed by quenching by radicals formed under irradiation rather than energy transfer. However, in our system, which contains a heavy inorganic ion as the fluorescent material in contrast with the above work, we think that energy transfer from water, sulfuric acid, or subexcitation electrons would be the most reasonable interpretation. The presence of heavy ions in large concentrations may increase the likelihood of energy transfer in their neighborhood, a fact which has also been mentioned in the above work to explain the results in the presence of Br^- and Cs^+ ions. Therefore, there is no real contradiction in the mechanisms in the above work and ours.

None of these explanations rule out a chemiluminescent process such as that occurring in fluorescein solutions.[21,22] However, on the basis of the evidence obtained so far, chemiluminescent processes are unlikely. The high acidities convert e_{aq}^- into H atoms. Also, we have done some experiments with solutions containing 0.1 *M* oxygen in the pulse radiolysis setup. There is no decrease in the UO_2^{2+} emission intensity at 513 nm by the O_2, an excellent H atom scavenger. Thus H atoms are unlikely precursors of emission. In fact, some of our experiments suggest that there may be a slight intensification of the emission in the high-pressure oxygen solutions as compared with the air-saturated solutions. Unfortunately, this O_2 enhancement is difficult to establish because of experimental difficulties with high-pressure cells. If future work confirms this O_2 intensification, an important clue to the mechanism of energy transfer will be provided. We are continuing the work on frozen systems containing ^3HOH also with a view of further understanding the processes involved.

Acknowledgments. We are grateful to S. Petrek and R. M. Clarke for technical assistance and to Professor R. L. Platzman for reminding us of the possible role of subexcitation electrons. C. G. is grateful to Bhabha Atomic Research Centre, Bombay, India, for leave of absence and to Dr. J. Shankar, head of the Chemistry Division, Bhabha Atomic Research Centre, for encouragement.

(16) C. Gopinathan, P. N. Moorthy, and K. N. Rao, *Indian J. Chem.*, **6**, 749 (1968).
(17) P. N. Moorthy, C. Gopinathan, and K. N. Rao, *Radiat. Eff.*, **2**, 175 (1970).
(18) C. Gopinathan, *Proc. Symp. Radiat. Chem., Trombay, India, Bhabha Atomic Research Center Report 489*, 28 (1970).
(19) G. Stein and M. Tomkiewicz, *Trans. Faraday Soc.*, **67**, 1678 (1971).
(20) G. Stein and M. Tomkiewicz, *Trans. Faraday Soc.*, **67**, 1009 (1971).
(21) W. Prütz, K. Sommermeyer, and E. J. Land, *Nature (London)*, **212**, 1043 (1966).
(22) L. I. Grossweiner and A. F. Rodde, Jr., *J. Phys. Chem.*, **72**, 756 (1968).

Pulse Radiolysis of the Aqueous Ferro-Ferricyanide System. I. The Reactions of OH, HO_2, and O_2^- Radicals

Dov Zehavi and Joseph Rabani*

Department of Physical Chemistry, The Hebrew University of Jerusalem, Jerusalem 91 000, Israel *(Received March 24, 1972)*

Pulse radiolysis of ferro and ferricyanide aqueous solutions is investigated at various H^+ and salt concentrations. It has been found that association and ion pair formation may affect the reactivity toward OH, HO_2, and O_2^- radicals. The following reaction rate constants were determined (in units of M^{-1} sec^{-1}): $k((OH + Fe(CN)_6^{4-})) = (1.25 \pm 0.1) \times 10^{10}$; $k((OH + HFe(CN)_6^{3-})) = (9.0 \pm 0.9) \times 10^9$; $k((OH + H_2Fe(CN)_6^{2-})) = (1.7 \pm 0.5) \times 10^9$; $k((HO_2 + Fe(CN)_6^{4-})) = (3.0 \pm 1.5) \times 10^4$; $k((HO_2 + HFe(CN)_6^{3-})) = (1.4 \pm 0.1) \times 10^5$; $k((HO_2 + H_2Fe(CN)_6^{2-})) = (1.0 \pm 0.3) \times 10^4$; $k((HO_2 + KFe(CN)_6^{3-})) = (3.0 \pm 1.5) \times 10^4$; $k((O_2^- + Fe(CN)_6^{3-})) = (2.7 \pm 0.9) \times 10^2$; $k((O_2^- + KFe(CN)_6^{2-})) = (6.2 \pm 0.6) \times 10^3$. The last two values are calculated for zero ionic strength. The formation of ion pairs has only a little effect (~10% decrease) on the reactivity of ferrocyanide toward OH radicals.

Introduction

In recent years, extensive work has been published on the steady (γ and X-rays) and pulse radiolysis of aqueous ferro- and ferricyanide solutions.[1-15] This system has been used for the determination of radical and molecular yields in the radiolysis of water and as a dosimeter in pulse radiolysis studies of aqueous solutions.

The radiolysis of water can be expressed by

$$H_2O \rightsquigarrow e_{aq}^-, H, OH, H_3O^+, OH^-, H_2, H_2O_2 \quad (1)$$

It is generally assumed that in the ferro-ferricyanide system, the OH radicals oxidize ferrocyanide and the e_{aq}^- and H radicals reduce ferricyanide according to reactions 2-4, while H_2 does not react with ferrocyanide nor ferricyanide.

$$Fe(CN)_6^{4-} + OH \rightarrow Fe(CN)_6^{3-} + OH^- \quad (2)$$

$$Fe(CN)_6^{3-} + e_{aq}^- \rightarrow Fe(CN)_6^{4-} \quad (3)$$

$$Fe(CN)_6^{3-} + H \rightarrow Fe(CN)_6^{4-} + H^+ \quad (4)$$

Absolute rate constants for the OH radical,[8] the H radical,[11] and the e_{aq}^- radical ion[4] reactions in this system were measured by the pulse radiolysis technique. Hydrogen peroxide oxidizes ferrocyanide to ferricyanide in acidic solutions and reduces ferricyanide to ferrocyanide in basic solutions, but these processes are slow in comparison with reactions 2-4.[16] In aerated solutions of ferrocyanide, e_{aq}^- and H radicals react with oxygen to form peroxy radicals. The peroxy radicals oxidize ferrocyanide only when sufficient acid concentrations are present [7] according to

$$Fe(CN)_6^{4-} + HO_2 \rightarrow Fe(CN)_6^{3-} + HO_2^- \quad (5)$$

It has been proposed that the $[Fe(CN)_5H_2O]^{3-}$ complex is formed together with $Fe(CN)_6^{4-}$ in the reduction of ferricyanide by e_{aq}^-,[5,9] H,[5] and O_2^-.[5] The aquapentacyanoferrate(II) has a peak of absorption at ~445 nm in neutral solutions.[17-19] It absorbs light at 420 nm where ferricyanide is usually measured by its peak absorption, and at wavelengths longer than 500 nm.[5b,17-19] In addition to the aquapentacyanoferrate(II), small yields of aquapentacyanoferrate(III) have been proposed.[5a]

In acid solutions ferrocyanide ions become protonated.[20,21] This fact has been disregarded in previous radiation chemistry work. Consequently, the possibility of the effect of pH on the reactivity of ferrocyanide has not been considered. The purpose of this work is to elucidate the mechanism of the OH and peroxy radicals reactions in the ferro-ferricyanide aqueous system, in both neutral and acid media.

Experimental Section

The experimental procedure for the pulse irradiation has been described elsewhere.[22] A linear accelerator was used as an electron pulse source of 5 MeV and 200 mA. The pulse duration was varied between 0.1 and 1.5 μsec. The inductive current obtained by the electron beam in a coil was used to

(1) J. Rabani and G. Stein, *Trans. Faraday Soc.*, **58**, 2150 (1962).
(2) (a) F. S. Dainton and W. S. Watt, *Nature (London)*, **195**, 1294 (1962); (b) F. S. Dainton and W. S. Watt, *Proc. Roy. Soc., Ser. A*, **275**, 447 (1963).
(3) (a) G. Hughes and C. Willis, *J. Chem. Soc.*, 4848 (1962); (b) G. Hughes and C. Willis, *Discuss. Faraday Soc.*, **36**, 223 (1963).
(4) (a) S. Gordon, E. J. Hart, M. S. Matheson, J. Rabani, and J. K. Thomas, *J. Amer. Chem. Soc.*, **85**, 1375 (1963); (b) S. Gordon, E. J. Hart, M. S. Matheson, J. Rabani, and J. K. Thomas, *Discuss. Faraday Soc.*, **36**, 193 (1963).
(5) (a) E. Masri and M. Haissinsky, *J. Chim. Phys.*, **60**, 397 (1963); (b) M. Haissinsky, A. M. Koulkès, and E. Masri, *ibid.*, **63**, 1129 (1966).
(6) (a) E. Hayon, *Trans. Faraday Soc.*, **61**, 723 (1965); (b) E. Hayon, *ibid.*, **61**, 734 (1965).
(7) G. E. Adams, J. W. Boag, and B. D. Michael, *Trans. Faraday Soc.*, **61**, 492 (1965).
(8) (a) J. Rabani and M. S. Matheson, *J. Amer. Chem. Soc.*, **86**, 3175 (1964); (b) J. Rabani and M. S. Matheson, *J. Phys. Chem.*, **70**, 761 (1966).
(9) C. E. Burchill, F. S. Dainton, and D. Smithies, *Trans. Faraday Soc.*, **63**, 932 (1967).
(10) S. Ohno and G. Tsuchihashi, *Radioisotopes*, **16**, 26 (1967).
(11) J. Rabani and D. Meyerstein, *J. Phys. Chem.*, **72**, 1599 (1968).
(12) G. Czapski and E. Peled, *Isr. J. Chem.*, **6**, 421 (1968).
(13) J. Sobkowski, *Nukleonika*, **14**, 253 (1969).
(14) G. E. Adams and R. L. Willson, *Trans. Faraday Soc.*, **65**, 2981 (1969).
(15) G. C. Barker, P. Fowles, and B. Stringer, *Trans. Faraday Soc.*, **66**, 1509 (1970).
(16) J. Sobkowski, *Roczn. Chem.* **43**, 1729 (1969).
(17) M. Ottolenghi and J. Rabani, *J. Phys. Chem.*, **72**, 593 (1968).
(18) G. Emschwiller, *Colloq. Int. Cent. Nat. Rech. Sci.*, **191**, 307 (1970).
(19) (a) G. Stein, *Isr. J. Chem.*, **8**, 691 (1970); (b) M. Shirom and G. Stein, *J. Chem. Phys.*, **55**, 3379 (1971).
(20) J. Jordan and G. J. Ewing, *Inorg. Chem.*, **1**, 587 (1962).
(21) G. I. H. Hanania, D. H. Irvine, W. A. Eaton, and P. George, *J. Phys. Chem.*, **71**, 2022 (1967).
(22) D. Zehavi and J. Rabani, *J. Phys. Chem.*, **75**, 1738 (1971).

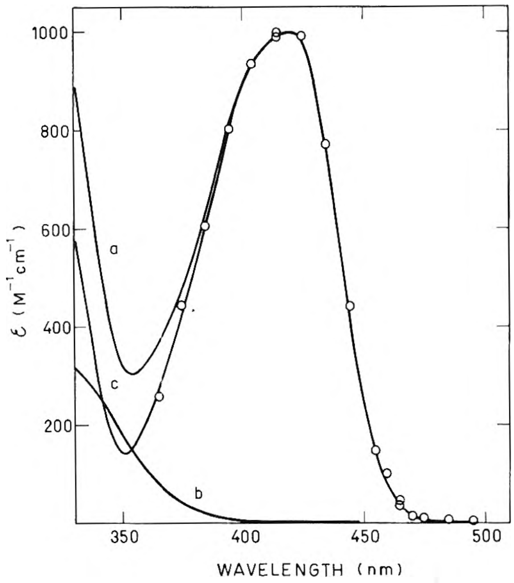

Figure 1. The spectra of ferricyanide and ferrocyanide in neutral aqueous solutions: a, absorption spectrum of ferricyanide (5×10^{-4} M); b, absorption spectrum of ferrocyanide (10^{-3} M); c, a difference spectrum (a − b); O, the spectrum in the pulse irradiation of 10^{-3} M $K_4Fe(CN)_6$ in oxygenated neutral solutions. The optical density at 420 nm is 0.04.

monitor the pulse intensity. A 150-W Osram xenon lamp, a halogen lamp (for the long time range) and D_2 lamp (for the uv range) produced the analyzing light. A 4-cm cell with 12.2-cm light path was used unless otherwise stated. An IP28A photomultiplier, a Bausch and Lomb high-intensity monochromator, and a Tektronix 556 double-beam oscilloscope were used. Spectra were recorded using a split analyzing light beam. One light beam at constant wavelength (normally at the peak of the absorption) served as a pulse intensity monitor.

Ferrocyanide and ferricyanide solutions undergo thermal and photochemical decompositions. In addition, ferrocyanide is oxidized by oxygen. These processes are enhanced in both acid solutions and at relatively concentrated neutral solutions. To minimize these effects, the following precautions were taken. (a) The solutions were prepared in syringes just before irradiation and were irradiated within about 20 min. Ferrocyanide was dissolved only after saturating the solutions with the appropriate gas and the removal of air (by bubbling the solutions with Ar, N_2O, or O_2 for 20 min). Gas chromatographic measurements showed that less than 2×10^{-7} M residual O_2 was left after 20 min bubbling with Ar. (b) Appropriate light filters (Corning or Schott and Gen.) were used between the light source and the irradiation cell. (c) A shutter, operated mechanically, was used between the irradiation cell and the light source. The solutions were exposed for periods of less than 1 sec before irradiation. (d) The analyzing light signals were recorded simultaneously with the corresponding absorption traces, so that errors in the optical density due to photoproduction of small concentrations of products before pulsing were eliminated. (e) The syringes, the filling system, and the irradiation cell were protected from light.

Materials were of AR grade. $K_4Fe(CN)_6 \cdot 3H_2O$ (Mallinckrodt), $K_3Fe(CN)_6$ (BDH), $HClO_4$ (Merck), H_2SO_4 (BDH), K_2SO_4 (H & W), and KOH (Riedel-De Haën) was used without further purification. The water used was triple distilled. Ultrahigh-purity argon and oxygen (Matheson Co.) were used. N_2O (Matheson Co.) was purified by the procedure described before.[8b] The temperature was 23 ± 2°. A Beckman Model H3 pH meter was used for pH measurements with standard Beckman buffer solutions for calibrations. A CD6400 computer was employed for the calculations of complex kinetics, using Schmidt's[23] program.

Results

1. The Reaction of OH with Ferrocyanide in Neutral and Acid Solutions. Rabani and Matheson[8] reported $k_2 = (1.07 \pm 0.10) \times 10^{10}$ M^{-1} sec^{-1} in the pulse radiolysis of neutral and acid (pH ~3) solutions of ferrocyanide. Irradiations in the presence of 0.3 M Na_2SO_4 in neutral solution gave similar results.[8] It was assumed that ferricyanide was the only reaction product absorbing at 420 nm.

In order to check whether the reaction of ferrocyanide with OH produces exclusively ferricyanide, neutral and acid solutions of ferrocyanide were irradiated and the optical absorption spectrum in the visible region was determined. The results are presented in Figure 1. We have found that the spectrum of ferricyanide in the range 330 to 500 nm does not depend on the presence of ferrocyanide (checked in 0.1 M ferrocyanide) or on the pH (examined at pH 3 and 1). The optical absorption of ferrocyanide changes with the pH due to protonation but it does not influence the difference spectrum (c) above 400 nm. Under the conditions of Figure 1 the OH radicals react with ferrocyanide while the e_{aq}^- and H radicals react with O_2. The absorption formed is stable for at least 100 µsec. Identical spectra have been obtained in the irradiations of (a) 10^{-3} M ferrocyanide in N_2O-saturated neutral solutions (about 1 µsec after the electron pulse) and (b) 10^{-3} M ferrocyanide in oxygenated $HClO_4$ solution at pH 1 and 5×10^{-4} M ferrocyanide in air-saturated 3 M $HClO_4$ solutions (1 µsec after the electron pulse). In all these experiments no absorption was found in the range of 500 to 700 nm. ($D < 5 \times 10^{-4}$ for electron pulses identical with those of Figure 1). This indicates that the only product formed under these conditions is ferricyanide.

In Table I we present the reaction rate constant k_2 measured in neutral and acid solutions. Values of k_2 were determined from plots of ln $(D_2 - D_t)$ vs. t, where D_t and D_2 are the optical densities at time t and at the end of the reaction 2, respectively. D_2 was measured before any decay of the ferricyanide had taken place, or corrected for it. In solutions containing O_2, electrons and H atoms produce O_2^- and HO_2, respectively. These products maintain a pH dependent equilibrium.[24] Under our conditions the reactions of ferricyanide or ferrocyanide with HO_2 or O_2^- are well separated in time from reaction 2, so that D_2 could be measured directly. In neutral solutions containing N_2O, electrons are quickly converted to OH radicals. H atoms (G ~0.6) may reduce ferricyanide (reaction 4 in competition with recombination reaction 7).

$$N_2O + e_{aq}^- \xrightarrow{H_2O} N_2 + OH + OH^- \qquad (6)$$

$$H + H \rightarrow H_2 \quad (k_7 = 7.8 \times 10^9\ M^{-1}\ sec^{-1}\ ^{25}) \qquad (7)$$

In acid solutions, reaction 4 becomes more important owing to the formation of additional H atoms by reaction 8. In

$$e_{aq}^- + H_{aq}^+ \rightarrow H \qquad (8)$$

(23) K. H. Schmidt, ANL Report 7199, Argonne National Laboratory, Argonne, Ill., 1966.

(24) (a) J. Rabani and S. O. Nielsen, *J. Phys. Chem.*, **73**, 3736 (1969). (b) D. Behar, G. Czapski, J. Rabani, L. M. Dorfman, and H. A. Schwarz, *ibid.*, **74**, 3209 (1970).

(25) P. Pagsberg, H. Christensen, J. Rabani, G. Nilsson, J. Fenger, and S. O. Nielsen, *J. Phys. Chem.*, **73**, 1029 (1969).

TABLE I: Rate Constants for the OH + Ferrocyanide Reaction

$10^4[K_4Fe(CN)_6]$, *M*	Additives[a]	pH[b]	D_2[c]	$10^{-10}k_2$,[d] M^{-1} sec^{-1}
0.3	N_2O 1 atm	Near neutral	0.037	1.19
0.5	N_2O 1 atm	Near neutral	0.039	1.26
1.0	O_2 1 atm or N_2O 1 atm	Near neutral	0.048	1.27
2.0	N_2O 1 atm	Near neutral	0.045	1.29
1.0	O_2 1 atm + 1 × 10^{-5} *M* H^+	5.5	0.046	1.24
1.01	N_2O 1 atm + 4 × 10^{-5} *M* H^+	4.5	0.057	1.16
1.0	O_2 1 atm + 1 × 10^{-4} *M* H^+	4.27	0.045	1.17
1.01	N_2O 1 atm + 2 × 10^{-4} *M* H^+	3.82	0.056	0.99
2.6	O_2 0.8 atm + 9.3 × 10^{-4} *M* H^+	3.11	0.037	0.79
2.56	N_2O 0.8 atm + 9.3 × 10^{-4} *M* H^+	3.16	0.075	0.89
1.01	O_2 1 atm + 1 × 10^{-3} *M* H^+	3.08	0.026	0.78
1.0	Air saturated + 1 × 10^{-3} *M* H^+	3.04	0.043	0.83
2.6	O_2 0.8 atm + 2.8 × 10^{-3} *M* H^+	2.57	0.037	0.66
2.56	N_2O 0.8 atm + 9.3 × 10^{-3} *M* H^+	2.04	0.051	0.71
2.6	O_2 0.8 atm + 9.3 × 10^{-3} *M* H^+	2.07	0.036	0.59
5.0	O_2 0.8 atm + 2.8 × 10^{-2} *M* H^+	1.65	0.038	0.39
5.0	O_2 0.8 atm + 9.3 × 10^{-2} *M* H^+	1.17	0.038	0.31
2.56	N_2O 0.8 atm + 9.3 × 10^{-2} *M* H^+	1.18	0.037	0.36
2.6	0.46 *M* H^+	0.45	0.033	0.23
2.6	0.46 *M* H^+	0.45	0.016	0.25
2.6	O_2 0.8 atm + 0.46 *M* H^+	0.45	0.017	0.23
2.6	O_2 0.8 atm + 0.46 *M* H^+	0.45	0.036	0.22
5.0	O_2 0.8 atm + 0.465 *M* H^+	0.45	0.038	0.23
5.0	Air saturated + 1 *M* H^+	0.1	0.049	0.18
5.0	Air saturated + 3 *M* H^+	0.4	0.052	0.13

[a] $HClO_4$ was used to obtain acid pH values. [b] Measured before irradiation. The pH of the 3 *M* solution is an extrapolated value from a pH *vs.* $[H^+]$ plot. Values were corrected according to pH = $-\log a_{H^+}$ = pH (measured) + 0.009[4−pH (measured)] for pH <4 (R. A. Robinson, "Handbook of Chemistry and Physics," The Chemical Rubber Co.). [c] Optical density at the end of reaction 2 measured at 420 nm. D_2 can also be used as an indicator to the pulse intensity. [d] Corrected values (see text). Each value is an average of 3-5 parallel determinations. In most cases, two separate samples of solid ferrocyanide were used for the preparation of each concentration.

these cases the values of D_2 were obtained by extrapolation methods. In the calculations of k_2 we have noted the possibility of OH recombination and reaction with HO_2 and O_2^-.

$$OH + OH \rightarrow H_2O_2 \quad (k_9 = 6.3 \times 10^9\ M^{-1}\ sec^{-1}\ {}^{18}) \quad (9)$$

$$OH + HO_2 \rightarrow H_2O_3(H_2O + O_2) \quad (k_{10} = 7.1 \times 10^9\ M^{-1}\ sec^{-1}\ {}^{26}) \quad (10)$$

$$OH + O_2^- \rightarrow OH^- + O_2 \quad (k_{11} = 1.0 \times 10^{10}\ M^{-1}\ sec^{-1}\ {}^{26}) \quad (11)$$

Computations have shown that in all the experiments (in Table I) less than 5% of the OH radicals disappeared by reaction 9 and less than 6% by reactions 10 and 11. Appropriate corrections have been made.

The results in Table I show that the apparent reaction rate constant of OH with ferrocyanide, "k_2," increases with the pH. In Figure 2 we demonstrate that the effect of pH can be attributed to different reactivities of $Fe(CN)_6^{4-}$, $HFe(CN)_6^{3-}$, and $H_2Fe(CN)_6^{2-}$ toward OH radicals. The best agreement of the calculated curve and experimental results is obtained with $k((OH + Fe(CN)_6^{4-})) = (1.25 \pm 0.1) \times 10^{10}$, $k((OH + HFe(CN)_6^{3-})) = (9.0 \pm 0.9) \times 10^9$, and $k((OH + H_2Fe(CN)_6^{2-})) = (1.7 \pm 0.5) \times 10^9\ M^{-1}$ sec^{-1}. We have used the equations obtained by Hanania, *et al.*,[21] for the calculations of the fractions of the various ferrocyanide ions.

$$pK_4 = 4.28 - 3.56 \frac{\mu^{1/2}}{1 + 1.5\mu^{1/2}};\ K_4 = \frac{a_{H^+}[Fe(CN)_6^{4-}]}{[HFe(CN)_6^{3-}]} \quad (I)$$

$$pK_3 = 2.3 - 2.55 \frac{\mu^{1/2}}{1 + 1.5\mu^{1/2}};\ K_3 = \frac{a_{H^+}[HFe(CN)_6^{3-}]}{[H_2Fe(CN)_6^{2-}]} \quad (II)$$

The activity of H^+ was calculated from the pH values. The ionic strength was calculated from eq III (by successive approximations using eq I and II).

$$\mu = [H^+]_0 + 10[Fe(CN)_6^{4-}] + 6[HFe(CN)_6^{3-}] + 3[H_2Fe(CN)_6^{2-}] \quad (III)$$

$[H^+]_0$ is the acid ($HClO_4$) concentration added. The association of $Fe(CN)_6^{4-}$ with K^+ was neglected. It amounts to less than 6% of the ferrocyanide (calculated according to Eaton, *et al.*[27]). The $KFe(CN)_6^{3-}$ fraction is included in the $Fe(CN)_6^{4-}$ fraction. Figure 2 shows excellent agreement between the results and the calculated curve down to pH 0.5. The deviations below this pH may be due to deviations in eq I and II in this range, or to an additional association of ferrocyanide with H^+.[20]

Rabani and Matheson[8] reported $k_2 = 1.07 \times 10^{10}\ M^{-1}$ sec^{-1}, averaging results obtained in both near neutral and acid solutions. When k_2 values[8] are recalculated so that only results in neutral solutions and with no other salts added are included, an average value $k_2 = 1.2 \times 10^{10}\ M^{-1}$ sec^{-1} is obtained, which is in very good agreement with our value. These values are slightly higher than the value $k_2 = (9.3 \pm 0.5) \times 10^9\ M^{-1}$ sec^{-1} recently reported by Willson, *et al.*[28]

(26) K. Sehested, O. L. Rasmussen, and H. Fricke, *J. Phys. Chem.*, **72**, 626 (1968).
(27) W. A. Eaton, P. George, and G. I. H. Hanania, *J. Phys. Chem.*, **71**, 2016 (1967).
(28) R. L. Willson, C. L. Greenstock, G. E. Adams, R. Wageman, and L. M. Dorfman, *Int. J. Radiat. Phys. Chem.*, **3**, 211 (1971).

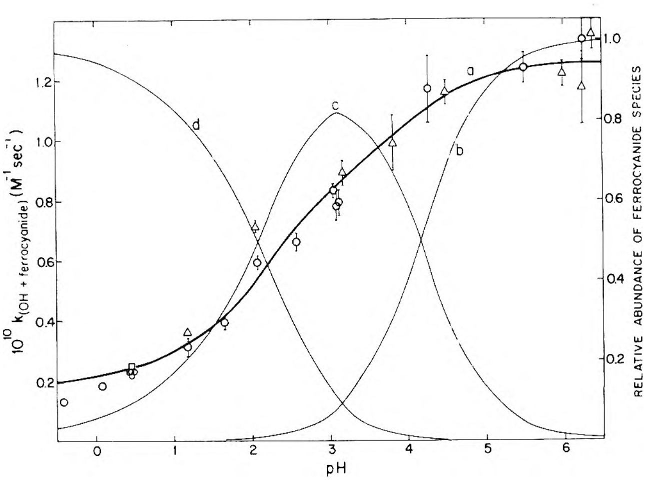

Figure 2. The dependence of the apparent $k_{(OH+ferrocyanide)}$ on the pH ($HClO_4$). The experimental results are those of Table I: O, oxygen or air saturated solutions; Δ, N_2O saturated solutions; □, deaerated (Ar saturated) solutions; a, calculated curve for the apparent $k_{(OH+ferrocyanide)}$; b, the fraction of ferrocyanide present as $Fe(CN)_6^{4-}$; c, the fraction of ferrocyanide present as $HFe(CN)_6^{3-}$; d, the fraction of ferrocyanide present as $H_2Fe(CN)_6^{2-}$.

Association of ferrocyanide with positive ions to form ion pairs has a small effect on k_2. Some results are presented in Table II. In the Li^+ solutions, about 50% of the ferrocyanide is present as ion pairs. In all other solutions there is practically a full association with one ion.[29] The ion pairs are by about 10% less reactive toward OH radicals as compared with free ferrocyanide ions.

Rabani and Matheson[8] reported $pK_{OH} = 11.9 \pm 0.2$ (K_{OH} is the equilibrium constant of $OH \rightleftarrows O^- + H^+$). This value is based on $k_2 = 1.07 \times 10^{10}\ M^{-1}\ sec^{-1}$. Using the revised value $k_2 = 1.25 \times 10^{10}\ M^{-1}\ sec^{-1}$ and taking $k((OH + NaFe(CN)_6^{3-})) = 1.15 \times 10^{10}\ M^{-1}\ sec^{-1}$, $pK_{OH} = 11.85$ results.

2. *The Reaction of HO_2 Radicals with Ferrocyanide in Acid Solutions.* Adams, Boag, and Michael[7] reported $k_5 = 1.64 \times 10^5\ M^{-1}\ sec^{-1}$ in $10^{-2}\ N\ H_2SO_4$ oxygenated solutions and assumed that the reaction product was ferricyanide. We have irradiated oxygenated solutions of ferrocyanide in the pH range 0.46 to 4.37 ($HClO_4$ or H_2SO_4). In these solutions the OH radicals react very rapidly with ferrocyanide (reaction 2), while the e_{aq}^- and H radicals are converted into peroxy radicals, HO_2 and O_2^-. HO_2 and O_2^- are in equilibrium, determined by the pK of HO_2, which is 4.8.[24]

TABLE II: The Effect of Ion Pair Formation on $k_{(OH+ferrocyanide)}$ in Neutral Solutions[a]

Additive	D_2[b]	$10^{-10}\ k_2$,[c] $M^{-1}\ sec^{-1}$
None	0.042	1.25
0.05 M Li_2SO_4	0.042	1.28
0.5 M Li_2SO_4	0.042	1.21
0.5 M $NaClO_4$	0.043	1.15
0.05 M K_2SO_4	0.041	1.16
0.5 M K_2SO_4	0.043	1.04
0.05 M Cs_2SO_4	0.042	1.15
0.5 M Cs_2SO_4	0.041	1.18
0.025 M $MgSO_4$	0.042	1.10
0.025 M $Ca(ClO_4)_2$	0.040	1.12
0.025 M $BaCl_2$	0.041	1.14

[a] The solutions were saturated with N_2O and contained $1 \times 10^{-4}\ M$ potassium ferrocyanide. [b] All the results are normalized to the same dose. [c] Corrected for the recombination of OH radicals (reaction 9).

Neither H_2O_2 nor O_2^- is reactive toward ferrocyanide under our conditions.[7,16] We have confirmed this by pulse irradiations of $10^{-2}\ M$ ferrocyanide in oxygenated neutral solutions and 0.1 M ferrocyanide in oxygenated slightly basic (pH 9.6) solutions. After reaction 2 has been completed, no further change in the optical absorption has been noticed (at 420 nm) up to 10 msec in the neutral solutions. In the basic solutions, a partial decay ($t_{1/2} \sim 1$ sec) was observed, which can be attributed to the reaction of ferricyanide with O_2^- (this will be discussed later). In conclusion, under our conditions, the oxidation of ferrocyanide *via* reaction 5 is well separated in time from other reactions of ferri- and ferrocyanide.

We have examined the spectrum of the product of reaction 5. The ratio D_5/D_2 (where D_2 is the optical density at the end of reaction 2 before any oxidation by HO_2 radicals had begun and D_5 is the optical density at the end of reaction 5), determined in $2.5 \times 10^{-3}\ M$ ferrocyanide solutions in acid range, did not change with the wavelength in the range 400–500 nm. No absorbance had been noticed in the range 500–700 nm. This indicates that ferricyanide is the only product of reaction 5.

The kinetic results are given in Table III. Values of the overall reaction rate constant of peroxy radicals were determined from plots of ln $(D_5 - D_t)$ *vs.* t, which showed linear dependence in all the experiments (Figure 3). In calculating k_5, corrections have been made for reactions 12a and 12b as well as corrections for impurity effects on HO_2 and O_2^-, based on an empirical rate constant (from blank experiments) for a presumed reaction 13.

$$HO_2 + HO_2 \rightarrow H_2O_2 + O_2 \quad (k = 0.76 \times 10^6\ M^{-1}\ sec^{-1}) \tag{12a}$$

$$HO_2 + O_2^- \rightarrow HO_2^- + O_2 \quad (k = 8.5 \times 10^7\ M^{-1}\ sec^{-1}) \tag{12b}$$

$$\text{“}HO_2\text{”} + X \rightarrow P \tag{13}$$

The contributions of reactions 12a, 12b, and 13 increase with pH. The relative amount of these reactions, in comparison with reaction 5 is indicated by the ratio $(D_5 - D_2)/D_2$. When reactions 12a, 12b, and 13 can be neglected, this ratio equals to G(peroxy radicals)/G(OH) = $(G_e + G_H)/G_{OH} = 1.23$ at low [ferrocyanide]. Table III shows that the limiting ratio is approached below pH 2.5 ($HClO_4$). The ratio of the experimental $(D_5 - D_2)/D_2$ divided by 1.23 is approximately equal to the ratio “k_5”/k_{exptl}, where “k_5” is the apparent pseudo-first-order rate constant of the reaction of the total peroxy radicals ($HO_2 + O_2^-$) with ferrocyanide. In solutions containing $10^{-2}\ M$ ferrocyanide the value G(peroxy radicals)/G(OH) = 1.13 was used in the corrections for reactions 12a, 12b, and 13. The ratio $(G_e + G_H)/G_{OH}$ is expected to decrease as the ferrocyanide concentration increases due to the increase in G_{OH}.[3b]

The values of k_5 were derived with the aid of eq IV, in which K is the equilibrium constant of $HO_2 \rightleftarrows O_2^- + H^+$.

$$k_5 = \text{“}k_5\text{”}\left(1 + \frac{K}{[H^+]}\right) \tag{IV}$$

The results of Table III show that the presence of ferricyanide in the solutions did not affect the rate of reaction 5.

(29) "Stability Constants," The Chemical Society, London, 1957, 1964, 1971.

Experiments in the presence of 10^{-2} M formate and 10^{-3} M ferricyanide at pH 2 (not included in Table III) showed no reduction of ferricyanide due to HO_2 within experimental error. From these experiments an upper limit $k((HO_2 + Fe(CN)_6^{3-})) < 500\ M^{-1}\ sec^{-1}$ can be calculated. This agrees with the lack of ferricyanide effect.

For the calculation of the fractions of the different ferrocyanide species, eq I, II, and V (from Eaton, *et al.*[27]) were used.

$$\log K_1 = 2.35 - 4.08\frac{\mu^{1/2}}{1 + 1.5\mu^{1/2}};\ K_1 = \frac{[KFe(CN)_6^{3-}]}{[K^+][Fe(CN)_6^{4-}]} \qquad (V)$$

Equation III was modified into VI for the calculations of ionic strengths in the $HClO_4$ solutions. (In experiments where K_2SO_4 was added, a term $3[K_2SO_4]$ was added to the right-hand side of eq VI.)

$$\mu = [H+]_0 + 10[Fe(CN)_6^{4-}] + 6[KFe(CN)_6^{3-}] + 6[HFe(CN)_6^{3-}] + 3[H_2Fe(CN)_6^{2-}] \qquad (VI)$$

TABLE III: Rate Constants for the HO_2 + Ferrocyanide Reaction in O_2-Saturated Solutions[a]

$[H^+]$, M	pH[b]	D_2[c]	$(D_5 - D_2)/D_2$[d]	$10^{-4}k_5$,[e] $M^{-1}\ sec^{-1}$
		$HClO_4$		
5.0×10^{-4}	4.37	0.032	0.78	5.3 ± 0.3
5.0×10^{-4}	4.37	0.034	0.85	5.3 ± 0.3
5.1×10^{-4}[i]	4.20	0.036	0.79	3.6 ± 0.1
1.0×10^{-3}	3.95	0.032	0.95	6.9 ± 0.2
1.0×10^{-3}	3.95	0.036	1.01	7.3 ± 0.2
1.02×10^{-3}	3.88	0.037	0.98	6.5 ± 0.2
1.02×10^{-3}[i]	3.87	0.037	0.98	5.2 ± 0.1
2.0×10^{-3}	3.44	0.032	1.09	10.1 ± 0.5
2.0×10^{-3}	3.44	0.036	1.07	8.8 ± 0.2
2.0×10^{-3}	3.44	0.061	0.96	9.2 ± 0.1
4.0×10^{-3}[i]	3.00	0.036	1.15	9.4 ± 0.1
4.0×10^{-3}	2.88	0.037	1.23	11.1 ± 0.1
4.0×10^{-3}	2.84	0.033	1.14	11.5 ± 0.3
7.0×10^{-3}	2.45	0.033	1.18	10.7 ± 0.3
1.0×10^{-2}	2.23	0.032	1.19	9.8 ± 0.5
2.0×10^{-2}	1.89	0.033	1.18	7.0 ± 0.2
5.0×10^{-2}	1.51	0.033	1.19	5.2 ± 0.2
0.10	1.22	0.034	1.21	4.0 ± 0.2
0.20	0.92	0.034	1.22	3.2 ± 0.1
0.50	0.61	0.034	1.20	2.3 ± 0.1
0.80	0.46	0.034	1.18	1.8 ± 0.1
		H_2SO_4		
5.0×10^{-3}	3.53	0.099	0.83	7.9 ± 0.3
1.0×10^{-2}	2.91	0.090	1.10	10.5 ± 0.1
2.0×10^{-2}	2.38	0.102	1.08	10.3 ± 0.2
4.0×10^{-2}	1.82	0.110	1.13	8.5 ± 0.3
4.0×10^{-2}[f]	1.82	0.100	1.13	8.2 ± 0.2
8.0×10^{-2}	1.50	0.108	1.06	6.0 ± 0.1
0.20	1.20	0.108	1.12	4.3 ± 0.2
0.60	0.83	0.109	1.07	2.7 ± 0.1
0.10[g]	1.24	0.096	0.89	3.9 ± 0.1
0.10[h]	1.24	. . .	0.90	4.0 ± 0.3

[a] Unless otherwise stated, $HClO_4$ solutions contained 2.5×10^{-3} M potassium ferrocyanide. H_2SO_4 solutions contained 1.0×10^{-2} M potassium ferrocyanide. [b] See footnote *b* of Table I. [c] Optical densities (at 420 nm) at the end of reaction 2. [d] D_5 is the optical density (at 420 nm) at the end of reaction 5. [e] Corrected values. Each value is an average of 3–6 determinations. Most measurements were carried out at 420 nm, but occasionally also at longer wavelengths up to 460 nm. [f] 10^{-4} M ferricyanide present. [g] 10^{-3} M $K_4Fe(CN)_6$. [h] 10^{-3} M $K_4Fe(CN)_6$ and 2×10^{-3} M $K_3Fe(CN)_6$. [i] 2×10^{-2} M K_2SO_4 added.

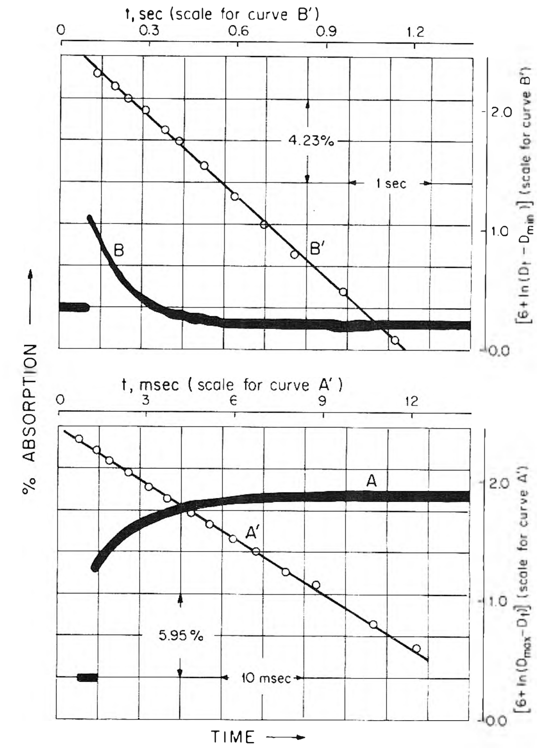

Figure 3. Oscilloscope traces for reactions of HO_2 radicals with ferrocyanide ions (curve A) and of O_2^- radical ions with ferricyanide (curve B) in oxygenated solutions. Curves A' and B' show the derivation of the pseudo-first-order rate constants. Curve A, 2.5×10^{-3} M ferrocyanide at pH 4.37 ($HClO_4$) irradiated with 0.4-μsec pulse at 420 nm. Curve B, 4.8×10^{-4} M ferricyanide + 6.9×10^{-4} M ferrocyanide + 1.8×10^{-2} M K_2SO_4 at pH 9.7, irradiated with 1.5-μsec pulses at 420 nm (2-cm light path).

Equation VII was used for the calculations of the ionic strengths in H_2SO_4 solutions.

$$\mu = 2[H^+] - [H_2SO_4]_0 + 10[Fe(CN)_6^{4-}] + 6[KFe(CN)_6^{3-}] + 8[HFe(CN)_6^{3-}] + 7[H_2Fe(CN)_6^{2-}] \qquad (VII)$$

$[H_2SO_4]_0$ is the total H_2SO_4 concentration added. $[H^+]$ was calculated for each solution according to Lindstrom and Wirth[30] (eq VIII) using the material balance equation (IX).

$$\log Q = \log 0.0102 + 2.036\mu^{1/2} - 1.376\mu + 0.886\mu^{3/2} - 0.217\mu^2;\quad Q = \frac{[H^+][SO_4^{2-}]}{[HSO_4^-]} \qquad (VIII)$$

$$[H_2SO_4]_0 = [HSO_4^-] + [SO_4^{2-}] = \tfrac{1}{2}[H^+] + \tfrac{1}{2}[HSO_4^-] + \tfrac{1}{2}[HFe(CN)_6^{3-}] + [H_2Fe(CN)_6^{2-}] \qquad (IX)$$

The results of Table III are plotted in Figure 4. The best agreement between the calculated curves and the experimental results is obtained with $0.6k((HO_2 + Fe(CN)_6^{4-})) + 0.4k((HO_2 + KFe(CN)_6^{3-})) = (3.4 \pm 0.3) \times 10^4$ (based on $HClO_4$ solutions), $k((HO_2 + HFe(CN)_6^{3-})) = (1.40 \pm 0.1) \times 10^5$, and $k((HO_2 + H_2Fe(CN)_6^{2-})) = (1.0 \pm 0.3) \times 10^4$ $M^{-1}\ sec^{-1}$.

From experiments in the presence of 0.02 M K_2SO_4 (Table III), it is possible to calculate $0.37k((HO_2 + Fe(CN)_6^{4-})) + 0.63k((HO_2 + KFe(CN)_6^{3-})) = 3.3 \times 10^4$.

(30) R. E. Lindstrom and H. E. Wirth, *J. Phys. Chem.*, **73**, 218 (1969).

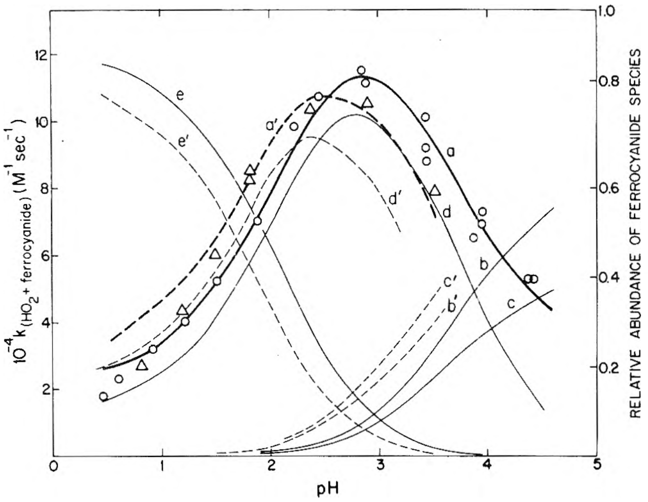

Figure 4. The dependence of the apparent "k_5" on the pH (Table II). The points O and full lines are for 2.5×10^{-3} M ferrocyanide in $HClO_4$ solutions. The points Δ and dotted lines are for 10^{-2} M ferrocyanide in H_2SO_4 solutions: a, a', calculated curves for the apparent "k_5"; b, b', the fraction (f) of ferrocyanide present as $Fe(CN)_6^{4-}$; c, c', f present as $KFe(CN)_6^{3-}$; d, d', f present as $HFe(CN)_6^{3-}$; e, e', f present as $H_2Fe(CN)_6^{2-}$.

From this, $k((HO_2 + Fe(CN)_6^{4-})) \simeq 3 \times 10^4$ M^{-1} sec^{-1} (error limits 50%). The deviations at low pH values, especially in H_2SO_4 solutions, are not surprising, since the equations used for the determination of the different ferrocyanide species are accurate only for low ionic strengths.

3. The Reaction of O_2^- Radical Ions with Ferricyanide Ions and Ion Pairs. O_2^- radical ions reduce ferricyanide ions and ion pairs according to reactions 14a and 14b, respectively.

$$O_2^- + Fe(CN)_6^{3-} \rightarrow O_2 + Fe(CN)_6^{4-} \quad (14a)$$

$$O_2^- + KFe(CN)_6^{2-} \rightarrow O_2 + KFe(CN)_6^{3-} \quad (14b)$$

Figure 3b demonstrates these processes. Ferricyanide concentrations ranging from 5×10^{-4} to 2×10^{-3} M have been pulse irradiated in a 2-cm cell (light path 2 cm, λ 420–440 nm). All the solutions contained 0.5–1 mM ferrocyanide. Ferrocyanide reacted with OH radicals according to reaction 2. As ferricyanide, which is already present, is the product of 2, OH radicals are eliminated without the formation of new species. After a relatively short time, the system contains only ferri- and ferrocyanide ions, as well as O_2^- radical ions. In Table IV we present results at pH 9.5–9.7. This high pH was used in order to suppress the disproportionation reactions of O_2^- and HO_2. O_2^- is relatively very stable in alkaline solutions,[24] when catalysis by impurities can be neglected. To minimize impurities, we have used five- instead of three-times distilled water. Control experiments in the absence of ferricyanide still indicated some catalysis. This might have contributed up to about 20% to the rate of O_2^- decay when ferricyanide was added. However, the results in the presence of ferricyanide seemed to indicate that under our conditions the reaction rate was strictly first order in both O_2^- and ferricyanide. This can be concluded from experiments in Table IV in which the fraction of ion pairs was kept constant, while the total concentration of ferricyanide varied. In such experiments, k_{exptl}, the pseudo-first-order rate constant for the decay of O_2^-, was proportional to the total ferricyanide concentration. In addition, the final optical densities, D_{14}, showed that practically all the O_2^- radical ions reduced ferricyanide. $\Delta D_{14}/\Delta D_2$ = 1.1 to 1.25 was always found in this system. (ΔD_i is the absorbance change during reaction i). This is expected if O_2^- reacts exclusively with ferricyanide.

TABLE IV: Determination of k_{14a} and k_{14b} at pH 9.5–9.7 in Oxygenated Solutions[a]

$10^4[K_4Fe(CN)_6]$, M	$10^3[K_3Fe(CN)_6]$, M	μ	$10^4[KFe(CN)_6^{2-}]$ M, calcd	k_{exptl},[b] sec^{-1}
5.8	0.55	0.0085	0.33	0.74
7.0	1.09	0.012	0.86	1.79
7.0	1.96	0.017	1.94	4.90
6.7	0.52	0.035[c]	0.96	1.79
6.7	1.04	0.038[c]	1.97	3.24
6.7	1.88	0.043[c]	3.69	8.21
6.9	0.48	0.062[d]	1.16	2.06
6.9	1.10	0.065[d]	2.70	5.37
6.9	2.14	0.071[d]	5.38	10.5
7.6	0.50	0.077[e]	1.34	2.59
7.6	1.55	0.083[e]	4.19	7.55

[a] Pulse duration 1.5 μsec; light path 2 cm, 420–440 nm. 1.4×10^{-5} M O_2^- formed per pulse. Adjustment of pH by adding KOH. [b] k_{exptl} is defined as (d/dt) (ln $(D - D_\infty)$). Each value is an average of at least three determinations. [c] 9.1×10^{-3} M K_2SO_4 added. [d] 1.81×10^{-2} M K_2SO_4 added. [e] 2.3×10^{-2} M K_2SO_4 added.

On the basis of eq V, X, XI[27] and the general Brönsted–Bjerrum eq XII, it is possible to show that eq XIII results.

$$\mu = 6[Fe(CN)_6^{3-}] + 3[KFe(CN)_6^{2-}] + 10[Fe(CN)_6^{4-}] + 6[KFe(CN)_6^{3-}] + 3[K_2SO_4] + [KOH] \quad (X)$$

$$\log K_2 = 1.46 - 3.06\frac{\sqrt{\mu}}{1 + 1.5\sqrt{\mu}};\ K_2 = \frac{[KFe(CN)_6^{2-}]}{[K^+][Fe(CN)_6^{3-}]} \quad (XI)$$

$$\log \frac{k^{\mu}_{14}}{k^0_{14}} = 1.02Z\frac{\sqrt{\mu}}{1 + \alpha\sqrt{\mu}} \quad (XII)$$

$$\frac{ak_{\text{exptl}}}{[Fe(CN)_6^{3-}]} = k^0_{14a} + bk^0_{14b}\frac{[KFe(CN)_6^{2-}]}{[Fe(CN)_6^{3-}]} \quad (XIII)$$

In the above equations μ is the ionic strength, Z is the charge of the corresponding ferricyanide ions ($Fe(CN)_6^{3-}$ or $KFe(CN)_6^{2-}$), and α was taken as 1.5 for both reactions 14a and 14b. This corresponds to an encounter radius of 4.5 Å, which agrees with a radius of 2.77 Å for ferrocyanide[31] and 1.7 Å for O_2^-.[32] k^{μ} is the reaction rate constant at an ionic strength μ. The values a and b are defined from eq XIV and XV, respectively.

$$a = 10^{-3.06\sqrt{\mu}/(1+1.5\sqrt{\mu})} \quad (XIV)$$

$$b = 10^{-1.02\sqrt{\mu}/(1+1.5\sqrt{\mu})} \quad (XV)$$

The results of Table IV were plotted according to eq XIII (Figure 5). The values $k^\circ_{14a} = (2.7 \pm 0.9) \times 10^2$ and $k^\circ_{14b} = (6.2 \pm 0.6) \times 10^3$ M^{-1} sec^{-1} were calculated.

Discussion

The reactivity of ferro- and ferricyanide toward OH, HO_2, and O_2^- is affected by the presence of unreactive ions. The formation of ion pairs has only little effect (10% to 20% decrease) on $k_{(OH+\text{ferrocyanide})}$ and $k_{(HO_2+\text{ferrocyanide})}$. The effect on $k_{(O_2^-+\text{ferricyanide})}$ is larger. In this case the forma-

(31) C. W. Gibby and C. B. Monk, *Trans. Faraday Soc.*, **48**, 632 (1952).
(32) (a) W. Kassatochkin, *Dokl. Akad. Nauk SSSR*, **47**, 199 (1945); (b) A. Helmes and W. Klemm, *Z. Anorg. Allg. Chem.*, **241**, 97 (1939).

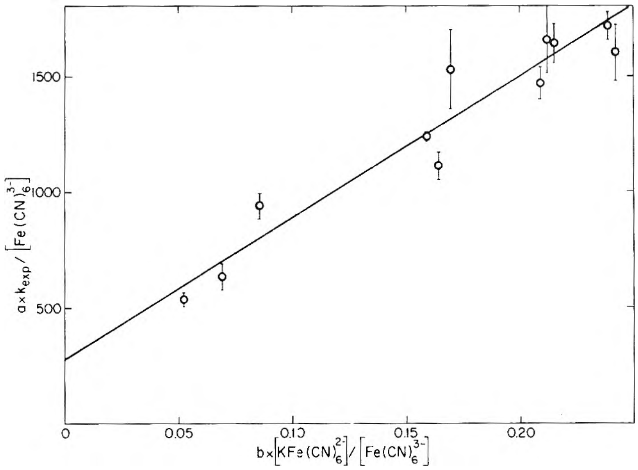

Figure 5. Determination of the rate constants of O_2^- radical ions with $Fe(CN)_6^{3-}$ (k°_{14a}) and $KFe(CN)_6^{2-}$ (k°_{14b}).

tion of the ion pairs $KFe(CN)_6^{2-}$ is expected to enhance the reaction rate because of the effect on the charge. The increase of ionic strength alone cannot account for this enhancement. When log k^{μ}_{14} is plotted *vs.* $\sqrt{\mu}/(1 + 1.5\sqrt{\mu})$ a straight line is obtained within experimental error. The slope is 4.8 compared with a slope of 3.06 which is required by the Brönsted–Bjerrum theory for the reaction between O_2^- and $Fe(CN)_6^{3-}$ ions. The formation of ion pairs may resolve the contradiction only if the ion pair has a much higher reactivity toward O_2^- as compared with the reactivity of $Fe(CN)_6^{3-}$. A different situation was found for the reaction of e_{aq}^- with ferricyanide, where ion-pair formation did not affect much the reactivities.[33] The difference may be due to the fact that the reaction with e_{aq}^- is diffusion controlled, while the reaction with O_2^- is activation controlled.

The reaction of ferrocyanide with OH radicals is a diffusion-controlled electron transfer reaction. Its reaction rate constant, $1.25 \times 10^{10}\ M^{-1}\ sec^{-1}$, is similar to the rates of other reactions which are considered to be diffusion controlled. We find a reduced reactivity of OH toward $Fe(CN)_6H_n^{-4+n}$ as n increases. A possible explanation is based on the attachment of OH to the ferrocyanide, followed by electron transfer. HO-HNCFe— is formed from a protonated group. This is followed by an electron transfer. This transfer may be much slower as compared with the analogous process which follows the formation of HO-NCFe— from OH and unprotonated cyanide. A similar process has been proposed by Halpern[34] for the reduction of complexes by atomic hydrogen.

The reaction of HO_2 with ferrocyanide is activation controlled. The effect of the first protonation is to enhance the reaction rate. Direct formation of H_2O_2 from the activated complex may perhaps decrease the activation energy and enhance the reaction rate

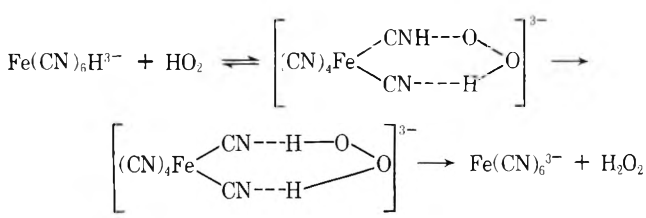

The formation of the complex similar to

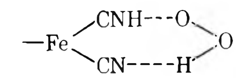

is less likely when a second proton is added to ferrocyanide. This may explain the lower reactivity of the doubly protonated ferrocyanide.

Acknowledgment. The authors are indebted to Mr. Y. Ogdan for his invaluable support in the operation, maintenance, and improvement of the system. This work was supported by U. S. Atomic Energy Commission Contract AT (30-1)-3753.

(33) M. S. Matheson and L. M. Dorfman, "Pulse Radiolysis," MIT Press, Cambridge, Mass., 1969, pp 66, 67.
(34) J. Halpern, *Discuss. Faraday Soc.* **29**, 252 (1960).

Emission from Aromatic Radicals in Ion Recombination Luminescence

B. Brocklehurst,* J. S. Robinson, and D. N. Tawn

Department of Chemistry, The University, Sheffield, S3 7HF, United Kingdom *(Received March 31, 1972)*

Thermoluminescence occurs when solutions of aromatic hydrocarbons are irradiated with γ rays or ultraviolet light and then allowed to warm up, releasing trapped ions. The luminescence spectra consist of emissions from the solute molecules and from related radicals, *e.g.*, benzyl from toluene: loss or gain of a hydrogen atom may occur. Carbanions are likely precursors of the excited radicals since infrared stimulated emission comes from the molecules, not the radicals, in most cases. At high doses, ground state radicals are formed and then trap charge in a second radiation-dependent step. Surprisingly, radical emission is sometimes observed at low doses (down to 1.5 krads): possible mechanisms are discussed.

Introduction

Ions can be trapped in organic glasses at 77 K:[1-4] they can be produced by high-energy radiation or ultraviolet light; the latter usually requires a long-lived triplet state which is ionized by a second photon. Recombination of the ions, especially in alkane glasses, often produces luminescence[3,4] which can be used to study the mechanisms involved. Some recombination takes place at 77 K (isothermal luminescence) because of the slow diffusion of electrons; this can be speeded up by irradiating in the absorption bands of electrons or anions (infrared stimulated emission; prolonged exposure to visible or infrared light bleaches out the ions). Recombination also occurs on warming (thermoluminescence) when molecular ions as well as electrons become mobile.

Burton and others[3-5] have studied the weak ion recombination luminescence of the pure alkanes, where the identity of the emitters is still uncertain:[6] they may be radicals. When aromatic solutes are added, positive and negative charge is transferred to them from the solvent[1,2] and the luminescence usually consists of fluorescence and phosphorescence of the solute.[3,4] In some cases, the emitter may be a radical derived from the solute: *e.g.*, toluene solutions give benzyl emission in thermoluminescence after both photolysis[7] and radiolysis;[8] durene similarly loses a hydrogen atom to give duryl.[9,10] Styrene, on the other hand, gains a hydrogen atom: its thermoluminescence in the green has been shown to be due to the α-methylbenzyl radical.[11] By analogy, similar emission from phenylacetylene solutions is probably due to the α-styryl radical.[12]

Formation of ground state radicals by photolysis and radiolysis is well known, but the mechanisms by which excited radicals are produced in ion recombination are not yet clear. In some of the previous work, very high doses were used so that trapping of charge by previously formed radicals was likely.[9,11] In this paper, results obtained mainly at very low doses are presented.

Experimental Section

Some of the methods used have been described previously.[12,13] In brief, 25-cm^3 samples were made up in high-purity silica tubes (internal diameter, 15 mm) and degassed by repeated freezing and pumping. A 2:1 mixture of methylcyclohexane and isopentane was used as the solvent. Indene was shaken with 6 N HCl, refluxed with 40% sodium hydroxide for 2 hr, and passed twice down a silica gel column. After distillation under nitrogen at reduced pressure, it was used as quickly as possible to avoid polymerization. This procedure greatly reduced the initially observed phosphorescence, probably due to carbazole impurity. Phenylacetylene was purified by gas-liquid chromatography Toluene (Analar reagent grade) and other solutes were used as received. Sulfur hexafluoride was distilled on the vacuum line. Samples were radiolyzed with a ^{60}Co source, dose rate approximately 750 rads/min; exposure to light was reduced as far as possible to avoid bleaching.

Photoelectric intensity measurements were usually made with an Aminco spectrofluorimeter, with the excitation source off for thermoluminescence and isothermal luminescence, or set to 750 nm with a red filter inserted for infrared stimulated emission. Quoted wavelengths have not been corrected for instrument response. For thermoluminescence measurements, samples were allowed to warm up quite quickly (see Figure 1) in a precooled empty dewar: temperatures were measured with a thermocouple at the center of the sample in a separate experiment. The method has disadvantages: there is a temperature gradient inside the sample which partly blurs out details of the glow curves and the sample thickness is such that significant reabsorption of fluorescence occurs. On the other

(1) W. H. Hamill in "Radical Ions," E. T. Kaiser and L. Kevan, Ed., Interscience, New York, N. Y., 1968.
(2) J. E. Willard, *Mol Cryst. Liquid Cryst.*, **9**, 135 (1969)
(3) F. Kieffer and M. Magat in "Actions Chimiques Biologiques des Radiations," Vol. 14, M. Haissinsky, Ed., Masson et Cie, Paris, 1970, p 135.
(4) B. Brocklehurst, *Radiat. Res. Rev.*, **2**, 149 (1970).
(5) M. Burton and K. Funabashi, *Mol. Cryst. Liquid Cryst.* **9**, 153 (1969).
(6) B. Brocklehurst and J. S. Robinson, *Chem. Phys. Lett.*, **10**, 277 (1971).
(7) W. A. Gibbons, G. Porter, and M. I. Savadatti, *Nature (London)*, **206**, 1355 (1965).
(8) B. Brocklehurst, R. D. Russell, and M. I. Savadatti, *Trans. Faraday Soc.*, **62**, 1129 (1966).
(9) C. Deniau, A. Déroulède, F. Kieffer, and J. Rigaut, *J. Lumin.*, **3**, 325 (1971).
(10) A. C. Albrecht and F. P. Schwarz, Proceedings of the Tenth Czechoslovak Annual Meeting on Radiation Chemistry, Mariánské Lázně, 1970, p 197.
(11) A. Déroulède, F. Kieffer, E. Migirdicyan, and J. Rigaut, *J. Chim. Phys.*, **67**, 1931 (1970).
(12) B. Brocklehurst, J. S. Robinson, and D. N. Tawn, *Chem. Phys. Lett.*, **12**, 610 (1972).
(13) B. Brocklehurst and R. D. Russell, *Trans. Faraday Soc.*, **65**, 2159 (1969).

hand, rapid warm-up of thick samples produces high light intensities so that spectra can be recorded easily at very low doses.

High intensities of ultraviolet light were obtained with a Rayonet photochemical reactor, but most photolysis measurements were made with a Hanovia coiled low-pressure mercury arc: intensities were measured with a ferrioxalate actinometer. Thermoluminescence intensities were much lower than with radiolysis; the intensity soon saturates because of the efficient bleaching out of trapped electrons. Spectra could be recorded on the fluorimeter at high doses: at low doses, a filter-photomultiplier combination was used to obtain greater sensitivity.

Partial bleaching of irradiated samples was carried out by placing the sample in a silica dewar surrounded by a Wratten gelatin filter at the center of a square of four 150-W tungsten lamps.

Results

(i) Toluene. Fluorescence and phosphorescence of toluene are readily identified in the thermoluminescence, after γ radiolysis, together with the fluorescence of the benzyl radical: the identity of the latter has been checked by photographing the spectrum, so resolving the vibrational structure.[12] In the case of naphthalene,[13] at high concentrations the monomer fluorescence early in the glow curves is replaced by excimer fluorescence later on: monomer cations, diffusing some distance, dimerize before neutralization. The toluene fluorescence shows a similar shift to longer wavelengths but the excimer emission could not be clearly separated at the low resolution of the photoelectric measurements: this is due in part to the low-fluorescence efficiency of the excimer and the relatively small shift in wavelength[14] and in part to the distortion of the monomer fluorescence by reabsorption (unusually large here because emission occurs uniformly through a thick sample).

Typical glow curves for low doses of γ rays are shown in Figure 1: measurements were made at 280 (fluorescence), 380 (phosphorescence), and 485 nm (benzyl): note the compressed intensity scale. Measurements were made over the concentration range, 10^{-4}–1 *M*. Between 10^{-3} and 10^{-2} *M*, benzyl emission can just be detected (intensity ~1% of the phosphorescence maximum at 5×10^{-3} *M*) at the very end of the glow curve: this is very difficult to study because of the rapid decay of intensity. It may be that the benzyl glow curve is similar to that in Figure 1b, but it is masked earlier by the strong phosphorescence (the benzyl glow curve is shifted slightly to later times, probably because of the lower mobility of the benzyl anion, see below).

As shown in Figure 1, there is a sudden change in behavior above 10^{-2} *M*. At first sight, benzyl emission appears to replace phosphorescence; however, this effect is coincidental. The behavior of the toluene emissions will be discussed elsewhere: here it suffices to state that the early part of the glow curve is due to cation–electron pairs with small separation, the later part to cation–anion recombination; the phosphorescence to fluorescence ratio falls as the temperature rises because of decreasing phosphorescence efficiency;[15,16] at high concentrations there is an even sharper fall because neutralization of dimer cations gives triplet excimers which undergo rapid quenching.[17] The rise in benzyl intensity is exaggerated by the

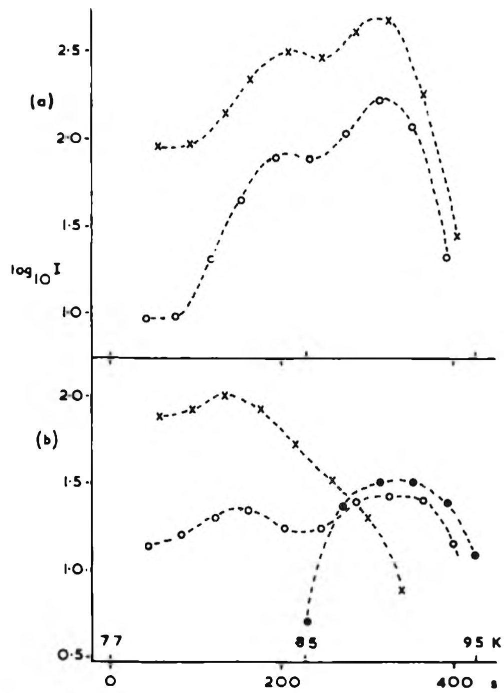

Figure 1. Glow curves: log (thermoluminescence intensity) *vs.* time; temperature calibration inserted. Intensities are not corrected for instrument response, but are comparable between a and b: (O, toluene fluorescence; ×, phosphorescence; ●, benzyl fluorescence; (a) 10^{-2} *M*. (b) 5×10^{-2} *M* toluene in 2:1 mixture of methylcyclohexane and isopentane; dose = 1.5 krads.

reduction in phosphorescence, but there is a steady increase up to 0.1 *M* after which the intensity levels off. Benzyl is not observed in the early part of the glow curve at any concentration.

Both above and below 10^{-2} *M*, the relative intensities of the three emissions are independent of dose from 1.5 krads up to at least 50 krads; benzyl is still increasing with dose at 600 krads while the toluene emissions pass through a maximum around 300 krads. Strong bleaching of the samples after the irradiation eventually removes all the thermoluminescence, but the toluene emissions were removed more quickly than benzyl. With less bleaching (15 sec, tungsten light above 600 nm) benzyl actually increased (× 3) while the others were reduced (× 10) compared with the nonbleached sample. Neither bleaching nor high doses affected the toluene fluorescence to phosphorescence ratios. The addition of sulfur hexafluoride to scavenge electrons had the same effect on the glow curves as in the case of naphthalene;[13] all intensities were reduced, toluene fluorescence most, benzyl least. Studies of isothermal luminescence and infrared stimulated emission showed only toluene emissions: benzyl could not be detected under any of the conditions used.

Fewer studies of photoionization have been made because of the low intensity of thermoluminescence: the intensity quickly levels off with dose because of bleaching. The results given here were obtained with exposures of 5

(14) J. B. Birks, "Photophysics of Aromatic Molecules," Wiley, London, 1970.
(15) N. G. Kilmer and J. D. Spangler, *J. Chem. Phys.*, **54**, 604 (1971).
(16) S. Fischer, *Chem. Phys. Lett.*, **10**, 397 (1971).
(17) R. B. Cundall and W. Tippett, *Trans. Faraday Soc.*, **66**, 350 (1970); R. B. Cundall, L. C. Pereira, and D. A. Robinson, *Chem. Phys. Lett.*, **13**, 257 (1972); R. V. Bensasson, J. T. Richards and J. K. Thomas, *ibid.*, **9**, 13 (1971).

to 60 sec at dose rates up to 1.5×10^{-9} einstein cm^{-1} sec^{-1} of mercury 254-nm radiation (sample 3.5 cm from the lamp). Qualitatively, the effect of concentration on the glow curves is the same as for γ irradiation. Intensities and intensity ratios (benzyl to toluene) were not easily reproducible, varying by a factor of 2 or 3: this may have been due to cracking of the sample and icing of the surface of the tube, affecting the rate of light absorption. However, at 5×10^{-2} *M*, it is clear that the ratio of benzyl and toluene intensities increases steadily with dose even at the shortest exposures and, within the considerable experimental error, may be zero initially. The lamp emits light at longer wavelengths (though in relatively small amounts[18]): when a glass filter was used to cut out 254 nm after a few seconds the benzyl intensity and the benzyl to toluene ratio again increased but more slowly. The addition of SF_6 reduced intensities but did not affect the ratios.

(ii) Other Compounds. Emission in the region 480–580 nm has been observed in the thermoluminescence of the following compounds: *p*-xylene, mesitylene, durene, hexamethylbenzene, indane, and diphenylmethane. Careful spectroscopic studies have not been made but it seems plausible to assign these to the fluorescence of radicals formed by loss of a hydrogen atom from the parent molecule: this has been established in the case of durene.[9,10] Insofar as studies have been made, these compounds behave like toluene, though the efficiency of radical emission is usually lower and is only easily seen late in the glow curves: indane and mesitylene readily give radical emissions at low γ-ray doses like toluene, while quite large doses (300 krads) are needed for *p*-xylene, durene, and hexamethylbenzene. The same differences were observed in photolysis experiments.

Phenylacetylene gives thermoluminescence peaks at about 300 (fluorescence), 430 (phosphorescence), and 480 nm; the latter has been ascribed tentatively to the α-styryl radical[12] formed by addition of a hydrogen atom (addition of a solvent radical is also possible) as in the case of styrene.[11] We have attempted to prepare this radical in other ways without success to date, but the identification remains plausible. The relative intensity of the radical emission increases at doses of a few hundred kilorads but the effect of concentration is much smaller: the amount of radical emission increases with concentration but the radical to molecule ratio changes only by a factor of 1.5 between 10^{-3} and 5×10^{-2} *M*. Again, the radical is not observed early in the glow curve or in infrared stimulated emissions (irse).

Indene gives a strong fluorescence peak at 315 nm, very weak emission around 400 nm (possibly the molecular phosphorescence[19]), and a strong peak at 500 nm. The 315- and 500-nm peaks were scarcely affected by the extensive purification procedures; the latter peak coincides with the long-wavelength emission from indane and is ascribed to the indanyl radical; the photographic method[12] confirms that the two radicals are identical. Indene then, appears to gain a hydrogen atom rather than lose one. Since indenyl is a nonalternant radical, its fluorescence, if any, would lie in a different spectral region from indanyl. The concentration dependence of thermoluminescence is similar to that of phenylacetylene, but indene differs in that the radical emission can be observed early in the glow curves and in irse (though less strongly). Attempts to photoionize indene and phenylacetylene were unsuccessful.

Discussion

Deniau, *et al.*,[9] have observed emission from the duryl radical in the thermoluminescence of durene solutions after γ radiolysis: at doses of 100 krads the radical emission is confined to the second peak of the glow curve which is due to cation–anion recombination (*n.b.*, their "thermal resolution" is better than ours); at doses > 1 Mrad, radical emission is observed in the first peak and in isothermal luminescence, both due to cation–electron recombination. They suppose that ground state radicals are first formed in the radiolysis, and subsequently trap charges; negative charge is trapped efficiently because of the great differences in electron affinity between durene and duryl; at high doses there are sufficient radicals to compete for positive charge as well. In our work at low doses, the radical to molecule luminescence ratio is independent of γ-ray dose between 50 and 1.5 krads; the latter dose gives concentrations of active species of $\sim 10^{-6}$ *M*: so processes involving two radiation-induced steps can be ruled out.

The absence at low doses of radical emission when cations recombine with electrons (irse, isothermal luminescence, early part of the glow curves) shows that benzyl cations are not present and that excited benzyl is not produced by dissociation of excited toluene. (This process has been observed in durene, but the efficiency is only 10^{-3}.[10]) Benzyl cations might be produced by reactions during the diffusion process, but the bleaching studies suggest that benzyl anions are involved.

In the highly viscous liquid produced by softening the glass (viscosity $\sim 10^6$ P), cation–anion neutralization takes place while the two ions are still separate.[13] One can regard the electron as tunnelling through the solvent: the highest energy electron will tunnel fastest leaving the anion in its ground state, the cation becoming excited. However, the two molecules may well be close enough for energy (both singlet and triplet) to be transferred back to the former anion; *i.e.*, toluene cation, benzyl anion recombination can lead exclusively to benzyl excitation. To test this hypothesis, a 10^{-2} *M* toluene solution containing 3×10^{-4} *M* naphthalene was irradiated: irse gave mainly toluene emission showing the predominance of toluene cations, while naphthalene emissions were much stronger in thermoluminescence ($C_7H_8^+ + C_{10}H_8^-$).[20]

The usual mechanism of "bleaching" is to excite electrons from their traps: eventually, this leads to recombination and the loss of thermoluminescence. The enhancement of benzyl emission by continued photolysis might be due to bleaching of toluene anions followed by retrapping on benzyl radicals. However, at the smallest exposures used the concentration of ground state radicals is very small; $\sim 10^{-8}$ *M* can be estimated.[21] It is difficult to believe that the radicals could trap electrons so efficiently; also the effect of SF_6 would be to reduce benzyl emission much more than toluene, but this is not observed. It seems necessary to postulate a different effect of the bleaching light.

$$C_7H_8^- + h\nu \rightarrow C_7H_7^- + H \quad (1)$$

(18) C. A. Parker, "Photoluminescence of Solutions," Elsevier, Amsterdam, 1968, p 162.

(19) M. Koyanagi and Y. Kanda, *Mem. Fac. Sci., Kyushu Univ., Ser. C.*, **6**, 109 (1968).

(20) B. Brocklehurst and J. P. Guerin, unpublished work.

(21) B. Brocklehurst, W. A. Gibbons, F. T. Lang, G. Porter, and M. I. Savadatti, *Trans. Faraday Soc.*, **62**, 1793 (1966).

The electron affinities of toluene[22] and benzyl[23] are not known with certainty but their difference is such that light of wavelength $\lesssim$1000 nm would give an exothermic reaction.

This mechanism does not immediately explain the radiolysis results: possibly a track or spur effect is involved in which excitation produced locally by the same γ ray is transferred between toluenes until it reaches a toluene anion. Such transfer would be efficient at the high toluene concentration. (Transfer of excitation to benzyl after recombination would give benzyl emission during irse, etc.) The reason for the need for high toluene concentration in the photolysis experiments is not clear. Perhaps electron loss is more efficient than reaction 1, so that efficient retrapping is necessary.

At the low temperatures and high concentrations used, considerable aggregation of the toluene molecules to form crystals or local concentrations may occur; Lipsky and Burton[24] suggested the existence of "domains" to explain the energy transfer properties of benzene–cyclohexane mixtures at room temperature. However, triplet states are very short lived in crystals and even in dimers;[17] photoionization, at any rate, must involve isolated molecules.

The preceding discussion applies mainly to the low-dose work. At doses > 1 Mrad, the result of Deniau, *et al.*,[9] show that radicals are acting as traps for positive charge. While negative charge will be more readily scavenged than positive, the increase in benzyl to toluene ratio above 100 krads can also be explained if benzyl anions are less readily bleached than toluene anions during continued γ irradiation. Either hypothesis will also explain the appearance of radicals from hexamethylbenzene, durene, and *p*-xylene in this region of dose, and the relative increase in other cases such as phenylacetylene. The differences between the methylbenzenes are a little surprising: measurements over a wider range of conditions will be needed to elucidate this.

The mechanism of radical excitation (at low doses) when the molecule has gained a hydrogen atom appears to be different from the hydrogen loss case, because of the different concentration dependence. Some, at least, of the indanyl radicals may have positive ions as precursors since the radical emission is observed weakly in irse; on the other hand, phenylacetylene apparently gives α-styryl anions only. Further measurements are again required before the mechanisms can be discussed further.

Conclusion

At high doses, both neutralization of carbonium ions by electrons or molecular anions, and of solute cations by carbanions can produce excited radicals; at low doses the latter process alone occurs (except, probably, in the case of indene). At high doses, radicals are formed and then act as traps for positive and negative charge: at low doses the carbanions must be formed in other ways: in the case of toluene this probably involves the loss of a hydrogen atom from an excited toluene anion.

Acknowledgment. The authors thank the Science Research Council (U. K.) for the award of maintenance grants to two of them (J. S. R. and D. N. T.).

(22) R. N. Compton, L. G. Christophorou, and R. H. Huebner, *Phys. Lett.*, **23**, 656 (1966).
(23) D. K. Bohme and L. B. Young, *Can. J. Chem.*, **49**, 2918 (1971).
(24) S. Lipsky and M. Burton, *J. Chem. Phys.*, **31**, 1221 (1959).

Stabilized Cluster. A Molecular Model for the Solvated Electron

G. Howat and B. C. Webster*

Department of Chemistry, The University of Glasgow, Glasgow, Scotland *(Received April 4, 1972)*

A model is proposed for solvated species generated radiolytically. A cluster of molecules, transiently stabilized, dresses the electron and sustains it until solvation is completed. Calculations are presented within the INDO molecular orbital approximation. The formation and stability of some dimer and tetramer clusters, comprised of water and ammonia molecules, are examined. Spectral properties are determined together with esr line widths. Dilation phenomena are interpreted.

Introduction

Solvation of electrons in polar liquids is now a well-established phenomenon. Elegant observations upon the properties of such species become ever more abundant.[1] Yet there is no single theory in terms of which the observations may be rationalized and fresh phenomena predicted.

No lack of attempts to construct such a theory is evident. Ever since Pekar quantified the polaron model of Landau, within the adiabatic and the self-consistent field approximation, and Ogg suggested the surplus electrons are self trapped in physical cavities inherent or created in the medium, theoretical formulations have accumulated.[2] Among the most recent the semicontinuum models have proved the most successful for correlating spectral properties. The theory has been developed by Copeland, Kestner, and Jortner within the adiabatic approximation and applied predominantly to the ammoniated electron.[3] Fueki, Feng, and Kevan working within the self-consistent field formulation have treated the hydrated electron.[4]

Such semicontinuum approaches differ from the earlier continuum theories in that some recognition is taken of the molecular character of the solvent. In the studies mentioned, a single solvation sheath comprising of four, six, eight, or twelve molecules is interposed between the electron and the remainder of the liquid, which is regarded as an isotropic continuous dielectric. A shell of four molecules is judged to be the most favorable for both the hydrated and ammoniated electron, although in the latter case the distinction between four and a larger number of molecules is a marginal one.

The viewpoint to be propagated in this investigation is that the behavior of electrons solvated in a polar medium is a reflection of the interaction of the surplus electron with a surrounding cluster of solvent molecules. This dresses the electron and sustains it in a solvated state. The number of molecules in each cluster may vary as also may their initial orientations. Through this facility the surplus electrons may occupy states of differing energies in the liquid.

Electron trapping by the transient stabilization of a cluster is envisaged. At such times when local molecular orientation may ensue, solvation in the proper sense of the term takes place. It is recognized that a range of relaxation times may exist dependent upon the mode of relaxation.[5]

In developing this hypothesis the techniques of molecular orbital theory are adopted. The hierachy of approximate molecular orbital methods extends from the *ab initio* calculation through INDO, MINDO, CNDO/2, CNDO, and extended Hückel to simple Hückel theory. The acronyms indicate the type of integral approximation involved in the method. INDO represents intermediate neglect of differential overlap. The formulation of such methods is described well in the text of Pople and Beveridge[6] and does not require repetition here. Where the magnitude of a problem precludes the performance of an *ab initio* calculation, perhaps the INDO method is preferred, especially if radicals are involved. In part, it is a matter of taste.

Traces of the molecular orbital viewpoint in the study of solvated electrons are discerned in the work of Kaplan and Kittel, Paoloni, and Raff and Pohl among others.[7] Extended Hückel calculations have been made by McAloon and Webster upon some dimer models for the hydrated and ammoniated electron.[8] These are deficient in that the total energy is not open to direct evaluation. It is therefore not possible to obtain the equilibrium geometries of the species studied or to ascertain whether such entities are energetically stable with respect to their component molecules. Further, the application of extended Hückel theory to charged systems is not admissible. Within the INDO method the total energy may be examined and properties of the systems computed in a more realistic fashion.

Dimer Models

(a) Formation and Stability. Our study begins with a consideration of the behavior of clusters comprised of only

(1) U. Schindewolf, *Angew. Chem., Int. Ed. Engl.*, **7**, 190 (1968); E. J. Hart and M. Anbar, "The Hydrated Electron," Wiley New York, N. Y., 1970; G. Scholes, *Annu. Rep. Chem. Soc.*, **67A**, 169 (1970); M. J. Bronskill, R. K. Wolff, and J. W. Hunt, *J. Chem. Phys.*, **53**, 4201, 4211 (1970); **55**, 530 (1971).
(2) S. Pekar, *J. Phys. (USSR)*, **X**, 341, 347 (1946); R. A. Ogg, Jr., *Phys. Rev.*, **69**, 668 (1946).
(3) D. A. Copeland, N. R. Kestner, and J. Jortner, *J. Chem. Phys.*, **53**, 1189 (1970).
(4) K. Fueki, D. F. Feng, L. Kevan, and R. E. Christoffersen, *J. Phys. Chem.*, **75**, 2297 (1971).
(5) J. Crossley, *Advan. Mol. Relaxation Processes*, **2**, 69 (1970); M. Davies, *Annu. Rep. Chem. Soc.*, **67A**, 65 (1970).
(6) J. A. Pople and D. L. Beveridge, "Approximate Molecular Orbital Theory," McGraw-Hill, New York, N. Y., 1970.
(7) J. Kaplan and C. Kittel, *J. Chem. Phys.*, **21**, 1429 (1953); L. Paoloni, *Proc. Colloq. Weyl. I*, 293 (1964); L. Raff and H. A. Pohl, *Advan. Chem Ser.*, **No. 50**, 173 (1965).
(8) B. J. McAloon and B. C. Webster, *Theor. Chim. Acta*, **15**, 385 (1969).

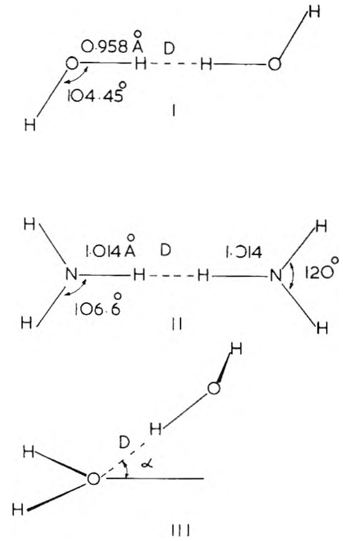

Figure 1. Three dimer models for solvated species. Pyramidal and planar geometries are noted for II. In structure III one molecule is orientated by α° with respect to the second which lies in the plane. For each case the intermolecular separation is D(Å).

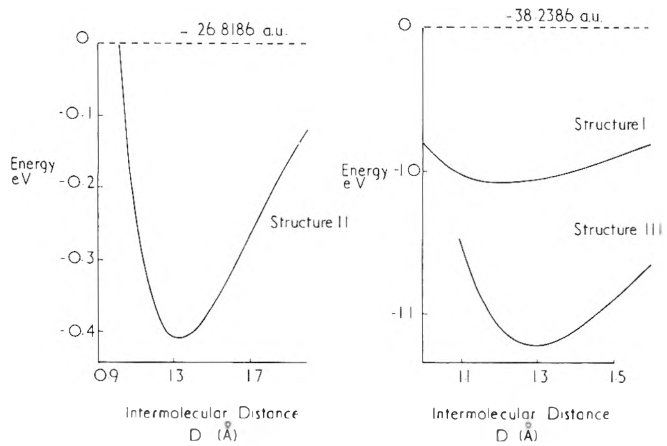

Figure 2. Variation in the total energy E with intermolecular separation D for the planar dimer structures. Reference state is equal to $E(H_2O + H_2O^-)$ and $E(NH_3 + NH_3^-)$, respectively.

TABLE I: Variation of the Total Energy E (au) with Intermolecular Separation D (Å) for the Planar Dimer Structures

Model					
I		II		III	
D	E	D	E	D	E
1.0	−38.2683	1.0	−26.8179	1.1	−38.2942
1.1	−38.2764	1.1	−26.8275	1.2	−38.3158
1.2	−38.2787	1.2	−26.8321	1.25	−38.3198
1.3	−38.2781	1.3	−26.8337	1.3	−38.3207
1.4	−38.2757	1.4	−26.8334	1.35	−38.3195
1.5	−38.2723	1.5	−26.8321	1.4	−38.3170
1.6	−38.2687	1.6	−26.8304	1.6	−38.2991

two molecules. Three dimer models are shown in Figure 1. Structures I and II are planar models for the hydrated and ammoniated electron, respectively. Differences in intramolecular dimensions on passing from the vapor state to the liquid are taken to be small, and geometries pertinent to the vapor are given. With the intramolecular geometries held constant, the energy is determined as a function of the intermolecular separation D. In the case of ice-like fragment III the intermolecular angle has been varied in the range 0–90°. Some results are given in Tables I and II.

The INDO calculations are performed in a conventional manner using a Slater basis set comprising of H(1s), O(2s, $2p_x$, $2p_y$, $2p_z$), and N(2s, $2p_x$, $2p_y$, $2p_z$) with orbital exponents of 1.2 for hydrogen, 2.275 for oxygen, and 1.95 for nitrogen, respectively. One-electron integrals have been evaluated rather than assigned empirical estimates. Clearly the calculations lie in the semiempirical mould. Although their inherent deficiences are recognized it is the hope that they are sufficiently meaningful as to allow some illumination of the problem to be perceived.

In Figure 2 the variation of the total energy with intermolecular separation shows that for each of the three dimers an equilibrum configuration persists. For planar water dimer I the equilibrium separation is 1.20 Å, for planar ammonia dimer II this distance is 1.33 Å. When $\alpha = 0°$ dimer III has a minimum energy at an intermolecular separation of 1.30 Å. Change of the intermolecular angle toward 90° results in a raising of the energy from −38.3207 ($\alpha = 0°$) to −38.3085 au ($\alpha = 90°$) with the equilibrium intermolecular distance slightly increasing to 1.35 Å ($\alpha = 90°$).

Also depicted in Figure 2 are the reference states for the dimer species. For stability a simple criterion is to require that the energy of the dimer dressing the electron $E(D^-)$ be lower than that of a system comprising of the component molecules and a surplus electron. This might be specified as $H_2O + H_2O^-$ for the hydrated electron, where the surplus electron is formally attached to one of the water molecules. For stability

$$SD = E(D^-) - E(H_2O^- + H_2O) < 0$$

Employing the total energies listed in Table III all three dimers are stable with respect to their components. Of the water dimers ice-like structure III is favored by 1.14 eV over structure I and this preference is maintained for all intermolecular angles.

The energy denoted by SD might for illustrative purposes be partitioned into three components. These are the energy involved in bringing the separated molecules together to form a cluster with the equilibrium geometry of the charged system, the electron affinity of the cluster, and the electron affinity of a single molecule. Accordingly

$$SD = E(D - 2H_2O) + A(D) - A(H_2O) < 0$$

where A(D), the dimer electron affinity, is defined by $E(D^-) - E(D)$ and $A(H_2O)$ is the electron affinity of a water molecule. Should the energy change involved in the cluster formation be very small then the dominant factor deciding the formation of the species will be the difference in affinity of the cluster for an electron as opposed to a single molecule.

Use of the criterion in the partitioned form requires the computation of a further item, the energy of the uncharged cluster E(D) at the equilibrium geometry of the charged system. This is −38.4953 au for dimer I and −27.0520 au for the ammonia dimer II, respectively.

In order to bring two water molecules into the geometry required of the charged dimer will involve accordingly an expenditure of +0.23 eV in energy. The electron affinity of

TABLE II: Variation of the Total Energy E (au) for the Wurtzite Dimer Fragment with Intermolecular Separation D(Å) and Orientation $\alpha°$

α	D 1.20	1.25	1.30	1.35	1.40
0	−38.3158	−38.3198	−38.3207	−38.3195	−38.3170
30	−38.3147	−38.3189	−38.3200	−38.3189	−38.3162
45	−38.3130	−38.3175	−38.3189	−38.3179	−38.3154
60	−38.3101	−38.3151	−38.3168	−38.3162	−38.3140
75	−38.3051	−38.3107	−38.3131	−38.3132	−38.3115
90	−38.2974		−38.3074	−38.3085	−38.3074

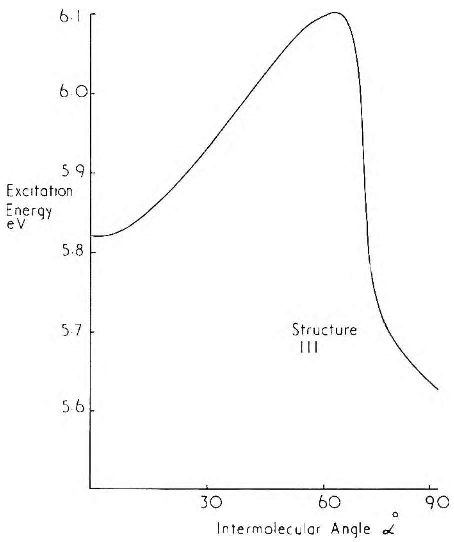

Figure 3. Variation in the excitation energy ΔE with intermolecular angle α for the dimer structure III.

the dimer so formed is 5.89 eV. The electron affinity of a water molecule is 7.21 eV. Structure I is thereby favored by 1.09 eV. This division of the energy is of course totally artificial and should not be regarded as representing a sequential process taking place during the solvation of an electron.

(b) Excitation Energies. If the excitation process of the surplus electron from the ground state to the first excited state is considered to take place without change in the nuclear coordinates and without significant alteration of the ground-state orbitals, then the excitation energy may be evaluated to an approximation from the virtual orbitals of the ground state. Proceeding in this manner the first excitation energy for the planar water dimer is calculated as 1.98 eV, and for the planar ammonia dimer as 1.10 eV. At standard temperature and pressure the absorption spectra attributed to these species have maxima which lie at 1.72 and 0.80 eV, respectively.

Table IV shows the variation in the excitation energy for intermolecular distances in the neighborhood of the equilibrium position. It may be seen that as the intermolecular separation is decreased the excitation energy increases. For structure I a change of 0.2 Å from the equilibrium position of 1.20 to 1.00 Å is accompanied by a rise in the excitation energy of 0.34 eV, the spectral shift being to the blue. Experimentally the maximum in the spectrum at 29 ± 3° changes from 1.71 eV by 0.06 eV/kbar until a pressure of 4.88 kbar is reached after which it remains nearly constant as the pressure is raised. At 6.62 kbar the spectrum has shifted by 0.29 eV to the blue.[9]

TABLE III: Total Energies of the Clusters and Their Component Molecules (au)

H_2O	−19.2519	I	−38.2787
H_2O^-	−18.9867	II	−26.8337
NH_3	−13.5299	III	−38.3207
NH_3^-	−13.2756	IV	−76.8242
NH_3 (planar)	−13.5261	V	−76.8024
NH_3^- (planar)	−13.2925	VI	−53.8888

TABLE IV: Variation in the Excitation Energy ΔE (eV) with Intermolecular Separation for the Planar Dimer Structures

I		II		III	
D, Å	ΔE, eV	D, Å	ΔE, eV	D, Å	ΔE, eV
1.0	2.32	1.0	1.53	1.1	7.20
1.1	2.16	1.1	1.38	1.2	6.50
1.2	1.98	1.2	1.23	1.25	6.18
1.3	1.80	1.3	1.10	1.3	5.82
1.4	1.63	1.4	0.98	1.35	5.47
1.5	1.46	1.5	0.87	1.4	5.13
1.6	1.30	1.6	0.77	1.6	3.92

For dimer structure III the variation in the excitation energy with intermolecular angle is shown in Figure 3, while the appropriate results are listed in Table V. Over all angles the excitation energy calculated is rather high being ~6 eV.

An interesting feature of Figure 3 is the manner in which the excitation energy exhibits a maximum at medi-

TABLE V: Variation in the Excitation Energy ΔE (eV) with Orientation α in the Neighborhood of the Equilibrium Conformations for Dimer Structure III

α	$\bar{R}$ 1.30	1.35	1.40
0	5.82	5.47	5.13
30	5.93	5.58	5.23
45	6.03	5.67	5.32
60	6.10	5.73	5.38
75	6.09	5.72	5.37
90	5.99	5.63	5.29

(9) R. R. Hentz, Farhataziz, and E. M. Hansen, *J. Chem. Phys.*, **55**, 4974 (1971).

an angles 45–70°, a range which encompasses the Wurtzite angle of 54.73°. In view of the high excitation energies it would be imprudent at present to emphasize this behavior. Yet should it be substantiated, then a simple rationalization becomes open for the spectral shifts observed when the bands are bleached with light of particular wavelengths, as has been mentioned elsewhere.[10]

On raising the temperature, increase in the vibrational motion of the molecules is anticipated together with a loosening of the molecular structure. Both effects will tend to lower the excitation energy. Qualitatively a red shift in the spectrum is indicated, as is observed.[11]

(c) Charge Distributions. In Figure 4 the charge distributions in the ground and first excited states are shown for the three dimer models. In contrast to the previous extended Hückel distributions,[8] the surplus electron in the ground state is delocalized over the two molecules for both the planar water and ammonia dimers, structures I and II. On excitation there is a slight transfer of charge to the peripheral hydrogen atoms.

Dimer structure III exhibits quite a different pattern. In the ground state the electron is localized almost entirely upon one molecule and on excitation is transferred to the second molecule. It is perhaps not so surprising therefore that for this case the computed excitation energy is so disparate from that observed, since considerable orbital reorganization is anticipated.

On deexcitation the charge may well transfer to a molecule other than that upon which it was originally sited, thereby providing a mechanism for photoconduction. Although such a photocurrent has not as yet been detected in radiolyzed water, photocurrents have been observed in γ irradiated alkaline ice.[12]

Tetramer Models

(a) Formation and Stability. One of the most popular descriptions for the structure of the hydrated electron is the tetrahedral defect model proposed by Natori and Watanabe.[13] In this the surplus electron is located at a defect formed by the absence, or removal, of a water molecule situated at the center of a tetrahedral array. The structure is shown in Figure 5, labeled IV, where it is seen that reorientation ot the water molecules is envisaged in such a manner that four hydrogen atoms, disposed in a tetrahedral manner, circumscribe the defect site. Recently a molecular orbital calculation performed within the CNDO/2 approximation upon this tetramer indicated that the structure is energetically unfavorable.[14] This conclusion is not corroborated within the INDO approximation.

With the intramolecular dimensions constrained as in the dimer studies, the variation in the energy of tetramer IV as a function of intermolecular separation is displayed in Figure 6. An equilibrium conformation is defined when the hydrogen atoms are 0.96 Å distant from the center of the tetrahedron. The total energy $E(T^-)$ of the defect tetramer dressing the electron at this distance is −76.824 au. For stability of the tetramer with respect to its components

$$E(T^-) - E(3H_2O + H_2O^-) < 0$$

Employing the values of the energies listed previously for H_2O and H_2O^- the tetramer is found to be stable by −2.224 eV. Again this energy term could be partitioned as

$$E(T - 4H_2O) + A(T) - A(H_2O)$$

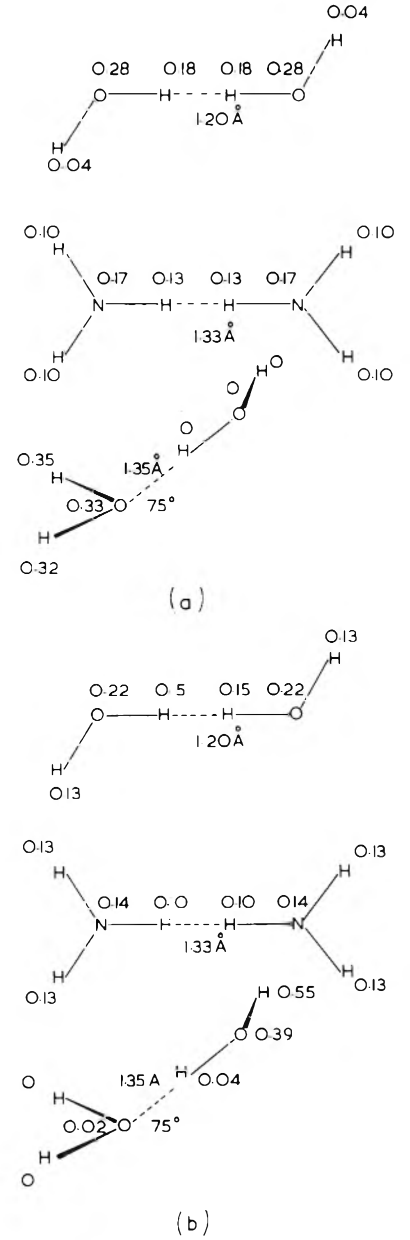

Figure 4. Charge density of the surplus electron for the dimer structures at the equilibrium separations, (a) ground state distribution and (b) excited state distribution.

It is this form which is adopted by Weissman and Cohen.[14] The first term expresses the energy involved in bringing four molecules into the tetrahedral array required of the defect structure. Since the energy term $E(T)$ is computed as −77.008 au, there is an energy gain of −0.006 eV in the creation of the tetramer. The difference in electron affinity of this structure for an electron, and of a water molecule, leads to a further energy gain of −2.218 eV.

Structure V for the hydrated electron arises when four molecules sited at the vertices of a tetrahedron are orien-

(10) B. C. Webster and G. Howat, *Radiat. Res. Rev.*, in press.
(11) B. D. Michael, E. J. Hart, and K. H. Schmidt, *J. Phys. Chem.*, **75**, 2798 (1971); R. K. Quinn and J. J. Lagowski, *ibid.*, **73**, 2326 (1969).
(12) I. Eisele, R. Lapple, and L. Kevan, *J. Amer. Chem. Soc.*, **91**, 6504 (1969); I. Eisele and L. Kevan, *J. Chem. Phys.*, **53**, 1867 (1970).
(13) M. Natori and T. Watanabe, *J. Phys. Soc. Jap.*, **21**, 1573 (1966).
(14) M. Weissman and N. V. Cohen, *Chem. Phys. Lett.*, **7**, 445 (1970).

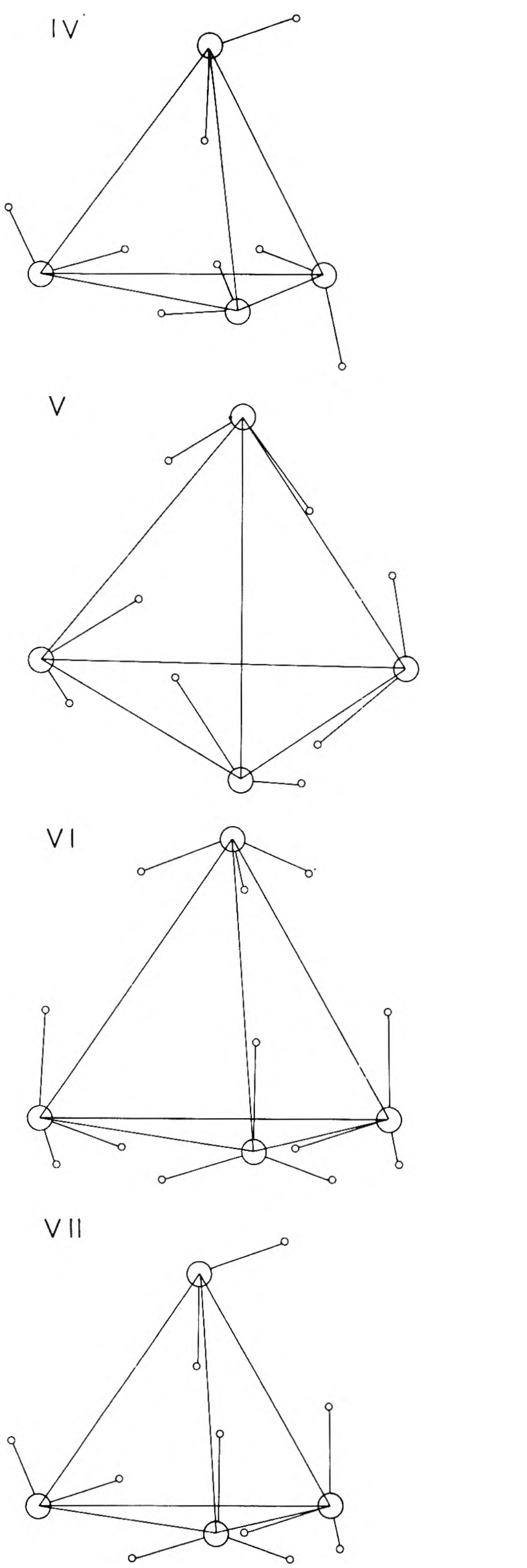

Figure 5. Four tetramer models for solvated species in water and ammonia. Structures IV and V pertain to the hydrated electron, structure VI to the ammoniated electron, and structure VII for a mixed H_2O-NH_3 system at mole fraction 0.5.

tated in such a manner that eight hydrogen atoms are inclined toward the center. Structure VI for the ammoniated electron is identical with structure V except that twelve hydrogen atoms are arrayed about the center.

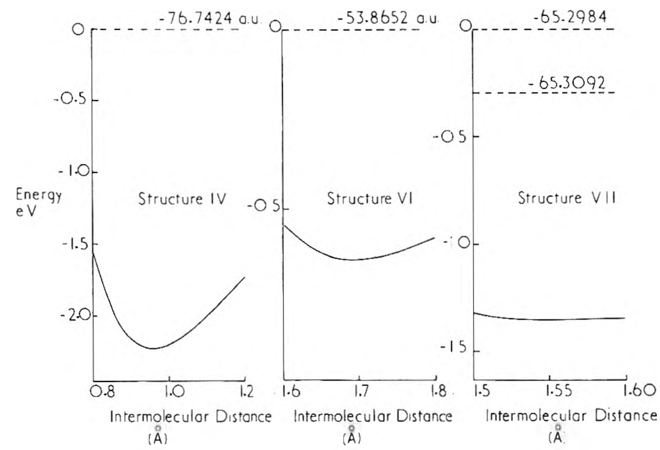

Figure 6. Variation in the total energy E with intermolecular separation for the tetramer structures. Reference states are $E(3H_2O + H_2O^-)$, $E(3NH_3 + NH_3^-)$, $E(2H_2O + NH_3 + NH_3^-)$, or $E(2NH_3 + H_2O + H_2O^-)$, respectively.

Structure VII is representative of those employed in the study of the mixed solvent system H_2O-NH_3. Apposite to a mixture of mole fraction 0.5, it is formed from two water molecules disposed as in structure IV and two ammonia molecules orientated as in structure VI. Similarly the structures used at mole fractions 0.25 and 0.75 are comprised from elements of structures IV and VI.

The behavior of the total energy when the intermolecular distance is varied may be seen in Figure 6 for each of the models. The pertinent data are presented in Table VI. It is apparent that an equilibrium configuration is formed in each case. For the water tetramer V this is attained when the distance from the tetrahedron center to the plane containing the hydrogen atoms is 1.09 Å. For the ammonia tetramer the distance from the center, to the plane containing the hydrogen atoms, is 1.70 Å, while for the mixed tetramer this distance is 1.56 Å at the equilibrium configurations.

Each equilibrium configuration is found to be stable with respect to the components in the sense of the criterion which already has been elaborated. The ammonia tetramer is stable by −0.64 eV. Of the two water tetramers the defect structure is the most favored as structure V has a stability of −1.63 eV. For the mixed dimer there is a dichotomy. The surplus electron may in the isolated state be formally associated with an ammonia or a water mole-

TABLE VI: Variation of the Total Energy E (au) with Intermolecular Separation R(Å) for the Tetramer Structures[a]

Model					
IV		VI		VII	
R	E	R	E	R	E
1.20	−76.8057	1.60	−53.8852	1.50	−65.3467
1.15	−76.8109	1.65	−53.8882	1.55	−65.3479
1.10	−76.8159	1.66	−53.8884	1.56	−65.3480
1.05	−76.8202	1.68	−53.8887	1.57	−65.3479
1.00	−76.8232	1.69	−53.8887	1.58	−65.3478
0.95	−76.8241	1.70	−53.8888	1.60	−65.3475
0.90	−76.8217	1.71	−53.8887		
0.85	−76.8141	1.75	−53.8881		
0.80	−76.7989	1.80	−53.8866		

[a] For structure IV R is the distance from the center of the tetrahedron to an internal hydrogen atom. For the other structures it is the distance to the plane containing the hydrogen atoms.

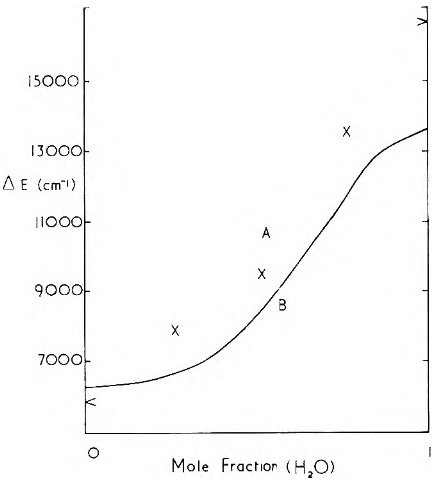

Figure 7. Variation of the excitation energy with mole fraction for the surplus electron in a H_2O-NH_3 mixture: points A computed, curve B experimental.

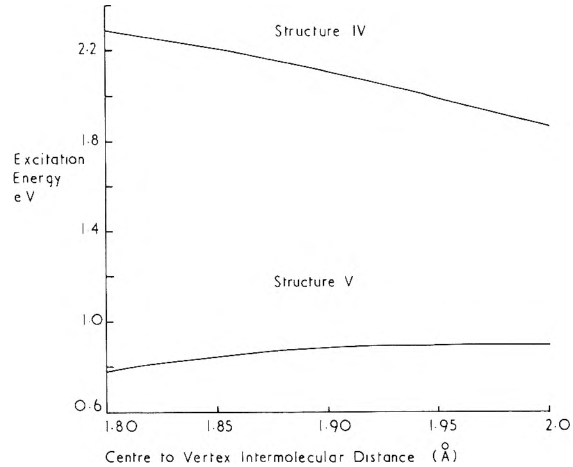

Figure 8. Variation of the excitation energy with intermolecular distance for two water tetramers. The distance is taken from the center of the tetrahedron to the oxygen atoms at the vertex.

cule. In the former case the tetramer is stable by -1.35 eV, in the latter by -1.05 eV.

(b) Excitation Energies. Within the level of approximation adopted the first excited state for the tetramer species is doubly degenerate. In the case of defect tetramer IV the transition energy as computed from the ground-state orbitals is 2.08 eV while for the ammonia tetramer a value of 0.72 eV is obtained. For the mixed tetramers H_2O-NH_3 the transition energies move smoothly between those found for the separate components. The theoretical variation of the excitation energy with mole fraction compares favorably with the behavior observed on the radiolysis of H_2O-NH_3 mixtures, as is seen in Figure 7. The experimental data are those of Dye, DeBacker, and Dorfman.[15]

Although the defect tetramer is found energetically favored over the other water tetramer examined, it might be envisaged that on increasing the temperature, the tetramer would deviate from IV and tend toward one with a fresh orientation of water molecules. Structure V is an extreme type of such reorientation. The transition energy for structure V is 0.86 eV at the equilibrium configuration. Accordingly under a temperature increase, such restructuring of the medium is accompanied by a red shift in the absorption spectrum.

The effect upon the excitation energy of compression in the case of the two water tetramers is illustrated in Figure 8, where the excitation energy is plotted against the distance from the center of the tetrahedron to the oxygen atom at the vertex. This distance is $R + 0.958$ Å (for structure IV) where R is the distance from the tetrahedral center to the internal hydrogen atoms. For structure IV the spectral shift under pressure is to the blue and would appear to become less marked at higher pressures. In contrast, the behavior of structure V suggests that under certain conditions of temperature and pressure, a reversal in the direction of the shift might take place. There seems to be no indication of such an effect in the spectrum of the hydrated electron observed by Michael, Hart, and Schmidt over a temperature range from -4 to 390°. Such a reversal has been recorded for dilute $K-NH_3$ and $KI-NH_3$ solutions at temperature in excess of 120°.[16]

(c) Charge Densities and Esr Spectra. For each of the tetramer models the charge density of the surplus electron in the ground state is displayed in Figure 9. Among the hydrogen atoms there is a preponderance of charge upon those atoms which lie closest to the center of the tetrahedron. However there is no strong localization at the center of the structure, the major portion of the charge is located upon the heteroatoms at the vertices.

The line width of an esr spectrum may be linked with the charge density ρ_i at nucleus i by the relation[17]

$$(\Delta H)^2 = \frac{64\pi^2}{27}\sum_i \mu_i^2 \; \frac{(I_i + 1)}{I_i}\rho_i^2 \quad \text{G}$$

When the hyperfine interactions fluctuate at a rate τ_c^{-1}, the line width is decreased as[18]

$$\delta H = \gamma(\Delta H)^2\tau_c$$

where γ is the magnetogyric ratio.

In determining the theoretical line widths the choice of the fluctuation rate is quite critical. Recognizing that such modulation rates proceed faster than molecular processes which are viscosity controlled,[19] upper limits to this quantity have been utilized. For water a dielectric relaxation time of 13.6 psec[20] at 278°K has been used while for ammonia 4.8 psec is taken.[21] The analysis of Hill suggests that in the latter case a value of 0.96 psec might be more appropriate.[22]

Some line widths are collected in Table VII. In consideration of the approximations which are involved agreement to an order of magnitude is anticipated. That the results are in better accord is regarded as fortuitous.

Volume Measurements

From the variation of the equilibrium constant with pressure for the reaction

$$\tfrac{1}{2}H_2 + NH_2^- = NH_3 + e^-$$

(15) J. L. Dye, M. G. DeBacker, and L. M. Dorfman, *J. Chem. Phys.*, **52,** 6251 (1970).
(16) R. Vogelsgesang and U. Schindewolf, *Ber. Bunsenges. Phys. Chem.*, **75,** 651 (1971).
(17) A. F. Kip, C. Kittel, R. A. Levy, and A. M. Portis, *Phys. Rev.*, **91,** 1066 (1953).
(18) N. Bloembergen, E. M. Purcell, and R. V. Pound, *Phys. Rev.*, **73,** 679 (1948).
(19) R. Catterall, *Proc. Colloq. Weyl, II,* 105 (1970); R. Catterall, L. P. Stodulski, and M. C. R. Symons, *ibid.*, 151 (1970).
(20) E. H. Grant, *J. Chem. Phys.*, **26,** 1575 (1957).
(21) V. L. Pollak, *J. Chem. Phys.*, **34,** 804 (1961).
(22) N. E. Hill, *Proc. Phys. Soc., London, Sect. B,* **67,** 149 (1954).

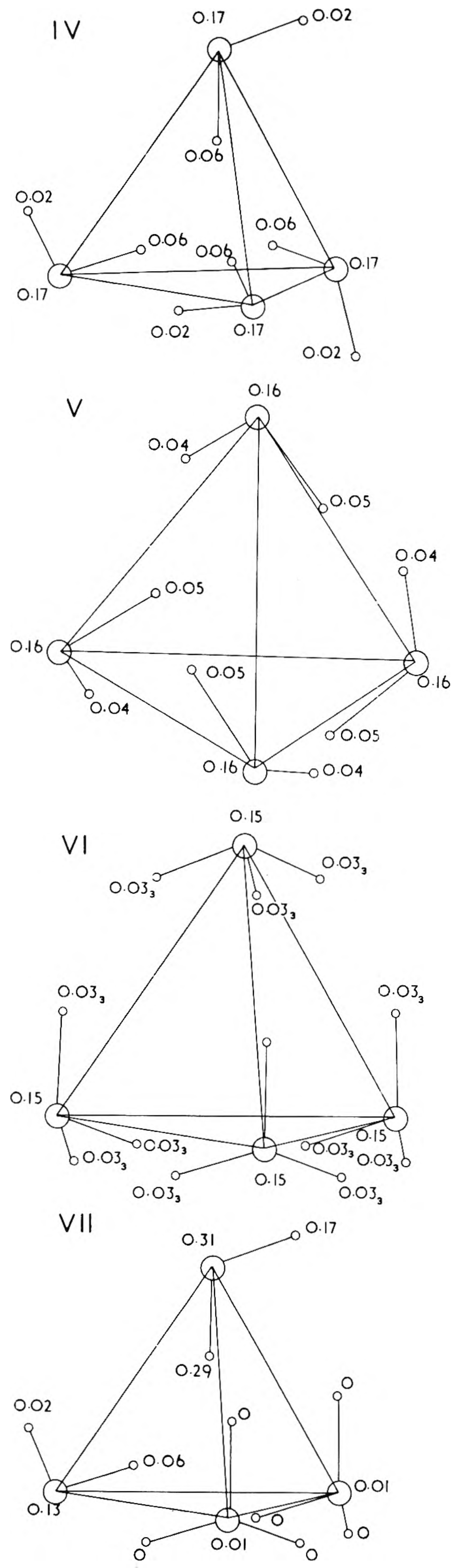

Figure 9. Charge density of the surplus electron in the ground state for the tetramer structures at their equilibrium separations.

the volume associated with the surplus electron in ammonia is assessed to be 84 ± 15 ml/mol at 240°.[23] In water the volume required by the electron would appear smaller.

TABLE VII: Comparison of the Theoretical and Observed Line Widths for the Esr Spectrum of the Solvated Electron

	Tetramer structure	T, °C	Relaxation time τ_c, psec	δH_{calcd}, ~G	δH_{obsd}, ~G
H_2O	IV	5	13.6	0.25	<0.5[a]
D_2O	IV	5	13.6	0.02	
NH_3	VI	20	4.8, 0.96	0.22, 0.045	~0.025[b]
ND_3	VI	20	4.8, 0.96	0.15, 0.031	

[a] E. C. Avery, J. R. Remko, and B. Smaller, *J. Chem. Phys.*, **49**, 951 (1968). [b] C. A. Hutchison and R. C. Pastor, *ibid.*, **21**, 1959 (1953).

Values of <20 ml/mol[23] and 1-6 ml/mol[24] have been suggested.

Such volume expansions have been cited as evidence to support the viewpoint that the surplus electron in the liquid is located in a cavity. Effective radii of spherical cavities have been adduced, while the cavity model is implanted in many discussions on the behavior of solvated species.

Yet the invocation of cavities is not necessary for the interpretation of the volume measurements. The measurements might be conceived better as being indicative of a type of lattice expansion. They are seen thereby as part of a general phenomenon, observed also in the irradiation of alkali halides or when potassium graphite is prepared.

Consider four water molecules located in a cell in the liquid. Such a cell is shown in Figure 10. The volume of the cell is 119.56 Å^3. In the presence of the electron the four molecules might adopt a tetrahedral array such as tetramer model IV already studied. To accommodate the electron an expansion of the cell occurs, and for the tetramer distance of 0.96 Å the expanded cell has a volume of 320.01 Å^3. The volume expansion is accordingly 30.19 ml/mol. Similarly for planar dimer I a cell with two molecules could be envisaged. Expansion of the cell unidirectionally along the line of the inner hydrogen atoms will result in a dilation of 11 ml/mol.

There is no cavity created in the conventional sense. The structure expands to accommodate the electron. About each electron there may be a domain within which other particles are excluded, rather like the Fermi hole about an electron in an atom. Yet there is no physical cavity involved. To interpret the tetramer result in terms of the cavity model and say the electron resides in a cavity of effective radius ~2.1 Å might seem more orthodox but is it a meaningful statement?

Should the tetramer ammonia structure VI be treated in terms of a lattice expansion, the dilation is 81 ml/mol. The density of ammonia at 240°K is taken as 0.6814 g/cc.

Concluding Discussion

It has been proposed that the behavior of surplus electrons in water and in ammonia is the concomitant effect of local microscopic interactions. The electron and a cluster of molecules are transiently stabilized. No initial molecular reorientation is involved. The surplus electron is held within a molecular cluster and its properties are determined by the number of molecules and the particular orientation of the molecules within the cluster.

At such times when molecular rotation may be effected, the cluster may attain to a more energetically favored

(23) U. Schindewolf, R. Vogelsgesang, and K. W. Boddeker, *Angew. Chem., Int. Ed. Engl.*, **6**, 1076 (1967).
(24) R. R. Hentz and D. W. Brazier, *J. Chem. Phys.*, **54**, 2777 (1971).

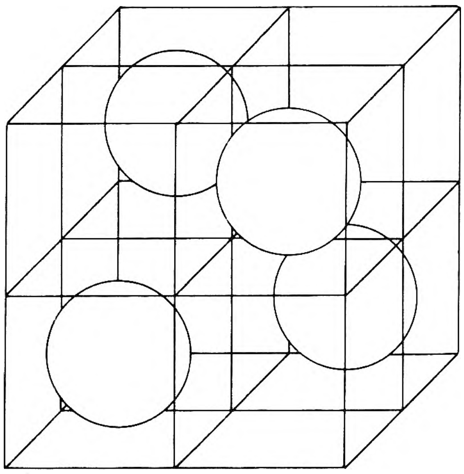

Figure 10. A cellular lattice model with the water molecules in a tetrahedral array.

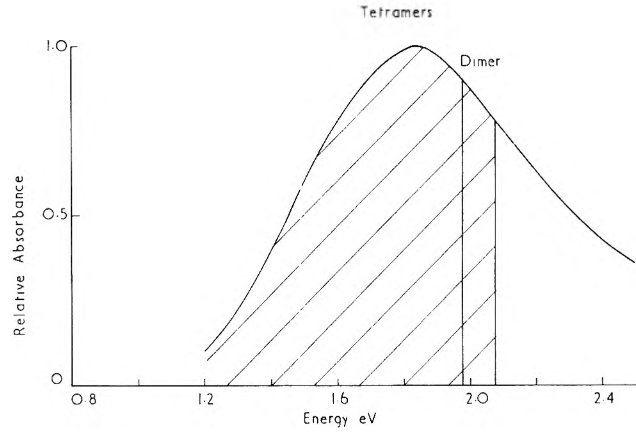

Figure 11. Possible contribution of dimer and tetramer structures to the absorption spectrum of the hydrated electron.

configuration. Accordingly the absorption spectrum observed at times prior to the onset of rotation should lie to the longer wavelength side of the spectrum recorded at times $\gtrsim 10^{-12}$ sec. This type of blue shift in the spectrum with the passage of time has been observed recently in the radiolysis of alcohol glasses.[25]

The concept of the stabilized cluster has been examined with the aid of an approximate molecular orbital method. Dimer and tetramer structures, taken as representing the stabilized cluster in which molecular reorientation has occurred, appear on the basis of such calculations capable of formation.

Computation of the excitation energies allows one to place upon the absorption spectrum for the solvated electron, the species which may be involved in the absorption process. Figure 11 shows the hydrated electron spectrum and the possible role of dimer and tetramer clusters. The central portion of the band appears to stem from the interaction of the surplus electron with two or four hydrogen atoms as nearest neighbors to the site where the electron is trapped and subsequently solvated.

Variations of the spectrum under temperature and pressure are obtained in accord with observation while consideration of the charge density on excitation allows some speculation as to a mechanism of photoconductivity. Evaluation of the line widths of the esr spectrum yields values in agreement to an order of magnitude with those observed. For the mixed solvent system H_2O–NH_3 the absorption maximum is found to follow the experimental results as the concentration of the mixture is altered.

The viewpoint of a stabilized cluster to simulate the structure of the solvated electron is naturally independent of the choice of method entailed in the elaboration of the concept. Application of the INDO method does appear to establish some points of contact between theory and observation. Among these the volume expansions which are obtained are quite striking. In evaluating the dilations, the liquid has been treated as being locally structured by the electron in such a manner that the cellular lattice model may be applicable. This serves to highlight a possible relation between the volume expansions in the liquid and similar phenomena in the solid state. The matter is under investigation. It also obviates the need to speak of physical cavities in the medium.

There are molecular traps in the medium. They are stabilized by the presence of the electron. At later times the energy may be further lowered by restructuring. The traps are thereby preformed and created.

Acknowledgments. One of us (G. H.) should like to thank the Carnegie Trust for the award of a scholarship. Also we are grateful to the referees for their constructive comments.

(25) L. Kevan, *J. Chem. Phys.*, **56**, 838 (1972).

Application of Charge Scavenging Kinetics to the Formation of Excited States in Irradiated Solutions of Aromatics in Cyclohexane[1]

Stefan J. Rzad

Radiation Research Laboratories and Center for Special Studies, Mellon Institute of Science, Carnegie-Mellon University, Pittsburgh, Pennsylvania 15213 *(Received April 12, 1972)*

Publication costs assisted by Carnegie-Mellon University and the U. S. Atomic Energy Commission

Charge scavenging kinetics established previously to account for the time dependence of the biphenylide ion in pulse-irradiated biphenyl–cyclohexane solutions are extended to the formation of excited states in such solutions. It is shown that given a particular reaction scheme one can describe the concentration dependence of the excited states in the steady-state radiolysis as well as their time dependence in pulse radiolysis. From the comparison of the predicted behavior and the experimental data available from the literature it is concluded that the triplets and singlets originate predominantly in the three different recombination processes: $S^+ + e$, $S^- + RH^+$, and $S^- + S^+$. Moreover λ, the constant characterizing the ion recombination processes in the pure solvent, can be interpreted to be $\sim 2 \times 10^{11}$ sec^{-1} which indicates that half of the original ions recombine in $\sim$3 psec. This in turn indicates that the rate constant for electron scavenging by biphenyl in cyclohexane is $\sim 3 \times 10^{12}$ M^{-1} sec^{-1}. Implications of these constants are discussed.

Introduction

The radiolysis of aromatics in hydrocarbon solutions has been studied for quite some time[2] by pulse and steady-state radiolysis methods. In particular Hunt and Thomas have shown that the pulse radiolysis of cyclohexane solutions of naphthalene and anthracene results in the formation of large yields of triplet states of the aromatics.[3] These triplets decrease in the presence of electron scavengers.[4] An emission characteristic of the fluorescence of these aromatics has also been observed.[3,5] This phenomenon has been confirmed by Land and Swallow,[6] Dainton and coworkers,[7] and Ludwig and Huque[8] who also showed that this fluorescence decreases with electron scavengers. It has also been shown that large yields of anions are produced in such systems,[4a] and in the case of anthracene it has been shown that the growth of the triplet follows the same kinetics as the decay of the anthracene negative ion.[4a] Very recently Baxendale and Wardman have correlated the 380-nm emission of biphenyl in isopentane at $-120°$ with the decay of the biphenylide ion monitored at 620 nm.[9,10] This fact together with a quantitative study of the formation of singlet and triplet states of biphenyl, anthracene, and naphthalene in cyclohexane prompted them to attribute those excited states to the reactions of $S^+ + S^-$ and $S^- + C^+$,[11] where S^+, S^-, and C^+ are the solute cation, solute anion, and solvent cation, respectively.

The importance of ionic precursors to the excited states is also manifest in steady-state experiments. Hentz and coworkers have shown that the isomerization of stilbene or of 1,2-diphenylpropenes in γ-irradiated cyclohexane solutions originates in the excited state of the solute produced by ion recombination.[12-14] The extent of isomerization was quantitatively accounted for[13] by using the charge scavenging expression proposed by Warman and coworkers.[15] Furthermore the luminescence from irradiated cyclohexane solutions of scintillators has been shown to be drastically decreased in the presence of charge scavengers.[16-18] Lipsky has shown recently[19] that liquid aliphatic hydrocarbons excited at 1470 Å fluoresce weakly. It is then quite possible that a small fraction of the excited states of the aromatic solute originate in excitation transfer from the aliphatic hydrocarbon solvent.[19] However all the information presented above points very strongly to ionic intermediates as major precursors to the formation of the excited states of these aromatics. A small contribution of solvent excited states will not affect the main conclusions of this paper.

Recently charge scavenging kinetics have been proposed which describe the decay of secondary negative ions of biphenyl in a 0.1 M solution of biphenyl in cyclohexane.[20] The application of these kinetics has further been extended by Hummel to more dilute solutions.[21] From these studies a lower limit of 2×10^{10} sec^{-1} has been obtained for the

(1) Supported in part by the U. S. Atomic Energy Commission. Some preliminary aspects of this work were presented at the 161st National Meeting of the American Chemical Society, Los Angeles, Calif., March 28–April 2, 1971.

(2) For a review see, *e.g.*, J. K. Thomas, *Annu. Rev. Phys. Chem.*, **21**, 17 (1970).
(3) J. W. Hunt and J. K. Thomas, *J. Chem. Phys.*, **46**, 2954 (1967).
(4) (a) J. K. Thomas, K. Johnson, T. Klippert, and R. Lowers, *J. Chem. Phys.*, **48**, 1608 (1968); (b) J. K. Thomas and I. Mani, *ibid.*, **51**, 1834 (1969).
(5) J. K. Thomas, *J. Chem. Phys.*, **51**, 770 (1969).
(6) E. J. Land and A. J. Swallow, *Trans. Faraday Soc.*, **64**, 1247 (1968).
(7) F. S. Dainton, G. A. Salmon, T. Morrow, and G. I. Thompson, *Chem. Commun.*, 326 (1968).
(8) P. K. Ludwig and M. M. Huque, *J. Chem. Phys.*, **49**, 805 (1968).
(9) J. H. Baxendale and P. Wardman, *Chem. Commun.*, 202 (1971).
(10) J. H. Baxendale and P. Wardman, *Int. J. Radiat. Phys. Chem.*, **3**, 377 (1971).
(11) J. H. Baxendale and P. Wardman, *Trans. Faraday Soc.*, **67**, 2997 (1971).
(12) R. R. Hentz, D. B. Peterson, S. B. Srivastava, H. T. Barzynski, and M. Burton, *J. Phys. Chem.*, **70**, 2362 (1966).
(13) R. R. Hentz and H. P. Lehmann, *J. Phys. Chem.*, **73**, 4283 (1969).
(14) R. R. Hentz and H. G. Altmiller, *J. Phys. Chem.*, **74**, 2646 (1970).
(15) J. M. Warman, K.-D. Asmus, and R. H. Schuler, *J. Phys. Chem.*, **73**, 931 (1969).
(16) R. R. Hentz and R. J. Knight, *J. Phys. Chem.*, **72**, 1783 (1968).
(17) T. Yoshida and S. Sato, *Bull. Chem. Soc. Jap.*, **40**, 2216 (1967).
(18) T. Saito, K. Takahashi, and S. Sato, *Bull. Chem. Soc. Jap.*, **41**, 2603 (1968).
(19) (a) F. Hirayama and S. Lipsky, *J. Chem. Phys.*, **51**, 3616 (1969); (b) F. Hirayama, W. Rothman, and S. Lipsky, *Chem. Phys. Letts.*, **5**, 296 (1970).
(20) S. J. Rzad, P. P. Infelta, J. M. Warman, and R. H. Schuler, *J. Chem. Phys.*, **52**, 3971 (1970).
(21) A. Hummel, *Proc. Int. Congr. Radiat. Res., 4th*, 1 (1970).

constant characterizing the recombination rate of the initial geminate ion pairs in cyclohexane.[20] Since it appears that excited states originate predominantly from ionic processes, it is the purpose of this work to apply the kinetic model of charge scavenging to the formation of excited states of aromatics in, for example, cyclohexane and to show that it can describe the phenomena. Moreover from comparison of experimental data available in the literature and the predicted behavior the time scale for ion recombination is defined more precisely.

Kinetics of Excited States Formation

Since upon irradiation of solutions of aromatics in aliphatic hydrocarbons, scavenging of both positive and negative charges occurs, the overall reaction scheme to be considered is the following

$$RH \longrightarrow RH^+ + e^- \quad (1)$$

$$e^- + S \longrightarrow S^- \quad (2)$$

$$RH^+ + S \longrightarrow S^+ + RH \quad (3)$$

$$RH^+ + e^- \longrightarrow RH^* \quad (4)$$

$$S^+ + e^- \xrightarrow{p_1} S^* \quad (5)$$

$$RH^+ + S^- \xrightarrow{p_2} S^* \quad (6)$$

$$S^+ + S^- \xrightarrow{p_3} S + S^* \quad (7)$$

The excited state S^* can be either a triplet or a singlet and p_1, p_2, and p_3 are the probabilities of obtaining a given excited state from a given recombination reaction. These excited states will decay by light emission, intersystem crossing, internal conversion, or formation of a stable product such as in the case of the isomerization of the stilbenes. From steady-state and pulse radiolysis experiments data are available for both the total yield of a given excited state and its time dependence. The yield of a given excited state and its dependence upon the concentration of S has been obtained, for instance, (i) from the isomerization of stilbenes,[12] (ii) from the absorption due to the triplets[3,4a,6,11] as measured on the microsecond time scale, and (iii) from the yield of fluorescence as measured by Baxendale and Wardman.[11] This type of experiments will be referred to as the steady-state radiolysis case. On the other hand nanosecond pulse radiolysis gives information on the time dependence of the excited state and will be referred to as the pulse radiolysis case.

Steady-State Radiolysis. Evidently reactions 1 through 7 apply to both free and geminate ions. Since these free ions are only a small fraction of the total ion yield and obey homogeneous kinetics we will concern ourselves with the geminate ions only (the free ions will be commented on later). This consideration is possible since the lifetime distribution function for these ion pairs has been obtained from the functional dependence of the scavenged charges on the scavenger concentration.[20] In the pure hydrocarbon this lifetime distribution function, *i.e.*, the fraction of ions which recombine between t and $t + \mathrm{d}t$, is interpreted to be

$$f(t) = \lambda\left[\left(\frac{1}{\pi\lambda t}\right)^{1/2} - e^{\lambda t}\,\mathrm{erfc}(\lambda t)^{1/2}\right] \quad (I)$$

where λ is a constant representing the recombination rate of the ion pairs and is equal to k/α where k is the second-order rate constant for charge scavenging and α is an empirical parameter obtained from the steady-state studies of charged scavenging.[20]

In the system under consideration the scavenger present at a concentration C scavenges electrons and positive ions with second-order rate constants k_n and k_p. At concentrations used in these systems pseudo-first-order kinetics can be applied as discussed previously[20] and in such an approximation the normalized rate of scavenging of a charged species of lifetime t is kCe^{-kCt}. Consequently the probability for an ion to be scavenged within time t is

$$\int_0^t kCe^{-kCt'}\mathrm{d}t' = 1 - e^{-kCt}$$

The three different recombination reactions (reactions 5, 6, and 7) have to be taken into consideration.

Reaction 5. $S^+ + e^-$. It is assumed here that the mobility of the positive ion does not change upon scavenging so that the probability for an electron of lifetime t to recombine with a scavenged positive ion is the product of the probability for this electron not to be scavenged at t, *i.e.*, e^{-k_nCt} and the probability for the positive ion to have been scavenged between 0 and t, *i.e.*, $1 - e^{-k_pCt}$. Summing this probability over the lifetime distribution and multiplying by the probability that such recombination will lead to a given excited state gives the total probability of obtaining such state through this recombination process

$$\pi_1 = p_1\int_0^\infty f(t)e^{-k_nCt}\left(1 - e^{-k_pCt}\right)\mathrm{d}t \quad (II)$$

Reaction 6. $S^- + RH^+$. Although this recombination is the opposite of the recombination treated above one complication arises due to the fact that the mobility of the negative species changes upon scavenging. As shown previously[20,22] one can take this effect into account by defining a new recombination time t'' such as

$$t'' = t' + (t - t')r_D \quad (III)$$

where t is the lifetime of the electron in the absence of scavenger, t' is the scavenging time, and r_D is a constant greater than unity and has been identified with the ratio of mutual ion mobilities before to that after scavenging. In other words, it is assumed that the residual lifetime $(t - t')$ of all ion pairs at the time of scavenging is extended by a factor r_D, so that the secondary negative ions exist from time t' to a time $t' + (t - t')r_D$.

In this second recombination process the fraction of electrons of initial lifetime t which are scavenged at t' and recombine with an unscavenged positive ion at t'' is the product of the probability for this electron to be scavenged between t' and $t' + \mathrm{d}t'$, *i.e.*, $(k_nCe^{-k_nCt'}\mathrm{d}t')$ and the probability for the positive ion to escape scavenging during the extended period of time available for scavenging $(e^{-k_pCt''})$. Since the scavenging of the electron can happen during its whole lifetime the probability for an electron of lifetime t in the absence of scavenger to be scavenged and to recombine as a secondary negative ion with an unscavenged positive ion is the sum over the lifetime of the electron of the above product. Summing this probability over the lifetime distribution and multiplying by the probability p_2 gives the total probability of obtaining a given state through this process

$$\pi_2 = p_2\int_0^\infty f(t)\int_0^t k_nCe^{-k_nCt'-k_pCt''}\,\mathrm{d}t'\mathrm{d}t \quad (IV)$$

Reaction 7. $S^+ + S^-$. In this case the reasoning is similar to that given for $S^- + RH^+$ but one wants here the

(22) S. J. Rzad, R. H. Schuler, and A. Hummel, *J. Chem. Phys.*, **51**, 1369 (1969).

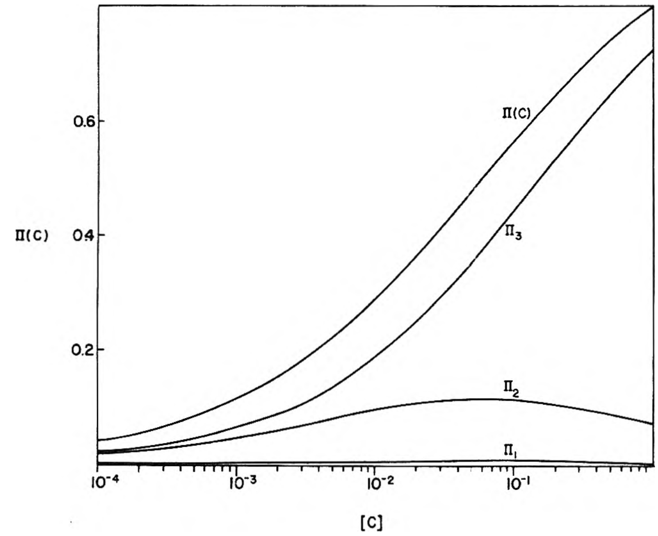

Figure 1. Concentration dependence of the total probability $\pi(C)$ and of its components π_1, π_2, and π_3.

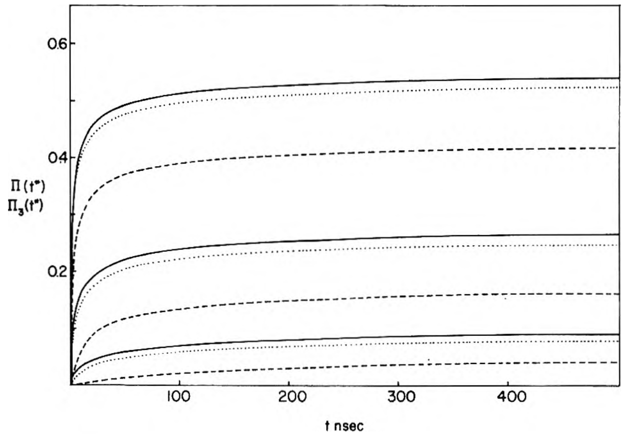

Figure 2. Time dependence of $\pi(t^*)$ and $\pi_3(t^*)$ ($\delta = 0$): (———) $\pi(t^*)$; $\lambda = 2 \times 10^{10}$ sec^{-1}, $r_D = 17$, and $\lambda = 6.9 \times 10^{11}$ sec^{-1}, $r_D = 588$; (- - -) $\pi_3(t^*)$; $\lambda = 2 \times 10^{10}$ sec^{-1}, $r_D = 17$; (· · · ·) $\pi_3(t^*)$; $\lambda = 6.9 \times 10^{11}$ sec^{-1}, $r_D = 588$; lower set of curves $C = 0.001$ M, middle set $C = 0.01$ M, upper set $C = 0.1$ M.

probability of a scavenged electron to recombine with a scavenged positive ion. It is sufficient therefore to replace $e^{-k_pCt''}$ by $1 - e^{-k_pCt''}$ and p_2 by p_3. One gets as a result

$$\pi_3 = p_3\int_0^{\infty} f(t)\int_0^{t} k_nCe^{-k_nCt'}\left(1 - e^{-k_pCt''}\right)dt'dt \qquad (V)$$

The total probability for producing a given excited state from one of the three recombination processes at a scavenger concentration C is then

$$\pi(C) = \pi_1 + \pi_2 + \pi_3$$

The introduction of $f(t)$, as given by eq I, and substitution of $t' + (t - t')r_D$ for t'' allow the evaluation of the different integrals and give for $\pi(C)$[23]

$$\pi(C) = p_1\left[\frac{1}{1 + (\alpha_nC)^{1/2}} - \frac{1}{1 + (\alpha_nC + \alpha_pC)^{1/2}}\right] + \frac{(p_2 - p_3)\alpha_nC}{\alpha_nC + \alpha_pC(1 - r_D)} \times \left[\frac{1}{1 + (\alpha_pCr_D)^{1/2}} - \frac{1}{1 + (\alpha_nC + \alpha_pC)^{1/2}}\right] + p_3\frac{(\alpha_nC)^{1/2}}{1 + (\alpha_nC)^{1/2}} \qquad (VI)$$

The yield of such excited state (neglecting the free ions) should be given by

$$G(S^*) = G_{gi}\pi(C) \qquad (VII)$$

Most of the parameters necessary for the evaluation of eq VI are known in cyclohexane. For a good electron scavenger $\alpha_n = 16$ M^{-1},[15] $\alpha_p = 1.0$ M^{-1},[24] and $r_D = 17$.[22] Although p_1, p_2, and p_3 are unknown one can assume as a first approximation that $p_1 = p_2 = p_3 = 1.0$.[13] For the purpose of illustration $\pi(C)$, π_1, π_2, and π_3 are plotted in Figure 1. As the concentration increases π_2 and π_1 go through a maximum as a result of the fact that more and more ions are scavenged at high concentrations so that reaction 7 dominates the recombination. In the case where $p_2 \simeq p_3$ the second term becomes unimportant and $\pi(C) \simeq p_3[\alpha_nC^{1/2}/(1 + \alpha_nC^{1/2})]$ which means that at a given concentration $\pi(C)$ is essentially equal to the fraction of scavenged electrons. It is not surprising, therefore, that Hentz and Lehmann[13] were able to fit the stilbene isomerization data by using simple electron scavenging kinetics.

Pulse Radiolysis. We will treat here the very general case where the excited state produced decays according to a first-order process characterized by a rate constant D. In order then to obtain the probability ($\pi(t^*)$) to observe a given excited state at a time t^* one has to consider the probability that the recombination process has occurred before t^* and that the excited state exists at t^*. Once this probability $\pi(t^*)$ is known it is easy to calculate the luminescence decay. The emitted light intensity at a time t^* is the rate of disappearance of the given excited state, *i.e.*, $-dN/dt = DN$ and therefore the normalized light intensity at t^* will be $I(t^*) = D\pi(t^*)$. As in the steady-state case three different recombination reactions have to be taken into account and the sum of their contribution at the observation time t^* gives $\pi(t^*)$, *i.e.*

$$\pi(t^*) = \pi_1(t^*) + \pi_2(t^*) + \pi_3(t^*)$$

Since the mathematics of the time dependence phenomena are considerably more complicated than in the steady-state case, the derivations of $\pi_1(t^*)$, $\pi_2(t^*)$, $\pi_3(t^*)$, and $\pi(t^*)$ are given in Appendix 1. For purpose of clarity two cases are considered when illustrating the properties of $\pi(t^*)$ as given by eq XII in the Appendix. First let us assume that the excited state produced does not decay, *i.e.*, $\delta = 0$. The behavior of $\pi(t^*)$ and $\pi_3(t^*)$ is then illustrated in Figure 2 for three different concentrations, *i.e.*, $C = 0.1$, 0.01, and 0.001 M, while that for $\pi_1(t^*)$ and $\pi_2(t^*)$ is given in Figures 3 and 4, respectively (note the different time scales). The parameters used in the calculation are $\alpha_n = 16$ M^{-1}, $\alpha_p = 1.0$ M^{-1}, $r_D = 17$, $\delta = 0$, $\lambda = 2 \times 10^{10}$ sec^{-1},[20] and $p_1 = p_2 = p_3 = 1.0$ (see below). It is readily noticed that $\pi_2(t^*)$ and $\pi_3(t^*)$ are the main components of $\pi(t^*)$ and that for reasonable concentrations, recombinations occurring through reactions 5 and 6 are finished within a few nanoseconds while those occurring through reaction 7 still occur at hundreds of nanoseconds. Another property of eq XII illustrated in Figures 2, 3, and 4 is that while, at times of the order of nanoseconds, $\pi(t^*)$ is independent of the absolute values of λ and r_D provided λ/r_D is kept constant, $\pi_1(t^*)$, $\pi_2(t^*)$, and $\pi_2(t^*)$ are very much dependent on the absolute values of λ and r_D for a given λ/r_D. Such a result is in fact expected since by increasing λ, in order to keep α

(23) All the integrals are of the form $\int_0^{\infty} f(t)e^{-St}dt$, which for $f(t)$ of eq I, gives, with $U = S/\lambda$, $\int_0^{\infty} f(t)e^{-St}dt = 1/(1 + U^{1/2})$.

(24) S. J. Rzad, Abstracts of the 158th National Meeting of the American Chemical Society, New York, N. Y., Sept. 1969, p 239.

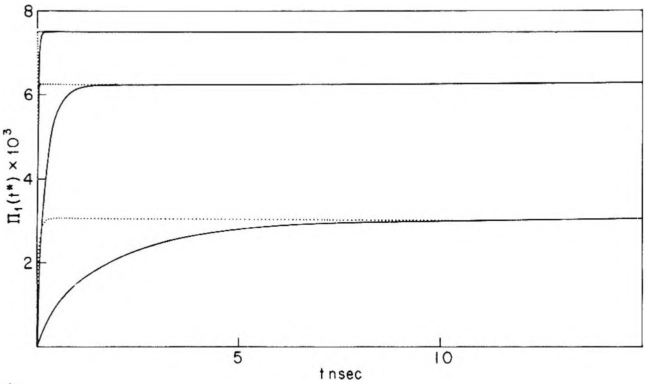

Figure 3. Time dependence of $\pi_1(t^*)$ ($\delta = 0$): (———) $\lambda = 2 \times 10^{10}$ sec^{-1}, $r_D = 17$; (· · · ·) $\lambda = 6.9 \times 10^{11}$ sec^{-1}, $r_D = 588$; lower set of curves $C = 0.001$ *M*, middle set $C = 0.01$ *M*, upper set $C = 0.1$ *M*.

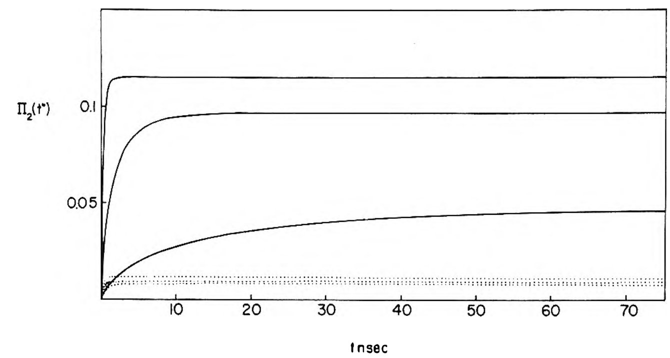

Figure 4. Time dependence of $\pi_2(t^*)$ ($\delta = 0$): (———) $\lambda = 2 \times 10^{10}$ sec^{-1}, $r_D = 17$; (· · · ·) $\lambda = 6.9 \times 10^{11}$ sec^{-1}, $r_D = 588$; lower solid line $C = 0.001$ *M*, middle $C = 0.01$ *M*, upper $C = 0.1$ *M*; lower dotted line $C = 0.001$ *M*, middle dotted line $C = 0.1$ *M*, upper dotted line $C = 0.01$ *M*.

constant, one has to increase k_n and k_p and hence processes which were occurring through reaction 6 will, at higher λ, occur through reaction 7. It should also be noted that the total fraction of processes occurring through reaction 5 is the same for a given λ/r_D and different values of λ but its time dependence is shifted to shorter times when λ increases. Since the contribution of reaction 5 to $\pi(t^*)$ is very small, at a given λ/r_D and for a higher value of λ, one will see a very small increase in $\pi(t^*)$ only at very short times.

The second illustration concerns the case where $\delta \neq 0$. This is shown in Figure 5 for a concentration of 10^{-3} *M* and an excited state decaying with a first-order rate constant $D = 4.4 \times 10^7$ sec^{-1} (this corresponds to a $\tau_{1/2}$ of 16 nsec as is the case for the biphenyl singlet) and all the other parameters the same as above. Again $\pi(t^*)$ and its component fractions are illustrated. It can be seen that due to the fact that recombination processes occur at longer and longer times when going from reaction 5 to 6 to 7 (Figures 2, 3, and 4) maxima in the luminescence intensity occur further out on the time scale for the same reason the apparent half-lives increase with time.

In order to apply eq XII to real systems one has to integrate this expression for a given pulse length. Such integration can be analytically performed but the length of the expression obtained makes its use quite impractical. It is much more convenient to integrate eq XII[25] numerically in a way similar to that done in the work on the decay of biphenyliole ion (Ph_2^-).[20]

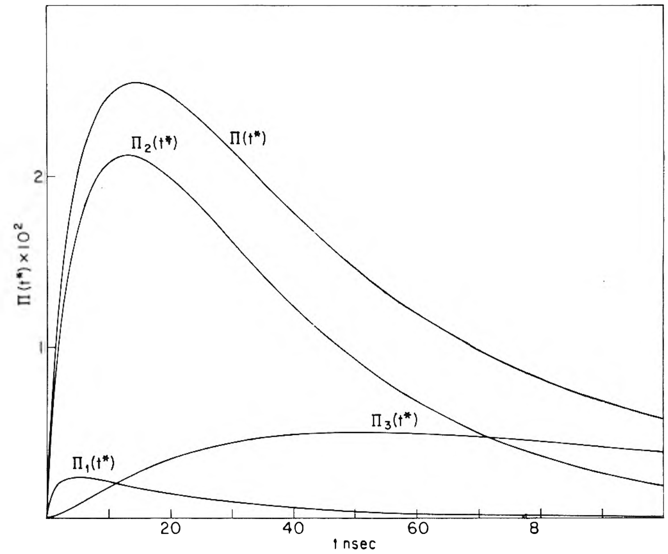

Figure 5. Time dependence of $\pi(t^*)$, $\pi_1(t^*)$, $\pi_2(t^*)$, and $\pi_3(t^*)$ for $\delta = 2.2 \times 10^{-3}$.

Comparison with Experiments

A problem which arises in comparing the above calculations with experiments is the fact that p_1, p_2, and p_3 are unknown. Although only their ratios are necessary for the calculation of the form of the growth or decay of an excited state, their absolute value is necessary for any quantitative prediction. Moreover while the maximum value of p_1 and p_2 is 1.0 that for p_3 could be one or two depending on whether one or two molecules of S are excited. This cannot be decided upon *a priori*. Baxendale and Wardman[11] after correction for the singlets crossing over to the triplets obtained a ratio of $G(\mathrm{T})/G(\mathrm{S}) \simeq 2.0$ for biphenyl and anthracene and $\simeq 1.0$ for naphthalene. Such a correction is justified since the cross over from singlets to triplets in irradiated systems has been previously pointed out by different authors.[5-7] Using a value of 2 for $G(\mathrm{T})/G(\mathrm{S})$ and a maximum value of 1.0 one gets $p_1 = p_2 = 0.67$ and 0.33 for triplets and singlets, respectively. One can obtain the maximum value for p_3 in the following fashion. In Figure 6 the yields of triplets of different aromatics in cyclohexane obtained from the literature are shown.[4a,5,6,11,26] These triplets were obtained by measuring the maximum triplet absorption after nanosecond or microsecond pulses. The G values were normalized to the latest accepted extinction coefficients of these species in cyclohexane.[27] These different extinction coefficients in units of M^{-1} cm^{-1} are as follows: biphenyl $\epsilon_{361.3}$ 42,800; anthracene ϵ_{425} 64,700; naphthalene ϵ_{415} 24,500; and 1,2-benzanthracene ϵ_{480} 28,800. The different G values agree quite well with each other and one should be able to calculate them using eq VII. But before doing so two more aspects should be discussed here. First since the dose rates used in the nanosecond or microsecond pulse radiolysis are 2 krads or less the half-life for recombination of the free ions is 5 μsec or more and therefore should not contribute to the excited state yields since the time of measurement was 1 μsec or less. Second, the singlets of the above mentioned compounds cross over to the triplets with a quantum efficiency $\phi_{\mathrm{S}\rightarrow\mathrm{T}} \simeq 0.7$,[28] which then gives for the triplets $p_1 =$

(25) Integrations have been carried out on a Hewlett-Packard 9100A calculator.

(26) T. J. Kemp and J. P. Roberts, *Trans. Faraday Soc.*, **65**, 725 (1969).
(27) R. Bensasson and E. J. Land, *Trans. Faraday Soc.*, **67**, 1904 (1971).
(28) J. B. Birks and I. H. Munro, *Progr. React. Kinet.*, **4**, 281 (1967).

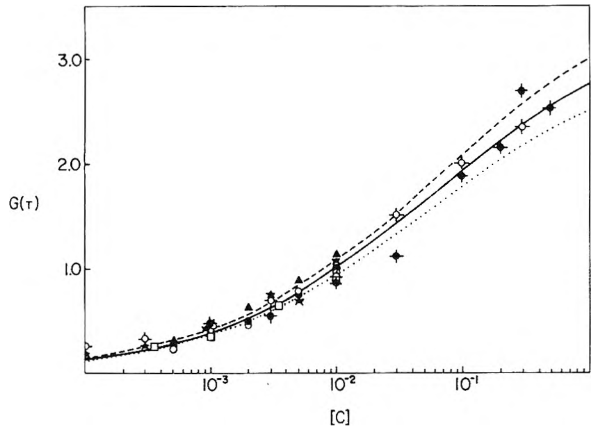

Figure 6. Concentration dependence of the yield of triplets for different solutions of aromatics in cyclohexane: ref 11 (●) biphenyl, (O) naphthalene, (▲) anthracene; ref 6 (-Ọ-) naphthalene, (★) anthracene; ref 3 (-◆-) biphenyl; ref 5 (□) 1,2-benzanthracene; ref 27 (-▲-) anthracene. Solid, dashed, and dotted lines calculated using eq VII with the parameters given in the text and p_3 = 1.0 (———), p_3 = 1.1 (- - - -), p_3 = 0.9 (· · · ·).

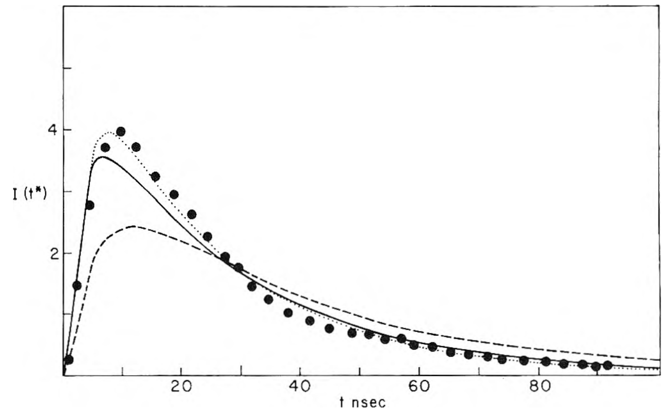

Figure 8. Time dependence of the biphenyl luminescence. $I(t^*)$ is in arbitrary units: (●) ref 11. Biphenyl triplet emission monitored at 340 nm of a solution of 0.01 M biphenyl in cyclohexane irradiated by a 5-nsec pulse of 10-MeV electrons. Solid dashed, and dotted lines calculated with eq XII the parameters given in the text and respectively $\lambda = 2 \times 10^{11}$ sec^{-1}, $p_1 = p_2 = p_3 = 0.33$ (———); $\lambda = 2 \times 10^{10}$ sec^{-1}, $p_1 = p_2 = p_3 = 0.33$ (----); and $\lambda = 2 \times 10^{10}$ sec^{-1}, $p_1 = p_2 = 0.33$, $p_3 = 0$ (····).

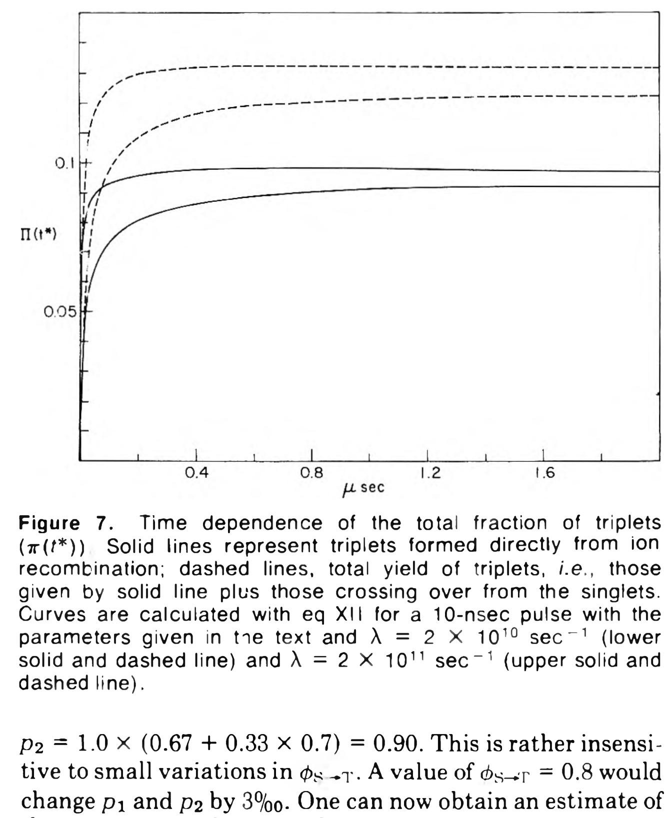

Figure 7. Time dependence of the total fraction of triplets ($\pi(t^*)$). Solid lines represent triplets formed directly from ion recombination; dashed lines, total yield of triplets, *i.e.*, those given by solid line plus those crossing over from the singlets. Curves are calculated with eq XII for a 10-nsec pulse with the parameters given in the text and $\lambda = 2 \times 10^{10}$ sec^{-1} (lower solid and dashed line) and $\lambda = 2 \times 10^{11}$ sec^{-1} (upper solid and dashed line).

$p_2 = 1.0 \times (0.67 + 0.33 \times 0.7) = 0.90$. This is rather insensitive to small variations in $\phi_{S\rightarrow T}$. A value of $\phi_{S\rightarrow T} = 0.8$ would change p_1 and p_2 by 3‰. One can now obtain an estimate of the maximum value of p_3 by fitting eq VII to the data of Figure 6 and remembering that p_3 = maximum value of $p_3 \times 0.9$ or that G(triplets) $= 0.9G_{gi}\pi$(C). The solid, dashed, and dotted lines are calculated in this fashion using p_3 = 1.0, 1.1, and 0.9, respectively, together with a_n = 16 16 M^{-1}, $\alpha_p = 1.0\ M^{-1}$, $r_D = 17$, and $G_{gi} = 3.8$. Obviously eq VI is a good description of the "steady-state case" and it can be readily seen that $p_3 = 1.0 \pm 0.1$ and in the following a value of $p_3 = 1.0$ will be used in the calculations.

As found earlier by Hunt and Thomas,[3] Baxendale and Wardman[11] have shown recently that in solution of naphthalene, biphenyl, or anthracene in cyclohexane, fluorescence is observed as well as a triplet absorption. Most of the triplet absorption for solutions of 2×10^{-3} M of the aromatic is present at the end of a 10-nsec pulse and only a small growth, following complex kinetics, occurs during approximately 500 nsec.[29] This has been pointed out previously by Thomas[3,4a] who has also shown that the growth of the anthracene triplet follows the decay of the anthracene negative ion.[4a] Equation XII with the pertinent parameters should describe this growth of triplets which have been shown to have a half-life of 30 μsec under the experimental conditions of Baxendale and Wardman.[10,11] Using $\lambda = 2 \times 10^{10}$,[20] $r_D = 17$, $\alpha_n = 16\ M^{-1}$, $\alpha_p = 1.0\ M^{-1}$, $\delta = 1.7 \times 10^{-6}$ ($\tau_{1/2} = 30$ μsec), and $p_1 = p_2 = p_3 = 0.67$ one calculates for a concentration $C = 2 \times 10^{-3}$ the lower solid line in Figure 7. It is readily seen that with such parameters the triplets grow during more than 1 μsec; this does not agree with the experimental results mentioned above. Moreover one can check this also from the singlet point of view. Figure 8 shows the biphenyl singlet emission as monitored at 340 nm[11] of a solution of 0.01 M biphenyl in cyclohexane irradiated by a 5-nsec pulse of 10-MeV electrons. Using a half-life of 16 nsec[28] for the biphenyl singlet ($\delta = 2.2 \times 10^{-3}$) and the other parameters as mentioned above one calculates the dashed curve in Figure 8. (Since the Y scale is arbitrary, the calculated curve has been made to fit the experimental data at 30 nsec.) Again the calculated curve does not represent the experimental data. This is due to the fact, mentioned previously, that ion recombination keeps generating singlets for times long after the end of the pulse and this increases the apparent half-life of the singlet. The apparent half-life from the experiments is of ~19 nsec[10,11] quite close to the uv excitation half-life of 16 nsec, indicating that most of the ion recombinations occur within a few nanoseconds. The only way to keep $\lambda = 2 \times 10^{10}$ sec^{-1} and explain the singlet fluorescence decay is to assume that singlets are generated only through the processes $S^- + RH^+$ and $S^+ + e^-$ which are over within a few nanoseconds (Figures 3 and 4). The dotted curve in Figure 8 is calculated in this way. Although the agreement is excellent this explanation has to be discarded for two reasons. First, the triplets would be generated only through $S^- + S^+$ which would not lead to any appreciable amount of immediate triplets (Figure 2)

(29) Data for the growth of triplets could not be read with any accuracy from the oscilloscope traces reproduced in Figure 1 of ref 11.

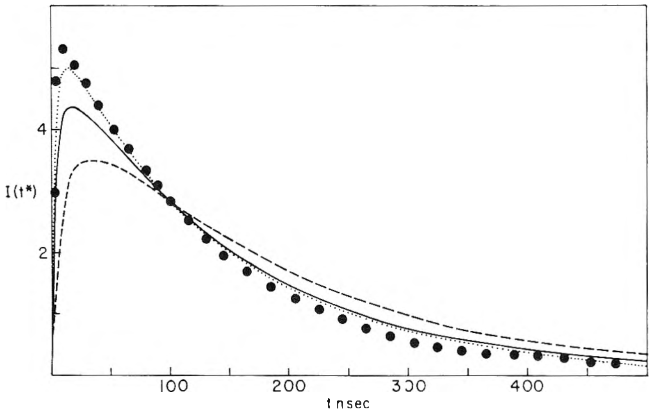

Figure 9. Time dependence of the naphthalene luminescence. $I(t^*)$ is in arbitrary units: (●) ref 11. Naphthalene singlet emission monitored at 360 nm of a solution of 5×10^{-3} M naphthalene in cyclohexane irradiated by a 5-nsec pulse of 10-MeV electrons. Solid, dashed, and dotted lines calculated with eq XII the parameters given in the text and respectively $\lambda = 2 \times 10^{11}$ sec^{-1}, $p_1 = p_2 = p_3 = 0.33$ (———); $\lambda = 2 \times 10^{10}$ sec^{-1}, $p_1 = p_2 = p_3 = 0.33$ (- - - -); and $\lambda = 2 \times 10^{10}$ sec^{-1}, $p_1 = p_2 = 0.33$, $p_3 = 0$ (····).

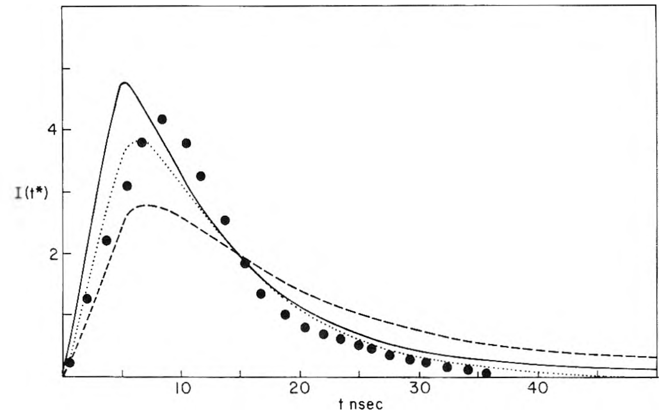

Figure 10. Time dependence of the anthracene luminescence. $I(t^*)$ is in arbitrary units: (●) ref 11. Anthracene singlet emission monitored at 440 nm of a solution of 5×10^{-3} M anthracene in cyclohexane irradiated by a 5-nsec pulse of 10-MeV electrons. Solid, dashed, and dotted lines calculated with eq XII the parameters given in the text and respectively $\lambda = 2 \times 10^{11}$ sec^{-1}, $p_1 = p_2 = p_3 = 0.33$ (———); $\lambda = 2 \times 10^{10}$ sec^{-1}, $p_1 = p_2 = p_3 = 0.33$ (- - - -); and $\lambda = 2 \times 10^{10}$ sec^{-1}, $p_1 = p_2 = 0.33$, $p_3 = 0$ (····).

and moreover the growth of the triplets would occur over too long of a period of time (Figures 2 and 7). Second, if singlets were formed only through reactions 5 and 6, the total yield of fluorescence (*i.e.*, total yield of singlets) should follow a concentration dependence characteristic of these two processes (Figure 1), *i.e.*, the yield should go through a maximum. This is not the case for the fluorescence yields of the naphthalene singlet measured by Land and Swallow[6] and Dainton, *et al.*[7] While the concentration dependence does not agree with the idea of the singlet formation only by reactions 5 and 6 it can be well described as in the case of the triplets, by the use of eq VII. Such a conclusion should be general since the yields for the fluorescence of biphenyl, anthracene, and naphthalene singlets as measured by Baxendale and Wardman[11] are similar. One can then conclude that triplets and singlets are formed through reactions 5, 6, and 7 with probabilities $p_1 = p_2 = p_3 = 0.67$ and 0.33, respectively. Finally it should be pointed out here that Ludwig and Huque[8] and more recently Baxendale and Wardman[10,11] have indicated that the luminescence has a long tail which should be the case if the three processes are leading to singlet formation but not so if only reactions 5 and 6 are producing singlets.

From the arguments given above (see also Figure 2) one has to use a higher value of λ/r_D, *i.e.*, higher value for λ if one wants to fit the experimental results obtained for the singlets. In Figure 8 the solid line is what one would calculate using expression XII with a $\lambda = 2 \times 10^{11}$ sec^{-1} and other parameters as given above. In Figures 9 and 10 are given the singlet emission decays obtained by Baxendale and Wardman[11] for solutions of 5×10^{-3} M naphthalene and 5×10^{-3} M anthracene in cyclohexane irradiated by a 5-nsec pulse of 10-MeV electrons and monitored at 360 and 440 nm, respectively. The dotted, dashed, and solid lines are calculated as in the three cases of biphenyl using eq XII with the pertinent parameters and a $\tau_{1/2} = 100$ and 5 nsec for the half-life of the singlets of naphthalene and anthracene, respectively.[28] The overall fit is rather good. It should be pointed out here that values of λ in the range of $1-4 \times 10^{11}$ sec^{-1} fit the singlet data rather well. However since a value of 2×10^{11} sec^{-1} gives the best overall fit to the three fluorescence decays considered (Figures 8, 9, and 10), it will be used in the following calculations. An uncertainty factor of $\sim$2 should be attributed to λ when considering the absolute time scale.

Using such value of $\lambda = 2 \times 10^{11}$ sec^{-1} one can now calculate with eq XII the growth of triplets and this is illustrated as the upper solid line in Figure 7. The contribution of the cross over from singlets to triplets using $\phi_{S \to T} = 0.7$ is also illustrated, as the dashed lines, in Figure 7. For 2×10^{-3} M biphenyl solution in cyclohexane the growth is expected to be complete within 500 nsec with approximately 50% of the triplets present at the end of the 10-nsec pulse. This agrees rather well with the experimental results.

At this point, although the calculated and experimental data for excited states agree, we are faced with the fact that the Ph_2^- decay has been fitted in cyclohexane with a value of 1.2×10^9 sec^{-1} for λ/r_D,[20] *i.e.*, a factor of 10 smaller than that obtained in this work. Our feeling is that the value obtained by fitting the triplet data is closer to the truth for the following reasons. Most important is the fact that the order of magnitude of $\lambda/r_D \simeq 1.2 \times 10^{10}$ sec^{-1} necessary to explain the very fast growth of triplets is completely independent of the absolute value (G value) of these triplets. This is due to the fact that there is no contribution of free ions to the triplets at the time scale involved in the measurements (<1 μsec) so that the growth of triplets with time reflects only the geminate ion recombination. The shape of this growth is then sufficient to obtain a value for λ/r_D. On the contrary the fitting of Ph_2^- decay is very much dependent upon the absolute yield since there is a free ion contribution of $\sim$30% to the total yield of Ph_2^- at $\sim$100 nsec.[20] The fact that Ph_2^+ absorption overlaps that of Ph_2^- and therefore complicates the accurate measurement of the latter has been pointed out by Thomas and coworkers.[4a,30] For example, at 600 nm where the measurements of Ph_2^- decay were made,[4a] approximately 30% of the absorption is due to positive ions. Any unaccounted contribution to the yield of Ph_2^- ions would mean that the actual yield is smaller requiring a higher value of the parameter λ/r_D for the calculation of the data according to eq 28 of ref 20. More-

(30) L. B. Magnusson, J. T. Richards, and J. K. Thomas, *Int. J. Radiat. Phys. Chem.*, 3, 295 (1971).

over very recently Richards and Thomas[30,31] have measured, in cyclohexane after a 10-nsec pulse of 3-MeV electrons, the Ph_2^- decay at 410 nm where the contribution of Ph_2^+ has been shown to be smaller.[30,31] At 100 nsec the yield of Ph_2^- is $G(Ph_2^-) \sim 0.18$.[30,31] Allowing for a yield of free ion of 0.12 gives a $G \sim 0.06$ for the geminate ions. It has been shown[20] that at times of the order of 100 nsec the yield of geminate ions is given by $G(Ph_2^-) \sim G_{gi}(r_D/\pi\lambda t)^{1/2}$ so that for 100 nsec and $G(Ph_2^-) \sim 0.06$, $\lambda/r_D \sim 1.3 \times 10^{10}$ sec^{-1}. This value is very close to the value of 1.2×10^{10} sec^{-1} proposed in this work. (In fact using $\lambda/r_D = 1.2 \times 10^{10}$ sec^{-1} in eq 28 of ref 20 with other parameters as given previously allows for the complete description of the Ph_2^- decay at 10^{-3} M as reported in ref 31 and 32.) Finally Hummel[21] has shown that, at 10^{-4} M biphenyl in cyclohexane, no growth of Ph_2^- occurs after a 10-nsec pulse. He explained the data using $\lambda/r_D = 1.2 \times 10^9$ sec^{-1} but with $\lambda = 1.1 \times 10^{12}$ and $r_D = 850$. However it has been shown (see Figure 2) that if one keeps λ/r_D = constant no change occurs in the overall growth of triplets. If one wants then to explain the lack of growth of Ph_2^- at 10^{-4} M one has to go again to higher ratios of λ/r_D.

As shown above the use of $\lambda = 2 \times 10^{11}$ sec^{-1} correlates the data for the formation of the excited states and the decay of the anion leading to these states.

Accepting a value of $\lambda = 2 \times 10^{11}$ sec^{-1} (within a factor of 2 as mentioned above) leads to the following conclusions.

(1) Half of the ion recombination processes occurs within $0.5915\ldots/\lambda$ [20] $= 3 \times 10^{-12}$ sec; this time scale is a factor of 10 shorter than that derived previously.[20]

(2) The rate constant for electron scavenging by biphenyl is $k_n = \lambda\alpha = 2 \times 10^{11} \times 16 \sim 3 \times 10^{12}$ M^{-1} sec^{-1}. This value should be compared to that of 2.6×10^{12} M^{-1} sec^{-1} measured by Beck and Thomas[32] and to that of 1×10^{12} M^{-1} sec^{-1} proposed by Mozumder.[33] Since it has been shown[34] as expected that k_n is proportional to the electron mobility one would expect from the rate constant obtained above that for n-hexane $k_n \sim (3 \times 10^{12} \times 0.09)/0.35$[35] $\sim 0.8 \times 10^{12}$ M^{-1} sec^{-1}. This value is to be compared with a value of 1×10^{12} M^{-1} sec^{-1} obtained for electron scavenging by biphenyl and carbon tetrachloride in n-hexane[36] and a value of 10^{12} M^{-1} sec^{-1} obtained for electron scavenging by pyrene and carbon tetrachloride in methylcyclohexane.[37]

(3) In a recent study Infelta and Schuler[38] have estimated from electron scavenging competitive studies an electron transfer parameter $\beta_e = k_e r_D/\lambda$. A typical value of this parameter is 0.5 M^{-1} ($CH_3Cl^- + SF_6 \rightarrow CH_3Cl + SF_6^-$). The previously accepted value of $\lambda/r_D = 1.2 \times 10^9$ sec^{-1} gives a $k_e = 6 \times 10^8$ M^{-1} sec^{-1} or an order of magnitude lower than that obtained by Richards and Thomas[30,31] for $k(Ph_2^- + SF_6) = 7.5 \times 10^9$ M^{-1} sec^{-1}. The value of λ/r_D obtained in this work leads to a rate constant of 6×10^9 M^{-1} sec^{-1} which agrees well with rate constants of the order of 10^{10} M^{-1} sec^{-1} reported in the literature.[30,31,39]

Acknowledgment. The author is very much indebted to Dr. P. P. Infelta for assisting in the derivation and evaluation of $[(\delta r_D)^{1/2}/i]\,\mathrm{erf}(i(\delta\lambda t)^{1/2})$.

Appendix

For an excited state to be observable at t^* the recombination of the ions leading to the formation of this state must have occurred before this time t^*. If this state decays with a characteristic first-order rate constant D it has also to be taken into consideration, *i.e.*, the excited state must not have decayed before t^*. The three recombination processes to be considered here are reactions 5, 6, and 7.

Reaction 5. $S^+ + e^-$. The probability for this reaction can be obtained directly from the steady-state case with only minor changes. The probability that an electron of lifetime t will recombine with a scavenged positive ion and that this recombination process will produce a given excited state which will exist at t^* is simply the probability for this process to occur and give such state, as obtained in the steady-state case, multiplied by the probability that the excited state would not have decayed during the interval from the time of its formation (t) to the observation time (t^*), *i.e.*, $e^{-D(t^*-t)}$. Since electrons with lifetimes longer than t^* will recombine after t^*, one wants to integrate from 0 to t^* over the lifetime distribution in order to obtain the probability of observing at t^* a given excited state originating in a recombination reaction such as reaction 5.

$$\pi_1(t^*) = p_1 \int_0^{t^*} f(t) e^{-k_n C t}\left(1 - e^{-k_p C t}\right) e^{-D(t^*-t)}\,dt \qquad \text{(VIII)}$$

Reaction 6. $S^- + RH^+$. In this case we start as previously with the fraction of electrons of lifetime t which are scavenged between t' and $t' + dt'$ and recombine at t'' with an unscavenged positive ion but we want to multiply this fraction by the probability that the resulting excited state did not decay from the time of its formation (t'') up to the time of observation t^*: $k_n C e^{-k_n C t' - k_p C t'' - D(t^*-t'')}dt'$. Here a complication arises due to the different portions of the electron lifetime distribution one has to consider. First, let us consider electrons with lifetimes from 0 up to t^*/r_D which when scavenged will always recombine before t^* and therefore one has to sum the fractional probability given above over the whole lifetime of a given electron and again over the pertinent lifetime distribution (first term in the bracket eq IX). The second portion of the lifetime distribution involves electrons with lifetimes between t^*/r_D and t^* and where the secondary ion will have recombined before t^* if scavenging occurs at or after a time $t_1 = (t^* - tr_D)/(1 - r_D)$ given by setting t'' equal to t^* in eq III. If scavenging occurs before t_1 the secondary ion will not have recombined before t^*. One wants then to sum the fractional probability over the interval t_1 to t of the lifetime of the electron and again over the pertinent lifetime distribution (second term in the bracket of eq IX). Ion pairs with lifetime longer than t^* will always recombine after t^* and therefore this portion need not be considered here. Now multiplying these two contributions by p_2 gives us the probability of observing a given excited state at time t^*.

$$\pi_2(t^*) = p_3\left[\int_0^{t^*/r_D} f(t)\int_0^t k_n C e^{-k_n C t' - k_p C t'' - D(t^*-t'')}\,dt'\,dt + \int_{t^*/r_D}^{t^*} f(t)\int_{t_1}^t k_n C e^{-k_n C t' - k_p C t'' - D(t^*-t'')}\,dt'\,dt\right] \qquad \text{(IX)}$$

(31) J. T. Richards and J. K. Thomas, *Chem. Phys. Letts.*, **10**, 317 (1971).
(32) G. Beck and J. K. Thomas, *J. Phys. Chem.*, in press (see proceedings of this conference).
(33) A. Mozumder, *J. Chem. Phys.*, **55**, 3026 (1971).
(34) S. J. Rzad and K. M. Bansal, *J. Phys. Chem.*, **76**, 2374 (1972).
(35) W. F. Schmidt and A. O. Allen, *J. Chem. Phys.*, **52**, 4788 (1970).
(36) G. Bakale, E. C. Gregg, and R. McCreary, *J. Chem. Phys.*, submitted for publication.
(37) J. H. Baxendale, C. Bell, and P. Wardman, *Chem. Phys. Letts.*, **12**, 347 (1971).
(38) P. P. Infelta and R. H. Schuler, *J. Phys. Chem.*, **76**, 987 (1972).
(39) S. Arai, D. A. Grev, and L. M. Dorfman, *J. Chem. Phys.*, **46**, 2572 (1967).

Reaction 7. $S^- + S^+$. The reasoning in this case is the same as for $S^- + RH^+$ but here one wants the probability of a scavenged electron to recombine with a scavenged positive ion. As for the steady-state case it is sufficient to replace $e^{-k_pCt''}$ by $(1 - e^{-k_pCt''})$ and p_2 by p_3. One gets then

$$\pi_3(t^*) = p_3\left[\int_0^{\frac{t^*}{r_D}} f(t)\int_0^{t} k_nCe^{-k_nCt'}\left(1 - e^{-k_pCt''}\right)e^{-D(t^*-t'')}dt'dt + \int_{\frac{t^*}{r_D}}^{t^*} f(t)\int_{t_1}^{t} k_nCe^{-k_pCt'}\left(1 - e^{-k_pCt''}\right)e^{-D(t^*-t'')}dt'dt\right] \quad \text{(X)}$$

The total probability of observing a given excited state at time t^* is the sum of the above probabilities.

$$\pi(t^*) = \pi_1(t^*) + \pi_2(t^*) + \pi_3(t^*)$$

Substituting $t' + (t - t')r_D$ for t'' and after preliminary integration one gets

$$\pi(t^*) = [p_1 - C_1]e^{-Dt^*}\int_0^{t^*} f(t)e^{-(k_nC-D)t}dt - [p_2 + C_2]e^{-Dt^*}\int_0^{t^*} f(t)e^{-(k_n+k_pC-D)t}dt + C_2e^{-Dt^*}\int_0^{\frac{t^*}{r_D}} f(t)e^{-(k_pC-D)tr_D}dt + \left(C_1 + C_2e^{-k_pCt^*}\right)e^{-(k_nCt^*/(1-r_D))} \times \int_{\frac{t^*}{r_D}}^{t^*} f(t)e^{-(k_nCtr_D/(r_D-1))}dt + C_1e^{-Dt^*}\int_0^{\frac{t^*}{r_D}} f(t)e^{Dtr_D}dt \quad \text{(XI)}$$

where $C_1 = p_3\alpha_nC/[\alpha_nC - \delta(1 - r_D)]$ and $C_2 = (p_2 - p_3)\alpha_nC/[\alpha_nC + \alpha_pC(1 - r_D) - \delta(1 - r_D)]$, where $\alpha_n = k_n/\lambda$, $\alpha_p = k_p/\lambda$, and $\delta = D/\lambda$.

Introducing f(t) as given in eq I into XI and solving the different integrals gives[40]

$$\pi(t^*) = \frac{(p_1 - C_1)\exp(-\delta\lambda t)}{1 - A}\left\{1 - A^{1/2}\mathrm{erf}(\lambda tA)^{1/2} - \exp\Big((1 - A)\lambda t\Big) \times \mathrm{erfc}\,(\lambda t)^{1/2}\right\} - \frac{(p_1 + C_2)\exp(-\delta\lambda t)}{1 - B}\left\{1 - B^{1/2}\mathrm{erf}(B\lambda t)^{1/2} - \exp\Big((1 - B)\lambda t\Big)\mathrm{erfc}(\lambda t)^{1/2}\right\} + \frac{C_2\exp(-\delta\lambda t)}{1 - D}\left\{1 - D^{1/2}\mathrm{erf}\left(\frac{D\lambda t}{r_D}\right)^{1/2} - \exp\left((1 - D)\frac{\lambda t}{r_D}\right)\mathrm{erfc}\left(\frac{\lambda t}{r_D}\right)^{1/2}\right\} + \frac{(C_1 + C_2\exp(-\alpha_pC\lambda t))}{1 - E}\left\{E^{1/2}\left[\exp\Big((E - \alpha_nC)\lambda t\Big)\mathrm{erfc}(E\lambda t)^{1/2} - \exp\left(\frac{E\lambda t}{r_D}\right)\mathrm{erfc}\left(\frac{E\lambda t}{r_D}\right)^{1/2}\right] + \exp\left(\frac{\lambda t}{r_D}\right)\mathrm{erfc}\left(\frac{\lambda t}{r_D}\right)^{1/2} - \exp\Big((1 - \alpha_nC)\lambda t\Big)\mathrm{erfc}(\lambda t)^{1/2}\right\} + \frac{C_1\exp(-\delta\lambda t)}{1 - \delta r_D}\left\{1 - \exp\left((1 + \delta r_D)\frac{\lambda t}{r_D}\right)\mathrm{erfc}\left(\frac{\lambda t}{r_D}\right)^{1/2} + \frac{(\delta r_D)^{1/2}}{i}\mathrm{erf}\left(i(\delta\lambda t)^{1/2}\right)\right\} \quad \text{(XII)}$$

with $A = \alpha_nC - \delta$; $B = (\alpha_n + \alpha_p)C - \delta$; $D = (\alpha_pC - \delta)r_D$; and $E = \alpha_nCr_D/(r_D - 1)$.

Equation XII reduces to eq VI if one considers that no decay is occurring and by setting $t^* = \infty$.

(40) Most integrals in eq XI are of the form $\int_a^b f(t)e^{-St}dt$. For an f(t) such as given by eq I, this integral gives with $U = S/\lambda$

$$\frac{1}{1 - U}\left[U^{1/2}\left(\mathrm{erf}(\lambda aU)^{1/2} - \mathrm{erf}(\lambda bU)^{1/2}\right) + e^{\lambda a(1-U)}\,\mathrm{erfc}\,(\lambda a)^{1/2} - e^{\lambda b(1-U)}\,\mathrm{erfc}\,(\lambda b)^{1/2}\right]$$

The integral of the form $\int_0^a f(t)e^{St}dt$ gives

$$\frac{1}{1 + U}\left[\frac{U^{1/2}}{i}\,\mathrm{erf}\left(i(\lambda aU)^{1/2}\right) + 1 - e^{\lambda a(1+A)}\,\mathrm{erfc}(\lambda a)^{1/2}\right]$$

Intermediate Phase Studies for Understanding Radiation Interaction with Condensed Media. The Electron Attachment Process[1]

L. G. Christophorou

Health Physics Division, Oak Ridge National Laboratory, Oak Ridge, Tennessee 37830 and Department of Physics, University of Tennessee, Knoxville, Tennessee 37916 *(Received April 12, 1972)*

Publication costs assisted by Oak Ridge National Laboratory

In this paper current efforts to bridge the gap in our existing knowledge on electron attachment processes in gases and liquids are discussed. The conclusions of a comprehensive study where gaseous data on electron attachment have been related to hydrated electron–molecule reaction rates are outlined. The first information on electron attachment to molecules in very high pressure gases is presented, with reference to electron attachment to molecular oxygen to form O_2^- in the presence of increasing pressures of N_2 (0.5 to 15 atm). A model is proposed to account for the latter results.

Intermediate phase studies, namely studies of radiation processes and effects as well as physicochemical reactions at densities between those corresponding to low-pressure gases and liquids, are fundamentally necessary for the development of a coherent understanding of radiation interaction with matter. There is need for uniting, linking together of our knowledge on radiation processes occurring in low-pressure gases with that in the condensed phase.

In this paper I wish to elaborate briefly on one aspect of this problem, namely on the efforts currently underway at our laboratory to bridge the gap in our existing knowledge on electron attachment processes in gases and liquids. I wish to report (A) the conclusions of a comprehensive study where gaseous data on electron attachment have been related to hydrated electron–molecule reaction rates and (B) the first information on electron attachment to molecules in very high pressure gases, with special reference to O_2. The latter studies are being performed with gas pressures between 0.5 and ~80 atm and will be accompanied by direct physical studies on liquids about which I will defer discussion.

A. Relevance of Quantities Describing Electron Attachment Processes in Gases to Hydrated Electron Reaction Rates, $R(e_{aq})$

The following physical quantities describing electron attachment processes in gases have been found[2,3] to be of interest in this study: parent negative ion lifetime τ_a, molecular electron affinity $(EA)_G$, cross section energy maximum, *i.e.*, the resonance energy ϵ_{max}. The following conclusions have been reached.[2a,b]

1. When $(EA)_G < 0$ eV or $\tau_a < 10^{-12}$ sec, $R(e_{aq})$ is much less than $10^{10}\ M^{-1}\ sec^{-1}$ (10^4 to $\sim 10^7\ M^{-1}\ sec^{-1}$). This suggests that for these molecules the electron affinity, $(EA)_L$, in the liquid environment is $\lesssim \frac{3}{2}kT$. However, when $(EA)_G \gtrsim -0.5$ eV, $R(e_{aq})$ is large (10^9 to $\sim 10^{10}\ M^{-1}\ sec^{-1}$) indicating that $(EA)_L > \frac{3}{2}kT$ (but small). This is due to the effect of solvation on the negative ion which increases its stability.

2. When $(EA)_G > \frac{3}{2}kT$ (and independent of the value of τ_a) and/or $\tau_a > 10^{-6}$ sec (*i.e.*, when a long-lived parent negative ion is formed in the field of the ground electronic state) and/or $\epsilon_{max} \lesssim \frac{3}{2}kT$ (*i.e.*, the cross section for the attachment process—dissociative or nondissociative—increases sharply at thermal energies with a possible maximum below $\frac{3}{2}kT$),[2] $R(e_{aq})$ is large, $\sim 3 \times 10^{10}\ M^{-1}\ sec^{-1}$, and most probably diffusion controlled. It appears that either of the above conditions [$(EA)_G > \frac{3}{2}kT$; $\tau_a > 10^{-6}$ sec; $\epsilon_{max} \lesssim \frac{3}{2}kT$] is sufficient for $R(e_{aq})$ to attain diffusion-controlled values.

3. The magnitude of $R(e_{aq})$ appears to be independent of $(EA)_G$ when $(EA)_G > 0$ eV (see Figure 1).

4. On the basis of conclusion 2 above, values of $R(e_{aq})$ can be predicted for a number of organic molecules for which gaseous data are available. Such predictions have been made[2] for 35 organic molecules.

B. Electron Attachment to Molecules in Very High Pressure Gases: O_2

The O_2^{-*} ion belongs to the group of transient molecular negative ions referred to as moderately short lived ($10^{-12} \lesssim \tau < 10^{-6}$ sec)[4] and hence it can easily be stabilized collisionally in a high-pressure (swarm) experiment. In Figure 2 the rate of electron attachment to O_2 in O_2–N_2 mixtures is plotted as a function of the mean electron energy, $\langle\epsilon\rangle$, for O_2 pressures $P_{O_2} \rightarrow 0$ and for N_2 pressures, P_{N_2}, as indicated in the figure. The attachment rates are seen to increase constantly with increasing P_{N_2}. For each P_{N_2} the maximum value of the attachment rate is attained at $\langle\epsilon\rangle \simeq 0.05$ eV. Using the actual experimental data points (solid circles in Figure 2) or the smoothed-out data (broken curves in Figure 2) the attachment cross sections shown in Figures 3 and 4 as closed and open circles, respectively, were obtained[5] by making use of the analytical methods we have described recently.[6] These methods[5,6] allow the deter-

(1) Research sponsored by the U. S. Atomic Energy Commission under contract with Union Carbide Corporation.

(2) (a) L. G. Christophorou, "Proceedings of the Third Tihany Conference on Radiation Chemistry," Tihany, Hungary, May 1971; (b) L. G. Christophorou and R. P. Blaunstein, *Chem. Phys. Lett.*, **12**, 173 (1971).

(3) It should be noted, also, that in both liquids and gases, electron capture reactions and their cross sections appear to be strongly dependent on specific functional groups and their reactivity.

(4) L. G. Christophorou, "Atomic and Molecular Radiation Physics," Wiley-Interscience, New York, N. Y., 1971.

(5) D. L. McCorkle, L. G. Christophorou, and V. E. Anderson, *Proc. Phys. Soc. London, At. Mol. Phys.*, **5**, 1211 (1972).

(6) L. G. Christophorou, D. L. McCorkle, and V. E. Anderson, *Proc. Phys. Soc. London, At. Mol. Phys.*, **5**, 1211 (1972).

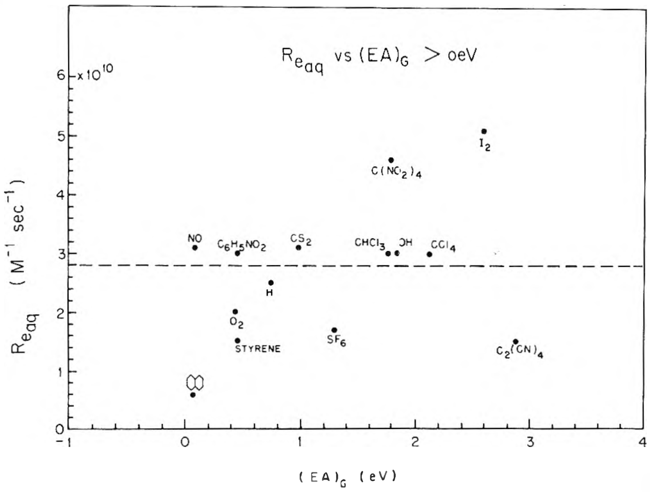

Figure 1. $R(e_{aq})$ *vs.* $(EA)_G$ (>0 eV). For detailed values of $(EA)_G$ (which spread considerably), see ref 4. The broken line represents the average value of $R(e_{aq})$ for the molecules shown in the figure.

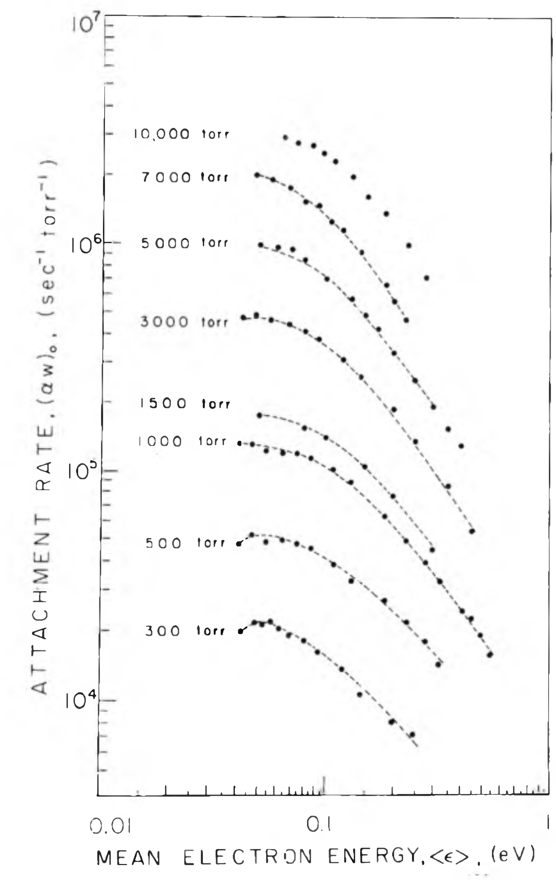

Figure 2. Attachment rates $(\alpha w)_0$, extrapolated to zero O_2 pressure, as a function of mean electron energy for various N_2 pressures.

mination of absolute electron attachment cross sections as a function of electron energy from electron attachment rate data obtained from very high pressure (swarm) experiments. They constitute a fundamental advancement in electron attachment studies.

The main features of the data in Figures 2–4 are (i) their absolute basis, (ii) the distinct structure in the cross section functions for P_{N_2} < 1000 Torr, and (iii) the gradual shift of

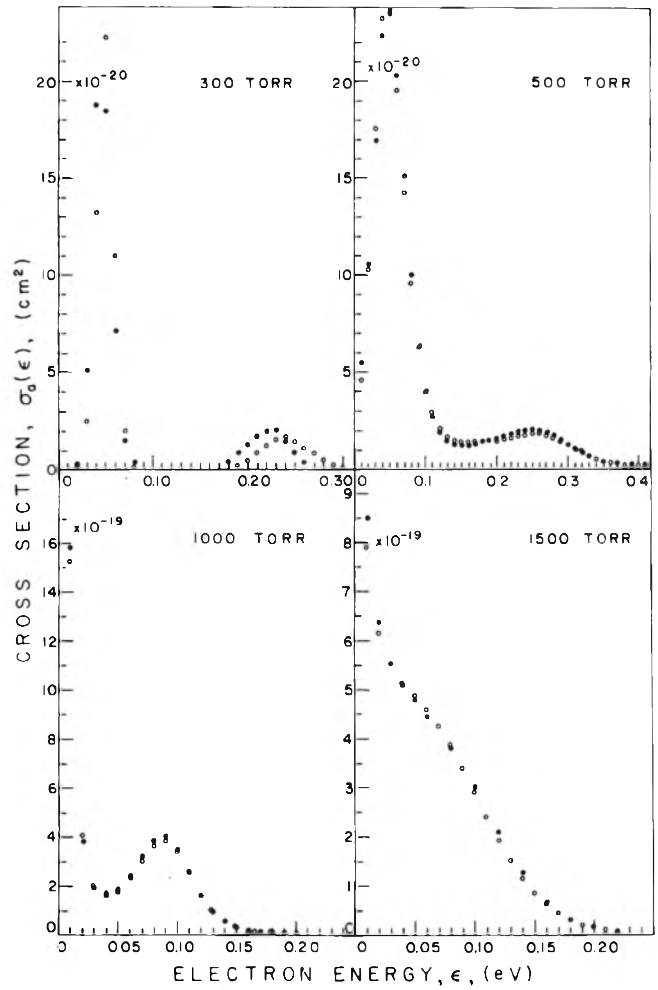

Figure 3. Attachment cross sections for O_2 in O_2–N_2 mixtures, as a function of electron energy for N_2 pressures 300, 500, 1000, and 1500 Torr. The solid circles were obtained using the data points in Figure 2 and the open circles using the smoothed-out data shown as broken curves in Figure 2.

the cross section functions toward thermal energies with the increasing of N_2 density. In Table I the energy integrated cross section, $\int_0^{\infty}\sigma_a(\epsilon)d\epsilon$, the maximum value of the attachment rate, $\alpha w(\langle\epsilon\rangle_{max})$, the values, $\langle\epsilon_{max}\rangle$, of the electron energy at which $\sigma_a(\epsilon)$ shows maxima or shoulders, and the energy separation, $\Delta\epsilon$, of the observed maxima or shoulders are given for various total pressures which are essentially those of N_2. Throughout this paper these total pressures will be referred to as N_2 pressures, P_{N_2}, since the percentage of O_2 is very small (in almost all measurements $5 \times 10^{-7} < P_{O_2}/P_{N_2} < 3 \times 10^{-3}$).

The two distinct peaks in the cross section function observed for the two lowest values of P_{N_2} (300 and 500 Torr) at 0.05 and 0.24 eV are interpreted,[5] respectively, as being due to the processes

$$e(\epsilon \simeq 0.05\text{ eV}) + O_2(X^3\Sigma_g^-, v = 0) \rightarrow O_2^{-*}(X^2\Pi_g, v' = 4) \quad (1)$$

and

$$e(\epsilon \simeq 0.24\text{ eV}) + O_2(X^3\Sigma_g^-, v = 0) \rightarrow O_2^{-*}(X^2\Pi_g, v' = 5) \quad (2)$$

i.e., capture of the electron into the fourth and fifth vibrational levels of O_2^- from the $v = 0$ vibrational level of O_2,

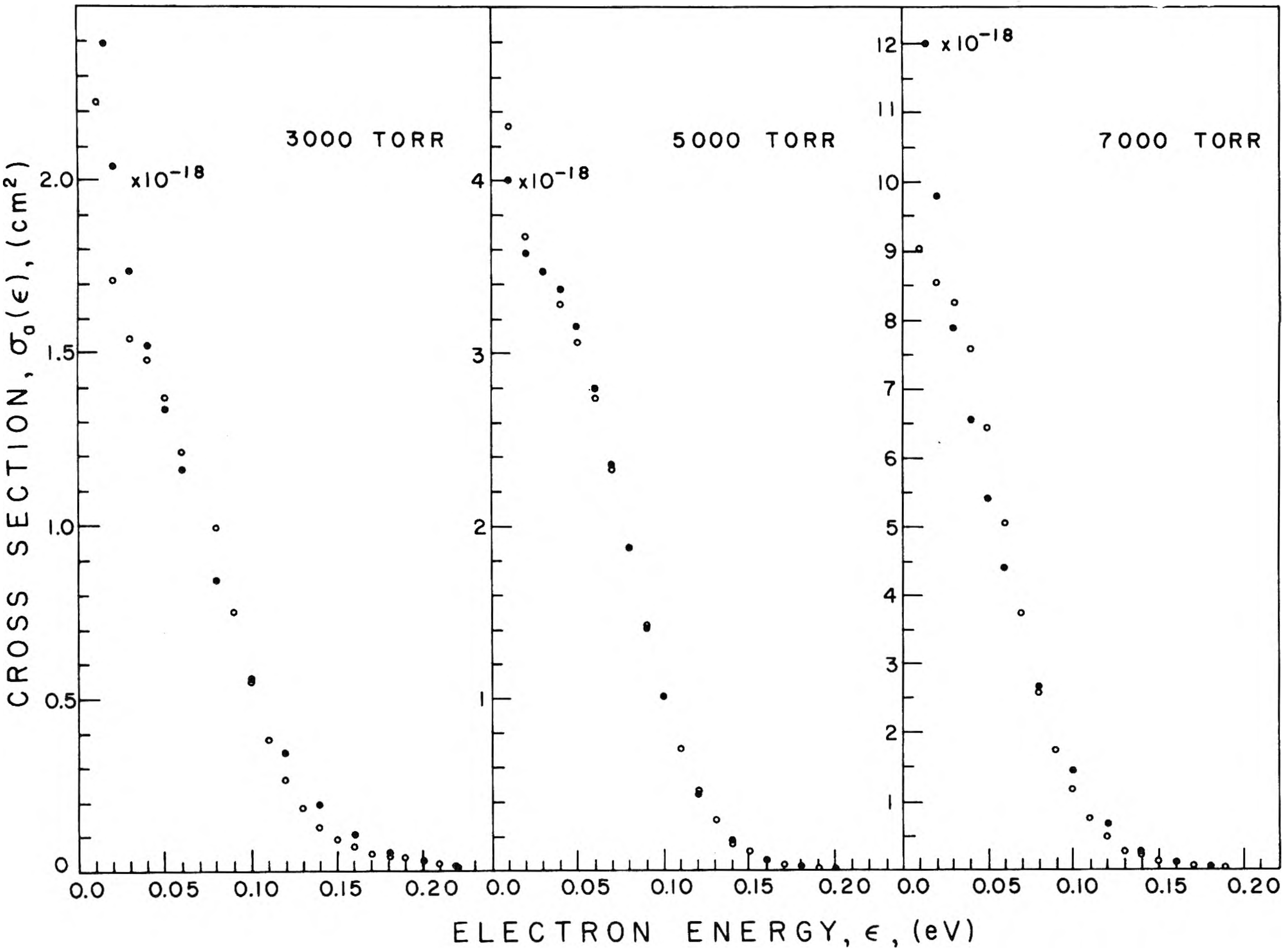

Figure 4. Attachment cross sections for O_2 in O_2–N_2 mixtures as a function of electron energy for N_2 pressures 3000, 5000, and 7000 Torr. The solid circles were obtained using the data points in Figure 2 and the open circles using the smoothed-out data shown as broken curves in Figure 2.

TABLE I: Electron Attachment Data for O_2 in O_2–N_2 Mixtures

Total pressure	$\alpha w(\langle\epsilon\rangle_{max})$,[a] $sec^{-1}\,Torr^{-1}$	$\int_0^\infty \sigma_a(\epsilon)d\epsilon$, eV cm^2	ϵ_{max}, eV	$\Delta\epsilon$,[b] eV
300	2.2×10^4	0.63×10^{-20}	0.05; 0.24	0.19
500	5.2×10^4	1.69×10^{-20}	0.05; 0.25	0.20
1,000	1.3×10^5	5.58×10^{-20}	<0.01; 0.09	. . .
1,500	1.75×10^5	6.49×10^{-20}	<0.01; ~0.07[c]	. . .
3,000	4.8×10^5	17.0×10^{-20}	<0.01; ~0.04[c]	. . .
5,000	9.7×10^5	32.0×10^{-20}	<0.01; ~0.04[c]	. . .
7,000	2×10^6	63.0×10^{-20}	<0.01; ~0.03[c]	. . .
10,000	3×10^6(?)	. . .	. . .	. . .

[a] $\langle\epsilon\rangle_{max} \simeq 0.05$ eV (see Figure 2). See additional data in Figure 5. [b] Energy difference between the two maxima in the cross section function (see Figure 4). [c] Shoulder.

with a subsequent stabilization of O_2^{-*} by an N_2 molecule, *viz.*

$$O_2^{-*} + N_2 \rightarrow O_2^- + N_2 + \text{energy} \quad (3)$$

where the N_2 molecule acts simply as an agent for removing excess energy. At low N_2 pressures instead of the sequential two-step process (reactions 1 or 2 followed by reaction 3), the electron attachment process to O_2 can be viewed as a one-step three-body electron attachment reaction

$$e + O_2 + N_2 \rightarrow O_2^- + N_2 + \text{energy} \quad (4)$$

in which the N_2 molecule acts as a third body removing energy in what may be called a "distant" collision, without perturbing the potential energy curves of O_2^- during capture. The continuous and gradual shift of the cross section functions toward thermal energies and the pronounced increase in their sharpness at near zero energies seen in Figures 3 and 4, however, suggest that as the N_2 density increases, electron attachment to O_2 cannot be described solely in this fashion and that N_2 does not act simply as a stabilizing third body in "distant" collisions. The observed consistent changes in $\sigma_a(\epsilon)$ seem to suggest that N_2 seriously perturbs the O_2^- potential energy curves during capture with a net downward shift in what may be called "hard" or "sticky" collisions, the effect becoming more dominant the higher the N_2 density. This brings to mind the familiar effect of solvation which apparently seems to be important from these densities.

On the basis of the trend exhibited by the cross section functions shown in Figures 3 and 4 one would expect the capture cross section to become a very sharp resonance at near zero energies in the limit of very high densities (efforts are currently in progress to investigate this for P_{N_2} up to ~80 atm). This would certainly be consistent with the conclusions in section A, namely that $R(e_{aq})$ attains diffusion-controlled values when $\sigma_a(\epsilon)$ is sharply peaking at thermal or subthermal energies.

Let us now assume that electron attachment to O_2 in O_2–N_2 mixtures proceeds *via* the mechanisms

$$\begin{aligned} e + O_2 &\xrightarrow{k_1} O_2^{-*} \\ O_2^{-*} &\xrightarrow{k_2} O_2 + e \\ O_2^{-*} + N_2 &\xrightarrow{k_3} O_2^- + N_2 + \text{energy} \\ &\xrightarrow{k_4} O_2 + N_2 + e \end{aligned} \qquad \text{(i)}$$

and

$$\begin{aligned} e + O_2 + N_2 &\xrightarrow{k_5} [O_2^{-*} - N_2] \\ [O_2^{-*} - N_2] &\xrightarrow{k_6} O_2 + N_2 + e \\ [O_2^{-*} - N_2] + N_2 &\xrightarrow{k_7} O_2^- + 2N_2 + \text{energy } \{[(NO^- + \\ &\qquad + NO \text{ or } N_2O_2^-) + N_2]?\} \\ &\xrightarrow{k_8} O_2 + 2N_2 + e \end{aligned} \qquad \text{(ii)}$$

The main difference between mechanisms i and ii is this: in mechanism i N_2 is assumed to act simply as a stabilizing third body in "distant" collisions, not affecting the O_2^- potential energy curves, while in mechanism ii N_2 is assumed to be involved in "hard," "sticky" collisions which result in a serious perturbation of the O_2^- potential energy curves during capture, with a possible formation of a transient complex $[O_2^{-*}$-$N_2]$ which can be destroyed by autoionization (or collision) or lead to O_2^- upon collision with a second N_2 molecule. At low pressures mechanism i could, of course, be viewed as a one-step three-body attachment process involving "distant" collisions. In mechanism i the reaction $O_2^{-*} \rightarrow O_2^- + h\nu$ has been neglected as it is insignificant.[4] Similarly, the reaction $[O_2^{-*}$-$N_2] \rightarrow O_2^- + N_2 + h\nu$ has been neglected. In both mechanisms i and ii, the effect of O_2 as a stabilizing third body has been neglected since we are considering $(\alpha w)_0$, *i.e.*, the attachment rates for $P_{O_2} \rightarrow 0$. We shall, further, restrict our discussion to values of $(\alpha w)_0$ at ~0.05 eV (see Figure 2), *i.e.*, to rates due to capture into the lowest vibrational level of O_2^- which lies above the level $v = 0$ of O_2.

If mechanisms i and ii are taken to be plausible, the rate of change of the electron density due to electron capture by O_2 can be expressed as

$$\frac{\partial n_e}{\partial t} = -\nu_a n_e = -k_1 n_{O_2} n_e \times \frac{k_3 n_{N_2}}{(k_3 + k_4)n_{N_2} + k_2} - k_5 n_{O_2} n_{N_2} n_e \frac{k_7 n_{N_2}}{(k_7 + k_8)n_{N_2} + k_6} \qquad (5)$$

In eq 5 ν_a is the overall attachment frequency, n_e, n_{O_2}, and n_{N_2} are the number densities for electrons, oxygen, and nitrogen molecules, respectively, and $k_1 \ldots k_8$ are the rate constants for the processes considered in (i) and (ii). From eq 5 we have

$$\frac{(\alpha w)_0}{n_{N_2}} = \frac{k_1 k_3}{(k_3 + k_4)n_{N_2} + k_2} + \frac{k_5 k_7 n_{N_2}}{(k_7 + k_8)n_{N_2} + k_6} \qquad (6)$$

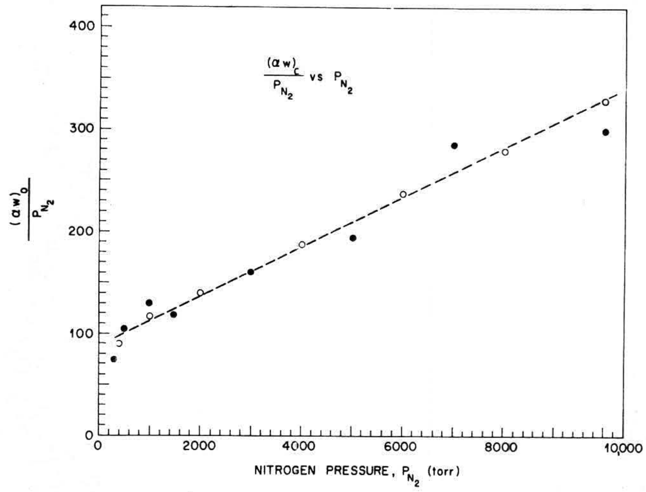

Figure 5. $(\alpha w)_0/P_{N_2}$ *vs.* P_{N_2}. The values of $(\alpha w)_0$ plotted are those for $\langle\epsilon\rangle \simeq 0.05$ eV, which basically correspond to the maximum value of $(\alpha w)_0$ at each P_{N_2} (see Table I). The solid points are the data of McCorkle, Christophorou, and Anderson[5] (Table I) and the open circles are the data of Goans and Christophorou.[7] The latter data have been taken with a much improved electronics system and are as follows: 3.6×10^4, 1.17×10^5, 2.8×10^5, 7.5×10^5, 1.43×10^6, 2.2×10^6, and 3.3×10^6 sec^{-1} Torr^{-1} for P_{N_2} 400, 1000, 2000, 4000, 6000, 8000, and 10,000 Torr, respectively.

If we now turn our attention to Figure 5, where $(\alpha w)_0/P_{N_2}$ is plotted as a function of P_{N_2}, we see that the experimental data can be represented by

$$\frac{(\alpha w)_0}{P_{N_2}} = A + BP_{N_2} \qquad (7)$$

where A and B are constants. Considering that $n_{N_2} \propto P_{N_2}$, eq 7 is consistent with eq 6 when

$$(k_3 + k_4)n_{N_2} \ll k_2;\ (k_7 + k_8)n_{N_2} \ll k_6 \qquad (8)$$

If we now assume that the cross section for O_2^{-*}, N_2 collisions is given by the Langevin expression for spiralling collisions,[4,8] we obtain for the average time between O_2^{-*}, N_2 collisions at 7000 Torr (T = 298°K) the value of $\sim 4 \times 10^{-12}$ sec. Hence, we have for the autoionization lifetime, $\tau_a(O_2^{-*})$, of O_2^{-*}

$$\tau_a(O_2^{-*}) = k_2^{-1} < [(k_3 + k_4)n_{N_2}]^{-1} \simeq 4 \times 10^{-12} \text{ sec} \qquad (9)$$

This value lies within the limits established by McCorkle, Christophorou, and Anderson,[5] who obtained an estimate of the upper limit of the lifetime of O_2^{-*} as follows. From the Breit–Wigner formula the cross section for the formation of all compound states with vibrational number n arising from the initial vibrational ground state 0 is

$$\int \sigma_c^n(0;\epsilon)d\epsilon = 2\pi^2 \lambda\!\!\!^-{}^2 \left(\frac{C^n}{g}\right)\Gamma_0^n \qquad (10)$$

In eq 10 $\lambda\!\!\!^-{}^2 = \hbar^2/2m\epsilon$, $2\pi\hbar$ is Planck's constant, m is the electron mass, and ϵ is the incident electron energy. For O_2, C^n/g = ⅔ (see ref 5 and 8) and since we are concerned with very low energies ($\epsilon < 0.1$ eV), n = 1 **and** $\Gamma_0^{n=1}$ is the total width. From eq 10 McCorkle, Christophorou, and Anderson[5] obtained $\Gamma_0^{n=1} = 4.9 \times 10^{-6}$ eV which yielded an upper limit for the autoionization lifetime of O_2^{-*} as

$$\tau_a(O_2^{-*}) < \frac{\hbar}{\Gamma_0^{n=1}} \simeq 1.3 \times 10^{-10} \text{ sec} \qquad (11)$$

using for the left-hand side of eq 10 the energy-integrated

(7) R. Goans and L. G. Christophorou, unpublished results.
(8) A. Herzenberg, *J. Chem. Phys.*, **51**, 4942 (1969).

cross section $\int_0^\infty \sigma_a(\epsilon)d\epsilon$ for P_{N_2} = 7000 Torr. For this pressure $\int_0^\infty \sigma_a(\epsilon)d\epsilon = 6.3 \times 10^{-19}$ eV cm^2 and $\epsilon_{max} \simeq 0.04$ eV (see Table I and Figure 4). It is to be noted, however, that the use of this value for the left-hand side of eq 10 overestimates[9] the upper limit of $\tau_a(O_2^{-*})$, since it basically assumes that each O_2^{-*}, N_2 collision results in the formation of O_2^-, *i.e.*, $k_4 = 0$. This is unlikely since at low P_{N_2} the three-body attachment coefficient for reaction 4 is[5] ~0.03 times that for

$$e + O_2 + O_2 \rightarrow O_2^- + O_2 + \text{energy} \quad (12)$$

for which it can be argued[10] that the probability of O_2^- formation is unity. If we assume that the upper limit for $\tau_a(O_2^{-*})$ obtained through eq 10 should be multiplied by a factor of 0.03, the upper limit for $\tau_a(O_2^{-*})$ in eq 11 becomes $\sim 4 \times 10^{-12}$ sec, which is in agreement with that in eq 9.

Similarly, from the second inequality (8) an upper limit to the autoionization lifetime of $[O_2^{-*}\text{-}N_2]$ can be estimated which is of the same order of magnitude as that for $\tau_a(O_2^{-*})$.

From a least-squares fitting to the data in Figure 5 we have

$$\frac{(\alpha w)_0}{P_{N_2}} = 88.3 + 0.025P_{N_2} \quad (13)$$

Hence

$$\frac{k_1k_3}{k_2} \simeq 88.3 \text{ sec}^{-1} \text{ Torr}^{-2}; \ \frac{k_5k_7}{k_6} \simeq 0.025 \text{ sec}^{-1} \text{ Torr}^{-3}$$

Finally, if it is assumed that eq 6 and 7 hold over all N_2 densities up to that (0.81 g cm^{-3}) of liquid N_2, from eq 13 we find that

$$(\alpha w)_0(\epsilon \simeq 0.04 \text{ eV}) \simeq 0.74 \times 10^{10} \text{ sec}^{-1} \text{ Torr}^{-1}$$

for O_2 in liquid N_2. This value compares well with the value (1.11×10^{10} sec^{-1} Torr^{-1}) one obtains from $\pi\lambda\!\!\!^{-2}$ where $\lambda\!\!\!^- = \lambda/2\pi$ is the deBroglie wavelength for a 0.04-eV electron. This is an interesting observation and may indicate that mechanisms i and ii describe reasonably well the process of electron capture by O_2 in the presence of N_2 throughout the whole range of N_2 densities up to that of the liquid. Efforts are in progress to investigate this by finding out the range of P_{N_2} over which a plot such as in Figure 5 holds.[11]

In conclusion, it has to be stressed once again that although high-pressure electron attachment (electron-molecule interaction processes in general) studies are experimentally very difficult, the detailed analyses are obscured by the complexities of high densities and the lack of direct information as to the products formed, and any generalizations have to consider carefully the effects of many specific environments on a given process, such studies are profoundly important in efforts to relate and unite our knowledge on radiation interaction with low-pressure gases and with condensed media.

(9) This was also pointed out in ref 5.
(10) This is a reasonable assumption as can be seen from the discussions in ref 4 (Chapter 6) and 8.
(11) Note Added in Proof: More recent data obtained[7] for nitrogen pressures up to 25,000 Torr show that a plot such as in Figure 5 holds very well.

Radiation Chemistry of CF_4–CCl_4 Mixtures in the Gas Phase

Ronald E. Marcotte and Robert J. Hanrahan*

Chemistry Department, University of Florida, Gainesville, Florida 32601 *(Received February 2, 1972)*

Publication costs assisted by the U. S. Atomic Energy Commission

A study has been made of the gas-phase γ radiolysis of CF_4-CCl_4 mixtures at 88° and a total pressure of 920 Torr. Effects of mixture composition, total dose, and added O_2 scavenger on the product yields were measured. The main products in this system are the three possible chlorofluoromethanes. Their yields all maximize in mixtures in which about 90% of the absorbed energy is deposited initially in CF_4; the values found are $G(CF_3Cl) = 2.13$, $G(CF_2Cl_2) = 0.62$, and $G(CFCl_3) = 6.9$. Other significant products are C_2Cl_6 and C_2Cl_4; their yields fall rather smoothly from maximum values of 0.38 and 0.24, respectively, as CF_4 is added to CCl_4. Typical yields of minor products in equimolar mixtures are as follows: C_2F_6, 0.006; $C_2F_3Cl_3$, 0.0003; $C_2F_4Cl_2$, 0.001; C_2F_5Cl, 0.003; Cl_2, 0.03. Since small amounts of added O_2 scavenge between 90 and 100% of all significant products in equimolar mixtures of CF_4 and CCl_4, it appears that the final products result almost completely from free-radical processes under these conditions. At the condition of maximum yield, however, O_2 scavenging is only about 70% effective, and a substantial contribution of ionic processes to final product yields is suggested.

Introduction

The interesting pattern of similarities and differences between CF_4 and CCl_4 suggested to us that it would be worthwhile to investigate the radiolysis of mixtures of these substances. Both compounds are entirely nonpolar and relatively volatile, and both show the peculiarity under electron bombardment in the mass spectrometer of giving zero intensity of the parent positive ion.[1] Instead,

(1) American Petroleum Institute Research Project 44, Catalog of Mass Spectral Data, Serial Number 401 and 603.

CF_3^+ and CCl_3^+ are formed, accompanied by the halogen atom or negative ion. Both CF_4[2-5] and CCl_4[6-11] show considerable yields for rupture of the C–X bond under radiolysis, but in both cases the net yield of C_2X_6 is small due to back-reaction with X_2. In both cases, the net yields of C_2X_6 and X_2 are very sensitive to addition of O_2. (The data for CCl_4 are primarily for the liquid phase, but similar behavior in the gas phase is likely.)

On the other hand, CF_4 is much more stable thermodynamically than CCl_4; the C–F and C–Cl bond dissociation energies are 121 and 68 kcal in CF_4 and CCl_4, respectively.[12] Although good data are rare because of the tendency of the compounds to give CX_3^+ rather than CX_4^+, it is clear that the first ionization potential of CF_4 must be at least 2 or 3 eV higher than CCl_4.[13] The lowest excitation potentials must be similarly related. Finally, although CF_4 is essentially inert to low-energy electrons,[16] CCl_4 readily undergoes bond rupture to give $CCl_3\cdot$ radicals and Cl^- ions.

As implied above, there have been several studies on the radiolysis of CF_4 in the gas phase.[2-5] There has been limited work on the radiolysis of gaseous CCl_4,[6] but the compound has been thoroughly studied in the liquid phase.[7-11] Although investigations of the radiolysis of CCl_4 and of CF_4 mixed with various other substances have been reported, no previous work on the radiolysis of CF_4-CCl_4 mixtures has been published.[17] However, an investigation of reactions of these compounds initiated by a glow discharge was recently completed in this laboratory.[18]

Experimental Section

Reagents. Mallinckrodt analytical reagent grade carbon tetrachloride was purified by irradiating a deaerated 2000-ml sample for 48 hr followed by distillation of the resulting mixture. The middle one-third of the distillate was dried over BaO and stored in a dark storage volume on a vacuum line. The only impurity found in this sample by flame ionization gas chromatography was chloroform at a concentration of less than 10 ppm. The Air Products Co. carbon tetrafluoride was dried over BaO and stored in a volume attached to the vacuum system. The only impurities found by gas chromatography were negligibly small ($<10^{-4}$ mol %) quantities of CF_3Cl and C_2F_6. The Phillips ethylene (99 mol % pure) was dried over BaO and deaerated prior to use. Most reagents used for chromatograph calibration were 99% pure and were used as received. The Linde acetylene was used as received taking into account that it was found to be only 93% pure.

Sample Preparation. Radiolysis samples were prepared on a conventional glass vacuum system. Kel-F grease was used on all stopcocks and joints. Samples were made up such that the total pressure in the radiolysis vessels would always be 920 Torr at 88°. At this temperature the vapor pressure of CCl_4 was 1065 Torr, thus ensuring that even in samples of pure CCl_4 only the vapor phase would be present. In preparing samples of a specific composition, the required amouunt of CF_4 was first metered out using a mercury manometer to monitor the pressure. The appropriate amount of CCl_4 was then metered out using *PVT* techniques and calibrated volumes on tbe vacuum line. Finally, the CCl_4 was vacuum transferred into the radiolysis vessels.

Sample Irradiations. Irradiations were carried out using 600 Ci of ^{60}Co in a "point source" geometry.[19] The irradiations were done in nickel radiolysis vessels equipped with Hoke monel bellows valves. The two vessels, fabricated from 0.040 in. thick ⅝ in. i.d. tubing, had volumes of 19.8 and 19.5 ml. The vessels were held in precise alignment during irradiations by a drilled aluminum block installed in a thermostated chamber. The temperature in the chamber was maintained at 88.0 ± 1°.

Gas-phase dosimetry was done by measuring the acetylene production from irradiated ethylene. The experimental conditions of temperature, pressure, radiation source, dose rate, and dose were almost identical with those of Sauer and Dorfman[20] who reported the G value for acetylene production to be 2.4 molecules/100 eV. Using this information, our dose rate in ethylene was found to be 1.4×10^{18} eV g^{-1} min^{-1}. Since the vessels were found to meet the criterion for a Bragg-Gray cavity as stated by Hine and Brownell,[21] the energy deposited in the dosimeter (E_d) could be related to that deposited in the CCl_4-CF_4 mixtures (E_s) by the ratio of their electron stopping powers (S_s/S_d) rather than their electron densities, as is usually done in liquid-phase radiolyses.

$$E_s = (S_s/S_d)E_d \tag{1}$$

The ratios of stopping powers were calculated using Bethe's equation[22] which can be rearranged to the form

$$\frac{S_s}{S_d} = \frac{N_sZ_s(k - \ln I_s^2)}{N_dZ_d(k - \ln I_d^2)} \tag{2}$$

where N is molecules/cm^3, Z is the electrons/molecule,

(2) W. C. Askew, T. M. Reed, and J. C. Mailen, *Radiat. Res.*, **33**, 282 (1968).
(3) W. C. Askew and T. M. Reed, *Nucl. Sci. Eng.*, **29**, 143 (1967).
(4) J. Fajer, D. R. MacKenzie, and F. W. Bloch, *J. Phys. Chem.*, **70**, 935 (1966).
(5) P. Y. Feng, W. A. Glasson, L. Mamula, K. Schmude, and S. Soffer, *Proc. Jap. Conf. Radioisotop., 4th*, 445 (1961).
(6) W. Mund, P. Huyskens, and J. Debaisieus, *Bull. Acad. Royal Belg.*, **41**, 929 (1956).
(7) A. V. Zimm and Z. S. Egonova, *Symp. Radiat. Chem., Moscow*, 207 (1955).
(8) J. Schulte, *J. Amer. Chem. Soc.*, **79**, 4643 (1957).
(9) W. Cooper and W. H. Stafford, *Proc. U. N. Int. Conf. Peaceful Uses At. Energy, 2nd*, **29**, 118 (1958).
(10) T. Chen, K. Wong, and F. Johnston, *J. Phys. Chem.*, **64**, 1023 (1960).
(11) F. P. Abramson, B. M. Buckhold, and R. F. Firestone, *J. Amer. Chem. Soc.*, **84**, 2285 (1962).
(12) T. L. Cottrell, "The Strengths of Chemical Bonds," 2nd ed, Academic Press, New York, N. Y., 1958.
(13) A recent tabulation by Franklin, *et al.*,[14] gives IP of CF_4 as 14.36 or 14.9, and CCl_4 as 11.47 ± 0.01. However, Majer[15] discusses the entire question of the ionization potential of CF_4 at some length, and argues for a higher value.
(14) J. L. Franklin, J. G. Dillard, H. M. Rosenstock, J. T. Herron, K. Draxl, and F. H. Field, "Ionization Potentials, Appearance Potentials, and Heats of Formation of Gaseous Positive Ions," NSRDS No. 26, National Bureau of Standards, Washington, D. C., 1969.
(15) J. R. Majer, *Advan. Fluorine Chem.*, **2**, 55 (1961).
(16) The effect of low-energy electrons on CCl_4 and CF_4 was studied by R. P. Blaustein and L. G. Christophorou, *J. Chem. Phys.*, **49**, 1526 (1968). Other perfluorocarbons have been studied by C. Lifshitz and R. Grajower, *Int. J. Mass Specrosc. Ion Phys.*, **3**, 211 (1969). Evidence is also provided by a study of the relative response of these compounds in an electron capture glc detector, reported by C. A. Clemons and A. P. Altshuller, *Anal. Chem.*, **38**, 133 (1966).
(17) Miscellaneous experiments on the radiolysis of CCl_4 and of CF_4 mixed with various substances are summarized in the Ph.D. Dissertation of R. E. Marcotte, University of Florida, 1968, available from University Microfilms.
(18) R. E. Marcotte and R. J. Hanrahan, *J. Fluorine Chem.*, **2**, 87 (1972).
(19) R. J. Hanrahan, *Int. J. Appl. Radiat. Isotop.*, **13**, 254 (1962).
(20) M. C. Sauer and L. M. Dorfman, *J. Phys. Chem.*, **66**, 322 (1962).
(21) G. J. Hine and G. L. Brownell, "Radiation Dosimetry," Academic Press, New York, N. Y., 1956, p 25.
(22) J. W. T. Spinks and R. J. Woods, "An Introduction to Radiation Chemistry," Wiley, New York, N. Y., 1964, p 41.

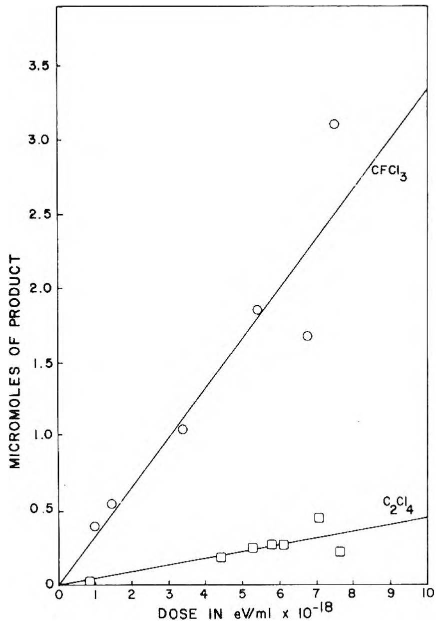

Figure 1. Yield of $CFCl_3$ and C_2Cl_4 as a function of dose in the γ radiolysis of equimolar gas-phase mixtures of CF_4 and CCl_4.

and I is the mean excitation potential. The term k represents the function

$$\ln \frac{m_0 \nu^2 E}{2(1-\beta^2)} - [2\sqrt{1-\beta^2} - 1 + \beta^2] \ln 2 + 1 - \beta^2 + \frac{1}{8}[1-\sqrt{1-\beta^2}]^2 \quad (3)$$

where m_0, ν, and E represent the rest mass, velocity, and energy of the incident electrons and β represents the ratio of their velocity to the speed of light in a vacuum, c. The term k was evaluated at 0.587 MeV, the average energy of the Compton electrons from ^{60}Co γ rays. The values of the mean excitation potentials for C_2H_4, CCl_4, and CF_4 were not available, but could be calculated from data on atomic excitation potentials (I_i) using the formula[23]

$$\ln I = \frac{\sum_i N_i Z_i \ln I_i}{\sum_i N_i Z_i} \quad (4)$$

where Z_i is the atomic number of element i and N_i is the number of atoms of element i per molecule. Thus, assuming ideal gases at the same temperature and pressure, the stopping power ratios were found to be

$$\frac{S(CCl_4)}{S(C_2H_4)} = 4.11 \quad (5)$$

and

$$\frac{S(CF_4)}{S(C_2H_4)} = 2.45 \quad (6)$$

All irradiations of CCl_4-CF_4 mixtures were carried out at 88° and a total pressure of 920 Torr. Equimolar mixtures of CCl_4 and CF_4 were irradiated to doses of 0.8×10^{18}–8×10^{18} eV/ml (1.6×10^{20}–1.6×10^{21} eV/g). All other samples were irradiated to a total dose of 4×10^{18} eV/ml. Irradiation times required to reach this dose were varied according to the total electron stopping power of the mixture.

Analytical Techniques. The primary analytical instrument was a MicroTek Model 2000 glc modified to include a vacuum transfer inlet system and a column effluent stream splitter/fraction collector. Qualitative identification of products was done by a combination of retention time and mass spectral analysis of the collected fractions. Quantitative analysis was performed on a 0.75 m silica gel column using peak area measurements. Sensitivity of the flame ionization detector to each of the radiolysis products was determined relative to that for CF_3Cl. Daily changes in sensitivity were monitored by making several injections of pure CF_3Cl. Variations in sensitivity seldom exceeded 5%.

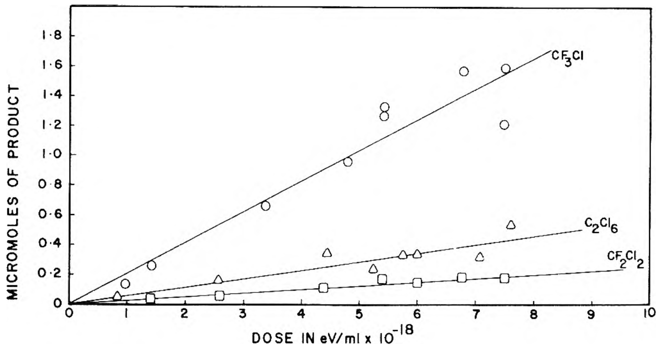

Figure 2. Yields of CF_3Cl, C_2Cl_6, and CF_2Cl_2 as a function of dose in the γ radiolysis of equimolar gas-phase mixtures of CF_4 and CCl_4.

Chlorine was measured spectrophotometrically. The contents of the radiolysis vessel were vacuum transferred into 0.5 ml of dry, deaerated CCl_4 contained in a Pyrex optical cell equipped with a Teflon vacuum stopcock. The chlorine concentration was measured by taking the optical density at 332 mμ using an extinction coefficient of 99 M^{-1} cm^{-1}.[24] The technique was checked by vacuum transferring known amounts of chlorine into the optical cell. The chlorine concentration found by spectrophotometry was within 6% of the amount predicted by *PVT* measurements. The possibility of interference by other radiolysis products was investigated by adding each compound to the optical cell and checking the optical density. No interference was observed at 332 mμ.

Results

Equimolar Mixtures of CCl_4 and CF_4. Irradiation of equimolar mixtures of CCl_4 and CF_4 was found to produce mainly CF_3Cl, CF_2Cl_2, $CFCl_3$, C_2Cl_4, and C_2Cl_6. The production of these compounds was studied over the range of doses from 0.8×10^{18} to 8×10^{18} eV/ml. Figures 1 and 2 show plots of the yield of each product in micromoles as a function of dose. Their yields were essentially linear with dose indicating that each was a primary radiolysis product that did not undergo further reaction once formed. The G values, or yields of molecules per 100 eV of energy absorbed by the system, were computed from these graphs and are summarized in Table I. The two most abundant products were found to be CF_3Cl and $CFCl_3$ with G values of 0.65 and 1.05, respectively. Trace amounts of other products were found by mass spectrometry to include C_2F_6, $C_2F_3Cl_3$, $C_2F_4Cl_2$, C_2F_5Cl, and Cl_2. The G values for these products were very small, ranging from 0.03 for Cl_2 down to 0.0003 for $C_2F_3Cl_3$. These and other G values are included in Table I to indicate that such

(23) G. J. Hine and G. L. Brownell, ref 22, p 98.
(24) A. E. Gillam and R. A. Morton, *Proc. Royal Soc., Sec. A*, **124**, 604 (1929).

TABLE I: Yields of Radiolysis Products in Equimolar Mixtures of CCl_4 and CF_4

Product	G value	Product	G value
$CFCl_3$	1.05	C_2F_6	0.006
CF_3Cl	0.65	$C_2F_3Cl_3$	0.0003
CF_2Cl_2	0.077	$C_2F_4Cl_2$	0.001
C_2Cl_4	0.14	C_2F_5Cl	0.003
C_2Cl_6	0.17	Cl_2	0.03

compounds were in fact detected, but only in very small amounts.

When 4 mol % oxygen was added to an equimolar CCl_4–CF_4 mixture and irradiated to a dose of 4×10^{18} eV/ml, the yields of all the major products were reduced by at least 90%. The measured G values in this experiment are summarized in Table II. Oxygen has been shown to act as a radical scavenger in irradiated carbon tetrachloride[25] by Spurny and in irradiated carbon tetrafluoride by Fajer, MacKenzie, and Bloch.[4] Thus it is indicated that the product precursors were primarily free radicals. The production of $COCl_2$ was also observed which is consistent with Spurny's observations that scavenging of the $CCl_3\cdot$ radicals ultimately leads to $COCl_2$ production.

TABLE II: Results of O_2 Scavenging in Equimolar Mixture of CCl_4 and CF_4

Product	G value, no oxygen	G value, 4% oxygen	Reduction of G value, %
CF_3Cl	0.65	0.024	97
CF_2Cl_2	0.08	0.006	93
$CFCl_3$	1.05	0.000	100
C_2Cl_4	0.14	0.003	98
C_2Cl_6	0.17	0.016	91

Effect of Composition in CCl_4-CF_4 Mixtures. A series of 12 mixtures whose composition ranged from pure CCl_4 to pure CF_4 were irradiated to a total dose of 4×10^{18} eV/ml. The exact compositions are shown in Table III in units of mole per cent, partial pressure, and the per cent of total absorbed energy initially deposited in the CCl_4. This last quantity is just the percentage of the total electron stopping power of the mixture that is attributable to CCl_4. Figures 3 and 4 show the G values for each of the major products plotted as a function of the per cent of the total absorbed energy initially deposited in the CCl_4. The

TABLE III: Composition of Irradiated Mixtures

Mixture no.	% of energy in CCl_4	% of energy in CF_4	$P(CCl_4)$,[a] mm	$P(CF_4)$, mm	Mol % CCl_4
1	0.0	100	0	760	0
1a	0.7	99	3.2	757	0.4
1b	2.0	98	9.0	751	1.2
2	10	90	47	713	6.2
3	25	75	126	634	16
5	40	60	216	544	28
5a	46	54	256	504	34
7a	63	37	380	380	50
9	75	25	487	273	64
11	90	10	641	119	84
13	100	0	760	0	100

[a] Pressure of CCl_4 at 24° assuming complete vaporization.

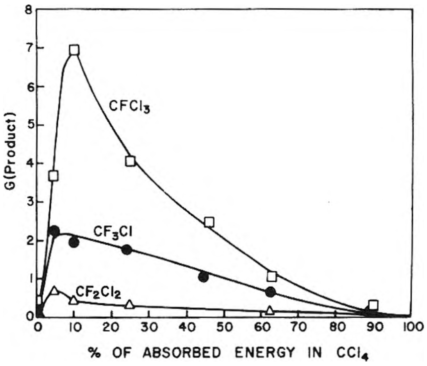

Figure 3. G values for production of $CFCl_3$, CF_3Cl, and CF_2Cl_2 as a function of mixture composition in the γ radiolysis of gas-phase mixtures of CF_4 and CCl_4 at a dose of 4×10^{18} eV/ml.

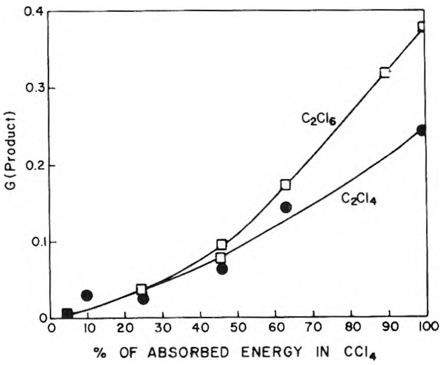

Figure 4. G values for production of C_2Cl_6 and C_2Cl_4 as a function of mixture composition in the γ radiolysis of gas-phase mixtures of CF_4 and CCl_4 at a dose of 4×10^{18} eV/ml.

yields of CF_3Cl, CF_2Cl_2, and $CFCl_3$ can be seen in Figure 3 to be strongly peaked in the region around 10% absorbed energy in CCl_4 (6.2 mol % CCl_4). By contrast, the yields of C_2Cl_4 and C_2Cl_6 (Figure 4) are small in this region and reach their maximum G values in pure CCl_4. The yields of minor products were measured for several of the irradiated mixtures and found to be similar to those found in the equimolar mixtures. The data are summarized in Table IV.

An examination of Figure 3 strongly suggests that the samples in which about 10% of the energy is absorbed in CCl_4 are likely to be more significant in understanding the radiolytic behavior of this system than are the equimolar mixtures. This suggested to us that the effect of oxygen scavenging should be investigated on such mixtures; the results are shown in Table V. It will be seen that oxygen scavenging is by no means complete in this case. Although over 92% of the CF_2Cl_2 is eliminated, scavenging of CF_3Cl and $CFCl_3$ is only about 70% complete. Mechanistic implications of these results are considered in the Discussion section.

Samples of pure CCl_4 were irradiated at 923 mm at 88° to a total dose of 4×10^{18} eV/ml. The only radiolysis products found were C_2Cl_4 (G = 0.24), C_2Cl_6 (G = 0.38), and chlorine (G = 0.03). This chlorine yield was checked on seven samples over a period of several months. In addition, the analytical techniques were checked on standard chlorine samples placed in the radiolysis vessels and were found to be quantitatively accurate. The value of the

(25) Z. Spurny, *Int. J. Appl. Radiat. Isotop.*, **14**, 337 (1963).

TABLE IV: *G* Values for Minor Products from Various Mixtures of CCl_4 and CF_4[a]

	% energy in CCl_4							
Product	0	5	10	25	46	63	75	100
C_2F_6	0.008	<0.001	<0.001	<0.001	<0.001	0.006		
C_2F_5Cl				0.003	0.002	0.003		
$C_2F_4Cl_2$			0.001	0.001		0.001		
$C_2F_3Cl_3$		0.001	0.004			<0.001		

[a] Besides the organic products listed here, all solutions containing 5% or more CCl_4 produced a small yield of Cl_2 (G = 0.01–0.03).

$G(Cl_2)$ is obviously low since a simple material balance argument leads to the equation

$$G(Cl_2) = 2G(C_2Cl_4) + G(C_2Cl_6) \quad (7)$$

which predicts a value for $G(Cl_2)$ of 0.86. This equation, of course, is based on the assumption that all chlorine-containing compounds have been identified. While it is felt that all volatile chlorine-containing molecules have been identified, there is evidence presented below that chlorine is being lost at the walls of the vessels. Thus it seems that under the present experimental conditions the G value for the accumulation of molecular Cl_2 in the gas phase is about 0.03.

TABLE V: O_2 Scavenging in Mixtures of 6 Mol % CCl_4 (10% Total Stopping Power Due to CCl_4)

Product	G value, no oxygen	G value, 4% oxygen	% of yield not scavenged
CF_3Cl	2.13	0.66	31
CF_2Cl_2	0.62	0.027	7.6
$CFCl_3$	6.9	1.40	27

Samples of pure CF_4 were also irradiated at 88° to a total dose of 4 × 10^{18} eV/ml. Initial attempts to measure the radiolysis products were hampered by the appearance of chlorine-containing products, chiefly CF_3Cl. Procedures such as rinsing the cell out with water, irradiating for extended periods of time (>48 hr) with high pressures of CF_4 (50 psig), or flaming out under high vacuum decreased the CF_3Cl yield only slightly. It was found that heating the vessels to about 600° under high vacuum in order to decompose any chlorine-containing polymer, then washing the vessels with distilled water and heating under high vacuum again reduced the yield of CF_3Cl by a factor of 30. Repetition of this treatment would not lower it further. The yield of C_2F_6 was not greatly affected by successive repetitions of the cleaning operations and the final value of $G(C_2F_6)$ was taken as 0.008.

Material Balance. The G value for the net transformation of each reactant into products can be calculated as one-fourth of the total yield of the corresponding halogen atom found in the products.

$$G(\text{incorporation } CCl_4) = \tfrac{1}{4}[3G(CFCl_3) + 2G(CF_2Cl_2) + G(CF_3Cl) + 4G(C_2Cl_4) + 6G(C_2Cl_6) + 2G(Cl_2)] \quad (8)$$

$$G(\text{incorporation } CF_4) = \tfrac{1}{4}[G(CFCl_3) + 2G(CF_2Cl_2) + 3G(CF_3Cl) + 6G(C_2F_6)] \quad (9)$$

These yields are shown respectively as open circles and triangles in Figure 5. In both cases, the yield for incorporation of CX_4 into product maximizes for mixtures containing 6 mol % CCl_4 (10% energy in CCl_4).

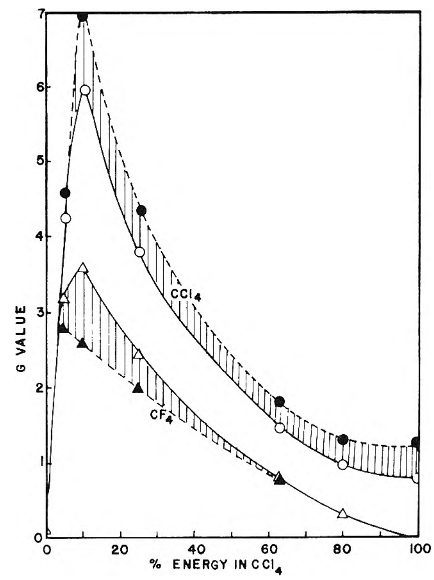

Figure 5. Material balance for incorporation of reactants into products in the γ radiolysis of gas-phase mixtures of CF_4 and CCl_4: (○, △) Cl and F incorporated into products; (●, ▲) carbon incorporated into products from CCl_4 and CF_4 (see text).

Calculation of the net rate of consumption of CCl_4 and CF_4 to give products can also be based on a count of carbon atoms, assumed to arise from the respective reactant molecule as postulated in the Discussion section.

$$G(\text{incorporation } CCl_4) = G(CFCl_3) + 2G(C_2Cl_4) + 2G(C_2Cl_6) \quad (10)$$

$$G(\text{incorporation } CF_4) = G(CF_3Cl) + G(CF_2Cl_2) + 2G(C_2F_6) \quad (11)$$

The resulting values are plotted in Figure 5 as filled circles and triangles, respectively.

It will be seen that the curve based on carbon count falls above the curve based on halogen count in the case of CCl_4, and below in the case of CF_4. This does not represent a true stoichiometric discrepancy, since reactions involving CF_4 and CCl_4 in the ratios 3:1, 1:1, and 1:3 can be written to give exclusive production of the three main products CF_3Cl, CF_2Cl_2, and $CFCl_3$, respectively. However, Figure 5 does represent a test of the extent to which the assumed mechanism is consistent with the observed yields, aside from polymer production.

Discussion

In spite of the relative simplicity of the reactants in the CF_4–CCl_4 system, a rather large number of reactions must be considered if an attempt is made to give a complete account ot the mechanism. In particular, several lines of evidence suggest that both ionic and free radical processes are involved. Mass spectrometric results[1] indicate that both CF_4 and CCl_4 dissociate under electron bombardment, giving virtually no parent ion. Accordingly, these fragmentation processes, and subsequent neutralization steps involving fragments rather than the parent molecules, must be considered. In addition, it is probable that CCl_4 acts as an electron scavenger in this system,[16] and this process leads to additional bond rupture.

It is also clear that the relative importance of the various primary processes must vary drastically across the composition range from pure CF_4 through pure CCl_4. The first indication of this behavior is given by the sharp peaking of the yield curves for the chlorofluoromethanes at high CF_4 concentration. Furthermore, Table V indicates that there is a substantial role of ionic (or other nonscavengeable) processes in the formation of the major products at high CF_4 concentrations, while Table II indicates that essentially only free-radical processes are involved in equimolar mixtures. Finally, we have unpublished results from experiments in high-pressure mass spectrometry, performed in this laboratory, that demonstrate the importance of a chloride ion transfer process in this system. Using a Bendix mass spectrometer with a high-pressure source modeled after the design of Futrell and coworkers,[26] we found strong evidence for a chloride ion transfer from CCl_4 to CF_3^+. This process, discovered in our laboratory, was subsequently confirmed by experiments on a tandem mass spectrometer in the Aerospace Research Laboratory, Wright-Patterson Air Force Base.[27]

Based on the above considerations, the following scheme is proposed to account for the initial reactions of ionized and excited species in this system

$$CF_4 \rightsquigarrow (CF_4^*) \longrightarrow CF_3\cdot + F\cdot \quad (12)$$

$$CF_4 \rightsquigarrow CF_3^+ + F\cdot + e^- \quad (13)$$

$$CF_4 \rightsquigarrow CF_2^+ + F_2\,(\text{or } 2F\cdot) + e^- \quad (14)$$

$$e^- + CCl_4 \longrightarrow CCl_3\cdot + Cl^- \quad (15)$$

$$CF_3^+ + Cl^- \longrightarrow (CF_3\cdot)^* + Cl\cdot \quad (16)$$

$$CF_2^+ + Cl^- \longrightarrow CF_2^* + Cl\cdot \quad (17)$$

$$(CF_3\cdot)^* \longrightarrow CF_2 + F\cdot \quad (18)$$

$$CF_2^* \longrightarrow CF\cdot + F\cdot \quad (19)$$

$$CF_3^+ + CCl_4 \longrightarrow CF_3Cl + CCl_3^+ \quad (20)$$

$$CCl_4 \rightsquigarrow (CCl_4^*) \longrightarrow CCl_3\cdot + Cl\cdot \quad (21)$$

$$CCl_4 \rightsquigarrow CCl_3^+ + Cl\cdot + e^- \quad (22)$$

$$CCl_3^+ + Cl^- \longrightarrow (CCl_3\cdot)^* + Cl\cdot \quad (23)$$

$$(CCl_3\cdot)^* \longrightarrow CCl_2 + Cl\cdot \quad (24)$$

$$(CCl_3\cdot)^* + CF_4 \longrightarrow CCl_3F + CF_3\cdot \quad (25)$$

Although this scheme is rather lengthy, it has been abbreviated in several respects. Obvious deactivation steps which would compete with reactions 12, 18, 19, 21, 24, and 25 are not shown. Initial fragmentation of CF_4 to give CF^+ as well as CF_2^+ and CF_3^+, and initial fragmentation of CCl_4 to give CCl_2^+ and CCl^+ must also occur, based on the mass spectra of these compounds. In fact, we wish to propose specifically that the yields of CF_2 and CF fragments are greater than the per cent abundance of CF_2^+ and CF^+ in the mass spectral fragmentation pattern would indicate.[28] This thesis is based on the assumption that neutralization of the ionic fragment feeds in additional energy which can lead to further fragmentation, as shown in the sequences 16,18 and 17,19. Similar considerations apply to the formation of CCl_2 and CCl. However, since Cl_2 is considered to be available as a radical scavenger, the fluorine-containing fragments are more significant in accounting for net product yields.

It is proposed that the various reactive fragments formed in primary processes lead to net product formation according to the following reaction scheme

$$CF_3\cdot + CCl_4 \rightarrow CF_3Cl + CCl_3\cdot \quad (26)$$

$$F\cdot + CCl_4 \rightarrow CFCl_3 + Cl\cdot \quad (27)$$

$$CF_2 + CCl_4 \rightarrow (CF_2ClCCl_3^*) \rightarrow CF_2Cl\cdot + CCl_3\cdot \quad (28)$$

$$CF\cdot + CCl_4 \rightarrow CFCl + CCl_3\cdot \quad (29)$$

$$CFCl + CCl_4 \rightarrow (CFCl_2CCl_3^*) \rightarrow CFCl_2\cdot + CCl_3\cdot \quad (30)$$

$$Cl\cdot + Cl\cdot \rightarrow Cl_2 \quad (31)$$

$$F\cdot + Cl\cdot \rightarrow ClF \quad (32)$$

$$CCl_3\cdot + Cl_2 \rightarrow CCl_4 + Cl\cdot \quad (33)$$

$$CCl_2F\cdot + Cl_2 \rightarrow CCl_3F + Cl\cdot \quad (34)$$

$$CF_2Cl\cdot + Cl_2 \rightarrow CF_2Cl_2 + Cl\cdot \quad (35)$$

$$CCl_3\cdot + CCl_3\cdot \rightarrow C_2Cl_6 \quad (36)$$

$$CCl_2 + CCl_4 \rightarrow (C_2Cl_6^*) \quad (37)$$

$$C_2Cl_6^* \rightarrow C_2Cl_4 + Cl_2 \quad (38)$$

$$ClF\,(\text{or } F_2) + CCl_4 \rightarrow CCl_3F + Cl_2\,(\text{or } ClF) \quad (39)$$

Again, although this set of reactions is quite lengthy there are several abbreviations. Thus fates of excited C_2Cl_6 formed in reaction 37 must include deactivation (stabilizing C_2Cl_6) and decomposition to two $CCl_3\cdot$ radicals.

In addition to the oxygen scavenger effects reported here, basing the scheme of secondary reactions on free-radical processes can be justified to a considerable extent from earlier work. It has been well established from scavenger studies[11] and studies of the radiolysis of CCl_4 mixed with alkanes[9] or chloroform[29] that trichloromethyl radicals and chlorine atoms are produced. Similarly, the irra-

(26) J. H. Futrell, T. O. Tiernan, R. P. Abramson, and C. Dean Miller, *Rev. Sci. Instrum.*, **39**, 340 (1968).

(27) B. M. Hughes, private communication.

(28) In the mass spectrometer, considerable time (typically several microseconds) is available during which vibrational quanta distributed throughout an excited ion can "collect" in a single bond, causing it to rupture. Under radiolysis conditions the time between collisions is several orders of magnitudes shorter than this, and excited ions may react or be deactivated before they can fragment. This model applies, however, only to species of moderate complexity, C_3 or C_4 hydrocarbons or beyond. The CF_4^+ ion has so few vibrational modes that any fragmentation process which is energetically possible should occur very rapidly. Hence, primary fragmentation of CF_4^+ may be nearly as great at 100 Torr as at 10^{-6} Torr.

(29) F. J. Johnston, T. Chen, and K. Wong, *J. Phys. Chem.*, **65**, 728 (1961).

diation of CF_4 has been shown to produce primarily trifluoromethyl radicals and fluorine atoms.[4,30]

Reactions 26-30 emphasize the reason why net product yields in this system maximize at high CF_4 concentrations—that is, fragments of CF_4 decomposition efficiently attack CCl_4 to yield observable products, whereas the products of CCl_4 fragmentation are relatively inert toward CF_4.[18] Reaction 26, previously proposed by Alcock and Whittle, is 15 kcal/mol exoergic, calculated from standard heats of formation.[32] We postulate that this is the usual fate of $CF_3\cdot$ radicals, although some reaction with Cl_2 might occur. We suggest that CCl_3, $CFCl_2$, and probably also CF_2Cl radicals usually react with Cl_2, as shown in eq 33, 34, and 35. A small portion of the $CCl_3\cdot$ radicals probably encounter each other before being scavenged, and combine to form C_2Cl_6 as shown in eq 36. This assumption has usually been made for the radiolysis of pure CCl_4 in the liquid phase.[8-11]

Direct attack on CCl_4 by fluorine atoms, shown in eq 27, appears to be an obvious route to production of CCl_3F. The reaction should be quite efficient since it can be calculated to be 31 kcal exoergic, and there is no reason to expect an unusually small steric factor. Analogous reactions have been proposed by Bigelow in the fluorination of various chlorocarbons.[33] There is likely to be some ClF present, formed by reaction 32 or in several other ways. We have also seen evidence for ClF in glow-discharge studies of the CCl_4–CF_4 system, as described elsewhere.[18] Murray[34] has observed direct fluorination of various chlorofluorobutanes by chlorine monofluoride in nickel vessels and it appears reasonable to represent the process as in eq 39. Both F_2 and ClF would doubtless be excellent free-radical scavengers in this system, but they are unlikely to persist or build up to appreciable concentration. Finally, we have seen some evidence[18] for production of CCl_3F by reaction of excited $CCl_3\cdot$ radicals with CF_4 (reaction 25), but this is not likely to account for a major portion of the substantial yield of this product.

It is difficult to envisage a one-step mechanism for the formation of CF_2Cl_2, and we suggest a sequential route *via* difluorocarbene, shown in eq 28 and 35. Not surprisingly, the yield of this compound is considerably lower than either CF_3Cl or CCl_3F.

Although we believe that the reaction scheme presented for the formation of the chlorofluoromethanes is qualitatively satisfactory, there are problems concerning the magnitudes of the yields. Although, as mentioned earlier, the results do not violate stoichiometry in the strict sense, the reaction scheme described would require certain relationships between the yields. In particular, the yield of CCl_3F should equal the yield of CF_3Cl plus twice the yield of CF_2Cl_2. For the maximum yield mixture this would be 2.13 plus twice 0.62, or a total predicted G value of 3.37. The actual yield, in contrast, is 6.9.

This dilemma can be solved in principle by assuming that some of the CCl_3F is formed *via* $CF\cdot$ fragments *via* the sequence 29, 30, 34. Since one $CF\cdot$ fragment would lead to production of four molecules of CCl_3F, a G value of 0.9 for CF fragments would account for all of the "surplus" of CCl_3F. Although we believe that there is a significant yield of $CF\cdot$ fragments in this system, the yield is not likely to be as large as 0.9. By comparison with the CCl_2F_2 yield of 0.62, which presumably represents CF_2 fragments, a yield of perhaps 0.2 or 0.3 would be more reasonable. This would account for at most a yield of 1.2 for CCl_3F, so that something over 2 G units of CCl_3F is still not accounted for.

It is postulated that the "extra" fluorine atom yield, which is required to form CCl_3F, corresponds to CF_2 (or CF) fragments involved in polymer formation. A polymer composed of $-(CF_2)-$ units with no cross linking and no chlorine bound in it, with a yield of about 1.0 for CF_2 units, would essentially solve the material balance problems. If there were some cross linking, or if the polymer contains some $-(CFCl)-$ units (which we suspect it does) then a yield somewhat below 1.0 would suffice.

In the Results section we mentioned some evidence tbat a polymer containing some chlorine accumulated in the radiolysis vessels. It can also be mentioned that rapid evolution of a gas was noted when the vessels were heated to about 500° under vacuum. This occurred whether or not the vessels had been under vacuum for 24 hr and subjected to mild heating (about 100 to 200°). Polymers of the general formula $(-CF-CF_2-)_n$ or $(-CF-CFCl-)_n$ would be expected to behave in this manner.[35] We have already postulated the role of CF_2, CFCl, and CCl_2 in this system. Difluorocarbene has been observed in numerous systems activated by thermolysis, photolysis, and a glow discharge, and is known to dimerize to C_2F_4 (which can then polymerize) or to add directly to a growing polymer chain.[36-38]

Dichlorocarbene has been reported by Wescott and Skell[39] in the pyrolysis of CCl_4 and by this laboratory[40] in photolysis below 2000 Å. These radicals are known to dimerize,[41] and it is reasonable to conclude that they could be bound into a growing polymer, as in the case of CF_2, although the dimer C_2Cl_4 shows only slight tendency to polymerize.[42] While there is no direct evidence on CFCl, it probably has properties similar to the other two carbenes.[43]

Turning to the two-carbon products, it is assumed that C_2Cl_6 is formed by combination of CCl_3 radicals, as mentioned above; this has been assumed in the liquid-phase radiolysis as well.[8-11] Insertion of CCl_2 into C–H bonds has been seen by Fields,[42] giving some justification for reaction 37. The formation of C_2Cl_4 from excited C_2Cl_6, shown in eq 38, was proposed previously by Firestone.[11]

The other ethanes, C_2F_6, C_2F_5Cl, $C_2F_4Cl_2$, and $C_2F_3Cl_3$, are extremely minor products. All of their yields are

(30) R. W. Fessenden and R. H. Schuler, *J. Chem. Phys.*, **43**, 2704 (1965).
(31) W. G. Alcock and E. Whittle, *Trans. Faraday Soc.*, **62**, 134 (1966).
(32) J. Heicklen, *Advan. Photochem.*, **7**, 57 (1969).
(33) Several references to work of this type are given in a review paper by L. A. Bigelow, "Fluorine Chemistry," Vol. 1, J. H. Simons, Ed., Academic Press, New York, N.Y., 1950, p 373.
(34) J. M. Muray, *J. Chem. Soc.*, 1884 (1959).
(35) C. R. Patrick, *Advan. Fluorine Chem.*, **2**, 1 (1961).
(36) F. W. Dalby, *J. Chem. Phys.*, **41**, 2297 (1964).
(37) W. J. Martin and H. A. McGee, *J. Phys. Chem.*, **72**, 739 (1968).
(38) L. Wescott and P. Skell, *J. Amer. Chem. Soc.*, **87**, 1721 (1965).
(39) D. D. Davis and R. J. Hanrahan, presented at the 153rd National Meeting of the American Chemical Society, Miami Beach, Fla., April 1967, Paper No. 89, Division of Physical Chemistry.
(40) J. S. Shapiro and F. P. Lossing, *J. Phys. Chem.*, **72**, 1552 (1968).
(41) G. Owen, J. Pearson, and M. Swarc, *Trans. Faraday Soc.*, **61**, 1722 (1965).
(42) E. K. Fields, *J. Amer. Chem. Soc.*, **84**, 1744 (1962).

(43) One of the referres suggested that the chlorine deficit is accounted for by formation of $NiCl_2$ on the walls. We feel that the possibility of chlorine reacting with the walls is greatly diminished by the fact that they are probably prefluorinated (due to radiolysis of CF_4) as well as coated with a rather inert fluorocarbon or chlorofluorocarbon polymer. Furthermore, the fact that chlorine was not effectively removed from the walls by simple washing, but was removed by pyrolysis followed by washing, argues strongly for organically rather than inorganically bound chlorine.

below 0.01 G units in all cases. Unfortunately, we were not able to make any conclusions about the effects of oxygen on their yields. In considering the formation of these compounds by radical combination, we note that the probable order of steady-state concentrations predicted by our reaction scheme, considering both rate of formation and reactivity, would probably be [$CCl_3\cdot$] > [$CF_3\cdot$] > [CF_2Cl] > [$CFCl_2$]. Thus it is reasonable to ascribe C_2Cl_6, CF_3CCl_3, and the rather uncertain yield of C_2F_6 to combination. However, there is doubt about the other cases, since (for example) CCl_3–CF_2Cl is not found yet $C_2F_4Cl_2$ does occur. We tentatively suggest that $C_2F_4Cl_2$ and C_2F_5Cl are formed by addition of Cl_2 and ClF to a small amount of C_2F_4 present in the steady state.

Returning briefly to the O_2 scavenging experiments, we propose that chloride ion transfer reaction 20 accounts for the nonscavengable yield of CF_3Cl in the 6% CCl_4 mixtures. The fact that CF_3Cl is completely scavengeable in equimolar mixtures presumably indicates that this reaction does not occur under these circumstances. Furthermore, reaction of fluorine atoms with substrate CCl_4 (eq 27) should be very hard to scavenge, yet the yield of $CFCl_3$ is also near zero when O_2 is added to equimolar mixtures. These observations strongly suggest that precursor states of CF_4, possibly the transient ion CF_4^+ or superexcited electronic states, are protected by the presence of high concentrations of CCl_4. Indeed, Figures 3–5 strongly suggest such behavior. The process would almost certainly be sacrificial protection, leading to fragmentation of CCl_4. We have seen in glow-discharge experiments that fragments from CCl_4 have some capacity to attack CF_4, but with much less efficiency than the inverse case (attack of fragments from CF_4 on CCl_4).[18] Reaction 25 would be followed by reaction 26, accounting for both CCl_3F and CF_3Cl. It is admitted that this scheme is speculative; a complete interpretation of the difference in O_2 scavenging in the 6% CCl_4 and 50% CCl_4 mixtures is, we feel, the main unanswered question in this work.

Acknowledgment. This work was supported by AEC Contract No. AT-(40-1)-3106 and by the University of Florida Nuclear Science Program. This is Document No. ORO-3106-40.

Dealkylation of Isopropylbenzene on γ-Irradiated Silica–Alumina. The Effect of Various Reagents on the Active Centers and on Their Yield

Enrique A. Rojo and Robert R. Hentz*

Comisión Nacional de Energía Atómica, Buenos Aires, Argentina, and Department of Chemistry and the Radiation Laboratory,[1] *University of Notre Dame, Notre Dame, Indiana 46556* *(Received April 14, 1972)*

Publication costs assisted by the U. S. Atomic Energy Commission

A silica–alumina gel was exposed to a gaseous reagent during or after γ irradiation, and the yield of benzene (molecules formed per gram of solid) on subsequent exposure to isopropylbenzene was determined. The following reagents were used: N_2, H_2, O_2, CO_2, N_2O, C_2H_4, NH_3, H_2S, CO, and SO_2. In general, effects of the reagents on the benzene yield correlate with previously reported effects of the same reagents (for corresponding conditions) on the positive-hole esr spectrum of the irradiated silica–alumina. The esr spectrum includes contributions from a positive hole trapped on a bridging oxygen atom bonded to a substitutional Al atom and from certain positive holes trapped on nonbridging oxygen. Certain of the results indicate that the yield of benzene from contact of isopropylbenzene with silica–alumina irradiated alone, like the yield of trapped positive holes seen in the esr spectrum, is limited by the number of preexisting electron traps in the silica–alumina matrix. The total results seem to require that electron transfer from isopropylbenzene to a trapped positive hole (of any kind contributing to the esr spectrum) be the primary process in isopropylbenzene dealkylation on γ-irradiated silica–alumina.

Introduction

Irradiation of silica–alumina gel with ^{60}Co γ rays imparts a very dark, essentially black, color to the solid, and subsequent introduction of isopropylbenzene bleaches the solid with concomitant formation of benzene.[2] With increase in radiation dose to the silica–alumina gel, the number of molecules of benzene produced per gram of solid increases to a limiting value designated the plateau yield.[3] Such phenomena are associated not with impurity content but with properties inherent in the structure or composition of the silica–alumina gel that are sensitive to variations in the preparation and pretreatment tech-

(1) The Radiation Laboratory of the University of Notre Dame is operated under contract with the U. S. Atomic Energy Commission. This is AEC Document No. COO-38-827.

(2) R. R. Hentz, *J. Phys. Chem.*, **66**, 2714 (1962).
(3) R. R. Hentz, *J. Phys. Chem.*, **68**, 2889 (1964).

niques[3] and to age of the solid (stored in a closed bottle with atmospheric gases at room temperature).[4] The results suggest that benzene yields are limited by the number of certain preexisting defects in the silica-alumina matrix (*e.g.*, traps for electrons or positive holes) that are populated by γ irradiation.[3,5] Moreover, though exposure of γ-irradiated silica-alumina to oxygen has no effect on either color of the solid or the amount of benzene formed on subsequent exposure to isopropylbenzene, exposure to hydrogen bleaches γ-irradiated silica-alumina and reduces the amount of benzene formed on subsequent exposure to isopropylbenzene.[4] The same reduced yield of benzene is obtained on exposure of thermally bleached γ-irradiated silica-alumina to isopropylbenzene.[4] Thus, the dealkylation of isopropylbenzene is associated with centers that do not absorb in the visible as well as with centers that do.

The esr spectrum of γ-irradiated silica-alumina gel consists of a narrow trapped-electron signal at g = 2.0010 and a broad (width of 44.5 G) positive-hole spectrum at g = 2.0088 which includes a partially resolved six-line component with a splitting of 8.5 G.[6] More than one kind of center contributes to the positive-hole esr spectrum. As noted with respect to the almost identical esr spectrum of irradiated aluminosilicate glasses,[7] the six-line component indicates presence of the center observed by Griffiths, *et al.*,[8] in irradiated quartz single crystals and identified by O'Brien and Pryce[8] as a positive hole trapped on a bridging oxygen atom that is bonded to a substitutional Al^- ion. The esr spectrum of this center, designated the Al positive-hole center, is removed by contact of irradiated silica-alumina gel with hydrogen[6] or by thermal annealing of irradiated aluminosilicate glass,[7] and a spectrum remains that is attributed to a positive hole trapped on nonbridging oxygen.[6,7,9]

In an esr study of γ-irradiated silica-alumina gel,[6] behavior of the esr signal of the Al positive-hole center was found, without exception, to parallel behavior of the visible coloration on exposure of the irradiated solid to each of 18 reagents and on irradiation in the presence of each of 12 reagents. Thus, as in irradiated quartz,[8] Al positive holes appear to be the centers that absorb in the visible. Further, results of the esr study indicate that the yield of trapped positive holes is limited by the availability of electron traps and that trapped positive holes can be neutralized by electron transfer from certain reagents (including isopropylbenzene).[10,11] Such results suggest that electron transfer from isopropylbenzene to a trapped positive hole (of any kind contributing to the esr spectrum) is the primary step in isopropylbenzene dealkylation on γ-irradiated silica-alumina gel. Then the yield of benzene, like the yield of trapped positive holes, should be limited by the availability of electron traps.

In the work reported in the present paper, inferences from the previous work[2-6] have been subjected to further test. Silica-alumina gel has been exposed during or after γ irradiation to ten of the reagents used in the esr study,[6] and the yield of benzene on subsequent exposure to isopropylbenzene has been determined. Effects of the reagents on the dealkylation yield and the esr spectrum, for corresponding conditions, are compared.

Experimental Section

The silica-alumina used in this work is a conventional catalyst with 10 wt % alumina and a surface area of 400 m^2/g (solid A of a previous publication in which its properties are described[3]). Purification of isopropylbenzene has been described.[12] All gases were obtained from Matheson Co. Gases noncondensable at 77°K were dried by passage through a silica gel column and through traps at 77°K. Condensable gases were passed through a silica gel column and were purified by trap-to-trap distillation at 77°K with the middle fraction being retained for use.

The general procedures, including dosimetry and gas-chromatographic determination of benzene, have been described.[2-6,13] A brief review of the most pertinent features follows. Materials were irradiated at room temperature with a ^{60}Co source. The silica-alumina was first heated for about 20 hr at 500° in air. Then 2 g of the solid in a 13-mm o.d. Pyrex tube with break-seal was evacuated at 10^{-6} Torr and 500° for 18-20 hr. Gaseous reagents were introduced, either before or after irradiation, at a pressure of 150 Torr as in the esr study.[6] Gases added after γ irradiation were kept in contact with the silica-alumina for 1 hr. Prior to introduction of another gas or isopropylbenzene, gas in contact with silica-alumina was removed by pumping the reaction cell on a high-vacuum line for 3-4 hr or until there was no increase in pressure for several minutes after isolation of the reaction cell from the pumping system. Removal of gaseous reagents or their reaction products was not always complete as shown by unusual color changes, in some cases, in subsequent treatment of the silica-alumina with isopropylbenzene and by the odor of NH_3 and SO_2, in experiments with these gases, in the recovered isopropylbenzene. Isopropylbenzene (0.2 g) was degassed by the conventional freeze-pump-thaw technique, dried over a fresh sodium surface, and transferred to the silica-alumina by means of liquid nitrogen on the reaction cell. Isopropylbenzene and silica-alumina remained in contact for 1 hr at room temperature. Then, a boiling-water bath was placed around the reaction cell and isopropylbenzene and products were collected for 1 hr in an adjacent trap at 77°K. Such a procedure gives quantitative recovery of benzene.

Results and Discussion

As observed in previous work, the silica-alumina is darkened by irradiation and with increase in dose the yield of benzene increases to a limiting value, the plateau yield. Table I gives benzene yields obtained from contact of γ-irradiated silica-alumina with isopropylbenzene after exposure of the solid to various reagents during or after irradiation. In all experiments in Table I, the dose exceeded that required ($\sim 1 \times 10^{21}$ eV g^{-1}) to attain the plateau yield of positive holes[6] and benzene. No benzene was ob-

(4) R. R. Hentz, L. M. Perkey, and R. H. Williams, *J. Phys. Chem.*, **70**, 731 (1966).
(5) E. A. Rojo and R. R. Hentz, *J. Phys. Chem.*, **70**, 2919 (1966).
(6) R. R. Hentz and D. K. Wickenden, *J. Phys. Chem.*, **73**, 817 (1969).
(7) S. Lee and P. J. Bray, *Phys. Chem. Glasses*, **3**, 37 (1962).
(8) J. H. E. Griffiths, J. Owen, and I. M. Ward, "Bristol Conference on Defects in Crystalline Solids," The Physical Society, London, 1955, p 81; M. C. M. O'Brien and M. H. L. Pryce, *ibid.*, p 88.
(9) J. Vedrine, G. Dalmai, C. Naccache, and B. Imelik, *J. Chim. Phys.*, **65**, 2129 (1968), suggest that six positive-hole centers, including the Al center, contribute to the positive-hole esr spectrum of irradiated silica-alumina gel.
(10) Disappearance of visible coloration and the Al positive-hole esr spectrum on exposure of γ-irradiated silica-alumina gel to various reagents is accompanied by a luminescence which has been attributed to neutralization of the Al positive-hole center by an electron donated by the reagent at the solid surface.[11]
(11) R. R. Hentz and S. B. Ziemecki, *J. Phys. Chem.*, **74**, 3552 (1970).
(12) R. R. Hentz, *J. Phys. Chem.*, **66**, 1622 (1962).
(13) R. R. Hentz, *J. Phys. Chem.*, **66**, 1625 (1962).

TABLE I: Benzene Yields Obtained from Contact of γ-Irradiated Silica–Alumina with Isopropylbenzene after Exposure of the Solid to Various Reagents during or after Irradiation[a]

Expt no.	Reagent[b] A	Reagent[b] B	Benzene yield[c]
1	. .	. .	8.6
2	N_2	. .	8.5
3	. .	N_2	8.7
4	. .	H_2	5.3
5	H_2	. .	1.5
6	O_2	. .	26.0
7[d]	O_2	. .	26.0
8	O_2	H_2	5.6
9	CO_2	. .	24.8
10	CO_2	H_2	5.1
11	. .	CO_2	8.4
12	N_2O	. .	27.5
13	. .	N_2O	8.6
14	C_2H_4	. .	0.0
15[e]	. .	C_2H_4	0.0
16	NH_3	. .	0.0
17	. .	NH_3	0.0
18	H_2S	. .	0.0
19	. .	H_2S	0.0
20	CO	. .	8.6
21	. .	CO	7.8
22	SO_2	. .	8.8
23	. .	SO_2	7.9

[a] In all experiments the dose exceeded that required ($\sim 1 \times 10^{21}$ eV g^{-1}) to attain the plateau yield of positive holes and of benzene. [b] Reagents were present at 150 Torr; those in column A were present during irradiation and those in column B were introduced after irradiation. [c] Units are 10^{17} molecules of benzene per gram of silica–alumina. [d] After irradiation O_2 was removed and the silica–alumina was again irradiated to a saturation dose before addition of isopropylbenzene. [e] Owing to the large adsorption of C_2H_4, a second portion was required.

tained from contact of unirradiated silica–alumina with isopropylbenzene.

Discussion of the present results is facilitated by use of the following model which was proposed in the esr study[6] for interpretation of results obtained in radiation studies with silica–alumina gel. Radiation generates H atoms, mobile electrons, and mobile positive holes in the silica–alumina. The mobile positive hole may be thought of as an O^- ion the position of which moves through the solid by electron-transfer processes until the hole is trapped at a site of lower energy, *e.g.*, on a bridging oxygen atom bonded to a substitutional Al atom[7,8] or on some kind of nonbridging oxygen atom.[7,9] The Al positive-hole center absorbs in the visible and contributes the six-line component to the positive-hole esr spectrum; certain positive holes trapped on nonbridging oxygen, that do not absorb in the visible, are responsible for the positive-hole esr spectrum left after exposure of irradiated silica–alumina to hydrogen. An equal number of electrons is trapped and most of these are trapped in such a way as to escape detection in the esr spectrum. At room temperature, H atoms react with some kind of defect at which ionization occurs to give the tapped-electron signal at $g = 2.0010$.

The presence of N_2 during irradiation or the introduction of N_2 after irradiation has no effect on the visible coloration or esr spectrum of irradiated silica–alumina.[6] Thus, N_2 does not react with any of the mobile or trapped species. Accordingly, benzene yields in experiments 2 and 3 do not differ significantly from that in experiment 1.

The benzene yield in experiment 4 is substantial but is less than that in experiment 1. Because exposure of irradiated silica–alumina to isopropylbenzene removes the color and the *entire* positive-hole esr spectrum,[6] the result of experiment 4 indicates that benzene formation is associated with both the Al positive-hole centers and those positive holes trapped on nonbridging oxygen that are left after H_2 has neutralized the Al center. Comparison of the benzene yields in experiments 4 and 5 indicates that H_2 present during irradiation intercepts the mobile positive holes that are precursors of the trapped positive holes involved in benzene formation. In accord with such conclusions, irradiation of silica–alumina in the presence of H_2 gives no visible coloration and an ill-defined broad signal of very low intensity in the region of the positive-hole esr spectrum.[6]

The results in experiments 1 and 4 also confirm the earlier observation[4] that radiation-induced dealkylation activity associated with visible coloration decreases with age of the unirradiated silica–alumina while that not associated with visible coloration is not affected. The plateau yield of benzene in experiment 1 is 8.6×10^{17} molecules/g compared with that of 13×10^{17} molecules/g last obtained;[4] however, the yield in experiment 4 of 5.3×10^{17} molecules/g, after exposure of irradiated silica–alumina to H_2, is the same as that last obtained in such an experiment.[4] Consequently, the benzene yield associated with visible coloration is now 3×10^{17} molecules/g, compared with the earlier 8×10^{17} molecules/g, and is now less than the age-independent yield not associated with visible coloration.

The presence of C_2H_4, NH_3, or H_2S during irradiation of silica–alumina or their introduction after irradiation results in elimination of visible coloration and the *entire* positive-hole esr spectrum.[6] Consequently, the absence of detectable benzene formation in experiments 14–19 provides additional support for the identification of benzene formation with all positive-hole centers that contribute to the esr spectrum.

Exposure of irradiated silica–alumina to such effective electron scavengers as O_2, CO_2, or N_2O has no effect on the visible coloration or esr spectrum.[6] Accordingly, dealkylation yields are not affected by prior exposure of the irradiated solid to O_2 (as shown in previous work[4]) or to CO_2 or N_2O (as shown in experiments 11 and 13). However, when silica–alumina is irradiated in the presence of O_2, CO_2, or N_2O, the solid becomes very much darker and height of the positive-hole esr signal is 2–3 times greater than that obtained in irradiation of silica–alumina alone to the same dose.[6] From such results it was argued that the yield of trapped positive holes is limited by the availability of electron traps; O_2, CO_2, and N_2O, when present during irradiation, function as additional traps for mobile electrons and thereby enhance the visible coloration and positive-hole esr signal. Results obtained in the present work are consistent with such results and conclusions of the esr study and provide still more evidence for involvement of trapped positive holes in the dealkylation of isopropylbenzene. With increase in radiation dose to silica–alumina in the presence of O_2, it was found that the benzene yield (from subsequent exposure of the irradiated solid to isopropylbenzene) increases and attains a plateau at a dose about the same as that required for attainment of the plateau in irradiation of silica–alumina alone. The plateau yield obtained with O_2 present during irradiation, *cf.* experiment 6, is 3 times greater than that in experiment 1. Such results, and the results of experiments 9 and 12, indicate that the benzene yield from silica–alumina irradiated alone, like the yield of trapped positive holes, is limited by the number of preexisting electron traps. The approximate equality of plateau yields in experiments 6, 9 and 12 suggests that (1) O_2, CO_2, and N_2O trap mobile electrons only at certain surface sites (that are limited in number) and remain bound to, thereby blocking, the site or (2) the number of preexisting positive-hole traps becomes the limiting factor with the electron scavengers present during irradiation. It is interesting that, as shown in experiments 8 and 10, the presence of electron scavengers during irradiation enhances the yield of only those dealkylation centers that are removed by exposure to H_2. Experiment 7 shows that electrons trapped by irradiation in the presence of O_2 are not freed by a second irradiation after pumping O_2 from the reaction cell.

On exposure of irradiated silica–alumina to CO or SO_2, height of the positive-hole esr signal decreases to ~85% of the original value and there is a slight bleaching of the visible coloration;[6] as shown in experiments 21 and 23, there is a corresponding small reduction in benzene yield. Because of the absence of visible coloration on irradiation of silica–alumina in the presence of CO or SO_2 and the appearance of a very intense new esr signal attributed to CO_2^- or SO_3^-, respectively, it was suggested that CO and SO_2 are very effective traps for the mobile positive hole (unstabilized O^-).[6] Thus, equality of the benzene yields in experiments 1, 20, and 22 suggests that the positive holes trapped by CO and SO_2 also are effective in isopropylbenzene dealkylation (the total yield of trapped positive holes and, therefore, of benzene being limited by the number of preexisting electron traps).

Results of the present study, then, provide strong support for the ideas developed in previous work.[2-6] The yield of benzene from contact of isopropylbenzene with irradiated silica–alumina, like the yield of trapped positive holes, does indeed appear to be limited by the number of preexisting electron traps. The total results seem to require that electron transfer from isopropylbenzene to a trapped positive hole (of any kind contributing to the esr spectrum) be the primary process in isopropylbenzene dealkylation on γ-irradiated silica–alumina.

Electronic Spectra of Trapped Electrons in Organic Glasses at 4°K. III. Effect of an Electron Scavenger in Ethanol

Takenobu Higashimura,* Akira Namiki, Masato Noda, and Hirotomo Hase

Research Reactor Institute, Kyoto University, Kumatori-cho, Sennan-gun, Osaka, Japan *(Received April 18, 1972)*

Publication costs assisted by the Research Reactor Institute, Kyoto University

Optical absorption measurements were carried out on e_t^- and e_{sol}^- in ethanol glasses containing solute BzCl at 4 and 77°K. The electron scavenging efficiency for the γ radiolysis at 4°K is about 4 times larger than for the radiolysis at 77°K and depends slightly on the wavelength of the absorption band. The temperature dependence of the efficiency is tentatively attributed to that of the scavenging cross section obeying the $1/v$ law and/or to that of trapping cross section affected by lattice phonon interaction.

Introduction

At such a very low temperature as 4°K or in a very early stage at low temperature in organic glasses, electrons are stabilized in shallow traps where surrounding molecular dipoles are not relaxed.[1-10] Such trapped electrons in unrelaxed traps are confirmed by their optical absorption spectra[4-10] and esr spectra[1-3,6] which are much different from those of ordinary solvated electrons observed at 77°K. In glasses containing a small amount of electron scavenger, competitive reactions of electrons occur between the scavenger molecules, positive holes, and traps. Knowledge of the scavenging efficiency in these competetive processes affords information on the nature of electron traps because the efficiency will depend on both trapping and scavenging cross sections.

The efficiency of electron scavenging by biphenyl in 2-methyltetrahydrofuran glass was found to be about four times as large for irradiation at 4°K as that at 77°K.[11] The result implies that the efficiency of electron scavenging at 4°K is larger than at 77°K. However there remains

(1) D. R. Smith and J. J. Pieroni, *Can. J. Chem.*, **45**, 2723 (1967).
(2) H. Yoshida and T. Higashimura, *Can. J. Chem.*, **48**, 504 (1970).
(3) T. Higashimura, M. Noda, T. Warashina, and H. Yoshida, *J. Chem. Phys.*, **53**, 1152 (1970).
(4) H. Hase, M. Noda, and T. Higashimura, *J. Chem. Phys.*, **54**, 2975 (1971).
(5) H. Hase, M. Noda, T. Higashimura, and K. Fueki, *J. Chem. Phys.*, **55**, 5411 (1971).
(6) H. Hase, T. Warashina, M. Noda, A. Namiki, and T. Higashimura, *J. Chem. Phys.*, **57**, 1039 (1972).
(7) J. T. Richards and J. K. Thomas, *J. Chem. Phys.*, **53**, 218 (1970).
(8) J. H. Baxendale and P. Wardman, *Nature (London)*, **230**, 449 (1971).
(9) L. Kevan, *Chem. Phys. Lett.*, **11**, 140 (1971).
(10) L. Kevan, *J. Chem. Phys.*, **56**, 838 (1972).
(11) H. Yoshida, M. Ogasawara, T. Warashina, and T. Higashimura, *J. Chem. Phys.*, **56**, 4238 (1972).

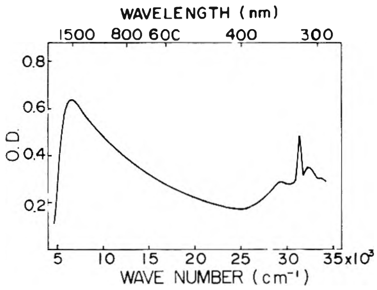

Figure 1. Optical absorption spectrum of ethanol glass containing 0.01 mol % BzCl. The γ irradiation and measurement were carried out at 4°K. The total dose was 0.23 Mrad.

another possibility that the higher efficiency may be caused from additional capture in the course of warming the sample from 4 to 77°K, because concentrations of trapped electrons and anions were determined by measurements at 77°K.

In this investigation, effects of solute benzyl chloride (BzCl) on the trapped electron band in ethanol glass at 4 and 77°K are reported and efficiency of electron scavenging is compared for irradiation and measurement at 4°K with those at 77°K. The temperature dependence of the efficiency is discussed according to the temperature dependence of scavenging and trapping cross sections.

Experimental Section

Reagent grade ethanol was used without further purification. Reagent grade BzCl was purified by ordinary fractional distillation methods. Disk samples of 0.2 cm thickness were made in liquid nitrogen and were then immersed and fixed in liquid helium.[4] Both irradiation by γ rays and optical absorption measurements at 4°K were performed with the same optical dewar as described before.[4] The total γ dose was 0.23 Mrad for the irradiation at 4°K and 0.34 Mrad at 77°K.

Results and Discussion

When ethanol glass containing a small amount of BzCl is irradiated and measured at 4°K, the observed optical absorption band extending from 2000 nm to 300 nm consists of two well separated bands as shown in Figure 1. The broad band extending from the near-infrared to the visible region is due to electrons in unrelaxed traps, and the sharp absorption band around 310 nm is for benzyl radicals.[12] As the concentration of BzCl increases, the band of benzyl radicals increases in intensity. Concomitantly, the electron band decreases in intensity over the whole region as shown in Figure 2. It is noted that the infrared part of the band which is responsible for electrons in shallow, unrelaxed traps is quenched more efficiently than the visible part responsible for electrons in deep, unrelaxed traps.

The decrease of the trapped electron band and consequently the increase of the radical bands in intensity are much more sensitive to a change in concentration of BzCl for radiolysis at 4°K than for radiolysis at 77°K. The electron band is almost eliminated at a concentration of 0.10 mol % BzCl at 4°K, whereas the band decreases in intensity to half of that in pure ethanol glass at the same concentration of BzCl at 77°K.

Because the detrapping process which can compete with the trap relaxation is not important,[6] the behavior of mobile electrons, until they are stabilized or disappear, in

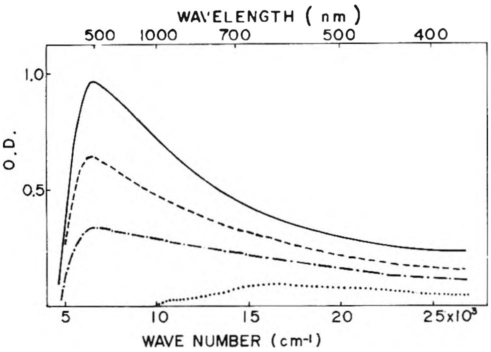

Figure 2. Optical absorption spectra of ethanol glass containing 0.01 (- - - -), 0.03 (- · - · -) and 0.1 mol % (· · · ·) BzCl, together with the spectrum for pure ethanol (——). The γ irradiation and measurements were carried out at 4°K. Total γ dose was 0.23 Mrad for each sample.

ethanol glass containing BzCl is described as

$$e_m^- \longrightarrow \begin{cases} e_t^- \longrightarrow e_{sol}^- & (1) \\ \text{neutralization} & (2) \\ \text{captured by BzCl} \longrightarrow \text{benzyl radicals} & (3) \end{cases}$$

where e_t^- and e_{sol}^- denote the electrons in unrelaxed and relaxed traps, respectively.

Reactions 1 and 3 obey second-order kinetics with rates of $k_t[\mathrm{T}]$ and $k_s[\mathrm{S}]$, where [T] and [S] denote concentration of preformed, unrelaxed traps and of scavenger molecules, respectively. Reaction 2 includes recombination with both the parent cations $C_2H_5OH^+$ and cations $C_2H_5OH_2^+$. These cations are expected to distribute spatially close to each other. Reaction 2 is regarded as a first-order reaction with rate constant of k_r. Thus the yield of e_t^- is given by

$$G(e_t^-) = G(e_m^-)\,\frac{k_t[\mathrm{T}]}{k_t[\mathrm{T}] + k_r + k_s[\mathrm{S}]} \tag{4}$$

The efficiency of electron scavenging, α, is defined as the initial slope of the scavenging curve of $[e_t^-]$ against [S], and is expressed as

$$\alpha = \frac{-1}{G_0(e_t^-)}\left(\frac{\mathrm{d}G(e_t^-)}{\mathrm{d[S]}}\right)_{[\mathrm{S}]=0} \tag{5}$$

Thus it follows from eq 4 and 5 that

$$\alpha = \frac{k_s}{k_t[\mathrm{T}] + k_r} \tag{6}$$

Because the yield of trapped electrons in pure ethanol glass is independent of the temperature of radiolysis,[6] the ratio of the efficiency of electron scavenging at 4°K to that at 77°K is given by

$$\frac{\alpha(4°\mathrm{K})}{\alpha(77°\mathrm{K})} \doteqdot \frac{k_s(4°\mathrm{K})}{k_s(77°\mathrm{K})}\,\frac{k_t(77°\mathrm{K})}{k_t(4°\mathrm{K})} = \frac{\sigma_s(4°\mathrm{K})}{\sigma_s(77°\mathrm{K})}\,\frac{\sigma_t(77°\mathrm{K})}{\sigma_t(4°\mathrm{K})} \tag{7}$$

where σ_s and σ_t are the cross sections of electron scavenging by BzCl molecules and of electron trapping by preformed traps, respectively.

For practical evaluation of the value α from the actual scavenging curves, it is better to use the relation

$$\alpha = \frac{1}{[\mathrm{S}]_{1/2}} \tag{8}$$

where $[\mathrm{S}]_{1/2}$ denotes the concentration of scavenger mole-

(12) F. S. Dainton, G. A. Salmon, and J. Teply, *Proc. Roy. Soc. London*, **286**, 27 (1965).

TABLE I: Efficiency of Electron Scavenging at 4 and 77°K

Temp. of irradiation and measurement	Wavelength, nm	Efficiency of electron scavenging, α, $(\text{mol }\%)^{-1} \times 10$
4°K	1500	5.3 ± 0.5
	1250	5.3 ± 0.5
	1000	4.8 ± 0.5
	800	4.2 ± 0.4
	700	3.6 ± 0.4
	540	2.9 ± 0.3
	400	3.3 ± 0.3
77°K	650	0.77 ± 0.05
	540	1.00 ± 0.05
	450	0.83 ± 0.04

cules when $G(e_t^-)$ is half of $G_0(e_t^-)$. The values of α thus obtained at the different wavelengths of the absorption band at 4 and 77°K are listed in Table I. It follows from Table I that α(4°K) depends slightly on the wavelength of the band, while α(77°K) is independent of the wavelength of the band. Thus the value of α(4°K)/α(77°K) lies between 3 and 5.

If the interaction between mobile electrons and scavenger molecules is of induced dipole type, the interaction would be inversely proportional to the distance to the power of 4 and the cross section for electron scavenging would be inversely proportional to the velocity of electrons. If this cross section is averaged over a Maxwell–Boltzmann distribution of the velocity of thermalized electrons, the average cross section becomes inversely proportional to the square root of the temperature of the system.[13] Therefore, if the trapping cross section is independent of the velocity of the electrons, the efficiency of electron scavenging would become inversely proportional to the square root of the temperature of the system, and thus the value of α(4°K)/α(77°K) would be about 4.5, agreeing approximately with the experimental result. It should be noted that the previous result for 2-methyltetrahydrofuran gives this ratio as 4.[11]

The unrelaxed traps might be surrounded by molecular dipoles orienting favorably to form shallow potential wells. When mobile electrons come close to these traps, they will be interfered with by potential barriers around the traps. Therefore, electrons must penetrate the barriers in order to be trapped. Transmission of this process would depend on the kinetic energy of the electrons, and therefore mobile electrons at 4°K may have less transmission than that at 77°K.

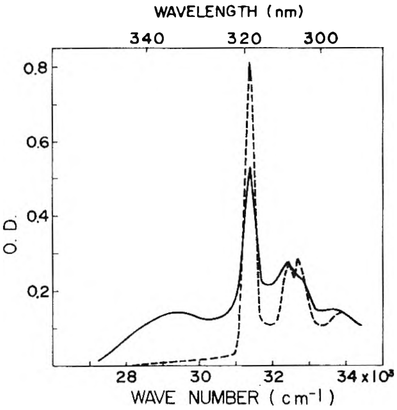

Figure 3. Optical absorption spectra of 0.10 mol % BzCl in ethanol glass irradiated at 4°K. Total γ dose was 0.11 Mrad. Solid line spectrum was obtained after trapped electrons were completely photobleached at 4°K. Broken line spectrum was obtained after subsequently warming the glass rapidly to 77°K. All absorption measurements were carried out at 4°K.

It is probable that the trapping cross section depends on the interaction of electrons with lattice phonons and that the matrix element of the interaction is smaller at the reduced temperature. This may result in a smaller cross section for trapping at 4°K than at 77°K, thereby contributing to the temperature dependence of the efficiency of electron scavenging.

Finally, it is noted that the spectrum of the radicals obtained for irradiation and measurement at 4°K is not identical with that for the radiolysis at 77°K, as shown in Figure 3. The spectrum at 4°K has a peak at 340 nm in addition to the sharp peaks reported in the radiolysis study at 77°K.[12] The new peak disappears at about 55°K in the course of warming the glass from 4°K, being accompanied by growth of the sharp peaks. At 77°K, intensity of the 318-nm peak grows to about two times the initial intensity. Cooling the glass down again to 4°K causes no further changes in the spectrum. Such an irreversible change suggests that a precursor of the benzyl radical is responsible for this new peak.

Acknowledgment. The authors wish to express their sincere thanks to Professors T. Watanabe and K. Fueki for their kind discussions and suggestions on the electron trapping mechanism.

(13) J. M. Wardman, and M. C. Sauer, Jr., *J. Radiat. Phys. Chem.*, **3**, 273 (1971).

Dissociative Electron Attachment to Dimethyl Ether in Irradiated 3-Methylpentane Glass

Hiroshi Yoshida,* Masahiro Irie, Osamu Shimada, and Koichiro Hayashi

Faculty of Engineering, Hokkaido University, Sapporo, Japan *(Received April 19, 1972)*

Publication costs assisted by Hokkaido University

The trapped electron in γ-irradiated 3-methylpentane glass containing dimethyl ether shows an esr spectrum of 3.7 G width and an optical absorption band with a maximum at 1250 nm. It is bleached with light of a wavelength shorter than 1170 nm. The photobleaching is followed by the formation of methyl radical. The conversion efficiency from a trapped electron to a methyl radical is found to be *independent* of the wavelength in the range examined (1170–600 nm). All experimental results indicated that the methyl radical is formed by dissociative electron attachment to dimethyl ether which occurs only when the trapped electron is photobleached but does not occur during γ irradiation. According to gas-phase data, the reaction is expected to be endothermic by about 0.7 eV, although this value may be decreased somewhat in the glassy matrix. Therefore, the results seem to lead to the amazing conclusion that all electrons detrapped by light have an appreciable amount of kinetic energy independent of the photon energy of the light.

Introduction

Dissociative electron attachment in irradiated glassy matrix was extensively studied for toluene derivatives[1] and alkyl halides[2,3] by optical absorption and electron spin resonance (esr) measurements. In these investigations where the bond dissociation energy is smaller than the electron affinity of the leaving group such as halogen atoms, the electron attachment occured very rapidly during γ irradiation to form benzyl and alkyl radicals. Bonin, *et al.*, found a different feature of dissociative electron attachment to acetonitrile in a 2-methyltetrahydrofuran matrix.[4] Although the reaction did not occur during irradiation, the formation of methyl radical through dissociative electron attachment was observed by esr when the trapped electron was photobleached. This was attributed to the reaction of "photoexcited electrons."

A similar observation was reported by the present authors for the dissociative electron attachment to methyl vinyl ether in irradiated 3-methylpentane and 2-methyltetrahydrofuran matrices.[5] Methyl radical, the product of the attachment reaction, was found only when the trapped electron in the glasses was bleached by light. This was interpreted as due to a very small cross section of methyl vinyl ether for the attachment process, though values of the bond dissociation energy and the electron affinity concerned were unknown.

In the present investigation, the study of this peculiar feature of dissociative electron attachment was extended to dimethyl ether in 3-methylpentane glass, for which the CH_3O–CH_3 bond dissociation energy and the electron affinity of CH_3O are known from gas-phase data. Although, according to these data, the dissociative electron attachment is not expected to occur to dimethyl ether with electrons of thermal energy, it was found to occur in the glassy matrix by observing the formation of methyl radical when the trapped electron was photobleached. Deuterated methanol was also studied for comparison.

Experimental Section

3-Methylpentane and 3-methylhexane were purified as described elsewhere[5b] and were dried with calcium hydride and then with sodium–potassium alloy. Analytical grade dimethyl ether, naphthalene, and biphenyl were used as received without further purification. The isotopic purity of deuterated methanol, CH_3OD, was higher than 95%. It was also used as received.

Sample solutions were sealed in esr sample tubes of pure quartz under a pressure of less than 10^{-5} Torr, irradiated to a dose of 4.0×10^5 rads with ^{60}Co γ rays at 77°K in the dark, and subjected to esr measurement at 77°K. Photobleaching of the sample was carried out mostly with the monochromatic light from a slide projector through adequate combinations of a band-pass filter and a cut-off filter (half-width of about 20 nm) and a quartz lens attached to an optical port in the esr cavity wall. Esr and optical absorption measurements were carried out with a conventional X-band spectrometer (JEOL, Model JES-ME-2X) and a conventional recording spectrophotometer (Hitachi. Model EPS-3T).

Results

3-Methylpentane glass containing 5 vol % dimethyl ether gives an esr signal as shown in Figure 1a after γ irradiation. The signal consists of a broad six-line spectrum and a sharp single line spectrum of a width, ΔH_{ms}, of 3.7 G. The former is due to a 3-methylpentyl radical formed from a glass matrix molecule and the latter is due to a trapped electron. Free radicals from dimethyl ether give a spectrum too weak to be distinguished. When the trapped

(1) J. B. Gallivan and W. H. Hamill, *Trans. Faraday Soc.*, **61**, 1960 (1965).
(2) D. W. Skelly, R. G. Hayes, and W. H. Hamill, *J. Chem. Phys.*, **43**, 2795 (1965).
(3) (a) R. C. F. Claridge and J. E. Willard, *J. Amer. Chem. Soc.*, **87**, 4992 (1965); (b) H. W. Fenrick, N. B. Nazhat, P. J. Ogren, and J. E. Willard, *J. Phys. Chem.*, **75**, 472 (1971).
(4) M. A. Bonin, J. Lin, K. Tsuji, and F. Williams, *Advan. Chem. Ser.*, **No. 82**, 269 (1968).
(5) (a) M. Irie, K. Hayashi, S. Okamura, and H. Yoshida, *J. Phys. Chem.*, **75**, 476 (1971); (b) M. Irie, K. Hayashi, S. Okamura, and H. Yoshida, *Int. J. Radiat. Phys. Chem.* **1**, 297 (1969).

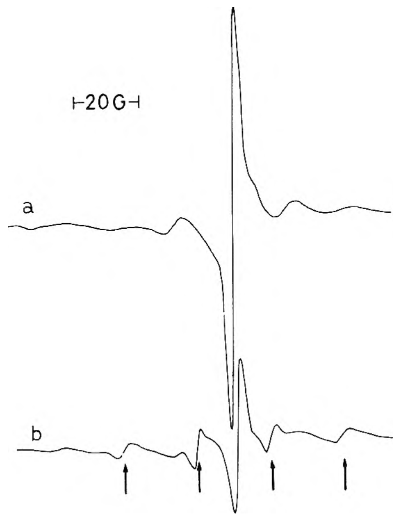

Figure 1. Esr spectra of 3-methylpentane glass containing 5 vol % dimethyl ether irradiated to a dose of 4.0×10^5 rads at 77°K: (a) measured immediately after the irradiation; (b) after photobleaching the trapped electron by light (>800 nm).

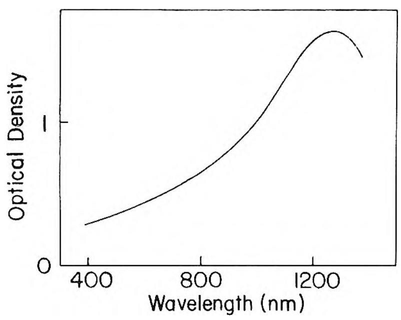

Figure 2. Optical absorption spectrum of 3-methylhexane glass containing 5 vol % dimethyl ether irradiated to a dose of 1.0×10^5 rads at 77°K. Instead of 3-methylpentane, 3-methylhexane glass was studied in detail because the trapped electron is much more stable. However, the absorption spectrum was found to be the same in 3-methylpentane glass.

electron spectrum is photobleached, a four-line spectrum with a hyperfine separation of 23 G appears as shown in Figure 1b (indicated by arrows), which is attributed to a methyl radical.

The irradiated glass shows an optical absorption with a maximum at 1250 nm due to the trapped electron, as shown in Figure 2. Because of the presence of dimethyl ether, the maximum shifts to shorter wavelengths than that in neat 3-methylpentane glass, as reported previously for the trapped electron in 3-methylpentane glass containing alcohol.[6] The bleaching rate of the trapped electron decreases with increasing wavelength of the light, and the trapped electron was found to be bleached with light of 1170 nm but not with light of 1250 nm corresponding to the maximum. This observation is very similar to the bleaching of the trapped electron reported for neat 3-methylpentane and 2-methyltetrahydrofuran glasses.[7,8]

Figure 3 shows the formation and decay of the methyl radical during photobleaching along with the decay of the trapped electron for the wavelengths 602 and 1170 nm. The concentration of the methyl radical reaches a maximum and then gradually decreases. The formation of methyl radical is observed whenever the trapped electron is bleached regardless of the wavelength of the light. The

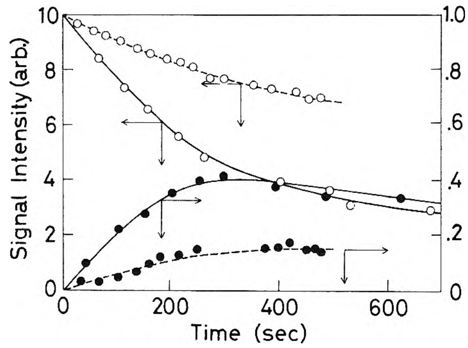

Figure 3. Photobleaching of the trapped electron (O) and simultaneous formation of the methyl radical (●) by light of 1170 nm (- - - -) and 602 nm (——) in 3-methylpentane glass containing 5 vol % dimethyl ether irradiated to a dose of 4.0×10^5 rads at 77°K.

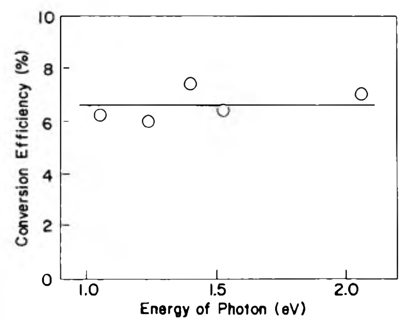

Figure 4. Conversion efficiency of the trapped electron to the methyl radical in irradiated 3-methylpentane glass containing 5 vol % dimethyl ether at 77°K as a function of photon energy of the bleaching light.

conversion efficiency of the trapped electron to the methyl radical is derived from the initial slope of the curves in Figure 3, which is 6.6% and is independent of the wavelength from 602 nm (the shortest wavelength examined) to 1170 nm, as shown in Figure 4.

The conversion efficiency is dependent on the fraction of dimethyl ether in the glass. It is found to be 6.6, 2.0, and 1.8% for 5.0, 1.6, and 1.4 vol % of dimethyl ether, respectively, when the trapped electron is bleached by light of wavelength longer than 480 nm. These values show that the conversion efficiency is linearly proportional to the concentration of dimethyl ether in the glass.

The half-life of methyl radical after turning off the light depends on the photobleaching time and, therefore, on its initial concentration, and the decay follows the second order reaction as shown in Figure 5. This observation contrasts to the behavior of the alkyl radical formed by dissociative electron attachment to alkyl halides (in this case, the half-life was independent of the initial concentration)[2] and indicates the recombination of methyl radicals with each other. The second-order decay of methyl radical was also observed for the dissociative electron attachment to methyl vinyl ether in the glassy matrices.[5a]

If a small amount of aromatic compound such as biphenyl and naphthalene is present in the glass (occasion-

(6) A. Ekstrom and J. E. Willard, *J. Phys. Chem.*, **72**, 4599 (1968).

(7) D. W. Skelly and W. H. Hamill, *J. Chem. Phys.*, **44**, 2891 (1966).

(8) (a) P. J. Dyne and O. A. Miller, *Can. J. Chem.*, **43**, 2696 (1965); (b) K. F. Baverstock and P. J. Dyne, *ibid.*, **48**, 2182 (1970); (c) T. Huang, I. Eisele, D. P. Lin, and L. Kevan, *J. Chem. Phys.*, **56**, 4702 (1972).

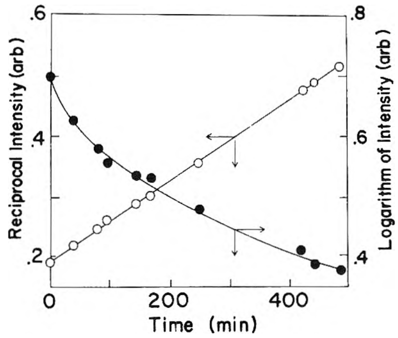

Figure 5. Decay of the methyl radical at 77°K in 3-methylpentane glass containing 5 vol % dimethyl ether irradiated to a dose of 4.0×10^5 rads.

ally of 3-methylhexane instead of 3-methylpentane), the trapped electron spectrum is replaced by that of the aromatic anion, as shown in Figure 6a representatively for biphenyl. Biphenyl anion is known to have two absorption bands in the visible region at 655 and 410 nm.[9] By bleaching the anion with the light of wavelength corresponding to either of the bands, the formation of the methyl radical is evidenced by observing the four-line spectrum as shown in Figure 6b. Similar behavior is observed for naphthalene.

The irradiated 3-methylpentane glass containing 5 vol % of deuterated methanol, CH_3OD, gives an esr signal very similar to that shown in Figure 1a, consisting of a spectrum due to 3-methylpentyl radical and that of the width of 4.5 G due to the trapped electron. When the glass is bleached by light of wavelength longer than 450 nm, the trapped electron decays and a new spectrum appears. It is a three-line spectrum with a hyperfine separation of 17 G and agrees with the spectrum attributed to CH_2OD formed by ultraviolet irradiation of polycrystalline CH_3OD,[10] except that the width of each component is about 3 G which is narrower in the glass than in the polycrystalline matrix. The narrow width enables us to distinguish the CH_2OD spectrum from the 3-methylpentyl radical spectrum overlapping it.

When the electron is formed by photoionization of a small amount of tetramethyl-*p*-phenylenediamine in the glass instead of by γ irradiation, the formation of methyl radical and CH_2OD radical is found in the presence of dimethyl ether and deuterated methanol, respectively. Recently, it was reported that the methyl radical was formed by direct photolysis of tetramethyl-*p*-phenylenediamine after a long photolysis time in the glass matrix.[11] However, in the present investigation, the photolysis time was so short that the methyl radical was not observed in the absence of dimethyl ether.

Discussion

The formation of the methyl radical in the present investigation is reasonably attributed to dissociative electron attachment to dimethyl ether, because methyl radical formation involves electron transfer when the electron is photo-released from aromatic anions and tetramethyl-*p*-phenylenediamine. Furthermore, the latter case excludes an alternative interpretation that the methyl radical might be formed by a charge recombination reaction between an electron and protonated dimethyl ether, because the ionization potential of tetramethyl-*p*-phenylenediamine (<7.0 eV)[12] is much lower than that of dimethyl ether, 10.0 eV,[13] and the cationic entity is exclusively tet-

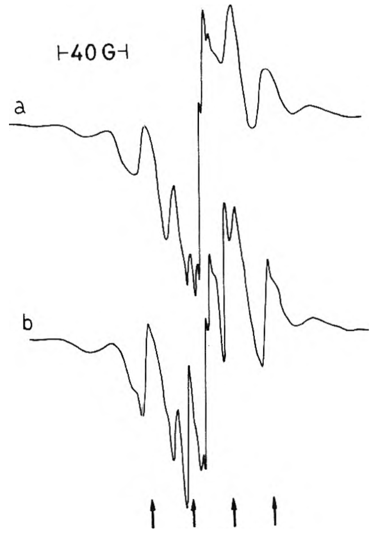

Figure 6. Esr spectra of 3-methylhexane glass containing 5 vol % dimethyl ether and 0.1 mol % biphenyl at 77°K irradiated to a dose of 4.0×10^5 rads and measured: (a) immediately after the irradiation; (b) after photobleaching biphenyl anion by light of 670 nm.

ramethyl-*p*-phenylenediamine cation. The dependence of the conversion efficiency from electron to methyl radical on the fraction of dimethyl ether may indicate the reaction of electron released from its trapping site with a dimethyl ether molecule in the bulk glassy matrix.[14]

The CH_2OD radical formation in the presence of deuterated methanol in 3-methylpentane is thought to be due to dissociative electron attachment to methanol, $CH_3OD + e^- \rightarrow CH_3O^- + D$, followed by the hydrogen abstraction reaction, $CH_3OD + D \rightarrow CH_2OD + HD$. This can be compared with the reaction of a photoexcited trapped electron in pure alcohol glasses with the alcohol molecules of the trapping site.[15] Fujii and Willard suggested the possibility of $e^- + 2CH_3CH_2OH \rightarrow CH_3CH_2O^- + CH_3CHOH + H_2$ in ethanol glass as one of the pathways of decay of the trapped electron,[16] which may be interpreted as due to the dissociative electron attachment as interpreted here.

The energy relationship for the dissociative electron attachment is expressed as follows for dimethyl ether in the gas phase

$$E(e^-) = DE(CH_3O\text{-}CH_3) - EA(CH_3O) + E^* \quad (1)$$

where *DE* and *EA* are the bond dissociation energy and the electron affinity, respectively. E^* is the sum of kinetic and internal energies of the reaction products. $E(e^-)$ is the kinetic energy required for the electron to bring about

(9) M. R. Ronayne, J. P. Guarino, and W. H. Hamill, *J. Amer. Chem Soc.*, **84**, 4230 (1962).
(10) (a) B. Smaller and M. S. Matheson, *J. Chem. Phys.*, **28**, 1169 (1958); (b) R. S. Alger, T. H. Anderson, and L. A. Webb, *ibid.*, **30**, 695 (1959).
(11) P. J. Bekowies and A. C. Albrecht, *J. Phys. Chem.*, **75**, 431 (1971).
(12) R. Foster, *Nature (London)*, **183**, 1253 (1959).
(13) K. Watanabe, *J. Chem. Phys.*, **24**, 623 (1956).
(14) The dependence of the conversion efficiency on the solute concentration was discussed in detail previously (see eq 4 and Figure 7 in ref 5a). When the cross section of the solute for dissociative electron attachment is small enough, the conversion efficiency is approximated to be linearly proportional to the solute concentration.
(15) A. Habersberzerova, Lj. Josimovic, and J. Teply, *Trans. Faraday Soc.*, **66**, 656 (1970).
(16) S. Fujii and J. E. Willard, *J. Phys. Chem.*, **74**, 4313 (1970).

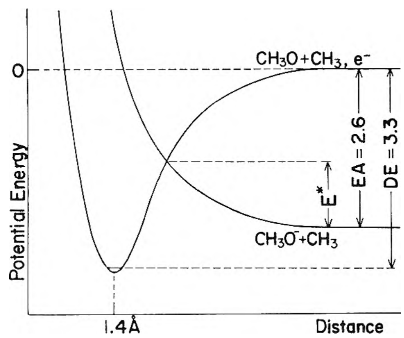

Figure 7. Potential energy diagram for $CH_3O + CH_3$ and $CH_3O^- + CH_3$. The shape of the curves is arbitrary except for the limits indicated.

the attachment process and corresponds to the appearance potential in mass spectroscopic experiments. The *DE* value is derived from the heat of formation of dimethyl ether, CH_3O and CH_3[17] to be 3.3 eV. The *EA* value was determined to be 2.6 eV by a mass spectroscopic study.[18] These gas-phase data lead to the value of 0.7 eV for $E(e^-) - E^*$. The relationship is schematically shown by potential energy-internuclear distance curves for dimethyl ether and its anion in Figure 7.

In the gas phase it is known that the dissociative electron attachment to alkyl halides occurs through a vertical transition from the equilibrium distance of carbon-halogen atoms from electron beam experiments.[19] In the liquid phase, dissociative electron attachment proceeds as a thermal activation process passing through the crossing point between the two potential energy-internuclear distance curves as deduced from electron scavenger experiments.[20] Even if the latter process is presumed for dimethyl ether in the glassy matrix, the energy required for $E(e^-)$ may be much higher than 0.7 eV as suggested in Figure 7. The above argument leads to the amazing conclusion that the electron photo-released from its trap in the glass has a considerable amount of kinetic energy independent of the photon energy of the bleaching light.

The $E(e^-)$ value may be modified in the glass matrix, because the stabilization energy of the product ion should be subtracted from the right-hand side of eq 1. Although the reorientation of molecular dipoles is ineffective for the stabilization. because of the long relaxation time for this process (of the order of microseconds or more in glass matrices at 77°K[21]), stabilization results from the electronic polarization of the glass matrix molecules surrounding the product ion. According to the observed effect of matrix polarization on the photodetachment of electrons in liquid hydrocarbons,[22] the stabilization energy is presumed to be about 1 eV. Although there are no data at the moment available to estimate the extent of modifying the $E(e^-)$ value unambiguously, it appears probable that its value is considerably higher than the thermal energy of the electron in the glassy matrix. If $E(e^-)$ were to be small enough, the dissociative electron attachment should occur so readily that the methyl radical is formed during γ irradiation as is the case for alkyl halides.[2,3]

According to the semicontinuum model,[23] the short-range charge-dipole interaction as well as the long-range polarization interaction is responsible for electron trapping not only in the liquid but also in glass matrices. The dipole orientation due to the former interaction necessarily forms a potential barrier around the electron traps. When the electron is excited vertically and conducts into the bulk matrix, it probably gains an excess kinetic energy at least equal to the barrier height with reference to the bottom of a conduction band state (in other words, the quasi-free state) in the matrix. This is one of the reasons why the electron reacts with dimethyl ether even when it is bleached with the light of threshold wavelength. As a matter of fact, the barrier height was calculated, as a difference of conduction levels between the configuration of glass matrix for the trapped electron in the ground state and the nonperturbed glass matrix, to be 0.7-0.9 and 0.1-0.3 eV for ethanol[23b] and 2-methyltetrahydrofuran glass,[23c] respectively.

The dissociative electron attachment is a resonant process, so that only an electron having an appropriate kinetic energy can give rise to the process. Therefore, the electron has only a small chance to react with dimethyl ether during the course of energy degradation from its formation until trapping. This is completely the same for an electron released from the trap by light as long as it initially gains an energy higher than $E(e^-)$. It is expected that the amount of methyl radical formed during the photobleaching of trapped electrons is n times as much as that formed during γ irradiation where n is the average number of detrapping-retrapping cycles which the electron undergoes before charge recombination. The present results indicate, though not quantitatively, that n is appreciably larger than unity, in agreement with the small quantum efficiency of photobleaching trapped electrons observed for several organic glasses.[7,8]

The dependence of the formation of CH_2OD in 3-methylpentane-deuterated methanol glass on the bleaching wavelength was not determined in detail because the weak CH_2OD spectrum could not be distinguished quantitatively from the overlapping spectrum of the 3-methylpentyl radical. However, the $E(e^-)$ value is calculated to be as high as 1.8 eV for the dissociative electron attachment to methanol in the frame of argument given for dimethyl ether.

Acknowledgment. The authors express their thanks to Professor Larry Kevan for his kind reading of the manuscript and invaluable discussion.

(17) V. I. Vedeneyev, *et al.*, "Bond Energies, Ionization Potentials and Electron Affinities," (English translation) St. Martin's Press, New York, N. Y., 1966, p 123.
(18) S. Tsuda and W. H. Hamill, *Advan. Mass Spectrom.*, **3**, 249 (1966).
(19) J. J. DeCorpo, D. A. Babus, and J. L. Franklin, *J. Chem. Phys.*, **54**, 1592 (1971).
(20) W. E. Wentworth, R. George, and H. Keith, *J. Chem. Phys.*, **51**, 1791 (1969).
(21) (a) J. T. Richards and J. K. Thomas, *J. Chem. Phys.*, **53**, 218 (1970); (b) L. Kevan, *Chem. Phys. Lett.*, **11**, 140 (1971); *J. Chem. Phys.*, **56**, 838 (1972).
(22) C. Vermeill, M. Matheson, S. Leach, and F. Muller, *J. Chim. Phys.*, **61**, 596 (1964).
(23) (a) K. Fueki, D-F. Feng, L. Kevan, and R. E. Christoffersen, *J. Phys. Chem.*, **75**, 2297 (1971); (b) K. Fueki, D-F. Feng, and L. Kevan, to be published; (c) K. Fueki, D-F. Feng, and L. Kevan, unpublished data.

Kinetics of Defect and Radiolytic Product Formation in Single Crystal Sodium Bromate Determined from Color-Center Measurements[1]

P. W. Levy,* M. Goldberg,

Brookhaven National Laboratory, Upton, New York 11973

and P. J. Herley

Explosives Laboratory, Picatinny Arsenal, Dover, New Jersey and Material Science Department, State University of New York at Stony Brook, New York 11970 *(Received April 20, 1972)*

Publication costs assisted by Brookhaven National Laboratory

The kinetics of defect and/or radiolysis product formation in single crystal $NaBrO_3$ have been studied using color-center, *i.e.*, optical absorption, techniques. Samples were exposed to X-rays, γ-rays, or ultraviolet light at liquid helium, liquid nitrogen, and room temperatures. The radiation-induced absorption depends on the irradiation temperatures and the type of radiation used. The observed spectra can be resolved into six prominent and one, two, or three weak Gaussian-shaped absorption bands. Some of these bands are described in the literature and appear to be correlated with specific radiolysis products. The various observed growth curves can be grouped into distinct categories broadly characterized as linear which is possibly a special case of a saturating exponential, linear plus saturating exponential, concave, and sigmoid. Expressions for these curves can be derived from very simple kinetic models involving defect, *i.e.*, precursor, formation and subsequent charge transfer. The experimentally determined curves are accurately described by these expressions.

Color-center measurements are a potentially powerful tool for studying the kinetics of radiolysis and radiation damage processes. Yet, after nearly 3 decades of intensive study on the effects of radiation on numerous solid substances, relatively few radiolysis studies have been completed which make use of color-center techniques. This paper summarizes some of the more interesting results obtained by applying color-center measurement techniques to determine the kinetics of radiolysis product formation, or more specifically, the formation of radiation-induced species, in high purity crystalline sodium bromate. Very briefly, it will be shown that this material becomes colored when exposed to ultraviolet light, X-rays, or γ-rays. The induced optical absorption spectrum can be resolved into individual absorption bands. The coloring curves for each of these bands, *i.e.*, curves of optical absorption *vs.* dose and/or irradiation time, depend on both the sample temperature and the type of radiation employed. Furthermore, these curves group into various categories which can be attributed to relatively simple kinetic processes.

The published information on color centers in crystalline $NaBrO_3$ is relatively sparse. Among the first to study the effects of irradiation on single crystals were Ramasastry and Murti[2a] who reported that the X-ray induced optical absorption spectra, at room temperature, contained bands at 280, 330, and 420 nm. They searched for but did not detect paramagnetic centers in crystals irradiated and measured at room temperature. However, Andersen, Byberg, and Olsen,[2b] using samples bombarded with 10-MeV electrons, produced a paramagnetic center at $-78°$ which could be detected after annealing for several days at 80–100°. They attributed this center, called the A center, to O_3^- localized at a BrO_3^- site. Recently Andersen, *et al.*,[3] published a single optical absorption spectrum of $NaBrO_3$ crystals, after 10-MeV electron irradiation, containing bands at 290, 350, and 440 nm. Considerably more information is available from the extensive radiolytic decomposition studies of the alkali bromates by Boyd, *et al.*[4-6] After subjecting crystals to a variety of irradiations at room temperature, the following products were found when the crystals were dissolved in water: oxygen gas, Br^-, BrO_2^-, BrO^-, and (possibly) BrO_2.

Most of the investigations described above used radiations in the MeV range, *i.e.*, uv irradiations were not attempted. Also, they contain little data, or curves, showing product concentration as a function of dose or sample temperature.

Experimental Section

All measurements were made on $NaBrO_3$ single crystals grown by slow cooling from a seeded saturated aqueous solution. Individual samples, approximately 10 × 20 × 0.5–2 mm with their largest faces perpendicular to the (100) direction, were cut from large 9 × 9 × 9 cm single crystals and the largest faces were polished to a window glass finish. All samples were water clear and free of optical imperfections. Potassium was the only impurity detected by emission spectroscopy. After polishing all samples were kept desiccated in the dark. Optical absorption measurements were made with a Cary 14R spectrophotometer. The spectra were recorded digitally at fixed incre-

(1) Research performed primarily at Brookhaven National Laboratory and supported jointly by Picatinny Arsenal and the U. S. Atomic Energy Commission.

(2) (a) C. Ramasastry and Y. V. G. S. Murti, *Indian J. Pure Appl. Phys.*, **2**, 35 (1964); (b) T. Andersen, J. R. Byberg, and K. J. Olsen, *J. Phys. Chem.*, **71**, 4129 (1967).
(3) T. Andersen, H. E. Lundager Madsen, and K. Olesen, *Trans. Faraday Soc.*, **62**, 2409 (1966). Also, T. Andersen, Ph.D. Thesis, University of Aarhus, 1968.
(4) J. Chase and G. E. Boyd, *ASTM Spec. Tech. Publ.*, **No. 400**, 17 (1966).
(5) G. E. Boyd and Q. V. Larson, *J. Phys. Chem.*, **68**, 2627 (1964).
(6) J. W. Chase and G. E. Boyd, *J. Phys. Chem.*, **70**, 1031 (1966).

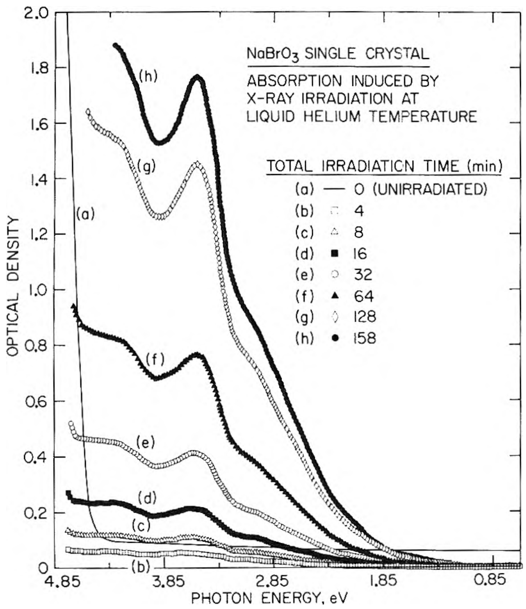

Figure 1. Optical absorption induced in crystalline $NaBrO_3$ by X-ray irradiations at liquid helium temperatures. Continuous curve shows absorption of the crystal before irradiation. The spectra shown are differences between this curve and absorption after irradiation.

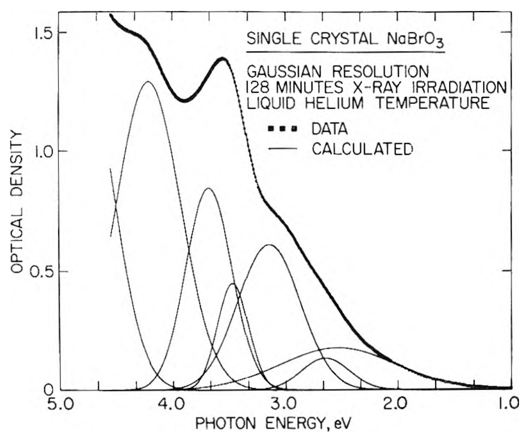

Figure 2. Resolution of 128-min absorption spectrum from Figure 1 into Gaussian bands. The peak energy of the resolved bands occurs at 4.2, 3.7, 3.5, 3.1, 2.8, and 2.5 eV.

ments of wavelength as close as 2 Å. The data were processed on a large computer; including the preparation of optical absorption spectra. These spectra were resolved into component Gaussian-shaped absorption bands using a best-fit procedure.[7]

Ultraviolet irradiations were carried out *in vacuo* using filtered light from a high-pressure mercury lamp.[8] Samples were irradiated with ^{60}Co γ-rays at a dose rate of 1.08×10^6 rads hr^{-1}, at room temperature (30°), in air, and in the dark. X-Ray irradiations were obtained from a tungsten target, beryllium window, tube operated at 60 kV and 30 mA.

Absorption Spectrum Measurements and Analysis

Absorption spectra measurements were made on crystals irradiated at room temperature, at liquid nitrogen temperature, and at liquid helium temperature after exposure to ultraviolet light, X-rays, or to ^{60}Co γ-ray irradiation. A detailed description of all of these measurements is much too long to include here and will appear in subsequent publications. Consequently, only those measurements will be described which are essential for outlining the procedure used to obtain data describing the kinetics of radiolysis product formation. This will include brief descriptions of the X-ray induced coloring at liquid helium temperature, the room temperature γ-ray induced coloring, and a considerably more detailed description of the room temperature ultraviolet light induced coloring.

A typical example of X-ray induced absorption spectra obtained by irradiating and measuring at liquid helium temperature is shown in Figure 1. Curve a, in this figure, is the absorption of the crystal prior to any irradiation. The remaining curves show the absorption induced by the indicated X-ray irradiations. Specifically, the remaining curves were obtained by subtracting the pristine crystal absorption from the absorption measured after each irradiation. Each absorption spectrum was resolved into component Gaussian-shaped absorption bands. An analysis of the various absorption spectra, as well as additional spectra which are not shown, suggests that five individual components must be present. However, when the observed spectra are resolved into component Gaussian-shaped absorption bands it is found that six bands are present. In addition, a certain amount of band-edge absorption must be included to account for all of the observed absorption. At the present time, it is not known if the band edge is "real" or is an apparent edge attributable to a very intense absorption band. However, in both cases it is appropriate to approximate the band-edge absorption by the "tail" of an additional Gaussian-shaped absorption band. A typical example of an X-ray induced absorption spectrum at liquid helium temperature is shown in Figure 2. Actually, this figure shows the data points, the individual absorption bands obtained by resolving the observed spectrum into component Gaussian-shaped bands, and a solid line, which is difficult to discern, passing through the data points. The line through the data represents a superposition, *i.e.*, the sum of the individual absorption bands.

From data, such as is shown in Figure 1, it is possible to construct growth or coloring curves describing the intensity of each band as a function of dose and/or irradiation time. First, it is essential to resolve each of the individual absorption spectra into component bands. This resolution was carried out for each of the spectra shown in Figure 1 and it was determined that all of the spectra could be fitted with a set of six individual bands. Furthermore, the relative intensity of each of these bands was found to vary systematically with irradiation time. The resulting growth curve is shown in Figure 3. Obviously, to a relatively high degree of accuracy, the intensity of each of the bands is a linear function of irradiation time.

These linear growth curves can be attributed to a very simple mechanism for radiolysis product formation. Namely, as the radiation progresses products or defects are formed in direct proportion to the total dose. However, as will be explained below, linear growth curves are consistent with a large variety of relatively simple defect formation mechanisms. A large number of these mechanisms leads to theoretical coloring curves which can be approximated by straight lines in the low total dose region. A more detailed discussion of linear growth curves is contained in the section on mechanisms.

(7) R. E. Biggers, J. T. Bell, L. C. Long, and O. W. Russ, Oak Ridge National Laboratory Report 3834.
(8) P. J. Herley and P. W. Levy, *J. Chem. Phys.*, **46**, 627 (1967).

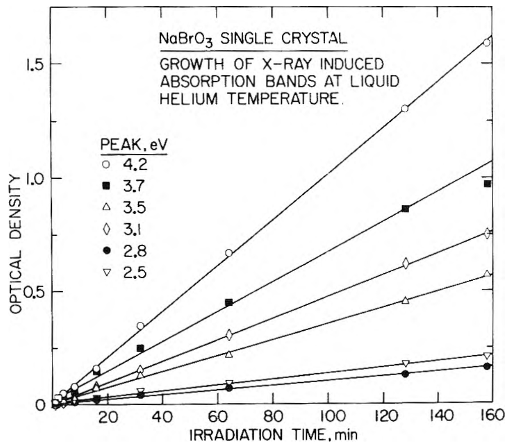

Figure 3. Growth curves for the various bands introduced by X-ray irradiation at liquid helium temperatures. The intensities were obtained by resolving each of the spectra shown in Figure 1 into the components shown in Figure 2.

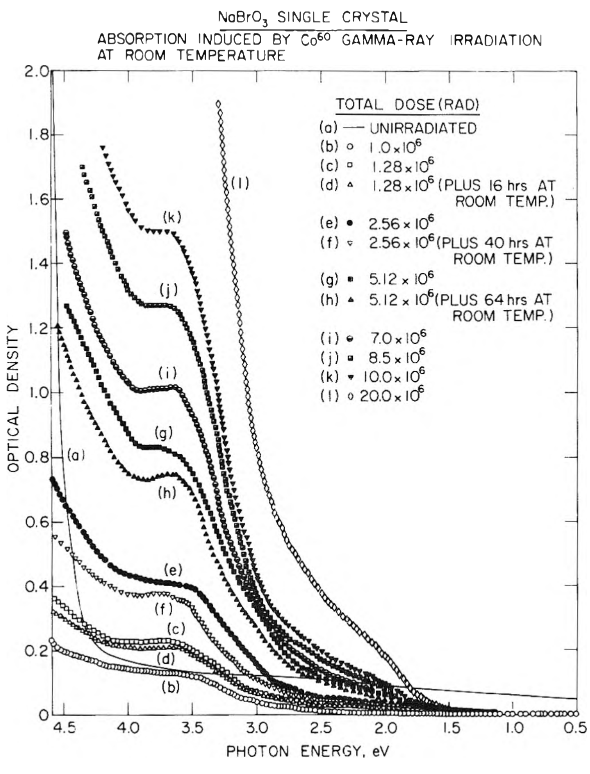

Figure 4. Optical absorption induced in crystalline $NaBrO_3$ by exposure to ^{60}Co γ-rays at room temperature. The continuous curve shows the absorption of the crystal before irradiation. The spectra shown are differences between this curve and absorption after each irradiation.

The absorption spectra obtained by irradiating with X-rays or ultraviolet light at liquid nitrogen temperature resemble the spectra obtained at liquid helium temperatures. They can be fitted with the same set of individual bands obtained from the liquid helium temperature data. However, the peak energy and full widths obtained from the liquid nitrogen temperature data differ slightly from the corresponding parameters obtained from the liquid helium temperature data. This is in accord with the expectation that the full width and peak energy of these bands will depend on sample temperatures. Interestingly, the overall growth rate for these bands, *i.e.*, the rate of formation of color centers or defects, appears to be greater

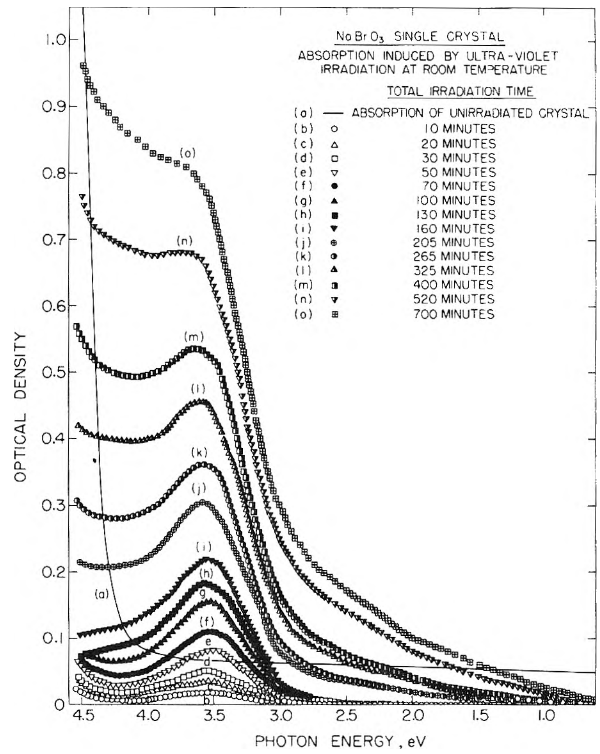

Figure 5. Optical absorption induced in crystalline $NaBrO_3$ by exposure to 2537 Å light at room temperature. Continuous curve shows absorption of the crystal before illumination. The spectra shown are differences between this curve and absorption after each exposure.

at liquid nitrogen temperature than at either room temperature or liquid helium temperature.[9] Both the data and analysis of the temperature dependent effects are too extensive for inclusion in this paper and will be published elsewhere. However, the data presented in this paper have been carefully chosen to illustrate kinetic features which remain valid when considered in the framework of the more general temperature-dependent effects.

The spectra obtained by both irradiating and making absorption measurements at room temperature depend on the type of irradiation which is used. This point can be demonstrated by comparing Figures 4 and 5. The first of these contains spectra obtained from γ-ray irradiated samples and the second applies to crystals exposed to ultraviolet light. The spectra are superficially similar but differ in several respects. First, the ultraviolet light irradiated crystals develop absorption bands at about 1.5 eV which are not observed in the γ-ray irradiated samples. Second, in the ultraviolet light irradiated crystals there is comparatively little color center formation in the 4.0- to 4.5-eV region during the initial stages of the exposure. This can be stated in another way; the initial ultraviolet light induced absorption is confined to a band, or bands, in the 3.5-eV region. Third, at relatively high ultraviolet light and γ-ray irradiation the spectra become quite similar except for the absorption below 1.5 eV which is produced only by ultraviolet light exposure. Spectra obtained by X-ray irradiation, which are not illustrated, can be characterized as intermediate between γ-ray and uv cases. Again, however, the broad absorption at 1.5 eV and longer wavelengths introduced by ultraviolet light is not observed after X-ray irradiation.

(9) M. Goldberg, P. W. Levy, and P. J. Herley, *Bull. Amer. Phys. Soc., Ser. 2*, **14**, 376 (1969); **15**, 371 (1970); **16**, 441 (1971).

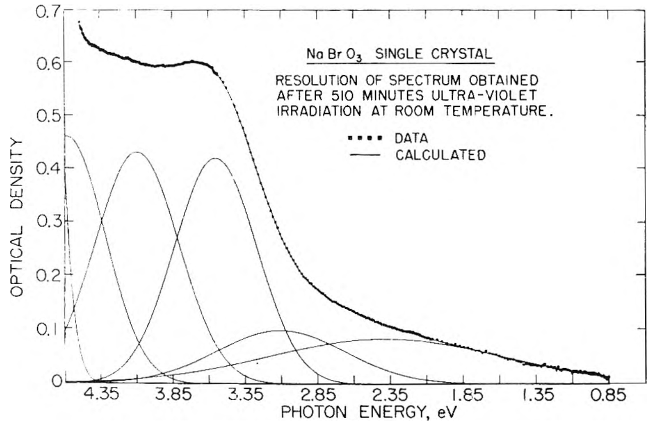

Figure 6. Resolution of 510-min curve from Figure 5 into Gaussian-shaped bands. At the lower doses only the bands at 4.8, 4.5, 4.0, and 3.5 eV can be detected; those at 3.0 and 2.3 eV are not intense enough to be observed. The band at 3.0 eV appears only after 20-min exposure and the 2.3-eV band is detectable only after 150-min exposure.

Numerous spectra obtained by X-ray or γ-ray irradiation at room temperature were resolved into component Gaussian absorption bands. The spectra introduced by uv at room temperature can be resolved into components consisting of a large fraction of the bands observed at other temperatures. More specifically, the room temperature uv spectrum consists of four, or possibly five, of the bands observed in room temperature X-ray and γ-ray induced spectra plus an additional band at approximately 2.38 eV which accounts for the additional long-wavelength-induced absorption at 1.0–1.5 eV. This last mentioned band is also observed at low temperatures, *e.g.*, it is quite apparent in the liquid helium X-ray induced spectrum, Figure 2. Finally, a small band appears at 2.12 eV after very long uv exposure at room temperature.

A typical analysis of the room temperature uv induced absorption is shown in Figure 6 and a comparison of this data with Figure 2 illustrates one of the principal difficulties which arises when spectra are resolved into component bands. Note that Figure 2 contains bands near 2.5, 2.8, and 3.1 eV but, in this region, Figure 6 contains a single broad band whose peak is near 3.0 eV. Since absorption bands are expected to narrow as the crystal temperature is reduced it is likely that the single broad band near 3.0 eV at room temperature is in reality a superposition of the three bands which occur in this region at liquid helium temperature. Similarly the two bands near 4.2 and 3.7 eV at liquid helium temperature may superimpose to form the single broad band observed near 4.0 eV at room temperature. The band near 3.5 eV is so intense it appears as a single band at all temperatures.

Another difficulty inherent in the procedure for resolving the spectra into components should be mentioned. Unfortunately, the observed absorption does *not* consist of isolated bands. Consequently, it is often difficult to ascertain the peak energy and full width which should be assigned to each band at various temperatures. More specifically, when two or more approximately equal intensity bands lie close together the computerized best-fit procedure will assign somewhat different values to spectra measured under different conditions. Thus, in these cases the parameters obtained from the resolution of different spectra will tend to cluster around an average value. In favorable cases, *e.g.*, the band at approximately 3.5 eV, the spread is very small.

TABLE I: Nominal Parameters for the Optical Absorption Bands Observed in $NaBrO_3$ Single Crystals Irradiated at Various Temperatures

Peak energy, eV	Full width at half max., eV	Measurement[a] temperature RT	LNT	LHT	Remarks
4.85	0.65	×	×	×	Edge
4.55	0.59	×	×	–	$Br{-}BrO_3^-$, BrO_2^- [b] $BrO_2{-}BrO_3^-$
4.20	0.74	–	×	×	
4.05	0.71	×	–	–	
3.70	0.49	–	×	×	
3.55	0.63	×	×	×	BrO^- [b]
3.20	0.55	–	×	×	
2.90	0.91	×	–	×	Br_2, O_3^- [b]
2.70	0.54	–	×	–	
2.60	1.11	–	×	×	
2.35	1.49	×	×	–	Produced only by uv
(2.10)	0.61	×	–	–	Only at large uv doses

[a] × = observed, – = not detected, RT = room temperature, LNT = liquid nitrogen temperature, LHT = liquid helium temperature. [b] See Table II.

All of the various color centers which have been observed, during the course of this work, are summarized in Table I. In preparing this table only nominal values for the peak energy and full width have been given. They were obtained from numerous spectra such as those shown in Figures 1, 2, 4, 5, and 6.

At the present time relatively few of the bands observed in irradiated sodium bromate have been attributed to specific defects. The available information is summarized in Table II. Because of the scarcity of information, measurements on absorption spectra obtained by dissolving irradiated crystals in various solvents were also included. Clearly the applicability of such data may be questionable. However, in some instances where the absorption spectrum of a known species was measured both in a crystalline matrix and in various solvents the agreement was surprisingly good.

The room temperature ultraviolet induced coloring data were also used to construct growth curves for each observed absorption band. First, the spectra shown in Figure 5 were resolved into component absorption bands using the bands shown in Figure 6. The "goodness of fit" illustrated by Figure 6 is typical of that obtained for each curve. Actually, the fitting procedure varied the intensity, the peak energy, and the full width of each of the bands. The variations in peak energy, obtained from the spectra in Figure 5, were negligibly small. The variations in band width were larger but quite satisfactory for this type of procedure. Most importantly, the band intensities were found to increase monotonically with irradiation time. The resulting growth curves, *i.e.*, curves of defect or absorption band intensity *vs.* dose, are contained in Figure 7. Clearly, these curves group into three categories: curves a and b in one, curve c in a second, and curves d and e in a third. The linear growth curves illustrated by Figure 3 may be considered to constitute a fourth category. Some simple mechanisms accounting for the shape of each of these curves will be described in the next section. However, it is worthwhile pointing out that similarly shaped curves in all four categories have been observed previously and attributed to color-center formation in various crystals. Curve c is an example of a growth curve very often

TABLE II: Species Attributed to Bands Observed at Room Temperature

Peak energy, eV	Attributed to	Ref	Comment
4.54 (273 nm)	BrO_2^-–BrO_3^- (280 nm)	2a	X-Ray, single crystal $NaBrO_3$
	BrO_2^- (285 nm)	5	X-Ray, aqueous solution of $CsBrO_3$ and $Sr(BrO_3)_2$
	Br–BrO_3^- (290 nm)	2b	Electron, solid $KBrO_3$
	(285 nm)		Electron, $KBrO_3$ dissolved in water
3.53 (351 nm)	BrO^- (330 nm)	2a	X-Ray, single crystal $NaBrO_3$
	BrO^- (330 nm)	5	X-Ray, $CsBrO_3$ and $Sr(BrO_3)_2$ crystals dissolved in water at 35°
	BrO^- (350 nm) (solid) (330 nm) (solution)	2b	Electron, solid $KBrO_3$ crystals dissolved in water
2.90 (427 nm)	Br_2 or nonparamagnetic oxide of bromine (420 nm)	2a	X-Ray, single crystal $NaBrO_3$
	Br_2 (410 nm)	2b	Electron, solid $KBrO_3$ dissolved in H_2O extracted in CCl_4
	O_3^- (440 nm)	3	Electron, solid $KBrO_3$

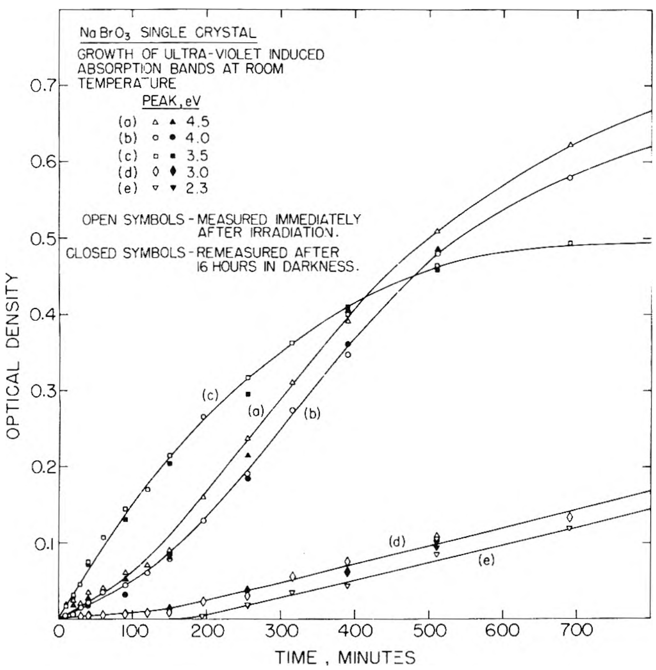

Figure 7. Growth curves for the bands introduced by uv exposure at room temperature. The intensities were obtained by resolving the spectra shown in Figure 5 into the components shown in Figure 6. The effect of allowing the crystal to stand for 16 hr in the dark is also shown.

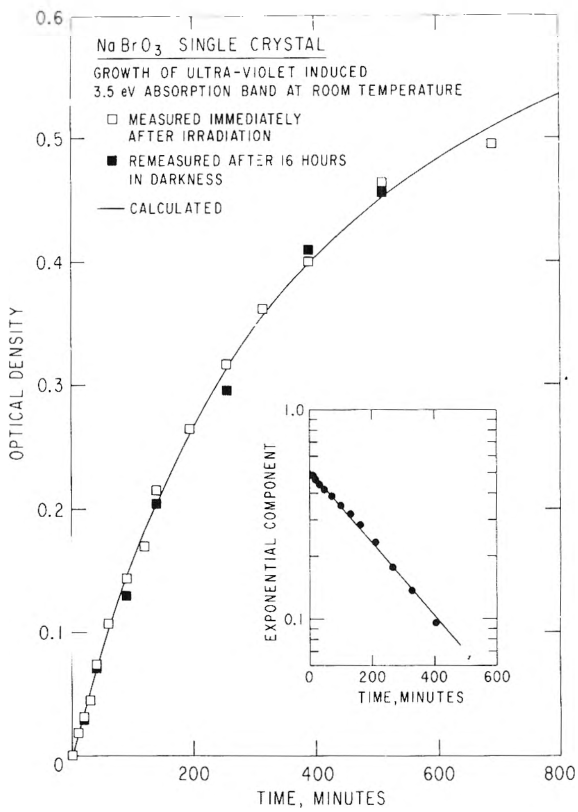

Figure 8. Analysis of the 3.5-eV band growth curve shown in Figure 7. The points in the insert were obtained by taking the difference between the data points and a line extrapolated from the "linear" portion of the data curve observed at large times. This demonstrates that the growth curve contains one saturating exponential and one linear component. The solid line was computed from parameters obtained from the semilog plot.

observed in alkali halides and a variety of oxides.[10-13] Usually the alkali halide and aluminum oxide growth curves consist of one, two, or three saturating exponential components and a single linear component. In its simplest form such a curve consists of a single saturating exponential region near the origin and becomes linear when the irradiation time or dose becomes large. If the linear data region is extrapolated to the vertical axis and the difference between the data and the extrapolated line is plotted on semilog paper a single straight line is obtained. The data for curve c on Figure 7 were analyzed in this manner. This is illustrated by Figure 8 which contains the curve c data plotted on a larger scale. The insert on this figure shows the semilog analysis described above. Thus, one concludes

(10) P. W. Levy, P. L. Mattern, and K. Lengweiler, *Phys. Rev. Lett.*, **24**, 13 (1970).
(11) P. L. Mattern, K. Lengweiler, and P. W. Levy, *Solid State Commun.*, **9**, 935 (1971).
(12) K. Lengweiler, P. L. Mattern, and P. W. Levy, *Phys. Rev. Lett.*, **26**, 1375 (1971).
(13) (a) J. L. Alvarez Rivas and P. W. Levy, *Phys. Rev.*, **162**, 816 (1967); (b) P. W. Levy, *Phys. Rev.*, **123**, 1226 (1961).

that curve c consists of a single saturating exponential component and a single linear component.

This figure, as well as Figures 4 and 7, illustrates some of the temperature related effects mentioned above. They indicate that the room temperature induced coloring is not completely stable and that it decays slowly after irradiation. This room temperature decay can be attributed to several different processes. The most likely processes are related to the thermal untrapping of charges from defects which act as hole or electron traps. The thermal trapping effects indicated in Figures 4, 7, and 8 are relatively small and consequently they are not included in the discussion on kinetics which follows. When included in the kinetics they improve the agreement between the theoretical kinetic curves and the data. For example, when applied to Figure 8 they have the effect of "straightening out" the data points in the insert.

Furthermore, the temperature dependent effects, especially the decrease in optical absorption which occurs when the crystals are allowed to stand in the dark at room temperature, indicate that all of the absorption bands are due to color centers or possibly other defects such as trapped molecules. Figure 4 indicates that all of the absorption bands formed by irradiation at room temperature are unstable to some extent. Stated another way, these effects provide evidence for concluding that the observed absorption does not contain an appreciable contribution from scattering centers such as colloid particles and/or voids. The observed decay is typical color-center behavior. If one or more of the observed bands were due to voids or colloid particles one would expect them to be stable, or if they changed at all, to increase in size. As mentioned above, the temperature-dependent effects will be included in a separate paper.

Kinetic Mechanisms

The various radiolysis product, defect, or color-center growth curves obtained can be described by a variety of simple mechanisms. These mechanisms can be shown to be special cases of more general treatments which are similar but differ in details.[14] Furthermore, when the equations obtained from different general treatments are simplified, by utilizing approximations, the resulting equations often have exactly the same *form*, with the constants having slightly different meaning. Only one simplified mechanism will be described in detail. This choice was based on several considerations. First, it can be derived from relatively simple assumptions. Second, the mathematical description of the mechanism is relatively simple; a general equation is obtained and all of the observed curves can be shown to be special cases of the general solution. Third, although the mechanism to be described immediately has been used only rarely to describe radiolysis experiments it has been shown to apply to a variety of color-center growth measurements. In particular, during the past 2 years it has been shown to apply to a variety of growth curves obtained by making color-center measurements during irradiation with γ-rays.[10-13] In fact, because of the high density of data points which were obtained, these recent measurements constitute a severe test of the kinetic equations given below.

Before proceeding it is essential to briefly describe one type of radiolysis mechanism which must occur in some materials but is excluded from the mechanism to be described below. This is the process whereby the radiolysis product is formed immediately as a primary result of the interaction of the radiation field and the solid to be considered. For example, consider that a BrO_3^- ion interacts strongly enough with an incident γ-ray to remove a neutral oxygen atom from the ion and deposit it some tens of lattice spaces from the initial interaction. If the BrO_2^- reaction product were to form an absorption band, *i.e.*, a color center, it would increase linearly with irradiation time or dose. Of course, this particular mechanism would occur exactly as described only if all alternative processes for forming BrO_2^- ions were excluded. Also, as the reaction proceeds one might expect that BrO_2^- ions would be removed by a variety of secondary processes such as back reactions or electronic reactions which would change the charge state of the ion. As is well known, in this case, the kinetic equation would contain one production term and a back reaction term. The resulting color center *vs.* time or dose equation would be a simple saturating exponential term which would reach a saturation value or plateau. This primitive saturating exponential behavior, *i.e.*, a saturating exponential component *not* superimposed on a linear component, has not been observed with sodium bromate, as far as can be determined. However, as mentioned above, the linear growth observed at liquid helium temperatures may be a special case of this process corresponding to the situation when only the initial portion of the growth curve has been observed.

The assumptions leading to the kinetic equation to be given in detail are as follows.

(1) The observable radiolysis product, *i.e.*, a color center, is formed in a two-step process. The initial step is the formation of a color-center precursor. For example, the initial step may be the formation of a lattice defect.

(2) The second step, which occurs at some undetermined time after the first step, is the conversion of the precursor into a color center. For example, the precursor may be a defect which is converted into a color center by capturing an electron or an (electronic) hole.

Although the processes described in assumptions 1 and 2, above, have been discussed for many years it is difficult to cite examples clearly in accord with this model. Recently, this model has been shown to apply to the formation of F centers in KCl crystals when they are irradiated with γ-rays at liquid nitrogen temperatures.[12] In fact, in addition to predicting the observed form of the F center *vs.* dose curve, an obvious extension of the model correctly accounted for the observed dose rate dependences. Before deriving the kinetic equation based on the assumptions given above it is essential to point out that the model may apply to a large number of different processes. More specifically, these equations provide useful information about the growth of a certain absorption band. They do not in themselves specify the particular mechanism, nor the particular defect associated with a specific absorption band. Consequently to emphasize the unspecified nature of these mechanisms, the entities will be referred to as precursors and color centers and an attempt will not be made to associate them with any specific defect.

Let P represent the concentration of precursors of a particular color center and P_0 the concentration of precursors at time $t = 0$. Likewise N represents the color-center concentration and N_0 the value of N at $t = 0$, usually $N_0 = 0$. In addition to the original precursors assume additional ones are formed during the irradiation, at a rate of K per unit time. Consider next the possibility that precursors

(14) P. W. Levy, to be submitted for publication.

TABLE III: Growth Curve Equations

Approx.[a]	Equation	Curve shape	Examples		
			Band, eV	Temp	Radiation
None	$N = [1/(f-p)]\{(P_0f - K)(1-e^{-ft}) - (P_0f - (f/p)K)(1-e^{-pt})\}$	Sigmoid	4.5, 4.0	RT	Uv
$p = 0$	$N = (P_0 - (K/f))(1-e^{-ft}) + Kt$	Linear plus saturating exponential	3.5	RT	UV
$p = 0, P_c = 0$	$N = Kt - (K/f)(1-e^{-ft})$	Concave	3.0, 2.3	RT	Uv
$p^2 \ll p$, $f^2 \ll f$	$N = P_cft$	Linear	All	LHT	Uv, X-ray
$p = 0, P_c = 0$, $1 \ll f$	$N = Kt$	Linear	All	LHT	Uv, X-ray
$p = 0, K = 0$	$N = P_c(1-e^{-ft})$	Saturating exponential	Not observed		

[a] All $N = 0$ at $t = 0$.

are destroyed or rendered inoperable during irradiation. For example, if the precursor is a vacancy it could disappear by capturing a radiation-produced interstitial and this could occur whether or not the vacancy was a color center. Alternatively, if the precursor is an impurity atom, it could be rendered inoperable as a precursor by a valence change, the removal or capture of a charge compensating atom in a nearby site, etc. It is assumed in this treatment that the removal rate is given by pP where p is the rate (fraction per unit time) of removal of the precursors during irradiation. During irradiation the differential equation for P becomes

$$dP/dt = K - pP \tag{1}$$

whose solution is

$$P = (K/p)(1 - e^{-pt}) + P_0e^{-pt} \tag{2}$$

Next, assume that the rate that precursors are converted to color centers is given by

$$dN/dt = f(P - N) \tag{3}$$

i.e., the rate of formation of color centers is proportional to the number of uncolored precursors. Substituting (2) in (3) one obtains

$$dN/dt = f[(k/p)(1 - e^{-pt}) + P_0e^{-pt} - N] \tag{4}$$

The solution of this equation is, using $N = N_0 = 0$ at $t = 0$

$$N = A(1 - e^{-ft}) - A_D(1 - e^{-pt}) \tag{5}$$

where

$$A_I = (1/(f-p))(P_0f - K) \tag{6}$$

and

$$A_D = (1/(f-p))(P_0f - (f/p)K) \tag{7}$$

Equation 5 is the most general case of the color center, *i.e.*, absorption band, growth curves which result from these simple kinetic considerations. One may expect to obtain color-center growth curves described by eq 5 and, in addition, curves which represent various approximations and special cases of this equation. For example, it is reasonable to consider cases where $p = 0$, $P_0 = 0$, and/or $K = 0$. The most likely special cases and approximations are summarized in Table III. With one exception all of the cases considered occur among the $NaBrO_3$ color-center growth curves described above. The exception is the simple saturating exponential.

The absence of a simple saturating exponential is relatively easy to explain. This case occurs when there is a fixed number of precursors which can be converted into color centers. The most likely situation arising from a fixed precursor concentration is the formation of color centers by charge trapping on impurities. As mentioned above, the measurements were made on high purity $NaBrO_3$ crystals. Consequently, it would be unlikely that a significant number of impurity related color centers would be formed. However, one would expect growth curves attributable to radiation-induced precursor formation and this is actually what is observed.

As stated above the $NaBrO_3$ growth curves can be associated with the general solution and four approximations or special cases. Actually some additional special cases exist which are not exemplified by this data. For example, $N = (\text{constant})t^2$ could occur but is not observed. Furthermore, it is possible for N to increase monotonically to a maximum value and then decrease as the irradiation time becomes large.[15] The latter possibility could occur in $NaBrO_3$ but would, most likely, require longer irradiations than those used.

In summary, exposure to radiation produces at least six color centers in $NaBrO_3$ single crystals. The literature ascribes some of these bands to specific defects. The band parameters (peak energy and full width) appear to be functions of the sample temperature. Individual bands present at low temperature may superimpose to form what may appear to be single broad bands at room temperature. However, it is possible to resolve all the radiation induced absorption spectra into individual Gaussian-shaped bands. The resolved spectra contain five or six prominent absorption bands and indications that one, two, or three additional weak bands may also be present.

(15) P. W. Levy, P. L. Mattern, K. Lengweiler, and A. M. Bishay, *J. Amer. Ceram. Soc.*, submitted for publication.

Color center, *i.e.*, absorption, *vs.* dose or irradiation time curves were obtained for the prominent bands in $NaBrO_3$ at liquid helium, liquid nitrogen, and room temperature. The observed growth curves can be grouped into four categories describable as linear, concave, linear plus saturating exponential, and sigmoid. The various growth curves represent different cases of the relatively simple mechanism for radiation induced defect, color center, and/or radiolysis product formation. The mechanism is based on the assumption that the observed color centers result from a two-stage process; first, defects or color-center precursors are formed, and second, these defects or precursors are converted to color centers by charge trapping.

Finally, the measurements and analyses described above appear to support the contention that color-center techniques are potentially quite useful for studying the kinetics of radiolysis product formation in solids.

Application of Electron Cyclotron Resonance Technique in Studies of Electron Capture Processes in the Thermal Energy Range

K. G. Mothes, E. Schultes, and R. N. Schindler*

Institut für Physikalische Chemie der Kernforschungsanlage Julich GmbH, D 517 Julich, West Germany *(Received April 21, 1972)*

Publication costs assisted by Kernforschungsanlage Julich GmbH

A method is described by which absolute cross sections can be determined for the capture of thermal electrons in the gas phase. Also the energy dependence for the attachment process can be followed in the energy range of 1 to $10kT$. The method is based on electron cyclotron resonance (ecr) measurements of photochemically produced electrons in a fast-flow system. A short account is given of the physical background of the ecr technique. The thermalization of the electrons and the influence of pressure and power on the signal parameters are discussed. Absolute rate constants for the attachment of thermal electrons are reported for the following groups of molecules: (a) very effective electron scavengers, CCl_4, SF_6, C_4F_8, and C_7F_{14}; (b) the CN containing compounds, ICN, ClCN, BrCN, CNCN, HCN, CH_3CN, and C_2H_3CN; and (c) the molecules NF_3, N_2F_4, CF_2Cl_2, $C_2F_4Cl_2$, HBr, and CH_3Br. Electron affinities for SF_6 and C_4F_8 have been calculated with the absolute values of the thermal rate constants. Three typical examples for the energy dependence of the cross section are given.

Introduction

The study of attachment reactions of free, low-energy electrons ($E \sim E_{\text{therm}}$) to molecules has gained increasing interest in the past few years. The investigation of these processes is stimulated by practical aspects, *e.g.* by the search for effective electron scavengers. It provides an abundance of new information concerning the interaction of low-energy electrons with various molecular structures. An excellent survey of the field is given by Christophorou.[1]

In this contribution we describe a new experimental method, with which very accurate quantitative information can be obtained on the elementary step of electron capture in the gas phase. Absolute rate constants and changes of cross sections as a function of electron energy are obtained from measurements of cyclotron resonance (ecr) signals of the free electrons.

The paper contains a brief description of the experimental setup. The ecr signal and its dependence on pressure in the flow system are discussed. A short account is given of the signal line shape and the calibration of ecr signals. The change of electron energy by variation of the microwave power is reported. Rate constants for a number of well-known electron scavengers have been measured. The results are compared with data obtained by other groups. Results are included in this report on the energy dependence of the attachment cross section in the low energy region (1 to $\sim 10kT$).

Experimental Section

The apparatus is shown in Figure 1. It consists of a conventional flow system with flow rates of 20–65 m/sec in the pressure range of 2–50 Torr. Argon or nitrogen are used as a carrier gas, respectively. The flow tube is made of quartz and is provided with pressure measuring devices, flow meters, mixing chamber, etc.

(1) L. G. Christophorou, "Atomic and Molecular Radiation Physics," Wiley-Interscience, London, 1971.

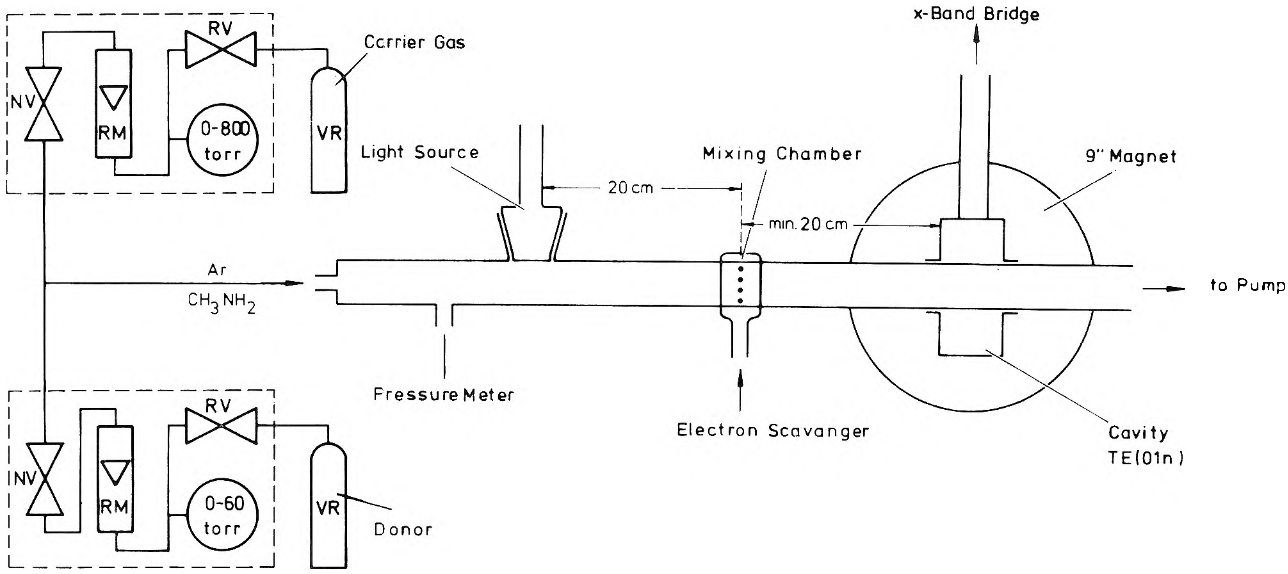

Figure 1. Flow system: NV, needle valve; RV, pressure regulation valve; RM, rotameter; VR, gas tank.

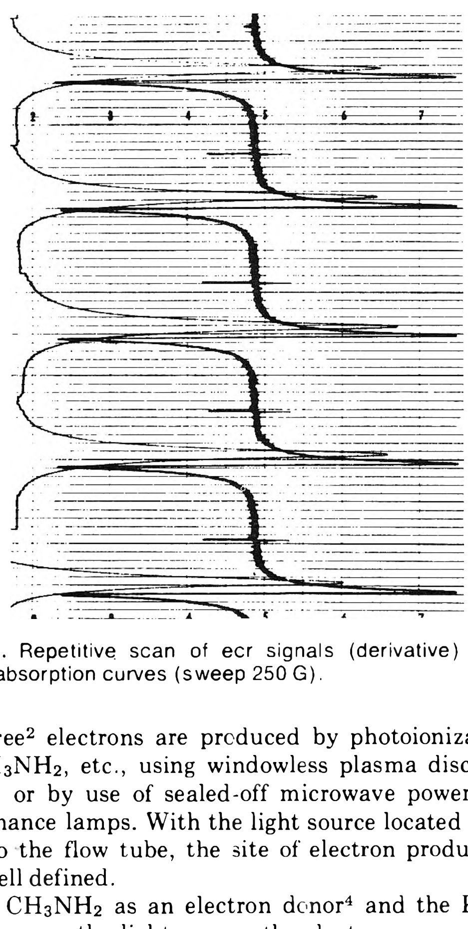

Figure 2. Repetitive scan of ecr signals (derivative) together with the absorption curves (sweep 250 G).

The free[2] electrons are produced by photoionization of NO, CH_3NH_2, etc., using windowless plasma discharges[3] in argon or by use of sealed-off microwave powered rare gas resonance lamps. With the light source located at right angles to the flow tube, the site of electron production is rather well defined.

Using CH_3NH_2 as an electron donor[4] and the Kr resonance lamp as the light source, the electrons are produced with an excess energy of about 1 eV. The thermalization of the electrons occurs in collisions with the buffer gas molecules.[5-7]

The electron concentration is measured with a conventional Varian esr spectrometer, Type 4500-42, with 100-kHz modulation. A cylindrical cavity Type V4535 operating in the TE(01n) mode served as the electron detector. The cavity together with the magnet could be moved along the flow tube.

The cavity consists of two parts: the coupling part and a section carrying the modulation coils. For the measurement of thermal rate constants the latter section pointed toward the mixing chamber. This way microwave heating of the electrons in the cavity was negligible. For the investigation of the energy dependence of cross sections the cavity was rotated so that the coupling part was next to the mixing chamber. In this setup the electrons are heated before entering the detection region. Microwave power was varied between <1 and about 300 μW. Measurement of the power input P_{MW} was carried out with a Hewlett-Packard power meter, Type 4316.

A repetitive scan of a typical ecr signal (derivative) is shown in Figure 2. It demonstrates the constancy of the output. The signal to noise ratio was better than 100:1 in most experiments. The second curve represents the true absorption signal. It was received by electronic integration of the ecr signal.[8] The area under this curve is a direct

(2) Electrons produced by ionization may be recaptured or can escape their parent ions. In the absence of external electric fields the probability for the escape of the electrons depends on the kinetic energy of the particles and on the attractive mutual electric field between ion and electron. The distance for which the potential energy of the electric field equals the thermal kinetic energy kT is given by: $d_{th} = q^2/\epsilon kT$ where q is the electronic charge and ϵ is the dielectric constant. For $T = 25°$ a value $d_{th} = 600$ Å is obtained. If the electron is thermalized beyond this distance d_{th} it will escape its positive ion and will be considered free. On the other hand, if the average distance of thermalization is smaller than d_{th}, recapture is dominant. The thermalization distance for 100 eV electrons in a gas of 1 atm pressure is greater than 10^4 Å. Thus at pressures of 2–50 Torr electrons produced with 1 eV energy can be considered free. This assumption is supported by a rough calculation carried out by S. G. Elkomoss and J. L. Magee, *J. Chem. Phys.*, **36**, 256 (1962).

(3) R. N. Schindler, "Proceedings of the 10th Czechoslovak Annual Meeting on Radiation Chemistry, Marianske Lazne 1970," Vol. I, J. Teply, Ed., Prague, 1971, p 125. K. G. Mothes, Thesis, University of Bonn, Bonn, West Germany, 1970.

(4) Although CH_3NH_2 gives the best electron yields in our system, it cannot be used indiscriminately as an electron donor. Care must be exercised because of possible chemical reactions with the scavenger. In determinations of k values for HBr, HCl, etc., formation of a slight deposit of the ammonium salt along the flow tube was observed. In all these cases NO was used as a donor.

(5) H. J. Oskam, *Philips Res. Rep.*, **13**, 355 (1958).

(6) J. M. Warman and M. C. Sauer Jr., *J. Chem. Phys.*, **52**, 6428 (1970).

(7) V. A. J. van Lint, *IEEE Trans. Nucl. Sci.*, **NS-11**, 266 (1964); V. A. J. van Lint, J. Parez, D. Trueblood, and M. E. Wyatt, *Rev. Sci. Instrum.*, **36**, 521 (1965).

(8) P. Tiedemann, K. G. Mothes and R. N. Schindler, *Messechnik*, **78**, 203 (1970).

measure of the electron concentration in the flow tube (see below).

The sensitivity of the ecr technique allows us to measure electron concentrations down to 10^2 cm^{-3}. The electron concentration in typical experiments was 10^5 to 10^6 cm^{-3}. The disappearance of electrons along the flow tube occurs predominantly *via* free diffusion. Ambipolar diffusion may be excluded under our experimental conditions.[5]

To determine absolute cross sections at thermal energies for the electron capture process, measured amounts of electron scavengers were leaked into the flow system. The mixing chamber was located 20 cm downstream of the site of electron production (Figure 1). Very effective electron scavengers such as CCl_4, SF_6, C_4F_8, C_7F_{14}, etc., were diluted with argon or diethyl ether, respectively, to slow down the reaction. First-order plots of signal intensity *vs.* scavenger concentration yield very good straight lines from the slope of which the rate constant for the reaction is calculated. For the determination of the energy dependence the relative intensity of the absorption signal was measured as a function of the incident microwave power.

Ecr Signal

1. Assignment of the Absorption Signal. In a static magnetic field H a free charged particle will execute circular orbits with a rotational frequency of

$$\omega_c = (e/mc)H \tag{1}$$

where e is the electronic charge, m is the electronic mass, and c is the speed of light. In the case of a free electron, e/mc = 2.799 MHz/G.

Because of the frequency range of our klystron of 9000 ± 500 MHz, cyclotron resonance of the free electron is expected to occur at 3200 ± 200 G. In all experiments we received an intensive absorption signal at a magnetic field of 3150–3200 G depending on the tuning of the cavity.

In principle, three processes may be responsible for this strong energy absorption: (a) spin resonance from positive ions and free electrons; (b) spin resonance of neutral atoms and radicals; and (c) cyclotron resonance from the motion of free electrons. Electron resonances due to processes (a) and (c) will occur at only slightly different magnetic fields due to the fact that g_e is not exactly 2. It has been shown[9] that the probability for a cyclotron transition is proportional to the effective dipole moment, which is given by the product of the charge of the dipole unit times the distance separating the dipolar charges. For the electron in a magnetic field $\mu_e = e \times$ average radius of orbits $\simeq 5 \times 10^{-13}$ erg/G is obtained. This is much greater than the magnetic dipole moment $\mu_B \simeq 10^{-20}$ erg/G which determines the electronic spin flip transition probability. Thus the orbital transition is about 5×10^7 times more probable than the spin flip.[10] In addition, the total number of free electrons contribute to the diamagnetic process, whereas only the statistical excess ($\simeq \mu H/nkT$) is effective in the Zeeman case. Therefore, the possible contributions from spin resonance would be "lost" in the much stronger cyclotron transition.

Another proof that the measured signal could not be attributed to atoms or radicals has been given in recent reports.[3] Further support for the assignment of this signal to the electron cyclotron resonance can be derived from the line shape and the intensity of the absorption signal on variation of microwave power P_{MW} and pressure as described below.

2. Energy Absorption. When an electric field of frequency ω acts on charged particles like electrons, the system will behave like a driven oscillator which resonates when ω approaches the resonance frequency ω_c. In a cylindrical cavity TE(01n) with the uniform magnetic field always at right angles to the alternating electric field $E = E_0 \cos \omega_0 t$, the average real power $\bar{P}$ absorbed by the free electrons in resonance is

$$P = \tfrac{1}{2}\chi''\omega_0 E^2 \tag{2}$$

where ω_0 is the microwave frequency[11] and χ'' is the electric susceptibility. Substitution of the electric susceptibility[12]

$$\chi'' = \frac{N_e e^2}{2m_e\omega_0}\left[\frac{\nu}{\nu^2 + (\omega_0 + \omega_c)^2} + \frac{\nu}{\nu^2 + (\omega_0 - \omega_c)^2}\right] \tag{3}$$

in eq 2 yields[13]

$$P = \frac{N_e e^2 E^2}{4m_e}\left[\frac{\nu}{\nu^2 + (\omega_0 + \omega_c)^2} + \frac{\nu}{\nu^2 + (\omega_0 - \omega_c)^2}\right] \tag{4}$$

Here N_e is the number of electrons, ω_0 is the microwave frequency, and ν is the collision frequency of the electrons with the buffer gas. The collision frequency ν is a function of the electron energy which without an external field applied will assume a Maxwell distribution. If the perturbation by the field is negligible the experimentally observed absorption signal will be the envelope over the individual Lorentz lines described by (3) weighted with a Maxwellian speed distribution of the electrons.

By power absorption in the microwave probe the quality factor of the cavity

$$Q = (\text{energy stored})/\omega_0 \times (\text{energy absorbed})$$

is changed. This alternates the damping of the microwaves by the resonator. The damping results from energy loss in the probe and in the sample. The change in damping due to electron absorption D_e is then given by

$$D_e = \frac{1}{Q_e} = \frac{\tfrac{1}{2}\omega_0 \chi'' E^2}{\tfrac{1}{2}\omega_0 \int_{V_{cav}} E^2 dV} \tag{5}$$

It follows that

$$D_e = \frac{\chi''}{V_{eff}} \tag{6}$$

where

$$V_{eff} = \int_{V_{cav}} E^2 dV/E^2$$

is the effective volume of the cavity. According to eq 6 the signal observed depends on the electric susceptibility of the sample.

(9) R. B. Dingle, *Proc. Roy. Soc., Ser. A*, **212**, 38 (1952).

(10) It is shown by Jones (R. V. Jones, Doctoral Thesis, University of California, Berkeley, Calif., 1956) that for spin resonance and cyclotron resonance signals of equal intensity the ratio of densities is given by $n_s/n_c = 4 \times 10^{13}$. For this calculation $J = \tfrac{1}{2}$ and $g = 2$ has been assumed. Since the limit of detection of spin signals in the gas phase is roughly 10^{11} spins/cm^3, densities of some hundred electrons/cm^3 should be detectable by the ecr technique.

(11) In our measurements the uniform magnetic field H is swept slowly through a range of 100 G/min while the microwave frequency ω is kept constant.

(12) A. A. Westenberg and de Haas, *J. Chem. Phys.*, **40**, 3087 (1964); **43**, 1550 (1965).

(13) D. C. Kelly, H. Margenau, and S. C. Brown, *Phys. Rev.*, **108**, 1367 (1957).

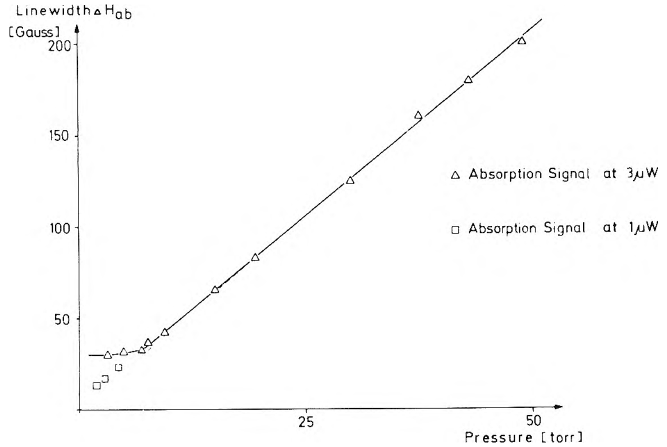

Figure 3. Pressure dependence (in argon) of ecr absorption line width.

In our experiments the change of the electric susceptibility was measured as function of the magnetic field. By use of 100-kHz field modulation and phase sensitive detection, signals corresponding to the derivative $d\chi''/dH$ were obtained. In this way a signal is obtained that corresponds to the derivative of the susceptibility $d\chi''/dH$. Integration of this signal gives the real absorption curve. The area under this line

$$\int_0^{\infty} \chi''_{(H)} dH = \frac{1}{2} \frac{\Pi ec}{\omega_0} N_e \tag{7}$$

is proportional to the electron density in the sample. In addition, it should be stated that the area is independent of P_{MW} (see section on power dependence).

Absolute electron concentrations were obtained by comparing the intensities of an ecr absorption signal and an esr signal of a standard probe which shows intense electric dipole transitions. Following a suggestion of Westenberg, *et al.*,[12] NO was used as a standard.

3. Signal Parameters and Their Dependence on Experimental Conditions. In the following section changes in the absorption signal will be described due to variation in microwave power and in total gas pressure, respectively. Also, the disappearance of electron signal along the flow tube will be considered. The analysis of the line shape, the line width, and the intensity of the absorption signal or its derivative is of great interest. As will be shown, the discussion of these line parameters provides us with information concerning the electron energy distribution in the flow system.

Line Width. Assuming a constant mean lifetime of the electrons in the system, the line width of a resonance absorption signal is a linear function of the collision frequency. In our experiments the collision number can be varied by both the gas pressure and the microwave power incident on the cavity.

Pressure Dependence. In the experiments illustrated in Figure 3, the dependence of line width on gas pressure was studied at a constant microwave power of 3 μW and a modulation amplitude of 0.5 G. The line width was determined from the peak to peak distance ΔH_{pp} of the derivative and from the half-width of the absorption curve ΔH_{ab}, respectively. The reproducibility of ΔH_{ab} and ΔH_{pp} was about 10%. Only H_{ab} is given in Figure 3.

The line width of the ecr signal and hence the collision frequency ν is shown to be a linear function of the pressure in the region of 7–50 Torr but stays constant at pressures <7 Torr. A cross section for the electron–argon collision of 0.7 Å^2 can be determined from the slope of Figure 3.[14] This is in good agreement with the value of 0.6 Å^2 found by microwave technique.[15]

TABLE I: Power Dependence of the Ecr Signal

P_{MW}, μW	ΔH_{ab}, G	ΔH_{pp}, G
0.3	4.6	15
0.6	4.6	15
1.0	4.6	15
1.5	4.6	15
7.5	4.6	16
18.0	5.5	20
60.0	10.5	33
120.0	15.0	43
230.0	19.0	55
300.0	22.0	60

The constancy of ΔH_{ab} at lower total pressures is not an experimental artifact but depends on the microwave power input. At a power input of 1 μW a linear dependence between ΔH_{ab} and pressure exists even down to 2 Torr (Figure 3). This pressure-independent and power-determined plateau can be attributed to non-thermal electrons, the energy distribution of which is dominated by power heating in the cavity (see section on line shape).

Power Dependence. The power dependence of the ecr signal was studied by varying the incident microwave power P_{MW} between 1 and 300 μW at a constant pressure of 3 Torr. The results are given in Table I. As indicated in Table I the width of the ecr signal increases with microwave power input. For P_{MW} < 5 μW the main contribution to line width results from pressure broadening and not from heating of electrons in the cavity.

Line Shape. The line shape of an absorbing system is determined by the interactions between the spin system and its environment. The width of the signal depends on the strength of the interaction and the lifetimes of the states involved. Theory predicts that the line shape of esr signals should be Lorentzian in a homogeneous system in which thermal equilibrium is maintained throughout the resonance process. If the system will not reach thermal equilibrium because the particles cannot loose their excess energy in collisions with the environment, the absorption line will assume Gaussian shape.

In this investigation two sets of experiments were carried out to study the line shape of the ecr signal as a function of electron energy distribution. In one set, the incident microwave power was varied to observe the effect of electron heating by energy absorption. In the second set, the line shape is recorded as a function of thermalization time along the tube at constant power input.

Figure 4 shows the change of line shape as a function of P_{MW}. The derivative signals are normalized in height and width and are compared with pure Lorentzian and Gaussian curves as well as with a Maxwellian curve. The Maxwellian line shape is received by averaging the Lorentzian lines obtained for each range of electron speeds between v and $v + dv$ over a Maxwellian speed distribution.[16] Good

(14) K. G. Mothes, D. Mihelcic, and R. N. Schindler, *Ber. Bunsenges. Phys. Chem.*, **75**, 9 (1971).
(15) A. V. Phelps, O. T. Fundingsland, and S. G. Brown, *Phys. Rev.*, **84**, 559 (1951).
(16) K. D. Bayes, D. Kivelson, and S. C. Wong, *J. Chem. Phys.*, **37**, 1217 (1962).

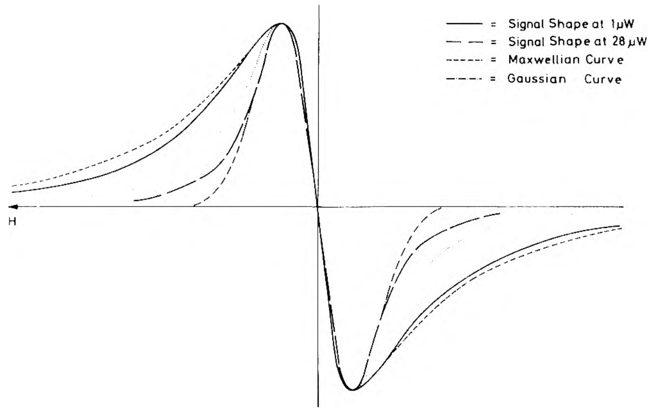

Figure 4. Comparison of the line shape of an ecr signal at 1 and 28 μW.

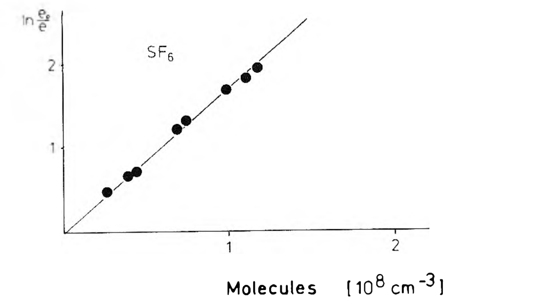

Figure 5. First-order plot for the reaction of thermal electrons with SF_6.

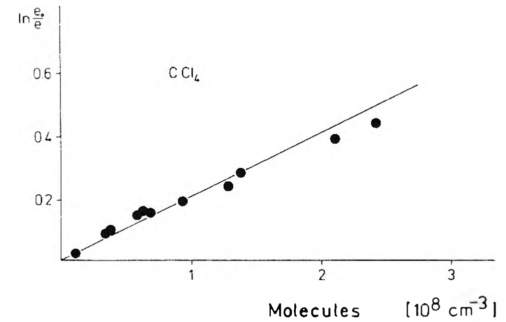

Figure 6. First-order plot for the reaction of thermal electrons with CCl_4.

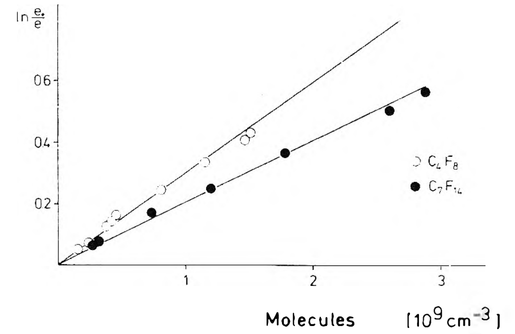

Figure 7. First-order plot for the reaction of thermal electrons with C_4F_8 and C_7F_{14}.

agreement is obtained between the experimental ecr signal and such a Maxwellian curve at 1 μW power input, whereas for 28 μW microwave power a different distribution is obtained which apparently is better described by a Gaussian curve. Therefore, all determinations of thermal rate constants (see below) were carried out at ≤ 1 μW power input. This power is also justified by a rough calculation of the electron heating in the electric microwave field. It has been shown[14,17] that for a pressure >3 Torr the collision number in the system will be high enough to prevent an appreciable increase in electron energy in the cavity.

Using windowless plasma discharges as a light source a number of experiments were carried out in which the ecr signal was measured at various distances (50–10 cm) between the site of electron production and the cavity. The results indicate that for distances >20 cm at 2 Torr of argon the line shape agrees well with the Maxwellian curve shown in Figure 4. This is taken as evidence that thermal equilibrium is practically obtained after this distance. With a Kr resonance lamp as light source the electrons are thermalized within a distance of about 10 cm at 3 Torr of argon. Calculations of the rate of thermalization in argon according to the method described by Oskam[5] yield similar values for this distance.

Measurements of Rate Constants

1. Reinvestigation of Very Effective Electron Scavangers. In this chapter measurements are reported[18] for thermal electron attachment to CCl_4 and a number of fluorine containing compounds. Absolute rate constants are obtained from an analysis of ecr signal intensity as a function of scavenger concentration (see Experimental Section). First-order plots yield very good straight lines in all cases (see Figures 5–7). The single points in the plots are averages of at least five signals. Rate constants for the elementary electron capture process are calculated from the slopes of the straight lines. More than three runs were carried out for each rate constant given below. The experimental scatter is usually approximately 2% within one run and differs less than 5% from run to run.

Our rate constant for thermal electron capture by SF_6 which is attributed to the process

$$SF_6 + e \rightarrow [SF_6^-]^* \rightarrow SF_6^- \qquad (I)$$

together with the values reported by other authors is given in Table II.[19-31] There is general agreement that the values given in the lower part of the table are too low. The values at the top are in the range of 2.2×10^{-7} to 2.7×10^{-7} cm^3/sec. Christophorou's values of 2.7×10^{-7} and 2.8×10^{-7} cm^3/sec, respectively, are obtained by mathematical extrapolation to thermal electron energies.

(17) E. Schultes, Thesis, University of Bonn, Bonn, West Germany, 1970.
(18) K. G. Mothes and R. N. Schindler, *Ber. Bunsenges. Phys. Chem.*, **75**, 936 (1971).
(19) G. E. Young, University of California Radiation Laboratory Report, M.C.R.L.-17171 (1966).
(20) L. G. Christophorou, D. L. McCorkle, and J. G. Carter, *J. Chem. Phys.*, **54**, 253 (1971).
(21) C. L. Chen and P. J. Chantry, Abstracts of 22nd Gaseous Electronics Conference, Gatlinburg Tenn., Oct 27–31, 1969, Paper J3, p 39.
(22) F. C. Fehsenfeld, *J. Chem. Phys.*, **53**, 2000 (1970).
(23) F. J. Davis and D. R. Nelson, *Chem. Phys. Lett.* **6**, 277 (1970).
(24) R. W. Fessenden and K. M. Bansal, *J. Chem. Phys.*, **53**, 3468 (1970).
(25) R. N. Compton, L. G. Christophorou, G. S. Hurst, and P. W. Reinhardt, *J. Chem. Phys.*, **45**, 4634 (1966).
(26) G. R. Freeman, *Radiat. Res. Rev.*, **1**, 1 (1968).
(27) J. B. Hasted and S. Beg, *Brit. J. Appl. Phys.*, **16**, 74 (1965).
(28) D. Rapp and D. D. Briglia, *J. Chem. Phys.*, **43**, 1480 (1965).
(29) R. K. Asundi and J. D. Craggs, *Proc. Phys. Soc.*, **83**, 611 (1963).
(30) N. S. Buchelnikova, *Zh. Eksper. Teor. Fiz.*, **35**, 1119 (1959).
(31) W. M. Hickam and R. E. Fox, *J. Chem. Phys.*, **25**, 642 (1956).

TABLE II: Rate Constants k (cm^3/sec) for the Capture of Thermal Electrons by SF_6 (T = 300°K)

k	Carrier gas	Method	Ref
2.6×10^{-7}	Ar	Cyclotron resonance	18
2.7×10^{-7}	He	Microwave	19
2.7×10^{-7}	N_2	Electron swarm	20
2.8×10^{-7}	C_2H_4	Electron swarm	20
2.42×10^{-7}	90% Ar + 10% CH_4	Pulse sampling	21
2.21×10^{-7}	He	Flowing afterglow	22
2.16×10^{-7}	He	Electron swarm[a]	23
2.21×10^{-7}	C_3H_8	Microwave	24
3.85×10^{-8}	C_2H_4	Electron swarm[b]	25
3.82×10^{-12}	C_7F_{14}	Radiolysis[c]	26
2.9×10^{-13}	Xe	Flowing afterglow	27
5.0×10^{-9}		Total ion current[d]	28
1.5×10^{-9}		Total ion current[d]	29
6.8×10^{-9}		Total ion current[d]	30
6.8×10^{-8}		Mass spectrometry	31

[a] Besides He, Davis and Nelson used N_2, H_2, CO_2, CH_4, CH_4 + Ar, CF_4, C_2H_2, C_2H_4, C_2F_6, *cis*-C_4H_8, and C_4H_{10} as carrier gases. Average is 2.0×10^{-7} cm^3/sec. [b] This value is too low due to an error in the pressure measurements.[20] [c] Temperature 380°K. [d] Calculated from the cross section in the maximum.

TABLE III: Rate Constants k (cm^3/sec) for the Capture of Thermal Electrons by CCl_4 (T = 300°K)

k	Carrier gas	Method	Ref
4.1×10^{-7}	Ar	Cyclotron resonance	18
4.0×10^{-7}	*n*-Hexane	Microwave	6
2.9×10^{-7}	N_2	Electron swarm	32
2.9×10^{-7}	a	Electron swarm	33

[a] The rate constant given is the average for the carrier gases C_2H_2, CO_2, and CH_3OH.

For the dissociative thermal electron capture by CCl_4

$$CCl_4 + e \rightarrow CCl_3 + Cl^- \qquad (II)$$

a rate constant of 4.1×10^{-7} cm^3/sec was obtained. It is listed together with the k values of other authors in Table III.[32,33] Our value is in excellent agreement with the rate constant reported by Warman, *et al.*[6] The rate constants measured by electron swarm technique are about 30% lower than these values. We attribute this to a higher than thermal electron energy in those experiments.

Further very critical and most efficient electron scavengers are the compounds C_7F_{14} and C_4F_8. The rate constants for the capture processes

$$C_7F_{14} + e \rightarrow [C_7F_{14}^-]^* \rightarrow C_7F_{14}^- \qquad (III)$$

$$C_4F_8 + e \rightarrow [C_4F_8^-]^* \rightarrow C_4F_8^- \qquad (IV)$$

are compared with the values obtained by other methods in Table IV.[34] The discrepancy between our k value for C_7F_{14} and the other values is attributed to the fact that cross sections at thermal energies are measured by ecr technique with a very narrow energy distribution. If the energy spread of the electrons is 0.2–0.3 eV wide, as for instance in some beam experiments, contributions from the adjacent maximum will result in a higher measured rate constant. The C_4F_8 value given by Kurepa[34] is reported not to be reliable since the $C_4F_8^-$ ion currents have not been normalized correctly.[35]

From the measured rate constants for SF_6 and C_4F_8 together with known data for the lifetime of the corresponding negative parent ions the electron affinities ϵ for the two molecules were calculated. The calculation is based on a model for the non-dissociative electron attachment proposed by Compton, *et al.*,[36] with the vibrational frequencies taken from ref 37 and 38. The following values were obtained: $\epsilon(SF_6)$ = 1.3 eV; $\epsilon(C_4F_8)$ = 0.61 eV. The molecules CCl_4 and SF_6 have a sharp peak for electron capture near thermal energies. Thus their absolute cross section in the maximum can only be measured with electrons of well defined thermal energies.

2. Further Measurements of Rate Constants. Rate constants for compounds which do not react as effectively with thermal electrons as SF_6 or CCl_4 are more convenient to measure. However, it must be taken into account that even very small impurities of an effective scavenger might alter the absolute value of the rate constant markedly. Thus very sensitive chemical analysis to assure the absence of effectively scavenging impurities is required.

In Table V[39,40] a number of rate constants are given for the attachment of thermal electrons to simple halogen- or CN-containing compounds. Except for methyl bromide no other data are available from the literature for comparison.

3. Energy Dependence of Cross Sections. The energy dependence of the capture process was studied by variation of microwave power input into the cavity. The results of a series of experiments are reported in Figure 8. The electron energy in the flow system at constant pressure is a function of the average electric field strength in the cavity. Since the modulus of the E vector is directly proportional to the square root of P_{MW}, a linear energy scale is obtained if $P_{MW}^{1/2}$ is plotted as the abscissa. In the ordinate relative changes of the cross section are plotted.

(32) R. P. Blaunstein and L. G. Christophorou, *J. Chem. Phys.*, **49**, 1526 (1968).
(33) L. Bouby, F. Fiquet-Fayard, and H. Abgrall *C. R. Acad. Sci., Paris*, **261**, 4059 (1965).
(34) M. V. Kurepa, *Proc. 3rd Czech. Conf. Electron. Vacuum Phys. Trans., Prague*, 107 (1965).
(35) W. T. Naff, C. D. Cooper, and R. N. Compton, *J. Chem. Phys.*, **49**, 2784 (1968).
(36) R. N. Compton, G. S. Hurst, L. G. Christophorou, and P. W. Reinhardt, ORNL-TM-1409 (March 1966).
(37) C. W. F. T. Pistorius, *J. Chem. Phys.*, **29**, 1328 (1959).
(38) H. H. Claasen, *J. Chem. Phys.*, **18**, 543 (1950).
(39) K. M. Bansal and R. W. Fessenden, *Chem. Phys. Lett.* in press.
(40) A. A. Christodulides and L. G. Christophorou, *J. Chem. Phys.*, **54**, 4691 (1971).

TABLE IV: Rate Constants k (cm^3/sec) for the Capture of Thermal Electrons by C_7F_{14} and C_4F_8 (T = 300°K)

Scavenger	k	Carrier gas	Method	Ref
C_7F_{14}	5.2×10^{-8}	Ar	Cyclotron resonance	18
C_7F_{14}	8.8×10^{-8}	He	Microwave	19
C_7F_{14}	8.2×10^{-8}	a	Total ion current	29
C_7F_{14}	7.98×10^{-8}	90%Ar + 10%CH_4	Pulse sampling	21
C_4F_8	1.1×10^{-7}	Ar	Cyclotron resonance	18
C_4F_8	2.4×10^{-10}		Total ion current	34

[a] Calculated from cross section in the maximum.

TABLE V: Rate Constants k (cm^3/sec) for the Capture of Thermal Electrons by CN- or Haolgen-Containing Molecules (T = 300°K)

Scavenger	k
ICN	2.1×10^{-9}
BrCN	1.8×10^{-7}
ClCN	1.1×10^{-10}
CNCN	4.6×10^{-11}
CH_3CN	7.2×10^{-12}
C_2H_3CN	5.6×10^{-11}
HCN	9.1×10^{-11}
NF_3	2.4×10^{-11}
N_2F_4	3.8×10^{-9}
CF_2Cl_2	8.3×10^{-10}
$C_2F_4Cl_2$	1.2×10^{-10}
HBr	9.6×10^{-11}
CH_3Br	3.6×10^{-12a}

[a] Other reported values: $k = 1.0 \times 10^{-11}$, Schindler,[3] $k = 7.0 \times 10^{-12}$, Fessenden,[39] $k = 1.0 \times 10^{-9}$ (E = 0.05eV), Christophorou.[40]

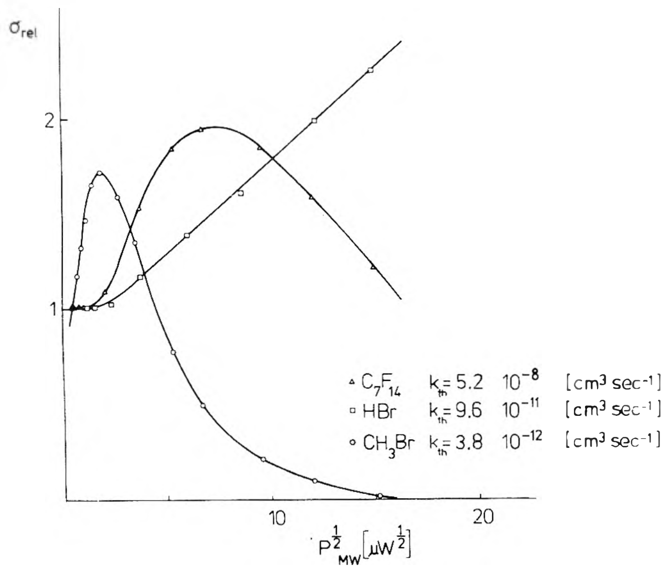

Figure 8. Energy dependence of the attachment cross section for CH_3Br, C_7F_{14}, and HBr. The curves are normalized at P = 0.3 μW incident powe-.

A correlation between $P_{MW}^{1/2}$ and absolute energy values is obtained by comparing the energy for a maximum or minimum in the cross section curve measured by ecr technique with results from beam experiments.[41] This scaling reveals that, *e.g.*, $P_{MW}^{1/2}$ = 7.5 $\mu W^{1/2}$ corresponds to (0.15 ± 0.05) eV or (6 ± 2)kT. A detailed discussion of the electron energy distribution in the cavity indicates that the energy spread for electrons having mean velocities of 1-6kT is narrower in ecr experiments than in beam experiments. For electron energies >6kT mass spectrometric data give more detailed information than ecr results. Since from the chemical point of view information on reactive cross sections for temperatures <3000°K ≡ 10kT are of high practical interest, the data obtained in the energy range accessible to ecr experiments are considered chemically relevant.

Figure 8 shows three characteristically different examples of the variation of the attachment cross section with energy. The curves are normalized at the lowest incident P_{MW} = 0.3 μW, *i.e.*, at minimal electrical perturbation. For methyl bromide a sharp peak with a maximum around 0.05 eV is observed. A half-width of <0.1 eV can be taken from the figure. For C_7F_{14} a half-width of <0.3 eV is estimated. In HBr only an increase in cross section is obtained with the ecr technique, although energies up to about 0.4 eV should be accessible for measurements with this method.[41]

Final Remarks

Evidence has been presented that the ecr method is a rather convenient and direct technique for the measurement of capture rate constants of thermal electrons to suitable molecules. Values obtained with this technique for CCl_4 as well as for SF_6 agree very well with the largest measured rate constants. This supports our finding that the electrons which are produced photochemically and are transported by the carrier gas down the flow tube possess a narrow thermal energy distribution when entering the reaction zone. Also, the arrangement can be adjusted to study the energy dependence of attachment processes in the chemically relevant range up to roughly 10kT. For C_7F_{14} a stronger energy dependence of the attachment cross section was found below 0.15 eV ≡ 6kT than in beam experiments. This is corroborated by the fact that a smaller cross section for electron attachment at thermal energies is measured with the ecr technique. In methyl bromide a fully resolved attachment peak with a maximum around 0.05 eV was obtained. The reported maximum in the HBr case is experimentally not accessible with this technique. More details on rate constants, activation energies, and energy dependences, respectively, in cyanides and halides will be given elsewhere.[41-43]

(41) K. G. Mothes, E. Schultes, and R. N. Schindler, *Ber. Bunsenges. Phys. Chem.*, in press.
(42) E. Schultes, K. G. Mothes, and R. N. Schindler, submitted for publication in *Ber. Bunsenges. Phys. Chem.*
(43) K. G. Mothes, Doctoral Thesis, University of Bonn, Bonn, West Germany, 1972; E. Schultes, Doctoral Thesis, University of Bonn, Bonn, West Germany, 1973.

Solvated Electrons in Irradiated Concentrated Alkaline Methanol and Water–Methanol Mixtures

A. K. Pikaev,* T. P. Zhestkova, and G. K. Sibirskaya

Institute of Physical Chemistry of Academy of Sciences of the U.S.S.R., Moscow, U.S.S.R. *(Received April 21, 1972)*

The properties of solvated electrons (e_s^-) in concentrated alkaline methanol and water–methanol mixtures with emphasis on their optical absorption spectra, decay kinetics, and yields have been studied by the pulse radiolysis method. In methanol at $[CH_3ONa] \geq 3.5$ *M* a maximum (λ_{max}) of e_s^- optical band is shifted slightly to the shorter wavelengths. In alkaline water–methanol mixtures λ_{max} has an intermediate position between pure alkaline methanol and water. In some cases the optical band of e_s^- also has a shoulder at longer wavelengths, which seems to belong to a particle of the type $Me^+\cdots e_s^-$. The e_s^- decay in alkaline methanol occurs in a reaction of pseudo-first order; in water–methanol mixtures the kinetics of this process is complex. The rate constants $k(H + CH_3O^-)$ in alkaline methanol and $2k(e_s^- + e_s^-)$ in water–methanol mixtures have been evaluated. The first rate constant is equal to $\sim 1.2 \times 10^7$ M^{-1} sec^{-1}; the second is dependent on water content in the mixture, increasing from $\leq 10^9$ M^{-1} sec^{-1} for 5.5 *M* methanolic solution of CH_3ONa to $\sim$ (3-4) $\times 10^9$ M^{-1} sec^{-1} for 6 *M* aqueous solution of NaOH. The values of $G(e_s^-)\epsilon_{max}$ (ϵ_{max} is molar extinction coefficient of e_s^- at λ_{max}) have been measured. It has been estimated that in alkaline methanol ϵ_{max} is equal to 9.7×10^3 M^{-1} cm^{-1}. It is increased with the growth of water content in the mixture, reaching 1.6×10^4 M^{-1} cm^{-1} for 6 *M* aqueous solution of NaOH.

Introduction

It is well known (see, *e.g.*, ref 1 and 2) that upon irradiation of water, alcohols, and water–alcohol mixtures the solvated electron (e_s^-) is formed as one of the main products of the radiolysis. However, the properties of this particle have been studied mainly in neutral liquids. In alkaline medium the behavior of e_s^- can be quite different in comparison with the neutral medium. Recently[3,4] it was found that in water in the presence of ions of alkaline metals the solvated electron seems to form particles of type $Me^+\cdots e_s^-$ (Me^+ is a cation). In alkaline alcohols and water–alcohol mixtures this effect has not been studied. This is one of the reasons for carrying out the present investigation. Methanol has been chosen because of better solubility of alcoholate and alkali in this alcohol in comparison with other alcohols. Besides, in the case of alcohols it was found[5-8] that in alkaline medium $G(e_s^-)$ and the lifetime of e_s^- are higher than in neutral medium. In particular, in sufficiently concentrated alkaline solutions $G(e_s^-)$ is equal to the yield of initial ionization of alcohol.[6,8] Further, in alkaline methanol the e_s^- decay is a pseudo-first-order reaction[5,6,8]. However, in alkaline water this process is more complex (see, *e.g.*, ref 9-11). Obviously, it is interesting to study the possible influence of water addition on the yields and stability of e_s^- in alkaline alcohol. In our work the pulse radiolysis method with optical registration of short-lived species has been used for the investigation of e_s^- properties.

Experimental Section

The linear electron accelerator U-12 was used as a source of pulse-ionizing radiation. The energy of electrons is 5 MeV and pulse duration is 2.3×10^{-6} sec. The measurement of optical absorption of solvated electrons and the study of decay kinetics of these species were achieved by a means of the pulse radiolysis apparatus.[8]

Methyl alcohol used was of Chemically Pure grade and contained about 1.5% water. It was purified by refluxing with 2,4-dinitrophenylhydrazine in the presence of sulfuric acid; then it was twice distilled in a nitrogen atmosphere, middle fractions being retained. Triple distilled water was used for a preparation of the mixtures. Sodium metal, KOH, and RbOH were of Chemically Pure grade and were not subjected to any additional purification. Sodium hydroxide was of Chemically Pure grade and was purified by recrystallization. Alkaline methanol and water–methanol mixtures were prepared by the addition of sodium metal in inert atmosphere or by the dissolution of alkali. Before irradiation the solutions were saturated with argon of Especially Pure grade by prolonged bubbling.

The solutions were irradiated in quartz cylindrical cells (volume 2 ml) at room temperature. The dose in solution along the path of analyzing light was determined by means of a 5×10^{-3} *M* solution of KCNS saturated with oxygen. The values of the molar extinction coefficient of $(CNS)_2^-$ at λ_{max} 475 nm and $G[(CNS)_2^-]$ were taken to be equal to 7.3×10^3 M^{-1} cm^{-1} [12,13] and 2.9 radicals/100 eV.[12] The charge collected on a platinum wire in solution or on a metal holder of the cell was used as a secondary standard. The doses per pulse were from 2 to 11 krads.

(1) A. K. Pikaev, "Sol'vatirovannyi elektron v radiatsionnoi khimii," Izdatel'stvo "Nauka", Moskva, 1969.
(2) E. J. Hart and M. Anbar, "The Hydrated Electron," Wiley-Interscience, New York, N. Y., 1970.
(3) C. Gopinathan, E. J. Hart, and K. H. Schmidt, *J. Phys. Chem.*, **74**, 4169 (1970).
(4) S. A. Kabakchi and V. N. Shubin, *Int. J. Radiat. Phys. Chem.*, **4**, 1 (1972).
(5) S. Arai, A. Kira, and I. Imamura, *J. Phys. Chem.*, **74**, 2102 (1970).
(6) J. W. Fletcher, P. J. Richards, and W. A. Seddon, *Can. J. Chem.*, **48**, 1645 (1970).
(7) G. K. Sibirskaya and A. K. Pikaev, *Khim. Vys. Energ.*, **4**, 472 (1970).
(8) A. K. Pikaev, G. K. Sibirskaya, E. M. Shirshov, P. Ya. Glazunov, and V. I. Spitsyn, *Dokl. Akad. Nauk SSSR*, **200**, 383 (1971).
(9) M. S. Matheson and J. Rabani, *J. Phys. Chem.*, **69**, 1324 (1965).
(10) S. Gordon, E. J. Hart, M. S. Matheson, J. Rabani, and J. K. Thomas, *Discuss. Faraday Soc.*, **85**, 1375 (1963).
(11) W. C. Gottschall and E. J. Hart, *J. Phys. Chem.*, **71**, 2101 (1967).
(12) G. E. Adams, J. W. Boag, J. Currant, and B. D. Michael, "Pulse Radiolysis," M. Ebert, *et al.*, Ed., Academic Press, New York, N. Y., 1965, p 117.
(13) J. H. Baxendale, P. L. T. Bevan, and D. A. Stott, *Trans. Faraday Soc.*, **64**, 2389 (1968).

Results and Discussion

In the case of methanol containing ~1.5% water it was possible to study the properties of e_s^- at concentration of CH_3ONa up to ~5.5 *M*. It was found that the maximum (λ_{max}) of the e_s^- optical band at $[CH_3ONa] \geq 3.5$ *M* is shifted slightly to the shorter wavelengths. In Figure 1 are compared as an example the e_s^- optical spectra in neutral methanol and methanol containing 5.5 *M* CH_3ONa. The λ_{max} values of e_s^- optical absorption bands in methanol at different concentrations of CH_3ONa are given in Table I. Let us note that in neutral methanol λ_{max} = 640 nm. This agrees with previous measurements (see ref 1). Perhaps, as in the case of hydrated electrons (e_{aq}^-),[14] the shift of λ_{max} is due to the decrease of size of "cavities" in which the electrons are localized.

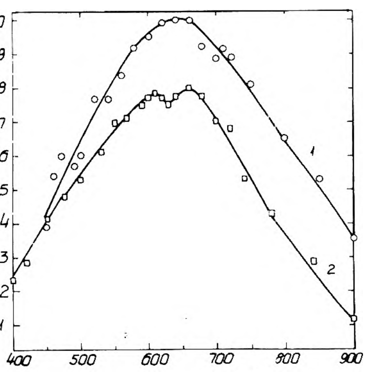

Figure 1. Optical absorption spectra of solvated electron in (1) neutral methanol (*n* = 0) and (2) methanol containing 5.5 *M* CH_3ONa (*n* = 0.2). Here and in Figure 2 and 3 D_{max} is the optical density of λ_{max}.

TABLE I: Influence of KOH or CH_3ONa on Optical Characteristics of Solvated Electron in Irradiated Methanol[a]

Solute	λ_{max}, nm	$W_{1/2}$, eV
	640 ± 10	1.23 ± 0.04[b]
2.7 *M* CH_3ONa	640 ± 10	1.30 ± 0.04
3 *M* KOH	640 ± 10	1.26 ± 0.05
3.6 *M* CH_3ONa	630 ± 10	1.28 ± 0.05
5.5 *M* CH_3ONa	610 ± 10	1.35 ± 0.05

[a] $W_{1/2}$ means half-width of optical absorption band. [b] Literature data (M. C. Sauer, S. Arai, and L. M. Dorfman, *J. Chem. Phys.*, **42**, 708 (1965); F. S. Dainton, J. P. Keene, T. J. Kemp, G. A. Salmon, and J. Teply, *Proc. Chem. Soc., London*, 265 (1964)) for neutral methanol are the following: λ_{max} 630–650 nm; $W_{1/2}$ = 1.29 eV.

Besides the e_s^- maximum, the optical absorption spectrum of irradiated methyl alcohol containing 5.5 *M* CH_3ONa has a shoulder at the longer wavelengths (see Figure 1). In this system it is at ~670–700 nm. This effect is more distinct in ~8 *M* methanolic solution of RbOH and in water–methanol mixture of 1:1 (by volume) composition containing 8 *M* KOH (see Figure 2). In Figure 2 is also shown for a comparison the optical absorption spectrum of irradiated 16 *M* aqueous solution of KOH. This spectrum is similar to the spectrum which was reported earlier.[4,15]

The introduction of water into alkaline methanol (the investigation was carried out with the mixtures in which 6 *M* Na were dissolved) causes the narrowing the e_s^- band and the shift of λ_{max} to the longer wavelengths (see Table II). Similar phenomenon was described earlier[16] for neutral water–methanol mixtures. Because of this effect the overlapping of the e_s^- maximum and the shoulder under consideration takes place with the increase of water content in the mixture. In particular, the shoulder is not observed in the mixtures in which the concentration of water is equal to 40–60 vol %. In the spectra of alkaline mixtures of composition of 75–85% H_2O and 25–15% CH_3OH (by volume) and in 6 *M* aqueous solution of NaOH there is a bend in the region 700–750 nm. The optical absorption spectra of alkaline water–methanol mixtures are shown in Figure 3.

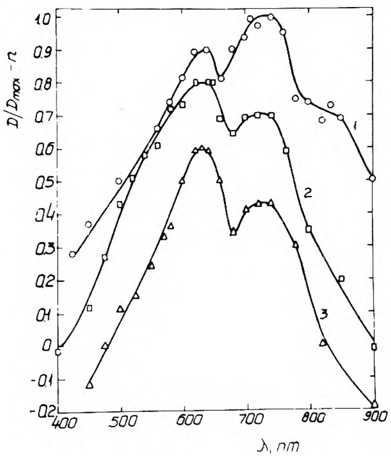

Figure 2. Optical absorption spectra of solvated electron in (1) ~8 *M* solution of RbOH in methanol (*n* = 0), (2) water–methanol mixture of 1:1 composition (by volume) containing 8 *M* KOH (*n* = 0.2), and (3) 16 *M* aqueous solution of KOH (*n* = 0.4).

TABLE II: Characteristics of Optical Absorption Spectra of Solvated Electron in Water-Methanol Mixtures Containing 6 *M* CH_3ONa and/or NaOH[a]

Mixture composition, vol %	λ_{max}, nm	$W_{1/2}$, eV
85% CH_3OH–15% H_2O	620 ± 10	1.26 ± 0.04
75% CH_3OH–25% H_2O	630 ± 10	1.12 ± 0.04
60% CH_3OH–40% H_2O	640 ± 10	1.04 ± 0.04
50% CH_3OH–50% H_2O	650 ± 10	0.98 ± 0.04
40% CH_3OH–60% H_2O	660 ± 10	0.95 ± 0.05
25% CH_3OH–75% H_2O	665 ± 10	0.95 ± 0.04
15% CH_3OH–85% H_2O	670 ± 10	0.92 ± 0.04
100% H_2O[b]	675 ± 10	0.95 ± 0.04

[a] The e_s^- band in the mixture of composition of 40% CH_3OH and 60% H_2O containing 9.2 *M* NaOH has λ_{max} 640 nm and $W_{1/2}$ = 1.03 eV. [b] Literature data (E. J. Hart and J. W. Boag, *J. Amer. Chem. Soc.*, **84**, 4090 (1962); J. P. Keene, *Radiat. Res.*, **22**, 1 (1964)) for neutral water are the following: λ_{max} 720 nm and $W_{1/2}$ = 0.92 eV.

The maximum and the shoulder (or the second maximum in highly concentrated alkaline solutions) seem to belong to the two different species. By analogy with alkaline aqueous solutions[4] it can be supposed that the shoulder (or the second maximum) under consideration is due to the particle of type $Me^+ \cdots e_s^-$.

The solvated electron in methanolic solutions of CH_3ONa over the whole studied range of concentrations (to

(14) M. Anbar and E. J. Hart, *J. Phys. Chem.*, **69**, 1244 (1965).
(15) S. A. Kabakchi, *Khim. Vys. Energ.*, **5**, 180 (1971).
(16) S. Arai and M. S. Sauer, *J. Chem. Phys.*, **44**, 2297 (1966).

TABLE III: Observed Rate Constants k' of e_s^- Decay in Alkaline Methanol[a]

Solute	k', sec^{-1} $\times 10^{-4}$	Solute	k', sec^{-1} $\times 10^{-4}$
	~ 35[b]		
2.7 M CH_3ONa	9.8	3.7 M KOH	6.3
3.0 M CH_3ONa	9.8	4.4 M CH_3ONa	7.8
3.0 M KOH	7.0	5.0 M CH_3ONa	7.4
3.3 M CH_3ONa	9.3	5.5 M CH_3ONa	6.1
3.6 M CH_3ONa	8.6	~ 8 M RbOH	4.0

[a] The precision of k' measurements is equal to ±20%. [b] Value taken from ref 8.

~ 5.5 M) decays during the process of pseudo-first order. The observed rate constants k' of this process are given in Table III. Usually the e_s^- decay was monitored at 600 nm. The kinetics was also measured by using the wavelengths 525, 700, and 800 nm, when identical results were obtained. The rate constants are independent of the dose per pulse (it was changed from 2 to 1: krads). From this it follows that the e_s^- decay reactions of second order are practically absent. Hence it may be concluded that in alkaline methanol the role of reaction 1 under studied conditions is negligible.

$$e_s^- + e_s^- + 2CH_3OH \rightarrow H_2 + 2CH_3O^- \qquad (1)$$

Obviously, the e_s^- disappearance during the process of pseudo-first order is mainly due to the reaction of the solvated electron with methyl alcohol

$$e_s^- + CH_3OH \rightarrow H + CH_3O^- \qquad (2)$$

Earlier[8] it was found that the rate constant of the e_s^- decay in alkaline methanol is independent of the concentration of CH_3ONa and KOH over the range of concentrations 0.1–2 and 0.1–1.5 M, respectively. Under such conditions it is equal to $\sim 2 \times 10^5$ sec^{-1}. From this it was concluded that $k_2 \sim 8 \times 10^3$ M^{-1} sec^{-1}. This value is close to the rate constant of the reaction of the solvated electron with ethyl alcohol, which is equal to $(7\text{–}10) \times 10^3$ M^{-1} sec^{-1},[6,8] but is much higher than the rate constant of the e_{aq}^- reaction with water (16 M^{-1} sec^{-1}).[17] From the results of the present work it follows that the rate constant of the e_s^- decay in more concentrated solutions of CH_3ONa or KOH is noticeably less than the k_2 value. This effect can be explained by the competition of reactions 3–5 in such solutions.

$$H + CH_3OH \rightarrow H_2 + CH_2OH \qquad (3)$$

$$H + CH_3O^- \rightarrow H_2 + CH_2O^- \qquad (4)$$

$$H + CH_3O^- \rightarrow e_s^- + CH_3OH \qquad (5)$$

Let us assume that e_s^- reacts with CH_3O^- ions much slower than with CH_3OH and that $k_3 = k_4$. Then k' is approximately equal to

$$k' \sim k_2[CH_3OH]/(1 + \frac{k_5[CH_3O^-]}{k_3[CH_3OH + CH_3O^-]}) \qquad (6)$$

From eq 6 and the experimental dependence of k' values on CH_3O^- concentration the rate constant of reaction 5 can be evaluated. In the calculations it is proposed that the k_3 values in methanol and water are identical (in the case of water k_3 is known and equal to 1.6×10^6 M^{-1} sec^{-1}).[18] From this one obtains $k_5 \sim 1.2 \times 10^7$ M^{-1} sec^{-1}.

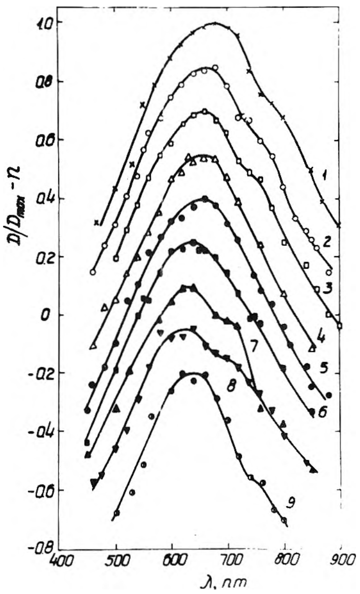

Figure 3. Optical absorption spectra of solvated electron in (1) 6 M aqueous solution of NaOH (n = 0), water–methanol mixtures (volume per cents) in which 6 M Na was dissolved (2) 85% H_2O–15% CH_3OH (n = 0.15), (3) 75% H_2O–25% CH_3OH (n = 0.3), (4) 60% H_2O–40% CH_3OH (n = 0.45), (5) 50% H_2O–50% CH_3OH (n = 0.6), (6) 40% H_2O–60% CH_3OH (n = 0.75), (7) 25% H_2O–75% CH_3OH (n = 0.9), (8) 15% H_2O–85% CH_3OH (n = 1.05), and (9) 9.2 M solution of NaOH in the mixture of composition 40% CH_3OH–60% H_2O (n = 1.2).

This approximate value is close to the rate constant of similar reaction in water

$$H + OH^- \rightarrow e_{aq}^- + H_2O \qquad (7)$$

which equals $(1.8\text{–}2.3) \times 10^7$ M^{-1} sec^{-1}.[9,17]

Another possible reason for the k' decrease in concentrated methanolic solutions of CH_3ONa is the formation of the particle of type $Me^+ \cdots e_s^-$ and the presence of equilibrium

$$Me^+ \cdots e_s^- \rightleftharpoons Me^+ + e_s^- \qquad (8)$$

Such an equilibrium was postulated in the work[4] on concentrated alkaline aqueous solutions. However, in our case the Me^+ concentration is not so high; because of this the concentration of $Me^+ \cdots e_s^-$ is comparatively low, and such particles do not have any noticeable effect on the rate of the e_s^- decay. This conclusion is confirmed by the identity of the rate of the e_s^- band disappearance over the range of wavelengths 525–800 nm.

The half-life ($t_{1/2}$) of solvated electron in alkaline water–methanol mixtures containing 6 M CH_3ONa and/or NaOH is dependent on the mixture composition. At first $t_{1/2}$ increases with increasing water content, reaching the maximum value in the mixtures which contain 40–60 vol % water, then $t_{1/2}$ decreases. The values of $t_{1/2}$ are shown in Figure 4.

The kinetics of e_s^- decay in alkaline water–methanol mixtures which were studied is complex. In mixtures containing up to 25 vol % water the observed rate constant of this process is practically independent of the dose per pulse (or on initial optical density D_0 of solution within the e_s^- band). At the higher water content such a depen-

(17) E. J. Hart, S. Gordon, and E. M. Fielden, *J. Phys. Chem.*, **70**, 150 (1966).
(18) P. Neta, R. Fessenden, and R. H. Schuler, *J. Phys. Chem.*, **75**, 1654 (1971).

TABLE IV: Values of k_{I}, $k_{\mathrm{eff}}/\epsilon$, and $2k_{11}$ for Alkaline Solutions[a]

Composition of system[b]	k_{I}, sec^{-1}	$k_{\mathrm{eff}}/\epsilon$, cm sec^{-1}	Value of ϵ used at 600 nm,[c] M^{-1} cm^{-1}	$2k_{11}$, M^{-1} sec^{-1}
5.5 M solution of CH_3ONa in CH_3OH	$(6.1 \pm 1.3) \times 10^4$			
85% CH_3OH–15% H_2O–6 M Na	$(5.7 \pm 1.2) \times 10^4$			
75% CH_3OH–25% H_2O–6 M Na	$(3.2 \pm 0.7) \times 10^4$			
60% CH_3OH–40% H_2O–6 M Na	$(3 \pm 2) \times 10^4$	$(1.1 \pm 0.6) \times 10^5$	1.1×10^4	$(1.2 \pm 0.7) \times 10^9$
50% CH_3OH–50% H_2O–6 M Na	$(2.9 \pm 1.5) \times 10^4$	$(8 \pm 3) \times 10^5$	1.1×10^4	$(9 \pm 3) \times 10^8$
40% CH_3OH–60% H_2O–6 M Na	$(1.5 \pm 1.1) \times 10^4$	$(1.7 \pm 0.4) \times 10^5$	1.3×10^4	$(2.2 \pm 0.5) \times 10^9$
25% CH_3OH–75% H_2O–6 M Na	$(3 \pm 2) \times 10^4$	$(2.2 \pm 0.6) \times 10^5$	1.4×10^4	$(3.1 \pm 0.8) \times 10^9$
15% CH_3OH–85% H_2O–6 M Na	$(1.3 \pm 0.7) \times 10^4$	$(2.6 \pm 0.4) \times 10^5$	1.4×10^4	$(3.6 \pm 0.8) \times 10^9$
40% CH_3OH–60% H_2O–9.2 M NaOH	$(1.5 \pm 0.6) \times 10^4$	$(1.0 \pm 0.4) \times 10^5$	1.3×10^4	$(1.3 \pm 0.5) \times 10^9$
6 M solution of NaOH in H_2O[d]	$(5 \pm 4) \times 10^4$	$(1.2 \pm 0.2) \times 10^6$	1.4×10^4	

[a] Decay was monitored at 600 nm; experimental results were treated by a method of the least squares. [b] Volume per cents. [c] Choice of ϵ is discussed in text of the paper. [d] k_{eff} for this system includes rate constants of some reactions (see text).

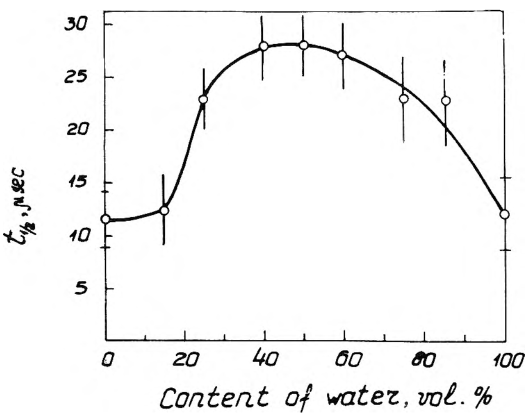

Figure 4. Half-life ($t_{1/2}$) of solvated electron in 5.5 M solution of CH_3ONa in methanol and water–methanol mixtures in which 6 M Na was dissolved (the composition is given in volume per cent) and 6 M aqueous solution of NaOH. The dose is 2–2.5 krads per pulse; the decay was monitored at 600 nm.

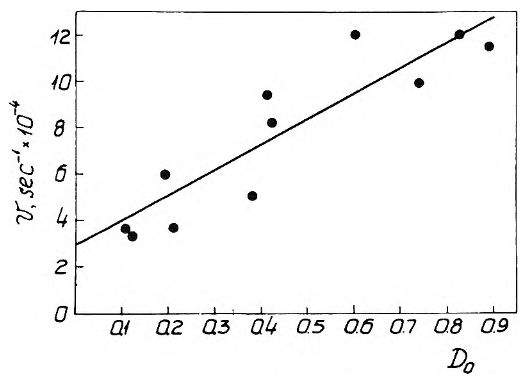

Figure 5. Dependence of v on D_0 (λ 600 nm) for the mixture 25% CH_3OH–75% H_2O (volume per cent) in which 6 M Na was dissolved.

dence takes place. In this case the decay curves were treated by the method of normalized concentrations which was used in work[19] during the study of the decay kinetics of hydrated electron in irradiated crystalline ice. Under some conditions this method gives the possibility of the determination of rate constant of first- (or pseudo-first) order reaction (*e.g.*, rate constant of the e_s^- reaction with solvent or impurity) and effective rate constant of second-order reactions. In the case of the e_s^- decay the determination of such constants is based on the graphical solution of the equation

$$-\frac{d}{dt}\left(\frac{[e_s^-]}{[e_s^-]_0}\right)\bigg|_{t=0} = k_{\mathrm{I}} + k_{\mathrm{eff}}[e_s^-]_0 \qquad (9)$$

where k_{I} is the rate constant of first- (or pseudo-first) order reaction, $[e_s^-]_0$ is the initial concentration of e_s^- (*i.e.*, at time $t = 0$) and $k_{\mathrm{eff}} = \Sigma_{i=1}^{n} k_i([x_i]/[e_s^-]_0)$ (k_i is the rate constant of second-order reaction of solvated electron with radical x_i).

Equation 9 is true if only a small fraction of solvated electrons decays during the pulse. Obviously, D_0 can be taken instead of $[e_s^-]_0$. Then

$$-\frac{d}{dt}\left(\frac{D}{D_0}\right)\bigg|_{t=0} = k_{\mathrm{I}} + k_{\mathrm{eff}}\frac{D_0}{\epsilon l} \qquad (10)$$

where ϵ is molar extinction coefficient of solvated electron and l is optical path length.

In Figure 5 is shown as an example the dependence of $v = -d/dt(D/D_0)|_{t=0}$ on D_0 (λ 600 nm) for the alkaline mixture of composition 25% CH_3OH and 75% H_2O. The calculated values of k_{I} and $k_{\mathrm{eff}}/\epsilon$ (in the experiments l was equal to 2 cm) are given in Table IV.

For the alkaline water-methanol mixtures k_{eff} is, most probably, the rate constant of reaction

$$e_s^- + e_s^- + 2CH_3OH\ (\text{and/or } 2H_2O) \rightarrow H_2 + 2CH_3O^-\ (\text{and/or } 2OH^-) \qquad (11)$$

i.e., $k_{\mathrm{eff}} \sim 2k_{11}$. The OH radicals formed from water or the products of their ionic dissociation (O^- radical ions) react with methyl alcohol

$$OH\ (\text{or } O^-) + CH_3OH \rightarrow H_2O\ (\text{or } OH^-) + CH_2OH \qquad (12)$$

and the resulting radicals are relatively inert toward solvated electrons.[20]

For the determination of $2k_{11}$ it is necessary to know the ϵ values. The latter were evaluated from the values of $G(e_s^-)\epsilon$ (see below). The values of $2k_{11}$ calculated by such a manner are given in Table IV. From this table it is seen that $2k_{11}$ is increased with the growth of water content in the mixture. Because of relatively high rate constant k' in alkaline methanol it is impossible to determine the value of $2k_{11}$ for this system at the doses used. However, from the data on kinetics of the e_s^- decay in alkaline water-

(19) T. E. Pernikova, S. A. Kabakchi, V. N. Shubin, and P. I. Dolin, *Radiat. Eff.*, **5**, 133 (1970).
(20) M. Anbar and D. Meyerstein, *Trans. Faraday Soc.*, **62**, 2121 (1966).

methanol mixtures it can be concluded that in methyl alcohol containing 5.5 M CH_3ONa $2k_{11} \leq 10^9$ M^{-1} sec^{-1}. For the determination of the exact value of this constant it is necessary to use the higher doses per pulse. Obviously, the upper limit of $2k_{11}$ values for alkaline mixtures of composition 75–85% CH_3OH and 25–15% H_2O is the same. Earlier[21] it was estimated that the value of $2k_{11}$ in weakly alkaline methanol is equal to $(6.6 \pm 4) \times 10^9$ M^{-1} sec^{-1}. The decrease of $2k_{11}$ in concentrated alkaline methanol may be due to the increase of viscosity of the system.

Alkaline mixture of composition 85% water–15% methanol-6 M NaOH contains ~4 M methanol and more than 40 M water. Therefore it is reasonable to assume that the value of $2k_{11}$ is the same for this mixture and 6 M aqueous solution of NaOH. In water at pH 10.9–13.3 $2k_{11}$ = (0.9–1.26) $\times 10^{10}$ M^{-1} sec^{-1}.[9-11] Our value (~3.6×10^9 M^{-1} sec^{-1}) is much less. Apparently, this effect is due to the increase of viscosity of concentrated alkaline aqueous solutions. It must be noted that a similar effect was observed earlier[22] for the rate constant of recombination of radical ions $(CNS)_2^-$ in aqueous solutions of KCNS.

In alkaline aqueous solutions in the absence of alcohol the predominant second-order processes of e_{aq}^- decay are the reactions 11 and 13

$$e_{aq}^- + O^- \rightarrow O^{2-} \tag{13}$$

In this case

$$k_{eff} \sim 2k_{11} + k_{13}\frac{[O^-]_0}{[e_{aq}^-]_0} \tag{14}$$

Obviously, in alkaline water $[O^-]_0/[e_{aq}^-]_0 = G_{O^-}/(g_H + G_{e_{aq}^-})$. It can be taken in the first approximation that this ratio of yields for 6 M aqueous solution of NaOH is equal to the ratio for water at pH 13. For water at pH 13 the ratio under consideration is equal to 0.8–0.9.[9,23] If we assume further that the value of $2k_{11}$ is the same both in the mixture of composition 85% water–15% CH_3OH, in which 6 M Na were dissolved, and in 6 M aqueous solution of NaOH, then $k_{13} \sim 1.3 \times 10^{10}$ M^{-1} sec^{-1}. In water at pH 13 $k_{13} = 2.2 \times 10^{10}$ M^{-1} sec^{-1}.[9] Similar results were obtained by using the method of linear anamorphoses of kinetic curves. From the initial slopes of plots $1/D_t$ *vs.* t at doses ~10 krads per pulse it was found that $k_{eff} = 1.4 \times 10^{10}$ M^{-1} sec^{-1}. Hence $k_{13} \sim 1.2 \times 10^{10}$ M^{-1} sec^{-1}.

The kinetics of disappearance of the optical absorption at wavelengths corresponding to the maximum of e_s^- band and to the shoulder (or to the second maximum) is the same even in ~8 M methanolic solution of RbOH and in the mixture of composition of 40% CH_3OH–60% H_2O (by volume) containing 9.2 M NaOH. However, in other work[4] it was found that the kinetics is different in the case of 14.5 M aqueous solution of KOH. Apparently in the systems which were investigated by us the concentration of formed particles which are responsible for the additional optical absorption is relatively low, and they do not affect appreciably the kinetics of e_s^- decay.

The values of $G(e_s^-)\epsilon_{max}$ (ϵ_{max} is molar extinction coefficient of e_s^- at λ_{max}) were measured for concentrated alkaline methanol and water–methanol mixtures. In the case of methanolic solutions of CH_3ONa the initial optical density at the maximum of e_s^- band for the same electron current per pulse increases by ~20% in 5.5 M methanolic solution of CH_3ONa in comparison with 2.9 M solution. However it is not equivalent to the increase of $G(e_s^-)$ since in our experiments the width of irradiated layer of liquid was less by a factor 1.5–2 than the range of electrons. Taking into account the increase of the density of solutions with the growth of CH_3ONa concentration it has to give the increase of the dose at equal currents per pulse. In Figure 6 is shown the dependence of $G(e_s^-)\epsilon_{max}$ on CH_3ONa concentration at equal doses per pulse and with the corrections taking into account the e_s^- decay during the pulse. In these calculations of dose a correction was applied for the difference between the densities of the solutions under consideration and the solution of KCNS which was used in dosimetry. It was taken that the dose is proportional to the density of solution. The corrections for the e_s^- decay during the pulse were calculated by a means of the equation

Figure 6. Dependence of $G(e_s^-)\epsilon_{max}$ for solvated electron in methanol on concentration of CH_3ONa at the dose 5 krads per pulse.

$$\frac{D}{D_0} = \frac{1}{k'\tau}(1 - e^{-k'\tau}) \tag{15}$$

where D is the observed optical density of solution at λ_{max} immediately after the pulse, D_0 is the optical density with such a correction, k' is the observed rate constant of e_s^- decay (sec^{-1}), and τ is the duration of the pulse.

The data on the values of $G(e_s^-)\epsilon_{max}$ for water–methanol mixtures are given in Table V. In calculations of these values the corrections taking into account the difference between the densities of mixtures and the decay of solvated electrons during the pulse were applied. The values of $G(e_s^-)\epsilon_{max}$ were obtained at the doses 2–3 krads per pulse. At such doses the plot ln D_t *vs.* t is a straight line. The k' values which were found from such plots were used for the calculations of corrections associated with the e_s^- decay during the pulse.

From Figure 6 is seen that $G(e_s^-)\epsilon_{max}$ for the methanolic solutions of CH_3ONa does not depend significantly on the concentration of methylate over the concentration range under investigation. Ions CH_3O^- which are the scavengers of positive ions $CH_3OH_2^+$

$$CH_3O^- + CH_3OH_2^+ \rightarrow 2CH_3OH \tag{16}$$

suppress the process of geminate recombination occurring in "spurs"[5,6,8]

$$e_s^- + CH_3OH_2^+ \rightarrow H + CH_3OH \tag{17}$$

It should be noted that $CH_3OH_2^+$ is formed from parent

(21) J. W. Fletcher and P. J. Richards, *Can. J. Chem.*, **49**, 2275 (1971).
(22) T. P. Zhestkova, A. K. Pikaev, and V. I. Spitsyn, *Dokl. Akad. Nauk SSSR*, **204**, 1147 (1972).
(23) E. M. Fielden and E. J. Hart, *Radiat. Res.*, **32**, 564 (1967).

TABLE V: Values of $G(e_s^-)\epsilon_{max}$, $G(e_s^-)$, and ϵ_{max} for e_s^- in Alkaline Water–Methanol Mixtures[a]

Mixture composition, vol %	$G(e_s^-)\epsilon_{max}$, electrons/100eV M^{-1} cm^{-1}	$G(e_s^-)$, electrons/ 100 eV[b]	ϵ_{max}, M^{-1} cm^{-1}
5.5 M CH_3ONa in CH_3OH	4.2×10^4	4.3	9.7×10^3
85% CH_3OH–15% H_2O–6 M Na	4.4×10^4	4.3	1.0×10^4
75% CH_3OH–25% H_2O–6 M Na	4.6×10^4	4.3	1.1×10^4
60% CH_3OH–40% H_2O–6 M Na	5.1×10^4	4.3	1.2×10^4
50% CH_3OH–50% H_2O–6 M Na	5.0×10^4	4.3	1.2×10^4
40% CH_3OH–60% H_2O–6 M Na	6.0×10^4	4.3	1.4×10^4
25% CH_3OH–75% H_2O–6 M Na	6.3×10^4	4.3	1.5×10^4
15% CH_3OH–85% H_2O–6 M Na	7.0×10^4	4.3	1.6×10^4
6 M NaOH in H_2O	5.6×10^4	3.6	1.6×10^4
40% CH_3OH–60% H_2O–9.2 M NaOH	6.1×10^4	4.3	1.4×10^4

[a] Precision of $G(e_s^-)\epsilon_{max}$ measurements is equal to ±10%. [b] Choice of $G(e_s^-)$ values is discussed in text of the paper.

positive ion CH_3OH^+ by reactions

$$CH_3OH^+ + CH_3OH \rightarrow CH_3OH_2^+ + CH_2OH \quad (18)$$

$$CH_3OH^+ + CH_3OH \rightarrow CH_3OH_2^+ + CH_3O \quad (19)$$

Therefore a positive "hole" in methanol consists of $CH_3OH_2^+$ and CH_2OH or CH_3O. Because of this the solvated electrons can undergo geminate recombination also with CH_3O radicals (CH_2OH radicals are relatively inert toward e_s^-[20])

$$e_s^- + CH_3O \rightarrow CH_3O^- \quad (20)$$

However, in alkaline solutions the radicals CH_3O are transformed into radical ions CH_2O^-

$$CH_3O + CH_3O^- \rightarrow CH_2O^- + CH_3OH \quad (21)$$

According to work[24] in ethanol the rate constant of reaction of type 21 is $>8 \times 10^7$ M^{-1} sec^{-1}. The radical ion CH_2O^- should be less reactive toward e_s^- than even the radical CH_2OH. Besides, it is not excluded that k_{20} is less than k_{17}. Obviously, at sufficiently high concentrations of CH_3O^- reactions 17 and 20 must be suppressed completely, and $G(e_s^-)$ has to be equal to the yield of initial ionization of alcohol. Since $G(e_s^-)\epsilon_{max}$ in the concentration range under consideration does not depend on CH_3ONa concentration, it is reasonable to assume that under such conditions reactions 17 and 20 are suppressed completely. The yield of initial ionization of methyl and ethyl alcohols is equal to 4.3 ions/100 eV.[6,8,25,26] From this it follows that the molar extinction coefficient of solvated electron at λ_{max} in alkaline methanol is 9.7×10^3 M^{-1} cm^{-1}. This is much less than the λ_{max} value 1.7×10^4 M^{-1} cm^{-1} for neutral methanol measured earlier in work.[27] Our value of λ_{max} is confirmed by the following facts. First, recently[28] it was found that the molar extinction coefficients of trapped electrons in glassy methanol, ethanol, and 2-propanol at 77°K are characterized by the relatively low values ($\sim 4 \times 10^3$ M^{-1} cm^{-1} at λ_{max}. Second, the $G(e_s^-)\epsilon_{max}$ value for alkaline water–methanol mixtures is increased with the growth of water content in the mixture (see Table V). For 6 M aqueous solution of NaOH $G(e_{aq}^-)\epsilon_{max}$ is equal to 5.6×10^4 electrons/100 eV M^{-1} cm^{-1}. Let us propose that $G(e_{aq}^-)$ is the same both in water at pH 13 and in 6 M aqueous solution of NaOH. According to work[23] in water at pH 13 $G(e_{aq}^-)$ taking into account reaction 7 is equal to 3.6 electrons/100 eV. Then the molar extinction coefficient of hydrated electron at λ_{max} in 6 M aqueous solution of NaOH is 1.6×10^4 M^{-1} cm^{-1}. This coefficient for neutral water is equal to (1.6–1.8) $\times 10^4$ M^{-1} cm^{-1}.[23,29] Let us note that in concentrated alkaline aqueous solutions ϵ_{max} has to be slightly less. From other work[14] it follows that ϵ for 15 M aqueous solutions of KOH or NaOH is equal to 90–93% of the extinction coefficient for neutral water. Since the mixture of composition 85% water–15% CH_3OH (by volume) in which 6 M Na were dissolved contains only about 4 M CH_3OH, it may be taken that ϵ_{max} for this mixture is the same as for 6 M aqueous solution of NaOH. Then $G(e_s^-)$ in this mixture is equal to 4.3 electrons/100 eV. Hence, in the mixture under consideration there is the increase of the yield in comparison with 6 M aqueous solution of NaOH. Such an increase can be explained by suppressing reaction 13, which occurs in "spurs," with methyl alcohol. In this mixture the only process occuring in "spurs" is the reaction

$$e_{aq}^- + e_{aq}^- + 2H_2O \rightarrow H_2 + 2OH^- \quad (22)$$

In the case of neutral and slightly alkaline water G_{H_2} = 0.4–0.45 molecules/100 eV.[30] In 6 M aqueous solution of NaOH the role of reaction 22 in "spurs" must be less than in neutral or slightly alkaline water, since in concentrated aqueous solution of alkali the rate constant of reaction 22 is lower. From this it may be concluded that the maximum value of $G(e_{aq}^-)$ is within the limits of 4.3–5.2 electrons/100 eV. Let us note that the maximum value of the electron yield for concentrated alkaline and acid aqueous media, which has been reported,[31,32] is equal to 5.0–5.1 electrons/100 eV.

In accordance with the described data it may be taken that for alkaline water–methanol mixtures $G(e_s^-)$ is also equal to 4.3 electrons/100 eV. The values of ϵ_{max} calculated on this basis are given in Table V.

(24) J. W. Fletcher, P. J. Richards, and W. A. Seddon, *Can. J. Chem.*, **48**, 3765 (1970).
(25) G. R. Freeman, "Actions Chimiques et Biologiques des Radiations," 14 Serie, M. Haissinsky, Ed., Masson et Cie, Paris, 1969, p 73.
(26) S. J. Rzad and J. H. Fendler, *J. Chem. Phys.*, **52**, 5395 (1970).
(27) M. C. Sauer, S. Arai, and L. M. Dorfman, *J. Chem. Phys.*, **42**, 708 (1965).
(28) Z. A. Sinitsina and Kh. S. Bagdasar'yan, *Khim. Vys. Energ.* **5**, 140 (1971).
(29) J. Rabani, W. A. Mulac, and M. S. Matheson, *J. Phys. Chem.*, **69**, 53 (1965).
(30) A. O. Allen, "The Radiation Chemistry of Water and Aqueous Solutions," Van Nostrand, Princeton, N. J., 1962.
(31) G. V. Buxton, F. C. Cattell, F. S. Dainton, T. E. Lantz, and F. P. Sargent, "International Discussion on Progress and Problems in Contemporary Radiation Chemistry," Vol. 2, J. Teplý, *et al.*, Ed., Prague, 1971, p 295.
(32) E. J. Hart, ref 31, p 326.

Therefore our experimental data testify that the properties of solvated electrons in strong alkaline methanol and strong alkaline water are different. The main differences are the following: the extinction coefficient of e_s^- in methanol is appreciably less than in water and the recombination of e_s^- in alkaline water occurs faster than in alkaline methanol. These differences are gradually removed with the increase of water content in the water–methanol mixtures.

Acknowledgments. We wish to express our indebtedness to A. Kulakov and A. Konopeshko for careful Linac operation and Dr. P. Glazunov and E. Shirshov for maintenance of electronic equipment.

Excitons Bound to Ionized Impurities in Inorganic Crystals

S. G. Elkomoss

Laboratoire de Soectroscopie at d'Optique du Corps Solide,[1] Institut de Physique, Strasbourg, France *(Received April 21, 1972)*

Pekeris' method for helium atom generalized recently by Frost for the three-particle systems has been developed extensively to apply to excitons bound to ionized impurities in inorganic crystals. Haken's exciton potential, where the dielectric constant between the two particles is a function of the interparticle distance, the optical and static dielectric constants, the electron and hole effective masses m_e^* and m_h^*, respectively, and the longitudinal vibrational frequency of the lattice, has been generalized for the three particles. This potential shows the important effect of the polarizability. A considerable long recursion relation of 57 terms has been derived. In exciton–ionized-donor complexes, the binding energy of the system is a function of the mass ratio m_e^*/m_h^*. This complex has been studied for real systems such as CdS, ZnO, CuCl, CuBr, CuI, ZnSe, ZnTe, CdTe, SiC 6H, TlCl, and TlBr. The agreement with experiment is better than that obtained by the previous authors where the polarizability has been neglected. The calculations have also been carried out for exciton–ionized acceptor. In this case the results are given in terms of the mass ratio m_h^*/m_e^*. For known inorganic crystals, this mass ratio is usually high, and consequently it is highly improbable to find such a stable complex for these crystals.

Introduction

In inorganic crystals, experimental evidence[2] has shown the existence of excitons bound to ionized donors. It is of interest to carry out some exact calculations for these complexes. The method given by Pekeris[3] for the helium atom and generalized recently by Frost[4-6] for the three-particle system has been developed further. Haken's exciton potential[7] in which the effect of the polarizability is included has been used in these calculations. For exciton–ionized-donor complexes the results are given in terms of the mass ratio $\sigma = m_e^*/m_h^*$ where m_e^* and m_h^* are the effective masses of the electron and the hole, respectively. In the case of the exciton–ionized-acceptor complexes the binding energies are function of the ratio $\delta_a = m_h^*/m_e^*$. Comparison with experiment is also carried out for some real systems.

Form of the Potential

As described by Haken,[7] the dielectric constant $K(r_{23})$ between the hole and the electron of a delocalized exciton is a function[2] of the distance (r_{23}) separating the two particles, of their effective masses, of the optical (K_0) and the static (K_s) dielectric constants, and of the longitudinal vibrational frequency (ω) of the lattice. As atomic units in terms of a certain effective dielectric constant K_{eff} are usually adopted, the generalized Haken's potential[2] for any two particles i and j of effective masses m_i^* and m_j^* in a crystal can be written in the following form

$$\frac{1}{K(r_{ij})} = \frac{1}{K_{eff}}\left\{\frac{K_{eff}}{K_s}\left[1 - \frac{\zeta_{ij}}{2}\right] + \frac{K_{eff}}{K_o}\frac{\zeta_{ij}}{2}\right\} \tag{1}$$

with

$$\zeta_{ij} = e^{-\kappa_i r_{ij}} + e^{-\kappa_j r_{ij}} \tag{2a}$$

$$\kappa_i = (2m_i^*\omega/\hbar)^{1/2} \tag{2b}$$

$$\kappa_j = (2m_j^*\omega/\hbar)^{1/2} \tag{2c}$$

For the complex exciton–ionized donor given in Figure 1,

(1) Research group associated with the Centre Nationale de la Recherche Scientifique (CNRS), France.
(2) For full review on the experimental evidence of exciton–ionized-donor complex, see the references given in S. G. Elkomoss, *Phys. Rev. B*, **4**, 3411 (1971).
(3) C. L. Pekeris, *Phys. Rev.*, **112**, 1649 (1958).
(4) A. A. Frost, *J. Chem. Phys.*, **41**, 478 (1964).
(5) A. A. Frost, M. Inokuti, and J. P. Lowe, *J. Chem. Phys.*, **41**, 482 (1964).
(6) A. A. Frost, D. K. Harris, and J. D. Scargle, *J. Chem. Phys.*, **41**, 489 (1964).
(7) H. Haken, *Z. Naturforsch. A*, **9**, 228 (1954); "Halbeiter Probleme," Vol. I, W. Shottky, Ed. Vieweg, Braunschweig, 1954, p 72; "Halbleiter Probleme," Vol. II, W. Shottky, Ed., Vieweg, Braunschweig, 1955, p 1; *J. Phys. Radium*, **17**, 826 (1956); *J. Chim. Phys.*, **55**, 643 (1958); *J. Phys. Chem. Solids*, **8**, 166 (1959).

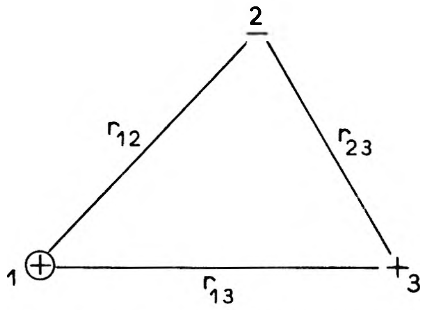

Figure 1. Exciton–ionized-donor complex.

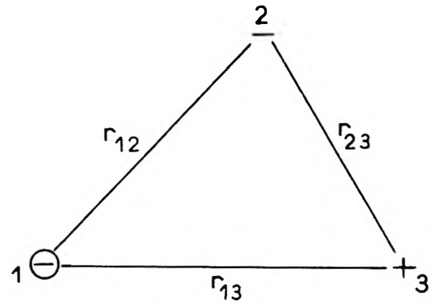

Figure 2. Exciton–ionized-acceptor complex.

the potential energy of the system is

$$V(r_{12},r_{13},r_{23}) = \frac{1}{2}\sum_{i=1}^{N}\sum_{j\neq i}^{N} e^2\lambda_{ij}/(K_{\rm eff})r_{ij} \qquad (3)$$

where λ_{12}, λ_{13}, and λ_{23} are the coefficients of the terms $1/r_{12}$, $1/r_{13}$, and $1/r_{23}$ given by eq 1. For the complex exciton–ionized acceptor of Figure 2, the potential energy is given by eq 3 where λ_{12} and λ_{13} are of opposite signs to those for the exciton–ionized-donor complex of Figure 1.

Due to the difficulties that may occur in solving the problems of exciton complexes using the general potential of eq 1, 2, and 3, mean values of λ_{ij}'s should be considered. Knowing the wave function Ψ of the system, one can write

$$\bar{\lambda}_{ij} = \frac{K_{\rm eff}}{K_{\rm s}} + \frac{1}{2}K_{\rm eff}\left[\frac{1}{K_{\rm o}} - \frac{1}{K_{\rm s}}\right]\left[\int \Psi\zeta_{ij}\Psi{\rm d}\tau/\int\Psi\Psi{\rm d}\tau\right] \qquad (4)$$

The mean values $\bar{\lambda}_{ij}$ are denoted by λ, μ, and ν, respectively. The values of λ, μ, and ν depend on the fundamental constants m_e^*, m_h^*, K_s, K_o, and ω.

The binding energy of the complex given in Figure 1 can be calculated in terms of the neutral donor binding energy E_D

$$E_D = -m_e^*e^4/2K_D^2\hbar^2 \qquad (5)$$

The dielectric constant $K_D = K(r_{12}) = K_{\rm eff}$ and is evaluated using $\lambda = 1$. In this case the atomic units $K_{\rm eff}\hbar^2/e^2m_e^*$ and $m_e^*e^4/\hbar^2K_{\rm eff}^2$ will be adopted for length and energy, respectively, and the units $m_e^* = \hbar = 1$ and $e^2/K_{\rm eff} = 1$ will be used. The binding energy E_D is simply then equal to 0.5 au.

For the exciton–ionized-acceptor complex of Figure 2, the binding energies are calculated in terms of the neutral acceptor binding energy E_A

$$E_A = -m_h^*e^4/2K_A^2\hbar^2 \qquad (6)$$

The dielectric constant $K_A = K(r_{13}) = K_{\rm eff}$ for the system of Figure 2 and is evaluated using $\mu = -1$. In this case the atomic units $K_{\rm eff}\hbar^2/e^2m_h^*$ and $m_h^*e^4/\hbar^2 K_{\rm eff}^2$ are usually adopted for length and energy, respectively, with $m_h^* = \hbar = e^2/K_{\rm eff} = 1$. The binding energy E_A of eq 6 is then simply equal to 0.5 au.

In most of the inorganic crystals where the exciton–ionized-donor complexes have been observed, the binding energy E_D of the neutral donor is not well determined. The binding energies of such complex are usually given in terms of the exciton binding energy E_x

$$E_x = -Me^4/2K_x^2\hbar^2 \qquad (7)$$

where M is the exciton reduced mass and $K_x = K_{\rm eff} = K(r_{23})$, evaluated from $\nu = 1$. In this case the atomic units $K_{\rm eff}\hbar^2/e^2M$ and $Me^4/K_{\rm eff}^2\hbar^2$ can be considered for length and energy, respectively with $M = \hbar = e^2/K_{\rm eff} = 1$. The exciton binding energy E_x of eq 7 is simply 0.5 au. Notice that the atomic units corresponding to eq 5, 6, and 7 are different from each other.

For these different cases corresponding to the complexes given in Figures 1 and 2, the nonrelativistic Schrodinger equation takes one of the following three forms depending on the choice of the above atomic units

$$\sum_i \nabla_{ei}^2\Psi + \sigma\sum_j \nabla_{hj}^2\Psi + 2(E - V)\Psi = 0 \text{ donor} \qquad (8)$$

$$\delta_a\sum_i \nabla_{ei}^2\Psi + \sum_j \nabla_{hj}^2\Psi + 2(E - V)\Psi = 0 \text{ acceptor} \qquad (9)$$

$$\sum_i \nabla_{ei}^2\Psi + \delta_x\sum_j \nabla_{hj}^2\Psi + 2(1 + \delta_x)(E - V)\Psi = 0 \text{ exciton} \qquad (10)$$

For the systems where the calculations are carried out in terms of E_D, eq 8 is used. In this case the electron effective mass m_e^* is considered to be unity and the mass ratio σ is equal to $1/m_h^*$ au. For those cases in which the calculations are to be expressed in terms of E_A, it is eq 9 that has to be solved. In this case the atomic units are those that correspond to $m_h^* = 1$ and the mass ratio δ_a is equal to $1/m_e^*$ au. For the systems where the computations are given in terms of E_x, eq 10 has to be used. In this case the exciton reduced mass M is considered to be unity and the mass ratio δ_x is equal to m_e^*/m_h^*. Note that the atomic units used in the three cases are different. In eq 8, 9, and 10, the potential V is given by eq 4 and 3 transformed into the appropriate atomic units, ∇_{ei}^2 is the Laplacian for the electron i, ∇_{hj}^2 is that for the hole j, and E is the total energy of the system expressed in terms of the atomic units used.

Method of Solution

Consider eq 8 corresponding to Figure 1. Use the classical method of Hylleraas,[8] and introduce the perimetric coordinates u, v, and w. These coordinates[2] depend on three variational parameters α, β, and γ. Put

$$\Psi = e^{-(1/2)(u+v+w)}F(u,v,w) \qquad (11)$$

with

$$F(u,v,w) = \sum_{l,m,n}^{\infty} A(l,m,n)L_l(u)L_m(v)L_n(w) \qquad (12)$$

where L_l, L_m, and L_n denote, respectively, the normalized Laguerre polynomials of order l, m, and n. Using the different relations between these polynomials and their derivatives, one obtains[2] a considerable long 57-term recursion

(8) E. A. Hylleraas, *Z. Phys.*, 54, 347 (1929).

TABLE I

$\lambda = 1$	$\mu = 1$	$\nu = 1$	$\lambda = 1$	$\mu = 0.95$	$\nu = 1$
$\lambda = 1$	$\mu = 0.9$	$\nu = 1$	$\lambda = 1$	$\mu = 0.85$	$\nu = 1$
$\lambda = 1$	$\mu = 0.8$	$\nu = 1$	$\lambda = 1$	$\mu = 0.75$	$\nu = 1$
$\lambda = 1$	$\mu = 0.7$	$\nu = 1$	$\lambda = 1$	$\mu = 0.65$	$\nu = 1$
$\lambda = 1.05$	$\mu = 1$	$\nu = 1$	$\lambda = 1.1$	$\mu = 1$	$\nu = 1$
$\lambda = 1.15$	$\mu = 1$	$\nu = 1$	$\lambda = 1$	$\mu = 1$	$\nu = 1.05$
$\lambda = 1$	$\mu = 1$	$\nu = 1.1$	$\lambda = 1$	$\mu = 1$	$\nu = 1.2$
$\lambda = 1.05$	$\mu = 1$	$\nu = 1.1$	$\lambda = 1.05$	$\mu = 0.95$	$\nu = 1.1$
$\lambda = 1.05$	$\mu = 1.05$	$\nu = 1.1$	$\lambda = 2$	$\mu = 2$	$\nu = 1$
$\lambda = 2$	$\mu = 1.9$	$\nu = 1$	$\lambda = 3$	$\mu = 3$	$\nu = 1$

relation between the coefficients $A(l,m,n)$. The solution of this recursion relation gives the energy ratio E/E_D as a function of $1/m_h^*$ for different values of λ, μ, and ν.

Computations and Results

The recursion relation takes the form of the eigenvalue problem

$$H + \epsilon(P + \sigma Q) = 0 \tag{13}$$

The procedure of computation is given in detail in ref 2. The results of ϵ in the determinants of eq 13 converge to four decimals. The maximum order attained for these determinants is 50. The first part of this work is to show whether the effect of the polarizability expressed in terms of λ, μ, and ν has an important effect or not. Computations were performed in double precision for different cases with different values of λ, μ, and ν. Some of these cases correspond to the values of λ, μ, and ν shown in Table I. For these cases the values of E/E_D are represented in Figure 3 as a function of the mass ratio $\sigma = 1/m_h^*$ au. The values of $\alpha = 0.72$, $\beta = 1.5$, and $\gamma = 0.55$ that correspond to the minimization of energy for the case $\lambda = \mu = \nu = 1$ have been considered the same for all the curves given in Figure 3 with different values of λ, μ, and ν and for different values of σ. This approximation has been adopted to save considerably the computer time involved in such elaborate long computations. The results

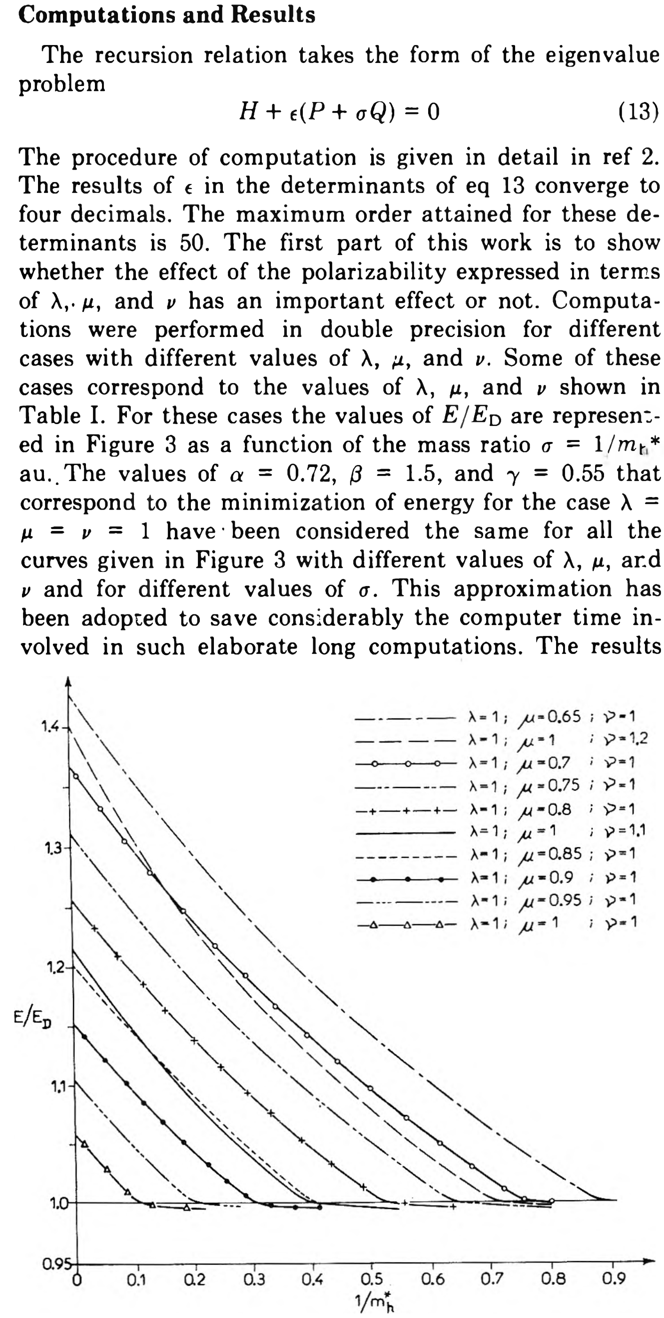

Figure 3. Plots of E/E_D vs. $1/m_h^*$ for different values of λ, μ, and ν.

are strongly dependent on the values of λ, μ, and ν. This means that the variation in the dielectric constant due to the polarizability between the three particles makes an important contribution. The intersections between the curves $E/E_D = f(\sigma)$ and $E/E_D = 1$ give critical values σ_c for the mass ratios. The systems are stable for $\sigma \leq \sigma_c$ and unstable otherwise. From Figure 3 one can notice that the values of σ_c are also a function of λ, μ, and ν.

The exponential part[2] of the wave function 11 can be written in terms of r_{12}, r_{13}, and r_{23} as follows

$$\Psi = e^{-\epsilon(a r_{12} - b r_{13} + c r_{23})} F(u, v, w) \tag{14}$$

where a, b, and c are given by the following expressions

$$\begin{aligned} a &= (1/2)(-\alpha + \beta + \gamma) \\ b &= (1/2)(\alpha - \beta + \gamma) \\ c &= (1/2)(\alpha + \beta - \gamma) \end{aligned} \tag{15}$$

Taking $\alpha = 0.72$, $\beta = 1.5$, and $\gamma = 0.55$, the corresponding values of a, b, and c are 0.665, 0.115, and 0.835, respectively, all positive numbers. These values of a, b, and c show that the repulsion between the hole and the donor has a smaller effect than the attractions along the directions of r_{12} and r_{23}. Another important feature is the positive sign of the r_{13} term in the exponential of eq 14. This sign has a significant physical meaning in that it explains the repulsive forces between the hole of the exciton and the donor. The two negative signs of r_{12} and r_{23} in the exponential represent, of course, the attractive forces between the electron and the donor, as well as between the two exciton particles, respectively. The wave function 14 still converges since the value of b is much smaller than that of a or c. This has been demonstrated by studying the integrals of eq 4 used for calculating the values of λ, μ, and σ which are necessary for comparing experiment and theory. Notice that the coefficients a, b, and c of the exponential part of the wave function given in eq 14 as well as the energy ϵ and consequently the total energy E of the system are all determined from the long-recursion relation of eq 13.

Comparison with Experiment

To carry out the comparison between theory and experiment for a specific inorganic crystal, the corresponding mean values λ, μ, and ν given in eq 4 have to be calculated. For these computations one needs to know the wave function Ψ. The calculations concerning the wave function 14 are quite elaborate. For simplifications only the exponential part of this eq 14 has been used to evaluate the integrals of eq 4 and consequently to calculate the values of λ, μ, and ν. Using elliptical coordinates for integration, the values of λ, μ, and ν for a given crystal are

TABLE II: Fundamental Constants and the Computed Values of $(E - E_D)/E_D$ for Exciton–Ionized-Donor Complex in CdS, ZnO, ZnSe, ZnTe, CdTe, SiC 6H, TlCl, and TlBr

	m_e^*	$m_{h\perp}^*$	$m_{h\parallel}^*$	$K_{s\perp}$	$K_{s\parallel}$	K_o	σ	ω	$(E - E_D)/E_D \times 10^2$
			$\lambda = 1$, $\mu = 1.0017$, $\nu = 1.06568$						
CdS	0.205^a	$0.7^{a,b}$	5^a	9.2^c		5.24^d	0.207	306	3.524
			$\lambda = 1$, $\mu = 1.0012$, $\nu = 1.0697$						
ZnO	0.29^e	1.8^d		8.5^e	11	4.59^d	0.1611	580	6.4
			$\lambda = 1$, $\mu = 1.00057$, $\nu = 1.03242$						
ZnSe	0.1^d	0.6^d		9.2^f		5.75^g	0.167	253	1.158
			$\lambda = 1$, $\mu = 1.00044$, $\nu = 1.02763$						
ZnTe	0.096^h	0.6^i		10.38^j		6.7^k	0.16	206	0.875
			$\lambda = 1$, $\mu = 1.00038$, $\nu = 1.02792$						
CdTe	$0.096^{d,l}$	0.68		10.6^m		7.13^m	0.1412	168	1.827
			$\lambda = 1$, $\mu = 1.00017$, $\nu = 1.021$						
SiC 6H	$0.25^{n,q}$, $1.5^{n,r}$	3.5^n		9.66^o	10.03^o	6.7^o	0.1	967^o	3.007
			$\lambda = 1$, $\mu = 1.00338$, $\nu = 1.21155$						
TlCl	0.53^p	2.72^p		37.6^p		5.1^p	0.1915	174^p	25.446
			$\lambda = 1$, $\mu = 1.0051$, $\nu = 1.15727$						
TlBr	0.28^p	0.72^p		35.1^p		5.4^p	0.3889	116^p	6.73

[a] Reference 9 and J. O. Dimmock, *Int. Conf. II–VI Semiconduct. Compounds, 1967*, 2 (1968); B. Segali, *ibid.*, 327 (1968). [b] J. J. Hopfield, *J. Appl. Phys. Suppl.*, **32**, 2277 (1961). [c] R. E. Halsted, M. R. Lorenz, and B. Segall, *J. Phys. Chem. Solids*, **22**, 109 (1961). [d] See ref 10. [e] See ref 1. [f] S. S. Mitra, *J. Phys. Soc. Jap. Suppl.*, **21**, 61 (1966). [g] M. Aven, D. T. F Marple, and B. Segall, *J. Appl. Phys. Suppl.*, **32**, 226 (1961). [h] R. L. Bowers and G. D. Mahan, *Phys. Rev.*, **185**, 1073 (1969). [i] D. T. F. Marple and M. Aven, *Int. Conf. II–VI Semiconduct. Compounds, 1967*, 315 (1968). [j] S. Narita, H. Harada, and K. Nagasaka, *J. Phys. Soc. Jap.*, **22**, 1176 (1967). [k] A. Nitsuishi in United States–Japanese Cooperative Seminar on Far-Infrared Spectroscopy, Columbus, Ohio, 1965 (urpublished. [l] K. K. Kanazawa and F. C. Brown, *Phys. Rev.*, **135**, A1757 (1964). [m] D. De Nobel, *Philips Res. Rept.*, **14**, 357 (1959); **14**, 430 (1959); S. Yamada, *J. Phys. Soc. Jap.*, **15**, 1940 (1960). [n] B. Ellis and T. S. Moss, *Proc. Roy. Soc.*, **299**, 383 (1967); H. J. Van Daal, W. F. Knippenberg and J. D. Wasscher, *J. Phys. Chem. Solids*, **24**, 109 (1963). [o] L. Patrick and W. J. Choyke, Westinghouse Scientific Paper No. 70-9J3-OPGAP-P1, 1970 (unpublished). [p] See ref 24. [q] $m_{e\perp}^*$. [r] $m_{e\parallel}^*$.

given by the following expressions

$$\lambda = (K_{eff}/K_s) + (1/2)K_{eff}[(1/K_o) - (1/K_s)]\{(SF)/[R(c + a_1)^3(c - a_1)^3]\}$$

$$\mu = (K_{eff}/K_s) + (1/2)K_{eff}[(1/K_o) - (1/K_s)](T/R)$$

$$\nu = (K_{eff}/K_s) + (1/2)K_{eff}[(1/K_o) - (1/K_s)]\{(U + W)F/[R(c_1 + a)^3(c_1 \ a)^3]\}$$

where

$$a_1 = a + (\kappa_e/2\epsilon);\ a_2 = a + (\kappa_h/2\epsilon);\ c_1 = c + (\kappa_e/2\epsilon)$$

$$c_2 = c + (\kappa_h/2\epsilon);\ G_1 = (c_1 - b)^3;\ G_2 = (c_2 - b)^3$$

$$F = (c^2 - a^2)^3;\ G = (a - b)^3;\ J = (c - b)^3$$

$$R = [c(c^2 - 3a^2 + 2ab)/G] + [a(3c^2 - a^2 - 2cb)/J]$$

$$S = \{[c(c^2 - 3a_1^2 + 2ba_1)]/(a_1 - b)^3\} + \{[ac^2 - aa_1^2 + 2ca_1(c - b)]/J\}$$

$$T = [c(c^2 - 3a^2 + 2ab_2)/(a_2 - b)^3] + [a(3c^2 - a^2 - 2cb_2)/(c_2 - b)^3]$$

$$U = \{c_1[c^2 + (c\kappa_e/2\epsilon) - 3a^2 + (\kappa_e/2\epsilon)^2 + 2ab]/G\} + \{a[3c^2 + 3(c\kappa_e/2\epsilon) - a^2 + 3(\kappa_e/2\epsilon)^2 - 2cb - b(\kappa_e/\epsilon)]/G_1\}$$

$$W = \{[c^2 + (c\kappa_h/\epsilon) - 3a^2 + (\kappa_h/2\epsilon)^2 + 2ab]/G\} + \{a[3c^2 + 3(c\kappa_h/\epsilon) - a^2 + 3(\kappa_h/2\epsilon)^2 - 2cb - (b\kappa_h/\epsilon)]/G_2\} \quad (16)$$

where κ_e and κ_h are given by eq 2. The values of λ, μ, and ν depend not only on the fundamental constants but are also a function of the energy ϵ of the complex. This energy has been calculated using the determinant 13. In this case the computations have to be self-consistent as described in detail in ref 2.

For a particular material, different values of effective masses and dielectric constants are available in the literature. The computations corresponding to a particular substance are carried out for these different effective masses and dielectric constants. In Table II, the fundamental constants and the computed values of $(E - E_D)/E_D$ for some of the cases that correspond to the best agreement with experiment in CdS, ZnO, ZnSe, ZnTe, CdTe, SiC 6H, TlCl, and TlBr are given. The problem of anisotropy for the effective masses and the dielectric constants is eliminated by taking mean values for these constants using the formulas of Hopfield and Thomas.[9]

$$1/m_h^* = (1/3)[(2/m_{h\perp}^*) + (1/m_{h\parallel}^*)(K_{s\perp}/K_{s\parallel})]$$

$$1/m_e^* = (1/3)[(2/m_{e\perp}^*) + (1/m_{e\parallel}^*)(K_{s\perp}/K_{s\parallel})] \quad (17)$$

$$K_s = (K_{s\perp}K_{s\parallel})^{1/2}$$

The stability of the exciton–ionized-donor complex calculated in Table II for these materials agrees with observations.[10-19] The value $(E - E_D)/E_D = 3.524 \times 10^{-2}$ com-

(9) J. J. Hopfield and D. G. Thomas, *Phys. Rev.*, **122**, 35 (1961).
(10) D. C. Reynolds, C. W. Litton, and T. C. Collins, *Phys. Status Solidi*, **9**, 645 (1965).
(11) D. C. Reynolds, C. W. Litton, and T. C. Collins, *Phys. Rev.*, **174**, 8459 (1968).

TABLE III: Fundamental Constants and the Computed Values of $(E - E_x)/E_x$ for Exciton–Ionized-Donor Complex in CuCl, CuBr, and CuI

	m_e^*	m_h^*	K_s	K_0	δ_x	ω	$(E - E_x)/E_x \times 10^2$
			$\lambda = 0.98$, $\mu = 0.89$, $\nu = 1$				
CuCl	0.5[a]	13[a,b]	7.43[c,d]	4.84[e]	0.03846	216[c]	0.146
			$\lambda = 1.01$, $\mu = 0.925$, $\nu = 1$				
CuBr	0.415[c,d]	20[c,d]	5.7[d]	4.4[d]	0.02075	160	0.15
			$\lambda = 1.002$ $\mu = 0.935$, $\nu = 1$				
CuI	0.415	20	4.85[e]	6.2[e]	0.02075	150	0.13

[a] K. S. Song, Thesis, Strasbourg, 1967. [b] M. A. Khan, *J. Phys. Chem. Solids*, **31**, 2309 (1970). [c] See ref 25. [d] S. Lewonczuk, J. Fingeissen, and S. Nikitine. *J. Phys.*, **32**, 941 (1971). [e] C. Caraoatos, B. Prevot, and M. Leroy, *C. R. Acad. Sci.*, **274**, 707 (1972).

puted for CdS in Table II is in better agreement with experiment[16] (2.5×10^{-2}) than the best previous value (4.04×10^{-2}), calculated recently by Suffczynski, *et al.*,[20,21] using Rotenberg and Stein's[22] wave function. For ZnO, the computed value 6.4×10^{-2} is again in better agreement with experiment[16,23] (9.61×10^{-2}) than the previous best value 5.085×10^{-2} calculated recently by Suffczynski, *et al.*,[21] using also Rotenberg and Stein's wave function. For the materials ZnSe, ZnTe, and CdTe, in spite of the observation of such a complex and which is confirmed by the calculations given in Table II for these crystals, the corresponding experimental values of $(E - E_D)/E_D$ are not well determined. Taking $\nu = 1.21155$ and 1.15727 given respectively for TlCl and TlBr in Table II, the corresponding exciton binding energies for these materials are 6.312 and 2.95 meV. These energies are in very good agreement with the experimental values (11 ± 2) and (6 ± 1) meV given by Bachrach and Brown[24] for TlCl and TlBr, respectively.

For CuCl, CuBr, and CuI the neutral donor binding energy E_D is not well determined. The experimental data are given in terms of the exciton binding energy E_x. For these materials, the atomic units corresponding to Schrodinger eq 10 have been adopted. The self-consistent calculations have been carried out. The values of α, β, and γ are determined from the minimization of energy. For these three materials there are three different sets of values for λ, μ, and ν as well as three different sets of values for α, β, and γ. In Table III, the fundamental constants and the computed values of $(E - E_x)/E_x$ are given for these materials. For CuBr the effective masses given by Ringeissen, *et al.*, for CuCl have been considered. For CuCl and CuBr the computed values of $(E - E_x)/E_x$ are in good agreement with experiment 0.2[25,26] and 0.175,[27-29] respectively. For CuI the experimental value of $(E - E_x)/E_x$ is not well determined. But the computed value 0.13 for this material in Table III compared to the corresponding values in CuCl and CuBr seems to be satisfactory. Equation 10 has also been considered for CdS and an agreement of the same order with experiment similar to that given in Table II has been obtained.

For TlBr, Grabner[30] observed recently two peaks, B_1 and B_2, which he interpreted as bound excitons to unknown defects. The peak B_1 may correspond to exciton–ionized-donor complex as predicted by the calculations given in Table II for this material. The measurements[30] are given in terms of the free exciton binding energy E_x. Equation 10 has then to be considered and computations similar to those for CuCl, CuBr, and CuI mentioned above

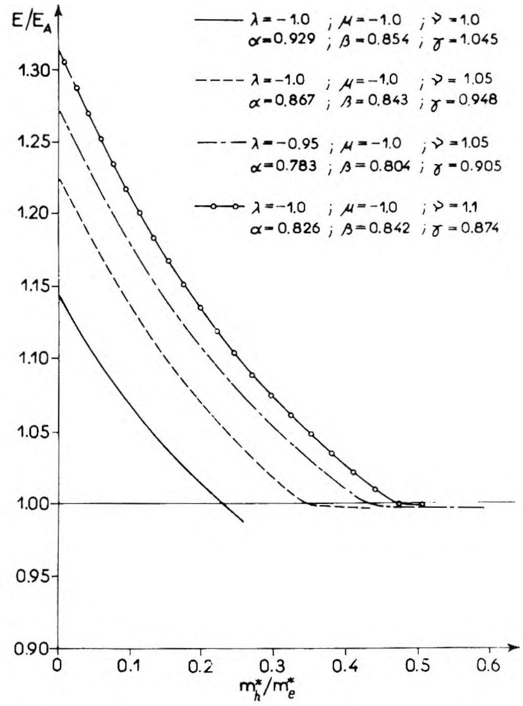

Figure 4. Plots of E/E_A vs. $1/m_e^*$ for different values of λ, μ, and ν.

(12) M. A. Gilleo, P. T. Bailey, and D. E. Hill, *Phys. Rev.*, **174**, 898 (1968).
(13) E. Hal Boardus and H. B. Bebb, *Phys. Rev.*, **176**, 993 (1968).
(14) D. C. Reynolds and T. C. Collins, *Z. Naturforsch.*, 249, 1311 (1969).
(15) D. C. Reynolds, "Electronic Structures in Solids," Plenum, New York, N. Y., (1969, p 110.
(16) D. C. Reynolds, "Optical Properties of Solids," Plenum, New York, N. Y., 1969, Chapter 10, p 239.
(17) J. Conradi and R. R. Haering, *Phys. Rev.*, **185**, 1088 (1969).
(18) D. E. Hill, *Phys. Rev. B*, **1**, 1863 (1970).
(19) W. J. Choyke, *Mater. Res. Bull.*, **4**, S141 (1969).
(20) M. Suffczynski and W. Gorzkowski, *Acta Phys. Pol.*, **A38**, 441 (1970).
(21) M. Suffczynski, W. Gorzkowski, and T. Skettrup. Internal Report of the Institute of Theoretical Physics, Warsaw University, and the Technical University of Denmark, Lyngby, 1970 (unpublished).
(22) M. Rotenberg and J. Stein, *Phys. Rev.*, **182**, 1 (1969).
(23) Y. S. Park, C. W. Litton, T. C. Collins, and D. C. Reynolds, *Phys. Rev.*, **143**, 512 (1966).
(24) R. Z. Bachrach and F. C. Brown, *Phys. Rev. B*, **1**, 818 (1970).
(25) J. Ringeissen, Thesis, Strasbourg, 1967.
(26) M. Certier, Thesis, Strasbourg, 1969.
(27) A. Mysyrowicz, R. Heimburger, J. B. Grun, and S. Nikitine, *C. R. Acad. Sci.*, **263**, 1116 (1966).
(28) C. Wecker, Thesis 3ème Cycle, University Louis Pasteur, Strasbourg, Science Section, 1972.
(29) T. Goto and M. Ueta, *J. Phys. Soc. Jap.*, **22**, 488 (1967).
(30) L. Grabner, to be submitted for publication. I wish to thank Dr. R. Z. Bachrach who brought this reference to my attention.

are carried out. Using the fundamental constants given in Table II for this material, the three sets of values for λ, μ, and ν obtained from the self-consistent computations are 1.05, 1, and 1, respectively. The corresponding calculated value $(E - E_x)/E_x = 0.53$ is in good agreement with experiment 0.61.[30]

For the exciton-ionized-acceptor complex the atomic units corresponding to Schrodinger eq 9 have been considered. The total energy E of the system is calculated in terms of the neutral acceptor binding energy E_A. In this case the recursion relation of eq 13 takes the form

$$H' + \epsilon(\delta_a P + Q) = 0 \tag{18}$$

The matrix H' is a function of λ, μ, and ν. The values of λ and μ have opposite signs to those corresponding to the exciton-ionized-donor complex. Four different cases with different values of λ, μ, and ν have been considered in Figure 4. In these calculations the values of α, β, and γ corresponding to specific values of λ, μ, and ν are determined from the minimization of the energy for this specific case. In Figure 4 the values of α, β, and γ corresponding to the specific values of λ, μ, and ν are given. This figure shows again the important contribution of the polarizability expressed in terms of λ, μ, and ν. As either the value of λ or μ or ν changes, one gets different results for E/E_A as function of $1/m_e^*$ au. The intersections of $E/E_A = f(\delta_a)$ with $E/E_A = 1$ give critical mass ratios σ_{ac} below which the system is stable, otherwise it is unstable. In most known inorganic crystals the values of δ_a are high and it is highly improbable that such a complex exist in such materials.

The terminology of trapped hole and trapped electron in radiation chemistry could correspond to the same terminology of ionized donor and ionized acceptor, respectively, treated in this paper. It may be possible that similar treatment to that given in this paper leads to an explanation for the physical phenomena of trapped hole and trapped electron in radiation chemistry, particularly, in the radiation of glasses.

Acknowledgments. The computations have been carried out at the Computer Center of Cronenbourg-Strasbourg. I wish to thank Professor G. Monsonego, director of the Computer Center, and the personnel, in particular M. Gendner, for their considerable help.

Polaron Yields in Low-Temperature Pulse Radiolysis of Chemically Inert Aqueous Matrices

V. N. Shubin,* Yu. I. Sharanin, T. E. Pernikova, and G. A. Vinogradov

Institute of Electrochemistry of the Academy of Sciences of the U.S.S.R., Moscow, U.S.S.R. *(Received April 21, 1972)*

The competition between the recombination of activated electrons with parent positive ions and the formation of localized electrons (polarons) is considered. The equation obtained as the result of a physico-mathematical analysis gives a satisfactory explanation of the dependence of the polaron yield on temperature, experimentally observed in crystalline ice. The calculated value of the activation energy is equal to 0.12 eV, which suggests the localization process have an energy threshold. The possibility of polaron formation as result of dissociation of an excited state in alkaline glasses is postulated. This can be the reason for the anomalous dependence of $G(e_s^-)$ on temperature in 10 M alkaline solutions. Energetic characteristics of the water excited state were estimated. The calculated excitation potential is equal to 9.3 eV.

At present the existing theories of an electron in a local state ignore completely the kinetics of free electron transitions into localized state and the inverse processes. Nevertheless, it is possible that the quantitative characteristics (and, in particular, the polaron yield) are determined precisely by the competition between different kinds of electron stabilization processes (on a single molecule or on whole groups). Taking into account this approach, an attempt at a physico-mathematical analysis of such competition was carried out for frozen matrices.

The interaction of ionizing radiation with substance leads to activation of molecular or atomic electrons into the conduction band of a dielectric. Since, however, along with electron, there appears also a positive hole with which it will rapidly or slowly recombine, the kinetics of polaron formation in such a system has some specific features, as compared with the classical model of the "excess" electron in crystal. Some of these features were pointed out in previous papers.[1,2]

If the number of the band electrons in unit volume is N^-

(1) V. N. Shubin, V. A. Zhigunov, V. I. Zolotarevsky, and P. I. Dolin, *Nature (London)*, **212**, 1002 (1966).
(2) V. M. Biakov, Yu. I. Sharanin, V. N. Shubin, *Ber. Bunsenges. Phys. Chem.*, 271 (1971).

and the number of holes, accordingly, N^+, the probability of their recombination is proportional to the product of these quantities $P_1N^-N^+$. It can be assumed with certainty that the electron will be trapped by the Coulombian field of the hole if it comes into its vicinity of radius

$$r_B = e^2/2\epsilon kT \qquad (1)$$

The "thermal" electron itself having the velocity

$$\bar{v} = (2kT/m_e)^{1/2}$$

during the time Δt is "localized" in the sphere of radius[3] $r_L = \bar{v}\Delta t$. The probability of partial or total overlapping of these spheres (which leads to recombination) is proportional to the products of the volumes

$$W_1 = \beta v_B v_L = \beta \frac{4}{3}\pi r_B{}^3 \frac{4}{3}\pi r_L{}^3 = \beta \frac{16\pi^2}{9}\left(\frac{e^2}{2\epsilon kT}\right)^3\left(\frac{2kT\Delta t^2}{m_e}\right)^{3/2} \qquad (2)$$

Since in the final analysis the dependence of G_p on T is determined, it would be expedient to combine all the coefficients into one and write

$$W_1 = \delta(kT)^{-3/2} \qquad (3)$$

Apart from recombination, there exists a possibility, first pointed out by Landau,[4] that from an unstable band state the electron will transform into a specific local state such as polaron. Having carried out a physico-mathematical analysis, Pekar[5] arrived at the concept that the band electron of dielectrics will be autolocalized into the optimum polaron state as the result of monotonic deepening of the polarization potential well at the expense of energy of the electron field. It is not impossible, however, that near the top edge of the polaron band there should exist some intermediate region from which the electron, loosely bound with the medium, may be transferred, due to thermal or some other fluctuations, with equal probability either to the conduction band or to the polaron state. For this reason, the electron transition into the polaron state will be of a jumpwise (threshold) nature, *i.e.*, the medium will constitute a stable trap for the electron only starting from a certain definite energy value of the polarization potential well E_0.[6]

If E_0 is a trap of minimum depth in which electron can be stabilized and account is taken of the fact that the probability[7] of the electron being captured by the trap is proportional to its depth (see Appendix I) and the number of the traps with an energy E, the Boltzmann factor, the following expression is valid

$$W_{E \geq E_0} = \alpha \int_{E_0}^{\infty} Ee^{-E/kT}\,dE = \alpha e^{-E_0/kT}(kT)^2\left(1 + \frac{E_0}{kT}\right) \qquad (4)$$

Here $W_{E \geq E_0}$ is the probability of the electron being captured by all traps of depth $E \geq E_0$ and α is the proportionality factor. Since it would be reasonable to assume $E_0 \gg kT$, expression 4 can be restricted to the second term, so that

$$W_2 = \rho(kT)e^{-E_0/kT} \qquad (5)$$

The total probability of transition into the polaron state is proportional to the total number of electrons formed during ionization, so that the electron formation–decay equilibrium during the pulse action can be written as[8]

$$\delta(kT)^{-3/2}N^-N^+ + \rho(kT)e^{-E_0/kT}N^- = G_0\left(\frac{I}{100N}\right) \qquad (6)$$

where N is the Avogadro value and G_0 the primary ionization yield. Using this expression we can obtain an equation for the radiation yield of detected polarons, determining a definite dependence of the polarone yield, G_p, on the temperature of a dielectric

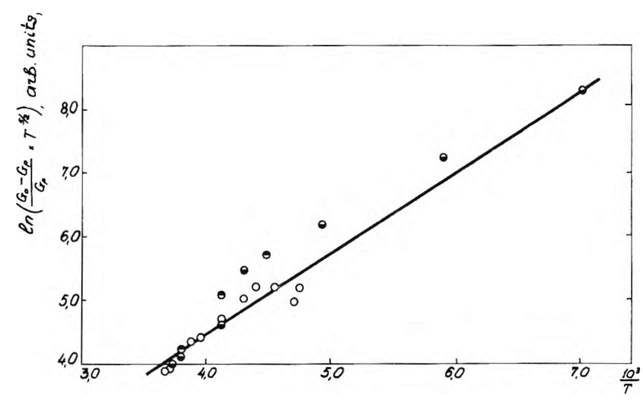

Figure 1. Graphical solution of eq 8 from the experimental data of the authors and ref 9 and 11: O, this paper, ●, ref 11; ⊖, ref 9. The straight line has been constructed using the least-squares method.

$$G_p = G_0 \frac{\rho(kT)e^{-E_0/kT}}{\delta(kT)^{-3/2}N^+ + \rho(kT)e^{-E_0/kT}} \qquad (7)$$

Combining all the unknown constant coefficients into one constant and writing out the dependence of the yield on temperature in an explicit form, we finally obtain

$$\frac{G_0 - G_p}{G_p} = \text{constant} \times T^{-5/2}e^{E_0/kT} \qquad (8)$$

In Figure 1 this equation is solved by plotting it as ln $\{[(G_0 - G_p)/G_p]T^{5/2}\}$ *vs.* $1/T$ using the data of the authors as well as the results[10] of other papers.[9,11] It can be seen that eq 8 agrees satisfactorily with experiment at E_0 = 0.12 eV ±15%, which corresponds to the upper boundary of the librational (rotational) spectrum, equal to ~0.125 eV.[12]

This confirms the concept advanced earlier[2,14] that interaction with phonons has a determining effect on a number of properties of the electron local state in crystalline ice and liquid water. A radically new conclusion is drawn here, namely, that electron localization does not take place at all if the energy of the polarization well is less than the upper boundary of the phonon spectrum, *i.e.*, the maximum energy of an optical phonon. If this is the case an electron can be ejected from the trap after an interaction with a phonon.

(3) It is convenient to believe an electron which relaxes with a positive hole is an excited state equivalent which has a half-life Δt and an indeterminate energy ΔE. Then according to the principle of indeterminacy $\Delta E_e \Delta t = h = \Delta P \Delta x$ or $\Delta(m_e V^2/2)\Delta t = \Delta(m_e \bar{V})\Delta x$ so that $\Delta x = r_L = \bar{V}\Delta t \cong 100$ Å at the temperature 273°K.

(4) L. D. Landau, *Phys. Z. Sowjetunion*. **3**, 664 (1933).

(5) S. I. Pekar, *Issled. Elektron. Teor. Kristall.*, (1951).

(6) One can see that if an electron is autolocalized during the process of monotonic deepening of the polarization potential well then the energy value E_0 will be equal to zero simply.

(7) A. S. Davydov, "Kvantovaya mechanica," PhisMathGIS, Moscow, 1963.

(8) Radical OH does not form a Coulombian trap for electron and OH^- can appear only if the time of an electron passing the hydroxyl radical, equal to $t = r_{OH}/V \simeq 10^{-14}$ sec, exceeds the time of the energy losses through dipole radiation (see Appendix I) $t = (\hbar^4 c^3/e^2 a^2 E^3{}_{OH^-}) \cong 10^{-9}$ sec. Here E_{OH^-} is the ionization potential of OH^- and a, the trap size. As one can see, the condition is not fulfilled and the OH^- formation, because of an electron interaction with hydroxyl radical, does not take place. That is confirmed experimentally.[9]

(9) I. A. Taub and K. Eiben, *J. Chem. Phys.*, **42**, 2499 (1968).

(10) The values of G_p obtained by different authors were normalized to the value of G_p = 0.8 ion/100 eV at 263°K, obtained by direct electrochemical measurements.[13]

(11) G. Nilsson, H. C. Christensen, I. Fenger, P. Pagsberg, and S. O. Nielsen, *Advan. Chem. Ser.*, **No. 81**, 71 (1968).

(12) I. E. Bertie and E. Whalley, *J. Chem. Phys.*, **40**, 1637 (1964).

(13) Yu. I. Sharanin, V. N. Shubin, and P. I. Dolin, *Dokl. Acad. Nauk SSSR*, **195**, 896 (1970).

(14) V. N. Shubin and S. A. Kabakchi. "Teoriya i metody radiatsionnoy khimii vody," "Nauka," Moscow, 1969.

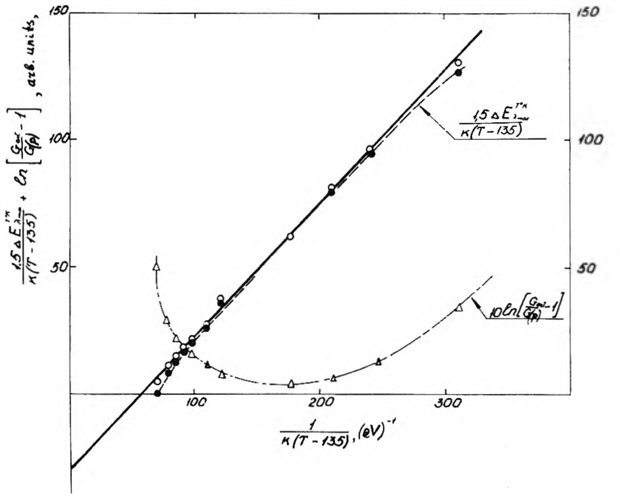

Figure 2. Graphical solution of eq 12 from the experimental data of ref 19. The straight line has been constructed using the least-squares method. The dashed lines illustrate the change with temperature of the first (- - - -) and the second (-·-·-·-) terms of the equation.

Apart from ionization, radiation can lead to appearance of the excited states of water molecules. In such states an activated electron is on a discrete level located much deeper than the lower boundary of the conduction band. For this reason thermal dissociation of such "excitons" to form a band electron appears to be extremely problematic.

Apparently, Frank[15] was the first to suggest that thermal fluctuation can transfer an excited electron into the polaron state (or e_{aq}^-). According to Frank, having absorbed an energy quantum, the electron can (a) be thermally transferred into the polaron state with the probability $\sim e^{-E_1/kT}$, where E_1 is the difference of energies of two levels, and (b) recombine with the hole radiating light with the probability independent of temperature.

This leads to the expression for the quantum polaron yield (compare also ref 16).

$$\eta(T) = 1/(1 + Ae^{-E_{kT}}) \tag{9}$$

As it was first pointed out earlier,[2] the residence of the polaron in the field of alkali metal cations resulted in appreciable (up to 13%, see ref 17) deepening of the polarization potential well. This affects the change in the value of E_1 characterizing the difference between the electron energies on a discrete exciton level, and in the polaron state. Moreover, the value of E_1, as it follows from the results of numerous (see, *e.g.*, ref 18) experimental investigations, should be a function of temperature. As a consequence, one can see from analysis of expression 9, the observed polaron yield obtained upon cooling of the sample may increase. This phenomenon was experimentally observed by Buxton, Cattell, and Dainton[19] during pulse radiolysis of a 10 *M* NaOH-KOH mixture in the temperature range 300–77°K. With temperature decreasing from 300 to $\sim$200°K, the observed yield of e_{solv}^- at first increases smoothly from 3.3 to $\sim$5 ion/100 eV, and subsequently drops to previous values ($\sim$3) with further temperature decrease. According to ref 19, this drop correlates with complete disappearance at $T_\infty = 135$°K of translations of water molecules favoring spatial separation of charges[20] during exciton dissociation. Due to steric difficulties arising in this case, the recombination phenomena begin to prevail in the competing processes, which results in a corresponding decrease of the detected yield of localized electrons.

Assuming, after the authors of ref 19, this temperature to be the arbitrary zero of the temperature scale and taking into consideration all that has been said above about the dependence of E on T, let us transform expression 9 into the form

$$G_{(p)} = \frac{G_{ext}}{1 + Ae^{E(T)/k(T-T_\infty)}} \tag{10}$$

Here $G_{(p)}$ and G_{ext} are the yield of the electrons transferred from the discrete level to the polaron state[21] and the primary yield of excited states (excitons), respectively. The value of the energy gap $E(T)$, which is a function of the sample temperature, can be for convenience rewritten as

$$E(T) = E_{300°K} - \Delta E_{T°K} \tag{11}$$

Here $E_{300°K}$ is the gap width at 300°K and $\Delta E_{T°K}$, the change in its value when the temperature drops from 300°K to a lower value. The value of $\Delta E_{T°K}$ can be determined using the data on the shift of $E_{\lambda_{max}}$ upon cooling of the sample,[19] since $\Delta E_{T°K} = 1.5\,\Delta E_{\lambda_{max}}^{T°K}$.[14] Then writing out the dependence on temperature in an explicit form, we obtain finally instead of (10) an equation that can be conveniently solved graphically

$$\frac{E_{300°K}}{k(T - T_\infty)} = \frac{1.5\,\Delta E_{\lambda_{max}}^{T°K}}{k(T - T_\infty)} + \ln\left[\frac{G_{ext}}{G_{(p)}} - 1\right] \tag{12}$$

As it follows from the solution results (Figure 2), eq 12 agrees satisfactorily with experiment at $G_{ext} = 7$. This value agrees closely with the value of the exciton yield estimated earlier in analysis of the anomalous behavior of the radiation-induced electrical conductivity of crystalline ice.[22]

From the slope of the straight line obtained, it is possible to estimate the energy characteristics of the dissociative transition exciton–polaron and the energy of the electron excitation to the exciton state. The value of the energy gap at 300°K, calculated from analysis of the experimental data, is 0.52 eV ± 10%.

Adding the calculated value of the energy gap to the polaron well depth at this temperature and subtracting the quantity obtained from the ionization potential of a water molecule,[23] we obtain

$$E_{ext} = 12.56 - (E_{300°K} + 1.5E_{\lambda_{max}}^{300°K}) = 12.56 - (0.52 + 2.74) = 9.30\text{ eV}$$

The calculated value closely coincides with the energy of one of excited levels of a water molecule given in ref 24 and is equal to 9.2 eV. Thus the results of the estimation carried out support the hypothesis that polaron is anion of an excited state (exciton).

Acknowledgment. The authors wish to thank Professor R. R. Dogonadze for discussion of this paper and valuable remarks.

(15) J. Frank, unpublished, cited in R. Livingston, "Chemical Reactions Caused by Ionizing Radiation," in coll. "Radiobiology," Moscow, 1955.
(16) N. F. Mott, *Proc. Roy. Soc.*, **167**, 384 (1938).
(17) S. A. Kabakchi, *Khim. Vys. Energ.*, **5**, 180 (1971).
(18) A. K. Pikaev, "Solvatirovannyy electron v radiatsionnoy khimii," "Nauka," Moscow, 1970.
(19) G. V. Buxton, F. G. R. Cattell, and F. S. Dainton, *Trans. Faraday Soc.*, **67**, 687 (1971).
(20) E. Koldin, "Kinetics of Fast Reactions in Solution," "Nauka," Moscow, 1966.
(21) Less the yield of the electrons formed as the result of ionization and completely transformed into e_{aq}^- (see in more detail),[19] *i.e.*, $G_{(p)} = G(e_s^-)^{total} - G(e_s^-)^{ioniz}$.
(22) Yu. I. Sharanin, V. N. Shubin, T. E. Pernikova, and V. I. Zolotarevsky, P. I. Dolin, *Nature (London)*, **234**, 15 (1971).
(23) W. C. Price, *J. Chem. Phys.*, **4**, 149 (1936).
(24) C. I. Hochanadel, "Comparative Effect of Radiation," M. Burton, *et al.*, Ed., Wiley, New York, N.Y., 1960, p 151.

Appendix I

It is possible to estimate the probability of electron filling the traps of different depth which is equivalent to the determination of the problem of photon energy radiation during the electron transition from the zonal state to the lowest level of the trap. Suppose that the initial electron state is weakly bound with the trap. Then the radiation process can be calculated with the help of the first-order matrix. The equation for the matrix element will be

$$S_{i\to f} = -e\int \bar{\psi}_2 \hat{A}\psi_1\, \mathrm{d}x\sqrt{N+1}$$

where $\hat{A}$ is the electromagnetic field potential and ψ_1 and ψ_2 are the wave functions of the initial and final states. Since these are steady states, ψ_1 and ψ_2 include the time in the form of $e^{-i\omega_1 t}$ and $e^{-i\omega_2 t}$ so that the matrix element will be

$$S_{i\to f} = -2\pi i U_{i\to f}\,\delta(\epsilon_1 - \epsilon_2 - \omega)$$

where

$$U_{i\to f} = -e\sqrt{\frac{\omega \mathrm{d}\omega}{\pi}}\, i^l\sqrt{\frac{l+1}{l}}\,\frac{\omega^l}{(2l+1)!!}\int \psi_2{}^*\psi_1 r^l J_{lm}{}^*\mathrm{d}r$$

and ω is the frequence of the electron oscillation into the trap with an energy E, and δ the δ-function.

Since the dipole radiation at $l = 1$ is the most likely one, the probability of such transition can be written as

$$|U_{i\to f}|^2 = \frac{4\omega^3}{3\hbar c^3}\int \psi_2{}^*\psi_1 r J_{lm}{}^*\mathrm{d}r$$

Then taking into account that the Legendre adjoint polynomial is equal to 1, and the integrand corresponds to the matrix unit of the dipole moment, the probability of transition in time unit will be

$$P_{i\to f} = (e^2\omega/\hbar c)(\omega a/c)^2 \equiv e^2a^2E_{\mathrm{trap}}{}^3/\hbar^4c^3$$

where a is a characteristic trap size and c, the light velocity. Consequently, the traps are not filled uniformly, but proportionally to their depth cubed.

For a system with the Coulombian interaction $a = (e^2/\hbar\omega)$ so that the obtained equation one can simplify to

$$P_{if} = (e^2\hbar c)\omega(\omega a/c)^2 = \omega/(\hbar c/e^2)^3 = \omega/(137)^3$$

The mean energy of the electron interaction with the induced polarization is equal to $E = {}^4/_3E_{1s}$ where E_{1s} is the polaron energy in the ground state. Then using the equation of the usual theory of the hydrogen-like atom

$$E = {}^4/_3E_{1s} = I\omega^2$$
$$I\omega = n\hbar$$

one can estimate the electron frequence in the polaron state

$$\omega = {}^4/_3(E_{1s}/\hbar)$$

Evidently that the relation between the probabilities of a thermalized electron being captured by a proton, P_{H^+}, or a polarization trap, P_p, will be

$$\frac{P_{H^+}}{P_p} = \frac{2E_H}{{}^4/_3E_{1s}} = \frac{2E_H}{2E_{\lambda_{max}}} \simeq 8$$

where E_H is the ionization potential of hydrogen atom. It is clear that when the concentrations of "free" protons and polarization traps become equal the observed yield of e_{aq}^- should be essentially less then the primary ionization yield as it takes place in the cristalline ice.[1,9,11] In the case of liquid water the same effect was observed experimentally by Kenney and Walker.[25]

(25) G. A. Kenney and D. C. Walker, *J. Chem. Phys.*, **50**, 4074 (1969).

Cerenkov Reabsorption Spectroscopy for Subnanosecond Pulse Radiolysis Studies

Stephen C. Wallace and David C. Walker*

Chemistry Department, University of British Columbia, Vancouver, Canada *(Received April 24, 1972)*

Publication costs assisted by the National Research Council of Canada

Cerenkov reabsorption spectroscopy involves the measurement of absorption by radiation-produced species of the system's own Cerenkov light when subjected to a pulse of high energy electrons. Absorption spectra are obtained as the difference between the partially reabsorbed Cerenkov spectrum and the true Cerenkov emission spectrum. The enormous dose rate provided by the 3-nsec pulse of 600-kV electrons from a Febetron accelerator provides very considerable sensitivity, enabling, for instance, the absorption spectrum of the hydrated electron to be observed in 3 M $HClO_4$ solutions where the mean lifetime of e_{aq}^- is only $\sim 3 \times 10^{-11}$ sec. Thus while utilizing comparatively simple spectrographic or nanosecond spectrophotometric detection systems, the picosecond events of radiolysis may be examined. Several experimental methods and the theoretical treatment of the data are presented in detail. The measured absorption is shown to be related to the product $G\epsilon\tau$ for the absorbing species in different ways depending on the experimental conditions. Results are given which demonstrate the potentialities of the method and corroborate some of the important results obtained by Hunt, *et al.*, on the picosecond time scale for water. These include the measurement of a primary yield of e_{aq}^- of 3.2 ± 0.8 for the pH range 0–7, presolvation scavenging by solutes except H^+, the absorption spectrum in the presence of molar concentrations of scavengers, lack of evidence for time-dependent pseudo-first-order rate constants at ~ 1 M concentration, and relative yields of solvated electrons in aliphatic alcohols.

Introduction

The investigation of radiation-induced chemical processes in liquids on the 10^{-11} to 10^{-9} sec time scale has recently been reported using the very elegant, but experimentally complex, stroboscopic pulse radiolysis technique.[1-4] Some of the results of those studies have had a reviviscent impact on theoretical treatments of the primary radiation chemical processes.

In this paper we demonstrate that this same time domain is also accessible using a method described as Cerenkov reabsorption spectroscopy (CRS) which utilizes the enormous dose rates available from a Febetron accelerator. A preliminary report of such measurements has already been given[5] where it was dubbed a "self-portrait" method because spectrographic measurements were made of the self-absorption spectra of the system's own Cerenkov light. A comprehensive review is presented here of the experimental methodology and the theoretical treatment of data.

The inherent simplicity of the experimental procedures of Cerenkov reabsorption spectroscopy is one of its principal advantages, coupled with a need for only a few milliliters of the liquid being studied. Its main limitation is that it does not provide direct kinetic information on the decay rate of the absorbing species except when both the radiation yield (G) and extinction coefficient (ϵ) are already known. In terms of its sensitivity for detection of very short-lived species it is comparable to the stroboscopic method, requiring $G\epsilon \simeq 2000$ when $\tau \simeq 10^{-10}$ sec. For longer-lived species it is more sensitive.

Since the method involves measuring the difference between the Cerenkov light intensity transmitted through an absorbing solution with that of the pure Cerenkov intensity, limitations to the sensitivity are imposed by the pulse-to-pulse reproducibility of the accelerator and the accuracy with which these different intensities may be evaluated. In practice this means that the "absorbance" must exceed ~ 0.1. For this reason the dose rate provided by the electron pulse from a 600-kV Febetron is particularly advantageous. This accelerator provides a pulse <3 nsec width at half-height with a maximum beam current of ~ 5000 A cm^{-2}. About 7 J cm^{-2} of energy is deposited within a 2-mm depth of unit density material resulting in dose rates greater than 10^{29} eV g^{-1} sec^{-1}. The internally synchronized Cerenkov light pulse is partially reabsorbed by the high concentration of radiation-produced species, and the "effective absorption path length" is less than 1.5 mm. Nanosecond pulsed electron beams of much higher kinetic energy, but lower current, could be adopted this same way—the lower dose rate being partially compensated by a longer light absorption path length—and the geometric factors stemming from the predominant direction of Cerenkov emission could be used to advantage. However, on high energy linear accelerators the Cerenkov light pulses may be generated separately and redirected through the radiation cell, as in the stroboscopic method,[1-4] thereby affording kinetic information as well.

Theoretical Section

For the electron beam used in this work the Cerenkov light produced in a liquid sample is given off predominantly in the direction of the electron beam, and it originates from the first few tenths of a millimeter from the electron window of the irradiation cell. Consequently, the Cerenkov light which emerges through the quartz window at the rear of the cell has had to pass through a region of liquid in which a large fraction of the dose was deposited.

(1) M. J. Bronskill, R. K. Wolff, and J. W. Hunt, *J. Phys. Chem.*, **73**, 1175 (1969).
(2) M. J. Bronskill, R. K. Wolff, and J. W. Hunt, *J. Chem. Phys.*, **53**, 4201 (1970).
(3) R. K. Wolff, M. J. Bronskill, and J. W. Hunt, *J. Chem. Phys.*, **53**, 4211 (1970).
(4) J. E. Aldrich, M. J. Bronskill, R. K. Wolff, and J. W. Hunt, *J. Chem. Phys.*, **55**, 530 (1971).
(5) D. C. Walker and S. C. Wallace, *Chem. Phys. Lett.*, **6**, 111 (1970).

The experimental observables in Cerenkov reabsorption measurements are the emitted fluxes of Cerenkov photons from the irradiated material with and without reabsorption by radiation-produced transient species. These functions, denoted $I(t)$ and $I_0(t)$, respectively, may be measured as a function of wavelength as explicit time variables using a photomultiplier-oscilloscope detection system, or they may be conveniently integrated over the pulse by the photographic film in a spectrograph. At a given wavelength the total number of photons per pulse in the absence of any reabsorption—called reference Cerenkov—is given by

$$I_0 = \int_0^{\tau_c} I_0(t)\mathrm{d}t \tag{1}$$

and the total number of photons per pulse with reabsorption—called absorbed Cerenkov—by

$$I = \int_0^{\tau_c} I(t)\mathrm{d}t \tag{2}$$

where τ_c is the duration of the Cerenkov emission pulse. In this work both the ratio of I_0 to I (defined as S) and the logarithm of this ratio (defined as U) have been measured, the former being directly available from spectrophotometric measurements and the latter a consequence of the spectrographic method of detection.

Unfortunately the current and energy of the electron beam are not constant during the pulse. This confers a complicated time dependence during the pulse on both the intensity of Cerenkov emission and concentration of absorbing species. Thus the parameter S cannot simply be related to the inverse of the transmittance of the irradiated solution nor U to the absorbance. The situation is further aggravated by spatial considerations. The Cerenkov light source overlaps with a portion of the dose distribution so that the "effective optical absorption path length" (l) is not immediately available. In fact l could be evaluated empirically in an independent experiment providing one knew with certainty for some species the radiation yield on a 1-nsec time scale (G), the extinction coefficient (ϵ), and the lifetime (τ). There is in addition a time dependence superimposed upon the spatial distributions because of the changing energy of the electron beam during the pulse. It transpires that this is not particularly serious because it mainly affects only the leading and trailing edges of the pulse when the Cerenkov intensity is particularly low and which therefore contribute very little to I and I_0. In practice we can use a measured dose distribution obtained for the total pulse and calculate the intensity of Cerenkov emission as a function of depth based on the mean electron energy (500 kV) to which the observed depth–dose distribution corresponds.

Just as I and I_0 depend on the temporal- and spatial-dose functions so does the instantaneous concentration of absorbing species $c(x, t)$. At one extreme, when the lifetime τ of the species is long ($>10^{-8}$ sec) compared to the pulse duration, the concentration at time t can be related to the accumulated dose up to time t and is independent of τ. At the other extreme, when $\tau < 10^{-10}$ sec, the instantaneous concentration is proportional to the product of dose rate times lifetime. For the general case we treat $c(t)$ as an explicit function of t based on a pseudo-first-order rate constant. Since we are in general dealing with primary species of the radiolysis (or those formed in $<10^{-10}$ sec by first-order processes), the spatial dependence of concentration is the same as the dose or dose rate distributions.

Taking Beer's law to apply to photons originating at depth x within the cell at time t during the pulse one has

$$I(x,t) = I_0(x,t)\exp[-\alpha\int_x^{a_d} c(x',t)\mathrm{d}x'] \tag{3}$$

where x' is the depth of dose deposition through which the photons pass, a_d the depth at which the dose deposition becomes zero, and $\alpha = 2.303\epsilon$. In this equation the integrand gives the product of concentration times optical path length for photons originating at depth x. For the total pulse this yields

$$I = \int_0^{\tau_c}\int_0^{a_c} I_0(x,t)\exp[-\alpha\int_x^{a_d} c(x',t)\,\mathrm{d}x']\mathrm{d}x\mathrm{d}t \tag{4}$$

$$I_0 = \int_0^{\tau_c}\int_0^{a_c} I_0(x,t)\mathrm{d}x\mathrm{d}t \tag{5}$$

where a_c is the depth at which Cerenkov emission becomes zero.[6] S and U are hence the ratio of eq 5 to eq 4 and the logarithm of this ratio, respectively.

The purpose of the following theoretical treatment then is to relate the magnitude of the Cerenkov reabsorption, as measured by the parameters S and U, to such physical properties of the absorbing species as the $G\epsilon$ product and the rate of disappearance. However, commensurate with certain types of measurements that can be made we will firstly show two ways in which the treatment may be approximated without introducing serious errors for specified cases before attempting the general integration of eq 4 and 5 using explicit functions of x and t.

A. Measurement of Peak Light Fluxes (for Short-Lived Species Only). For cases in which the absorbing species are very short-lived (specifically $\tau < 10^{-10}$ sec) they will exist at radiation-stationary levels during the pulse. At the pulse peak, which is fairly flat for ~0.5 nsec, they will have steady-state concentrations governed by the maximum dose rate and by their mean lifetimes. The maximum in the dose pulse coincides with *both* the maximum in $I_0(t)$ and in the maximum absorbance. Consequently, by measuring only the peak values of $I_0(t)$ and $I(t)$ (their ratio will be called $(I_0/I)_{\max}$) there is no time dependence involved. Furthermore the electron beam is monoenergetic at the peak so that a correction for the spatial overlap of light source and dose deposition may be applied by specifying that only a certain fraction, γ, of the total dose is available for generating species that may contribute to absorption. γ can be estimated from the Cerenkov and dose distributions synthesized later. For 550-kV electrons (mean peak energy incident upon the liquid) penetrating water γ has a value of 0.7 ± 0.1.

From Beer's law one derives

$$(I_0/I)_{\max} = \exp[\sigma\gamma\int_0^{a_d} c'(x)\mathrm{d}x] \tag{6}$$

where γ corrects for the fraction of species not available for absorption (equivalent to correcting for the "effective" path length), σ is the absorption cross section in square centimeters per mole (*i.e.*, $\sigma = 2.303\epsilon$) and $c'(x)$ is the steady-state concentration in moles per liter of species at distance x during the pulse peak.

Because of the stationary-state condition it follows that the total number of species present in the cell per unit area

(6) Since a_c is substantially smaller than a_d, the actual depth–dose distribution between a_c and a_d is unimportant. All species produced in this region at time t contribute to absorption for all photons; *i.e.*, one could evaluate the dose deposited between a_c and a_d, regard that as only a time-dependent parameter, rewrite x' as $x'' = a_c - x$ and then integrate $c(x)$ between x and a_c. However, we treat it this way because it transpires that both $I(x)$ and $c(x')$ may be represented by fairly simple functions, and this method compensates better for the time dependence of the depth–dose function.

normal to the electron beam under an incident radiation intensity R (electron volts per square centimeter per second) is given by

$$\int_0^{a_d} c'(x)\mathrm{d}x = RG\tau/N_0 \times 10^2 \qquad (7)$$

for a first-order decay process, where N_0 is Avogadro's number and τ the lifetime of the species.

Combining eq 6 and 7 yields the relationships 8 and 9

$$(I_0/I)_{\max} = \exp[23.03R\gamma G\epsilon\tau/N_0] \qquad (8)$$

$$\log(I_0/I)_{\max} = G\epsilon\tau(10R\gamma/N_0) \qquad (9)$$

The peak incident radiation intensity R may readily be obtained for a Febetron accelerator either by (i) measuring the peak beam current using a suitably shaped Faraday cup placed behind the cell's electron window, or (ii) measuring the total incident radiation per pulse by adiabatic calorimetry and calculating the maximum flux from the dose waveform. Unless τ can be evaluated independently one cannot separate $G\epsilon$ and τ from these measurements. However, for a single species one can readily obtain the absorption spectrum of the species by plotting log $(I_0/I)_{\max}$ against wavelength.

Although this method is quite straightforward, it is limited at the present time because it requires a detection system which is sufficiently fast to properly display the maxima in the light signals $I_0(t)$ and $I(t)$. Whereas a sluggish detection system (risetime ~2 nsec) may adequately represent, from the measured areas on the oscillograms, the true ratio $\int_0^{\tau_c} I_0(t)\mathrm{d}t/\int_0^{\tau_c} I(t)\mathrm{d}t$, it is not clear that the ratio of the observed trace maxima can confidently be equated to the real ratio $(I_0/I)_{\max}$. Sampling methods would be extremely tedious using a Febetron.

B. Absorption Spectra by an Approximate Method (for Species with $\tau > 10^{-8}$ Sec). For the purpose of obtaining only the absorption spectrum of species which do not decay appreciably during the pulse one can make the following approximations without introducing serious distortions to those spectra: (i) that the Cerenkov light waveform and dose waveforms are the same and coincident; and (ii) that a correction γ, as in A, may be applied separately to account for the spatial distributions. For the total pulse, including its low energy regions, γ is estimated to be 0.75 ± 0.1 for the case of water.

As before the use of γ permits one to ignore the depth distribution of concentration and to consider only the number of species per unit area present in the cell under a given incident radiation flux. Applying Beer's law one derives eq 10 for this case

$$I(t) = I_0(t)\exp[-\sigma\gamma\int_0^t n(t)\mathrm{d}t] \qquad (10)$$

where $n(t)$ is the number of moles per square centimeter *created* in time interval dt at time t (the integral in eq 10 is hence the number of moles per square centimeter present at time t since decay is taken to be insignificant). The dose rate and light pulses are taken to have the same time dependence ($g(t)$) so that the accumulated incident radiation intensity at time t, $F(t)$, and reference Cerenkov intensity $I_0(t)$ may be written as in

$$F(t) = \xi\int_0^t g(t)\mathrm{d}t \qquad (11)$$

$$I_0(t) = bg(t) \qquad (12)$$

where ξ is a constant converting the time-dependence function, $g(t)$, to incident radiation (electron volts per

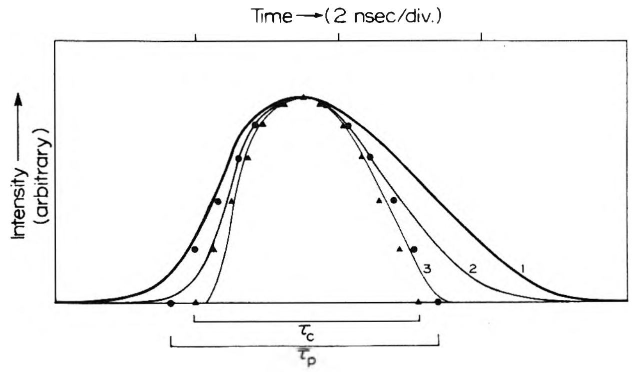

Figure 1. Time profiles of current, dose, and Cerenkov light intensity. Curve 1, oscilloscope tracing of the current pulse as measured with a Faraday cup and recorded on a 1-GHz oscilloscope. Curve 2, expected dose pulse, being curve 1 squared and normalized at the peak. Curve 3, calculated Cerenkov light pulse based on current and voltage pulses represented by curve 1, again normalized at the peak. The sine functions, sin $\pi t/\tau$, are indicated by ● for τ_p = 3.8 nsec which should be compared with the dose curve 2; ▲ for τ_c = 3.2 nsec for comparison with the Cerenkov curve 3.

square centimeter), and b likewise converts $g(t)$ to a light flux.

Since $n(t)$ is given by the accumulated incident radiation, one has

$$n(t) = \frac{G}{N_0 10^2}\xi\int_0^t g(t)\mathrm{d}t \qquad (13)$$

Now, the measurable parameter is

$$S = \int_0^{\tau_p} I_0(t)\mathrm{d}t/\int_0^{\tau_p} I(t)\mathrm{d}t$$

so that, by substitution of (12) and (13) in (10), one obtains

$$S = b\int_0^{\tau_c} g(t)dt/b\int_0^{\tau_c} g(t)\exp\left[\frac{-\sigma\gamma G\xi}{N_0 10^2}\int_0^t g(t)\mathrm{d}t\right]\mathrm{d}t \qquad (14)$$

Since all integrals involve the same time function, $g(t)$, eq 14 may be solved by calling $h(t) = \int_0^t g(t)\mathrm{d}t$ and $h_{\tau_c} = h(t)$ for $t = \tau_c$. Integration between $h(t) = 0$ and $h(t) = h_{\tau_c}$ then yields

$$S = \omega\xi h_{\tau_c}/[1 - \exp(-\omega\xi h_{\tau_c})] \qquad (15)$$

where $\omega = \sigma\gamma G/10^2N_0 = 23.03\gamma G\epsilon/N_0$. In this ξh_{τ_c} is simply $\int_0^{\tau_c}\xi g(t)\mathrm{d}t$ which is the total radiation per pulse, D_p, in electron volts per square centimeter as measured by adiabatic calorimetry. Therefore one has

$$S = \omega D_p/(1 - e^{-\omega D_p}) \qquad (16)$$

S must always be greater than unity, and in general $\omega D_p \gg 1$ so that (16) reduces to

$$S = G\epsilon(23.03\gamma D_p/N_0) \qquad (17)$$

and the spectrum may be obtained simply by plotting S against wavelength, correcting for the slight variations of dose per pulse.

It is normally more convenient to use a spectrograph to obtain the visible and uv spectrum on one pulse, in which case one plots antilog U against λ. Using this approach we have published absorption spectra in a few media.[5,7] Our results for the absorption spectra of solvated electrons in methanol and ethylene glycol and for the benzene excimer in irradiated benzene demonstrate that data obtained in this way compare very favorably with data obtained by conventional microsecond pulse radiolysis methods. For the

(7) D. C. Walker and S. C. Wallace, *Can J. Chem.*, **49**, 3398 (1971).

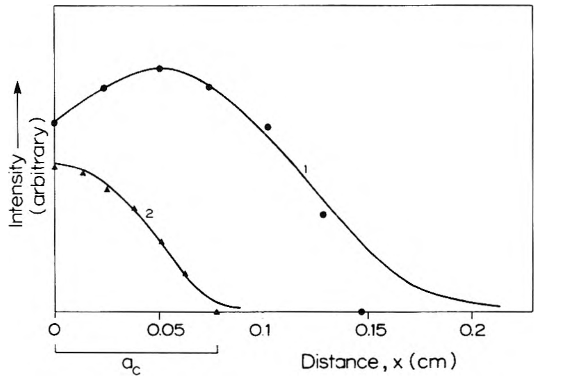

Figure 2. Depth-dose and depth-Cerenkov light distributions for water. Curve 1, depth-dose distributions estimated for water based on measurements using blue-cellophane dosimetry between Al spaces.[8a] Curve 2, expected Cerenkov light emission as a function of depth based on monoenergetic incident energy of 500 kV as discussed in the text. ●, values for $\sin(\pi/c_2)(x + c_3)$ with $c_2 = 0.20$ and $c_3 = 0.055$ cm. (The divergence from line 1 at $x > a_c$ is not very important because all this dose is deposited beyond the region of light generation and therefore all of it contributes to absorption regardless of the distribution.) ▲, values for $\cos \pi x/2a_c$ with $a_c = 0.080$ cm.

spectra in the alcohols the reference Cerenkov light intensities, I_0, were obtained by chemically quenching the absorbing species by the addition of 2 *M* $CHCl_3$ to the alcohols. For the benzene case the Cerenkov emission from cyclohexane was used for reference. The spectra of I_0 were shown to give the expected Cerenkov λ^{-2} dependence in all cases.

This treatment is relatively simple because of approximation i, namely that the dose rate and Cerenkov light waveforms were the same. Thus S and U became entirely independent of that waveform, and no knowledge of it was required, because the transmittance reduced to a form in which only the total dose per pulse was involved. However, if one wishes to obtain accurate *absolute* values for $G\epsilon$ or $G\epsilon\tau$, one must take into account these waveforms and the spatial distributions. The treatment that follows uses functions based on calculated and empirical data to describe these parameters.

C. The General Case. The equation to be solved is, from (4) and (5)

$$S = \int_0^{\tau_c}\int_0^{a_c} I_0(x,t)\mathrm{d}x\mathrm{d}t \Big/ \int_0^{\tau_c}\int_0^{a_c} I_0(x,t)\, \exp\Big[-\alpha \int_x^{a_d} c(x',t)\mathrm{d}x'\Big]\mathrm{d}x\mathrm{d}t \quad (18)$$

Consequently one needs expressions for $I_0(x, t)$ and $c(x, t)$. The only experimental data available are the beam current waveform and the depth-dose curve. These may be combined with the Bethe stopping power relationship and the Franck–Tamm theoretical treatment of Cerenkov emission to derive the expected curves shown in Figures 1 and 2. This information could be used in eq 18 either as data profiles for numerical integration by the computer or described by representative explicit functions for analytical solution. We have chosen the latter approach because (i) within the uncertainty with which the information is obtained simple trigonometrical functions describe it quite well and (ii) the closed analytical form enables small variations in τ_p, τ_c, a_d, and a_c to be readily applied and examined.

Treatment of eq 18 firstly requires $c(x', t)$. Specifying again that the absorbing species is either a primary product of the radiation or formed in a first-order process extremely rapidly ($<10^{-10}$ sec), its rate of formation is proportional to the dose rate function. We will describe its rate of disappearance as a pseudo-first-order decay process given by $kc(x', t)$ because in the experiments we present later high concentrations of scavengers are added. [For some systems, particularly those that may involve excited states which undergo rapid bimolecular annihilation processes, second-order decay processes may be more important; but it is too complicated to treat both first- and second-order processes here, and we are primarily interested in studies involving solute additions.] Thus one obtains

$$\frac{\partial c}{\partial t'}(x,t') = \phi D(x,t') - kc(x,t') \quad (19)$$

where $D(x, t')$ is the spatio-temporal dose-rate function and ϕ is a constant converting dose to concentration. It should be noted that the variable t', which is not necessarily equal to t representing Cerenkov light, is used in this equation because this is the general derivation, and the time dependence of the Cerenkov emission may not even be proportional to the dose-rate function.

In the following treatment we introduce a small error by making the approximation that the variables x and t may be separated to perform the integrations. This separation of the variables implies that we ignore the time dependence of the depth distributions, so it permits us to treat the time dependence properly and then apply depth distributions based on the mean energy of the pulse. Without this separation procedure we could not handle the mathematics so it is applied out of necessity; but in fact it introduces only a small error. As the initial electron energy changes during the pulse, the dose-depth and Cerenkov-depth distributions change, but they change in the same direction, so that the "effective optical path length" does not change very much (it could remain constant only if the electron energy were constant). The error introduced on separating x and t is probably comparable to the percentage difference ($\sim$10%) between the value of $\gamma = 0.7$ in A, where no assumption was invoked, and $\gamma = 0.75$ in B, which was calculated using the assumption.

On separating the variables x and t the dose function in eq 19 may be written as

$$\phi D(x,t') = \zeta_d D(x),\ \zeta_n g(t') \quad (20)$$

where $D(x)$ and $g(t')$ are the dose-depth and dose-rate functions and ζ_d and ζ_n are constants chosen so that $\int_0^{\tau_p}\int_0^{a_d} D(x,t')\mathrm{d}x\mathrm{d}t'$ is equal to the experimentally observed total incident radiation flux per pulse, D_p. (τ_p is the dose pulse width, defined later through a sine function.)

On rewriting eq 19 and 20 with t'' instead of t', combining them, and multiplying by the integrating factor, $e^{kt''}$, gives

$$e^{kt''}\frac{\partial c}{\partial t''}(x,t'') + kc(x,t'')e^{kt''} = \zeta_d\zeta_n g(t'')D(x)e^{kt''}$$

Since the left-hand side of this is equivalent to

$$\frac{\partial}{\partial t''}(c(x,t'')e^{kt''})$$

integration from $t = 0$ to t' gives

$$c(x,t') = e^{-kt'}\int_0^{t'} \zeta_d\zeta_n g(t'')D(x)e^{kt''}\mathrm{d}t''$$

Since

$$\phi D_p = \int_0^{a_d} \zeta_d D(x)\mathrm{d}x \int_0^{\tau_p} \zeta_n g(t'')\mathrm{d}t''$$

and $\phi = 10G/N_0$, upon substitution, one arrives at

$$c(x,t') = \frac{10G}{N_0}\frac{D_pD^*(x)e^{-kt'}}{\int_0^{\tau_p} g(t')\mathrm{d}t'}\int_0^{t'} e^{kt''} g(t'')\,\mathrm{d}t'' \qquad (21)$$

in which $D^*(x) = D(x)/\int_0^{a_d} D(x)\mathrm{d}x$, being the fraction of the total dose deposited at distance x.

The Cerenkov emission function may be written as

$$I_0(x,t) = \lambda l(x)\Lambda m(t) \qquad (22)$$

by also separating the depth and time variables. In (22) $l(x)$ and $m(t)$ are the spatial- and time-dependent functions of Cerenkov light emission in the solution with the constants λ and Λ converting these functions to light intensity. Substituting (21) and (22) into (18) yields

$$S = \int_0^{\tau_c}\int_0^{a_c} \lambda l(x)m(t)\mathrm{d}x\mathrm{d}t \Big/ \int_0^{\tau_c}\int_0^{a_c} \lambda l(x)m(t) \times \exp\left\{\left[\frac{-10G\alpha D_p}{N_0}\int_x^{a_d} D^*(x')\mathrm{d}x'\right] \times \left[(e^{-kt'}/\int_0^{\tau_p} g(t')\mathrm{d}t')\right]\int_0^{t'} e^{kt''}g(t'')\mathrm{d}t''\right\}\mathrm{d}x\mathrm{d}t \qquad (23)$$

It is now necessary to choose the best functions for $l(x)$, $m(t)$, $D^*(x)$, and $g(t')$ from our knowledge of the pulse characteristics.

Figure 1 shows the current pulse profile as measured directly using a very fast Faraday cup–oscilloscope combination as described later. The observed current waveform has a width at half-height of 3.0 ± 0.1 nsec and agrees very well with the manufacturer's data.[8] During discharge the electron tube of the Febetron is believed to have constant impedance; thus the voltage waveform should coincide with that of the current. (Direct measurements of the voltage pulse through a constant impedance by the manufacturers corroborate this.[8b] The time profile of the dose pulse should thus be given by the current waveform squared. This is shown in Figure 1 and has been normalized at the pulse peak. It has a width-at-half-height of 2.3 nsec. Apart from the leading and trailing edges this waveform may be quite well described by a sine function

$$g(t) = \sin \pi t/\tau_p \qquad (24)$$

as demonstrated in Figure 1. The trailing edge of the dose waveform is entirely unimportant because it contributes dose *after* the Cerenkov light pulse is over so no absorption results from it. The leading edge contributes a small constant dose, $\lesssim$5% of the total dose, prior to the Cerenkov pulse.

Unfortunately we have not been able to observe directly the Cerenkov light pulse on a sufficiently fast detection system. Using an H.P. 4207 photodiode and a 250-MHz oscilloscope we have observed Cerenkov light pulses with width at half-height of 2.7 nsec, but this was obviously broadened by the detection system (risetime ~1.5 nsec). Instead we have used the Frank–Tamm theoretical treatment of Cerenkov emission[9] to calculate the Cerenkov pulse shape based on the observed current waveform. For each electron the number of Cerenkov photons emitted between wavelengths λ_1 and λ_2 per unit distance traveled ($\mathrm{d}N/\mathrm{d}x$) in a dielectric medium of refractive index n (assumed to be constant between λ_1 and λ_2) is given by[9,10]

$$\mathrm{d}N/\mathrm{d}x = \frac{2\pi e^2}{\hbar c}\left(\frac{1}{\lambda_2}-\frac{1}{\lambda_1}\right)\left(1-\frac{1}{\beta^2n^2}\right) \qquad (25)$$

where β is the velocity of the electron divided by the velocity of light *in vacuo* (c), which is related to its kinetic energy (E) by the relativistic relationship.

$$E = m_0c^2[(1-\beta^2)^{-1/2} - 1] \qquad (26)$$

Computations based on (25) and (26), in combination with the current and energy profiles of Figure 1 and integrating over electron energies, provide the Cerenkov light profile shown in Figure 1. This can be seen to be substantially narrower than the dose pulse, being 2.1 nsec at half-height. The reason for this is evident from (25), the higher energy electrons generate more photons than do the low energy ones, and in fact $\beta n = 1$ for water in the visible region of the spectrum at the Cerenkov threshold of 270 kV. Thus essentially no light is generated during the leading and trailing edges of the dose pulse. This Cerenkov light profile may also be well represented by a sine function so that the Cerenkov light function which can be used is

$$m(t) = \sin \pi t/\tau_c$$

Now t and t' can be related by

$$t' = t + (\tau_p - \tau_c)/2$$

It is most expedient to integrate 23 with respect to t first; this is done in Appendix A. The results for fast and slow decays are given by eq 27 and 28.

When $k \geq 5 \times 10^9\ \mathrm{sec}^{-1}$

$$S = \int_0^{a_c} l(x)\mathrm{d}x \Big/ \int_0^{a_c} l(x)\left(1 - a'f + \frac{b'f^2}{2!} - \frac{c'f^3}{3!}\cdots\right)\mathrm{d}x \qquad (27)$$

where

$$f = \frac{23.03D_pG\epsilon}{N_0kg}\int_x^{a_d} D^*(x')\mathrm{d}x'$$

$$g = \int_0^{\tau_p} g(t)\mathrm{d}t = 2\tau_d/\pi$$

and a', b', and c' are constants given in Appendix A.

When $k \leq 10^8\ \mathrm{sec}^{-1}$

$$I = \frac{\tau_p^2}{\tau_c}\frac{\Lambda\lambda}{2\pi r}\exp[-f'(1-r)]\int_0^{a_c} l(x) \times \left[\frac{1}{f'} - \frac{s}{2}\left(\frac{\pi}{f'r}\right)^{1/2}\exp\left\{\frac{s^2f'}{4r}\right\}\left(1 - \mathrm{erf}\left\{\left(\frac{f'}{r}\right)^{1/2}\frac{s}{2}\right\}\right)\right]\mathrm{d}x \qquad (28)$$

where

$$f' = \frac{23.03D_pG\epsilon}{2N_0}\int_x^{a_d} D^*(x')\mathrm{d}x'$$

$$r = \cos\frac{\pi}{2}\left(1-\frac{\tau_c}{\tau_p}\right)$$

and

$$s = \sin\frac{\pi}{2}\left(1-\frac{\tau_c}{\tau_p}\right)$$

The spatial dependence of dose-deposition and Cerenkov emission are estimated for the specific conditions of the Febetron pulse and illustrated in Figure 2. The depth–dose curve is based on dosimetry using bleachable dyed cellophane sheets placed between aluminum spacers.[8a] The data correspond closely to the distribution expected for an electron beam having a *mean* energy of 500 keV.[8] It also compares favorably with actual *in situ* measurements of hy-

(8) (a) Technical information supplied by the manufacturers of the Febetron, Field Emission Corp., McMinnville, Ore.; (b) F. M. Charbonnier, private communications.

(9) I. M. Frank and I. Tamm, *Dokl. Acad. Nauk SSSR*, **14**, 109 (1937).

(10) J. V. Jelley, "Cerenkov Radiation," Pergamon Press, Elmsford, N.Y., 1958.

drated electrons produced at the end of the pulse as a function of depth, for fairly broad beam irradiations.[11] Very narrow and well-defined regions of depth may be investigated by this latter method because it utilizes a very small pinhole which may be moved by a micrometer screw across the 2-mm beam of a He/Ne laser directed through the liquid just behind the electron window.

The Cerenkov emission distribution is calculated by combining the Bethe stopping-power equation with eq 25 and integrating over all energies. The total number of photons (N) generated within the wavelength range λ_1 to λ_2 by an electron having an initial velocity β_m as it enters a material thick enough to completely stop it is given by[12]

$$N = \frac{2\pi m_0^2c^3}{he^2n^2ZAB}\left(\frac{1}{\lambda_2} - \frac{1}{\lambda_1}\right)\left[\frac{\beta_m^2n^2 - 1}{(1-\beta_m^2)^{1/2}} + 2n^2(1-\beta_m^2)^{1/2} - 2n(n^2-1)^{1/2}\right] \quad (29)$$

where Z is the mean nuclear charge of the molecules of the medium, A the number of electrons per cubic centimeter, and B is the mean Bethe stopping constant of the medium for electrons of 600 to 260 kV. (This equation involves the simplifying assumption that the dependence of B upon β can be disregarded as a good first approximation.) By subdividing the voltage pulse into a number of energy ranges entering various depths a complete histogram can be constructed from eq 29. Curve 2 of Figure 2 was constructed from a histogram of this sort for a distribution of initial electron energies given by curve 1 of Figure 1. A similar curve was created for a monoenergetic beam of 550-kV electrons. The values of γ used in A and B were evaluated from Figure 2 (and its equivalent for 550-kV electrons) simply by determining the fraction of the total dose deposited at depths greater than $\bar{x}$, the mean depth representing the Cerenkov light source. It is interesting to note that $\bar{x}$ moves to smaller values of x faster than does the mean depth of dose deposition as the electron energy is decreased, in this energy range. This effect, together with the broader dose distribution of a nonmonoenergetic beam, accounts for the larger value of γ in B than in A.

It has been shown by the use of 180° cameras that the Cerenkov emission forms one broad lobe in the direction of the electron beam. This is in accord with expectations when it is noted that (i) the maximum Cerenkov angle for 600-kV electrons is only 28° and that as they slow down this angle approaches zero, and (ii) for 600-kV electrons considerable elastic scattering will be caused by the cell's electron window and by the liquid under investigation.

As indicated in Figure 2 these distributions can be represented quite satisfactorily by the following functions

$$D^*(x) = c_1 \sin \frac{\pi}{c_2}(x + c_3)$$

$$l(x) = \cos \pi x/2a_c$$

where values for the constants c_1, c_2, c_3, and a_c are obtained from the actual distributions presented in Figure 2. Final evaluation of eq 23 involves the integration of (27) and (28) with respect to x using these functions. This is given in Appendix B for the case of $k \geq 5 \times 10^9$ sec^{-1} which represents the conditions used in the scavenger studies for which data are presented later. In this analysis the power series resulting from the time integration (eq 27) is shown to approximate the McLaurin expansion of an exponential in $(G\epsilon/k)$ so that one finally obtains

$$S = \exp\left[\frac{G\epsilon}{k}\left(\frac{23D_p}{N_0}\right)\left(\frac{1}{\tau_p + \tau_c}\right)\left(\frac{\pi c_3 a_c}{c_2^2 - 4a_c^2} + 1\right)\frac{\pi^2}{3.3}\right] \quad (30)$$

Thus the spectrographic observable, U, is simply given by

$$U = \log I_0/I = \frac{G\epsilon}{k}\left(\rho D_p\right) \quad (31)$$

where ρ is described by the constants in (30) which are characteristics of the electron pulse. D_p is the incident radiation intensity per square centimeter per pulse as measured by adiabatic calorimetry. The validity of this equation will be established later by showing that $U \propto k^{-1}$ for the hydrated electron over a range of H_{aq}^+ concentrations where $k \geq 5 \times 10^9$ sec^{-1} and from the slope of this plot obtaining a numerical value for $G(e_{aq}^-)$ which is in agreement with the data of Wolff, *et al.*, for this time scale.[3]

For longer-lived species ($\tau > 5 \times 10^{-9}$ sec) analytical solutions are not readily available because of the complicated form of eq 28 and the intermediate cases. Thus the most satisfactory procedure for calculating the $G\epsilon$ product was a computer simulation of eq 23 using double gaussian quadrature.[13] The imput data includes the depth-dose and Cerenkov distributions of Figure 2, the dose rate function given in Figure 1, and values for k corresponding to the addition of electron scavengers at various concentrations. For the intraspur decay of e_{aq}^- in pure water a rate constant of 5×10^8 sec^{-1} was used as suggested by Schwarz.[14] Curves showing the variation of U with k were computed numerically for various values of $G\epsilon$, and curve fitting to the experimental data enabled the best value of the $G\epsilon$ product to be obtained. This method is used later to evaluate $G(e_{aq}^-)$ over the pH range 0 to 7. Families of curves constructed for various values of τ_p and τ_c showed that the calculated $G\epsilon$ is quite sensitive to the differences between τ_p and τ_c when k is comparatively small ($<\sim 3 \times 10^9$ sec^{-1}), but not responsive to small changes in $\tau_p - \tau_c$ at higher values of k.

Later we present data on the relative values of $G\epsilon$ obtained for water and aliphatic alcohols. On the basis that the picosecond and microsecond yields of solvated electrons in alcohols are the same,[4] we have assumed that decay during the pulse may be ignored. Using the numerical integration mentioned above for $\tau > 5 \times 10^{-9}$ sec the functional relationship between S and $G\epsilon$ may be expressed by $S \propto (G\epsilon)^n$, where n varies from 1 to 2 depending on the magnitude of $G\epsilon$. This arises because these calculations take into account the difference between τ_p and τ_c. (When $\tau_p = \tau_c$, then $n = 1$ as in eq 17 for all values of $G\epsilon$.)

Both the time dependence and the spatial distributions contribute to the uncertainty in the measurement of absolute $G\epsilon$ values. The magnitude of the error also depends on the value of k, the theoretical treatment used, as well as uncertainties in the functions shown in Figures 1 and 2. The Cerenkov-depth function $l(x)$ is probably the principal source of error, but even with it very reasonable values of γ were obtained for A and B. We therefore estimate that the error involved in measuring an absolute $G\epsilon$ is probably about ±25%. By invoking eq 29 to calculate and use curve 2 of Figure 2 one is assuming that the same fraction of Cerenkov light generated in the cell would be picked up by the col-

(11) G. A. Kenney and D. C. Walker, *J. Chem. Phys.*, **53**, 1282 (1970).
(12) E. A. Shaede and D. C. Walker, *Int. J. Radiat. Phys. Chem.*, **1**, 307 (1969).
(13) Evaluated using the subroutine DBGAUSS Library Program at the University of British Columbia Computing Centre.
(14) H. A. Schwarz, quoted as private communication in ref 2.

lection lens for all electron energies from the incident energy down to the Cerenkov threshold. In fact, as they slow down (*i.e.*, move deeper in the cell), the solid angle of the "forward lobe" should increase slightly. However since the number of Cerenkov photons falls sharply as the electron energy decreases, the systematic error arising from this change in the overall shape of the Cerenkov lobe during the pulse should be very small. This is corroborated by direct measurements on photographic film of the light distribution from the cell. As the accelerating voltage was changed, no discernible alteration in the distribution occurred.

Problems arising from spatial distributions could be completely circumvented by using a thin ($\sim$0.3 mm) Spectrosil quartz electron window on the irradiation cell, rather than the 1/1000-in. stainless steel sheet. With this cell the electron energy would degrade to below the Cerenkov threshold before the electrons entered the liquid under study. Consequently, all the Cerenkov light would be generated in the nonabsorbing quartz window and all species, regardless of the dose distribution, would contribute to absorption, thus eliminating any need to know the "effective optical absorption path length." A disadvantage is that the quartz would also absorb $\sim$70% of the total incident energy thereby reducing appreciably the number of species formed and hence the "sensitivity" of the method. In addition, the Cerenkov light pulse then would be longer than the dose pulse, thus further diminishing the measured absorbance.

D. Summary. The equations to be used and an indication of their sensitivity may be summarized as follows.

1. For short-lived species ($\tau < 10^{-10}$ sec), measuring only the peak maxima, one has

$$\log(I_0/I)_{\max} = G\epsilon\tau(10R\gamma/N_0) \qquad (9)$$

Typically for the Febetron 706, $R = 1.4 \times 10^{28}$ eV sec^{-1} cm^{-2} and $\gamma = 0.7$ (for water). Assuming that a 15% difference between I_0 and I can be measured sufficiently accurately, one has a limit of sensitivity given by

$$G\epsilon\tau = 3.6 \times 10^{-7}$$

where G is in mol (100 eV)$^{-1}$, ϵ in M^{-1} cm^{-1}, and τ in sec. Consequently, for $\tau < 10^{-10}$ sec, $G\epsilon$ must be greater than 3600.

2. For long-lived species ($\tau > 10^{-8}$ sec) by approximations i and ii eq 17 applies, no knowledge of the pulse shape or τ being required

$$\text{antilog } U = S = G\epsilon(23\gamma D_p/N_0) \qquad (17)$$

Using spectrographic measurements the practical limitation for U is 0.1 on the linear part of the characteristic curve. For the total pulse $D_p = 3.4 \times 10^{19}$ eV cm^{-2} and $\gamma = 0.75$; thus the limit in this case is that $G\epsilon$ must exceed $\sim$1250.

3. For short-lived species ($\tau < 2 \times 10^{-10}$ sec) using the functions indicated in Figures 1 and 2 for the temporal and spatial dependence of both the dose and light one has

$$\text{antilog } U = S = \exp\left[\frac{G\epsilon}{k}\left(\frac{23D_p}{N_0}\right)\left(\frac{1}{\tau_p + \tau_c}\right)\left(\frac{\pi c_3 a_c}{c_2^2 - 4a_c^2} + 1\right)\frac{\pi^2}{3.3}\right] \qquad (30)$$

Using the following values, $\tau_p = 3.8$ nsec, $\tau_c = 3.2$ nsec, $c_2 = 0.2$, $c_3 = 0.055$, $a_c = 0.08$ cm and setting a lower practical limit on $S = 1.25$ (or $U = 0.1$), one requires $G\epsilon$ to exceed $\sim$1100. This limit of course gets larger as k increases.

For longer-lived species the computer simulation procedure yields limits of sensitivity varying between those estimated in 3 and 2 above, depending on the particular value of k involved. A direct comparison between methods A and C may be made simply from the constants in eq 9 and 30 noting that $R = D_p\pi/2\tau_p$ when $g(t)$ is given by the sine function as indicated in Figure 1.

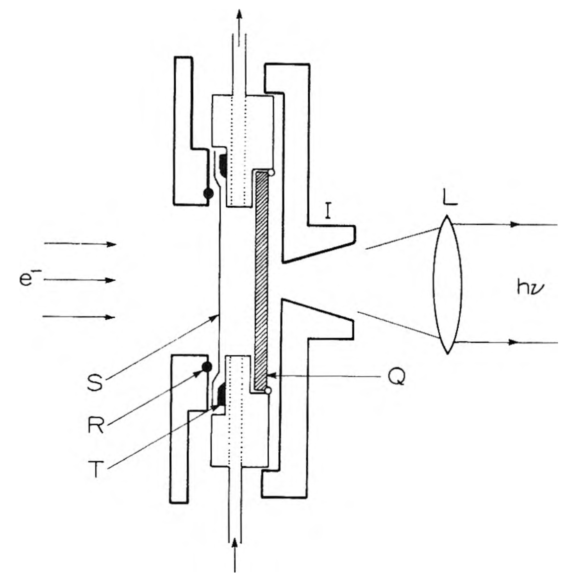

Figure 3. Irradiation cell (not drawn to scale): S, stainless steel electron window to cell; Q, Suprasil quartz window; I, light-constricting iris and electrical noise shield; L, light collecting lens, focus $\sim$0.1 cm behind S; R, isoprene O-ring; T, Teflon O-ring.

Thus for e_{aq}^-, for instance, where $G \sim 3$ the entire visible spectrum ($\epsilon > 10^3$) can be observed in >1 M H_{aq}^+ solution where $\tau < 10^{-10}$ sec by method A or C as shown later. Indeed, several of the very short-lived ($\tau \simeq 10^{-10}$ sec) primary radiation-produced excited states, radicals, ions. and electrons in various liquids may have values of $G\epsilon \gg 10^3$.

Experimental Section

Cerenkov reabsorption spectroscopy can be applied to the subnanosecond temporal domain because of the very high rate of energy deposition provided by the 600-kV Febetron (Model 730/2667, equivalent to 706).[8a] This accelerator produces a short pulse of electrons having peak energies of 600 kV and peak currents of $\sim$5000 A cm^{-2}. Each pulse deposits about 7 J cm^{-2} with dose rates in excess of 10^{15} rads sec^{-1}. The current waveform of the electron pulse was measured directly using a logarithmetrically tapered Faraday cup. A collection aperture (0.5-mm diameter) permitted a very small sample of the electron beam to strike the Faraday cup which was coupled through impedance matched attenuators to the 125-Ω imput resistance of a 1-GHz oscilloscope (Tektronix 519). These data are shown in Figure 1. As discussed already the dose-waveform is expected to be proportional to $I(t)^2$ as illustrated in Figure 1, where the curves are normalized at the peaks.

Values for the total incident radiation intensity per pulse were obtained by adiabatic calorimetry.[8a,15] A small aluminum disk, equal in shape, area, and position to the liquid sample from which emitted light was collected and sufficiently thick to completely absorb the electrons, was placed behind the electron window of the irradiation cell. A thermocouple attached to this calorimeter permitted the tem-

(15) (a) See, *e.g.*, C. Willis, O. A. Miller, A. E. Rothwell, and A. W. Boyd, *Radiat. Res.*, **35**, 428 (1968); (b) G. A. Kenney-Wallace, E. A. Shaede, D. C. Walker, and S. C. Wallace, *Int. J. Radiat. Phys. Chem.*, **4**, 209 (1972).

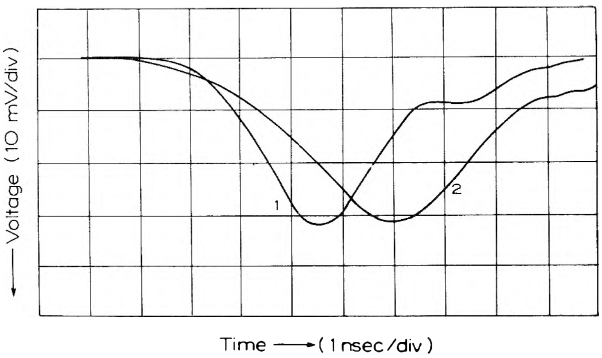

Figure 4. Typical spectrophotometric oscilloscope traces of absorbed and reference Cerenkov, showing absorption by hydrated electrons at 620 nm. Curve 1 represents the time profile of the Cerenkov light pulse transmitted through irradiated water at pH 7 (absorbed Cerenkov profile). Curve 2 was obtained from 3 *M* H_2O_2 in water, the light intensity having been attenuated by a neutral density film of optical density = 1.7 (reference Cerenkov profile). The real intensity before attenuation in 2 was consequently 50 times that in 1, the attenuation having been selected to produce comparable peak heights as seen by the detector. The two curves have been overlapped where the traces start to leave the base line. It is evident that the peak in curve 1 is narrower and precedes that in curve 2. The detection system consisted of a monochromater set at λ 620 nm, a 1P28 photomultiplier with 50-Ω termination and a 250-MHz oscilloscope. This detection system clearly broadened the trace quite substantially, the width at half-height of curve 2 being 3.6 nsec compared with about 2.1 nsec expected from Figure 1. Slight impedance mismatch caused some ringing on the tails of these traces.

perature jump resulting from an electron pulse to be measured on an oscilloscope after suitable amplification by an operational preamplifier. The incident energy per pulse per unit area measured in this way corresponds to the values of D_p required for use in eq 17 and 30, while the incident maximum flux (R in eq 9) was calculated from D_p using the dose waveform of Figure 1.

The spatial anisotropy of Cerenkov emission was shown to take the form of a single broad lobe in the forward direction, rather than the characteristic Cerenkov cone which would be expected only for an unscattered monoenergetic beam of electrons entering a sample much thinner than the electron range. Thus the cell depicted in Figure 3 was used for these studies. Emitted Cerenkov light was collected from a region of the solution defined by the iris using a simple wide-aperture quartz optical system collinear with the electron beam. Transmitted light was directed onto the slits of either a spectrograph or a monochromator–photomultiplier detection system.

The irradiation cell of Figure 3 consisted of a shallow (0.5 cm) annular stainless steel body containing entrance and exit ports with stainless steel to glass seals to enable the irradiated liquid to be replenished by fresh solution supplied from an all-glass, He-pressurized flow system in which the liquid was deoxygenated. An electron window on the front of the cell consisted of a 0.025-mm thick stainless steel sheet tautened between the cell and an aluminum flange which was bolted to the face of the Febetron. The pressure exerted by the O ring of the flange against the thin electron window created an adequate liquid seal to prevent the sample in the cell touching the outer Teflon ring seal. At the rear of the cell a quartz window was sealed to the stainless steel using epoxy resin on the outside only. Liquids under study made contact only with glass and stainless steel. A tightly fitting aluminum cap fastened over the quartz window functioned both as a containment-shield for electrical noise created by the electron beam and also as an iris to restrict the observed light emission to that originating in the small volume defined by the aperture of the first lens.

Absorbed and reference Cerenkov light intensities emerging from the irradiation cell were measured spectrophotometrically or spectrographically. For the former the light was focused into the entrance slit of a 0.25 m grating monochromator (Jarrel-Ash) having a fast photomultiplier (RCA 1P28 or Hamamatsu R213) at the exit slit. The light pulse waveform was displayed on a 250-MHz oscilloscope (Hewlett-Packard 183A) having 50-Ω imput impedance. The risetime of the detector was typically $\sim$2 nsec so that waveforms were broadened slightly by this detector system. A wide selection of neutral density filters were used to insert in the light beam of the reference Cerenkov to reduce its intensity to approximately that of the absorbed Cerenkov. In this way the photomultiplier was made to respond to similar peak light intensities for both the absorbed and reference Cerenkov experiments. Distortions of the signals caused by the photomultiplier–oscilloscope risetime would then be quite similar for the two cases so that the ratio of the areas under the oscilloscope traces would be proportional to I_0/I to a good approximation.

Figure 4 shows typical waveforms for absorbed and reference Cerenkov intensities in pure water and 3 *M* aqueous H_2O_2, respectively, measured at 620 nm using an RCA 1P28 photomultiplier. The reference Cerenkov signal was attenuated by a neutral density film having an optical density of 1.7 so that the reference intensity had been reduced 50-fold relative to the Cerenkov light transmitted through the solution of radiation-produced hydrated electrons in the pure water. Waveforms in Figure 4 are superposed at the point where they were seen to leave the baseline. It is evident that the absorbed Cerenkov pulse was substantially narrower and its peak occurred earlier than in the reference pulse. This is entirely consistent with the treatment given earlier because in pure water e_{aq}^- would be comparatively long-lived, and hence its concentration would build-up throughout the electron pulse causing much more absorption of the latter part of the Cerenkov light pulse.

Spectrographic measurements have two advantages: firstly, a complete spectrum is recorded in a single event and secondly, the photographic emulsion conveniently integrates the Cerenkov light intensity over the duration of the pulse. Two spectrographs were used in this work: for the uv and visible a small Hilger and Watts quartz prism instrument was used in conjunction with Kodak 2475 recording film; and for the visible and near-ir, a grating spectrograph on the design of Bass and Kessler[16] (used in first order with a dispersion of 60 nm/mm) and Kodak high-speed infrared film.

Reciprocity law failure of the photographic film to these very short time scale and intense light pulses, and any variation of this with wavelength, does not present a serious problem for two reasons: firstly, because we are only concerned with the *ratio* of the reference to absorbed Cerenkov and secondly, because we simply measured the number of absorbed Cerenkov light pulses which produced the same film density as did one reference Cerenkov pulse. To achieve this we established characteristic curves (film density against log exposure) by measuring the film density produced by 1, 2, 4, 6, 8, etc., pulses of absorbed Cerenkov light at each wavelength and plotted film density against the

(16) A. M. Bass and K. G. Kessler, *J. Opt. Soc. Amer.*, **49**, 1223 (1959).

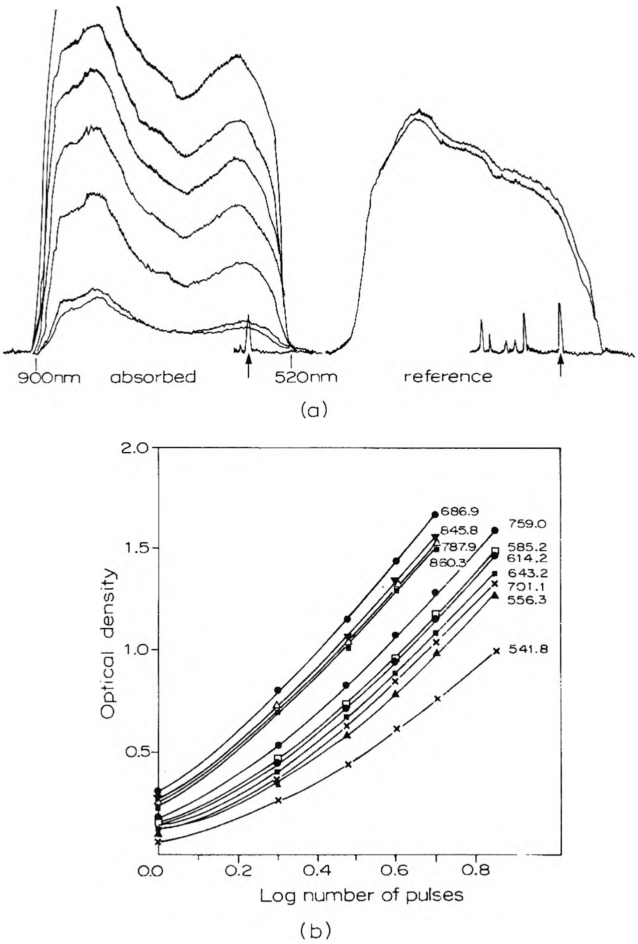

Figure 5. Spectrographic treatment of data. (a) Microdensitometer tracings of the film density after exposure to absorbed and reference Cerenkov light pulses. The absorbed Cerenkov traces correspond to 1 (twice), 2, 3, 4, 5, and 7 successive absorbed Cerenkov light pulses from 1.0 M $HClO_4$ solution. The reference Cerenkov was obtained from 1 (twice) light pulse from 3 M H_2O_2 solution in water. The line spectrum and arrow indicate wavelength markers from a Ne lamp. (b) Characteristic curves of the photographic film at various wavelengths, plotted as optical density of the film against the logarithm of the number of absorbed Cerenkov pulses. The absorbance of a solution may be equated directly with the logarithm of the number of absorbed Cerenkov pulses which produces the same film density as one pulse of reference Cerenkov (see text).

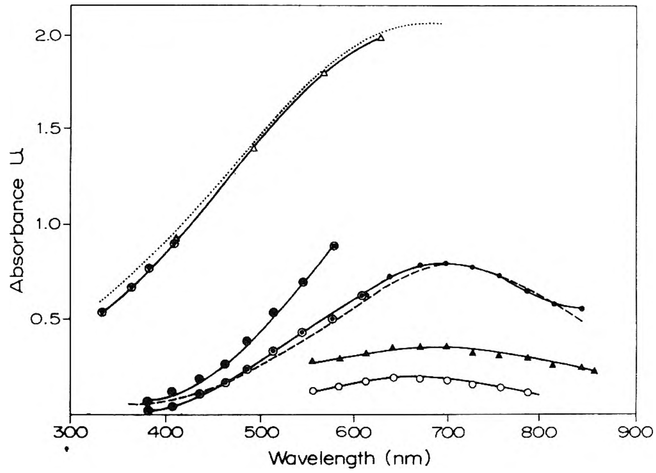

Figure 6. Absorption spectrum (U against λ) of the hydrated electron in concentrated $HClO_4$ solutions and in pure H_2O: O, 3 M $HClO_4$ (Bass Kessler spectrograph); ▲, 2 M $HClO_4$ (Bass Kessler spectrograph); ●, 1 M $HClO_4$ (Bass Kessler spectrograph); ⊙, 1 M $HClO_4$ (Hilger spectrograph); ◉, 0.5 M $HClO_4$ (Hilger spectrograph); ⊙, pure water (Hilger spectrograph); Δ, pure water (spectrophotometric measurements). Dashed line is the published microsecond pulse radiolysis spectrum of e_{aq}^- in pure water. Dotted line gives the values of U calculated from eq 23 based on published $G\epsilon$ data for e_{aq}^-. H_2O_2 solutions (3 M) were used for the reference Cerenkov.

logarithm of the number of pulses. The film density observed for one reference Cerenkov pulse was then deduced from this characteristic curve to be equivalent to the exposure to "n" absorbed Cerenkov pulses. It follows that $U = \log (I_0/I)$ may be obtained directly from these measurements and is numerically equal to log n. An example of raw data in the form of microdensitometer traces for several groups of absorbed Cerenkov pulses and one reference Cerenkov pulse are shown in Figure 5a, with the resulting characteristic curves in Figure 5b. Absorption spectra of e_{aq}^- in concentrated H^+ and H_2O_2 solutions obtained in this way are presented later.

The principal limitation to this spectrographic method is that its dynamic range is limited to $U \lesssim 1.4$. Above this the method seems to overestimate the absorbance when compared with the photometric method; but again, when the reference intensity very greatly exceeds the absorbed Cerenkov, the reference signal may be reduced by a known factor using neutral density attenuators. This multipulse method of establishing characteristic curves also tends to average out small variations in the pulse-to-pulse reproducibility of the accelerator. Having established the characteristic curve it is necessary only to obtain a good average value for the film density per pulse from several individual reference Cerenkov spectra to determine how many absorbed Cerenkov pulses produce this film density.

Reference Cerenkov data were obtained by three methods: (i) chemically destroying the absorbing species in the medium under study—addition of 3 M H_2O_2 essentially completely eliminates e_{aq}^- in water as demonstrated by the data portrayed in Figure 4; (ii) by constructing a reference spectrum from the theoretical Cerenkov relationship (eq 25) based on the light intensity observed at a wavelength where none of the radiation-produced species appear to absorb; and (iii) by comparison of the emission from a liquid of similar refractive index and density which does not however produce absorbing species. (For instance, cyclohexane was used for the reference spectrum of the benzene excimer,[5] small theoretical corrections being applied for the differences in refractive index and density.)

Aqueous solutions were prepared from doubly distilled water, the second stage being from dilute potassium dichromate. All other chemicals were reagent grade or better and used without further purification. Solutions were deaerated in a closed system connected directly to the irradiation cell by vigorous bubbling with high-purity helium.

Results

To demonstrate the method and the theoretical treatment of data, we present results on the formation of solvated electrons in aliphatic alcohols, in water, and in aqueous solutions containing high concentrations of scavengers of e_{aq}^-, using both spectrographic and spectrophotometric methods.

A. Highly Concentrated Aqueous Solutions. The effect of high concentrations of electron scavengers on the absorption spectrum, radiation yield and lifetime of e_{aq}^- were studied in $HClO_4$ and H_2O_2 solutions for concentrations up

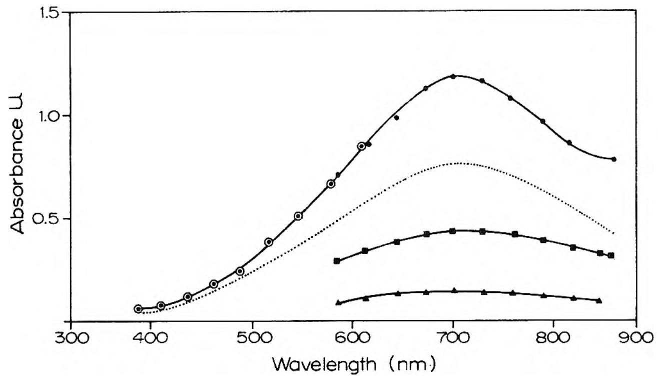

Figure 7. Absorption spectrum (U against λ) of the hydrated electron in concentrated H_2O_2 solutions: ▲, 2.0 M H_2O_2 (Bass Kessler spectrograph); ■, 1.0 M H_2O_2 (Bass Kessler spectrograph); ●, 0.5 M H_2O_2 (Bass Kessler spectrograph); ⊙, 0.5 M H_2O_2 (Hilger spectrograph). Dotted line is the published microsecond pulse radiolysis spectrum of e_{aq}^- in pure water. H_2O_2 solutions (3 M) were used for reference Cerenkov.

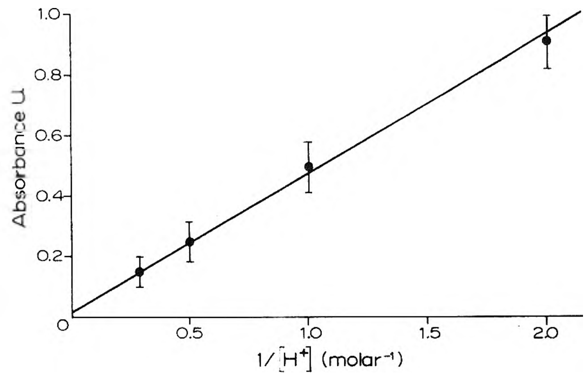

Figure 8. Plot of U at 580 nm against $1/[H^+]$ for concentrated acid solutions.

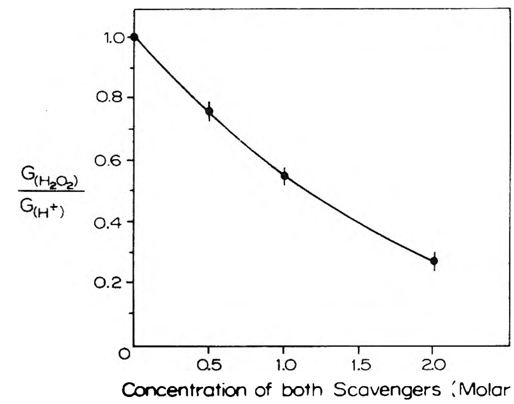

Figure 9. Plot of the relative initial yield of hydrated electrons in H_2O_2 compared to H^+ solutions as a function of concentration. Data points represent the values of $U_{H_2O_2}.k_2/U_{H^+}.k_1$ obtained from separate experiments in which the same concentrations of H_2O_2 and H^+ were studied, namely, 0.5, 1.0, and 2.0 M. The ratio k_2/k_1 was taken to be 1.1 in accordance with the subnanosecond value of k_1. (If this ratio should be the microsecond value, 0.5, then it merely alters the scale of the ordinate.)

to 3 M (in 3 M $HClO_4$ the lifetime of e_{aq}^- is ~30 psec). An entire absorption spectrum was recorded spectrographically at each concentration using the data for 3 M H_2O_2 as the reference Cerenkov. These spectra are plotted as absorbance U against wavelength in Figures 6 and 7. Data for pure water at pH 7 are also given in Figure 6, these data being obtained using spectrophotometric detection (limited to 630 nm) because of the large values of U involved.

The dashed lines in Figures 6 and 7 represent the published absorption spectrum of e_{aq}^- obtained by microsecond pulse radiolysis methods.[17] They can be seen to match very well the spectra obtained by Cerenkov reabsorption spectroscopy thereby demonstrating that U is proportional to ϵ at these high scavenger concentrations (in accordance with eq 31).

The dotted line in Figure 6 shows values of U calculated by the computer simulation method described earlier using the published data of $G\epsilon$ for e_{aq}^- at pH 7.[17] This curve was normalized at 630 nm to the spectrophotometrically observed data of U. The agreement demonstrates the validity of the theoretical treatment of data, this time for comparatively long-lived species.

Further justification for the use of

$$U = \frac{G\epsilon}{k}(\rho D_p) \tag{31}$$

for $k \geq 5 \times 10^9$ sec^{-1} is indicated by Figure 8, which shows a plot of U against $1/[H^+]$ at 580 nm. The linearity of this plot is consistent with (i) $U \propto 1/k$ as in eq 31 and (ii) the primary yield of e_{aq}^- (G) being independent of $[H^+]$ over the range of 0.5 to 3 M, as found by Wolff, *et al.*[3]

Adiabatic calorimetry showed that for the central part of the electron beam, for which these data were obtained, the incident radiation energy density per pulse (D_p) was 3.4 × 10^{19} eV cm^{-2}. Combining this with τ_c = 3.2 nsec, τ_p = 3.8 nsec, c_2 = 0.2 cm, a_c = 0.08 cm, and c_3 = 0.055 cm, from Figures 1 and 2, enables one to evaluate the constants in eq 30. This information may be used in conjunction with the known values of ϵ and k to evaluate $G(e_{aq}^-)$ from the slope of the plot in Figure 8. Using values of ϵ of 1.1 × 10^4 M^{-1} cm^{-1} at 580 nm and k = 1.1 × 10^{10} M^{-1} sec^{-1} [3] gives a value of 3.2 for the primary yield of e_{aq}^- in these strongly acid solutions. The principal absolute error in this value arises from the semiempirical spatial distributions of dose and Cerenkov light and comparatively little from the values of τ_c and τ_d estimated. At present we feel these will collectively contribute an absolute error as large as ±25%.

The internal consistency of the analysis and agreement with the stroboscopic work[2,4] is further corroborated by the relative primary radiation yields of e_{aq}^- in H_2O_2 as compared to H_{aq}^+ solutions (*i.e.*, $G_{(H_2O_2)}/G_{(H^+)}$). It follows from eq 31 that

$$G_{(H_2O_2)}/G_{(H^+)} = U_{(H_2O_2)}k_2[H_2O_2]/U_{(H^+)}k_1[H^+]$$

where k_1 and k_2 are the rate constants for the reaction of e_{aq}^- with H_{aq}^+ and H_2O_2, respectively, and are taken to be 1.1 × 10^{10} and 1.2 × 10^{10} M^{-1} sec^{-1}. Figure 9 shows the plot of $[U_{(H_2O_2)}k_2/U_{(H^+)}k_1]$ against concentration for the same 0.5, 1.0, and 2.0 M concentrations of H_2O_2 and H^+. The ordinate thus represents the relative primary yield which is seen to decrease very markedly with increasing solute concentrations. These observations are similar to those of Aldrich, *et al.*,[4] and which have been interpreted by them as indicating presolvation scavenging by H_2O_2 but not by H^+.

B. Dilute Aqueous Solutions. For the cases of pure water or aqueous solutions containing <1 M concentrations of scavengers, where k < 5 × 10^9 sec^{-1}, eq 30 does not apply. For these a computer simulation as outlined earlier, based on eq 23, was used to derive numerical values of U over a range of lifetimes, using $G\epsilon$ as the variable parameter.

(17) E. M. Fielden and E. J. Hart, *Trans. Faraday Soc.*, **63**, 2975 (1967).

TABLE I: Data, Correction Factors, and Relative Yields for Solvated Electrons in Aliphatic Alcohols and Water [a]

Compounds	S	λ^b	$\lambda_{max}{}^c$	Correction factor	$G\epsilon_{max}$	G^d	$G\epsilon_{max}$ published psec^e	$G\epsilon_{max}$ published μsec^f	Dielectric constant (static)
Water	87.1	630	720	1.27	1.0	1.0	1.0	1.0	80
Methanol	26.9	630	630	1.0	0.39	0.43	0.37	0.36	34
1-Propanol	28.8	630	740	1.18	0.42	0.59	0.29	0.25	21
2-Propanol	23.6	630	850	1.40	0.44	0.58	0.25	0.27	19
1-Butanol	27.1	630	660	1.05	0.36				17
1,2-Ethanediol	30.9^g	580	580	0.60^g	0.39	0.51	0.36	0.32	39
1,2,3-Propanetriol	30.6^g	550	550	0.47^g	0.42				43

^{a} The yields are compared with published values (all yields are relative to 1.0 for water). ^{b} Wavelength of measurement. ^{c} Wavelength of absorption band maximum. ^{d} This work. Calculated relative to water from known extinction coefficients. ^{e} Published data from ref 2 (picosecond). ^{f} Published data from ref 18 (microsecond). ^{g} These data were determined relative to water at the wavelengths 580 and 550 nm. The correction factors were consequently less than unity.

Figure 10 shows the data obtained for various values of k in the pH range 0 to 7 taking $k_1 = 1.1 \times 10^{10}\ M^{-1}\ \text{sec}^{-1}$. The experimental values of U at λ 580 nm (obtained spectrographically) are indicated by the data points. Computed curves for three values of $G\epsilon$ are shown. The best fit is obtained for $G\epsilon = 3.5 \times 10^4$, from which one calculates $G(e_{aq}^-) = 3.2$ over this pH range, since $\epsilon(e_{aq}^-) = 1.1 \times 10^4$ $M^{-1}\ \text{cm}^{-1}$ at 580 nm. The uncertainty to be attached to this value is again $\sim$25% because the same functions for the spatial and temporal dependences were employed.

C. Pure Aliphatic Alcohols. Solvated electron yields were also measured in a number of pure alcohols, relative to the primary yield of hydrated electrons in neutral water. Because of the large absorbances obtained in the absence of scavengers more accurate comparisons could be made spectrophotometrically. These were all done either at the known λ_{max} for the solvated electron or at 630 nm followed by a correction to the value of ϵ at λ_{max} using published spectra obtained by microsecond pulse radiolysis.[18] As noted earlier, Cerenkov reabsorption spectroscopy gives spectra[5] which conform very closely to the published microsecond data. Reference Cerenkov data were obtained using 2 M $CHCl_3$ in the alcohols and 3 M H_2O_2 in water. For the pure systems it is assumed that the rate of disappearance of solvated electrons does not exceed $5 \times 10^8\ \text{sec}^{-1}$,[3] so that the functional relationship between S and $G\epsilon$ is nearly independent of k. Numerical integration of eq 23 shows that for $10^4 < G\epsilon < 5 \times 10^4$ with $\tau_c = 3.2$ nsec and $\tau_d = 3.8$ nsec and for $k < 5 \times 10^8\ \text{sec}^{-1}$ relationship

$$S \propto (G\epsilon)^{1.7} \tag{33}$$

applies. Table 1 shows the data obtained for the experimental values of S and the derived values of $G\epsilon_{max}$ and G relative to that obtained for water. These results are also compared with published data from picosecond and microsecond studies.

Discussion

The method of Cerenkov reabsorption spectroscopy has been shown to be quite straightforward experimentally and to be extremely sensitive, capable of observing strongly absorbing species whose mean lifetime is in the range 10^{-11} to 10^{-10} sec. Spectra which are in good agreement with published data may readily be obtained through simple treatment of the observables S and U by eq 9 and 17. Their quantitative relationship to the $G\epsilon$ or $G\epsilon\tau$ products, however, is more complex and, except for peak height measurements, has to be based on semiempirical temporal and spatial functions for both dose deposition and Cerenkov emission.

Results are presented on solvated electrons which agree with several of the important findings of Hunt, *et al.*,[1-4] on the picosecond time scale of events in the radiolysis of water and aliphatic alcohols. The agreement demonstrates the validity of the quantitative treatment of data used here. The overall self-consistency corroborates the conclusions drawn regarding the picosecond observations.

A. Spectrum of e_{aq}^- at Short Times. Figures 6 and 7 demonstrate that the spectrum of the hydrated electron is not significantly changed by the addition of high concentrations of H^+ or H_2O_2, which reduce the electron's lifetime to $<10^{-10}$ sec at >1 M. There is no indication then that those reactions which occur prior to normal diffusion involve solvated electron species which contribute predominantly to one region of the spectrum; *i.e.*, if the broad spectrum of e_{aq}^- arises from absorption by species in different energy environments there is no evidence that those in the weaker traps are preferentially involved in the first 10^{-10} sec of decay.

B. Presolvation Scavenging. The presence of high concentrations of H_{aq}^+ does not change the yield of e_{aq}^- initially formed, as shown by Figures 8 and 10. In contrast added H_2O_2 in the same concentration range markedly diminishes the yield of e_{aq}^- (see Figure 9). Similar observations to these and with other scavengers have been attributed to presolvation scavenging.[2,4] At 1 M concentration the mean separation of scavenger molecules is only $\sim$1 nm, or two or three molecular diameters, so that presolvation scavenging of electrons by solutes which possess an electron affinity is not surprising. What is more surprising at first sight is that H_{aq}^+ does not do this. Hamill has suggested that the presolvated electron (the "dry" electron) is simply unreactive towards H_{aq}^+.[19] Perhaps this implies that the reaction between H_{aq}^+ and an electron should be properly described as a proton transfer reaction (rather than an electron transfer, or addition, as with most other reactive solutes) which is only favored when the electron has been immobilized momentarily in a solvation trap.

The fact that the spectrum is unaltered by the occurrence of presolvation scavenging by H_2O_2 at $\sim$1 M concentration (Figure 7) further implies that the whole spectrum builds in at the same rate, so that electrons which quickly find a deep trap are not less susceptible to presolvation scavenging than those that must eventually settle for a shallower trap,

(18) M. C. Sauer, S. Arai, and L. M. Dorfman, *J. Chem. Phys.*, **42**, 708 (1965).
(19) W. H. Hamill, *J. Phys. Chem.*, **73**, 1341 (1969).

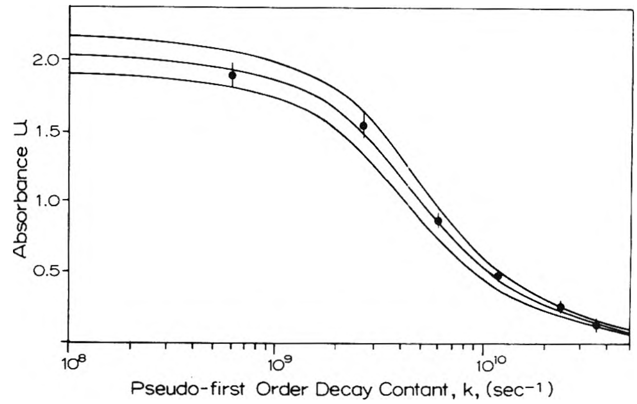

Figure 10. Plot of U against k. Data points represent the measured absorbance in water at various concentrations of $HClO_4$ (k_1 taken to be 1.1×10^{10} M^{-1} sec^{-1}). Lines are calculated by computer simulation (see text) for three values of $G\epsilon$; upper, middle, and lower lines referring to $G\epsilon$ values of 4.0×10^4, 3.5×10^4, and 3.0×10^4 M^{-1} cm^{-1} $(100\ eV)^{-1}$, respectively.

if these different types of traps exist. In low-temperature liquid alcohols there are strong indications that the spectrum shifts to lower wavelengths as the electrons either slowly find deeper traps or progressively dig them deeper.[20] If analogous successive steps occur in liquid water at 25°, then they must occur in $<\sim 10^{-10}$ sec.

C. Initial $G(e_{aq}^-)$. At pH <0 and for the whole pH range 0 to 7 we find that the absorbance data can be described by one value of $G(e_{aq}^-) = 3.2 \pm 0.8$. (This value is based on the high concentration value for k_1 which is taken to be 1.1×10^{10} M^{-1} sec^{-1}.[2]) It is in very close agreement with values obtained by Hunt, *et al.*;[21] but it is contrary to several scavenging studies[22] and to the yield observed after 7 nsec by pulse radiolysis of alkaline alcoholic aqueous solutions[23] where values of $G(e_{aq}^-)$ up to 5 are reported. These different results may arise because of the effect of the scavengers on the hydrated electron precursors, on the geminate recombination processes, or simply on the survival probability of e_{aq}^- within the spur.

It is worth noting, however, that the fine structure pulse of a linear accelerator gives a dose rate of $\sim 10^{13}$ rads sec^{-1} and the Febetron 10^{13} to 10^{15} rads sec^{-1}, whereas a Van de Graaff's dose rate is a few orders of magnitude smaller. Conceivably there are extra very rapid annihilation processes occurring under these highest dose-rate conditions.

D. No Time-Dependent Rate Constants. In Figure 8 it is shown that U is proportional to k^{-1} for the addition of H^+ in the concentration range 0.5 to 3 M. This is entirely in accord with eq 30 and corroborates the validity of the analysis used. But it can only arise if the effective rate constant for the reaction of e_{aq}^- with H_{aq}^+ did not vary with time. Furthermore, Bronskill, *et al.*,[2] have directly observed the decay of e_{aq}^- in the presence of acid at these concentrations and obtained linear first-order plots. There is no evidence then of time-dependent rate constants for the time scale 10^{-11} to 10^{-10} sec even though the scavenger molecules are separated by only two to five molecular diameters. At these concentrations the mean initial separation of e_{aq}^- from a solute molecule is comparable to the reaction radius.

Perhaps the detailed mechanism of hydrated electron diffusion is involved here. If this diffusion arises from quantum mechanical tunneling, or extensive but infrequent leaps to new sites,[24] then an exponential decay of e_{aq}^- would be expected, even at these scavenger concentrations.

E. Electron Yields in Alcohols. Table I shows that the yields of solvated electrons in six aliphatic alcohols (including mono-, di-, and trihydroxy compounds) are approximately 50% that found in water, and the yield does not progress in accordance with their respective static dielectric constants. Since no time dependence was included in the treatment of these data, it is impossible to decide if these represent the relative *initial yields* as compared to water, or if intraspur decay during the pulse is much more important for the alcohols. However Hunt, *et al.*,[4] have reported similar values, though ~25% lower, for the primary yields in some of these alcohols and also noted that their formation was complete within ~10 psec. Again, as in water, there appears to be a serious discrepancy between the yields of solvated electrons obtained by direct observation by subnanosecond pulse radiolysis and yields deduced from scavenger studies at high solute concentration (where $G(e_s^-)$ approaches 4 or 5[25]).

Acknowledgments. We are most grateful to Dr. B. Shizgal for assistance with some of the mathematical manipulations and to the National Research Council of Canada for financial support and for postgraduate scholarships to S. C. W.

Appendix A

Integration of Equation 23 *over Time.* Separating eq 23 into its I_0 and I components and placing the x dependency terms with the other constants, we have

$$I = \int_0^{a_c} \Lambda' \int_0^{\tau_c} m(t) \exp\left[-\frac{\eta G\epsilon}{g} \epsilon^{-kt'} \int_0^{t'} e^{kt''} g(t'')dt''\right] dt dx \qquad (A1)$$

and

$$I_0 = \int_0^{a_c} \Lambda' \int_0^{\tau_c} m(t) dt dx \qquad (A2)$$

where

$$\Lambda' = \Lambda\lambda l(x)$$

$$\eta = (23.03 D_p/N_0) \int_x^{a_d} D^*(x')dx'$$

$$g = \int_0^{\tau_p} g(t)dt$$

and

$$t' = t + (\tau_p - \tau_c)/2 = t + q$$

When one expands the integral in the exponential in (A1) using integration by parts, the argument of the exponential has the following form

$$\arg = \frac{-\eta G\epsilon}{g}\left\{\frac{1}{k}\left[g(t+q) - \frac{g'}{k}(t+q) + \frac{g''(t+q)}{k_2} \cdots \frac{(-1)^n g^n(t+q)}{k^n}\right] \times \frac{-e^{-k(t+g)}}{k}\left[\frac{-g'(0)}{k^2} + \frac{g''(0)}{k^2} \cdots \frac{(-1)^n g^n(0)}{k^n}\right]\right\} \qquad (A3)$$

(20) J. H. Baxendale and P. Wardman, *Nature (London)*, **230**, 449 (1971).
(21) M. J. Bronskill, R. K. Wolff, J. E. Aldrich, and J. W. Hunt, unpublished data quoted in ref 4.
(22) See, *e.g.*, (a) D. A. Head and D. C. Walker, *Can. J. Chem.*, **45**, 2051 (1967); (b) J. C. Russell and G. R. Freeman, *J. Chem. Phys.*, **48**, 90 (1968).
(23) G. V. Buxton, *Proc. Roy. Soc., Ser. A*, **328**, 9 (1972).
(24) D. C. Walker, *Quart. Rev. (Chem. Soc.)*, **21**, 79 (1967).
(25) See, *e.g.*, G. R. Freeman in "Actions Chimiques et Biologiques Radiations," Vol. 14, M. Haissinski, Ed., Masson et Cie, Paris, 1970, p 73.

When $k \geq 5 \times 10^9$ sec^{-1} both series in (A3) rapidly converge, but the terms in t predominate because of the factor $e^{-k(t+q)}/k$ ahead of the series in $g^n(0)$. Thus the argument of the exponential is to a good approximation

$$\arg = \frac{-\eta G\epsilon}{gk}\left[g(t+q) - \frac{q'}{k}(t+q)\right] \quad \text{(A4)}$$

and the temporal portion of (A1) becomes

$$I' = \int_0^{\tau_c} I'(t)\mathrm{d}t =$$

$$\int_0^{\tau_c} m(t)\exp\left\{-\frac{\eta G\epsilon}{gk}\left[g(t+q) - \frac{q'}{k}(t+q)\right]\right\}\mathrm{d}t \quad \text{(A5)}$$

As indicated in the text $m(t)$ and $g(t)$ are given by

$$m(t) = \sin \pi t/\tau_c \quad \text{(A6)}$$

$$g(t) = \sin \pi t/\tau_p \quad \text{(A7)}$$

which may now be substituted in (A5).

This integral can be evaluated by expanding the exponential in a Taylor series about the origin in powers of $\eta G\epsilon/gk$. This parameter is never very large for $k \geq 5 \times 10^9$ sec^{-1} and $G\epsilon \leq 6 \times 10^4$, so that the series converges fairly rapidly (it converges for all finite values of $\eta G\epsilon/gk$).

The significant terms of this series remaining after integration over t are

$$I' = \frac{2\tau_c}{\pi}\left[1 - \sin\frac{\pi}{2}\left(1 - \frac{\tau_c}{\tau_p}\right)\left(\frac{\tau_d^2}{\tau_p^2 - \tau_c^2}\right)\left(\frac{\eta G\epsilon}{gk}\right) + \frac{1}{2!}\left(\frac{2\tau_d\tau_c}{4\tau_c^2 - \tau_p^2}\right)\left(\frac{\eta G\epsilon}{gk}\right)^2 - \frac{1}{3!}\sin\frac{\pi}{2}\left(1 - \frac{\tau_c}{\tau_p}\right) \times \left(\frac{6\tau_p^2}{\tau_p^2 - \tau_c^2}\right)\left(\frac{\tau_c^2}{9\tau_c^2 - \tau_p^2}\right)\left(\frac{\eta G\epsilon}{gk}\right)^3 \ldots\right. \quad \text{(A8)}$$

and substituting into (A1) gives

$$I = \int_0^{a_c} \frac{2\tau_c}{\pi}\Lambda\lambda l(x)\left[1 - a'\left(\frac{\eta G\epsilon}{gk}\right) + \frac{b!}{2!}\left(\frac{\eta G\epsilon}{gk}\right)^2 - \frac{c!}{3!}\left(\frac{\eta G\epsilon}{gk}\right)^3 \ldots\right]\mathrm{d}x \quad \text{(A9)}$$

where a', b', and c' are the coefficients of the $(\eta G\epsilon/gk)$ terms in eq A8.

Integration of (A2) gives

$$I_c = \int_0^{a_c} \frac{2\tau_c}{\pi}\Lambda\lambda l(x)\mathrm{d}x \quad \text{(A10)}$$

Combination of (A9) and (A10) yields eq 27 presented in the text for the condition $k \geq 5 \times 10^9$ sec^{-1}.

When $k < 5 \times 10^9$ sec^{-1}, the terms in $g(0)$ in (A3) cannot be entirely ignored. Analytic solutions are not easily obtained so that numerical integration is much more satisfactory.

One situation, however, is worth pursuing further, namely when $k \leq 10^8$ sec^{-1}, because in this case the decay of the absorbing species can be ignored and the $e^{-kt'}$ and $e^{kt''}$ become unity. (A1) now simplifies to

$$I = \int_0^{a_c}\Lambda'\int_0^{\tau_c} m(t)\exp\left[-\frac{\eta G\epsilon}{g}\int_0^{\tau+q} g(t'')\mathrm{d}t''\right]\mathrm{d}t\mathrm{d}x \quad \text{(A11)}$$

Carrying out the integration in the argument of the exponential using (A6) and (A7), eq A11 has the following time dependence

$$I'' = \int_0^{\tau_c} I''(t)\mathrm{d}t = \int_0^{\tau_c}\sin\frac{\pi t}{\tau_c}\exp\left[\frac{-\eta G\epsilon}{g}\left(1 - \cos\frac{\pi}{\tau_p}(t+q)\right)\right]\mathrm{d}t \quad \text{(A12)}$$

To perform this integration one observes that $I''(t)$ decreases very rapidly with time because of the large values of $\eta G\epsilon$ (normally >20) which are obtained in many of these studies. The geometric functions may be expanded in power series with the integration performed over a small range of t ($0 < t < \tau^*$) so that (A12) becomes

$$I'' = \exp\left[-\eta'(1-r)\frac{\pi}{\tau_c}\right] \times \int_0^{\tau^*} t\exp\left(-\eta' r\frac{\pi^2}{\tau_p^2}t^2\right)\exp\left(-\eta' s\frac{\pi}{\tau_p}t\right)\mathrm{d}t \quad \text{(A13)}$$

where $\eta' = \eta G\epsilon/g$, $r = \cos(\pi/2)(1 - \tau_c/\tau_p)$, and $s = \sin(\pi/2)(1 - \tau_c/\tau_p)$.

Integration of this yields

$$I'' = \frac{\tau_p^2}{\tau_c^2\pi c}\left[\frac{1}{\eta'} - \frac{s}{2}\sqrt{\frac{\pi}{\eta' r}}\exp\left(\frac{s^2\eta'}{4r}\right) \times \left(1 - \mathrm{erf}\left(\sqrt{\frac{\eta'}{c}\frac{s}{2}}\right)\exp\left[-\eta'(1-c)\right]\right)\right] \quad \text{(A14)}$$

as the terms of τ^* disappear. [It should be noted that when τ_c approaches τ_p, $r \to 1$ and $s \to 0$, so that the expression simplifies to $I'' = \tau_p/2\pi\eta'$ and S is independent of pulse shape as in approximation B in the text.]

Substitution of (A14) into (A1) and integration of (A2) finally gives eq 28 in the text for the condition $k < 10^8$ sec^{-1}.

Appendix B

Integration over Distance. One requires the integration of (A9)

$$I = \int_0^{a_c}\frac{2\tau_c}{\pi}\Lambda\lambda l(x)\left\{1 - a'\left(\frac{\eta G\epsilon}{gk}\right) + \frac{b'}{2!}\left(\frac{\eta G\epsilon}{gk}\right)^2 - \frac{c'}{3!}\left(\frac{\eta G\epsilon}{gk}\right)^3 + \cdots\right\}\mathrm{d}x \quad \text{(B1)}$$

where

$$\eta = \frac{23.03}{N_0}D_p\int_x^{a_d} D^*(x')\mathrm{d}x' \quad \text{(B2)}$$

and the dose and light intensity functions from the text are

$$D^*(x) = c_1\sin\frac{\pi}{c_2}(x + c_3) \quad \text{(B3)}$$

$$l(x) = \cos \pi x/2a_c \quad \text{(B4)}$$

The constant c_1 in (B3) must be such that

$$\int_0^{a_d} c_1\sin\frac{\pi}{c_2}(x + c_3)\mathrm{d}x = 1 \quad \text{(B5)}$$

therefore

$$c_1 = \frac{\pi}{c_2}\left(\frac{1}{1 + \cos\pi c_3/c_2}\right) \quad \text{(B6)}$$

Substituting (B6) into (B3) gives

$$\int_x^{a_d} D^*(x')\mathrm{d}x' = [\cos(\pi/c_2)(x + c_3) + 1]/(\cos\pi c_3/c_2 + 1) \quad \text{(B7)}$$

Letting

$$\eta = \eta^*[\cos(\pi/c_2)(x + c_3) + 1]$$

(B1) becomes

$$I = \frac{2\tau_c}{\pi}\Lambda\lambda\left\{\int_0^{a_c}\cos\frac{\pi x}{2a}\,dx - a'\left(\frac{\eta^* G\epsilon}{gk}\right)\int_0^{a_c}\left(\cos\frac{\pi x}{2a_c}\right)\times\right.$$
$$\left[\cos\frac{\pi}{c_2}(x + c_3) + 1\right]dx +$$
$$\frac{b'}{2!}\left(\frac{\eta^* G\epsilon}{gk}\right)^2\int_0^{a_c}\left(\cos\frac{\pi x}{2a_c}\right)\left[\cos\frac{\pi}{c_2}(x + c_3) + 1\right]^2 dx - \frac{c'}{3!}\times$$
$$\left(\frac{\eta^* G\epsilon}{gk}\right)^3\int_0^{a_c}\left(\cos\frac{\pi x}{2a_c}\right)\left[\cos\frac{\pi}{c_2}(x + c_3) + 1\right]^3 dx + \cdots \quad \text{(B8)}$$

Carrying out the integration of these first three integrals in (B8), one obtains

$$\int_0^{a_c}\cos\frac{\pi x}{2a_c}dx = \frac{2a_c}{\pi} \quad \text{(B9)}$$

$$\int_0^{a_c}\left(\cos\frac{\pi x}{2a_c}\right)\left[\cos\frac{\pi}{c_2}(x + c_3) + 1\right]dx =$$
$$\frac{2a_c}{\pi}\left\{\left(\frac{c_2^2}{c_2^2 - 4a_c^2}\right)\left[\cos\frac{\pi}{c_2}(a_c + c_3) + \frac{2a_c}{c_2}\sin\frac{\pi c_3}{c_2}\right] + 1\right\} \quad \text{(B10)}$$

$$\int_0^{a_c}\cos\frac{\pi x}{2a_c}\left[\cos\frac{\pi}{c_2}(x + c_3) + 1\right]^2 dx =$$
$$\frac{2a_c}{\pi}\left\{\left(\frac{c_2^2}{c_2^2 - 4a_c^2}\right)\left[\cos^2\frac{\pi}{c_2}(a_c + c_3) + 2\cos\frac{\pi}{c_2}(a_c + c_3) +\right.\right.$$
$$\left.\left.4\frac{a_c}{c_2}\sin\frac{\pi c_3}{c_2}\left(1 + \cos\frac{\pi c_3}{c_2}\right)\right] + 2\right\} \quad \text{(B11)}$$

The terms in $\cos(\pi/c_2)(a_c + c_3)$ may be ignored relative to the terms in $\sin \pi c_3/c_2$.

Equations B9, B10, and B11 may now be substituted into (B8) and then combined with eq A8 to give (B12)

$$I = \frac{2\tau_c}{\pi}\frac{2a_c}{\pi}\Lambda\lambda\left\{1 - \left(\frac{\eta G\epsilon\pi}{2k}\right)\left(\frac{\tau_p}{\tau_p^2 - \tau_c^2}\right)\sin\frac{\pi}{2}\left(1 - \frac{\tau_c}{\tau_p}\right)\times\right.$$
$$\left(\frac{1}{1 + \cos\pi c_3/c_2}\right)\left[\left(\frac{c_2}{c_2^2 - 4a_c^2}\right)2a_c\sin\pi c_3/c_2 + 1\right] +$$
$$\frac{1}{2}\left(\frac{\eta G\epsilon\pi}{2k}\right)^2\left(\frac{\tau_c}{\tau_p(4\tau_c^2 - \tau_p^2)}\right)\left(\frac{1}{1 + \cos\pi c_3/c_2}\right)^2\times$$
$$\left.\left[\left(\frac{c_2}{c_2^2 - 4a_c^2}\right)4a_c\sin\pi c_3/c_2(1 + \cos\pi c_3/c_2) + 2\right] + \cdots\right\} \quad \text{(B12)}$$

Several simplifications can be made in (B12) because of the functions shown in Figures 1 and 2. For instance

$$\sin\frac{\pi}{2}\left(1 - \frac{\tau_c}{\tau_p}\right) \approx \frac{\pi}{2}\left(1 - \frac{\tau_c}{\tau_p}\right), \sin\frac{\pi c_3}{c_2} \approx \frac{\pi c_3}{c_2}$$

and $\cos \pi c_3/c_2 = 0.65$. Thus (B12) simplifies to

$$I = \frac{4\tau_c a_c}{\pi^2}\Lambda\lambda\left\{1 - \frac{\eta G\epsilon}{k}\left[\frac{\pi^2}{3.3}\left(\frac{1}{\tau_c + \tau_p}\right)\left[\frac{\pi c_3 a_c}{c_2^2 - 4a_c^2} + 1\right]\right] +\right.$$
$$\left.\frac{1}{2}\left(\frac{\eta G\epsilon}{k}\right)^2\left[\frac{\pi^2}{4}\left(\frac{\tau_c}{\tau_p(4\tau_c^2 - \tau_p^2)}\right)\right]\left[\frac{2a_c c_3\pi}{c_2^2 - 4a_c^2} + 2\right] + \cdots\right\} \quad \text{(B13)}$$

It turns out that on substitution of numerical values for the coefficients of $(\eta G\epsilon/k)^n$ this series is to a good approximation the McLaurin expansion of an exponential in $\eta G\epsilon/k$. Thus it is finally obtained that

$$I =$$
$$\frac{4\tau_c a_c}{\pi^2}\Lambda\lambda\exp\left[-\left(\frac{\eta G\epsilon}{k}\right)\left(\frac{\pi^2}{3.3}\right)\left(\frac{1}{\tau_p + \tau_c}\right)\left(\frac{\pi c_3 a_c}{c_2^2 - 4a_c^2} + 1\right)\right] \quad \text{(B14)}$$

I_0 is obtained from the substitution of (B4) into (10A) followed by integration which yields

$$I_0 = 4\tau_c a_c \Lambda\lambda/\pi^2 \quad \text{(B15)}$$

Combination of (B14) and (B15) yields eq 30 presented in the text for $k \geq 5 \times 10^9\ \text{sec}^{-1}$.

Ranges of Photoinjected Electrons in Dielectric Liquids[1]

R. A. Holroyd,* B. K. Dietrich, and H. A. Schwarz

Chemistry Department, Brookhaven National Laboratory, Upton, New York 11973 *(Received April 21, 1972)*

Publication costs assisted by Brookhaven National Laboratory

Measurements of the current efficiency of liquid-filled phototubes are used to determine the ranges of low-energy (0.1–0.5 eV) electrons in liquids. The efficiency depends on the applied field as well as on the nature of the liquid but is not affected by low concentrations of electron trapping solutes. Certain liquids such as neopentane and tetramethylsilane yield currents comparable to the vacuum current at an electric field of 10^4 V/cm, whereas n-hexane and n-pentane yield currents a few orders of magnitude less. The differences in current for various liquids are attributed to the differences in thermalization ranges of the photoinjected electrons. The model used to analyze the results assumes that the injected charges diffuse subject to the concentration and potential gradients, where the potential is the sum of the applied and image potentials. This model successfully accounts for the observed voltage dependence of the currents and shows that low-energy electrons penetrate considerable distances into the liquids and thermalize without significant back scattering. The observed values of b for a Gaussian distribution of ranges are: for n-pentane, 36 Å; cyclopentane, 77 Å; neopentane, 147 Å; n-hexane, 42 Å; 2-methylpentane, 58 Å; 3-methylpentane, 50 Å; 2,2,4-trimethylpentane, 102 Å; and tetramethylsilane, 177 Å. These values are comparable to the ranges of the more energetic electrons formed in X-irradiated liquids and demonstrate that most of the range of such electrons is attained at epithermal energies.

Introduction

Measurements of the ranges of electrons in various liquids are important to a basic understanding of radiation chemistry. When a molecule is ionized the energetic electron produced will travel some distance from the positive charge. The magnitudes of the free ion yield and the time required for geminate ion recombination depend critically on this distance. Reliable range data exist only for electrons with considerable energy ($>10^3$ eV), and extrapolation of such data down to low energies leads to erroneous values. It has been suggested that electrons with subvibrational energies lose energy inefficiently and consequently that a large fraction of the range of an energetic electron must be obtained at low energies.[2,3] Measurements of free ion yields[4,5] have been used to calculate the thermalization range of energetic electrons produced in the X irradiation of various dielectric liquids. In terms of a Gaussian distribution of ranges, values of the b parameter for hydrocarbons vary from 60–70 Å for n-alkanes to a high of 178 Å for neopentane.

Previous to this study very little has been published on the ranges of subvibrational electrons in dielectric liquids. From a study of the photoionization of TMPD in n-hexane,[6] Houser and Jarnagin conclude that the ejected electron can travel in excess of 100 Å before thermalization. A value of 250 Å was reported for the range of photoinjected electrons in n-hexane.[7] These large values are inconsistent with the value derived from free-ion measurements. Some information is also available on the penetration of photoelectrons through solid hydrocarbon films.[8] Silver and Smejtek[9a] find a thermalization distance of 55 Å in liquid nitrogen.

The idea that the photoefficiency of liquid-filled phototubes could be used to measure ranges was suggested in an earlier study.[10] Electrons injected into a liquid are subjected to the combined applied and image potentials, and there is a maximum in this potential at a distance x_m from the cathode (see Figure 1). In their study of injection of electrons into liquid He, Onn and Silver[9b] considered this maximum to be a gate such that electrons injected beyond this distance would be collected. This concept, which was suitable for He at 4°K, was later applied to n-hexane at 25°.[7] However, a detailed analysis (see Discussion) shows that diffusion must also be considered at higher temperatures. Silver and Smejtek[9a] have included diffusion effects in a later treatment of liquid nitrogen for the specific case in which the hot electron flux decreases exponentially with distance from the electrode. It is shown here that a model involving diffusion of the electron under the influence of the potential and concentration gradients accounts quantitatively for the photoinjected currents.

Experimental Section

All hydrocarbons used were Phillips Research grade; tetramethylsilane (TMS) was NMR grade obtained from Peninsular Chemresearch, Inc. All liquids were first dried on a column of silica gel, which was previously activated at 400° for 24 hr and then transferred to a vacuum line and stirred over NaK for at least 24 hr. Before use, the samples were degassed by trap-to-trap distillation and passed over an NaK mirror before transfer to the phototube.

(1) Work performed under the auspices of the U. S. Atomic Energy Commission.
(2) A. Hummel, A. O. Allen, and F. H. Watson, Jr., *J. Chem. Phys.*, **44**, 3431 (1966).
(3) A. Mozumder and J. L. Magee, *J. Chem. Phys.*, **47**, 939 (1970).
(4) (a) W. F. Schmidt and A. O. Allen, *J. Phys. Chem.*, **72**, 3730 (1968); (b) *J. Chem. Phys.*, **52**, 2345 (1970).
(5) G. R. Freeman and J. M. Fayadh, *J. Chem. Phys.*, **43**, 86 (1965).
(6) N. Houser and R. C. Jarnagin, *J. Chem. Phys.*, **52**, 1069 (1970).
(7) R. M. Minday, L. D. Schmidt, and H. T. Davis, *J. Chem. Phys.*, **54**, 3112 (1971).
(8) W. B. Berry, *J. Electrochem. Soc.*, **118**, 597 (1971).
(9) (a) M. Silver and P. Smejtek in "Conduction in Low Mobility Materials," Klein, Tannhauser, and Pollack, Ed., Taylor and Francis, London, 1971, p 435 (b) D. G. Onn and M. Silver, *Phys. Rev.*, **183**, 295 (1969).
(10) R. A. Holroyd and M. Allen, *J. Chem. Phys.*, **54**, 5014 (1971).

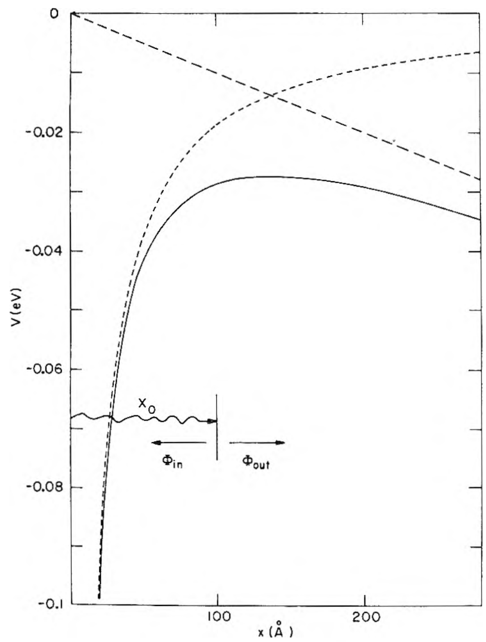

Figure 1. Potential diagram: - - -, applied potential $E = 10^4$ V/cm; · · · ·, image potential; ——, total potential.

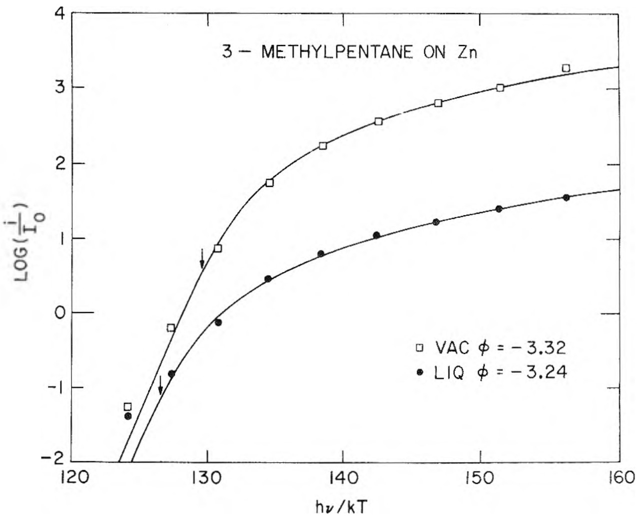

Figure 2. Spectral response of cell filled with 3-methylpentane, E = 8.3 kV/cm; •, liquid; □, vacuum response. Arrows indicate computed work functions.

The cells used for most of the work were diodes in which the electrode spacing was 0.48 cm. The cathode was a 3-cm diameter gold-plated brass disk. The anode was also 3 cm in outer diameter, with a 1.5-cm diameter central hole covered by a 0.025-mm tungsten mesh. Two varieties of cells were used. In one the cathode was further coated with zinc by vaporizing a small foil of zinc wrapped on a tungsten filament. This filament was removed from the interelectrode space after coating. This cell was made of Pyrex and allowed measurements only above 290 nm. A second cell, made of quartz, allowed measurements of the photoelectric effect of the gold surface without further coating.

Light from a 500-W xenon arc was focused on the entrance slit of a high-intensity Bausch and Lomb monochromator. The emerging beam was filtered to remove scattered light of shorter wavelengths and was focused on the hole in the anode of the photocell. The mesh across the hole was 80% transparent. The light beam impinged on the central area of the cathode so that the outer part was in effect a guard ring, minimizing effects due to field inhomogeneities.

Current measurements from the liquid-filled cell were made with the cathode at 0.1–10 kV negative potential. Current was measured at the anode with a Kiethley micro-microammeter. The inside surface of the cell, coated everywhere but at the window with tin oxide, was at ground potential.

For vacuum measurements, the polarity was reversed; a positive voltage was applied to the anode and the current measured to the cathode, which was at ground potential. This configuration was necessary since if the cathode were negative a fraction of the electrons would pass through the mesh in the anode. The vacuum current (i_V) was measured as a function of voltage and extrapolated to zero voltage on a log current *vs.* $E^{1/2}$ plot (Schottky plot). An Amperex 1003 PM tube was used to monitor light intensity; corrections were applied to the observed intensities to correct for PM tube spectral response and for transmission losses in the windows.

Calculation of work functions (ϕ) was done by computer using a least-squares fit of the data to the Fowler spectral response curve.[10] A typical result for 3-methylpentane is shown in Figure 2. Work function shifts ($\Delta\phi$) determined in this study were in general within 0.05 eV of those measured in an earlier study.[10] That the spectral response of photocurrents fits the Fowler function for dielectric liquids has been shown empirically.[10] Also Brodskii and Gurevich in a theoretical study have shown that for mediums of low dielectric constant the Fowler spectral response is expected to apply.[11]

Results

Typical current efficiency *vs.* field results are shown in Figures 3–7 for various liquids. The points are experimental, and all solid lines are one-parameter theoretical fits (see Discussion). The current efficiency (i/i_V) is the ratio of the current collected in the liquid to the total current injected from the cathode. The latter quantity is assumed equal to the current observed in the vacuum (at zero voltage—see Experimental Section) at a *corresponding* wavelength. *Corresponding* means eq 1 is satisfied.

$$h\nu_{vac} - \phi_{vac} = h\nu_{liq} - \phi_{liq} \quad (1)$$

That is, the vacuum current is measured at a wavelength such that the photon energy ($h\nu_{vac}$) exceeds the vacuum work function by the same amount that $h\nu_{liq}$ exceeds the liquid work function. For several liquids, n-pentane, n-hexane, 2-methylpentane, and 3-methylpentane, $\Delta\phi \sim 0$, and the vacuum measurements are at approximately the same wavelength as the liquid.[12]

The magnitude of the current efficiency is markedly different for various liquids. At an applied field of 10^4 V/cm the current efficiency is of the order of 1% for n-alkanes, about 15% for neopentane and TMS, and intermediate for cyclopentane. The highest measured efficiency is 25% for neopentane and TMS at fields of the order of 20 kV/cm.

(11) A. M. Brodskii and Y. Y. Gurevich, *Sov. Phys. JETP*, **27**, 114 (1968).

(12) Note that because of the large $\Delta\phi$ in liquids like neopentane the efficiency would exceed 100% if the vacuum measurement were made at the *same* wavelength.

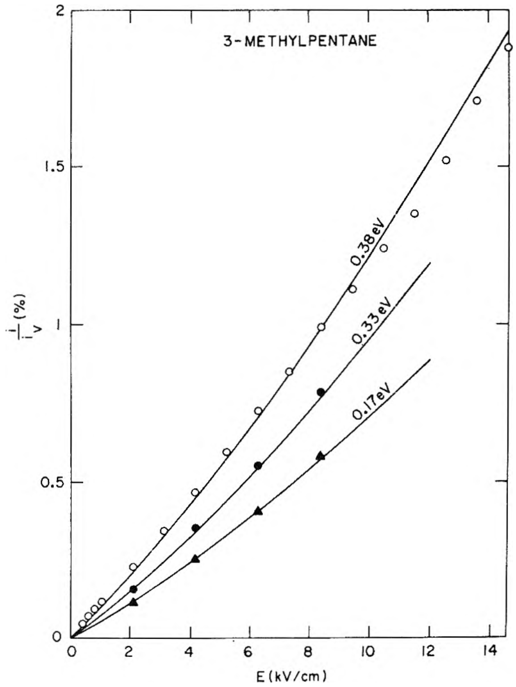

Figure 3. Current efficiency *vs.* field for 3-methylpentane; ○, 0.38-eV electrons, solid line calculated for b = 53 Å; ●, 0.33-eV electrons, solid line calculated for b = 48 Å; △, 0.17-eV electrons, solid line calculated for b = 43 Å.

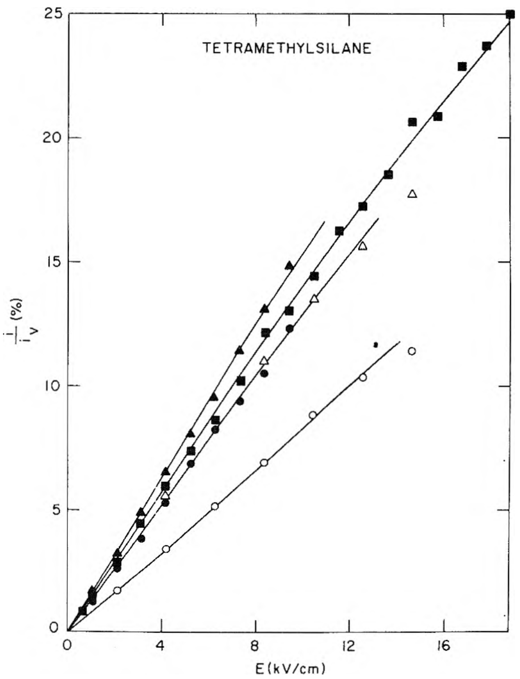

Figure 4. Current efficiency *vs.* field for tetramethylsilane: ■, 0.25-eV electrons, solid line calculated for b = 186 Å; ▲, 0.2-eV electrons, solid line calculated for b = 198 Å; ●, 0.08-eV electrons, solid line calculated for b = 176 Å. Open points refer to a solution of naphthalene (4 mM) in TMS: △, 0.23-eV electrons, solid line calculated for b = 176 Å; ○, 0.08-eV electrons, solid line calculated for b = 133 Å.

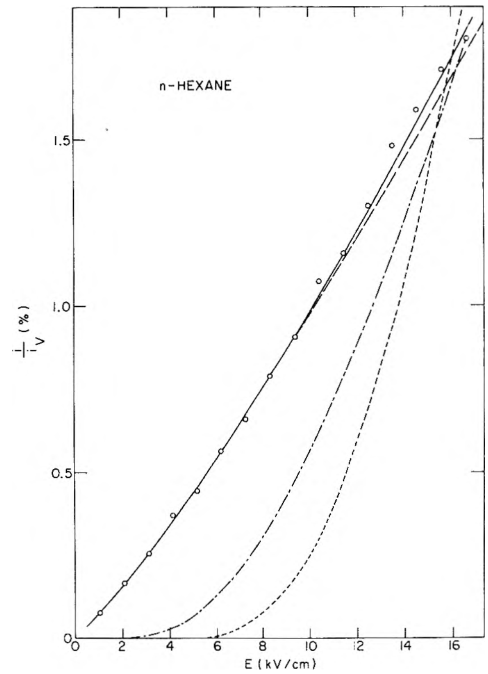

Figure 5. Current efficiency *vs.* field for n-hexane. Points are experimental for 0.36-eV electrons: ——, diffusion model for gaussian distribution with b = 49 Å; - - - -, diffusion model for 1-dimensional exponential distribution, R = 24 Å; · · · ·, gate model for gaussian distribution, b = 45.3 Å; –· –·, gate model for exponential distribution, R = 26.4 Å.

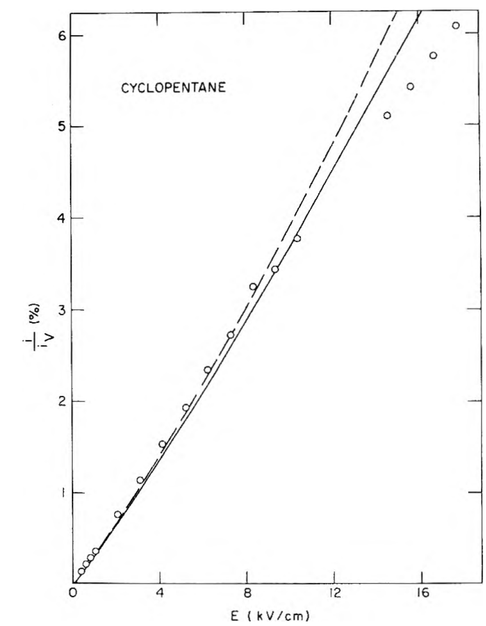

Figure 6. Current efficiency *vs.* field for cyclopentane: ○, 0.47-eV electrons, solid line for gaussian distribution with b = 84 Å; dotted line for isotropic single range distribution of 102 Å.

A casual inspection of the figures suggests the current *vs.* voltage plots are linear (ohmic) but there are subtle but quite real deviations from linearity which must be accounted for. In liquids of low efficiency the plots are slightly concave upward throughout the range studied (Figures 3 and 5). In the efficient liquids the curvature is just the opposite; the points fall off at higher voltage (see Figures 4 and 7).

The effect of varying the energy[13] of the injected electrons is also investigated. Individual experiments sometimes show a decreasing efficiency with decreasing energy

(13) An average energy of 0.6 of the maximum energy is assumed, based on vacuum measurements; see L. B. Loeb, "Basic Processes of Gaseous Electronics," 2nd ed, University of California Press, Berkeley, Calif., 1960, Chapter 7.

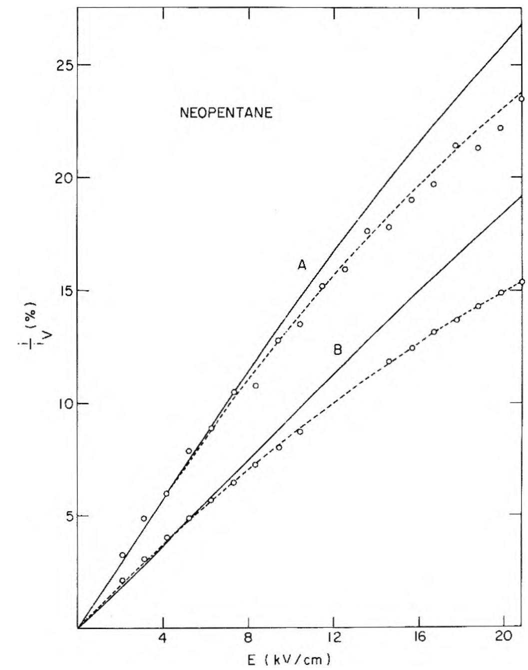

Figure 7. Current efficiency *vs.* field for neopentane. Points are experimental: ●, 0.34-eV electrons; O, 0.23-eV electrons. Solid lines are calculated for gaussian distribution and (A) b = 188 Å; (B) b = 145 Å. Upper dotted curve (A) calculated assuming injected current is 33% back-scattered and b = 245 Å. Lower dotted curve (B) calculated assuming two gaussians with b = 65 Å (70%) and b = 286 Å (30%).

(*e.g.*, see Figure 3). However, the effect is slight. In other cases the efficiency is the same, within the experimental uncertainty, for all electron energies (*e.g.*, see Figure 4). Determinations at very low energies, that is close to the work function, are difficult because of the lower currents measured and more uncertain because any uncertainty in the work function leads to a large error in i_V.

There are several other possible sources of error in the measurements. One is the role of impurities. In general this must not be important because measurements in this laboratory on different samples of liquid by three different investigators yielded comparable results. In one case the efficiency was first measured on a sample of pure TMS and then 5 m*M* naphthalene was added (to the TMS) and the efficiency *vs.* field curve was remeasured. The results with the additive were the same as with pure TMS for 0.27-eV electrons and slightly lower for 0.09-eV electrons (see Figure 4).

The effect of space charge on the liquid current is negligible, since the current is found to be directly proportional to light intensity. The current densities are generally less than 10^{-8} A/cm^2 at the highest field employed and much lower at low fields, which is well below the space charge limit.

The effect of surface roughness which leads to field inhomogeneities[14] is difficult to evaluate. To minimize this effect the cathode was highly polished and the light beam illuminated only the central area of the cathode so that edge inhomogeneities were eliminated.

Discussion

Diffusion Model. The results are interpreted in terms of a diffusion model which treats the motion of the electrons after thermalization in the liquid. The electrons leave the metal with excess kinetic energy. They are scattered by collisions in the liquid and eventually are thermalized. It is expected that a certain fraction of the "hot" electrons are scattered back to the cathode before thermalization.[9b] As is discussed below, our results indicate that this fraction is small.

Electrons are thermalized at various distances from the metal and some characteristic distribution of such distances is assumed. We first calculate the probability of escape of an electron at a distance x_0 from the metal and then integrate this probability over the distribution assumed. Thus the current observed is a function of a parameter of the distribution function; for example, the b parameter for the Gaussian.

In the liquid the electron is in the field of the applied potential, given at any point by $-Ex$, and of the image potential,[15] given by $-e/\epsilon 4x$ (see Figure 1). The total potential is

$$V(x) = -Ex - e/\epsilon 4x \tag{2}$$

where ϵ is the dielectric constant of the liquid. Electrons will diffuse in the liquid under the influence of the concentration gradient $\mathrm{d}c/\mathrm{d}x$ and under the influence of the potential gradient $\mathrm{d}V/\mathrm{d}x$; thus at any point the current flux of electrons ϕ is given by

$$\phi = -D\mathrm{d}c/\mathrm{d}x - \mu c\mathrm{d}V/\mathrm{d}x \tag{3}$$

Since $\mu = eD/kT$, then the basic diffusion equation becomes

$$\phi/D = -\mathrm{d}c/\mathrm{d}x - (c/kT)\cdot e\mathrm{d}V/\mathrm{d}x \tag{4}$$

If the substitution $c = ye^{-eV(x)/kT}$ is made, eq 4 is transformed to eq 5. The variable y will approach 0 as $x \rightarrow 0$

$$\frac{\mathrm{d}y}{\mathrm{d}x} = -\phi/De^{eV(x)/kT} \tag{5}$$

and $x \rightarrow \infty$ because $-V(x)$ is infinite at these points. Equation 5 was solved in two regions: (A) between the metal and x_0 and (B) from x_0 to ∞. In region A there will be a net flux of electrons back to the metal ($-\phi_{\mathrm{in}}$). In region B there will be a net flux toward the anode (ϕ_{out}) (see Figure 1). The total injected flux is, by definition, $\phi_{\mathrm{out}} + (-\phi_{\mathrm{in}})$. For region A, where $0 < x < x_0$ the solution of (5) is

$$y_{\mathrm{A}} = +\frac{(-\phi_{\mathrm{in}})}{D}\int_0^{x_0} e^{eV(x)/kT}\mathrm{d}x \tag{6}$$

For region B, where $x_0 < x < \infty$ the solution is

$$y_{\mathrm{B}} = +\frac{\phi_{\mathrm{out}}}{D}\int_{x_0}^{\infty} e^{eV(x)/kT}\mathrm{d}x \tag{7}$$

Since the function y must be continuous, y_{A} must be equal to y_{B} at x_0 or

$$(-\phi_{\mathrm{in}})/\phi_{\mathrm{out}} = \frac{\int_{x_0}^{\infty} e^{eV(x)/kT}\mathrm{d}x}{\int_0^{x_0} e^{eV(x)/kT}\mathrm{d}x} \tag{8}$$

Thus the escape probability of an electron thermalized at a distance x_0 from the cathode, given by the flux out divided by the total injected current, is

$$P(x_0) = \frac{\phi_{\mathrm{out}}}{\phi_{\mathrm{out}} + (-\phi_{\mathrm{in}})} = \frac{\int_0^{x_0} e^{eV(x)/kT}\mathrm{d}x}{\int_0^{\infty} e^{eV(x)/kT}\mathrm{d}x} \tag{9}$$

(14) R. Gomer, *Accounts Chem. Res.*, **5**, 41 (1972).
(15) R. P. Feynman, R. B. Leighton, and M. Sands, "The Feynman Lectures on Physics," Vol. 2, Addison Wesley, Reading, Mass., 1964, pp 6-9.

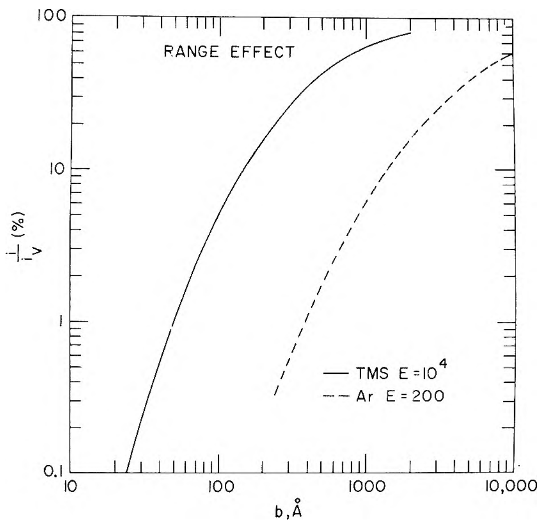

Figure 8. Theoretical current efficiency *vs.* range according to eq 8 as a function of the width of the gaussian distribution. Solid line for a liquid of ϵ = 1.84 at a field of 10^4 V/cm and T = 298°K. Dotted line for argon, ϵ = 1.53, E = 200 V/cm and T = 85°K.

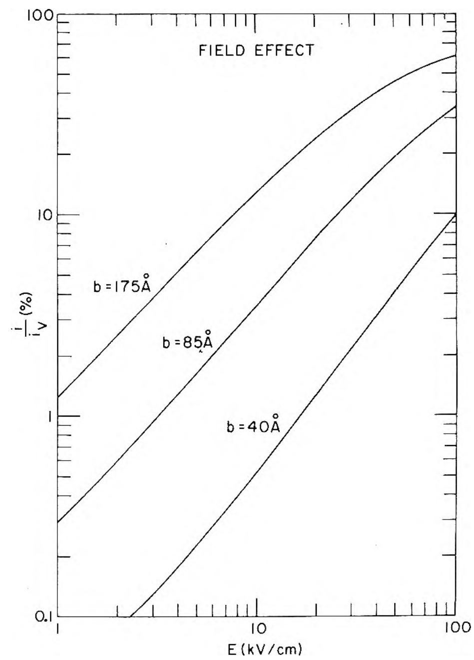

Figure 9. Theoretical current efficiency *vs.* field for different values of b = 40, 85, and 175 Å.

The integral in the denominator of eq 9 is a modified Bessel function, $K_1(z)$, for which a polynomial approximation is available.[16] The numerator is evaluated by a Simpson's rule integration.

The calculated efficiency of the phototube is given by the integral over distance of the product of $P(x_0)$ and an assumed distribution function, $D(x_0)$

$$i/i_v = \int_0^\infty P(x_0)\, D(x_0)\, dx_0 \tag{10}$$

If $D(x_0)$ is gaussian, then

$$i/i_v = \frac{2}{b\sqrt{\pi}} \int_0^\infty P(x_0)\, e^{-x_0^2/b^2} dx_0 \tag{11}$$

If some of the current, i_{BS}, is assumed to be back-scattered into the cathode before thermalization, i/i_v may be obtained by multiplying the right-hand side of eq 11 by (1 − i_{BS}/i_v). Figures 8 and 9 are plots of eq 11 for various conditions. Figure 8 shows how the efficiency varies as a function of b, the width of the gaussian distribution. The solid line is for TMS at 25° and a field of 10^4 V/cm.

The model predicts no current at zero field, in contrast to γ radiolysis where there is an ion yield at low field (the free-ion yield). The lack of a "free-ion" yield here is a consequence of the geometry. The electron can escape in only one direction (away from the cathode). Stated in another way, the volume element into which the electron can diffuse to escape is less in the case of photoinjection.

Figure 9 shows the predicted behavior of the efficiency *vs.* field dependence for various ranges. The model correctly predicts that for low ranges the dependence is concave upward (lower curve) and for large ranges concave downward (upper curve).

The model is compared with typical experimental results in the current *vs.* voltage plots (Figures 3–7). For most of the liquids the theoretical (solid) curves, as calculated from eq 11, give a very satisfactory fit to the experimental points. In general, standard deviations expressed in terms of σ are of the order of 1–2% of the b value for a given experiment (see Table I). For cyclopentane and neopentane the fit is worse; the value of σ is around 5%. This would still be considered a reasonable fit except that there is a definite trend in the data in that the current falls off faster than predicted at high fields.[17] Although a relatively good fit of the data is obtained in each experiment, Table I shows that the reproducibility between different experiments is not as good and the uncertainty to be associated with each b value is 10–15%. For the theoretical fits shown as solid lines in the figures and for the b values listed in Table I, back-scattering was assumed to be negligible. The average values of "b" obtained are: for n-pentane, 36 Å; cyclopentane, 77 Å; neopentane, 147 Å; n-hexane, 42 Å; 2-methylpentane, 58 Å; 3-methylpentane, 50 Å; 2,2,4-trimethylpentane, 102 Å; and TMS, 177 Å.

The only other comprehensive data to which our results can be compared are those available from free-ion measurements in radiation studies.[4,5] From these measurements b values are derived for the hot electrons released in ionization events. Such values from ref 4 are listed in the last column of Table I. In general the b value for photoinjected electrons is less than that for hot electrons formed in radiolysis (TMS and cyclopentane are exceptions). The average difference in the two sets of values is 17 Å. This shows that most of the range of hot electrons is attained while the electron has epithermal energies.

Other distributions of ranges are also considered to see if the shape of the distribution can be determined. The results for inefficient liquids are quite insensitive to the shape. The data for n-hexane in Figure 5 can be fit equally well by a one-dimensional exponential [$N(x) = x_c^{-1} \cdot e^{-x_0/x_c}$] as well as by an isotropic single range of 61 Å. However, the single range is not satisfactory for the more efficient liquids. As is shown in Figure 6, such a distribution gives a worse fit to the data than the gaussian. Here too one-dimensional or three-dimensional[18] exponential

(16) "Handbook of Mathematical Functions," National Bureau of Standards, Applied Math Series 55, M. Abramowitz and I. A. Stegun, Ed., 1964, p 379.

(17) An improved fit to the neopentane data can be obtained by assuming two gaussians, one rather tight and one with a larger b (Figure 7).

(18) What is meant is the x component of a three-dimensional exponential distribution of the form

$$D(x_0) = \frac{1}{2}\left(1 + \frac{x_0}{x_c}\right) e^{-x_0/x_c}$$

where x_c is the characteristic range.

TABLE I: Low-Energy Electron Range Data

Liquid	Cathode	ϕ_{vac}, eV	$\Delta\phi$,[a] eV	Electron energy,[b] eV	b, Å	Gaussian fit, σ%	b[c] X-rays, Å
			C_5				
n-Pentane	Zn	3.66	+0.09	0.15	36	1.2	72
	Zn	3.75	0.00	0.23	36	3.2	
Cyclopentane	Zn	3.12	−0.14	0.52	71	1.6	69
	Zn	3.17	−0.19	0.47	84	4.2	
Neopentane	Zn	3.61	−0.36	0.24	135	6.5	178
	Au	4.47	−0.35	0.23	132	5.6	
	Au	4.55	−0.35	0.34	178	4.3	
			C_6				
n-Hexane	Zn	3.40	+0.02	0.43	36	1.0	67
	Zn	3.43	−0.03	0.36	49	0.9	
2-Methylpentane	Zn	3.74	+0.04	0.30	68	1.4	71
				0.13	74	0.6	
	Au	4.42	−0.01	0.22	47	2.1	
3-Methylpentane	Zn	3.32	−0.08	0.38	53	1.9	70
	Zn	3.69	+0.03	0.33	48	1.4	
				0.17	43	0.8	
	Zn	3.77	+0.04	0.20	47	0.8	
			C_8				
2,2,4-Trimethylpentane	Au	4.48	−0.15	0.20	100	2.6	95
	Au	4.39	−0.12	0.24	103	1.5	
Tetramethylsilane	Zn	3.87	−0.53	0.25	186	1.3	159
	Zn	3.91	−0.57	0.25	142	0.8	
				0.12	160	1.3	
	Zn	3.75	−0.54	0.27	184	3.2	
				0.20	198	2.1	
				0.14	190	1.2	
				0.08	176	1.5	

[a] $\Delta\phi = \phi_{liq} - \phi_{vac}$. [b] K.E. = 0.6 × ($h\nu - \phi_{liq}$). [c] Reference 4.

distributions are almost as good as the gaussian.

Back-scattering. In the derivation of b values presented in Table I, it is assumed that all electrons leaving the electrode become thermalized in the liquid. However, it is more reasonable to expect that some of the "hot" electrons should be scattered back to the cathode where they would be trapped. In the case of liquid helium it was found that 90% of the electrons injected from a cold cathode emitter were scattered back.[10] The magnitude of this term is shown[10] to be related to the ratio of the mean free path to x_0. If this ratio is large, the back-scattering is less and if small the back-scattering is greater. Our results for neopentane and TMS, where i/i_v approaches 25% at high fields, clearly require that back-scattering be small in these liquids. An estimate of the upper limit of i_{BS}/i_v allowed by the data can be obtained by assuming differing amounts of back-scatter and fitting the results. For example, if the back-scattering is 50% the data in Figure 5 for n-hexane can be fit satisfactorily with b = 65 Å instead of b = 49 Å; or if the back-scattering is 75% a fit is obtained with b = 87 Å. For large percentages the fit is poor and even larger values of b must be assumed. However, large values of b can be ruled out by the data on free-ion yields in radiolysis.[4,5] Electrons released in radiolysis have much more energy than those obtained by photoinjection, and so b values derived from ion yield measurements (last column Table I) provide an upper limit for ranges measured here. Schmidt and Allen report a b value for n-hexane of 67 Å; thus we conclude that for n-hexane back-scattering cannot be greater than 50%.

The percentage is even less if we consider the neopentane data. The average b value is 147 Å. The maximum back-scattering allowed by the free-ion b value is 23%. If a similar calculation is made for the other liquids the maximum percentages of back-scattering allowed are for n-pentane 85%, 2-methylpentane 39%, and 3-methylpentane 57%. For cyclopentane, 2,2,4-trimethylpentane, and TMS the b value found for low-energy electrons is comparable to that derived from free-ion measurements and thus no back-scattering is allowed by the data on these liquids. Assuming a small amount of back-scatter has the virtue that a better fit is obtained to the neopentane data. As shown by the upper dashed curve in Figure 7, a good fit is obtained assuming 33% back-scatter and b = 245 Å, but this value is already much larger than the free-ion b value of 178 Å.

The lack of importance of back-scattering can be rationalized if we consider both the equivalent "mean free path" for energy loss, Λ_0, and for momentum loss, Λ_1. For low-energy electrons these will in general be different as was pointed out by Cohen and Lekner.[19] Recently, experimental values of V_0,[9] the ground-state energy of the electron, have been used to evaluate scattering lengths (a) for thermal electrons. The values derived are a = 2.18 Å for n-hexane and 1.92 Å for neopentane.[20,21] Comparable values of a have been obtained directly from electron mo-

(19) M. H. Cohen and J. Lekner, *Phys. Rev.*, **158**, 305 (1967).
(20) H. T. Davis, L. D. Schmidt, and R. M. Minday, *Chem. Phys. Lett.*, **13**, 413 (1972).
(21) K. Fueki, D.-F. Feng, and L. Kevan, *Chem. Phys. Lett.*, **13**, 616 (1972).

bility studies. The corresponding values of Λ_0 are 3.6 and 4.2 Å, respectively. The momentum transfer mean free paths are longer than Λ_0 by the factor $1/S(\mathrm{O})$, where $S(\mathrm{O})$ is the structure factor. Thus the mean free paths for momentum transfer can be calculated and are of the order of 100 Å for these liquids. We conclude that the properties of the low-energy electrons studied here are similar to thermal electrons in being characterized by large momentum mean free paths. Thus in the process of injection a low-energy electron loses small amounts of energy regularly to phonon excitations but travels a considerable distance before undergoing a scattering event in which there is a large change in direction.

Other Models. Another model which has been used to interpret electron injection data is the "gate" model. In this, the maximum in potential (see Figure 1) acts like a gate in that the position of the electron relative to the maximum upon thermalization determines the probability of escape; *i.e.*, diffusion is ignored. Onn and Silver[9b] showed that this model works well for liquid He and it has also been applied to liquid hydrocarbons.[7] A test of the applicability of this model to our results is shown in Figure 5. Regardless of the type of distribution assumed, the gate model predicts an entirely different dependence of current on voltage (lower dotted lines) than is observed. This theory also predicts that the log of the photocurrent should be linearly dependent on $E^{-1/2}$. Data obtained here, which show a nearly ohmic dependence, illustrate that this relation is invalid. The average value of $b = 42$ Å reported here for electrons photoinjected into n-hexane is clearly inconsistent with the range reported in ref 7 of 250 Å.[22] This value was arrived at assuming that the gate model applied.

Berry[8] has studied the penetration of 1-eV electrons through thin films of hydrocarbons deposited on a silver photocathode. He found an exponential attenuation with thickness and reports attenuation lengths of 59 and 65 Å for n-hexane and 3-methylpentane. These ranges are not to be compared directly with our b values since they refer to penetration of "hot" electrons through films at 77°, whereas our results refer to the distribution of ranges derived from diffusion of thermalized electrons. Nevertheless, Berry's results support our conclusion that low-energy electrons penetrate distances comparable to hot electrons before thermalization.

If our model is correct it should be applicable to other nonpolar liquids. Equation 11 can be used to predict the dependence of photoefficiency on range, given the temperature, dielectric constant, and field. As an example, we show in Figure 8 the calculated efficiency of a liquid argon-filled phototube as a function of b for an applied field of 200 V/cm. The conditions were chosen to match the experimental conditions in a recent study of photoinjection into liquid argon.[23] A ratio of liquid to vacuum current of $1/10$ was observed; if this ratio is equated to i/i_v, the range (b value) of a low-energy electron in liquid argon is 1400 Å (see Figure 8). This is in surprisingly good agreement with the value of $b = 1300$ Å determined from ion-yield measurements in the radiolysis of liquid argon.[24]

Acknowledgments. The authors wish to express their appreciation to A. O. Allen for many stimulating discussions, to C. Nawrocki, E. Ritter, J. Walsh, and K. Walther for construction of the phototubes, and to M. L. Perlman for suggesting the design of the anodes.

(22) A value of 250 Å was reported. However, if the dielectric constant of the medium is included in eq 6 of ref 7, then analysis of their data in terms of the gate model yields $x_0 = 175$ Å.

(23) B. Halpern, J. Lekner, S. A. Rice, and R. Gomer, *Phys. Rev.*, **156**, 351 (1967).

(24) P. G. Fuochi and G. R. Freeman, *J. Chem. Phys.*, **56**, 2333 (1972).

Triplet Formation in Ion Recombination in Spurs

John L. Magee* **and Jan-Tsyu J. Huang**

Department of Chemistry and the Radiation Laboratory,[1] University of Notre Dame, Notre Dame, Indiana 46556
(Received April 27, 1972)

Publication costs assisted by the U.S. Atomic Energy Commission

It is generally believed that ion recombination is an important mechanism for production of excited states in irradiated systems. In many such systems the recombination occurs within spurs and takes place before spin relaxation. Under such conditions the probability for triplet formation is a simple combinatorial problem and yields the result, $P_T = (3/4)[1 - 1/(2n - 1)]$, where n is the number of ion pairs in the spur. The direct impact excitation of triplet states in spurs alters this result. The general problem of ion recombination in spurs which also contain triplet molecules excited by subexcitation electrons is discussed and general formulas are presented. The average over spur size distribution and comparison with experiment are discussed.

I. Introduction

Recently there has been increasing interest in experimental investigation of excited electronic states, particularly triplet states, formed in irradiated systems.[2-4] It is usually assumed that the states excited initially by the primary particle are not themselves observed but are transformed through several generations of intermediates although the reaction sequences are not very well known.

In approximately chronological order the mechanisms of formation of triplet states in irradiated systems are (a) electron impact, (b) recombination of ions in spurs, and (c) intersystem crossing.

Only low-energy electrons have significant cross sections for triplet formation. Studies of the cross sections for this process have been carried out for gases[5] and solid thin films[6] recently. They suggest that impact excitation of triplets in organic liquids may play an important role in radiation chemistry.

Recombination in a completely relaxed system yields triplet to singlet ratios of 3/1. Relaxation of spin involves transitions which are induced by magnetic interactions and the extent of relaxation in any system depends upon the rate of its relaxation processes. The other extreme condition is conservation of spin, and under this condition recombination of a small number of ion pairs in a spur should yield triplet/singlet ratios very different from 3/1. In many organic liquids (such as hydrocarbons) in the vicinity of room temperature ion recombination occurs in times short compared with spin relaxation times. For these systems spin conservation applies to the recombination process.[7,8]

Excited singlet states formed on recombination may be converted by intersystem crossing into triplets (and *vice versa*). Thus the interpretation of experimental data requires careful analysis, taking into account the various mechanisms of triplet origin. Our work is concerned with the spur recombination problem which is required in the analysis. A brief discussion of this problem was given previously by Magee.[9] A more complete account of the statistical model of spur recombination (as affected by concomitant triplet production by slow electrons) is contained in the present paper.

II. Combinatorial Considerations

A characteristic of ionization in irradiated systems is that it occurs in tracks with high local concentration of charges. Mozumder and Magee[10] have discussed the structure of low LET tracks and have shown that they are composed of widely spaced entities (spurs) which on the average contain rather small numbers of ion pairs. It is also known that for the most part the ion pairs produced in the same spur recombine with each other.

Consider a spur in which n ionizations are produced. In the initial state (before ionization) the n electrons to be ionized form electron pair bonds with n other electrons in n separate molecules. Each molecule is singlet and so the entire system is clearly singlet. The ionization processes produce an intermediate state which is in the singlet subspace of the larger 2^{2n}-dimensional spin space for the $2n$

(1) The Radiation Laboratory of the University of Notre Dame is operated under contract with the U. S. Atomic Energy Commission. This is AEC Document No. COO-38-824.

(2) J. K. Thomas, *Annu. Rev. Phys. Chem.*, **21**, 17 (1970).

(3) F. S. Dainton, G. S. Salmon, T. Morrow, and G. F. Thompson, *Chem. Commun.*, 326 (1968); E. J. Land and A. J. Swallow, *Trans. Faraday Soc.*, **64**, 1247 (1968); S. Arai, A. Kira, and M. Imamura, *J. Chem. Phys.*, **54**, 5073 (1971); B. Brocklehurst and R. D. Russell, *Trans. Faraday Soc.*, **65**, 2159 (1969).

(4) J. H. Baxendale and P. Wardman, *Trans. Faraday Soc.*, **67**, 2997 (1971).

(5) A. Kuppermann, J. K. Rice, and S. Trajmar, *J. Phys. Chem.*, **72**, 3894 (1968); J. P. Doering, *J. Chem. Phys.*, **51**, 2866 (1969).

(6) D. Lewis and W. H. Hamill, *J. Chem. Phys.*, **51**, 456 (1969); P. B. Merkel and W. H. Hamill, *ibid.*, **55**, 1409 (1971).

(7) The applicability of conservation of spin can be seen as follows. To a good approximation the Hamiltonian H of the ion pairs recombining in a spur includes only electrostatic terms. Therefore the spin operators S^2 and S_z commute with H; both total spin and its z projection are constants of motion. Weak magnetic forces arise from the motion of the charges but spin relaxation cannot be induced in the recombination times.

(8) It should be noted that large cross sections may be found for electron spin exchange in slow electron collisions with atoms or molecules. This process occurs because of exchange interactions and maintains conservation of the total spin of the system. Following ionization of a molecule, the free electron produced may undergo exchange collisions. However, "spin flips" of the colliding electron must be compensated by spin flips in the target molecules. Thus if the molecules are all in singlet ground-states initially, a spin flip of the electron does not occur in a collision unless a triplet excitation takes place at the same time.

(9) J. L. Magee in "Comparative Effects of Radiation," M. Burton, J. S. Kirby-Smith, and J. L. Magee, Ed., Wiley, N. Y., N. Y., 1960, p 130.

(10) A. Mozumder and J. L. Magee, *J. Chem. Phys.*, **45**, 3332 (1966); *ibid.*, **47**, 939 (1967).

electron system. The recombination process leads to a final state which is again singlet in the total spin. But the recombined individual molecules can be triplet, if their spins are oriented with respect to one another to give zero total spin for the entire system.

According to Rumer[11] the number of singlet wave functions for a system of $2n$ electrons is

$$\omega_n = \frac{(2n)!}{(n+1)!n!} \tag{1}$$

and this is the dimension of the singlet subspace mentioned above. Each possible state of the total system can be represented by an orthonormal function Ψ_k where $k = 1,2,3 \ldots \omega_n$.

The ionization and recombination amounts to a permutation of electron spins. The final wave function Ψ_f can, therefore, be expressed as a linear combination of all the possible (total singlet) states

$$\Psi_i \rightarrow \Psi_f = \sum_{k=1}^{\omega_n} C_k \Psi_k \tag{2}$$

In any representation there is only one state Ψ_k in which all of the molecules are separately in singlet states and this state can be taken as Ψ_1. By hypothesis there are no energetic preferences and the absolute value of the coefficients $|C_k|$ in (2) must be taken as equal. This can be understood as follows. In spur development the positive ions are formed relatively closely together, perhaps in a region of diameter ~20 Å, and the electrons go out to turning points ~60–100 Å from the positive ions. For most of the time during which the charges are separated the energy of all of the ω_n spin states is essentially the same because it depends only on the coulombic integrals (the exchange integrals are negligible). Therefore during the time of charge separation it is impossible to assign any unique wave function to the system; all of the ω_n spin-allowed wave functions must be taken with equal statistical weights. We can say that there has been fast relaxation within the ω_n spin subspace; we call this process "combinatorial relaxation."[12] In order to maintain equal *a priori* weights for the final states, the requirement is only that there should be no activation energy needed for recombination leading either to singlet or triplet molecules.

We now consider the general question, what is the probability in all of the ω_n possible final states of the system that there will be a singlet bond[13] for a particular molecule PQ? The answer turns out to be simple. If a singlet bond exists at PQ, the other $(n - 1)$ bonds remain confined to a smaller singlet subspace so that there are ω_{n-1} possible functions associated with this possibility. In other words the fraction ω_{n-1}/ω_n of all possible final states has a singlet bond at PQ. The probability for triplet formation in the molecule PQ is therefore the remainder

$$P_T = 1 - \omega_{n-1}/\omega_n \tag{3}$$

The probability for triplet formation is clearly the same for any recombined molecule in the spur and is given by eq 3.

Use of eq 1 allows us to write an explicit formula

$$P_T = \frac{3}{4}\left(1 - \frac{1}{2n-1}\right) \tag{4}$$

which shows that the asymptotic limit for large n is 3/4. Table I lists various values of P_T as a function of the spur size n.

TABLE I: Fraction of Triplet Molecules Formed on Ion Recombination in Spur

n	$P_T = [3/4](1 - [1/2n - 1])$	$T/S = [3(n - 1)/(n + 1)]$
1	0.000	0.00
2	0.500	1.00
3	0.600	1.50
4	0.640	1.80
5	0.667	2.00
6	0.682	2.14
7	0.693	2.25
8	0.700	2.33
.		
.		
.		
∞	0.750	3.00

III. Theoretical T/S Ratios

It has been pointed out[10] that for low LET radiations such as electrons in the MeV range spurs with a single ion pair dominate. Under conservation of spin only spurs with two or more ion pairs can yield triplets. Using the spur distribution given for hexane by Mozumder and Magee,[10] we estimate a triplet/singlet ratio of 0.5 arising from ion recombination.

An implicit assumption has been made so far that the low-energy electrons generated in the development of the spur did not create any triplet molecules directly. Recent work of Hamill and Hiraoka[14] however makes it clear that such a process probably occurs in most of the systems of interest to us. We now consider the effect of the triplets produced by low-energy electron impacts on the recombination process itself.

In the process of direct triplet excitation by subexcitation electrons, the electron spin will be exchanged. However, there is only fast "combinatorial relaxation" involved and the total spin of the system is still conserved. In the simplest case if a spur contains one ion pair and one triplet molecule is directly excited by the electron before it recombines with the positive ion, the charge pair must recombine as triplet because the only possible singlet state for the entire system requires antiparallel triplet states for the two molecules. The general combinatorial consideration for various numbers of recombining charge pairs which have a finite spin arising from triplet excitation by low-energy electrons is similar to the treatment for zero spin. These cases do not lead to formulas as simple as that for zero spin given in eq 4 but the treatment is straightforward and is presented in Appendix A.

Real systems of interest have a principal component (solvent) M which undergoes all excitations and then transfers charge and/or excitation to a minor component (solute) N. The spin state of the spur as a whole is unaffected by these processes and remains singlet. Now let us consider a reaction scheme which involves triplet forma-

(11) T. Rumer, *Gottingen Nachr.*, 377 (1932). This topic is discussed in H. Eyring, J. Walter, and G. E. Kimball, "Quantum Chemistry," Wiley, New York, N. Y., 1944; R. McWeeny and B. T. Sutcliffe, "Methods in Molecular Quantum Mechanics," Academic Press, New York, N. Y., 1969.

(12) In this relaxation no violation of conservation of spin occurs, while in the slower relaxation processes involving magnetic interactions the total spin of a system is not conserved.

(13) In this treatment the molecule re-formed on recombination is represented by an electron pair bond.

(14) W. H. Hamill and K. Hiraoka, private communication; see also ref 6.

tion of solvent molecules by slow electrons.

$$M \rightsquigarrow M^+ + e^* \quad (A)$$

$$e^* + M \xrightarrow{f} e + M_T^* \quad (B1)$$

$$\xrightarrow{(1-f)} e + M_S' \quad (B2)$$

$$e + N \longrightarrow N^- \quad (C)$$

$$M^+ + N \longrightarrow M + N^+ \quad (D)$$

$$N^- + N^+ \text{ (or } M^+) \xrightarrow{f} N_T^* + N \text{ (or M)} \quad (E1)$$

$$\xrightarrow{(1-f)} N_S^* + N \text{ (or M)} \quad (E2)$$

where the asterisk in eq A, B, E1, and E2 indicates excess energy; f in eq B and E is the fraction of subexcitation electrons which excite triplet molecules during thermalization; and M_S' indicates thermal excitation. This formulation requires that the average number of triplets excited by a subexcitation electron shall be less than one. Let us define $P_T(j,k)$ as the probability for triplet formation on recombination of j ion pairs in a spur in which k triplet molecules have been excited by direct impact of subexcitation electrons. For a single ion pair the initial T/S ratio of solute from ion recombination will be

$$(T/S)_1 = \frac{fP_T(1,1) + (1-f)P_T(1,0)}{1 - [fP_T(1,1) + (1-f)P_T(1,0)]} \quad (5)$$

which leads to

$$(T/S)_1 = \frac{f}{1-f} \quad (5a)$$

because $P_T(1,0) = 0$ and $P_T(1,1) = 1$.

It has been assumed that the triplet states produced in the solvent (eq B1) are degraded in processes which do not lead to formation of solute triplets. Under the same conditions, the spur-averaged ratio $\langle T/S \rangle$ for each value of f is estimated (see Appendix B) and shown in Table II. These values are for complete scavenging of charge by the solute and therefore correspond to values extrapolated to high concentrations.

IV. Discussion

The considerations above are limited to the case in which there is no spin relaxation. Brocklehurst[15] has discussed spin–spin and spin–lattice relaxation for organic ions. These relaxation times are known in esr studies when magnetic fields are present, but not as much is known about field-free systems. However, it can be concluded that in liquid organic solutions relaxation times are of the order of 10^{-6} sec at nearly zero field.[15] Recombination time in the same systems is of the order of 10^{-11} sec. Thus spin relaxation is not expected to occur before recombination for organic liquid systems at room temperature and the treatment presented here should apply.

As suggested by Brocklehurst, ion recombination time may be increased by lowering the temperature to increase viscosity. If hyperfine interaction with protons is involved, the spin relaxation time may be as small as $\hbar/a_p \sim 10^{-9}$–10^{-8} sec (where a_p is the parameter in the electron spin–proton spin interaction Hamiltonian) although it is generally taken to be somewhat larger than this range of values. In the presence of an external magnetic field, hyperfine relaxation will then result in $(T/S)_1 = 1$ for a single ion pair and $\langle T/S \rangle \simeq 1.5$ for the spur average. Even if there is no external field, this same hyperfine relaxation would give $0 < (T/S)_1 < 3$ and $0.5 < \langle T/S \rangle < 3$. The exact value depends upon the number of protons involved and details of the electron motion which are not known. No consideration of the effects of relaxation on T/S ratios has been made for the case in which there is excitation of triplet molecules by subexcitation electrons.

Another relaxation mechanism is collision of electrons with molecules in doublet or triplet states. In such collisions "spin flips" can occur with zero threshold energy. Examples of molecules in doublet states are NO, NO_3, organic radicals, and "spin labeled" compounds;[16] and the most common triplet molecule is O_2. If the concentration of one of these species is large enough in the irradiated system to affect the relaxation, a special consideration must be made. In such case it is likely that the chemistry will also be altered so that a direct comparison of the effect of the relaxation with and without the additive is not straightforward. In any case the consideration of this paper neglects this possibility.

Collisions of electrons with molecules in singlet states can contribute to spin relaxation through spin flips induced by spin–orbit coupling. Kessler[17] has reviewed the situation with respect to the effect of collisions on the spin polarization of low-energy electron beams. The electron beams for which experimental results are available have much more energy (60–600 eV or more) than the electrons in a spur. Since the depolarization effects are small in low atomic number materials (less than 1% spin flipping in H_2O for electrons of a few hundred eV) it can be taken as an indication that relaxation for the lower energy electrons of spurs in the same materials is unlikely. The radiation chemistry of materials which contain higher Z atoms (such as halogens) is also of interest, and in such systems spin–orbit coupling is enhanced[18] and electron spin relaxation in spurs should be more probable.

Although some measurements of T/S ratios are available, comparison with our theoretical values is far from straightforward. The predictions given here refer to initial ratios of triplet and singlet *manifolds* but not the ratios of the first excited triplet and singlet as measured by absorption and emission, respectively. Corrections for intersystem crossing must be made. There are also other complications in the interpretation of experimental results as mentioned in ref 15. Nevertheless, our simplified model of effects of subexcitation electrons on ion recombination (see section III) seems to give a picture not inconsistent with experimental data. The fraction f (eq B1) is estimated to be much less than unity from relative cross sections[14] of triplet production in electron impacts. Thus, from Table II, $\langle T/S \rangle \ll 7$. This prediction is in agreement with observations.[2-4] Furthermore, it is tempting to note that a small fraction ($\sim$30%) of spin exchange by subexcitation electrons will lead to $\langle T/S \rangle \approx 1$. This may furnish a rough explanation of the fact that in some hydrocarbons ion recombination has produced approximately equal initial yields of triplet and singlet excited states.[2]

Another possibility for production of triplet solvent molecules in spurs involves energy transfer from excited positive ions. This mechanism has been suggested[19] but

(15) B. Brocklehurst, *Nature (London)*, **221**, 921 (1969).
(16) O. H. Griffith and A. S. Waggoner, *Accounts Chem. Res.*, **2**, 17 (1969).
(17) J. Kessler, *Rev. Mod. Phys.*, **41**, 3 (1969).
(18) U. Fano and W. C. Martin in "Topics in Modern Physics, A Tribute to E. U. Condon," W. F. Brittin and H. Odabasi, Ed., Colorado Associated University Press, Denver, Colorado, 1971, p 147.
(19) A. Mozumder, private communication.

TABLE II: Theoretical T/S Ratios[a]

f	$(T/S)_1 = [f/1 - f]$	$\langle T/S \rangle$
0.0	0	0.5
0.10	1/9	0.6
0.20	1/4	0.8
0.30	3/7	1.0
0.40	2/3	1.2
0.50	1/1	1.5
0.60	3/2	1.8
0.70	7/3	2.2
0.80	4/1	2.6
0.90	9/1	3.3
1.00	∞	7.1

[a] f is the fraction of subexcitation electrons which produces direct triplet excitation. $(T/S)_1$ is the triplet/singlet ratio for a single ion pair. $\langle T/S \rangle$ is an average over the spur distribution of Mozumder and Magee.[10]

experimental evidence for it is nonexistent. The treatment in section III could be extended to cover this possibility.

A more significant correlation between the theoretical model and experimental data requires further efforts in both areas.

Appendix A

We consider the triplet formation probability on ion recombination for a spur with n ion pairs and n_T triplet molecules directly excited by the subexcitation electrons. Let $P_T(n,n_T)$ designate this probability. It is obvious from eq 3 that

$$P_T(n,0) = \frac{\omega_n - \omega_{n-1}}{\omega_n} \tag{6}$$

In a more formal development we can define the triplet probability as an ensemble average over the accessible states, *e.g.*

$$P_T(n,0) = \frac{\sum_{k=1}^{\omega_n} n_k^T}{\sum_{k=1}^{\omega_n} (n_k^T + n_k^S)} = \frac{N_T}{N_T + N_S} \tag{7}$$

where n_k^T and n_k^S are respectively the number of triplet and singlet bonds[13] in the kth state. Of course, $n_k^T + n_k^S = n$ for all k, and N_T and N_S are total numbers of triplet and singlet bonds. The total number of bonds is $(N_T + N_S) = n\omega_n$ in this case. The number of triplet bonds is the difference between the total number of bonds and the number of singlet bonds, $N_T = n\omega_n - n\omega_n(\omega_{n-1}/\omega_n)$. Substitution of this expression into eq 7 leads to eq 6.

The most convenient way to obtain $P(n,1)$ is by means of an analysis of the spur with $(n + 1)$ ion pairs. Consider such a spur and imagine that one ion pair recombines first; there are two categories of resulting states.

(i) The re-formed molecule is singlet; there are ω_n states in this category.

(ii) The re-formed molecule is triplet; there are $(\omega_{n+1} - \omega_n)$ states in this category.

The states in the category ii are the ones which are accessible to the system which has one triplet molecule excited by electron impact. The total number of triplet bonds in the ensemble, N_T^{ii}, contains the molecule directly excited by impact $(\omega_{n+1} - \omega_n)$ times, and by definition we are counting only triplets formed in the n ion pairs and must subtract out the directly excited triplets. This consideration gives

$$P_T(n,1) = \frac{N_T^{ii} - (\omega_{n+1} - \omega_n)}{N_S^{ii} + N_T^{ii} - (\omega_{n+1} - \omega_n)} \tag{8}$$

and the values of N_S^{ii} and N_T^{ii} are obtained as follows.

$$N_S^{i} + N_S^{ii} = N_S = (n + 1)\omega_{n+1}\frac{\omega_n}{\omega_{n+1}}$$

and

$$N_T^{i} + N_T^{ii} = N_T = (n + 1)\omega_{n+1}\left(1 + \frac{\omega_n}{\omega_{n+1}}\right) \tag{9}$$

The number of singlet bonds in i is

$$N_S^{i} = \omega_n + n\omega_n\frac{\omega_{n+1}}{\omega_n} = \omega_n + n\omega_{n-1} \tag{10}$$

while that of triplet bonds in i is

$$N_T^{i} = 0 + n\omega_n\left(1 - \frac{\omega_{n-1}}{\omega_n}\right) = n(\omega_n - \omega_{n-1}) \tag{11}$$

The number of singlet bonds in ii can be calculated by difference between the total given in eq 9 and N_S^i in eq 10

$$N_S^{ii} = N_S - N_S^{i} = n(\omega_n - \omega_{n-1}) \tag{12}$$

Also the number of triplet bonds in ii can be obtained as the difference between eq 9 and 11

$$N_T^{ii} = N_T - N_T^{i} = (n + 1)\omega_{n+1} - (2n + 1)\omega_n + n\omega_{n-1} \tag{13}$$

Thus, substitution of (12) and (13) into eq 8 gives

$$P_T(n,1) = \frac{\omega_{n+1} - 2\omega_n + \omega_{n-1}}{\omega_{n+1} - \omega_n} \tag{14}$$

Using a similar procedure the following formulas can be obtained

$$P_T(n,2) = \frac{\omega_{n+2} - 3\omega_{n+1} + 3\omega_n - \omega_{n-1}}{\omega_{n+2} - 2\omega_{n+1} + \omega_n} \tag{15}$$

$$P_T(n,3) = \frac{\omega_{n+3} - 4\omega_{n+2} + 6\omega_{n+1} - 4\omega_n + \omega_{n-1}}{\omega_{n+3} - 3\omega_{n+2} + 3\omega_{n+1} - \omega} \tag{16}$$

By inspection of (14–16) it can be assumed that the general formula is

$$P_T(n,n_T) = [\omega_{n+n_T} - (n_T + 1)\omega_{n+n_T-1} + \frac{(n_T+1)n_T}{2!}\omega_{n+n_T-2} - \frac{(n_T+1)n_T(n_T-1)}{3!}\omega_{n+n_T-3} + \cdots - (-1)^{n_T}\omega_{n-1}]/[\omega_{n+n_T} - n_T\omega_{n+n_T-1} + \frac{n_T(n_T-1)}{2!}\omega_{n+n_T-2} - \frac{n_T(n_T-1)(n_T-2)}{3}\omega_{n+n_T-3} + \cdots + (-1)^{n_T}\omega_n] \tag{17}$$

In these formulas $\omega_0 = 1$. The ω_j's satisfy the general relationship

$$\lim_{j\to\infty}\frac{\omega_j}{\omega_{j+1}} = \frac{1}{4} \tag{18}$$

so that we have for all values of n_T

$$\lim_{n\to\infty} P_T(n,n_T) = \frac{3}{4} \tag{19}$$

The use of $f \leq 1$ (in section II) corresponds to $n_T \leq n$. The formulas of Appendix A, however, do not involve this restriction.

Appendix B

If $F(n)$ is the track-average fraction of ions produced in spurs which have n ion pairs, the average triplet formation probability is given by

$$\langle P_T\rangle = \sum_{n=1}^{\infty}[f^nP_T(n,n) + nf^{n-1}(1-f)P_T(n,n-1) + \cdots + (1-f)^nP_T(n,0)]F(n) \quad (20)$$

where it is assumed that $n_T \leq n$. Thus

$$\langle P_T\rangle \leq [fP_T(1,1) + (1-f)P_T(1,0)]F(1) + [f^2P_T(2,2) + 2f(1-f)P_T(2,1) + (1-f)^2P_T(2,0)]F(2) + [f^3P_T(3,3) + 3f^2(1-f)P_T(3,2) + 3f(1-f)^2P_T(3,1) + (1-f)^3P_T(3,0)]F(3) + \left[\frac{3}{4}\right]F(>4) \quad (21)$$

because for $n > 4$, all values of $P_T(n,n_T)$ are close to 3/4 which is also the upper bound for them. Then, it can be shown that

$$\langle P_T\rangle \lesssim 0.477f + 0.212\left[\frac{4}{5}f^2 + \frac{4}{3}f(1-f) + \frac{1}{2}(1-f)^2\right] + 0.071\left[\frac{30}{43}f^3 + \frac{39}{19}f^2(1-f) + 2f(1-f)^2 + \frac{3}{5}(1-f)^3\right] + 0.240\left[\frac{3}{4}\right] \quad (22)$$

Finally the spur-averaged ratio

$$\langle T/S\rangle = \frac{\langle P_T\rangle}{1-\langle P_T\rangle} \quad (23)$$

can be estimated from the approximate value of $\langle P_T\rangle$ given by (22). Equations 22 and 23 were used to obtain the third column in Table II.

Excited States in the Nanosecond Pulse Radiolysis and Laser Flash Photolysis of *N,N*-Dimethylaniline[1a,b]

E. J. Land,*[1c] J. T. Richards, and J. K. Thomas

Chemistry Division, Argonne National Laboratory, Argonne, Illinois 60439 *(Received April 28, 1972)*

Nanosecond pulse radiolysis and laser flash photolysis of dimethylaniline (DMA) and its solutions lead to the observation of excited states rather than ions. Both techniques were used to characterize the absorptions of singlet excited DMA, triplet excited DMA, and the DMA exciplexes of anthracene, 1,2-benzanthracene, biphenyl, naphthalene, and pyrene. After such exciplexes had decayed the hydrocarbon triplet absorptions alone remained. Singlet excited DMA ($t_{1/2} \sim 3$ nsec) absorbs in the infrared and is monomeric. Triplet excited DMA ($t_{1/2} = 250$ nsec in pure DMA) absorbs at 465 nm, ϵ 5000 M^{-1} cm^{-1}. The triplet half-life increases when the DMA is dissolved in benzene or cyclohexane. The singlet→triplet crossover efficiency of DMA was estimated to be 0.95. The primary yields of triplet and singlet excited DMA on radiolysis were estimated to be 3.1 and 0.9, respectively. The absorption spectra, extinction coefficients, singlet→triplet crossover efficiencies, rates of formation, and rates of decay of the DMA–aromatic hydrocarbon exciplexes were estimated. Studies of the system anthracene plus DMA in cyclohexane show a "grow-in" of anthracene triplet at a rate equal to the DMA–anthracene exciplex decay rate. Thus, contrary to the conclusions of previous workers, such exciplexes do appear to fit into the normal pattern of the aromatic hydrocarbon triplet originating from the thermalized fluorescent state, in this case of the exciplex.

Introduction

The short-lived species observed following nanosecond pulse radiolysis of benzene alone[2] and its alkyl derivatives[3,4] have been attributed to excited states or products of the reaction of excited states. Addition of various solutes leads to the observation of solute singlet and triplet excited states formed *via* solvent–solute excitation transfer. Only low yields of ionic species have been detected in such systems.[2a,4] The short-lived intermediates found after nanosecond pulse radiolysis of aniline alone, on the other hand, have been assigned to ionic species exclu-

(1) (a) Work performed under the auspices of the U. S. Atomic Energy Commission; (b) Presented at the Conference on Elementary Processes in Radiation Chemistry, Notre Dame, Ind, April 4–7, 1972. (c) Address correspondence to The Paterson Laboratories, Christie Hospital and Holt Radium Institute, Manchester M20 9BX, England.

(2) (a) R. Cooper and J. K. Thomas, *J. Chem. Phys.*, **48**, 5097 (1968); (b) J. K. Thomas and I. Mani, *ibid.*, **51**, 1834 (1969).

(3) R. V. Bensasson, J. T. Richards, T. Gangwer, and J. K. Thomas, *Chem. Phys. Lett.*, **14**, 430 (1972).

sively,[5] namely, the solvated electron and the aniline positive ion. Solute triplet excited states were observed on adding various solutes to aniline but these were attributed to ion-recombination processes rather than solvent–solute excitation transfer.

The present study of *N,N*-dimethylaniline (DMA) was undertaken in order to elucidate further the roles of charge transfer and excitation transfer in the radiolysis of aromatic compounds. Both the radical cation[6] and triplet[7,8] absorptions of DMA are known. Emissions attributed to exciplexes (complexes between an excited singlet of one molecule and a ground state of another) formed between aromatic hydrocarbons and *N*-alkylanilines have been characterized, notably by Weller and coworkers,[9] using fluorescence techniques. The ultraviolet output of a frequency-doubled ruby laser at 347.2 nm makes it possible to excite pure DMA even though the ground state singlet absorption of the amine has a low extinction coefficient at this wavelength, ϵ 0.1 M^{-1} cm^{-1}. Therefore, in addition to nanosecond pulse radiolysis experiments, complementary studies of DMA and its solutions were carried out using nanosecond laser flash photolysis.

Experimental Section

The DMA (free of *N*-methylaniline) was supplied by Eastman Organic Chemicals. It was purified immediately before use by distillation under a low pressure of argon and was shielded from light. The various solutes used were the purest available commercially, further purified where necessary by crystallization or distillation. Samples were prepared using standard syringe techniques.

The pulse radiolysis system utilizing 3-, 12-, and 33-nsec pulses from a 3-MeV electron Van de Graaff accelerator has been previously described.[10-12] RCA IP 28 and Hamamatsu R213 photomultipliers were used in the range 350–700 nm (net time response of the system ~2 nsec), and a Philco Ford LP 4200 photodiode between 700 and 1600 nm (net time response of the system ~10 nsec). Monochromator bandwidths of between 1 and 10 nm were used. Radiation doses were measured using the absorption of solvated electrons in deaerated ethanol at 600 nm, taking ϵ_{600} 13,400 M^{-1} cm^{-1} [13] and $G_{e^-solv} = 1.5$.[14] The laser flash photolysis system utilizing 25-nsec, 347.2-nm pulses from a frequency-doubled ruby laser, has also been previously described.[12,15] The same detectors were used for both pulse radiolysis and flash photolysis experiments. In many cases deflections due to light emission were superimposed upon changes in absorption. These were separated by examining oscilloscope traces with and without the analyzing light; the effect of fluorescence emission on absorption signals was also minimized by pulsing the analyzing 450-W Xenon lamp as described previously.[12]

Results

A. Pulse Radiolysis Studies. 1. Dimethylaniline Alone. Figure 1a shows the absorption spectrum of argon-flushed DMA in the range 350–1600 nm immediately after a 12-nsec pulse of electrons. The ground state absorption of the solvent itself prevented measurements being made at shorter wavelengths. Three distinct species could be identified in the wavelength range studied. The first could be detected between 350 and 400 nm. In this region a further 10% build-up of absorption occurred over ~100 nsec after the pulse, after which the transient absorption decayed by first-order kinetics with a rate constant, determined at

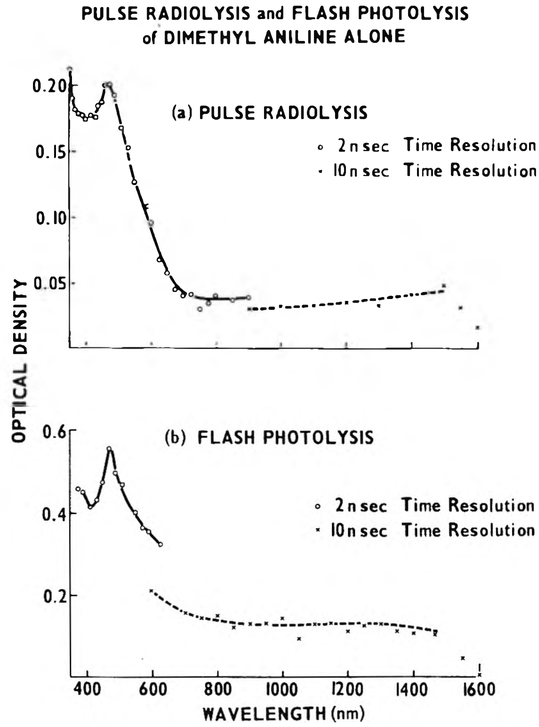

Figure 1. Transient absorption spectra after irradiation of pure DMA: (a) pulse radiolysis, immediately after 12-nsec pulse; O, response time ~2 nsec; ×, response time ~10 nsec; (b) laser flash photolysis, immediately after 25-nsec flash of 347.2-nm radiation; O, response time ~2 nsec; ×, response time ~10 nsec.

375 nm, of 1.6 × 10^6 sec^{-1}. The growth of absorption after the pulse in this region is reminiscent of the behavior of benzene and alkyl benzenes,[2b,3,4] where the corresponding species have been assigned to biradicals. Between 400 and 700 nm a second transient species was apparent. In this region no growth of absorption took place after the pulse and the species (λ_{max} 465 nm) decayed by first-order kinetics, $k_1 = 2.7 \times 10^6$ sec^{-1}. It seems likely that this species also possesses some absorption between 350 and 400 nm. Both the dimethylaniline cation radical[6] and DMA triplet[7,8] have peaks close to 465 nm. Above 700 nm a third much shorter lived transient intermediate was observed having a broad absorption stretching right up to the limit of the detection system (1600 nm). The observed decay rate of this species (<10 nsec) appeared to be determined by the response time of the detection system in this region. The short-lived absorption is similar in profile to that found with aniline itself, where the transient was assigned to the solvated electron.[5] The lifetime in DMA,

(4) J. T. Richards and J. K. Thomas, *J. Chem. Phys.*, **55**, 3636 (1971).
(5) R. Cooper and J. K. Thomas, *J. Chem. Phys.*, **48**, 5103 (1968).
(6) E. J. Land and G. Porter, *Trans. Faraday Soc.*, **59**, 2027 (1963).
(7) K. Kimura, S. Arimitsu, N. Yamamoto, and H. Tsubomura, *Bull. Chem. Soc. Jap.*, **41**, 1274 (1968).
(8) K. D. Cadogan and A. C. Albrecht, *J. Phys. Chem.*, **73**, 1868 (1969).
(9) H. Knibbe, D. Rehm, and A. Weller, *Ber. Bunsenges. Phys. Chem.*, **72**, 257 (1968).
(10) J. W. Hunt and J. K. Thomas, *J. Chem. Phys.*, **46**, 2954 (1967).
(11) J. K. Thomas, K. Johnson, T. Klippert, and R. Lowers, *J. Chem. Phys.*, **48**, 1608 (1968).
(12) J. K. Thomas, *J. Chem. Phys.*, **51**, 770 (1969).
(13) S. Arai and M. C. Sauer, *J. Chem. Phys.*, **44**, 2297 (1966).
(14) J. K. Thomas and R. V. Bensasson, *J. Chem. Phys.*, **46**, 4147 (1967).
(15) R. McNeil, J. T. Richards, and J. K. Thomas, *J. Phys. Chem.*, **74**, 2290 (1970).

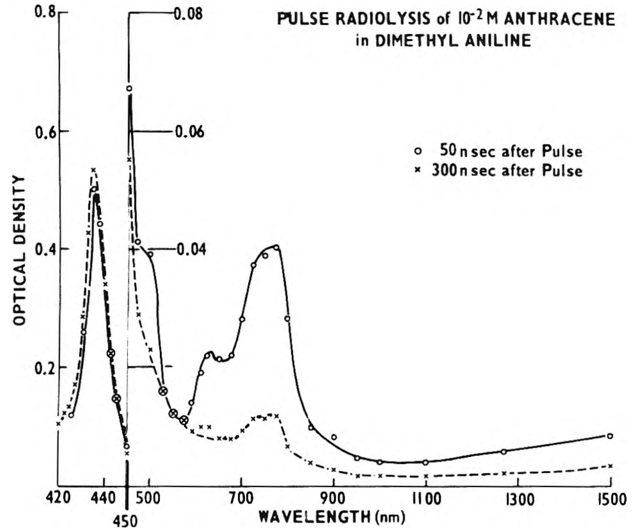

Figure 2. Transient absorption spectra after pulse radiolysis of 10^{-2} *M* anthracene in DMA, pulse length 3 nsec: O, 50 nsec after pulse; X, 300 nsec after pulse.

however, is much shorter than that observed in aniline ($t_{1/2} = 62.5$ nsec).

Between 350 and 400 nm an emission was detected on pulse radiolysis of DMA having a decay half-life of $\sim$3 nsec. No decrease in fluorescent light output occurred on increasing the temperature by $\sim$50°. An apparent decrease in the short-lived absorption intensity at 1500 nm on raising the temperature was explicable in terms of a decrease in lifetime rather than a decrease in initial absorption intensity.

2. *Anthracene Solutions in Dimethylaniline.* Addition of increasing amounts of anthracene to DMA caused a progressive increase in the decay rate of the 465-nm transient absorption, and an exactly corresponding growth of the intense anthracene triplet absorption with λ_{max} 435 nm in this solvent. These observations are explicable in terms of triplet energy transfer from DMA to anthracene and strongly suggest that the 465-nm absorption obtained here from DMA alone is due to DMA triplet–triplet absorption rather than absorption of the radical cation, $C_6H_5N(CH_3)_2^+$. The increase in 465-nm absorption decay on adding anthracene led to a rate constant for triplet energy transfer from DMA to anthracene of 1.4×10^{10} M^{-1} sec^{-1}. The same estimate for this rate constant was obtained from the growth of anthracene triplet absorption at 435 nm. This and other triplet energy transfer rates determined in this study using pulse radiolysis are collected in Table I. Figure 2 shows the full transient absorption spectrum in the range 420–1500 nm, 50 and 300 nsec after the pulse of 10^{-2} *M* anthracene in DMA. In addition to the anthracene triplet absorption, which lasts tens of microseconds, another shorter lived species with a maximum of 775 nm

TABLE I: Dimethylaniline Triplet Quenching Rate Constants in Dimethylaniline

Quencher	Rate constant, M^{-1} sec^{-1}
Anthracene	1.4×10^{10}
Biacetyl	5.9×10^{10}
Pyrene	9.0×10^{9}
Naphthalene	4.8×10^{9}
Piperylene	1.1×10^{10}

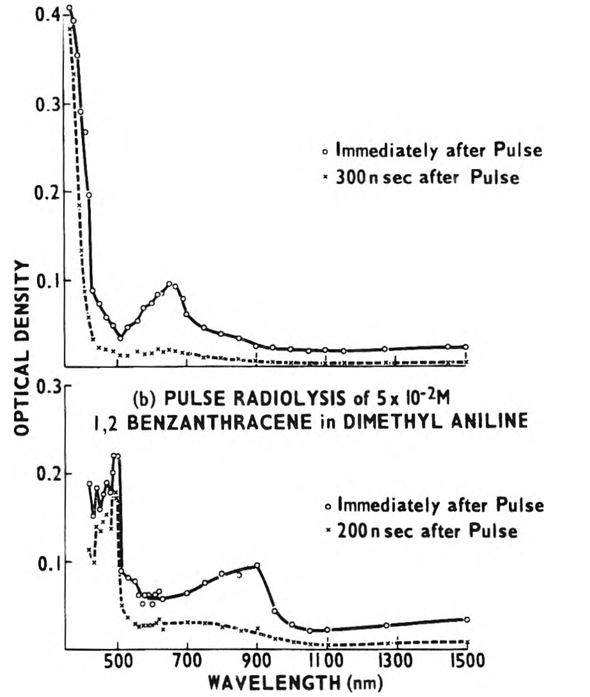

Figure 3. Transient absorption spectra after pulse radiolysis of (a) 10^{-1} *M* biphenyl in DMA, pulse length 3 nsec: O, immediately after pulse; X, 300 nsec after pulse; (b) 5×10^{-2} *M* 1,2-benzanthracene in DMA, pulse length 12 nsec: O, immediately after pulse; X, 200 nsec after pulse.

dominates the transient absorption in the range 600–1500 nm. Over the whole of this range the decay was first order, $k_1 = 1.3 \times 10^7$ sec^{-1}. The anthracene anion radical (and presumably also the corresponding cation radical) has a peak at 775 nm.[16] Such ions might be the cause of the 600–1500-nm absorption shown in Figure 2. However, a broad emission is observed on pulse radiolysis of 10^{-2} *M* anthracene in DMA which decays at exactly the same rate (1.3×10^7 sec^{-1}) as the absorption peak at 775 nm. Such emissions, which have been observed by Knibbe, *et al.*,[9] on photoexcitation of similar solutions, have been assigned to exciplexes, *i.e.*, singlet excited complexes between an aromatic hydrocarbon (acting as an acceptor of electrons) and an aromatic amine (acting as a donor of electrons). It is proposed, therefore, that the absorption with peak at 775 nm obtained on pulse radiolysis of anthracene in DMA is due to an exciplex formed between anthracene and DMA. Evidence in favour of this assignment is provided by the recent observation by Goldschmidt and Ottolenghi[17] of a similar absorption, with maxima at 740 and 630 nm, following the laser flash photolysis of a solution of anthracene ($\sim10^{-3}$ *M*) plus *N,N*-diethylaniline ($\sim$2 *M*) in toluene. This absorption, which again decayed at the same rate as an associated emission, was likewise attributed to the anthracene–diethylaniline exciplex.

3. *Biphenyl Solutions in Dimethylaniline.* Biphenyl is often used to detect ions in pulse radiolysis experiments with organic liquids[11] because of its scavenging ability and characteristic biphenyl anion absorption which occurs in a convenient region of the visible spectrum, λ_{max} 650 nm, ϵ 1.2×10^4 M^{-1} cm^{-1}.[16] Pulse radiolysis of 10^{-1} *M*

(16) K. H. Buschow, J. Dielman, and G. J. Hoijtink, *Mol. Phys.*, 7, 1 (1963).
(17) C. R. Goldschmidt and M. Ottolenghi, *Chem. Phys. Lett.*, 4, 570 (1970).

TABLE II: Dimethylaniline–Aromatic Hydrocarbon Exciplex Decay Constants

Aromatic hydrocarbon	Solvent	Technique[a]	Decay constant × 10^{-7} sec^{-1} Absorption	Emission
Anthracene	DMA	PR	1.3	1.3
Anthracene	Cyclohexane	FP	1.4	1.7
Naphthalene	DMA	PR	1.4	1.9
Naphthalene	Cyclohexane	FP	3.5	2.9
Biphenyl	DMA	PR	2.6	2.4
Biphenyl	Cyclohexane	FP	2.1	1.8
1,2-Benzanthracene	DMA	PR	1.8	1.4
1,2-Benzanthracene	Cyclohexane	FP	1.4	1.5
Pyrene	DMA	PR	1.2	1.0
Pyrene	Cyclohexane	FP	1.2	1.4
Pyrene	Benzene	PR		1.0

[a] PR = pulse radiolysis, FP = flash photolysis.

biphenyl in DMA (Figure 3a) did, in fact, lead to the observation of a transient absorption in the region where the biphenyl radical anion absorbs. The decay measured at 630 nm followed first-order kinetics, $k_1 = 2.6 \times 10^7$ sec^{-1}. Here again, however, a new broad emission appeared which decayed at the same rate (2.4×10^7 sec^{-1}) as the 630-nm absorption. It thus seems that the short-lived absorptions observed from aromatic solutions in DMA in the region where the corresponding radical anions absorb are predominantly due to exciplexes rather than simple radical anions or cations. Biphenyl triplet is also observed and the spectrum after 300 nsec (Figure 3a) is due exclusively to this species.

4. Other Solutions in Dimethylaniline. The spectra of solutions of 1,2-benzanthracene (5×10^{-2} *M*), naphthalene (10^{-1} *M*), and pyrene (3×10^{-2} *M*) in DMA following pulse radiolysis were also measured (Figures 3 and 4). In each case the spectra observed could be interpreted in terms of a combination of solvent–solute exciplex and solute triplet absorptions. The decay rates of the various exciplexes determined both in emission and absorption are collected in Table II.

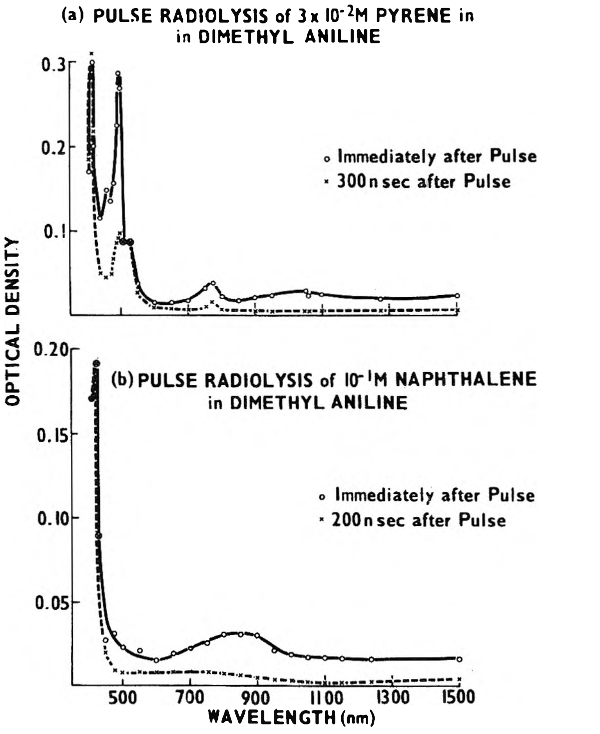

Figure 4. Transient absorption spectra after pulse radiolysis of (a) 3×10^{-2} *M* pyrene in DMA, pulse length 3 nsec: O, immediately after pulse; ×, 300 nsec after pulse; (b) 10^{-1} *M* naphthalene in DMA, pulse length 3 nsec: O, immediately after pulse; ×, 200 nsec after pulse.

Piperylene (10^{-1} *M*) was added to DMA alone since it is believed to quench triplet states more efficiently than singlet states.[18] This led to a 30% reduction in maximum fluorescence intensity, measured at 360 nm, and a 70% reduction in the maximum absorption intensity measured at 1460 nm. This difference in intensity reduction might exclude the possibility that the ir absorption and uv emission are due to the same species. However, it is clear that the response times of the detection system are not fast enough to allow unambiguous interpretation of the effect of scavengers on the very short-lived absorptions and emissions observed from DMA alone. Piperylene (10^{-1} *M*) did not affect the initial absorption intensity of DMA triplet although it did increase its rate of decay. The increase in decay rate, monitored at 465 nm, on adding 4×10^{-3} *M* piperylene led to a triplet quenching rate of 1.1×10^{10} M^{-1} sec^{-1}.

Saturation of DMA with the electron scavengers, N_2O and SF_6, led to an approximately 50% reduction in maximum fluorescence intensity and an approximately 80% reduction in the detected maximum intensity of short-lived infrared absorption. It is possible that these electron scavengers are behaving as singlet excited state quenchers here. N_2O apparently little affected the intensity or lifetime of DMA triplet absorption, whereas SF_6 decreased its lifetime from 370 to 70 nsec, although it did not affect its initial intensity. Addition of 10^{-1} and 1 *M* methanol, which has been used as a positive charge scavenger,[19] to DMA gave no significant change in the intensity or decay rate of triplet absorption at 465 nm. Addition of 10^{-4} *M* biacetyl to DMA resulted in an increase in the decay rate of the 465-nm triplet absorption. This gives a quenching rate constant of 5.9×10^{-10} M^{-1} sec^{-1}. The spectrum 50 nsec after pulse radiolysis of 10^{-2} *M* biacetyl showed no sharp peak at 465 nm[6] which might be due to the DMA positive ion. This indicates that biacetyl quenches DMA by energy transfer rather than charge transfer. Benzophenone also appeared to quench DMA triplet *via* energy

(18) A. A. Lamola, "Techniques of Organic Chemistry," Vol. XIV, P. A. Leermakers and A. Weissberger, Ed., Interscience, New York, N. Y., 1969, p 17.
(19) J. K. Thomas, *Annu. Rev. Phys. Chem.*, **21**, 17 (1970).

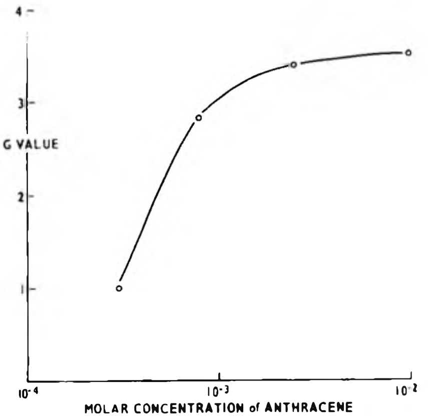

Figure 5. G value of anthracene triplet as a function of anthracene concentration in DMA.

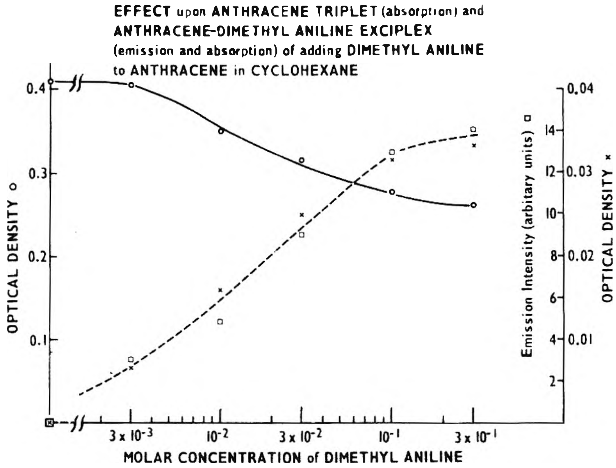

Figure 6. Effect upon anthracene triplet (absorption (430 nm, O)) and anthracene-DMA exciplex (emission (500 nm, □) and absorption (700 nm, ×)) of adding various amounts of DMA to 3.63×10^{-4} M anthracene in cyclohexane.

transfer rather than charge transfer. Xenon was also used as a solute since this molecule enhances intersystem crossing.[20] Saturation of 3×10^{-2} M pyrene in DMA with xenon did lead to some increase in the triplet yield, and a corresponding increase in exciplex decay rate. However, the rate constant for catalyzed intersystem crossing in this case is too small to cause complete S→T crossover under 1 atm pressure of xenon.

5. *Dimethylaniline in Other Solvents.* Pulse radiolysis of a solution of DMA in benzene and cyclohexane results in the formation of triplet DMA in both solvents. In benzene the decay rate at 465 nm ($k_1 = 2.6 \times 10^6$ sec^{-1}) is similar to that in pure DMA; in cyclohexane the lifetime is much longer ($k_1 \sim 6 \times 10^5$ sec^{-1}).

6. *Triplet Excited State G Values in Dimethylaniline.* Estimates of solute triplet yields in DMA were obtained from the extinction coefficients of the solute triplet–triplet transitions observed. In DMA the half-peak-height bandwidth of the anthracene triplet peak with maximum at 435 nm is 11 nm. In benzene the corresponding bandwidth is 12 nm[21] and the extinction coefficient is 45,550 M^{-1} cm^{-1}. On the assumption[21,22] that no change in oscillator strength occurs on changing the solvent from benzene to DMA, the corresponding maximum extinction coefficient in DMA is 49,700. Figure 5 shows the yield of anthracene triplet as a function of anthracene concentration employing this extinction coefficient. The maximum yield obtained at 10^{-2} M anthracene was $G = 3.5$. The yield of the triplet states of three other solutes were also estimated by taking their maximum triplet–triplet extinction coefficients to be likewise 9% above the corresponding values in benzene.[21] The values obtained were as follows: 10^{-1} M naphthalene, $G = 3.8$ (ϵ_{max} 14,400); 5×10^{-2} M 1,2-benzanthracene, $G = 3.5$ (ϵ_{max} 22,400); 3×10^{-2} M pyrene, $G = 3.6$ (ϵ_{max} 22,800).

B. Laser Flash Photolysis Studies. 1. Dimethylaniline Alone. Figure 1b shows the absorption spectrum of argon-flushed DMA in the range 375–1600 nm immediately after a 25-nsec flash of 347.2-nm radiation from the laser. This absorption spectrum is remarkably similar to that found after pulse radiolysis of DMA (Figure 1a), appearing to be made up of the same three transient species. Thus, between 375 and 400 nm the same small "grow-in" of absorption after the flash could be detected. A species with maximum at 465 nm was formed within the flash and decayed at the same rate (2.8×10^6 sec^{-1}) as the species with maximum at the same wavelength found using pulse radiolysis. Between 700 and 1600 nm a very short-lived species again occurred having a decay rate of ~10 nsec, the time resolution of the detection system in this region. Between 350 and 400 nm an emission (fluorescence) could be detected whose lifetime was short compared with that of the laser flash.

2. *Naphthalene Solutions in Dimethylaniline.* Naphthalene was chosen as a triplet scavenger to add to DMA as it absorbs only very weakly at the laser excitation wavelength of 347.2 nm. Addition of 3×10^{-2} M naphthalene (DMA absorbs 95% of the light in this solution) caused the rate of decay of 465-nm dimethylaniline transient absorption to increase, leading to a concurrent growth of intense absorption at 427.5 nm, the wavelength maximum of naphthalene triplet absorption. This observation confirms that the 465-nm transient absorption found on laser flash photolysis of DMA is due to triplet–triplet absorption, rather than the DMA positive ion, and leads to a DMA→naphthalene triplet transfer rate of 4.8×10^9 M^{-1} sec^{-1}. Comparison of the naphthalene triplet optical density at 427.5 nm (ϵ 14,400 M^{-1} cm^{-1}) caused by transfer from DMA triplet, with the DMA triplet optical density in the absence of naphthalene, gives[21] an estimate of 5000 M^{-1} cm^{-1} for the DMA triplet extinction at 465 nm.

3. *Anthracene with and without Dimethylaniline in Cyclohexane.* Addition of DMA to anthracene in a nonpolar solvent causes anthracene fluorescence to be quenched with the resultant appearance of anthracene–DMA exciplex emission.[9] Figure 6 shows the effect upon anthracene triplet absorption at 430 nm, anthracene–DMA exciplex emission at 500 nm, and the exciplex absorption at 700 nm, of adding increasing amounts of DMA, up to 3×10^{-1} M, to 3.63×10^{-4} M anthracene in cyclohexane. In such solutions nearly all the laser excitation light is absorbed by anthracene; even at 3×10^{-1} M DMA the amine absorbs less than 4% of the exciting light. Above 10^{-1} M DMA most of the anthracene singlets appear to be complexed. Figure 7 shows oscilloscope traces of the kinetics of growth of triplet absorption and decay of exci-

(20) T. Medinger and F. Wilkinson, *Trans. Faraday Soc.*, **61**, 620 (1965).
(21) R. Bensasson and E. J. Land, *Trans. Faraday Soc.*, **67**, 1904 (1971).
(22) D. Lavalette, R. Bensasson, B. Amand, and E. J. Land, *Chem. Phys. Lett.*, **10**, 331 (1971).

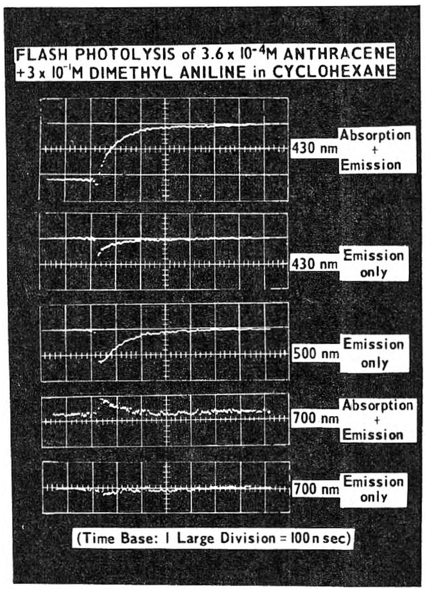

Figure 7. Oscilloscope traces of the flash photolysis of 3.63×10^{-4} M anthracene plus 3×10^{-1} M DMA in cyclohexane (time base: 1 large division = 100 nsec).

plex emission and absorption for 3.63×10^{-4} M anthracene plus 3×10^{-1} M DMA in cyclohexane.

Anthracene (3.63×10^{-4} M) in cyclohexane has an optical density (1.0) at 347.2 nm equal to that of DMA alone. Comparison of the triplet optical densities detected at 430 and 465 nm, respectively, on photolysis of each separately with equal energy flashes, gives[23] a S→T crossover efficiency for DMA of 0.95. This estimate was based on ϵ_{430} 64,700 M^{-1} cm^{-1} for anthracene triplet[21] and a S→T crossover efficiency for anthracene of 0.75.[20]

Comparison of the anthracene triplet optical density at 430 nm in the presence and absence of 3×10^{-1} M DMA (see Figure 6) likewise led to a S→T crossover efficiency estimate for the DMA-anthracene exciplex of $(0.26/0.41) \times 0.75 = 0.47$. This efficiency, together with the optical density at 700 nm observed in the presence of 3×10^{-1} M DMA, gives a value of 2700 M^{-1} cm^{-1} for the extinction coefficient of the DMA-anthracene exciplex at 700 nm, again based on ϵ_{430} 64,700 M^{-1} cm^{-1} for anthracene triplet.

4. Other Solutes Plus Dimethylaniline in Cyclohexane. The spectra of solutions of 1,2-benzanthracene (1.8×10^{-4} M) and pyrene (1.7×10^{-3} M) in cyclohexane containing 10^{-1} M DMA were measured immediately and several hundred nsec after the laser flash (Figure 8a and b). Comparison of the maximum triplet absorptions[21] from the above data with that obtained in the absence of DMA gives S→T crossover efficiencies of 0.46 and 0.38 for the DMA exciplexes of 1,2-benzanthracene and pyrene, respectively. These values were based on crossover efficiency estimates of 0.73[24] and 0.38[25] for 1,2-benzanthracene and pyrene, respectively, and the assumption that all singlets formed by the flash become exciplexes before decaying. These exciplex efficiencies together with the optical densities at 460 (1,2-benzanthracene) and 480 nm (pyrene), observed in the presence of 10^{-1} M DMA, give estimates of 11,600 and 9100 M^{-1} cm^{-1} for the corresponding exciplex extinction coefficients at 460 and 480 nm, respectively.

Saturation of 1.7×10^{-3} M pyrene plus 10^{-1} M DMA in cyclohexane with xenon led to a small increase in pyrene triplet yield, and corresponding increased exciplex decay rate, as found on pulse radiolysis of pyrene in DMA.

Discussion

1. Assignment of Transient Species. Three different species are observed on pulse radiolysis and flash photolysis of DMA alone. One has a peak at 465 nm, another absorbs in the infrared, and the third absorbs below 400 nm. Quenching of the 465-nm transient species by anthracene, leading to an exactly corresponding build-up of anthracene triplet absorption, shows that the 465-nm transient is due to a DMA triplet-triplet absorption. The short-lived infrared absorption could be due either to the solvated electron or an excited state. If it were an electron one might expect to observe the DMA positive ion at the same time. In view of the absence of absorption due to the positive ion, it is proposed that the species absorbing in the infrared is a singlet excited state. This assignment is supported by the consistency of the decay rate of the infrared absorption with the decay rate of the fluorescence. The lack of a temperature effect upon both fluorescence and infrared absorption intensities suggests that the singlet state is monomeric rather than excimeric. The species absorbing below 400 nm, from the delayed growth, appears to be similar to that found with benzene and alkyl benzenes and is assigned to a biradical.[2b,3,4]

Addition of various polycyclic aromatic solutes, *e.g.*, anthracene and biphenyl, to DMA in the case of pulse radiolysis, or to DMA in cyclohexane in the case of flash photolysis, results in the observation, together with solute triplet absorption, of solute-DMA exciplex absorptions.[17,26,27] Such exciplex absorptions are characterized by maxima close to the maxima belonging to the corresponding solute radical anions or cations. However, the kinetic characteristics of the absorptions and emissions detected (see Table II) suggest that the absorptions observed, both in the pulse radiolysis and flash photolysis experiments, are due predominantly to exciplexes rather than radical ions. It is interesting to note that the same exciplex absorptions were observed using pulse radiolysis, where the DMA is excited initially, and using laser flash photolysis, where the polycyclic aromatic is excited initially.

The lack of detection of absorptions due to ions contrasts with previous observations on the nanosecond pulse radiolysis of aniline[5] and its solutions. The observations in DMA in the time scale studied are much more similar to previous observations on benzene and its alkyl derivatives.[2-4,12]

2. Excited State G Values. Use of the extinction coefficient of 5000 M^{-1} cm^{-1} for the DMA triplet-triplet absorption at 465 nm gives a total DMA triplet G value of 4.0. Part of this triplet originates *via* intersystem crossing from singlet excited DMA, $G(S_0)$, the remainder being formed directly, $G(T_0)$. Estimates of $G(S_0)$ were obtained as follows: in pure DMA

$$G(T_0) + 0.95G(S_0) = 4.0$$

(23) J. T. Richards, G. West, and J. K. Thomas, *J. Phys. Chem.*, **74**, 4137 (1970).
(24) W. Heinzelmann and H. Labhart, *Chem. Phys. Lett.*, **4**, 20 (1969).
(25) A. R. Horrocks and F. Wilkinson, *Proc. Roy. Soc., Ser. A*, **306**, 257 (1968).
(26) C. R. Goldschmidt, R. Potashnik, and M. Ottolenghi, *J. Phys. Chem.*, **75**, 1025 (1971).
(27) R. Potashnik, C. R. Goldschmidt, M. Ottolenghi, and A. Weller, *J. Chem. Phys.*, **55**, 5344 (1971).

where 0.95 is the S→T crossover efficiency of DMA; in 10^{-2} *M* anthracene

$$G(T_0) + 0.47G(S_0) = 3.5$$

where 0.47 is the S→T crossover efficiency of the anthracene–DMA exciplex. Solving these two equations gives $G(S_0) = 1.0$ and $G(T_0) = 3.0$. Corresponding estimates for $G(S_0)$ of 1.0 and 0.7 and $G(T_0)$ of 3.0 and 3.3 were obtained from the data already given for 1,2-benzanthracene and pyrene, respectively. In principle, it would also be possible to estimate $G(S_0)$ using exciplex extinction coefficients but the values appropriate to DMA as solvent may differ widely from those obtained here in cyclohexane. Also, had the infrared time resolution been better, the extinction coefficient of singlet excited DMA could have been obtained and thus, together with the data of Figure 1, would have given rise to another estimate of $G(S_0)$.

Mean values for $G(S_0)$ of 0.9 ± 0.3 and $G(T_0)$ of 3.1 ± 0.4 will be taken. These *G* values appear to be somewhat lower than the corresponding values[28] found for benzene, $G(S_0) = 1.6$ and $G(T_0) = 4.2$. The present values in DMA may be less accurate in view of the uncertainties in the extinction coefficients and crossover efficiencies used. The total triplet yields are, however, certainly higher than those obtained in aniline;[5] no singlet yield data are available for this solvent.

3. Rates of Formation and Decay of Exciplexes. The data of Figure 6 may be used to obtain an estimate of the rate of quenching (k_q) of singlet excited anthracene by DMA in cyclohexane. The concentration of 2×10^{-2} *M* DMA corresponds to one-half the maximum intensity of exciplex absorption and emission. At such a concentration the decay of anthracene singlet to its ground state ($t_{1/2}$ = 4 nsec)[10] equals its decay rate *via* quenching by DMA. Hence, $k_q = 0.9 \times 10^{10}\ M^{-1}\ \text{sec}^{-1}$. This compares with the corresponding values of 0.88, 1.65, 0.19, and $2.1 \times 10^{10}\ M^{-1}\ \text{sec}^{-1}$ measured by Knibbe, *et al.*,[9] for anthracene singlet quenching by DMA in toluene, dimethoxyethane, amyl alcohol, and acetonitrile, respectively. The quenching of singlet excited perylene[29] and pyrene[30] by DMA also occurs at a rate close to diffusion controlled.

The rates of decay of the exciplexes observed in this study, both in absorption and emission, are collected in Table II. The value obtained here for the pyrene–DMA exciplex decay in cyclohexane (1.3×10^7 sec^{-1}) is rather lower than a previous estimate[30] of 2.3×10^7 sec^{-1} from emission measurements. A decay constant of 0.53×10^7 sec^{-1} has also been obtained previously[31] for this exciplex in *n*-hexane.

4. Intersystem Crossing in Exciplexes. Previous studies[26] using laser flash photolysis of anthracene (and several other aromatics) in the presence of diethylaniline revealed no "grow-in" of anthracene absorption at a rate consistent with the decay of exciplex emission. For 10^{-2} *M* anthracene plus 0.5 *M* diethylaniline in toluene all the anthracene triplet appeared within 15 nsec of the end of the flash, whereas the exciplex emission decayed with a half-life of ~50 nsec. These observations were taken to suggest that the usual assumption that singlet→triplet intersystem crossing in an aromatic molecule occurs from the thermalized lowest excited singlet state, in competition with fluorescence, does not hold for these exciplexes. A coincidental identity between exciplex and triplet absorption spectra was also recognized as a possibility to explain the lack of observation of triplet "grow-in," but was considered extremely unlikely. It was instead suggested[26] that here the S→T transition is induced by the very act of quenching the first excited singlet state of anthracene by diethylaniline. Accordingly, an alternative scheme was proposed to explain the formation of triplets independently of the relaxed fluorescent charge-transfer state of the exciplex. This scheme involved the formation of an encounter complex (^{1}A*D) between the singlet excited anthracene ^{1}A* and the diethylaniline (D). From this state, radiationless transitions take place rapidly *either* to the charge-transfer state (A$^-$D$^+$)* which emits, *or* to a dissociative "locally excited" triplet state (^{3}A*D) which yields triplet anthracene.

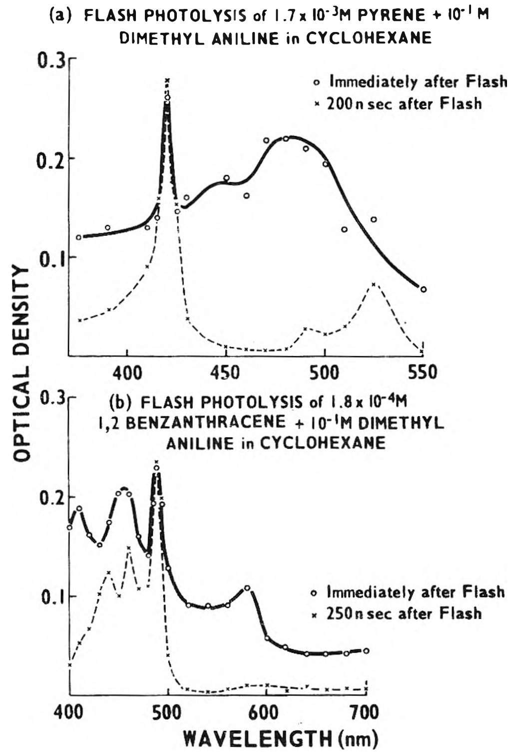

Figure 8. Transient absorption spectra after flash photolysis of (a) 1.7×10^{-3} *M* pyrene plus 10^{-1} *M* DMA in cyclohexane: O, immediately after flash: ×, 200 nsec after flash; (b) 1.8×10^{-4} *M* 1,2-benzanthracene plus 10^{-1} *M* DMA in cyclohexane; O, immediately after flash; ×, 250 nsec after flash.

The results obtained here for a similar system 3.6×10^{-4} *M* anthracene plus 3×10^{-1} *M* DMA in cyclohexane (Figure 7) show clearly that a "grow-in" of anthracene triplet, consistent with the decay of exciplex emission and absorption, *does* occur. The data of Figure 7 were obtained under experimental conditions where the interference of emission with absorption measurements was much less apparent than in the data of Goldschmidt, *et al.*[26] It is, therefore, suggested that such exciplexes do, in fact, fit into the normal pattern of the triplet state originating from the thermalized fluorescent state. Little apparent

(28) J. H. Baxendale and M. Fiti, *J. Chem. Soc., Faraday Trans. 2*, **68**, 218 (1972).
(29) W. R. Ware and H. P. Richter, *J. Chem. Phys.*, **48**, 1595 (1968).
(30) K. Yoshihara, T. Kasuya, A. Inoue, and S. Nagakura, *Chem. Phys. Lett.*, **9**, 469 (1971).
(31) N. Mataga, T. Okada, and N. Yamamoto, *Chem. Phys. Lett.*, **1**, 119 (1967).

"grow-in" of triplet was observed for exciplexes involving pyrene (Figure 8a), in agreement with Goldschmidt, *et al.*,[26] or with 1,2-benzanthracene (Figure 8b). This we attribute to coincidence of the corresponding triplet and exciplex absorptions.

Acknowledgments. E. J. L. wishes to thank Argonne National Laboratory for a Visiting Scientist Fellowship during which this work was carried out, and the Paterson Laboratories, Christie Hospital and Holt Radium Institute, Manchester, England, for a leave of absence.

Lifetime Distribution Function for Geminate Ion Pairs and Its Importance to the Kinetics of Ionic Reactions in the Radiolysis of Hydrocarbon Solutions[1]

Robert H. Schuler* and Pierre P. Infelta

Radiation Research Laboratories, Center for Special Studies and Department of Chemistry, Mellon Institute of Science, Carnegie-Mellon University, Pittsburgh, Pennsylvania 15213 *(Received May 1, 1971)*

Publication costs assisted by the U. S. Atomic Energy Commission and Carnegie-Mellon University

The concentration dependence for the reaction between ions produced in the radiolysis of hydrocarbons and solutes added to scavenge these ions can be related to the Laplace transform of the distribution of lifetimes of the ion pairs in the pure hydrocarbon. It is shown that this Laplace transform provides a phenomenological model which allows the derivation of the concentration dependence of secondary ionic reactions in a quite general way, even without an explicit expression for the lifetime distribution function. It is also shown that given an appropriate reaction scheme certain limitations are placed on the importance of secondary reactions as a natural result of the short lifetime ot most of the ion pairs. Measurements on electron scavenging by the alkyl halides have given an algebraic expression which appears to represent the concentration dependence for the scavenging process quite accurately. Use of this expression allows one to make quantitative predictions from the above mentioned relationships. A number of examples have already been considered and are summarized. Two new examples are treated here: the effect of electron scavengers on the HD yields from ND_3 solutions and the production of H_2 and I_2 from HI solutions. An explicit description for the distribution of ion pair lifetimes can be derived by taking the inverse Laplace transform of the observed scavenging dependence. Some general comments are made on the characteristics and consequences of this description as it applies to the direct observation of intermediates in pulse experiments.

It has now been generally recognized for a number of years that large yields of ions are produced in the radiolysis of hydrocarbons but that, for the most part, these ions recombine rapidly and enter into chemical reactions to a significant extent only with very reactive solutes present at relatively high concentrations. The present vigorous interest in ion scavenging kinetics dates back to about 1964 when Scholes and Simic[2] found large yields of nitrogen in the radiolysis of cyclohexane solutions of nitrous oxide and attributed the formation of this product to electron capture processes. At about the same time Williams[3] observed that HD was formed in the irradiation of ND_3 solutions and suggested proton transfer from solvent ions to the ND_3 as the source of this HD. Williams and Hamill[4] had, in fact, indicated 10 years earlier that for alkyl halide solutions dissociative electron capture by the solute could be responsible for large yields of alkyl radicals but uncertainties in distinguishing between the reactions of electrons and hydrogen atoms made kinetic experiments difficult to interpret.[5] This situation clarified in the late 1960's with improvement in analytical procedures which resulted in the accumulation of large amounts of accurate experimental information and it was possible to present a reasonably cohesive statement on electron scavenging processes at the time of the 1968 Argonne Conference on Radiation Chemistry.[6] At the present time a considerable amount of experimental information is available and a reasonably clear phenomenological picture has emerged. We are now in a position to use this picture to discuss quantitative aspects of various secondary ionic processes. It is the purpose of this contribution to discuss first some general ramifications of what can be called the phenomenological model of ion scavenging kinetics and then to summarize available information which makes it possible to apply this model analytically to a number of systems of interest. Finally we will review the significance

(1) Supported in part by the U. S. Atomic Energy Commission. Presented at the Conference on Elementary Processes in Radiation Chemistry, University of Notre Dame, Notre Dame, Ind., April 4–7, 1972.
(2) G. Scholes and M. Simic, *Nature (London)*, **202**, 895 (1964).
(3) T. F. Williams, *J. Amer. Chem. Soc.*, **86**, 3954 (1964).
(4) R. R. Williams, Jr., and W. H. Hamill, *Radiat. Res.*, **1**, 158 (1954).
(5) R. H. Schuler, *J. Phys. Chem.*, **61**, 1472 (1957).
(6) J. M. Warman, K.-D. Asmus, and R. H. Schuler, *Advan. Chem. Ser.*, **No. 82**, 25 (1968).

of the scavenging information as it applies to the lifetimes of ion pairs in the hydrocarbon itself.

Phenomenological Model

In the radiolysis of liquid hydrocarbons and other media of low dielectric constant, the majority of the electrons produced are thermalized at sufficiently short distances from their positive ion partners that the coulombic energy between the ions is considerably larger than their kinetic energy. Charge collection,[7] product analysis,[8] and pulse radiolytic[9] experiments all demonstrate quite conclusively that only a few per cent of the ions can be truly regarded as "free ions," *i.e.*, as having escaped the coulombic potential of their partner so that they become homogeneously distributed throughout the medium. The reactions of these free ions presumably can be treated by classical kinetic methods. The remaining ions, with which we are primarily concerned here, are present as charge pairs which are constrained by the coulombic potential between them and as a result will undergo charge recombination. The ions of these pairs have become known as "geminate ions." Recombination of these geminate ions is very rapid and significant reaction with a solute will occur only if both the rate constant for the reaction and the solute concentration are sufficiently high to allow competition with this recombination. This fact was reasonably clear even as early as 1957.[5] The kinetics of the reactions of these geminate ions is expected to be complicated since the ionic lifetimes depend upon the distances from the positive ion at which the electrons are thermalized. In any real radiation chemical system a distribution of distances will be represented. Following the initial example of Williams,[3] a number of workers have attempted to discuss the concentration dependence for scavenging in terms of a physical model of the ion recombination process which takes as its starting point a description of the ion pair separation distances. Kinetically speaking it is the period available for chemical reaction and not the separation distance *per se* that is important. Unfortunately there is not a 1:1 correspondence between these two quantities since for any given separation distance a distribution of lifetimes exists. Application of the physical model to scavenging kinetics involves either an implicit or explicit transformation of the distribution of initial ion pair separation distances into ionic lifetimes. No complete analytical solution has, as yet, been obtained, even for a given distribution of separation distances, although the limiting case of large separation distances has recently been treated rigorously.[10] It has, in fact, not even been demonstrated that the problem possesses a formal solution although, from very recent work,[11,12] it now appears possible to obtain some of the characteristics of a general solution by application of numerical methods. In the phenomenological approach outlined here one takes the concentration dependence of the yield observed for an appropriate scavenging reaction and deduces from the distribution of ion pair lifetimes. As is described below, this can be done in a very general way and the result provides us with a tool with which we can describe other ionic phenomena in which we are interested.

In the following we will make use of three functional dependences: (1) $F(\mathrm{S})$, the scavenging function which is taken as the fraction of ions of a particular type that react with a solute present at concentration [S]; (2) $F(t)$, the existence function representing the fraction of ion pairs that is extant in the hydrocarbon at time t in the absence of a reactive solute; and (3) $\mathrm{f}(t)$, the lifetime distribution function, the fraction of ions which recombine in the interval $\mathrm{d}t$ at time t, again in the pure hydrocarbon. The second and third dependences are directly related.

$$\mathrm{f}(t) = -\mathrm{d}F(t)/\mathrm{d}t \tag{1}$$

We will assume that the scavenging reaction is well described by pseudo-first-order kinetics[13] so that the probability that an ion which has a lifetime t in the pure hydrocarbon will react with a solute is

$$\int_0^t k[\mathrm{S}]e^{-k[\mathrm{S}]t'}\mathrm{d}t'$$

where k is the rate constant for the scavenging reaction. If we sum this quantity over all ion pairs we can directly write the total scavenging probability as

$$F(\mathrm{S}) = \int_0^\infty \mathrm{f}(t)(1 - e^{-k[\mathrm{S}]t})\mathrm{d}t$$
$$= 1 - \int_0^\infty \mathrm{f}(t)e^{-k[\mathrm{S}]t}\mathrm{d}t \tag{2}$$

The application of eq 2 to ion scavenging kinetics was first pointed out by Hummel[14] and other workers have since used this equation in the treatment of a number of specific problems. It is convenient to incorporate the rate constant k into the argument of the scavenging function so that $\mathfrak{F}(k[\mathrm{S}] = F(\mathrm{S})$ and rewrite eq 2 as

$$\int_0^\infty \mathrm{f}(t)e^{-k[\mathrm{S}]t}\mathrm{d}t = 1 - \mathfrak{F}(k[\mathrm{S}]) \tag{3}$$

in which case $\mathrm{f}(t)$ is the inverse Laplace transform of $1 - \mathfrak{F}(k[\mathrm{S}])$. It is a general property of Laplace transforms that inversion of the image function ($1 - \mathfrak{F}(k[\mathrm{S}])$ in this case) will give a unique description of the original function ($\mathrm{f}(t)$). Thus, the experimental determination of the scavenging function for any one solute gives the information necessary to specify the form of $\mathrm{f}(t)$ and it remains only to measure k to place $\mathrm{f}(t)$ on a correct absolute time scale. Equation 3 is the mathematical description of what is referred to here as the phenomenological model.

The existence function $F(t)$ can be obtained by summing all recombination processes which occur at times greater than t, *i.e.*

$$F(t) = \int_t^\infty \mathrm{f}(t)\mathrm{d}t \tag{4}$$

Equivalently one can invert the auxiliary transform

$$\int_0^\infty F(t)e^{-k[\mathrm{S}]t}\mathrm{d}t = \frac{\mathfrak{F}(k[\mathrm{S}])}{k[\mathrm{S}]} \tag{5}$$

Equation 5 can be derived from eq 1 and 3 if one integrates the left-hand side of eq 3 by parts or, alternatively, obtained directly by integrating the product of the frequency of the scavenging reaction ($k[\mathrm{S}]e^{-k[\mathrm{S}]t}$) and the

(7) W. F. Schmidt and A. O. Allen, *J. Phys. Chem.*, **72**, 3730 (1968).
(8) S. J. Rzad and J. M. Warman, *J. Chem. Phys.*, **49**, 2361 (1969).
(9) C. Capellos and A. O. Allen, *J. Phys. Chem.*, **74**, 840 (1970).
(10) J. L. Magee and A. B. Tayler, *J. Chem. Phys.*, **56**, 3061 (1972).
(11) G. Abell, A. Mozumder, and J. L. Magee, *J. Chem. Phys.*, **56**, 5422 (1972).
(12) P. P. Infelta, *J. Chim. Phys.*, in press.
(13) Strictly speaking the assumption of pseudo-first-order kinetics is not rigorously correct because ions are produced to a fair extent in multiple pairs. However at any particular scavenger concentration, the period for scavenging ($1/k[\mathrm{S}]$) is long with respect to the recombination period for most of the ions which are not scavenged so that effectively only single pairs exist in the vicinity of the scavenger at the time of reaction. Because of this, local depletion becomes relatively unimportant and a pseudo-first-order kinetic treatment should be a good approximation.
(14) A. Hummel, *J. Chem. Phys.*, **49**, 4840 (1968).

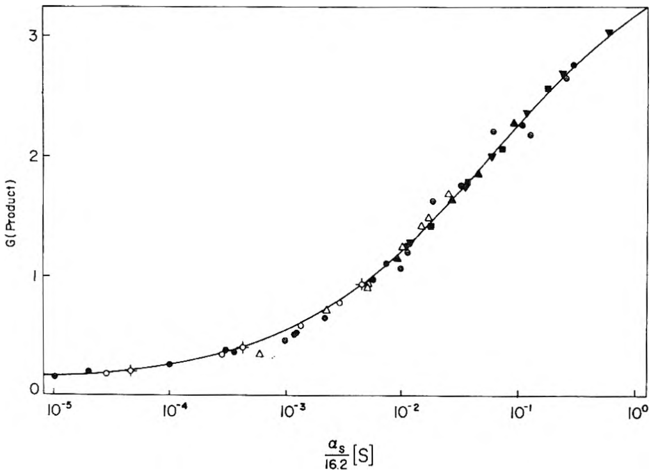

Figure 1. Concentration dependence of product yield from various scavengers in cyclohexane. Solid curve is a plot of eq 13 with G_{fi} = 0.12, G_{gi} = 3.80, and $\alpha(CH_3Br)$ = 16.2 M^{-1} and summarizes the results from ref 15 on CH_3Br, C_2H_5Br, and CH_3Cl solutions. Data for solutes other than CH_3Br are shifted on the concentration axis by multiplying the concentration by the appropriate α_S. Data represented are ●, independent data on CH_3Br (from reference 23); ▼, CF_3Br (present work, $\alpha(CF_3Br)$ = 19.5 M^{-1}); ■, CF_3Cl (present work, $\alpha(CF_3Cl)$ = 6.0 M^{-1}); ▲, C_2F_5Br (present work, $\alpha(C_2F_5Br)$ = 15.0 M^{-1}); ⊙, $C_6H_5CH_2Cl$ (from ref 25, α = 16 M^{-1}); △, ND_3 (ordinates are (4/3)HD yields, from ref 16, $\alpha(ND_3)$ = 0.85 M^{-1}); and ○, cyclopropane (total yields from ref 29, $\alpha(c\text{-}C_3H_6)$ = 0.40 M^{-1}). The points designated by ⌖ are for cyclopropane solutions containing a large concentration of CCl_4 and used to determine r_D (see eq 12 and ref 17).

fraction ($F(t)$) of ions extant at time t over all time (to give $\mathfrak{F}(k[S])$).

An algebraic description of the scavenging function was suggested by Warman, Asmus, and Schuler[6] and the application of this description makes it possible to treat certain types of experimental information analytically and in detail. We will review this approach below. However, before doing so we would like to present certain general arguments in order to emphasize the fact that many conclusions can be arrived at without knowledge of the algebraic form of either $f(t)$ or $F(S)$.

While it may at first seem peculiar, one must recognize that the results from experiments in which scavengers have been added to the system give information on the ionic lifetime in the absence of solutes. The lifetime distribution function applicable in eq 3 must, of course, be a characteristic of the hydrocarbon and cannot contain any quantity which pertains to the individual solutes. It follows directly that as long as scavenging involves a simple reaction with one of the ions *the form of the scavenging function cannot depend on the particular scavenger and will, in fact, be identical for the reactions of both positive ions and electrons.* As is seen in eq 3 the concentration must be scaled by a kinetic factor proportional to the rate constant k. Previously it was shown[15] that the concentration dependences for the production of methyl and ethyl radicals from methyl chloride, methyl bromide, and ethyl bromide are all of the same form with the kinetic factors being in the ratios of 5.4:16.2:7.8, respectively. The dependence observed in these cases is indicated by the solid curve in Figure 1. Superimposed on this curve are data for a number of additional electron and positive ion scavengers. It is seen that within experimental error all of these solutes do indeed exhibit a common concentration dependence.

Various situations which arise when two or more solutes are present can be analyzed in a very general way in terms of the experimentally observed scavenging function. For example, if two solutes S_1 and S_2 compete for reaction of either electrons or positive ions with respective rate constants k_1 and k_2 then one can determine the total probability for reaction $F(S_1,S_2)$ simply by integrating the probability that reaction will occur with either of the solutes $(1 - \exp(-(k_1[S_1] + k_2[S_2]t))$ over the distribution of lifetimes, *i.e.*

$$F(S_1,S_2) = \int_0^\infty f(t)(1 - e^{-(k_1[S_1]+k_2[S_2])t})dt = 1 - \int_0^\infty f(t)e^{-(k_1[S_1]+k_2[S_2])t}dt \quad (6)$$

The last integral of eq 6 is given by the Laplace transform $1 - \mathfrak{F}(k_1[S_1] + k_2[S_2])$ so that

$$F(S_1,S_2) = F([S_1] + \frac{k_2}{k_1}[S_2]) \quad (7)$$

Thus the total fractional scavenging can be determined from a master curve such as that given in Figure 1 by adding to the concentration of the first solute the concentration of the second one appropriately scaled to take into account the relative scavenging rates. It is these relative rates that are usually the most difficult to determine accurately but, where solutes can be examined directly, can be obtained from the relative concentrations required to effect the same fractional scavenging.

A very important problem, which can be formulated similarly, is the distribution of reaction between the two scavengers. Reaction with solute S_2 will occur with a frequency $k_2[S_2]\exp(-k_2[S_2]t)$ provided prior reaction has not occurred with S_1. Thus for electrons of lifetime t, the probability for scavenging by S_2 is

$$\int_0^t k_2[S_2]e^{-k_2[S_2]t'}e^{-k_1[S_1]t'}dt' = \frac{k_2[S_2]}{k_1[S_1] + k_2[S_2]}(1 - e^{-(k_2[S_2]+k_1[S_1])t}) \quad (8)$$

Integrating this quantity over the distribution of lifetimes gives $F(S_2)_{S_1}$, the probability for scavenging by S_2 in the presence of S_1.

$$F(S_2)_{S_1} = \frac{k_2[S_2]}{k_1[S_1] + k_2[S_2]}\int_0^\infty f(t)(1 - e^{-(k_2[S_2]+k_1[S_1])t})dt = \frac{1}{1 + \frac{k_1[S_1]}{k_2[S_2]}}(F(S_1,S_2)) \quad (9)$$

This probability can be determined from the master curve provided one knows the relative scavenging rates. For two scavengers $F(S_1,S_2) > F(S_1)$ so that as one adds a second scavenger the increase in product from it will be more rapid and the decrease from the first scavenger less rapid than would be estimated on the assumption that the yield was constant. Equations 7 and 9 are intuitively obvious but the above is given in order to emphasize that they can be derived without an explicit description of either $f(t)$ or $\mathfrak{F}(k[S])$.

Other more interesting cases can be treated in a similarly general way. If one assumes a particular reaction scheme then certain consequences must necessarily follow

(15) J. M. Warman, K.-D. Asmus, and R. H. Schuler, *J. Phys. Chem.*, **73**, 931 (1969).

as the result of the limited lifetime of the ion pairs. As examples we will consider here two cases involving the effect of electron scavengers on products from positive ion reactions. Both cases involve the general reaction scheme

$$RH \longrightarrow RH^+ + e^-$$

$$RH^+ + e^- \longrightarrow \text{products not observed}$$

$$RH^+ + P \xrightarrow{k_p} P^+$$

$$P^+ + e^- \longrightarrow \text{products observed}$$

$$e^- + N \xrightarrow{k_n} N^-$$

$$P^+ + N^- \longrightarrow \begin{matrix} \text{products not observed (case 1)} \\ \text{products observed} \quad \text{(case 2)} \end{matrix}$$

and differ only in the net chemical effect of the last reaction.

Case 1. First we will treat the case where measurable product is produced only when the secondary positive ion is neutralized by an electron. Asmus[16] has recently indicated that qualitatively this appears to be tbe case for the production of HD from ND_3 solutions in cyclohexane since the addition of electron scavengers substantially reduces the HD yield. For a given ion pair the probability that positive ion scavenging will occur is $1 - \exp(-k_p[S_p]t)$ and that electron scavenging will not occur is $\exp(-k_n[S_n]t)$. The fraction of the positive ions that will give the desired product in the presence of the electron scavenger is, therefore

$$F(P \rightarrow \text{products})_{S_n} = \int_0^\infty f(t)\left(1 - e^{-k_p[S_p]t}\right)\left(e^{-k_n[S_n]t}\right) dt$$
$$= \int_0^\infty f(t)e^{-k_n[S_n]t}dt - \int_0^\infty f(t)e^{-(k_p[S_p] + k_n[S_n])t}dt \tag{10}$$

The integrals of the right-hand side of eq 10 are given by their Laplace transforms $1 - \mathfrak{F}(k_n[S_n])$ and $1 - \mathfrak{F}(k_n[S_n] + k_p[S_p])$ so that the fractional yield expected is

$$F(P \rightarrow \text{products})_{S_n} = F\left([S_n] + \frac{k_p}{k_n}[S_p]\right) - F(S_n) \tag{11}$$

The general nature of this relationship is illustrated in Figure 2 in terms of the hypothetical scavenging function $F(S_n)$ given by the solid curve. The fractional yield expected from the proposed scheme is the difference between the values of $F(S_n)$ at the concentrations $[S_n] + (k_p/k_n)[S_p]$ and $[S_n]$. Equation 11 will be applied below to the experimental data after considering the analytical description of the scavenging function.

Case 2. The second limiting case concerns the situation when the same product is obtained from neutralization of the secondary positive ion by either an electron or secondary anion. It also is the case where the product is formed from the positive ion prior to neutralization. This case has been treated in detail in considering the effect of electron scavengers on the reaction of positive ions with cyclopropane.[17] Experimentally it is observed that addition of electron scavengers to cyclohexane solutions of cyclopropane results in an increased yield of product from the cyclopropane. If the time scale for neutralization were unaffected by the scavenging of electrons then the fraction of the positive ions which react would not be expected to change upon addition of an electron scavenger. However the yields do increase and it is obvious that the lifetimes of the positive ions are increased as a result of the conversion

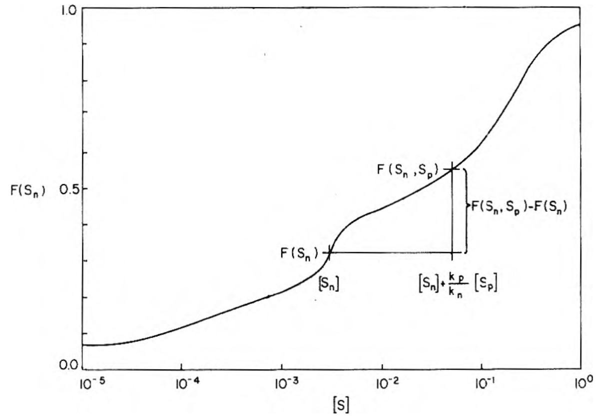

Figure 2. Hypothetical electron scavenging function. Application of the generalized approach in determining product yields is illustrated for the example when neutralization of the positive ions by secondary anions does not give product. The fractional yields are given by the difference in the scavenging function $F(S_n)$ at the concentration $[S_n] + k_p/k_n[S_p]$ and $[S_n]$ (see eq 11 in text).

of the electrons to massive less mobile negative ions. Effectively one can use the positive ion reaction to probe the change in the period required for neutralization which results from the conversion of electrons to less mobile negative ions.

This case can be treated exactly if it is assumed that positive ions having a lifetime t in the absence of scavenger will, if capture occurs at time t', have their remaining lifetime $t - t'$ extended by a constant factor r_D.[18] The appropriate integrals have been written previously.[17] All are reducible to Laplace transforms which can be evaluated in terms of the general scavenging function. The result in this case, in terms of the positive ion scavenging function $F(S_p)$, is

$$F(P)_{S_n} = F\left(S_p + \frac{k_n}{k_p}[S_n]\right) + \frac{1}{1 + \frac{k_p}{k_n}\frac{[S_p]}{[S_n]}(1 - r_D)} \times \left[F(r_D[S_p]) - F\left([S_p] + \frac{k_n}{k_p}[S_n]\right)\right] \tag{12}$$

One needs only to know k_p/k_n, r_D and the values of $F(S_p)$ at the equivalent concentrations $([S_p] + (k_n/k_p)[S_n])$ and $r_D[S_p]$ in order to determine the yields expected from the assumed scheme. One can see from eq 12 that at very high concentrations of electron scavenger, where $(k_p[S_p]/k_n[S_n](1 - r_D)$ approaches zero, the fractional reaction approaches the limit $F(r_D[S_p])$. Thus introducing a large concentration of electron scavenger affects the yields in a manner equivalent to increasing the positive ion scavenger concentration by the factor by which the lifetime has been extended and one needs only to determine the shift of the scavenging curve on a logarithmic concentration axis to determine r_D. This fact was previously pointed out[17] and used to obtain an estimate ~ 20 for r_D.

All cases where pseudo-first-order kinetics apply can be treated in a similarly general manner since the integrals

(16) K.-D. Asmus, *Int. J. Radiat. Phys. Chem.*, **3**, 419 (1971).

(17) S. J. Rzad, R. H. Schuler, and A. Hummel, *J. Chem. Phys.*, **51**, 1369 (1969).

(18) It can be demonstrated that the factor r_D is constant for all ion pair lifetimes and for all times of electron capture provided that the radius at which neutralization occurs is independent of whether the negative entity is an electron or negative ion (P. P. Infelta, Ph.D. Dissertation, Carnegie-Mellon University, 1971).

reduce to Laplace transforms which have experimentally definable values. One would mention here as typical chemical problems which are tractable secondary charge transfer reactions (such as can be important for multiple solute systems), reactions of ionic product with the ion scavenger itself (*e.g.*, the high nitrogen yields observed from nitrous oxide solutions indicate that a short ionic chain may be involved),[19] and situations involving the solute as both electron and positive ion scavengers (such as appears to be the case for HI solutions). The first two of these situations have already been treated in detail using an algebraic description of the scavenging function[19,20] but the more general approach outlined here is, in fact, just as applicable. In these previous studies we have attempted to stress that the conclusions were general and that algebraic methods were introduced purely as a convenience for computational purposes but it is easy to overlook this generality because attention tends to be focused on the rather involved expressions that result. In a report presented at this conference Rzad[21] treats the kinetics of the production of excited states as a result of various charge recombination processes. Again, while his treatment uses an explicit algebraic description for the scavenging function to discuss the expected concentration dependences, the treatment can, in fact, be made quite general.

Scavenging Function

It is convenient to have an algebraic description of $F(\mathrm{S})$ available for application of the more general model discussed above. It has rigorously been shown[10] that the limiting dependence at low solute concentrations must be linear in the square root of the solute concentration[22] but the dependence at the usual experimental concentrations is not known from first principles. Experimentally it has been found[14] that the radiation chemical yields of methyl and ethyl radicals from methyl bromide, methyl chloride, and ethyl bromide solutions in cyclohexane are described within experimental error by the expression

$$G(\mathrm{R}) = G_{\mathrm{fi}} + G_{\mathrm{gi}} \frac{\sqrt{\alpha_{\mathrm{S}}[S]}}{1 + \sqrt{\alpha_{\mathrm{S}}[S]}} \quad (13)$$

where G_{fi} and G_{gi} can be interpreted as the yields of free and geminate ion pairs and α_{S} is a parameter proportional to the rate constant of the scavenging reaction. Experimentally α_{S} is equal to the reciprocal of the concentration at which 50% of the geminate ions are scavenged. While eq 13 is not necessarily an exact description of the concentration dependence it does provide us with a means for working with the phenomenological model. The scavenging function which corresponds to this experimentally observed relationship is

$$F(\mathrm{S}) = \frac{\sqrt{\alpha_{\mathrm{S}}[S]}}{1 + \sqrt{\alpha_{\mathrm{S}}[S]}} \quad (14)$$

We will review here the experimental data which substantiate eq 13.

Alkyl Halides. The experimental studies on cyclohexane solutions of the alkyl halides carried out in these laboratories have been documented previously.[14] In the initial study,[14] various tests were carried out which demonstrated that the effect being examined was predominantly and very probably the exclusive result of electron capture by the solute. Over the concentration range 10^{-4}–0.5 M the yields observed in experiments where the radicals were trapped with iodine[14] are described to ~2% by eq 13 with $G_{\mathrm{fi}} = 0.12$ and $G_{\mathrm{gi}} = 3.8$ if α_{S} is taken as 16.2 M^{-1} for methyl bromide, 7.8 for ethyl bromide, and 5.4 for methyl chloride.[14] The dependence calculated for methyl bromide with the above parameters is given by the solid curve in Figure 1. The solid circles in the figure are the independent data of Warman and Rzad[23] determined by measuring the production of $^{14}CH_4$ from $^{14}CH_3Br$ solutions.

Perfluoroalkyl Halides. Previously unreported data on the concentration dependence of radical yields from the irradiation of cyclohexane solutions of perfluoromethyl and ethyl bromide and perfluoromethyl chloride are presented here. Radioiodine scavenging methods were employed and the yields of $CF_3{}^{131}I$ and $C_2F_5{}^{131}I$ were determined by separating these products gas chromatographically and trapping and counting them as previously described.[24] In this case a significant fraction of the CF_3 and C_2F_5 radicals abstract hydrogen from the solvent at the iodine scavenger concentrations (~1 mM) normally used in this type of experiment. The dependence of yield on iodine concentration was determined for solutions 0.1 M in CF_3Br or C_2F_5Br (see ref 24) and the data extrapolated to infinite iodine concentration by assuming a simple competitive scheme for the reactions of the radicals. Least-means-square treatment of these data indicates that the error involved in the extrapolation is ~3%. Correction factors were determined from these data ($1 + (2.94 \times 10^{-4})/[I_2]$ for CF_3 radicals and $1 + (1.5 \times 10^{-4})/[I_2]$ for C_2F_5 radicals) and were applied to the yields observed at other solute concentrations so that all data have been treated in a consistent fashion. The internal agreement can be seen from the corrected yields of 2.46, 2.39, 2.31, 2.32, 2.36, 2.34, 2.34, and 2.36 determined in eight measurements on 0.1 M CF_3Br with iodine concentrations ranging from 0.1 to 4 mM. Usually two or three determinations were made at each solute concentration. Since the agreement between experiments was mostly within a few per cent it is not possible to display the individual data easily and only the average value at any one concentration is plotted in Figure 1. It is seen that the data fall very nicely on the curve for the alkyl halides. The reactivity parameters determined from these measurements are $\alpha(CF_3Br) = 19.5\ M^{-1}$, $\alpha(CF_3Cl) = 6.0\ M^{-1}$, and $\alpha(C_2F_5Br) = 15.0\ M^{-1}$.

Benzyl Chloride. Prior to the studies on the alkyl halides mentioned above, Hagemann and Schwarz[25] examined benzyl chloride solutions in cyclohexane by pulse radiolytic methods. Their data on the production of benzyl radical are given by the doubled circles in Figure 1. While the experimental data show considerably more scatter than do the other results it is obvious that they fit the general framework outlined above quite well. Taking the yields at face value the reactivity parameter appears

(19) P. P. Infelta and R. H. Schuler, *Int. J. Rad. Phys. Chem.*, in press.
(20) P. P. Infelta and R. H. Schuler, *J. Phys. Chem.*, **76**, 987 (1972).
(21) S. J. Rzad, *J. Phys. Chem.*, **76**, 3722 (1972).
(22) Mozumder has commented that the square root dependence appears to be a general result of diffusion control of recombination processes in the long time limit and is applicable to ion recombination since at larger separation distances the coulombic terms involved cause only a small perturbation in the diffusional motion (A. Mozumder, *J. Chem. Phys.*, **55**, 3026 (1971)).
(23) J. M. Warman and S. J. Rzad, *J. Chem. Phys.*, **52**, 485 (1970).
(24) P. P. Infelta and R. H. Schuler, *J. Phys. Chem.*, **73**, 2083 (1969).
(25) R. J. Hagemann and H. A. Schwarz, *J. Phys. Chem.*, **71**, 2694 (1967).

to be very similar to that for methyl bromide (*i.e.*, ~16 M^{-1}).

Perfluorocyclohexane. Sagert, Reid, and Robinson[26] have published a very comprehensive study of the formation of $C_6F_{11}H$ in the radiolysis of cyclohexane solutions of perfluorocyclohexane. They attributed this product exclusively to electron capture by the perfluorocyclohexane and find that the form of the concentration dependence is described extremely well by eq 13. They give parameters of G_{fi} = 0.14, G_{gi} = 4.2, and $\alpha(C_6F_{12})$ = 30 M^{-1}. Since perfluorocyclohexane should be relatively inert to attack by radical species generated in this system this study helps considerably in assuring that extraneous chemical reactions of radicals do not significantly perturb the form of the scavenging function given by eq 13.

Ammonia. Williams was the first to attempt the quantitative interpretation of scavenging kinetics and his ideas were based on measurements of HD production from ND_3 solutions in cyclohexane.[3] In this early study he showed that the HD yield was approximately proportional to the square root of the ammonia concentration. More recent measurements by Asmus on this system[16] show slightly higher yields than reported by Williams at low ND_3 concentration but otherwise corroborate his values. The yields multiplied by a statistical factor of 4/3 (which assumes ND_3H^+ as an intermediate positive ion and neglects any isotope effect on the production of H or D atoms upon neutralization) are plotted in Figure 1. The reactivity parameter required to superimpose these data on the scavenging function is 0.85 M^{-1}. Rzad has measured $\alpha(NH_3)$ to be 1.0 M^{-1} by a competitive method.[27] With this latter value one can predict from eq 13 that a yield of 1.29 of secondary positive ions will be produced at an ND_3 concentration of 0.2 M. A comparison of this predicted value with the experimentally observed yield of 0.93(1.29/0.93 = 1.38) tends to substantiate the statistical factor of 1.33 introduced above. The form of the concentration dependence is seen to be that required by the scavenging function obtained from the electron scavenging experiments. One cannot, however, perform a meaningful exptrapolation to the high concentration limit since the practical region of measurement is restricted to concentrations where less than 50% of the geminate positive ions react.

Cyclopropane. Ausloos and coworkers demonstrated in 1966[28] that 1,1,2,2,3,3-hexadeuteriopropane is produced in the irradiation of hydrocarbon solutions of cyclopropane-d_6. Various observations suggested that a positive ion reaction was involved. The yield was found to be proportional to the square root of the cyclopropane concentration. Rzad and Schuler[29] carried out extensive studies on cyclopropane labeled with ^{14}C and showed that several other products were produced in reactions parallel to the formation of the propane. The yields of total product were determined in cyclohexane for cyclopropane concentrations from 10^{-4} to 10^{-1} M and are plotted in Figure 1. It is seen that these data also exhibit the same concentration dependence found in the other experiments. The parameter α_Δ = 0.40 M^{-1} is required to fit the data to the scavenging function.

Other Hydrocarbons. While much of the attention in scavenging kinetic studies has been directed toward cyclohexane solutions, various workers have examined other hydrocarbons. Rzad and Warman[23] applied the $^{14}CH_3Br$ technique to hexane and 2,2,4-trimethylpentane and more recently Rzad and Bansal[30] have studied 2,2,4-trimethylpentane further by both the $^{14}CH_3Br$ method and by radical trapping with $^{131}I_2$. Sagert and Reid[31] have examined perfluorocyclohexane solutions in hexane, 3-methylpentane, and 2,2,4-trimethylpentane. The present authors have studied methyl bromide solutions in 3-methyloctane both at room temperature and at lower temperatures (down to −160°).[32] All of these studies show a dependence on solute concentration similar in form to that for cyclohexane and it is found that with appropriate choice of parameters the data can be fitted within experimental error by eq 13.[33]

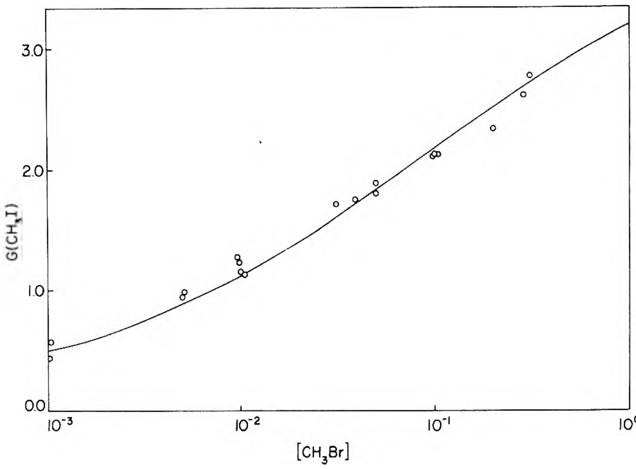

Figure 3. Concentration dependence of methyl radical yields from CH_3Br solutions in squalane as determined by the $^{131}I_2$ trapping technique. Solid curve corresponds to eq 13 with G_{fi} = 0.1, G_{gi} = 4.0, and α = 12 M^{-1}.

In order to examine possible effects of viscosity on the scavenging function we have measured the methyl radical yields from methyl bromide solutions in squalane and report the results here. Squalane ($C_{30}H_{62}$) is a high molecular weight liquid saturated hydrocarbon of high viscosity. The decay of electrons in it has been examined directly by Taub and Gillis[34] in pulse experiments at low temperature. Thomas[35] has also examined the decay of biphenylide anion from biphenyl solutions in this material at room temperature. In the present study the methyl radical yields were measured by the radioiodine trapping method[15] and the yields, after correction for a yield of 0.08 from the hydrocarbon itself, are plotted in Figure 3. Squalane is quite difficult to work with because of its viscosity and low vapor pressure. It was subjected to column chroma-

(26) N. H. Sagert, J. A. Reid, and R. W. Robinson, *Can. J. Chem.*, **47**, 2655 (1969).
(27) S. J. Rzad, Abstracts of the 185th National Meeting of the American Chemical Society, New York, N. Y., Sept 12–19, 1969.
(28) P. Ausloos, A. A. Scala, and S. G. Lias, *J. Amer. Chem. Soc.*, **88**, 1583 (1966); *ibid.*, **88**, 5701 (1966).
(29) S. J. Rzad and R. H. Schuler, *J. Phys. Chem.*, **72**, 228 (1968).
(30) S. J. Rzad and K. M. Bansal, *J. Phys. Chem.*, **76**, 2374 (1972).
(31) N. H. Sagert and J. A. Reid, *Can. J. Chem.*, **48**, 2429 (1970).
(32) P. P. Infelta and R. H. Schuler, to be submitted for publication.
(33) Measurements have been carried out on the production of N_2 from N_2O solution in a large variety of hydrocarbons (see, for example, M. G. Robinson and G. R. Freeman, *J. Chem. Phys.*, **48**, 983 (1968); **55**, 5644 (1971)). While the yields qualitatively exhibit the same form for the concentration dependence as given in Figure 1 the yields are, at a given solute concentration, considerably higher than those for other solutes and it seems almost certain that processes other than electron capture by the N_2O contribute (see ref 19). Because of this, these dependences are not taken as a good measure of the scavenging function.
(34) I. A. Taub and H. A. Gillis, *J. Amer. Chem. Soc.*, **91**, 6507 (1969).
(35) J. K. Thomas, private communication.

tography in an attempt to purify it and then outgassed at elevated temperature on a vacuum line. The radioiodine and methyl bromide were added to the outgassed sample directly on the vacuum line. While the data scatter somewhat more than in the cases of the other hydrocarbons it is clear that the form of the concentration dependence is described quite well by eq 13. The solid curve is a plot of this equation with G_{gi} taken as 4.0, $\alpha(CH_3Br)$ as 12 M^{-1}, and G_{fi} as 0.1 (from the results of clearing field experiments).[36]

Some General Comments on the Scavenging Function. At this point, since eq 13 is purely an empirical description of the experimental results, one should ask how well does it fit the data and whether or not additional terms are manifest in the experimental results. To this purpose we have examined the available data critically using a best-fit least-mean-square polynomial regression routine from the Hewlett-Packard 9100 Program Library.

At very low concentrations of scavenger the yield of ionic reaction should be linear in the square root of the scavenger concentration[10] and extrapolate to the free ion yield. Experimentally this appears to be the case.[8,31,37] The data of ref 15 and 23 on methyl radical production from CH_3Br solutions (27 points) were combined and fitted by polynomials in $[S]^{1/2}$. The result obtained for a sixth-order fit was

$$G(CH_3) = 0.123 + 14.3[S]^{1/2} - 47.4[S] + 167[S]^{3/2} - 484[S]^2 + 742[S]^{5/2} - 422[S]^3 \quad (15)$$

This expression describes the data extremely well (rms deviation between calculated and observed values of 0.02). It has no inflection point below 0.05 M so that in the low concentration region (<0.05 M) it represents a function with continuously decreasing slope (as required by eq 3 since $f(t)$ can never be negative). It compares quite well with the power series expansion of eq 13 which, with G_{gi} = 3.8 and α = 16.2 M^{-1}, gives

$$G(CH_3) = 0.12 + 15.2[S]^{1/2} - 61.5[S] + 247[S]^{3/2} - \ldots \quad (16)$$

The limiting slope at low concentrations (14.3) is seen to be within 10% of the value (15.2) required by the measurements at high concentrations. The slight difference reflects, to a certain extent, the truncation of the series in fitting the data to the polynomial (as also do the differences in the higher order terms). One can conclude that there is no significant departure from eq 13 up to a concentration corresponding to $\alpha[S]$ = 0.5. It should be noted that in eq 15 and 16 the third and fourth terms contribute significantly at all concentrations above $\sim 10^{-4}$ M so that a fall off from the square root dependence is important even at this low a concentration. It is obvious from this fact that the limiting case treated by Magee and Tayler[10] applies only to extremely low solute concentrations.

It is more important to detail the behavior of the scavenging function at high concentrations since the functional dependence in this region is not known from first principles. As the solute concentration is increased it is qualitatively expected that the yield will monotonically increase but that, because a competition is involved, the slope of a plot of yield *vs.* concentration should continuously decrease as the yield approaches the limiting value given by the total number of ions produced in the system. (As mentioned above this is required by the model since $f(t)$ must be positive.) In the region in which experimental information is usually accumulated the functional dependence must, as a result, be less than the limiting proportionality to the ½ power of the solute concentration and it is not too surprising that eq 13 is a good approximation to the observed yields. Since a plateau must be approached ultimately, no series involving positive powers of solute concentration can describe the high concentration data (eq 16, for example, does not converge for concentrations above 1/16.2 M). The data were, therefore, tested by examining $(G(CH_3) - G_{fi})^{-1}$ as a function of $[S]^{-1/2}$. If eq 13 applies the coefficients of all powers of $[S]^{-1/2}$ higher than one should be zero.

A difficulty in handling the data now arises since the change of variable results in an incorrect weighting of the experimental results. Attempts to fit the data over a wide concentration range to a polynomial in $[S]^{-1/2}$ produced curves with pronounced inflections as a result of very slight deviations of the data from a smooth function at low concentrations. This difficulty was avoided by using eq 15 to represent the smoothed data below 10^{-2} M. Combining values calculated from this expression for concentrations in the region 10^{-2} to 10^{-4} M with the experimental results above 10^{-2} M the solid curve of Figure 4 was obtained for the 6th order fit (eq 17).

$$(G(CH_3) - 0.123)^{-1} = 0.273 + 0.0588[S]^{-1/2} + 0.00092[S]^{-1} - 3.1 \times 10^{-5}[S]^{-3/2} + 5.3 \times 10^{-7}[S]^{-2} - 4.2 \times 10^{-9}[S]^{-5/2} + 1.3 \times 10^{-11}[S]^{-3} \quad (17)$$

It is seen that there is a very slight parabolic term which contributes $\sim$2% at a concentration of 10^{-1} M. The higher order terms are trivially small except for very high values of $[S]^{-1/2}$. There are no inflection points below $[S]^{-1/2}$ = 18 and the slope of the function for values of the argument from 10 to 100 is essentially constant. Qualitatively, therefore, eq 17 has the properties expected for a scavenging function. The solid curve of Figure 4 can be compared with the linear plot of eq 13 (given by the dashed curve with $1/G_{gi}$ = 0.263 and $1/(G_{gi}\sqrt{\alpha})$ = 0.0654). It is seen that the differences are small and well within experimental error.

Equation 15 describes the data in cyclohexane below 10^{-2} M CH_3Br and eq 17 the data above 10^{-4} M. Both are approximated very well by eq 13. *One concludes,* therefore, *that at both low and high solute concentrations eq 13 is a very accurate representation of the total phenomenological situation.* Such deviations as occur can affect derived conclusions only at very high solute concentrations ($\alpha[S] > 10$) and then only to second order. Deviations will principally be significant with respect to the time dependence of the ion population at very short times (see below) and to extrapolations of the observed data to infinite solute concentration. For example, the geminate ion yield obtained from an extrapolation *via* eq 17 is 3.67 or 0.13 units lower than obtained by the linear extrapolation implicit in eq 13. It seems unlikely that the dependence of Figure 4 can have any significant curvature that is not accounted for reasonably well by eq 17. Assuming that in these scavenging studies the radicals are produced with unit efficiency and that no other processes contribute to the yield, a value of 3.7 ± 0.2 is assigned to the geminate ion yield in cyclohexane. A nominal value of 3.8 for

(36) W. Schmidt and A. O. Allen, *J. Chem. Phys.*, **52**, 2345 (1970).
(37) S. J. Rzad and R. H. Schuler, *J. Phys. Chem.*, **72**, 228 (1968).

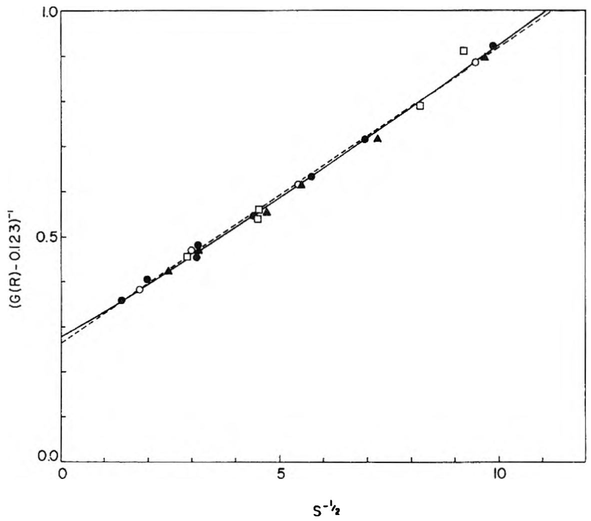

Figure 4. Competitive plot according to eq 13. Data are from ref 15 (, CH_3Br; ▲, C_2H_5Br; and □, CH_3Cl) and from 23 (o, CH_3Br). Concentrations of C_2H_5Br and CH_3Cl are multiplied by 8.7/16.2 and 5.4/16.2, respectively. Dashed line is the linear plot of eq 13 with G_{fi} = 0.12, G_{gi} = 3.80, and $\alpha(CH_3Br)$ = 16.2 M^{-1}. Solid curve is sixth-order best-fit polynomial given by eq 17. This curve is essentially linear in the region from $[S]^{-1/2}$ = 10–100 (see text).

G_{gi} is, however, recommended for use with eq 13. The value of $G_{gi}\sqrt{\alpha}$ (= 15.3 for CH_3Br) can be known quite accurately from the slope of plots such as those in Figure 4. The individual values of α will reflect the uncertainty in the extrapolated limit but different solutes can be intercompared quite well since this latter term cancels.

Application of the Scavenging Function to the Phenomenological Model

To date the scavenging function given by eq 13 has been applied to four cases involving secondary ionic processes: (1) the effect of electron scavengers on positive ion transfer to cyclopropane;[17] (2) a consideration of the competition between secondary electron transfer between different scavengers and both decay and neutralization of the anions initially produced;[20] (3) the possible production of nitrogen by secondary processes in N_2O solutions;[19] and (4) the production of excited states as a result of ion recombination.[21] The reader is referred to the various publications for details. Something of the algebraic complexity that can arise is illustrated by the result obtained in the second example. If electrons can be captured by two solutes S_1 and S_2 then in the case where the anion produced from S_1 has a lifetime τ and reacts with S_2 with a rate constant k_e the fraction of the electrons which are captured by S_1 but which are ultimately transferred to S_2 before the anion S_1^- dissociates or is neutralized is given by[20]

$$F_{exch}(S_2)_{S_1} = \int_0^\infty f(t)\mathrm{d}t \int_0^\infty k_1[S_1]e^{-(k_1[S_1]+k_2[S_2])t'}\mathrm{d}t' \times \int_0^{(t-t')r_D} e^{-t''/\tau}k_e[S_2]e^{-k_e[S_2]t''}\mathrm{d}t'' \quad (18)$$

(In an example such as this the appropriate integrals can be written quite readily with the aid of a diagram of the reaction time coordinate; see Figure 2 in ref 20.) The integrals can all be evaluated with the aid of eq 3 and 13. Taking into account the reactions involving the free ions, the yield of product from solute 1 in the presence of solute 2 is

$$G(S_1)_{S_2} = \frac{\alpha_1[S_1]}{\alpha_1[S_1]+\alpha_2[S_2]}\left[\left(1-\frac{\beta_e[S_2]}{\beta_e[S_2]+\delta_1}\right)G_{fi} + G_{gi} \times \frac{\sqrt{\alpha_1[S_1]+\alpha_2[S_2]}}{1+\sqrt{\alpha_1[S_1]+\alpha_2[S_2]}}\,Q\right] \quad (19)$$

where

$$Q = 1 - \frac{\beta_e[S_2]}{\beta_e[S_2]+\delta_1}\left[1 - \frac{\alpha_1[S_1]+\alpha_2[S_2]}{\alpha_1[S_1]+\alpha_2[S_2]-(\beta_e[S_2]+\delta_1)} \times \left(1 - \frac{\sqrt{\beta_e[S_2]+\delta_1}\,(1+\sqrt{\alpha_1[S_1]+\alpha_2[S_2]})}{1+\sqrt{\beta_e[S_2]+\delta_1}\,(\sqrt{\alpha_1[S_1]+\alpha_2[S_2]})}\right)\right] \quad (19a)$$

In eq 19 β_e is an exchange parameter related to α_1 by the relationship $\beta_e = (k_e/k_1)r_D\alpha_1$ and δ_1 is a lifetime parameter given by $\delta_1 = r_D\alpha_1(k_1\tau_1)^{-1}$. While eq 19 appears to be complicated, it can be evaluated in a quite straightforward manner (see ref 20) and is a complete description which follows directly from the reaction scheme assumed.

HD Yields from ND_3 Solutions. We will now consider several additional examples. The first is the effect of electron scavenging on the HD yield from ND_3 solutions. The general treatment was outlined above. With the aid of eq 13 to describe the scavenging function in eq 11, the HD yield is given by

$$G(\mathrm{HD}) = \frac{3}{4}G_{gi}\left(\frac{\sqrt{\alpha_n[S_n]+\alpha_p[S_p]}}{1+\sqrt{\alpha_n[S_n]+\alpha_p[S_p]}} - \frac{\sqrt{\alpha_n[S_n]}}{1+\sqrt{\alpha_n[S_n]}}\right) \quad (20)$$

According to the assumed reaction scheme the free ions do not contribute since positive ion neutralization will always occur with a secondary anion. All of the parameters of eq 20 are known from experiments on systems containing only ND_3 or electron scavenger so that an *a priori* prediction of the dependence of the HD yield on electron scavenger concentration can be made. This dependence is illustrated by the solid curves in Figure 5 for two concentrations of ND_3. It is seen from eq 20, that all electron scavenging should have the same effect when the yields

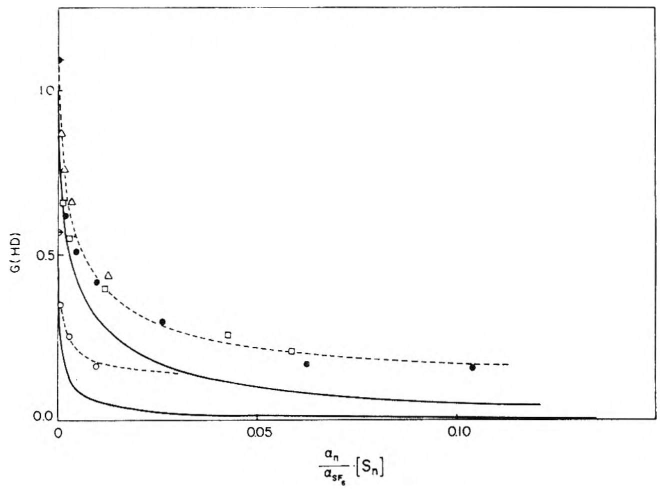

Figure 5. Dependence of HD yields from ND_3 solutions in cyclohexane on electron scavenger concentration: ● and O, SF_6; □, N_2O; and △, CH_3Cl. Data taken from ref 16. Lower data and curves are for ND_3 concentration of 0.045 M and upper data and curves for 0.33 M with $\alpha(N_2O)$ taken as 10 M^{-1} and $\alpha(CH_3Cl)$ as 5.4 M^{-1}. Solid curves are calculated from eq 20. Dashed curves are higher by the free ion component (0.12).

are plotted as a function of $\alpha[S]$. The data of Asmus[16] for the effect of SF_6, N_2O, and CH_3Cl are given in the figure and it is seen that within experimental error a common dependence is observed. The yields are, however, somewhat higher than the *a priori* prediction and it can be said rather definitively that there must be a contribution over and above that attributable to the scheme assumed. Two possibilities can be suggested. One is that a small fraction of the neutralization processes involving anions results in the formation of HD. It can be shown that this fraction cannot be more than ~5%. The second possibility, which seems more likely, is that the free ions, because of their relatively long lifetimes, always give HD as the result of some process that occurs before neutralization. The yields calculated on this basis are given by the dashed curves in the figure. It can be seen that a scheme based on this assumption describes the observed data extremely well.

Radiolysis of HI solutions. A second example is the radiolysis of HI solutions. It has been known since 1957[5] that the hydrogen yields from solutions of HI in cyclohexane are greater than those from pure cyclohexane (see also Nash and Hamill).[38] Electron scavenging by the HI certainly occurs. However, since positive ion-electron neutralization produces H_2 with near unit efficiency,[39] the production of hydrogen as a result of electron capture should be virtually cancelled by the reduction in hydrogen caused by the change in the neutralization process so that electron scavenging should have little effect on the hydrogen yield. It seems obvious at this point that positive ion scavenging by the HI must also be occurring. One can calculate the contribution of such positive ion reactions from eq 12 for the special case where the electron and positive ion scavenger concentrations are identical. Expressed as the yield of H_2 the result is

$$G(\mathrm{H_2}) = G(\mathrm{H_2})_0 + G_{fi} + G_{gi} \times \left\{ \frac{\sqrt{(\alpha_n + \alpha_p)[\mathrm{HI}]}}{1 + \sqrt{(\alpha_n + \alpha_p)[\mathrm{HI}]}} + \frac{1}{1 + \frac{\alpha_p}{\alpha_n}(1 - r_D)} \times \left[\frac{\sqrt{\alpha_p[\mathrm{HI}]}\,r_D}{1 + \sqrt{\alpha_p[\mathrm{HI}]r_D}} - \frac{\sqrt{(\alpha_n + \alpha_p)[\mathrm{HI}]}}{1 + \sqrt{(\alpha_n + \alpha_p)[\mathrm{HI}]}} \right] \right\} \quad (21)$$

where $G(H_2)_0$ is the hydrogen yield from the pure hydrocarbon. Taking $G(H_2)_0$ as 5.6 and estimating values of $\alpha_p = 0.8\ M^{-1}$ and $\alpha_n = 20\ M^{-1}$, one predicts that the hydrogen yield will increase as illustrated by the middle curve in Figure 6. A yield of 7.2 is calculated for an HI concentration of 0.08 M and can be compared with the measured yield of 7.0.[5] The data of Nash and Hamill[38] on the effect of HI on the hydrogen yield from perdeuteriocyclohexane are reproduced very well (*cf.* the lower curve) if it is assumed that the ionic processes are very similar in this solvent but that the molecular yield is 1.50 units lower.

It is also known that the initial yield of iodine from HI solutions also increases with HI concentration[40] and that yields of ~8 equiv are reached in the region of 0.03 M. Such a yield is far too high to be ascribable to radical or electron scavenging processes but is readily explained if charge or proton transfer occurs to the HI. In either case it is likely that reaction will ultimately lead to the formation of 2 equiv of iodine. The yields predicted with the appropriate modification of eq 21 are given by the upper curve in Figure 6. Again this is an *a priori* prediction based on an assumed reaction scheme. The data[40] are seen to be described quite well.

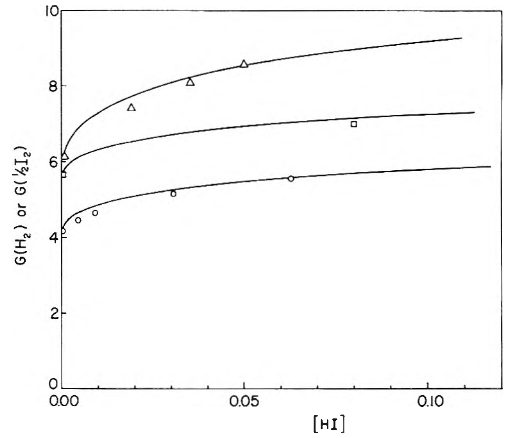

Figure 6. Radiolysis of HI solutions in cyclohexane: □, H_2 yield (ref 5) and Δ, initial production of I_2 (ref 40). Yields predicted on the basis of a scheme involving HI as both an electron and positive ion scavenger are given by the upper two curves (see text). The total hydrogen yields from solutions in deuteriocyclohexane (as measured by Nash and Hamill, ref 38) are also given (O) as well as the lower curve calculated on the assumption of a reduced yield from the pure material but otherwise similar ion scavenging kinetics.

Lifetime Distribution Function

Up to this point we have attempted to stress that explicit knowledge of the lifetime distribution function is not necessary for considering results from the usual sorts of chemical experiments. However if one is interested in time dependent phenomena, then descriptions of $f(t)$ and $F(t)$ from the scavenging results can provide many valuable clues toward interpretation of the experimental observations. A very detailed treatment of this subject has previously been given[41] and only the highlights and certain comments on the application to recent experimental work will be presented here.

As discussed previously[41] inversion of the experimental scavenging function represented by eq 14 gives for a description of $f(t)$

$$f(t) = \frac{k}{\alpha}\left[\left(\frac{\alpha}{\pi k t}\right)^{1/2} - e^{kt/\alpha}\,\mathrm{erfc}\left(\frac{kt}{\alpha}\right)^{1/2}\right] \quad (22)$$

It is seen in eq 22 that k and α appear only in their ratio. The model requires this to be the case since $f(t)$ must be a characteristic of the solvent only and any reference to a particular solute cannot appear in its description. Defining the ratio k/α as λ, we see that the scavenging parameter α, which had been introduced earlier for empirical reasons,[15] is in fact the ratio of a constant which describes the rate of scavenging to one which describes the rate of ion recombination.

$$\alpha = k/\lambda \quad (23)$$

Ion scavenging is important only for very fast reactions. Effectively the rate of the scavenging reaction will be controlled to a considerable extent by the diffusion coefficients of the reacting entities and that of ion recombination by the mobilities of the ionic partners. In the region

(38) J. R. Nash and W. H. Hamill, *J. Phys. Chem.*, **66**, 1097 (1962).
(39) K.-D. Asmus, J. M. Warman, and R. H. Schuler, *J. Phys. Chem.*, **74**, 246 (1970).
(40) D. Perner and R. H. Schuler, *J. Phys. Chem.*, **70**, 2224 (1966).
(41) S. J. Rzad, P. P. Infelta, J. M. Warman, and R. H. Schuler, *J. Chem. Phys.*, **52**, 3971 (1970).

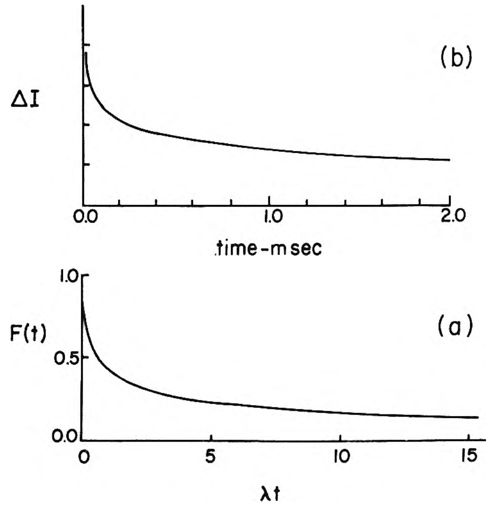

Figure 7. Decay of electrons (a) as predicted from scavenging data ($F(t) = e^{\lambda t}\ \mathrm{erfc}(\lambda t)^{1/2}$) and (b) as observed by Taub and Gillis in squalane at $-140°$ (ref 34). Note sharp initial drop and long tail.

where the ionic mobilities are independent of field strength these two quantities should be proportional and α should be constant and not strongly dependent on the nature of the hydrocarbon.

As indicated in the earlier discussion the decay of the ionic population can be obtained by integration of $f(t)$ given according to eq 4 or more simply and directly by inversion of the transform

$$\int_0^{\infty} F(t)e^{-k[S]t}dt = \frac{1}{\sqrt{k[S]}\left(\sqrt{\lambda} + \sqrt{k[S]}\right)} \tag{24}$$

This transform can be obtained by substituting eq 13 into eq 5 (remembering that $\alpha = k/\lambda$). The result is

$$F(t) = e^{\lambda t}\ \mathrm{erfc}(\lambda t)^{1/2} \tag{25}$$

A plot of eq 25 is given in Figure 7. It has two characteristic features: a sharp initial drop (50% decay occurs in a period $0.5915\ldots/\lambda$, see ref 41) and a long tail where the population decreases according to $t^{-1/2}$. The sharp initial drop is a characteristic which results from the form of the scavenging dependence used here and reflects the slow but continuous increase in yield at high solute concentration. Qualitatively the scavenging dependence given by eq 17 requires the initial drop to be slightly less sharp. The quantitative aspects are, however, evasive since the inverse transform of this expression cannot be obtained directly. The $t^{-1/2}$ dependence at long times is general since it is a characteristic of the inversion of any scavenging dependence which is linear in $[S]^{1/2}$ at low concentrations. As indicated above such a limiting dependence is a fundamental consequence of the competition between scavenging and diffusion-controlled recombination. Both Rzad, *et al.*,[41] and Mozumder[22,42] have previously commented on this point.

In cyclohexane λ has been estimated to have a value $\geq 2 \times 10^{10}$ sec^{-1}.[41] Because of this, decay is extremely rapid and in the pure material 50% of the ions will disappear by neutralization within a period ≤ 30 psec. Taub and Gillis[34] carried out experiments in squalane at $-140°$ in order to slow down the ion recombination. They observed an absorbing species in the near infrared which they attributed to solvated electrons. The decay reported by them[34] is reproduced in Figure 7. While there is considerable question about the quantitative aspects (the yield was estimated to be only 0.6) it is obvious that it has the rapid initial decay and long tail required by eq 25. In a very recent study Baxendale, *et al.*,[43] have carried out similar experiments on methylcyclohexane at $-113°$ and have reported a $t^{-1/2}$ dependence for the decay of the geminate electrons.

Various other features of time dependent phenomena can be derived from eq 25. For example, in the presence of an electron scavenger the probability that electrons will be present at time t is the product of the probabilities that they will neither have been neutralized nor have reacted with the solute, *i.e.*[44]

$$F(t)_S = F(t)\ e^{-k[S]t} \tag{26}$$

Combining eq 25 and 26 one obtains

$$F(t)_S = e^{(1-\alpha C)\lambda t}\ \mathrm{erfc}(\lambda t)^{1/2} \tag{27}$$

For values of $\alpha C \gg 1$ reaction with the scavenger dominates the decay at all times but in fact, because $F(t)$ varies only slowly at long times, decays can be expected to have an exponential appearance even for relatively low concentrations of solute (see Figure 3 in ref 41). In principle, according to eq 26, the electron scavenging rate constant can be determined from a comparison of the decay of electrons in the absence and presence of scavenger but such measurements have not as yet been carried out because of the short time scale involved.

Since the decay of the ions at room temperature is quite rapid with respect to the production and detection periods for all existing pulse apparatus one can ask what fraction of ions should be present at the end of a finite pulse. Integration of eq 25 over a square pulse of length τ leads to the expression for this fraction ($P(\tau)$)

$$P(\tau) = \frac{1}{\lambda\tau}\left\{e^{\lambda\tau}\ \mathrm{erfc}(\lambda\tau)^{1/2} - 1 + 2\left(\frac{\lambda\tau}{\pi}\right)^{1/2}\right\} \tag{28}$$

This fraction has been plotted as a function of pulse length in Figure 7 of ref 41 and it has been estimated that in ordinary hydrocarbons less than 20% of the ions will be present at the end of a 1-nsec pulse. At times where $\lambda\tau \gg 1$ eq 28 becomes

$$P(\tau) \simeq \frac{2}{(\pi\lambda\tau)^{1/2}} \tag{29}$$

i.e., the available fraction of ions decreases only with the square root of the pulse length. The total ionic concentration available at constant dose rate will, therefore, increase with the square root of the pulse length. Where one is interested in spectral properties this fact should be considered in the design of experiments.

Growth and Decay of Secondary Anions

As indicated above, the time scale for ion recombination will be lengthened by over an order of magnitude if the very mobile electrons are converted to anions by an appropriate scavenger. A considerable portion of the re-

(42) A. Mozumder, *J. Chem. Phys.*, **55**, 3020 (1971).
(43) J. H. Baxendale, C. Bell, and P. Wardman, *Chem. Phys. Lett.*, **12**, 347 (1971).
(44) It should be noted however that the relationship between the lifetime distribution functions $f(t)_S$ and $f(t)$ is much more complicated. By differentiation of eq 26 one obtains

$$f(t)_S = f(t)_0 + k[S]\int_t^{\infty} f(t)_0 dt\ e^{-k[S]t}$$

combination will therefore occur on the nanosecond time scale and be accessible to present day apparatus. It has been shown[41] that an explicit expression for the population of secondary anions as a function of time can be derived from eq 22 and therefore follows directly from the description of the scavenging function given by eq 14. The complete expression (eq 28 in ref 41) is very complicated in that it contains eight terms where each term consists of the product of factors involving an exponential and an error function complement. Evaluation effectively requires some computational aid and we have developed programs for use with a Hewlett-Packard 9100 calculator for this purpose. At long times it can be shown that the anion population decays according to the approximation

$$F_N(t)_{\lambda\tau \gg 1} \simeq \left(\frac{r_D}{\pi\lambda t}\right)^{1/2} \quad (30)$$

Since an estimate of r_D can be obtained from the studies on the effect of electron scavengers on the positive ion reactions with cyclopropane, determination of the fraction of the ions present as anions at a given time allows one to evaluate λ.

According to the work of Thomas, *et al.*,[45] on the decay of biphenylide anion in the pulse irradiation of biphenyl solutions in cyclohexane a yield of $\sim$0.2 is present at 100 nsec (where the approximation of eq 30 should apply). The subsequent decay follows the inverse square root dependence on time required (see ref 41). Taking $F_N(t)$ = 0.05 (*i.e.*, 0.2/4) at 100 nsec and r_D as 17 a value of 2×10^{10} sec^{-1} has been estimated for λ.[41,46] A value of $\sim 3 \times 10^{11}$ M^{-1} sec^{-1} is obtained for the rate constant of the scavenging process (since $k = \alpha\lambda$ and $\alpha \sim 15$ M^{-1}). This value is a factor of between 3 and 20 less than most recent estimates of electron scavenging rate constants.[43,47-49] It must, in any event, represent a lower limit.[46] It seems probable at this point that λ may be somewhat larger than 2×10^{10} sec^{-1} and that, therefore, the time scales for ion recombination may be even shorter than those given in the previous treatment.[41] It is noted that the fractional yield assigned to $F_N(t)$ appears as its square in the calculation of λ from eq 30. Interpretation of the biphenylide anion data is, therefore, extremely sensitive to the absolute yield scale. It hardly seems likely, however, that an error of more than a factor of 2 or 3 in λ can arise from this source so that an upper limit of $\sim 10^{12}$ M^{-1} sec^{-1} for the rate constant for biphenylide formation is indicated by this interpretation. Values similar to this have, in fact, been reported by Baxendale, *et al.*,[43] and by Bakale, *et al.*[48]

At this point two major difficulties arise. The first involves recent measurements which have shown that electrons have mobilities $\sim$0.1–0.2 cm^2 V^{-1} sec^{-1} in normal hydrocarbons.[40-52] Schmidt and Allen[51] have reported a value of 0.35 cm^2 V^{-1} sec^{-1} in cyclohexane. The latter value is a factor of $\sim$350 greater than the mobilities of most negative ions ($\sim 10^{-3}$ cm^2 V^{-1} sec^{-1})[53,54] in cyclohexane. If we identify r_D with the ratio of the mutual mobilities of the ions before and after electron capture, *i.e.*

$$r_D = \frac{\mu_e + \mu_+}{\mu_- + \mu_+} \quad (31)$$

(where μ_e is the mobility of the initial electron, μ_- that of the secondary anion, and μ_+ that of the positive ion) and take similar values for the mobilities of the positive ion and secondary anion then r_D should be $\sim$200. The change in the time scale indicated by the cyclopropane experiments[17] is, however, a factor of 10 less than this. Either the above definition of r_D does not apply in the chemical experiments or there is some fundamental difficulty in the interpretation of the experiments on cyclopropane. One possible solution to the problem is that the positive ions initially formed can readily undergo reversible charge exchange and as a result have an effective mobility considerably higher than those of the negative ions. If the positive ion mobility were $\sim$20 times that of the negative ions then the experimentally observed r_D would be accounted for. Our previous interpretation[41] of Thomas' pulse data would have to be modified to take this into account since biphenyl would act as a positive ion trap. If positive ion trapping is important in the biphenyl system then it is possible that the expansion of the time scale is an order of magnitude higher than the factor used in estimating λ and k and, accordingly, these constants could be correspondingly higher. Further considerations on the kinetic implications of possible changes in positive ion mobilities are currently in progress.[55]

The second difficulty, which is closely related to the above, involves the fact that the α parameters for positive ion scavenging are relatively large. For example, if one compares the value of 0.4 M^{-1} observed for the reaction of positive ions with cyclopropane with the value of 16 M^{-1} for electron capture by CH_3Br one concludes that the rate constants tor these two processes are approximately in the ratio of 1:40. If the rate constant for the electron scavenging reaction is taken as 3×10^{11} M^{-1} sec^{-1} then a value of $\sim 10^{10}$ M^{-1} sec^{-1} is estimated for the positive ion reaction and is reasonable for a diffusion-controlled reaction. Larger values for the rate constant of the electron scavenging process would require abnormally high rate constants for typical positive ion reactions, again implying a very high mobility for the positive ion. As of yet no positive ions with mobilities greater than $\sim 10^{-3}$ cm^2 V^{-1} sec^{-1} have been detected in hydrocarbons. In summary we can comment only that in cyclohexane the simplest conclusions from the chemical experiments indicate rate constants and electronic mobilities which are about an order of magnitude lower than those given by direct measurements. This discrepancy can be resolved if the mobilities of the positive ions initially produced are $\sim 10^{-2}$ cm^2 V^{-1} sec^{-1} but it is somewhat premature to say that such an explanation is necessarily involved. If the initial mobilities of the positive ions are as high as this then certain aspects of the scavenging kinetics must be reworked.

Experimental results are now starting to become available for very short irradiations and it is useful to project how these results should appear. Calculations for nanosecond and longer irradiation periods have already been

(45) J. K. Thomas, K. Johnson, T. Klippert, and R. Lowers, *J. Chem. Phys.*, **48**, 1608 (1968).
(46) S. J. Rzad, P. P. Infelta, J. M. Warman, and R. H. Schuler, *J. Chem. Phys.*, **50**, 5034 (1969).
(47) J. T. Richards and J. K. Thomas, *Chem. Phys. Lett.*, **10**, 317 (1971).
(48) G. Bakale, E. C. Gregg, and R. D. McCreary, *J. Chem. Phys.*, submitted for publication.
(49) A. Hummel, *Proc. Int. Congr. Radiat. Res., 4th*, (1970).
(50) E. E. Conrad and J. Silverman, *J. Chem. Phys.*, **51**, 450 (1969).
(51) W. F. Schmidt and A. O. Allen, *J. Chem. Phys.*, **52**, 4788 (1970).
(52) R. M. Minday, L. D. Schmidt, and H. T. Davis, *J. Chem. Phys.*, **54**, 3112 (1971).
(53) A. Hummel and A. O. Allen, *J. Chem. Phys.*, **44**, 3426 (1966).
(54) P. H. Tewari and G. R. Freeman, *J. Chem. Phys.*, **49**, 4394 (1968).
(55) P. P. Infelta and S. J. Rzad, to be submitted for publication.

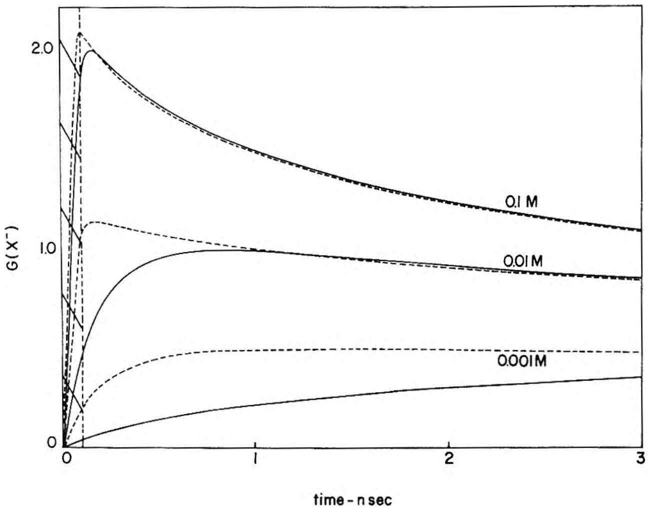

Figure 8. Growth and decay of secondary anions for the irradiation of 0.1, 0.01, and 0.001 M solutions of an electron scavenger with a 100-psec pulse. Curves obtained by numerical integration of eq 28 from ref 41. Parameters used are $\alpha = 15\ M^{-1}$ with $\lambda = 2 \times 10^{10}$, $r_D = 17$ (solid curves), and $\lambda = 2 \times 10^{11}$, $r_D = 170$ (dashed curves).

given.[41] In the previous discussion[41] it was shown that observations on the 10–1000-nsec time scale were of the form predicted by the scavenging experiments and that effectively one can quantitatively correlate the results from pulse and from scavenging experiments. At the times involved this correlation essentially involves only the quantity λ/r_D and avoids the difficulties indicated above in determining the individual values for λ and r_D. In Figure 8 we have plotted the time dependence of the secondary anion population for various concentrations of scavenger following a 100-psec pulse[56] with λ taken as 2×10^{10} sec^{-1} and $r_D = 17$ (the solid curves) and λ and r_D both an order of magnitude greater (the dashed curves). The calculation is based on eq 28 of ref 41 with an assumed value of 15 M^{-1} for α. A numerical integration has been carried out over the pulse as previously described. It is seen that except for measurements at very short times or low concentrations the individual values of λ and r_D are unimportant in determining the anion population and that it is the ratio which is all important. At very long times the population is not even strongly dependent on the solute concentration.[41] Increase of the ratio of λ/r_D by a factor of 3 reduces the yield at the peak of the curve for 0.1 M to 1.7 and makes the subsequent decay somewhat more rapid.

At this conference Thomas has reported[57] observing maximum yields in the subnanosecond region of 1.6 for biphenylide ion following the irradiation of solutions several tenths molar in biphenyl with very short pulses. Such yields are 30–40% lower than the total yield of anions expected from the scavenging experiments but this difference is readily accounted for by the decay that occurs within the growth period. The yields quoted are in reasonable agreement with the predictions of Figure 8 and could be completely accounted for by a slightly higher ratio of λ/r_D. Thus the scavenging and pulse experiments seem to complement each other quite nicely.

(56) The peak of the curve previously given for 0.1 M solutions in Figure 5 of ref 41 was somewhat lower than in the present figure. A truncation error in the Library subroutine for the error function complement used in the previous calculation was responsible. We have developed an error function complement subroutine for use with a Hewlett-Packard 9100 calculator which evaluates the function to 11 significant figures. In the previous work the calculation error was important only at short times and for the highest concentrations so that the curves at 0.01 M and below were essentially identical with those presented here.

(57) G. Beck and J. K. Thomas, *J. Phys. Chem.*, **76**, 3856 (1972).

Formation of Solvated Electrons in Dilute Solutions of Polar Molecules in Nonpolar Solvents

A. Mozumder

Department of Chemistry and the Radiation Laboratory,[1] University of Notre Dame, Notre Dame, Indiana 46556
(Received May 1, 1972)

Publication costs assisted by the Radiation Laboratory, University of Notre Dame

A theoretical model is presented for the time required to form solvated electrons in a dilute solution of polar molecules in a nonpolar solvent when irradiated by ionizing radiation. The polar molecules are assumed to exist as monomers; however, this assumption is not seen as a serious limitation to the applicability of the model. In the system considered an electron escaping geminate neutralization following an ionization event will eventually find itself attached to a polar molecule, which is the first step in the formation of the solvated electron. This process is always very fast. In the second step neighboring dipoles coagulate to the central negative charge. This process is relatively slow, consisting of dipole rotation and drift which contribute comparably to the so-defined microscopic relaxation time. The analysis presented here describes motions of electrons and dipoles in terms of drift velocities. The latter are obtained from instantaneous electric fields and linear and rotational mobilities. Concentration dependence of solvated electron formation time is evaluated and comparison with experiments is indicated.

Introduction

In the radiolysis of polar liquids formation of solvated electrons is a common occurrence. It is also a common belief or assumption that there is some kind of dielectric relaxation process associated with the formation of solvated electrons in such liquids. However, there are considerable difficulties in the interpretation of the relevant relaxation mechanism and therefore also in the evaluation of the time required to accomplish the process. In the first place, it is clear that a microscopic relaxation mechanism may be different, either partly or wholly, from the corresponding macroscopic counterpart.[2] In the second place, and this consideration is by no means trivial, even the macroscopic dielectric relaxation is in many cases only poorly understood.[3,4] The Debye theory, based on rotational Brownian motion, is the most commonly accepted model for macroscopic dielectric relaxation.[5] Even though in some cases calculations based on the Debye theory give relaxation times that are in fair agreement with experiments, the foundations of the theory are somewhat obscure.[3,4] Thus, it has been argued that (i) a pure rotation of a polar molecule in a continuum is at best a difficult concept since most significant polar liquids are hydrogen bonded and energy required to break the necessary number of hydrogen bonds is not available either from the heat bath or from the external field; (ii) to keep the layer of the liquid next to the molecule at rest (relative to the polar molecule), it is necessary to increase the molecular radius by at least a factor of 3 which increases the calculated relaxation time by more than an order of magnitude. There are also other difficulties such as associated with viscosity variation. Whereas the situation remains complicated and obscure with respect to macroscopic relaxation in neat polar liquids, the case of a dilute solution of polar molecules in nonpolar solvents is essentially simple. In the latter case the objections to the Debye theory which have just been described do not apply and the experimental situation is in good agreement with Debye's model.[6]

In an earlier attempt by the present author microscopic relaxation was described in a manner similar to the macroscopic description except in an essential change necessitated by the occurrence of ionization itself, *viz.*, the charge (or displacement) was kept constant rather than the field, the latter being the usual macroscopic restraint. This description results in a relaxation time shorter than the macroscopic value by a factor equal to the ratio of static to high-frequency dielectric constant. Such an analysis is in agreement with experiments on water and some alcohols but in other cases theory predicts too high relaxation times.[7a] Also, theory predicts a difference in the relaxation times of (say, for the sake of example) 1-propanol and 2-propanol which has not been experimentally observed. Thus, the case of dielectric relaxation remains somewhat obscure and largely not understood from both macroscopic and microscopic points of view. On the other hand, since macroscopic relaxation of dilute solutions of dipoles is a well-understood phenomenon, it is natural to expect that the formation of solvated electrons in such systems should similarly present a less complicated theoretical problem. In this paper we calculate the formation time for solvated electrons in dilute dipole solutions through basically a charge dipole interaction. A similar model involving dimers has been used by Raff and Pohl[7b] for electron binding and optical transition energy of solvated electrons in neat polar

(1) The Radiation Laboratory of the University of Notre Dame is operated under contract with the U. S. Atomic Energy Commission. This is AEC document No. COO-38-844.

(2) In the present context macroscopic relaxation refers to dielectric relaxation of the bulk medium in a (relatively) weak external field. The rapid relaxation process occurring in regions of molecular dimensions in the strong field surrounding an ionized electron will be called microscopic relaxation.

(3) W. Kauzmann, *Rev. Mod. Phys.*, **14**, 12 (1942).

(4) A. von Hippel, *J. Chem. Phys.*, **54**, 145 (1971).

(5) P. Debye, "Polar Molecules," The Chemical Catalog Co., New York, N. Y., 1929.

(6) W. Jackson and J. G. Powles, *Trans. Faraday Soc.*, **42A**, 101 (1946); see also H. Frohlich, "Theory of Dielectrics," 2nd ed, Oxford University Press, London, 1958, pp 120–121.

(7) (a) M. J. Bronskill, R. K. Wolff, and J. W. Hunt, *J. Chem. Phys.*, **53**, 4201 (1970); (b) L. Raff and H. A. Pohl, *Advan. Chem. Ser.*, **No. 50**, 173 (1965).

media. In a certain sense the present treatment is complementary to their work.

Model

In the present model formation of solvated electrons in a dilute dipolar solution evolves in two stages. In the first stage the electron is drawn to the nearest dipole with a favorable orientation. Since the electron is far more mobile than the polar molecule, the latter virtually remains stationary during this stage of motion.[8] In reality the electron sees the field at its own location contributed by all the surrounding dipoles. In practice, however, the field due to the nearest neighbor dominates because the charge–dipole interaction varies as r^{-3}, r being their separation. In this paper we will consider only the charge–nearest neighbor force, the residual part being assumed as negligible. Also since we are dealing with dilute solutions, polar molecules will be treated as point dipoles.

In the second stage of motion we consider the interaction of a dipole with a negative ion, the latter being just an electron attached to a polar molecule during the first stage of the motion. Again only the nearest neighbor dipole is considered, a certain amount of error in neglecting the other neighboring dipoles being explicitly acknowledged. However, in this stage, the ion and the dipole have comparable mobilities and we must consider their relative motion in terms of sum of their mobilities. Additionally, the torque acting on the dipole has time to orient the dipole along the radial direction and this motion competes with radial drift in producing the resultant polarization. The joining of dipoles in the second stage of motion will be called "dipole coagulation," this being the mechanism for the formation of solvated electrons in the present system.

Electron Attachment Time Scale

Figure 1 shows the diagram for the electron–dipole interaction. The force on the electron may be resolved into two components, $F_{\parallel}$ acting along the r direction and $F_{\perp}$ acting perpendicular to it. The perpendicular force changes the orientation θ even though the dipole remains stationary in the laboratory frame in this stage of motion. The electron motion will be described in terms of drift velocities, the drift velocity in any direction being equal to electron mobility times the field acting on the electron along the same direction. We thus get

$$\frac{\mathrm{d}r}{\mathrm{d}t} = -\frac{2\mu_e\mu\cos\theta}{\epsilon r^3} \qquad (1)$$

and

$$r\frac{\mathrm{d}\theta}{\mathrm{d}t} = -\frac{\mu_e\mu\sin\theta}{\epsilon r^3} \qquad (2)$$

where t is the lapse time and μ, μ_e, and ϵ refer respectively to the dipole moment of the molecule, mobility of the electron (*i.e.*, drift velocity per unit electric field), and the dielectric constant of the medium. A relationship between r

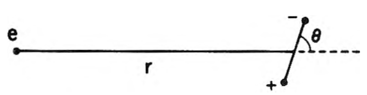

Figure 1. Charge–dipole interaction. The separation between the charge and the dipole is r, the vector being considered as positive when directed away from the charge. θ is the angle between the negative end of the dipole and the radius vector. The symbol e stands either for the electron or for the negative ion of same charge.

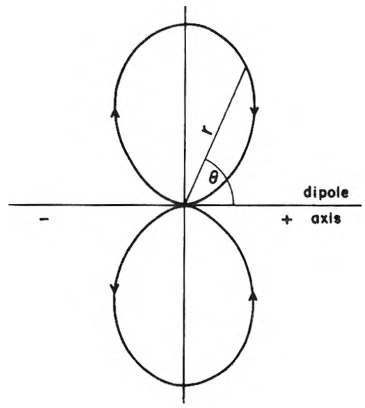

Figure 2. Polar plot of the curve $r = A\sin^2\theta$, A being chosen arbitrarily in the present case. If A is set equal to $r_0/\sin^2\theta_0$ where r_0 and θ_0 are initial separation and angle, respectively, then the curve will represent electron path in the attachment stage from the point (r_0, θ_0). Motion is clockwise above the line $\theta = 0, \pi$ and counterclockwise below it.

and θ may be obtained by eliminating t between (1) and (2) and integrating the resultant equation. With the initial condition, that at $t = 0$, $r = r_0$ and $\theta = \theta_0$, we then get

$$r = (r_0/\sin^2\theta_0)\sin^2\theta \qquad \sin\theta_0 \neq 0^9 \qquad (3)$$

Equation 3 shows that at attachment ($r = 0$) the electron arrives along the dipole direction ($\theta = 0$). It also shows that the electron follows the lines of force of the dipole which is a consequence of using instantaneous drift velocities. The situation is shown in Figure 2. However, eq 3 does not indicate the time required for the attachment process. For that we substitute (3) in (2) and obtain

$$\frac{\mathrm{d}\theta}{\mathrm{d}t} = -K/\sin^7\theta \qquad (4)$$

where

$$K = \mu_e\mu\sin^8\theta_0/\epsilon r_0^4 \qquad (5)$$

On the integration of eq 4, we get

$$Kt = \mathrm{f}(\theta) - \mathrm{f}(\theta_0) \qquad (6)$$

where

$$\mathrm{f}(\theta) = \cos\theta\,(a_1\sin^6\theta + a_2\sin^4\theta + a_3\sin^2\theta + a_4) \qquad (7)$$

and

$$a_1 = 1/7, a_2 = 6/35, a_3 = 8/35, a_4 = 16/35 \qquad (8)$$

The attachment time, t', for the electron may be obtained from (6), for a given initial position (r_0, θ_0), by letting $\theta = 0$. That is

$$t'(r_0, \theta_0) = 8t_f\mathrm{g}(\theta_0) \qquad (9)$$

where

$$\mathrm{g}(\theta_0) = [a_4 - \mathrm{f}(\theta_0)]/\sin^8\theta_0 \qquad (10)$$

and

$$t_f = \epsilon r_0^4/8\mu\mu_e \qquad (11)$$

(8) Measured electron mobilites in nonpolar, dielectric liquids are in the range ~0.1 to ~100 cm^2/V sec. See, for example, (a) R. M. Minday, L. D. Schmidt, and H. T. Davis, *J. Chem. Phys.*, **54**, 3112 (1971); (b) W. F. Schmidt and A. O. Allen, *ibid.*, **52**, 4788 (1970). Recently Freeman has found evidence for electron mobility in liquid methane as high as ~300 cm^2/V sec (see P. G. Fuochi and G. R. Freeman, *ibid.*, **56**, 2333 (1972)). By comparison, anion mobilities are of the order of 10^{-3} cm^2/V sec.

(9) If $\theta_0 = 0$, then θ is also zero at all times (see eq 2) and the radial equation is simply integrated from eq 1.

The quantity t_f measures the time scale of the attachment process. To get a significant measure of t' we must average eq 9 over a random distribution of θ_0 and also over a distribution of r_0 for a given concentration of the dipoles. The first averaging is done for $\theta_0 = -\pi/2$ to $+\pi/2$, *i.e.*, for initial orientations that are favorable for electron attraction. The residual initial orientations ($\theta_0 = \pi/2$ to $3\pi/2$) will cause the dipole to repel the electron initially. This repulsion usually makes r comparable to or greater than the mean separation between dipoles before the force on the electron becomes attractive by the necessary change of θ. It is reasonable to assume that about half the nearest neighbor dipoles are in the orientation $\theta_0 = -\pi/2$ to $\pi/2$ and the rest with $\theta_0 = \pi/2$ to $3\pi/2$. It is also reasonable to say that when an electron is repelled by the nearest neighbor because of unfavorable orientation it will find another neighbor to get attracted to. On these considerations the average attachment time is calculated here over a normalized population of dipoles with initial favorable orientations to the electron. We then obtain from eq 7, 9, and 10

$$\langle t' \rangle_{\theta_0} = 8t_f \lim_{\theta' \to 0} \int_0^{\cos\theta'} \left[\frac{a_4(1-z)}{(1-z^2)^4} - \frac{a_3 z}{(1-z^2)^3} - \frac{a_2 z}{(1-z^2)^2} - \frac{a_1 z}{(1-z^2)}\right] dz \qquad (12)$$

In eq 12, θ' is a small angle approaching the limit zero and $z = \cos\theta_0$. The integral appearing in eq 12 may be written as follows

$$I = a_1 I_1 - (a_2 I_2 + a_3 I_3 + a_4 I_4) + a_4 I_5 \qquad (13a)$$

where

$$I_1 = (1/2) \ln (1 - z^2) \qquad (13b)$$

$$I_2 = 1/2(1 - z^2) \qquad (13c)$$

$$I_3 = 1/4(1 - z^2)^2 \qquad (13d)$$

$$I_4 = 1/6(1 - z^2)^3 \qquad (13e)$$

and

$$I_5 = (1/48)\{(1 - z)^{-3} - (1 + z)^{-3}\} + (1/4)z/(1 - z^2)^2 + (5/16)z/(1 - z^2) + (5/32) \ln [(1 + z)/(1 - z)] \qquad (13f)$$

Substituting eq 13b–f in eq 13a and the last equation in eq 12 and evaluating the limit[10] $\theta' \to 0$ we get

$$(1/8t_f)\langle t' \rangle_{\theta_0} = (a_2/3) + (17a_3/90) + (413a_4/3780) + (5a_4/16) \ln 2 \qquad (14a)$$

Substituting the numerical values of the coefficients from eq 8 we get

$$\langle t' \rangle_{\theta_0} = 1.994t_f \qquad t_f = \epsilon r_0^4/8\mu\mu_e \qquad (15)$$

If the average dipole density be n per unit volume then, under random distribution, the probability of occurrence of a nearest neighbor dipole between distances r and $r + dr$ as seen from any arbitrary point is given by[11]

$$\omega(r)dr = 4\pi r^2 n \exp(-4\pi r^3 n/3)dr \qquad (16)$$

The average of $\langle t' \rangle_{\theta_0}$ over the distribution of r_0 is now given from eq 15 and 16 as follows

$$t_1 \equiv \left\langle \langle t' \rangle_{\theta_0} \right\rangle_{r_0} = 0.24929\left(\frac{\epsilon}{\mu\mu_e}\right)\left(\frac{3}{4\pi n}\right)^{4/3} \sqrt{(7/3)} = 4.395 \times 10^{-2} (\epsilon n^{-4/3}/\mu\mu_e) \qquad (17)$$

TABLE I: Concentration Dependence of Formation Times of Solvated Electrons in Dilute Dipolar Solutions

Concn, M	Attachment time t_1, psec	Coagulation time t_2, nsec	Comments
0.03	8.9	4.648	(1) Physical parameters used: $\epsilon = 2$, $\mu = 2$ D, and $\mu_e = 0.35\ cm^2/V$ sec
0.02	15.2	7.836	
0.01	38.4	19.136	
0.007	61.8	30.297	
0.005	96.8	46.735	(2) Attachment time is always negligible compared to the coagulation time
0.002	328	152.15	
0.001	827	371.58	

A sample calculation with $\epsilon = 2$, $\mu = 2$ D, $\mu_e = 0.35\ cm^2/V$ sec, and a density corresponding to a 20 mM solution ($n = 1.2 \times 10^{19}$ dipoles/ml) gives $t_1 = 15.24$ psec. The calculated variation of t_1 with the molarity of solution using otherwise the same physical parameters is shown in the second column of Table I. It is seen that electron attachment is always a fast process.

Dipole Coagulation

In this stage of the motion we consider coagulation of the nearest neighbor dipole with the central negative charge (*i.e.*, electron attached to a polar molecule). Figure 1 may still be deemed to represent the case, e now being interpreted as a negative ion. However, in this case, change of θ may be brought about by either the torque acting on the dipole or by the perpendicular component of the force, $F_\perp$. If these changes in the time interval dt be denoted by $d\theta_1$ and $d\theta_2$, respectively, then the equations for drift velocities may be written as follows[12]

$$\frac{d\theta_1}{dt} = -B_\theta\left(\frac{e\mu}{\epsilon r^2}\right)\sin\theta \qquad (18a)$$

$$r\frac{d\theta_2}{dt} = -B_r\left(\frac{e\mu}{\epsilon r^3}\right)\sin\theta \qquad (18b)$$

and

$$\frac{dr}{dt} = -B_r\left(\frac{2e\mu}{\epsilon r^3}\right)\cos\theta \qquad (18c)$$

Noting that $d\theta = d\theta_1 + d\theta_2$, the above equations may conveniently be put in a dimensionless form as given below

$$\frac{d\rho}{d\tau} = -\lambda\cos\theta/\rho^3 \qquad (19a)$$

$$\frac{d\theta}{d\tau} = -f(\rho)\sin\theta/\rho^2 \qquad (19b)$$

In eq 19a and 19b $\rho = r/r_0$, r_0 being the initial separation; $\tau = t/t_0$, where $t_0 = 8\pi\eta\epsilon a^3 r_0^2/e\mu$, a scaling factor having the dimension of time; a, the size parameter of the polar molecule; η, the viscosity of the medium; e, the magnitude

(10) At $\theta' = 0$, the various integrals appearing in eq 13a–f exhibit divergences of various orders. However the net result, as $\theta' \to 0$, is a neat cancellation of all divergences leaving only small finite terms. To see this it is necessary to expand each integral in powers of θ up to a nonvanishing, nondivergent term.

(11) See, for example, S. Chandrasekhar, *Rev. Mod. Phys.*, **15**, 1 (1943).

(12) Here generalized mobilities (B's) are defined as generalized velocities per unit generalized force (rather than electric field as was used in the electron attachment case). Thus B_θ is angular velocity per unit torque exercised on the system.

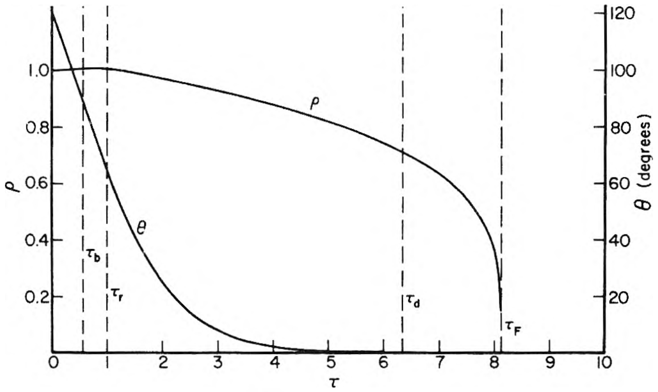

Figure 3. Evolution of ρ and θ in normalized time (τ) for r_0 = 24 Å and θ_0 = 120°. See text for values of physical parameters used; time scale t_0 = 0.483 nsec. Significance of the times shown on the curve are (i) τ_b, the boomerang time when the dipole starts retracting after an initial repulsion; (ii) τ_r, the time for orientational relaxation; (iii) τ_d, the beginning of the pure drift region, ($\theta \approx 0$); and (iv) τ_F, the final coagulation time.

of the electronic charge; $\lambda = 16a^2/3r_0^2$; and $f(\rho) = 1 + \lambda/2\rho^2$. Also, we have used[13] $B_r = (3\pi\eta a)^{-1}$ and $B_\theta = (8\pi\eta a^3)^{-1}$. The departure of $f(\rho)$ from unity measures the relative effect of $F_\perp$ in changing θ. Computer calculations in the worst case (highest concentration) show this effect to be only a few per cent. This means that essentially the rotation is effected through the torque only. The reason for this effect is, of course, to be found in the r-dependence (*cf.* eq 18a and 18b).

To compute the coagulation time we start at $t = 0$ with an initial separation r_0 and orientation θ_0. That is, eq 19a and 19b are solved numerically starting at $\tau = 0$ with $\rho = 1$ and $\theta = \theta_0$. Finally, arrival time (τ_F) is defined when $\rho = 2a/r_0$. However, since time is found to depend on a high power of distance (see later) the final distance is not critical as long as it is small compared to the initial value. Computer calculations show that in general both θ and ρ change significantly during the coagulation period. In fact, if θ_0 is not too large, $\theta \rightarrow 0$ substantially before the time τ_F so that there is a region of pure drift, which is defined in our program when $|\sin\theta| < 10^{-3}$. From eq 19a τ is proportional to ρ^4 in this region. In any case a time of orientational relaxation (τ_r) can always be defined such that at this time $\cos\theta = 1 - (1 - \cos\theta_0)\exp(-1)$, *i.e.*, $1/e$ of net required orientational polarization still remains to be achieved. Figure 3 shows computed evolution of ρ and θ in a typical case using the same physical parameters as before. The orientational relaxation time, pure drift region, and the final coagulation time are illustrated in this figure. Figure 4 shows the variation of coagulation time with initial angle for a fixed initial separation (24 Å). For θ_0 around ±180°, the dispersion of τ_F with θ_0 is also large which is a result of the fact that the dipole spends a lot of time in properly orienting itself for these starting angles before its separation from the negative ion changes significantly.

As in the electron attachment stage a significant measure of the coagulation time is obtained only after averaging over θ_0 and r_0. In the important region of initial separations, 16–32 Å, the angular averaging is performed numerically over 32 angles, 8 in each quadrant, such that their cosines are equally spaced. In this region it has always been found that there exists an angle close to 120° such that the arrival time for this initial angle is equal to the angle-averaged arrival time. Outside this region, then, we assume that the arrival

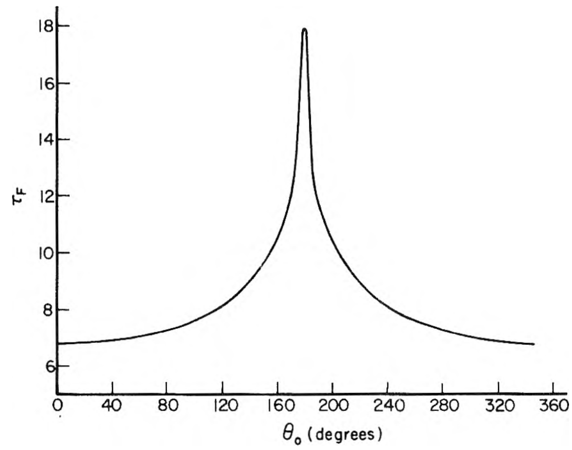

Figure 4. Plot of normalized coagulation time (τ_F) as a function of initial angle (θ_0) for a starting separation of 24 Å. The time scale in this case is t_0 = 0.483 nsec. See text for values of physical parameters used. The curve is symmetrica about θ_0 = ±180°; this symmetry can be seen from eq 19a and 19b by setting $\phi = 2\pi - \theta$.

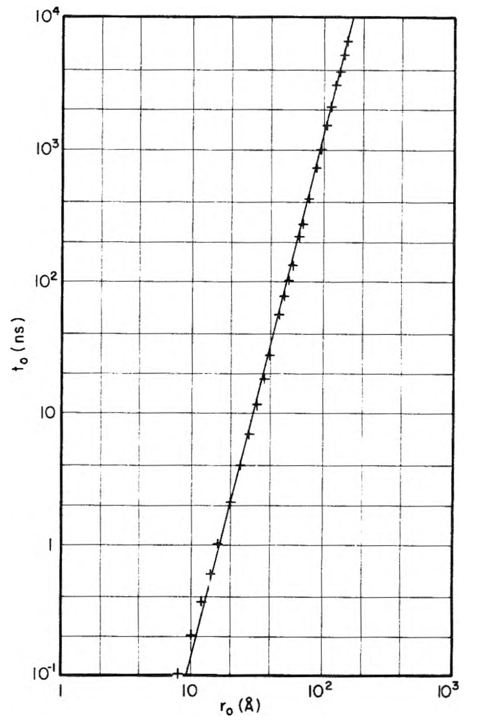

Figure 5. Variation of angle-averaged dipole coagulation time (nsec) with initial separation (Å) (log-log plot). The data are well represented by the line $t_a = 1.9613 \times 10^{-5} r_0^{3.8646}$. See text for values of physical parameters used.

time calculated for an initial angle of 120° represents the so-defined average value. Figure 5 shows the variation of this time (t_a) as a function of initial separation on a log–log scale. Same physical parameters are used here as applied before to convert the arrival time to absolute units. It is seen from this figure that the time-separation equation is well represented, except perhaps for very low separations, by a power relationship

$$t_a(\text{nsec}) = Ar_0(\text{Å})^m \tag{20a}$$

(13) B_θ is given by the Stokes–Debye equation (see ref 5). B_r is taken equal to twice the value given for a molecule of radius a by the Stokes–Einstein relation. This means that the linear mobilities of the ion and the dipole are taken equal.

where in this case

$$A = 1.9613 \times 10^{-5} \text{ and } m = 3.8646 \quad (20b)$$

Note that if the rotational relaxation was always very quick, we would have expected $m = 4$. Averaging t_a further over a distribution of initial distances for a given concentration n of dipoles is performed as before, *i.e.*, averaging eq 20a over the distribution of eq 16. The result is

$$t_2 \equiv \langle t_a \rangle_{r_0} = A(3/4\pi n)^{m/3}\sqrt{(1 + m/3)} \quad (21a)$$

or, in our case

$$t_2(\text{nsec}) = 0.050752M^{-1.2882} \quad (21b)$$

where in the last equation the molarity of the solution replaces the number concentration n. Table I shows the variation of t_2 with M which is significant even if not severe. We also notice that the attachment time t_1 is always insignificant compared to t_2, as perhaps expected. In fact, it is so short that mostly it will elude detection unless by specific design, *i.e.*, low-electron mobility, large initial separation, etc.

Discussion

The present model only underlines the essential basics of the theory without going into details of calculation or into an elaborate comparison with the few available experiments. No great accuracy is claimed but it is believed that the results are correct within their respective orders of magnitude. To keep the mathematical complexities to a minimum we have (i) assumed point dipoles, (ii) neglected bulk neutralization, and (iii) also assumed that in the dilute solution dipoles exist primarily as monomers. Improvements of the theory must be based on relaxing these simplifications to more realistic descriptions. Also, a more realistic field in the second stage of motion is indicated through the self-consistent mutual interaction of all the neighboring dipoles. Modifications due to these effects are difficult to make but they are highly desirable for comparison with experiment.

At a first sight it may appear that bulk neutralization will pose a lower limit on the dipole concentration for the practicability of the experiment. Taking a dose $\sim 10^{18}$ eV/ml and using a G value for escaped electrons ~ 0.1, we compute the initial concentration of electrons in volume as $c_0 \sim 10^{15}$/ml. Using the Debye equation for bulk neutralization (*i.e.*, $k = 4\pi D r_c$) with $D = 8.8 \times 10^{-3}$ cm^2/sec (from measured electron mobility in cyclohexane) and $r_c = 300$ Å, we get $k \sim 3 \times 10^{-7}$ ml/sec or that the first half-life of neutralization $= (kc_0)^{-1} \sim 3$ nsec. However, the electron-polar molecule attachment time for a concentration of 30 mM is ~ 10 psec (see Table I). Hence, it is clear that the bulk neutralization must be between the positive ion and the solvated electron. For the latter process, it may be argued that the positive ion is the more mobile species as some experiments require the existence of a mobile positive ion for interpretation.[14,15] Taking[15] $D_e/D_+ \sim 17$, we get $k_{+\text{to } e_s} \sim 1.76 \times 10^{-8}$ ml/sec and $t_{1/2} \sim 50$ nsec. Thus, the half-life for bulk neutralization is at least an order of magnitude greater than dipole coagulation time (see Table I) at the smallest experimental concentration. A high degree of coagulation should, therefore, set in before volume neutralization becomes significant. A crude estimation for lower concentration of dipoles from the neutralization point of view may be obtained by setting $\nu \times$ time for single coagulation $= t_{1/2}$ for neutralization, where ν is the number of dipoles required to approximate the structure of the solvated electron. Taking $\nu = 4$ (more or less arbitrarily) and using $t_{1/2} = 50$ nsec as before, we get coagulation time = 12.5 nsec which gives us a concentration, from eq 21b, ~ 14 mM. Experiments are usually done at much higher concentrations. We then come to the conclusion that the lower limit of concentration is not imposed by neutralization; it is more likely that the intensity of absorption of the solvated electron, *i.e.*, $G\epsilon$, imposes this lower limit. Actually our calculation puts the electron attachment time scale <10 psec for concentrations >30 mM. For this situation the polar molecules will scavenge not only the escaped electrons but some of the geminate fraction also.

An uncertain feature of solutions of polar molecules is polymerization or aggregate formation. Existence of polymers, up to octamers, has been argued from experiments with ultrasonics and nmr and also on the basis of thermodynamics. The basic question here seems to be the following: does the electron coagulate the monomers to form the solvated electron or does it simply get attached to a fairly large-sized entity already existing in solution? Our analysis shows that probably the first alternative applies in dilute solutions but it does not rule out the second possibility for concentrated solutions. In any case it may be safely stated that existence of large aggregates is not a prerequisite for the observation of the solvated electron. On the other hand, if they do exist then the yield (of the solvated electron) should exhibit a sharp concentration dependence in a certain region. This conclusion derives from the fact that the field of a higher order pole varies inversely as a high order of distance, the orientation being unimportant due to inherent angular averaging.

Electron attachment to a single polar molecule in the gas phase does not occur if the dipole moment is less than a critical value, ~ 1.6 D. On the other hand it may be argued that in the gas phase the electron can be preferentially ejected into the vacuum. In the solution, however, it can only be thrown into the bulk to be interacted upon electrostatically by a neighboring polar molecule. In this manner the concept of electron attachment by default evolves. In our model an absolute attachment in terms of negative energy is not a strict requirement. The model will work satisfactorily if the electron can be held near a polar molecule for sufficiently long time such that a significant coagulation can occur. If we assume for the sake of simplicity that only translational partition function is a relevant consideration and that only monomers and dimers exist in abundance in the dilute solution then we can simply calculate the monomer to dimer ratio. With $\mu = 2$ D, $a = 2$ Å, $T = 300$°K, and mass of polar molecule $= 4 \times 10^{-23}$ g, we then obtain the upper limit of dilute solutions as ~ 50 mM. At this concentration monomers outnumber dimers by six to one; however, this is barely high enough concentration for most experimental purposes. Also, the calculation just referred to tends to give a low value for the dimer fraction because of the use of dipolar model of a hydrogen bond. In principle it would be better to base the discussion on the free energies of hydrogen bond formation which, however, is not done here for the complexities and uncertainties involved.

Comments on Currently Available Experiments. At present only a few experiments[16-19] relate to the observa-

(14) M. Kondo, M. R. Ronayne, J. P. Guarino, and W. H. Hamill, *J. Amer. Chem. Soc.*, **86**, 1297 (1964); J. B. Gallivan and W. H. Hamill, *J. Chem. Phys.*, **44**, 2378 (1966); P. W. F. Louwrier and W. H. Hamill, *J. Phys. Chem.*, **72**, 3878 (1968).

(15) A. Mozumder, *J. Chem. Phys.*, **55**, 3026 (1971).

(16) T. J. Kemp, G. A. Salmon, and P. Wardman in "Pulse Radiolysis," M. Ebert, J. P. Keene, A. J. Swallow, and J. H. Baxendale, Ed., Academic Press, London, 1965, pp 247-257.

tion of solvated electron absorption spectra in solutions of polar molecules in nonpolar solvents. Of these, the work of Kemp, *et al.*,[16] seems to be the earliest. They use methanol dissolved in cyclohexane or THF in the concentration range 4% and up, the entire concentration range being high in our terminology. These experiments are probably not very quantitative; however, certain general features are already evident. They are (i) slight red shift of peak with dilution, (ii) half-width (but, note, not the shape) and lifetime independent of dilution, and (iii) $G\epsilon$ (and, therefore, by implication G) falling rapidly with dilution. We do not agree with the authors that their experiments indicate that polar aggregates must exist. On the other hand, since in some cases the yield is *ca.* six times greater than what would be obtained on mole fraction basis, it is reasonable to assume that a significant amount of coagulation has taken place in the presence of the electron.

In the experiments of Magnuson, *et al.*,[17] a fully developed spectrum is seen at the end of a 33-nsec pulse of irradiation. They further observe (i) small but systematic red shift of peak with dilution and (ii) spectral shift with concentration stated to be related with polymer formation. Their lowest concentrations fall in the category of dilute solutions in our terminology and their conclusion that trapping is determined by nearest dipole interaction is consistent with our findings. However, dipole coagulation may not be safely neglected in any of these experiments.

The experiments of Brown, *et al.*,[18] use fairly slow pulse (3.5 μsec) and a solution of ethanol in *n*-hexane at 22°. No spectral change is seen over the range of concentrations, 100–5 mol % of ethanol. Their smallest concentration is too high in our terminology. Faster pulse and more dilute solution are clearly indicated; however, as they are, these experiments indicate a fairly long life for the so-formed solvated electron.

In the experiments of Kenney-Wallace and Hentz[19] solutions of alcohols (C_1–C_{12}) in cyclohexane are used in the concentration range 0.1–0.5 M. After a 5-nsec pulse of irradiation they see a fully grown spectrum which is invariant in position and shape. This finding is consistent with our description (see Table I and eq 21b). In comparatively dilute solutions a red shift of the absorption spectrum is seen. The concentrations used in these experiments are rather high in our terminology but it is not seen as a serious obstacle in extrapolating eq 21b in the region of some of their lower concentrations.

In this paper we have only computed the formation time of solvated electrons. It is reasonable to expect that attachment followed by gradual coagulation will shift the absorption spectrum of the solvated electron to the blue. However, there is as yet no simple *a priori* way to calculate this effect quantitatively.

Values of physical parameters used in this work are for a typical polar molecule in a typical hydrocarbon at room temperature. However, from the experiments we desire to know the dependence of formation time and of the absorption spectrum on the concentration of the solution. We also expect to see a little of the evolution of the spectrum with time. With these factors in mind we should look into media of high viscosity and high yield for escaped electrons. The last item facilitates observation since in a zero-order approximation the yield of solvated electrons is equal to the yield of escaped electrons. With respect to time scale of observation we calculate $t_2 \sim 10$ nsec from eq 21b for a medium of $\eta \sim 0.2$ P ($t_2 \propto \eta$) and a concentration of 0.1 M. Such a system seems promising as it will put the experiment in a convenient time scale.

Acknowledgment. This paper is dedicated to Professor Milton Burton on the occasion of his seventieth birthday. A part of the material of this paper was presented at the Radiation Chemistry Conference held at the University of Notre Dame during April 4–7, 1972. The author benefited from numerous discussions with members of the Radiation Laboratory. In particular, he would like to thank Dr. G. Kenney-Wallace, Dr. Pierre P. Infelta, and Dr. G. C. Abell.

(17) L. B. Magnuson, J. T. Richards, and J. K. Thomas, *Int. J. Radiat. Phys. Chem.*, 3, 295 (1971).
(18) B. J. Brown, N. T. Barker, and D. F. Sangster, *J. Phys. Chem.*, 75, 3639 (1971).
(19) G. Kenney-Wallace and R. R. Hentz, private communication.

Energy Level Structure and Mobilities of Excess Electrons in Aqueous and Organic Glasses

Larry Kevan

Department of Chemistry, Wayne State University, Detroit, Michigan 48202 *(Received May 1, 1972)*

Publication costs assisted by the U. S. Atomic Energy Commission and the U. S. Air Force Office of Scientific Research

Recent photoconductivity and optical bleaching studies of trapped electrons (e_t^-) as a function of wavelength and temperature have delineated the energy level structure of electrons in matrices of varying polarity. Results are described for alkaline ice (10 M NaOH), 5 M K_2CO_3 ice, crystalline ice, methyltetrahydrofuran (MTHF), and 3-methylhexane (3MH) solid matrices. In alkaline ice no stable bound excited state exists for trapped electrons. This conclusion is based on a wavelength-independent quantum efficiency for bleaching in the e_t^- absorption band and on temperature-independent photoconductivity and optical bleaching responses between 77 and 4.2°K. In single crystal ice an excited state for e_t^- is found ~0.4 eV below the lowest conduction level from photobleaching quantum efficiency measurements. In MTHF two excited states of e_t^- have been found. One is optically allowed and is ~0.6 eV below the bottom of the conduction state in a vertical transition from the ground state. The other is optically forbidden and is ~1.1 eV below the bottom of the conduction state in a vertical transition from this optically forbidden state. If the ground state is described by a 1s type wave function, the optically allowed state can be described by a 2p function and the optically forbidden state by a 2s function. Photoconductivity can be generated by both one- and *two-photon* processes. The two-photon process can be interpreted to occur *via* a 2s state. The energy level structure of e_t^- in 3MH is similar to that in MTHF. The energy level structure in the different matrices can be semiquantitatively accounted for by the semicontinuum model for trapped electrons. Both Hall and drift mobilities have been measured for photoexcited electrons in alkaline ice. The results are well described by a band model and the main scattering mechanisms are identified as optical lattice phonon scattering and O^- Coulombic scattering. Drift mobilities of mobile electrons in MTHF indicate that the electron motion is best described by a hopping model from 40 to 77°K.

Introduction

In the last several years, electronic properties of disordered systems have arrested considerable interest among both chemists and physicists. Many advances have been made in both theory and experiment.[1] In liquid rare gases the high mobilities of injected electrons suggest that a band-type structure exists.[2] However, more attention has been focused on amorphous semiconductors like amorphous germanium, amorphous silicon, and the chalcogenide glasses. Energy bands and energy band gaps seem to exist in these amorphous materials.[3] Also electrical switching phenomena have been observed, particularly in the chalcogenide glasses, in which a reversible transition between a highly resistive to a conductive state is effected by an electric field.[4]

Radiation chemists have something significant to contribute to the general area of electronic properties of disordered systems from their extensive studies of excess electrons in aqueous and organic glasses.[5,6] The particular areas of most direct contribution are probably those of the energy level structure and mobilities of electrons in aqueous and organic glasses. Measurements of electron mobilities in liquid hydrocarbons[7,8] and their theoretical description[9] are also of considerable significance.

The energy level structure of trapped electrons in aqueous and organic glasses is reported here in terms of photoconductivity and optical bleaching studies as a function of wavelength and temperature. Results are included for glassy alkaline ice (10 M NaOH), glassy 5 M K_2CO_3, crystalline ice, methyltetrahydrofuran glass (MTHF), and 3-methylhexane glass (3MH). The experimental results are discussed within the theoretical framework of the semicontinuum model for trapped electrons.[10,11] The energy level structure of the trapped electrons in the different matrices can be semiquantitatively accounted for by this semicontinuum model.

The motion of photoexcited electrons in delocalized or conduction band like states in glassy matrices is characterized by the electron mobility. Both Hall and drift mobilities have been measured for photoexcited electrons in alkaline ice. The results are well described by a band model and the main scattering mechanisms can be identified. Drift mobilities of mobile electrons in MTHF and 3MH indicate that the electron motion in these organic glasses is best described by a hopping model over at least a limited temperature range.

(1) N. F. Mott and E. A. Davis, "Electronic Processes in Noncrystalline Materials," Oxford University Press, London, 1971.
(2) L. S. Miller, S. Howe, and W. E. Spear, *Phys. Rev.*, **166**, 871 (1968); H. Schnyders, S. A. Rice, and L. Meyer, *ibid.*, **150**, 127 (1966).
(3) T. M. Donovan and W. E. Spicer, *Phys. Rev. Lett.*, **21**, 1572 (1968); T. M. Donovan, W. E. Spicer, and J. M. Bennett, *ibid.*, **22**, 1058 (1969).
(4) S. R. Ovshinsky, *Phys. Rev. Lett.*, **21**, 1450 (1968).
(5) L. Kevan, *Actions Chim. Biol. Radiat.*, **13**, 57 (1969).
(6) L. Kevan, *Actions Chim. Biol. Radiat.*, **15**, 81 (1971).
(7) W. F. Schmidt and A. O. Allen, *J. Chem. Phys.*, **52**, 4788 (1970).
(8) R. M. Minday, L. D. Schmidt, and H. T. Davis, *J. Chem. Phys.*, **54**, 3112 (1971).
(9) K. Fueki, D. F. Feng, and L. Kevan, *Chem. Phys. Lett.*, **13**, 616 (1972).
(10) K. Fueki, D. F. Feng, L. Kevan, and R. Christoffersen, *J. Phys. Chem.*, **75**, 2297 (1971). The conduction bands calculated in this paper are incorrect and are too low. For ice with $N = 4$ and $V_0 = 0$ the corrected value of the photoconductivity threshold I is 2.4 eV.
(11) K. Fueki, D. F. Feng, and L. Kevan, *J. Chem. Phys.*, **56**, 5351 (1972).

Experimental Section

Sample preparation has been previously described for alkaline ice[12] and MTHF.[13] The K_2CO_3 glassy ice was made by rapidly freezing a 5 M K_2CO_3 solution to 77°K. Large single crystals of ice were prepared by slowly lowering a test tube of triply distilled water at a rate of about 1 mm/hr into a temperature bath at −4°. After removal from the test tube and shaping, the transparent ice crystals had to be cooled gradually in a cold nitrogen gas flow system to 80°K before immersing them in liquid nitrogen prior to γ irradiation. If this gradual cooling were not done the ice crystals cracked badly. Samples of 3MH were prepared in the same fashion as the MTHF samples.

All irradiations were carried out at 77°K at a nominal dose rate of 0.30 Mrad/hr in a ^{60}CO γ source.

The photoconductivity apparatus has been described.[13] Temperatures above 77°K were obtained by a cold nitrogen gas flow system and temperatures below 77°K were obtained by a cold helium gas flow system. In the aqueous glasses the wavelength dependence of the photocurrent was determined with monochromatic light. However in the organic glasses the photocurrents were too low to use this method and a differential filter method[13] was used. In the differential filter method a series of long-wave pass filters that transmit all light beyond a certain wavelength were used. The photocurrent at a particular wavelength is obtained by subtracting the results with two different long-wave pass filters, but it is important to realize that each individual measurement includes a range of photons and this leads to effective double-beam excitation under certain conditions.

Optical bleaching measurements as a function of wavelength were monitored by epr in MTHF and 3MH samples. Monochromatic light was used for bleaching. Optical bleaching experiments in single crystal ice were monitored by optical absorption of the trapped electron. Absolute light intensities at the position of the samples were measured with a radiometer.

Hall mobility measurements were made with a double modulation method newly developed for high-impedance photoconductors.[14] Drift mobility measurements were carried out by a time-of-flight method in which a xenon light flash produces mobile electrons near one electrode by optically detrapping some of the trapped electrons, the electrons drift under an applied field to the opposite positive electrode and the time dependence of this current is amplified and observed by an oscilloscope.[15]

Results and Discussion

I. Energy Level Structure of Trapped Electrons. A. Alkaline Ice. One of the most polar matrices in which electrons are readily trapped is 10 M NaOH ice which is commonly called alkaline ice. The trapped electron in this matrix at 77°K is characterized by an optical absorption band with a maximum at 580 nm and an epr singlet at g = 2.001 with a line width between points of maximum slope of about 13 G. Photocurrent associated with the trapped electrons is readily observed by excitation with visible light.[12] The wavelength dependence of the photocurrent is shown in Figure 1. The photocurrent magnitude per incident photon has the same wavelength dependence as the optical absorption band. In other words, the quantum efficiency of the photocurrent is constant across the absorption band. Absolute values of the quantum efficiency of the photocurrent are not known because all of the photoexcited electrons do not travel the full distance between the two electrodes. The observed wavelength dependence in Figure 1 suggests that the optical absorption band corresponds to excitation of electrons from a bound ground state to a delocalized state which can be considered as a state of conduction band type. It is also possible that the excited state is a localized one that autoionizes to a state of conduction band type. From the available data one cannot distinguish between these two possibilities.

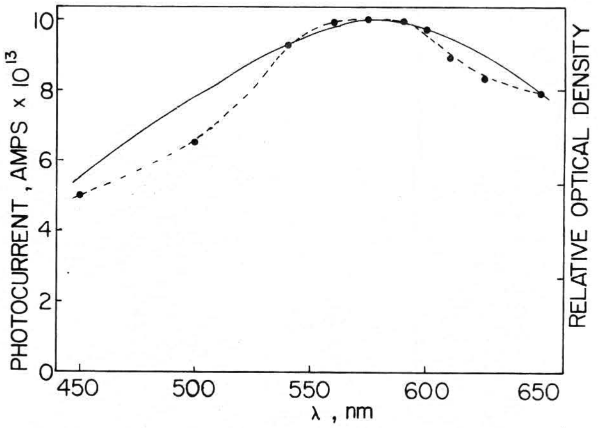

Figure 1. Wavelength dependence of photocurrent per incident photon in γ-irradiated (0.03 Mrad) 10 M NaOH at 77°K (dashed line). Optical absorption of trapped electrons in γ-irradiated 10 M NaOH at 77°K (solid line). The photocurrent curve maximum is normalized to the peak of the optical absorption curve.

One would also expect to be able to obtain similar data by looking at the wavelength dependence of the optical bleaching of electrons in the alkaline ice matrix, since this would correspond to loss of electrons from the ground state *presumably via* a delocalized state. The wavelength dependence of the optical bleaching has been studied.[16] However the band bleaches nonuniformly so the interpretation of the quantum efficiency of optical bleaching with wavelength is complex.

If the optical absorption band in alkaline ice really corresponds to direct excitation to a delocalized state or to an autoionizing state, then the rate of photoexcitation should be independent of temperature. This has been studied in two ways. The most straightforward method is to measure the temperature dependence of optical bleaching of the trapped electrons with broad band visible light excitation. Measurements made between 4 and 77°K in which the trapped electron concentration is monitored by epr show no temperature dependence.[17] The temperature dependence of the photocurrent has also been measured. This is more complex because the photocurrent I is given by eq 1

$$I = eF\mu\tau V/d \tag{1}$$

where F is the rate of photoexcitation, μ is the electron mobility, e is the electronic charge, τ is the average lifetime of an electron in the conduction band, V is the applied voltage, and d is the distance between the electrodes. Both F and μ may be temperature dependent; τ may also be temperature dependent but experiments show that it is independent of temperature below 77°K.[12] The temperature de-

(12) I. Eisele and L. Kevan, *J. Chem. Phys.*, **53**, 1867 (1970).
(13) T. Huang, I. Eisele, D. P. Lin, and L. Kevan, *J. Chem. Phys.*, **56**, 4702 (1972).
(14) I. Eisele and L. Kevan, *Rev. Sci., Instrum.*, **43**, 189 (1972).
(15) T. Huang, I. Eisele, and L. Kevan, *J. Phys. Chem.*, **76**, 1509 (1972).
(16) H. Hase and L. Kevan, *J. Chem. Phys.*, **54**, 908 (1971).
(17) P. Hamlet and L. Kevan, *J. Amer. Chem. Soc.*, **93**, 1102 (1971).

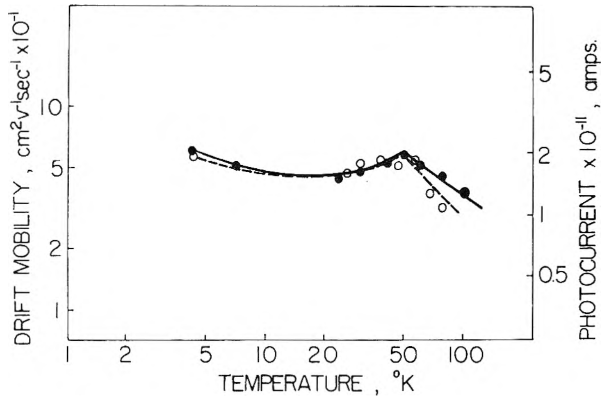

Figure 2. Temperature dependence of drift mobility (solid circles and solid line) and photocurrent (open circles and dashed line) of photoexcited electrons in γ-irradiated 10 *M* NaOH glassy ice. The photocurrent and drift mobility scales are adjusted to make the two sets of data coincide at 30°K (results by Huang of this laboratory).

pendence of the drift mobility of electrons in the alkaline ice matrix has been measured between 4 and 77°K.[15] The temperature dependence of the photocurrent has also been measured by Huang of this laboratory and his results together with the drift mobility results under the same experimental conditions are shown in Figure 2. It can be seen that the photocurrent varies in the same fashion as the drift mobility so that we may conclude that the rate of photoexcitation of electrons from the ground state to the delocalized or autoionizing state is independent of temperature.

From the above results we deduce the simple energy level diagram for the trapped electron in alkaline ice as shown in Figure 3. If the observed optical absorption corresponds to excitation to a conduction band state, then the threshold of the optical absorption band at about 830 nm (1.5 eV) is the photoconductivity threshold and is the energy from the ground state to the bottom of the conduction band state. One can interpret the maximum in the photocurrent response and the optical absorption band as corresponding to the maximum density of states in the conduction band as indicated in Figure 3. If an autoionizing state is involved, then the conduction band minimum may be either more or less than 1.5 eV above the ground state.

The only satisfactory theoretical model to explain the energy level structure in Figure 3 is a cubical or spherical well in which only short-range interactions are included. Any model in which long-range interactions, as represented by a polarization potential, are used and in which hydrogenic wave functions are used, will always predict bound excited states. On the basis of the semicontinuum model[10,11] the energy level structure in Figure 3 can be understood qualitatively as a limit in which only short-range charge dipole interactions are important.

B. 5 M K_2CO_3 Glassy Ice. Electrons are trapped in γ-irradiated 5 *M* K_2CO_3 glassy ice and are characterized by an absorption maximum at 540 nm. With visible light excitation, photocurrent associated with trapped electrons in this matrix can be observed. The wavelength dependence of the photocurrent per incident photon is shown in Figure 4 and compared with the optical absorption band as obtained by Noda in our laboratory. In contrast to the alkaline ice matrix the photocurrent wavelength dependence does not coincide with the optical absorption band. Instead it peaks at a slightly higher energy near 400 nm. There also appears

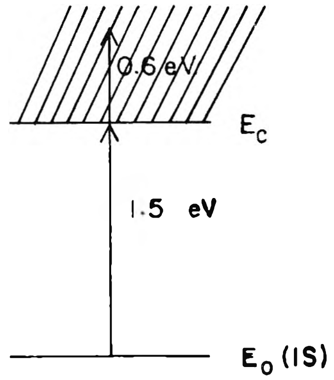

Figure 3. Energy level diagram for trapped electrons in 10 *M* NaOH glassy ice below 100°K. The threshold for photoconductivity is interpreted as the conduction band minimum, E_c.

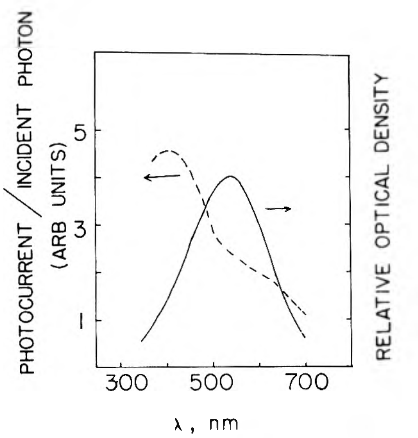

Figure 4. Wavelength dependence of photocurrent per incident photon (dashed line) and optical absorption of trapped electrons (solid line) in γ-irradiated 5 *M* K_2CO_3 glassy ice at 77°K (results by Noda of this laboratory).

to be a shoulder in the wavelength dependence of the photocurrent corresponding to the optical absorption band maximum. Since the wavelength dependence of the photocurrent does not coincide with the optical absorption band it seems that the optical absorption band at least partially corresponds to a transition from a bound ground state to a localized excited state. If we disregard the shoulder in the photocurrent response near 550 nm we can extrapolate the wavelength dependence of the photocurrent to a threshold near 600 nm. This energy is in fact less than the energy of the optical absorption maximum and suggests that there is little if any energy difference between the localized excited state and a conduction band state. The apparent shoulder in the wavelength dependence of the photocurrent may indicate transitions to the localized excited state which autoionize to the conduction band state. If this interpretation is correct, we can apparently distinguish between transitions to a localized autoionizing state and a delocalized conduction band state for trapped electrons in 5 *M* K_2CO_3 ice.

C. Single Crystal Ice. Only a very few electrons are trapped in crystalline ice. In fact, alkaline ice traps about 10^4 more electrons per unit radiation dose than does single crystal ice. This small yield makes it impossible to study the epr or the photocurrent associated with trapped electrons in crystalline ice. However, the optical absorption can be studied in large single crystals with a path length of 25 mm or longer. The optical absorption band has a peak at 640 nm as shown in Figure 5. The wavelength dependence of optical beleaching of electrons in crystalline at 77°K has

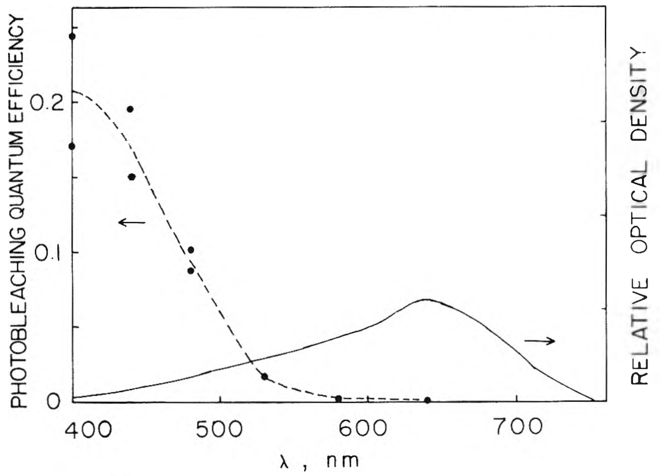

Figure 5. Wavelength dependence of photobleaching efficiency per absorbed photon (dashed line) and the optical absorption (solid line) of trapped electrons in γ-irradiated single crystal ice at 77°K (results by Ho of this laboratory).

recently been reported[18] and has also been studied by Ho in our laboratory. Our results are shown in Figure 5. It is clear that the quantum efficiency of optical bleaching has quite a different wavelength dependence than the optical absorption band. The trapped electrons are not significantly bleached until the exciting light energy is increased to that corresponding to the high-energy tail of the absorption band. From results in Figure 5 one can rather clearly assign the optical absorption band to a transition between a bound ground state to a stable bound excited state corresponding to 640 nm or 1.9 eV. The threshold of the bleaching quantum efficiency *vs.* wavelength curve is near 540 nm or 2.3 eV. This is interpreted as the energy corresponding to a transition from the bound ground state to the bottom of the conduction band state. Alternatively, an autoionizing state could be involved. The simple energy level diagram is shown in Figure 6.

It is interesting to compare the energy level diagram in Figure 6 with values calculated from the semicontinuum model for trapped and solvated electrons.[10,11] In this model the potential consists of short-range charge–dipole interactions and long-range polarization interactions. Hydrogenic wave functions are used with a variational parameter and treated by the self-consistent field method. The total energy of the system is calculated and configuration coordinate diagrams for the ground 1s state, the excited 2p state, and the conduction band state are determined. Four H_2O molecules are taken as the first solvation shell around the electron and the energy of the mobile electron in the conduction band (quasi-free electron state) is taken as $V_0 = -1$ eV. Then the configurational minimum of the ground state predicts an optical absorption maximum of $h\nu = 1.84$ eV and a photoionization threshold of $I = 2.4$ eV in excellent agreement with the experimental values shown in Figure 6. If six water molecules are taken as the first solvation shell around the electron, the calculated values are $h\nu = 1.85$ eV and $I = 2.4$ eV which are in equally good agreement with the experimental values. It is worth commenting that if only long-range polarization interactions are used in the framework of a dielectric continuum model, the calculated difference between I and $h\nu$ is much larger than the experimental values.[10] So short-range interactions are clearly an important and necessary part of an appropriate theoretical model for trapped and solvated electrons.

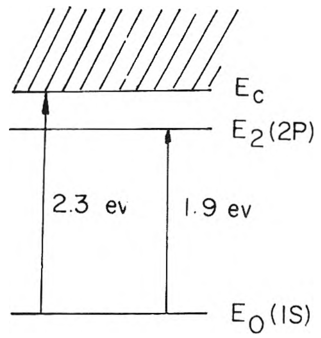

Figure 6. Energy level diagram for trapped electrons in single crystal ice at 77°K. Threshold for photobleaching is interpreted as the conduction band minimum, E_c.

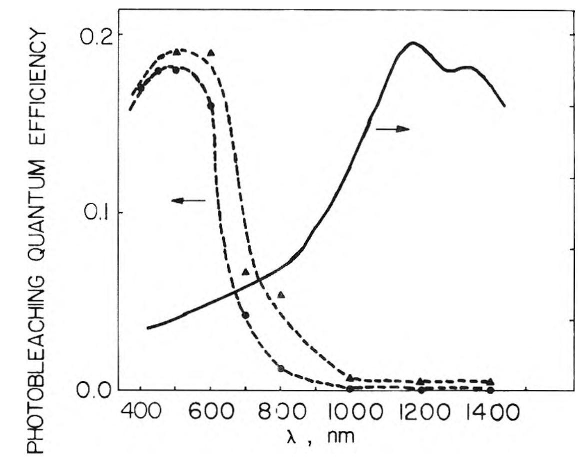

Figure 7. Wavelength dependence of photobleaching efficiency per absorbed photon (dashed lines) at 77 (▲) and 4.2°K (●), and the optical absorption (solid line) at 77°K of trapped electrons in γ-irradiated MTHF glass (ref 13).

The bound–conduction state transition for solvated or trapped electrons has also been considered by analogy to photoionization of hydrogen atoms by using hydrogenic wave functions.[19]

D. Methyltetrahydrofuran Glass. The trapped electron in MTHF glass is characterized by an optical absorption band with a maximum near 1180 nm and singlet epr spectrum at $g = 2.002$ with a width between points of maximum slope of 4.0 G. The optical absorption spectrum for trapped electrons in MTHF and the quantum efficiency of optical bleaching *vs.* wavelength are shown in Figure 7. The optical bleaching wavelength dependence is similar to what was found in crystalline ice and indicates that the optical absorption band corresponds to a transition between a bound ground state and a stable, bound excited state. The data in Figure 7 also indicate that direct transitions to a conduction band state or autoionizing state are possible at a threshold of about 800 nm. One would expect similar results by monitoring the wavelength dependence of the photocurrent, however, this is not possible with monochromatic light because the photocurrent magnitude is small. Instead, a differential filter method has been used to measure the wavelength dependence of the photocurrent associated with trapped electrons in MTHF glass. This method is effectively a double-beam excitation method.[13] Figure 8 shows

(18) K. Kawabata, *J. Chem. Phys.*, **55**, 3672 (1971).
(19) P. Delahay, *J. Chem. Phys.*, **55**, 4188 (1971).

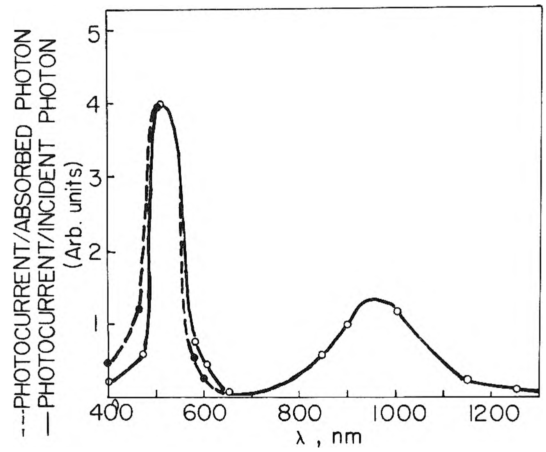

Figure 8. Wavelength dependence of photocurrent in γ-irradiated MTHF glass at 77°K and 8 kV/cm determined by the differential filter method with long-wave pass filters. The dashed line refers to photocurrent quantum efficiency and the solid line refers to photocurrent per incident photon. The peak near 520 nm is a one-photon transition and the peak near 950 nm is a two-photon transition. A quantum efficiency cannot be obtained in the ir region because the extinction coefficient of the intermediate state of the two-photon transition is unknown.

the wavelength dependence of the photocurrent in MTHF obtained by the differential filter method. In addition to the expected peak near 520 nm corresponding to direct excitation of electrons from the bound ground state to the conduction state, there is also a peak at 950 nm. Since the transition to the first excited state at 1180 nm is always excited under the conditions of our differential filter experiment, the 950-nm transition apparently represents a transition from an excited state to the conduction state. This is confirmed by the fact that the photocurrent magnitude near 950 nm depends on the square of the light intensity to within 10% (for data see ref 13). Thus, this represents a two photon transition. For comparison, it has been verified that the photocurrent at the 520-nm peak depends linearly on the light intensity.

A two-photon transition requires the existence of an intermediate state of significant lifetime. Additional evidence for the existence of such a state is indicated by the fact that the photocurrent associated with infrared light is characterized by a slow rise rather than an instantaneous peak. Photocurrent obtained with the visible light does show an instantaneous rise to a peak which is consistent with a direct one-photon transition to a conduction state.[13] The 950-nm transition can then be interpreted as one from an excited intermediate state directly to the conduction state or to an autoionizing state. The energy difference from the intermediate state to the bottom of the conduction band is then given by the threshold of the 950-nm band which occurs near 1150 nm = 1.08 eV.

In addition it has been found that there is a very small temperature dependence associated with the optical bleaching process by infrared light and also for the photocurrent excited by infrared light.[13] This temperature dependence corresponds to an activation energy of about 0.001 eV and is apparently associated with the population of the intermediate state. We can identify this temperature dependence with an activation energy for "intersystem" crossing from the excited state, to which the 1180-nm transition occurs, to the intermediate state, from which the 950-nm transition occurs. The intermediate state must be optically forbidden with respect to the ground state in order to achieve a sufficient population in it to allow an observable two-photon transition. So the intermediate state will have a different symmetry from the optically allowed state to which 1180-nm transition occurs.

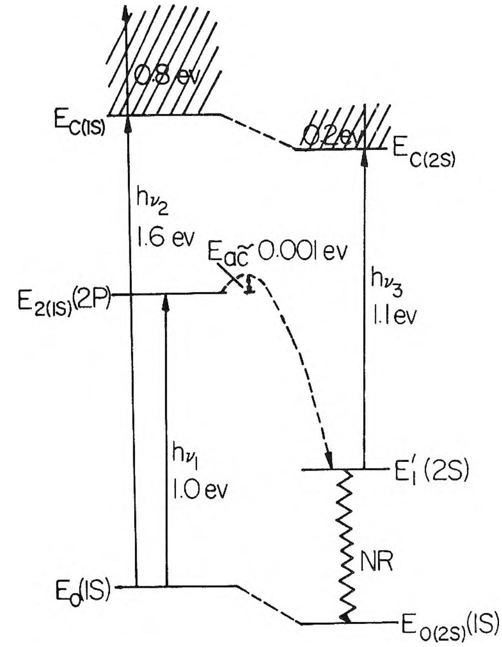

Figure 9. Energy level diagram for trapped electrons in MTHF glass at and below 77°K. 1s, 2s, and 2p refer to hydrogenic type wave functions; for vertical transitions to unrelaxed states the orbital in the subscript refers to the wave function which determines the orientational polarization of the matrix. NR refers to a possible nonradiative transition.

The above interpretation of the energy level structure of trapped electrons in MTHF is summarized in Figure 9. We identify the ground state E_0 as described by a 1s type wave function. The optical transition $h\nu_1$ must occur to an unrelaxed 2p type state E_2 due to the Franck-Condon principle. This unrelaxed state is one in which the orientational polarization of the matrix is determined by the ground state 1s type wave function as denoted by the 1s subscript. This unrelaxed 2p state then relaxes as the matrix nuclei respond to the 2p charge distribution and the orientation polarization of the matrix then becomes consistent with the 2p charge distribution. The right side of Figure 9 shows the relaxed 2s state and the vertical transitions from this state for the trapped electron system. We propose that the electron in the unrelaxed 2p state crosses with a small activation energy to the relaxed 2s state (E_1'). This temperature-dependent "intersystem" crossing presumably involves interaction with lattice vibrations of the MTHF matrix. Transition from the E_1' state is optically forbidden to the ground state but a nonradiative path (NR) may exist. Also an allowed optical transition $h\nu_3$ from E_1' to the conduction band E_c', which is consistent with the charge distribution of the E_1' state, is interpreted as the origin of the infrared photocurrent. If we interpret $h\nu_3$ as a direct transition to the conduction band, the wavelength dependence of the infrared photocurrent peak suggests that the maximum density of conduction band states lies about 0.2 eV above the bottom of the conduction band. In addition to $h\nu_1$ another transition from E_0 given as $h\nu_2$ is interpreted to occur directly to the conduction band E_c which is consistent with the charge distribution of the E_0 state. The visible photocurrent wavelength peak suggests that the maximum density of states in this

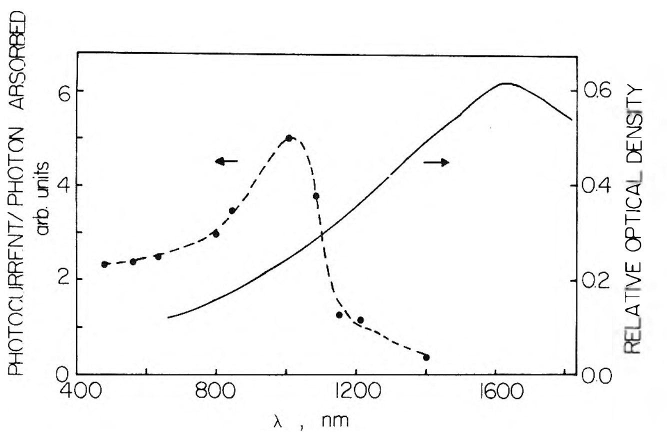

Figure 10. Wavelength dependence of photocurrent per absorbed photon (dashed line) and optical absorption band (solid line) of trapped electrons in γ-irradiated 3MH glass at 77°K (ref 20).

conduction band is about 0.8 eV above the bottom of the conduction band for vertical transitions from E_0. This can differ from the value for the vertical transitions from E_1' since the configuration coordinate and charge distributions are, in general, different. If autoionizing states are involved in the transitions to the conduction state, the qualitative features of Figure 9 will still be retained.

The semicontinuum model has been applied to trapped electrons in glassy MTHF at 77°K to compare with the experimental results by Feng, Fueki, and Kevan.[20] Four MTHF molecules are taken as the first solvation shell around the electron and the energy of the mobile electron in the conduction band (quasi-free electron state) is taken as $V_0 = -0.5$ eV. Configurational coordinate diagrams for various energy levels are determined. The configurational minimum of the ground state predicts an optical absorption maximum of $h\nu = 1.0$ eV in agreement with the experimental value $h\nu_1 = 1.0$ eV and an ionization threshold of $I = 1.4$ eV in agreement with the experimental value of $h\nu_2 = 1.6 \pm 0.2$ eV. Calculation of the configurationally relaxed 2s and 2p states shows that the relaxed 2s state lies above the relaxed 2p state by about 0.1 eV all along the configuration coordinate and that the relaxed 2s state crosses the unrelaxed 2p state near its configurational minimum. This calculation is remarkably consistent with the postulate that optical excitation from the ground 1s state ultimately carries the electron to a relaxed 2s state. Thus it appears that the semicontinuum model satisfactorily accounts for the observed two-photon transition in the MTHF system. The energy difference between the relaxed 2s state and the conduction band state consistent with the relaxed 2s state is 0.6 eV which is only fair agreement with the observed value of $h\nu_3 = 1.1$ eV. However the essential features of the energy level diagram in Figure 9 are accounted for remarkably well by the semicontinuum theoretical model.

E. 3-Methylhexane Glass. The trapped electron in the 3-methylhexane (3MH) glassy matrix is characterized by a broad optical band with a peak at 1650 nm and an epr line at $g = 2.002$ with a line width between points of maximum slope of about 3.7 G. Studies on the wavelength dependence of the photocurrent and the optical bleaching of trapped electrons in 3MH glass indicate a similar energy level structure to that found in MTHF.[21] Figure 10 shows the wavelength dependence of the photocurrent obtained by the differential filter method and the optical absorption band of electrons in 3MH. By analogy to the results in MTHF we can interpret the optical absorption band as occurring to a bound excited state and we can interpret the photocurrent peak as associated with direct transitions to a conduction band state. The threshold of the photocurrent peak occurs near 1300 nm which can be interpreted as the energy difference from the ground state to the bottom of the conduction band. In the wavelength range below 1200 nm the photocurrent depends linearly on light intensity. It is not possible to extend the photocurrent measurements to wavelengths longer than 1400 nm because the signal is too weak, however, it is possible to measure the light intensity dependence of the photocurrent produced by light from 1400 to 2000 nm. These results show quite definitely that the photocurrent in the region of the optical absorption maximum depends on the square of the light intensity. This result indicates that a two-photon transition also exists in the 3-methylhexane glass just as is found in the MTHF glass. The wavelength dependence of the optical bleaching carried out with monochromatic light confirms this by the observation of one peak at 1000 nm and another peak close to 1650–1700 nm.[21] We can therefore interpret the peak near 1650–1700 nm as a transition from an excited intermediate state to the conduction band. This peak can be observed by monochromatic light excitation because it fortuitously has the same photon energy as the transition from the ground state to the first excited state which is associated with the optical absorption band.

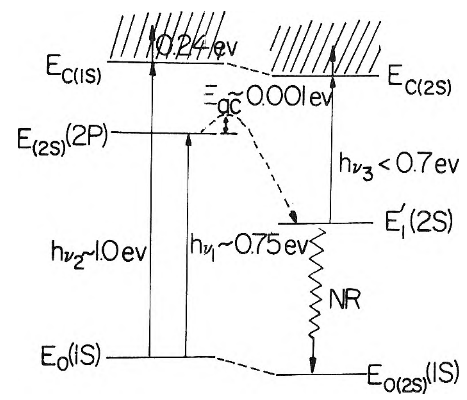

Figure 11. Energy level diagram for trapped electrons in 3MH glass at 77°K. 1s, 2s, and 2p refer to hydrogenic type wave functions; for vertical transitions to unrelaxed states the orbital in the subscript refers to the wave function which determines the orientational polarization of the matrix. NR refers to a possible nonradiative transition. The subscript for the 2p energy level should be 2(1s).

The temperature dependence of the optical bleaching rate constant was also measured.[21] There is little temperature dependence for light excitation at wavelengths shorter than 1200 nm, however, for longer wavelengths a temperature dependence is seen which extrapolates to an activation energy of 0.001 eV near 1650 nm. As in MTHF this temperature dependence can be associated with the population of the intermediate excited state associated with the two-photon transitions.

The results on the energy level structure of trapped electrons in 3MH can be summarized by the energy level diagram of Figure 11. The explanation and justification of this diagram are the same as for the MTHF energy level diagram in Figure 9. No comparison can be made with theoretical calculations for electrons in the 3MH matrix because the

(20) D. F. Feng, K. Fueki, and L. Kevan, submitted for publication.
(21) T. Huang and L. Kevan, submitted for publication.

semicontinuum model has not yet been extended to nonpolar media.

From the results found for the various matrices from alkaline ice to potassium carbonate ice to crystalline ice to MTHF and to 3MH, we have developed a general picture of the energy level structure of electrons in these various matrices. The example matrices span the entire range of matrix polarity and show a rather rich structure associated with the energy levels of trapped electrons in various matrices. In the polar ice matrices we have weakly bound excited states or no bound excited state at all as in the case of alkaline ice. No experimental evidence for two-photon transitions has been obtained although it is possible that in crystalline ice, for example, a two-photon transition does exist. It is difficult to observe this experimentally because the second photon presumably lies in the infrared which is the same region as that in which the ice matrix itself absorbs. In the MTHF matrix a bound excited state exists and also a two-photon pathway to the conduction band has been found. Even more pleasing is the fact that the semicontinuum model seems to satisfactorily account for all of the structure observed in the energy level diagram of trapped electrons in MTHF.

II. Mobility of Photoexcited Electrons. A. Electron Mobility in Alkaline Ice. Since trapped electrons can be photoexcited to a delocalized or conduction band type state to produce photocurrent, it is relevant to consider the motion of the photoexcited electrons in these conduction band states. Their motion is characterized by a mobility. Several types of mobility can be measured experimentally. The most fundamental information is given by the Hall mobility which corresponds to the electron motion in crossed electric and magnetic fields. The Hall mobility is intrinsically a microscopic mobility and is independent of trapping effects if they exist. It has recently been possible to measure Hall mobility of photoexcited electrons in the alkaline ice matrix.[22] Since the Hall voltage is extremely small and the impedance of the photoconducting glassy 10 M NaOH ice is of the order of 10^{10} ohms, it was necessary to develop a new double-modulation method for measuring Hall mobilities in high-impedance photoconductors.[14] In our method, the magnetic field is modulated at 3.3 Hz by rotating the sample in the magnetic field and the density of charge carriers is modulated at 90 Hz by chopping a light beam. A dc electric field is applied to the sample to produce the photocurrent and the resulting Hall voltage is detected with a lock-in detector at the sum frequency of 93.3 Hz. This method successfully discriminates against all error signals and has allowed the first measurement of Hall mobilities in such high-impedence photoconductors.[14]

The most accurate measurements of the electron Hall mobility in alkaline ice were made at 80°K and gave $\mu_H(80°K) = 4.7 \pm 1.9$ cm^2 V^{-1} sec^{-1}. This is a rather large microscopic mobility for electrons in a glassy or amorphous matrix. The magnitude alone suggests that the electrons can be regarded as traveling in a true energy band; this conjecture has been confirmed by measuring the temperature dependence of the mobility. Between 80 and 133°K the mobility increases with decreasing temperature. This is indicative of lattice phonon scattering and confirms that the electron motion can be treated in terms of a band model. Scattering of electrons by lattice phonons can be considered in terms of acoustical phonon and optical phonon interaction. The observed temperature dependence of the electron Hall mobility can be represented by either $\mu_H \propto \exp(131/T)$ or $\mu_H \propto T^{-1.3}$. For an ideal band structure these two temperature dependencies are characteristic of optical phonon scattering and acoustical phonon scattering, respectively. From the Hall mobility data alone a clear distinction between these two modes of phonon scattering cannot be made. However, from drift mobility results to be discussed below, it can be concluded that optical phonon scattering is the dominant interaction.

The second type of experimental mobility that has been measured for electrons in alkaline ice is the drift mobility. This is a macroscopic mobility measured across a finite sample distance, and it is subject to trapping effects. The drift mobility is measured with a time-of-flight method. A light flash produces mobile electrons near one electrode by photoexcitation of some of the trapped electrons produced in the alkaline ice sample by γ irradiation. The optical density is such that the electrons are only produced close to one electrode. These electrons then drift under an applied field to the positive electrode and the time dependence of this current is observed on an oscilloscope. The scope signal rises to a maximum within the response time of the amplifier, is constant while the mobile electrons move across the sample and decreases when they reach the opposite electrode. The time from the light flash to the break point for the decrease is taken as the transit time of mobile electrons. The drift mobility is calculated from $\mu_D = L^2/Vt$, where V is the applied voltage, t is the transit time, and L is the sample thickness. Many of the electrons are trapped in transit and do not make it to the other electrode, however, a few electrons do make the transit without being trapped, and it is the mobility of these electrons that is measured and is significant. At 77°K a field independent value of the drift mobility of 2 cm^2 V^{-1} sec^{-1} has been measured. This value agrees well with the Hall mobility and suggests that the drift mobility that we are measuring is indeed a true microscopic mobility characteristic of electron transport in a conduction band.

The most interesting result of the drift mobility data is that at fields of 10^3 V/cm and above the drift mobility is found to be field dependent. This means that the electrons can be heated-up somewhat above their thermal energy normally maintained by equilibrium with lattice interactions.

Before presenting the drift mobility results, it is useful to review the temperature and field dependencies expected for the mobility under different conditions. For ideal bands in which the conduction band minimum occurs at $\mathbf{k} = 0$ where $\mathbf{k}$ is the wave vector, acoustical phonon scattering leads to $\mu \propto T^{-3/2}$ and $\mu \propto F^{-1/2}$ for hot electrons where F is the field. For optical phonon scattering $\mu \propto \exp(\theta_0/T)$ for $T < \theta_0$ where θ_0 is the Debye temperature for optical modes, or $\mu \propto T^{-3/2}$ for $T > \theta_0$, and $\mu \propto F^{-1}$ for hot electrons.[23] For 10 M NaOH ice θ_0 has been estimated at 151°K.[22]

Another scattering mechanism that is found to be important for electrons in the alkaline ice matrix is ionic species scattering which is simply a Coulombic scattering interaction between the mobile electron and an ionic scattering center. The temperature dependence for this scattering mechanism is given by $\mu \propto T^{3/2}/\ln(1 + aT^2)$ where a depends upon characteristics of the lattice but is independent of temperature.[24] The field dependence for the scattering

(22) I. Eisele and L. Kevan, *J. Chem. Phys.*, 55, 5407 (1971).
(23) F. J. Blatt, "Physics of Electronic Conduction in Solids," McGraw-Hill, New York, N. Y., 1968, pp 254–258.
(24) E. Conwell and V. F. Wiesskopf, *Phys. Rev.*, 77, 388 (1950).

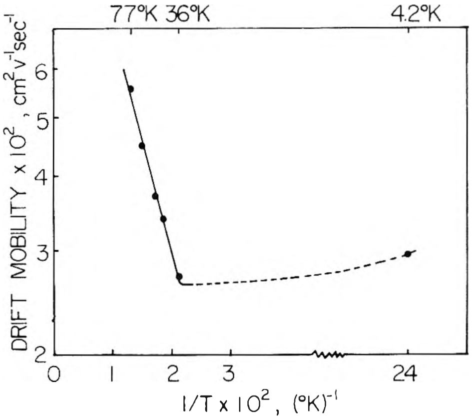

Figure 12. Temperature dependence of drift mobility of photoexcited electrons in γ-irradiated MTHF glass (ref 26).

mechanism is given as $\mu \propto F^3$ for hot electrons.[25]

The field and temperature effects on the electron drift mobility in alkaline ice can be summarized as follows.[13,26] At 77°K above fields of 5 kV/cm it is found that $\mu_D \propto F^{-1}$. This shows that optical phonon scattering is a dominant scattering mechanism and that it dominates all other mechanisms at very high fields. At lower fields around 0.6 kV/cm the mobility increases with increasing field in a manner consistent with the ionic species scattering mechanism. The temperature dependence of the drift mobility also indicates that both scattering mechanisms are operative. Above 50°K at low fields the drift mobility temperature dependence approaches $T^{3/2}$ which is consistent with lattice phonon scattering and is consistent with the Hall mobility measurements. Between 50 and 4°K at low fields the electron drift mobility varies in a manner consistent with the ionic species scattering mechanism.

It is also interesting to consider the identity of the ionic species that serve as scattering centers in the alkaline ice matrix. The most obvious candidates are the Na^+ and OH^- ions of the matrix. However, these ions do not serve as scattering centers because, according to estimates based on the Conwell-Weisskopf formula, such a high concentration of scattering centers is only consistent with mobility magnitudes 10^2–10^3 times lower than observed. The mobility magnitudes are in fact consistent with the concentration of O^- and e_t^- ions present in the matrix. O^- is confirmed to be one of the scattering species as shown by a decrease in the drift mobility as the O^-/e_t^- ratio is increased for constant e_t^- concentration.[15]

Thus for the alkaline ice matrix Hall and drift mobility measurements are able to confirm that the electrons can be described as moving in a conduction band, as being scattered by optical phonon interactions with the lattice and by ionic species scattering with O^- ions in the lattice, and as exhibiting hot electron effects.

B. Electron Mobility in MTHF and 3-Methylpentane (3MP) Glasses. Drift mobility measurements have been made for electrons in MTHF glass[27] and in 3MP glass.[28] Very low mobilities of less than 0 1 cm^2 V^{-1} sec^{-1} or less were observed in both matrices and no hot-electron effects were found up to fields of 40 kV/cm. In MTHF, drift mobility measurements were made as indicated above for the alkaline ice matrix from 77 to 4.2°K. The results are shown in Figure 12. Between 36 and 77° K the drift mobility increases with increasing temperature in contrast to the results found in alkaline ice, and it seems to be temperature activated with an Arrhenius activation energy of about 0.0035 eV. The measurement at 4.2°K is about the same as that at 36°K and suggests that there is little or no temperature dependence in this range. This conjecture is supported by the results in 3MP where several measurements were made between 30 and 4.2°K which indicated essentially no temperature dependence.

The drift mobility results for electrons in 3MP[28] are very similar to the results found for MTHF. For 3MP the experimental technique was slightly different in that the electrons were photoinjected into the 3MP glass from a layer of *N,N,-N′,N′*-tetramethyl-*p*-phenylenediamine (TMPD) film deposited on the surface of one electrode. Measurements were made between 4.2 and 77°K. Little or no temperature dependence was found between 4.2 and 35°K and between 35 and 77°K the mobility was temperature activated with an activation energy of about 0.01 eV. In 3MP the maximum mobility observed at 77°K is about 0.1 cm^2 V^{-1} sec^{-1} which is about twice as high as the mobility observed in MTHF at 77°K. At 4.2°K the mobility in 3MP is only about half the value of 0.03 cm^2 V^{-1} sec^{-1} for electrons in MTHF glass.

For a temperature activated mobility there are two different ways to interpret the transport mechanism. One way is to use a hopping model which was first treated by Holstein[29] and has been treated more completely by Munn and Siebrand.[30] Basically, one can say that charge transport occurs *via* electronic exchange interactions and that this transport is hindered by competing electron–phonon interactions. When electron–phonon interactions dominate, charge transport occurs by a series of uncorrelated phonon-assisted lattice jumps or, in other words, the transport is incoherent. This model is called the hopping model.

A second model that can explain temperature activated charge transport is a trapping model. In the trapping model, a set of trapping sites exist in the matrix independent of the position of the charge carrier. We can then think of the electrons as moving in a band subject to being localized in traps as they pass near them. The electron is simply considered to be in thermal equilibrium between a set of traps and a conduction band. In the trapping model there is no reason to expect that the temperature dependence of the mobility would abruptly change as the temperature is lowered as seems to be the case for the drift mobility in both MTHF and 3MP glasses near 35°K. Thus, we tentatively conclude that the trapping model is not consistent with the drift mobility data on electron motion in nonpolar organic glasses. It is worthwhile to comment that if successful electron Hall mobility measurements are made in MTHF or 3MP glass, the nonapplicability of the trapping model could be directly tested. Since the Hall mobility measures the microscopic mobility which would correspond to the electron mobility when moving between traps, the Hall mobility should be much larger than the measured drift mobility in MTHF or 3MP glass. Furthermore, the Hall mobility consistent with a trapping model should have a temperature dependence characteristic of band motion.

We choose to discuss the drift mobility results in nonpolar glasses in terms of a hopping model. The change in the temperature dependence near 35°K can be interpreted as follows. At lower temperatures, the electron–phonon interac-

(25) E. M. Conwell, *Phys. Rev.*, 90, 769 (1953).
(26) T. Huang and L. Kevan, to be submitted for publication.
(27) T. Huang and L. Kevan, to be submitted for publication.
(28) Y. Maruyama and K. Funabashi, *J. Chem. Phys.*, 56, 2342 (1972).
(29) T. Holstein, *Ann. Phys. (New York)*, 8, 343 (1959).
(30) R. W. Munn and Siebrand, *J. Chem. Phys.*, 52, 6391 (1970).

tions become less important relative to electronic exchange interactions. If electronic exchange interactions dominate completely, we have coherent transport which is the same as band motion. In Holstein's original work the change from hopping to band transport as the temperature was lowered was calculated to occur over a narrow temperature range since the transition region from incoherent to coherent motion was not adequately treated. Holstein's model would predict that the drift mobility should show a rather sharp rise between 35 and 4.2°K if indeed band transport were becoming important in that region. However, Munn and Siebrand have been able to treat the electron–phonon interactions in more detail and have been able to more adequately treat the region in which change from hopping to band transport occurs as the temperature is lowered. It is clear from their results that this transition region can be consistent with little or no temperature dependence as seems to be observed in the experimental results of the electron drift mobility in organic glasses.

It is clear that the transport mechanism for electrons is vastly different between aqueous and organic glasses. Since electron transport in the aqueous glasses can be treated in terms of a simple band model it seems to be relatively well understood at the moment. However in the organic glasses the electron transport mechanism is less well delineated. It is probable that Hall mobility measurements *vs.* temperature for the organic glasses would give sufficient information to definitively describe the electron transport mechanism in them.

Acknowledgment. This research was supported by the Air Force Office of Scientific Research under Grant No. AFOSR-70-1852 and by the U. S. Atomic Energy Commission under Contract No. AT(11-1)-2086. I am deeply indebted to the following students and colleagues who have contributed to this work: I. Eisele, D. F. Feng, K. Fueki, P. Hamlet, H. Hase, K. K. Ho, T. Huang, D. P. Lin, and S. Noda.

An Investigation of the Structure of the Hydrated Electron Based on Unpaired Electron Densities Calculated by the INDO Method[1]

Carolyn M. L. Kerr[*2a] **and Ffrancon Williams**[2b]

Department of Chemistry, University of Tennessee, Knoxville, Tennessee 37916 *(Received May 1, 1972)*

Spin density distributions have been calculated for a number of possible structures for the hydrated electron, and the total spin density associated with the hydrogen atoms compared with the value derived from esr experiments. Although the agreement with experiment is not close, the best results are obtained for a planar dimeric structure containing two central hydrogens close to one another. The structure of the hydrated electron may incorporate symmetrically placed units of this type.

I. Introduction

In this study the INDO method[3] has been employed to investigate the structure of the hydrated electron using a comparison of the experimental and theoretical spin densities on the hydrogen nuclei as a criterion of structural validity. This approach is used in preference to the conventional one of minimizing the energy of the system with respect to geometrical parameters for two reasons. First, the spin density distribution for a paramagnetic species is generally very sensitive to the molecular structure, and the INDO method has been shown to yield isotropic hyperfine coupling constants in good agreement with experiment for a wide variety of both σ and π radicals whose geometries can be reasonably well defined.[3c] The agreement is generally better for hydrogen than for second row elements. Second, the INDO method is not always reliable for predicting equilibrium geometries based on energy minimization. This is hardly surprising since the parameterization was intended to yield charge densities and spin densities rather than properties dependent on the molecular energies.[4]

The use of a completely molecular description instead of the familiar cavity or polaron models[5] of the hydrated electron stems from recent work in this laboratory on electron excess centers in acetonitrile[6] and sulfuryl chloride.[7] In

(1) This research was supported by the U. S. Atomic Energy Commission under Contract No. AT-(40-1)-2968, and this is AEC Document No. ORO-2968-75.

(2) (a) Author to whom correspondence should be addressed at the Department of Chemistry, The University, Southampton, S09 5NH, Hampshire, England. (b) John Simon Guggenheim Memorial Foundation Fellow, 1972–1973.

(3) (a) J. A. Pople and D. L. Beveridge, "Approximate Molecular Orbital Theory," McGraw-Hill, New York, N. Y., 1970. (b) Program 141, Quantum Chemistry Program Exchange, Department of Chemistry, Indiana University, Bloomington, Inc. 47401. Computations were carried out on an IBM System 360/65 digital computer. (c) J. A. Pople, D. L. Beveridge, and P. A. Dobosh, *J. Amer. Chem. Soc.*, **90**, 4201 (1968).

(4) J. N. Murrell and A. J. Harget, "Semi-empirical SCF Molecular Orbital Theory of Molecules," Wiley-Interscience, New York, N. Y., 1972, p. 57.

(5) J. Jortner in "Actions Chimiques et Biologiques des Radiations," Vol. 14, M. Haissinsky, Ed., Masson et Cie., Paris, 1970.

(6) E. D. Sprague, K. Takeda, and F. Williams, *Chem. Phys. Lett.*, **10**, 299 (1971).

(7) (a) C. M. L. Kerr and F. Williams, *J. Amer. Chem. Soc.*, **93**, 2805 (1971); (b) C. M. L. Kerr and F. Williams, *ibid.*, **94**, 5212 (1972).

acetonitrile, γ irradiation yields either the monomer or dimer radical anion depending upon the crystalline phase. The monomer radical anion is a typical σ radical with appreciable spin density in the 2s orbital of the nitrile carbon due to the bending of the molecule. On the other hand, the spin density distribution in the dimer radical anion indicates the unpaired electron is associated with two equivalent and essentially linear molecules, with most of the spin density in the p orbitals on nitrogen. According to a simple MO description, the dimer radical anion can be considered as a radical anion complex in which the unpaired electron occupies a supramolecular bonding orbital derived from the antibonding orbitals of two separate molecules. The radical anion of sulfuryl chloride can be described similarly, and in this case the molecular orbitals involved are essentially the lowest antibonding orbitals of adjacent sulfur dioxide and chlorine molecules.

In certain respects, the properties of the dimer radical anion of acetonitrile resemble those of trapped electrons in glasses. In particular, the esr signals of both these species saturate readily with microwave power and the optical absorption spectra are characteristically broad. These similarities suggest that in the case of trapped or solvated electrons, the excess electron may be confined to the orbitals of two or more solvent molecules rather than to an interstitial cavity. Accordingly, the hydrated electron can be formally represented as $(H_2O)_n\cdot^-$.

The esr spectrum of the trapped electron in aqueous solids is generally a broad singlet but hyperfine structure has been resolved in two instances.[8,9] Both in crystalline ice codeposited with alkali metals[8] and, more recently, in a γ-irradiated alkaline glass,[9] the spectrum was shown to consist of an odd multiplet with a splitting of approximately 5 G. From these results, it has been suggested that the trapped electron interacts with either four[8] or six[9] protons. In any event, the existence of resolved hyperfine features certainly points to a well-defined molecular structure for $(H_2O)_n\cdot^-$ rather than to a disordered cage of water molecules surrounding a trapped electron. A line-shape analysis[10] on the unresolved spectrum also indicates that the hyperfine interaction is limited to a relatively small number (8 ± 2) of protons. If eight protons can be considered an upper limit, the observed hfs of 5 G as compared to the value of *ca.* 500 G for the isolated H· atom indicates a total spin density on hydrogen for the complex of 8% or less. The aim of the present work has been to seek structures of $(H_2O)_n\cdot^-$ for which the calculated spin density distrubution approximates most closely to this experimental result.

2. Calculations

The INDO method employs a valence orbital basis set which in this case consists of the 1s orbitals on hydrogen and 2s and 2p orbitals on oxygen. The calculations yield the spin density distribution of the excess electron over the valence shell orbitals of the water molecules in the complex.

Bond orders between two atoms were calculated as the sum of all off-diagonal elements involving the atoms in the charge density matrix. While the numerical values obtained have no absolute significance, comparison of bond orders in a closed shell species and in the negatively charged open shell species with the same geometry can be used to determine the bond-breaking or bond-forming effect resulting from the addition of an electron.

3. Results

The results of calculations on the monomer, $H_2O\cdot^-$, are

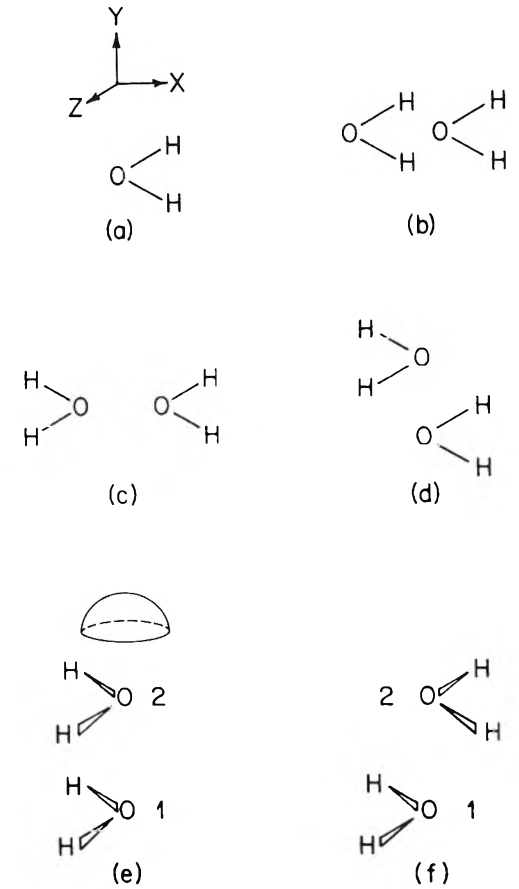

Figure 1. Models used in INDO calculations on the structure of the hydrated electron: (a) monomer shown in the *xy* plane with the coordinate axis system which defines the directions of the oxygen p orbitals for all models in this figure and in Figure 3; (b–f) represent various dimer models incorporating aligned oxygen p orbitals of the individual molecules.

presented first. For this species, the OH bond length was varied from 0.08 to 0.19 nm in increments of 0.01 nm, and the HOH angle from 60 to 180° in increments of 10°. The corresponding values for the neutral molecule are 0.096 nm and 105°.[11] Positive spin density is always obtained in the s orbitals of both hydrogen and oxygen. There is also considerable spin density in the oxygen p_x and p_y orbitals, but none in the p_z orbital (see Figure 1a). The spin densities in the p_x and p_y orbitals are always of opposite sign, and increase monotonically with the bond length. The positive spin density is associated with the p_y orbital for OH distances of 0.08–0.14 nm and for HOH angles of 60–90°, and with the p_x orbital for all other geometries. The total spin density on hydrogen, $\rho_H{}^T$, where this quantity is defined generally for multimeric species as

$$\rho_H{}^T = \sum_{\text{all H}} |\rho_H|$$

varies both with bond angle and bond length as shown in Figure 2. For the shorter bond lengths, minima occur in the curves for angles of 100 to 110°, but there is no corresponding optimum bond length, $\rho_H{}^T$ increasing regularly as the

(8) J. E. Bennett, B. Mile, and A. Thomas, *J. Chem. Soc. A*, 1393 (1967); 1502 (1969).
(9) K. Ohno, I. Takemura, and J. Sohma, *J. Chem. Phys.*, **56**, 1202 (1972).
(10) B. G. Ershov and A. K. Pikaev, *Radiat. Res. Rev.*, **2**, 1 (1969).
(11) L. Pauling, "The Nature of the Chemical Bond," 3rd ed, Cornell University Press, Ithaca, N. Y., 1960, pp. 110, 464.

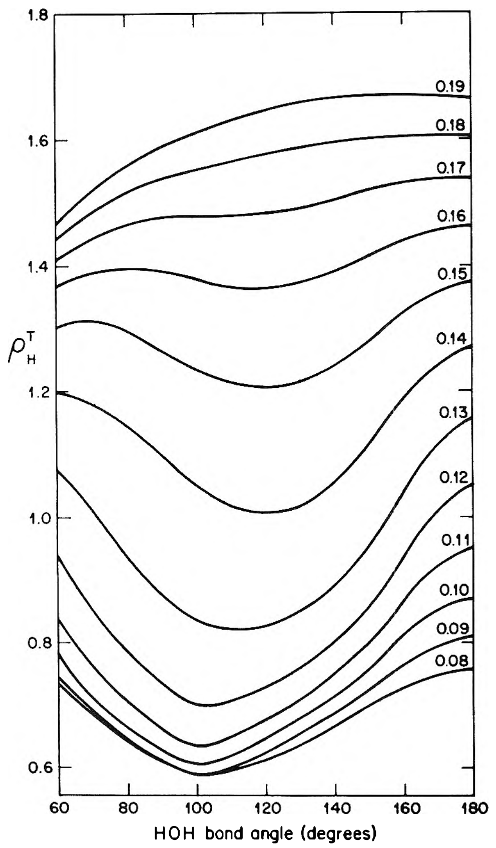

Figure 2. Variation of $\rho_H{}^T$ for $H_2O\cdot^-$ with the HOH angle for various OH bond lengths. Bond lengths are given in nm.

OH distance is increased. The O–H bond order decreases steadily with increasing bond length, and for bond lengths up to 0.14 nm, it has a value which is about 0.7 times that of the neutral molecule with the same geometry. For higher bond lengths, the bond orders for $H_2O\cdot^-$ and H_2O are both small. These factors and the high negative spin densities observed in the oxygen p orbitals suggest that the large values of $\rho_H{}^T$ and their variation with bond length reflect a progressive breakdown in the OH bonding.

The large $\rho_H{}^T$ found for $H_2O\cdot^-$ definitely excludes this as the structure of the hydrated electron. However, by analogy with acetonitrile where there are profound differences between the spin density distributions and structures of monomer and dimer radical anion, this does not rule out the possibility that suitable combinations of H_2O molecules could yield values of $\rho_H{}^T$ in closer accord with experiment. Based on this, our approach has involved the determination of $\rho_H{}^T$ for multimeric species $(H_2O)_n\cdot^-$. Since the values of $\rho_H{}^T$ for the monomer are extremely large, we have investigated various geometrical arrangements of molecules in $(H_2O)_n\cdot^-$ complexes to determine which configurations lead to a decrease in $\rho_H{}^T$.

Calculations have been done on a variety of different dimeric structures. The first set of structures are shown in Figure 1b–f. The distinguishing feature of these is that the oxygen p orbitals are aligned so that a strong overlap is possible. It has been shown previously[7] that an excess electron can be effectively shared between two molecules through positive overlap of antibonding orbitals from the separate molecules. An additional consideration in the present case is that bonding between the H_2O molecules through the oxygen p orbitals might redistribute the spin density in favor of these orbitals, thereby decreasing $\rho_H{}^T$.

For any particular structure, equivalent H_2O geometries were always employed. The OH bond length, the HOH angle, and d, the distance apart of the oxygen atoms, were varied independently over the ranges 0.09–0.12 nm, 90–135°, and 0.16–0.24 nm, respectively. The results showed that in structure b, there appeared to be no delocalization and the distribution was essentially that of the $H_2O\cdot^-$ monomer and a neutral H_2O molecule for all configurations; in all other structures, the unpaired electron was shared equally between the two molecules. For structures c and d, there was no reduction in $\rho_H{}^T$ whereas a reduction was found for structures e and f, this being larger in the case of the former for all configurations. A number of structures intermediate between e and f were generated by allowing the hydrogen atoms of the upper molecule to range over the surface of a hemisphere, as shown in Figure 1e. For all of these, $\rho_H{}^T$ was found to be greater than the value for structure e, suggesting that parallel alignment of the p orbitals is a contributing factor in reducing $\rho_H{}^T$.

The calculations were extended to trimer and tetramer for model e. Although there were some irregularities, in general $\rho_H{}^T$ decreased monotonically in going from monomer to tetramer and the largest decreases were observed for OH bond lengths of 0.11–0.12 nm, an HOH angle of 105°, and d = 0.18–0.20 nm. The results are summarized in Table I. For these geometries, the spin density on oxygen is largely in the p_x orbital with small negative contributions in the p_y and p_z orbitals, as shown in Table II. It can also be seen from the data given in this table that the overall distribution of the spin density in an individual molecule is not greatly altered between monomer and tetramer.

The models discussed above are somewhat unrealistic. Since the microstructure of an aqueous solid is controlled by hydrogen bonding, models in which molecules are linked by hydrogen bonding should also be considered. Although other configurations have been observed, hydrogen bonded systems generally involve linear or nearly linear O-----H—O units. A simple dimer incorporating this feature is shown in Figure 3a, the O-----H—O line making an approximately tetrahedral angle with the O–H bonds of molecule **2**. Calculations were performed for the same range of bond lengths and bond angles as previously and oxygen–oxygen distances of 0.24 to 0.30 nm (the corresponding distance in ice is 0.276 nm[11]). In all these cases, the unpaired electron was ef-

TABLE I: Values of $\rho_H{}^T$ for Model e Multimers[a]

OH bond length, nm	HOH angle, deg	O–O distance, nm	$\rho_H{}^T$				$\rho_H{}^T$ (tetramer) / $\rho_H{}^T$ (monomer)
			Monomer	Dimer	Trimer	Tetramer	
0.11	105	0.18	0.644	0.533	0.480	0.443	0.69
0.11	105	0.20	0.644	0.537	0.519	0.448	0.70
0.12	105	0.18	0.704	0.537	0.463	0.383	0.54

[a] These geometries yielded minimum values of $\rho_H{}^T$ for the tetramer.

TABLE II: Comparison of Spin Density Distributions for Monomers and Model e Tetramers with the Same Molecular Geometry[a]

OH bond length, nm	HOH angle, deg	O-O distance, nm	Species		ρ_H[b]	ρ_O^s	$\rho_O^{p_x}$	$\rho_O^{p_y}$	$\rho_O^{p_z}$
0.11	105		Monomer[c]		0.322	0.107	0.377	0.000	−0.128
0.11	105	0.18	Tetramer[d]	(1,4)	0.015	0.015	0.055	−0.003	−0.005
				(2,3)	0.096	0.055	0.203	−0.008	−0.033
				Total	0.222	0.140	0.516	−0.022	−0.076
0.11	105	0.20	Tetramer[d]	(1,4)	0.012	0.010	0.050	−0.001	−0.004
				(2,3)	0.101	0.052	0.207	−0.003	−0.036
				Total	0.226	0.124	0.514	−0.008	−0.080
0.12	105		Monomer[c]		0.352	0.085	0.397	0.000	−0.185
0.12	105	0.18	Tetramer[d]	(1,4)	0.003	0.007	0.064	−0.001	−0.001
				(2,3)	0.093	0.040	0.246	−0.004	−0.044
				Total	0.192	0.094	0.620	−0.010	−0.090

[a] These geometries yielded minimum values of ρ_H^T for the tetramers. [b] Refers to only one hydrogen nucleus. In all molecules the hydrogens are equivalent. [c] For comparison, the monomer is considered here to be in the xz plane as are the individual molecules of the tetramer (see Figure 1). [d] The molecules in the tetramer are equivalent in pairs.

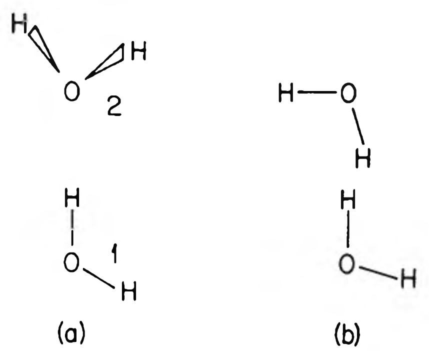

Figure 3. (a) A dimer model for the hydrated electron incorporating hydrogen bonding; (b) dimer model found to give lowest value of ρ_H^T. This model is planar with an OH bond length of 0.12 nm, an HOH angle of 105°, an oxygen-oxygen distance of 0.31 nm, and a distance between central hydrogens of 0.072 nm.

fectively localized on one molecule. Small rotations (up to 30°) of molecule **2** about the three coordinate axes (see Figure 1a) hardly affected the delocalization or the value of ρ_H^T, indicating that structures derived from a hydrogen-bonded fragment are unfavorable.

Further calculations were then carried out for an OH bond length of 0.11 nm, an HOH bond angle of 105°, an oxygen-oxygen distance of 0.27 nm, and configurations such that the position of molecule 1 and the linearity of the O-----H—O unit were retained and the hydrogen atoms of molecule 2 were rotated over the surface of a sphere. Over a small range of configurations, both delocalization and a decrease in ρ_H^T were observed. Once the configuration yielding the minimum value of ρ_H^T had been determined, ρ_H^T was minimized with respect to the bond length, bond angle, and oxygen-oxygen distance, these parameters being varied over the ranges 0.09 to 0.12 nm, 90 to 135°, and 0.23 to 0.35 nm, respectively. The lowest value of ρ_H^T was found for the configuration shown in Figure 3b with an OH bond length of 0.12 nm, a bond angle of 105°, and an oxygen-oxygen distance of 0.31 nm. The spin density distributions for this structure and for the monomer with the same molecular geometry are shown in Table III. A further limited number of calculations were performed with the above molecular geometry, but varying the orientations of both molecules and the distance between them. Spin densities close to the values obtained for the dimer in Figure 3b were found for dimers symmetrical about the oxygen-oxygen axis and with hydrogen-hydrogen distances of 0.08 to 0.09 nm. Slightly higher spin densities were obtained for symmetrical dimers containing linear O—H-----H—O units. The minimum values of ρ_H^T found for these structures are listed (Table III) with the associated structural parameters and spin densities.

From the data given in Table III, it can be seen that the distribution is substantially different for monomer and dimer, in contrast to the results obtained for model e. There is a marked shift of both spin density and charge density from hydrogen to oxygen in the dimer relative to the monomer. A further point to note is that the spin densities in all orbitals of the dimers in Table III are zero or positive.

TABLE III: Comparison of Spin Density Distributions for Monomer and Dimer Species Yielding Minimum ρ_H^T Values

Species[a]	O-O distance, nm	H-H distance, nm	ρ_H outer	ρ_H inner	ρ_O^s	$\rho_O^{p_x}$	$\rho_O^{p_y}$	$\rho_O^{p_z}$	ρ_H^T
Monomer			0.352	0.352	0.085	0.397	−0.185	0.000	0.704
Dimer	0.31	0.072	0.012	0.105	0.045	0.021	0.360	0.000	0.209
(as in Figure 3b)			0.013	0.079	0.040	0.071	0.256	0.000	
Symmetrical dimer[b,c]	0.31	0.079	0.012	0.092	0.043	0.043	0.310	0.000	0.208
Linear dimer[b,d]	0.33	0.090	0.018	0.091	0.041	0.064	0.287	0.000	0.217

[a] The molecular geometry is the same for all these species (OH bond distance = 0.12 nm, HOH angle = 105°). The monomer and the individual molecules of the dimer are in the xy plane (see Figures 1a and 3b). [b] The molecules are equivalent. The total spin density associated with any type of orbital is thus twice the quoted value. [c] Planar configuration as in Figure 3b except that the molecules have both been rotated until the center hydrogens are symmetrically placed with respect to the oxygen-oxygen axis. [d] Planar configurations as in Figure 3b except that molecule 2 has been rotated until both inner hydrogens are linear with the oxygens.

The proximity of the central hydrogen atoms appears to be an important feature of these structures. Low values of ρ_H^T were only observed for hydrogen-hydrogen distances in the range 0.07–0.10 nm, and these were associated with bond orders between the hydrogen atoms of 0.5–0.7. The bond orders in the corresponding neutral molecule dimer are almost a factor of 2 less than this, and the values for isolated hydrogen molecules are 1.0.

4. Discussion

In this paper we have examined the possibilities for determining the structure of the hydrated electron by comparison of theoretical and experimental unpaired electron densities. Although the investigations of the various structures are not exhaustive, they are reasonably detailed and lead to two general conclusions. First, dimers with certain configurations can yield values of ρ_H^T substantially less than that for the monomer with the same molecular geometry. Second, for a dimer structure which was shown to yield a reduced ρ_H^T, further reduction was obtained by increasing the number of molecules in the complex.

It is interesting that the optimum dimer model on the basis of spin densities is structurally similar to others proposed on other grounds. The dimer structure suggested by Raff and Pohl[12] consists essentially of an H_2^+ fragment perturbed by two OH^- ions. A degree of bonding is thus implied between the central hydrogens. This model yields a value for the optical excitation energy in good agreement with experiment. Webster and his coworkers[13] have investigated a similar model, *viz.*, a planar dimer containing a linear O—H-----H—O unit, using two different molecular orbital methods. In both cases, structures corresponding to the minimum energy give excitation energies close to the experimental value. However, the optimum hydrogen-hydrogen separations (0.12 nm for the INDO and 0.15 nm for the extended Hückel method) are somewhat larger than the range (0.07–0.10 nm) found in the present work.

While the dimer shown in Figure 3b clearly does not represent the complete structure of the hydrated electron, it has several favorable features which suggest that the complete structure may incorporate units of this type. Moreover, if a larger even number of molecules, *i.e.*, four or six, is used, symmetrical structures can be constructed which contain four or more equivalent protons as required by the esr results,[8-10] and calculations are currently in progress for these systems.

Acknowledgment. We would like to thank Dr. J. E. Bloor for his help and advice, and for lending us his INDO program.

(12) L. Raff and H. A. Pohl, *Advan. Chem. Ser.*, **No. 50**, 173 (1965).
(13) (a) B. J. McAloon and B. C. Webster, *Theor. Chim. Acta*, **15**, 385 (1969); (b) G. Howat and B. C. Webster, *Ber. Bunsenges. Phys. Chem.*, **75**, 626 (1971).

Precise Measurements of *W*, the Average Energy Required for Ion Pair Formation. II. Alcohols and Water[1]

G. G. Meisels* and D. R. Ethridge

Department of Chemistry, University of Houston, Houston, Texas 77004 *(Received May 1, 1972)*

Publication costs assisted by the U.S. Atomic Energy Commission

Ionization currents produced in simple alcohols by the decay of ^{63}Ni were measured with a reproducibility of about 0.01% at approximately 100 and 200° and over a pressure range of from 600 to 2500 Torr. In methanol and ethanol extrapolated and normalized ionization currents appear to decrease by approximately 5% over this range; this is ascribed to incomplete ion collection by applying a criterion for the attainment of saturation based on an analysis of slopes of current *vs.* potential curves. The following values of W relative to $W(N_2) = 34.6$ were obtained in the lower pressure range where ion collection is essentially complete: $W(H_2O) = 29.15 \pm 0.09$, $W(CH_3OH) = 25.02 \pm 0.09$, $W(C_2H_5OH) = 24.50 \pm 0.09$, $W(n\text{-}C_3H_7OH) = 23.86 \pm 0.08$, $W(i\text{-}C_3H_7OH) = 24.25 \pm 0.09$, $W(n\text{-}C_4H_9OH) = 23.53 \pm 0.12$, $W(2\text{-}C_4H_9OH) = 23.53 \pm 0.12$, and $W(i\text{-}C_4H_9OH) = 23.38 \pm 0.11$ eV per ion pair.

Introduction

The improvement of our insight into elementary processes in radiation chemistry, an endeavor which has made forceful strides as a result of the devotion of Professor M. Burton to this field, requires a continual reduction of the time span covered by the prime radiation chemical symbol, the wiggly arrow introduced by Burton. Modern pulse techniques are able to penetrate the picosecond range,[2] but details of the ionization process involving isolated molecules and their interaction with high-energy radiation are as yet not accessible.

Information on the ionization process can also be ob-

(1) Presented as part of a plenary lecture on "Ionization of Gases by High Energy Radiation" at the International Conference on Elementary Processes of Radiation Chemistry, held in honor of the 70th birthday of Professor Milton Burton at the University of Notre Dame, April 4–7, 1972.
(2) J. E. Aldrich, M. J. Bronskill, R. K. Wolff, and J. W. Hunt, *J. Chem. Phys.*, **55**, 530 (1971).

tained from the study of gross ionization in gases. Particularly the investigation of mixtures,[3-7] primarily using α-ray ionization chambers,[4-7] has resulted in a considerable increase of our understanding of second-order ionization processes and of the role and yield of excited states in the rare gases. These states are relatively long-lived or represent trapped resonance radiation. This kind of investigation has, however, not provided information on fast first-order ionization processes with picosecond lifetimes. At least in principle, this time range should be accessible from data on the change in the rate of ionization with pressure. For example, collisions may affect the branching between preionization and predissociation of a superexcited state[8] $M^*(E_j)$ with energy E_j greater than the ionization potential (I.P.) in a mechanism which may be summarized as

$$M \rightsquigarrow M^*(E_j) \quad (1)$$

$$M^*(E_j) + M \rightarrow M^*(E_{j+1}) + M \quad (2)$$

$$M^*(E_j) \rightarrow M^+ + e \quad (3j)$$

$$M^*(E_j) \rightarrow \text{neutral products} \quad (4j)$$

where reaction 2 removes energy from excited intermediates to yield states of lower excitation energy (E_{j+1}), etc.; k_{3j}/k_{4j} is a function of E_j, possibly discontinuous, and is obviously zero for $E_j <$ I.P. Provided that the lifetime of the $M^*(E_i)$ states is sufficient, increased gas density will effect a reduction in the mean excitation energy $\langle E_j \rangle$. Presumably $\langle k_{3j}/k_{4j} \rangle$ will decrease as $\langle E_j \rangle$ decreases since $k_{3j} = 0$ for $E_j <$ I.P.; one can express the effect of this change in the probability distribution of excitation energies by recognizing the dependence of the distribution on density ρ, *i.e.*, $P(E_j,\rho)$. Denoting the yield of all superexcitation processes as G_s and that of all direct ionization processes as G_d, the yield of ions in this formalism is

$$G_{\text{ions}} = G_d + G_s \sum_{E_j = \text{I.P.}}^{\infty} \{k_{3j}(E_j)/[k_{3j}(E_j) + k_{4j}(E_j)]\}P(E_j,\rho) \quad (A)$$

If only a single state ss were involved and if the first collision always were to cause a reduction of E_j to $E_{j+1} <$ I.P., the familiar expression

$$G_{\text{ions}} = G_d + G_{ss}[k_3/k_2[M + k_3 + k_4)] \quad (B)$$

would result. In any event, the change in ionization yield with density arises through $P(E_j,\rho)$.

Even if such a mechanism should be operative, preionization lifetimes could not be assessed directly because the rate constant of reaction 2 cannot be estimated directly from collision theory. Not only may not all collisions be strongly deactivating,[9] but the collision diameter of the species M^* is uncertain. Molecular autoionizing states are largely high-lying Rydberg series[10,11] with mean radii considerably greater than those of molecules in their ground electronic state. However, an effective deactivating collision should require interaction with the core to remove vibrational energy. Since the mean of the radial distribution function of Rydberg states decreases with increasing n, that is, the wave function becomes spread over a larger volume, the collision may also be approximated as occurring between a quasi-ion and a neutral molecule to give an upper limit to the rate constant.

In order for such a mechanism to manifest itself, autoionization rates must be sufficient to be detectable within the precision of the method. The first criterion seems to be fulfilled since theoretical considerations[10-12] have indicated that autoionization lifetimes in hydrogen should be in the range of 10^{-8} to 10^{-12} sec, and the magnitude should be comparable for more complex molecules particularly since lifetimes approach infinity, for transitions involving the same initial and final vibrational states, as the principal quantum number increases.[11,12] Yields, however, are probably small.

Recently Brehm, *et al.*,[13] have reported photoionization studies which suggest strongly that autoionization may be a substantial contributor to overall ionization in methanol and ethanol. Therefore, we have measured precise ionization rates in a series of alcohols and have investigated the dependence of total ionization currents in methanol on pressure between 600 and 2500 Torr at 200°, corresponding to collision-free periods of from 3 to 11 $\times$ 10^{-11} sec at the lower pressure and 0.8 to 2.8 $\times$ 10^{-11} sec at the higher pressure depending on whether one assumes a collision of hard spheres having molecular dimensions, or regards the collision as the interaction of a quasi-ion with a neutral molecule and employs the experimental ion-molecule reaction rate constant of 2.5 $\times$ 10^{-9} cm^3 sec^{-1} for reaction of CH_3OH^+ with CH_3OH.[14]

Experimental Section

Ionization produced by decay of ^{63}Ni plated on the central section of a parallel nickel wire grid, of 0.005-in. diameter, centered in a spherical chamber was measured as a function of applied voltage using a current to frequency converter by determining the period elapsed during the accumulation of a preset count. Details of the apparatus and procedure have been reported previously.[15] Minor changes included potting of the external portion of the triaxial feedthrough with General Electric RTV silicone resin to reduce arcing, and replacement of the mercury manometer with a Heise Model CMM-6, 0–4000-Torr pressure gauge accurate to 0.1% and reproducible to 0.02%.

All alcohols were the purest grade available from Matheson Coleman and Bell and were distilled on a 1 m $\times$ 1-cm glass bead column, the middle one-third being retained. Water was distilled from permanganate solution. Samples were degassed by pumping on the liquid at ambient temperature immediately prior to vaporization and introduction into the sample handling system.

Results

1. Relative Ionization in Alcohols. Contrary to earlier observations in hydrocarbons and nitrogen,[15] where the

(3) (a) W. P. Jesse, *J. Chem. Phys.*, **41**, 2060 (1964); (b) W. P. Jesse and R. L. Platzman, *Nature (London)*, **195**, 790 (1962).
(4) G. S. Hurst, T. E. Bortner, and R. E. Glick, *J. Chem. Phys.*, **42**, 713 (1965).
(5) T. D. Strickler, *J. Phys. Chem.*, **67**, 825 (1963).
(6) C. E. Klots, *J. Chem. Phys.*, **44**, 2715 (1966).
(7) L. M. Hunter and R. H. Johnsen, *J. Phys. Chem.*, **71**, 3228 (1967).
(8) R. L. Platzman, *Vortex*, **23**, (8), 372 (1962).
(9) S. C. Chan, J. T. Bryant, and B. S. Rabinovitch, *J. Phys. Chem.*, **74**, 2055 (1970).
(10) R. S. Berry, *J. Chem. Phys.* **45**, 1228 (1966).
(11) J. N. Bardsley, *Chem. Phys. Lett.*, 1, 229 (1967).
(12) (a) S. E. Nielsen and R. S. Berry, *Chem. Phys. Lett.*, **2**, 503 (1968); (b) G. B. Shaw and R. S. Berry, *J. Chem. Phys.*, **56**, 5808 (1972).
(13) B. Brehm, V. Fuchs, and P. Kebarle, *Int. J. Mass Spectrom. Ion Phys.*, **6**, 279 (1971).
(14) S. K. Gupta, E. G. Jones, A. G. Harrison, and J. J. Myher, *Can. J. Chem.*, **45**, 3107 (1967).
(15) T. A. Stoneham, D. R. Ethridge, and G. G. Meisels, *J. Chem. Phys.*, **54**, 4054 (1971).

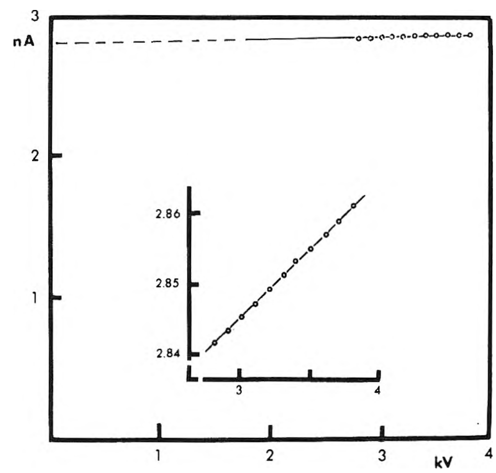

Figure 1. Variation of observed collector current i with applied potential. The insert is an expanded section and point size corresponds to approximately 0.01% of the ion current (isobutyl alcohol, 203°, 907 Torr).

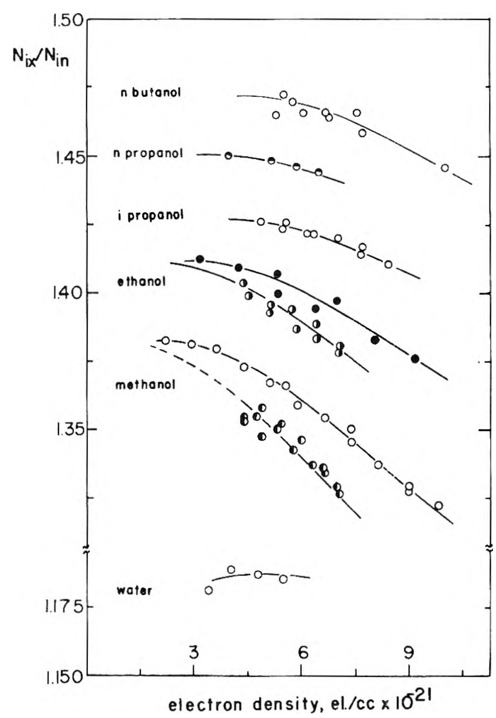

Figure 2. Variation of extrapolated ion current (N_{ix}) normalized to the extrapolated ion current in nitrogen at the same electron density (N_{in}) with electron density. Top to bottom: 1-butanol, 213°; 1-propanol, 236°; 2-propanol, 193°; ethanol, 203°; ethanol, 123°; methanol, 204°; methanol, 118°; water, 240°.

dependence of ion current on voltage is linear above 1–1.5 kV, apparent linearity was observed for the alcohols only at higher voltages. While the reproducibility of individual points was on the order of 0.005% and their deviation from a straight line in the region used for extrapolation was within the same magnitude, least-squares analysis of the data to assess the intercept showed typical standard deviations of the intercept to be 0.02 to 0.06%. An example of the saturation curve and the precision attainable are shown in Figure 1 for 2-methyl-1-propanol (isobutyl alcohol) at 203° and 907 Torr.

Intercepts obtained by this procedure (N_{ix}) were compared to those obtained on the same day for nitrogen at the same electron density (N_{in}) over a range of pressures and for methanol and ethanol, at two temperatures. Since errors which may result from incomplete energy loss of the β particle and back-scattering should be roughly related to electron density of the sample and to a lesser extent to the effective atomic number, our results are presented in Figure 2 as a function of electron density. Not shown are results for isobutyl alcohol which are nearly superimposable on those for 1-butanol and those for 2-butanol.

It is apparent that the relative extent of ionization decreases with increasing pressure or electron density for all alcohols, although the degree of dependence varies. No such variation was observed for alkanes over an even larger range of electron densities.[15] It was necessary therefore to investigate the possibility that this variation is an artifact resulting from incomplete ion collection which does not manifest itself in a deviation from linearity of current *vs.* voltage plots.

2. *Criterion for Total Ion Collection.* The apparent ion current can be expressed as the sum of a series of contributions, which include a resistive component R in the feedthrough assembly, and a number of energy terms: the mean effective β-ray energy, E_β, the energy associated with back-scatter into the grid wires, E_{BS}, that which is lost to adjacent wires or the chamber walls (E_{geom}), and energy gained (or lost) by electrons under the influence of the collecting field (E_{field}). In addition, total ion pair formation resulting from the energy terms may be reduced by incomplete collection and increased by ion multiplication. The ion current i is related to these parameters by the equation

$$i = \frac{V}{R} + \frac{DF}{N_A W}(E_\beta - E_{BS} - E_{geom} + E_{field})fM \quad (I)$$

where N_A is Avogadro's number, V is the applied potential, F is Faraday's constant, and D is the rate of disintegration of ^{63}Ni. W is the average energy per ion pair and is assumed to be independent of the source of energy, while f is the collection efficiency and M is the ion multiplication factor.

The first three energy terms do not affect relative measurements at the same electron density, while the energy gained by the field should be approximately proportional to the applied potential and the range of the electron.[16] Since the range is inversely proportional to electron density ρ, one may write

$$E_{field} = \frac{cV}{\rho} \quad (II)$$

where c is a proportionality constant.

The collection efficiency has been analyzed by Boag.[17] For spherical chambers in the limit where collection is nearly complete, it can be written as

$$f = 1 - \frac{C\rho_n P^2 k_r}{T^2 K_+^0 K_-^0 V^2} \quad (III)$$

where C is a constant, k_r is the recombination coefficient, K^0 represents the reduced mobility of the positive and negative species, respectively, and P is the pressure. The exponent n of ρ may be as large as 3 and arises from the variation in mean ionization density, which increases as the cube of stopping power of the medium for a point source. For our chamber, n is probably between 2 and 3.

(16) C. Wingate, W. Gross, and G. Failla, *Radiat. Res. Res.*, **8**, 411 (1958).
(17) J. Boag in "Radiation Dosimetry," G. J. Hine and G. L. Brownell, Ed., Academic Press, New York, N. Y., 1956, Chapter 4, p 153.

The P^2 term results from the pressure dependence of the mobility.

The ion multiplication factor is related to the first Townsend coefficient α[18,19] since multiplication is small

$$M = \exp(\alpha d) \approx 1 + \alpha d \qquad \text{(IV)}$$

Here d is the mean distance between ion pair formation and the chamber walls and somewhat, but not greatly, dependent on density since ion formation is always predominantly near the central grid structure. Substitution of the empirical form of α yields

$$M \cong 1 + AP\mathrm{d}\exp(-BP/V) \qquad \text{(V)}$$

where A and B are constants.

Insertion of all expressions into (I), neglect of the product of terms much smaller than unity, and combination of the first three energy terms into a net energy E_n, yields

$$i = V/R + [DF/(N_A W)](E_n + cV/\rho)[1 - C\rho^n P^2 k_r/(T^2 K_+{}^0 K_-{}^0 V^2) + AP\mathrm{d}\exp(-BP/V)] \qquad \text{(VI)}$$

Apparently the last two terms which allow for incomplete collection and ion multiplication are small enough not to reflect themselves in nonlinearity of plots of i *vs.* V. However, the extrapolation occurs over a substantial range, and even relatively minor systematic errors in the slope will amplify themselves in the extrapolation procedure. The slope of N_i *vs.* V plots should be given by the derivative of eq VI.

$$\frac{\mathrm{d}i}{\mathrm{d}V} = \frac{1}{R} + \frac{DF}{N_A W}\left[\frac{c}{\rho} + \frac{C\rho^n P^2 k_r}{T^2 K_+{}^0 K^0 V^2}\left(\frac{c}{\rho} + \frac{2E}{V}n\right) + Ad\left(\frac{cP}{\rho} - \frac{BcP}{V} - \frac{BP^2 E}{V^2}n\right)\exp\left(-\frac{BP}{V}\right)\right] \qquad \text{(VII)}$$

When complications from other factors are absent, only the first two terms contribute and a plot of slope *vs.* $1/\rho$ should yield a straight line with intercept $1/R$ and slope $DcF/(WN_A)$.

Equation VII was tested using propane as a standard; no apparent pressure effect has been observed for this gas at electron densities up to 1.2×10^{21} electrons cm^{-3}, and in fact a linear relationship is obtained over this density range (Figure 3). At high electron densities, however, even propane shows an increase in slope, and concomitant saturation ionization currents determined from intercepts decrease while W values so obtained increase. The deviation sets in at even lower electron densities in methanol and ethanol, and scatter as well as deviations from a line calculated using eq VII and the empirical values of R and c derived from the propane data are more dominant at the lower temperature. The deviation of the slope calculated for methanol at 10^{21} electrons cm^{-3} is about 25%; this is an order of magnitude larger and opposite in sign to that predicted from eq VII and the possible change of W indicated in Figure 2. However, good adherence to the relationship predicted for the absence of complications is observed at 200° and at electron densities less than 5×10^{20} electrons cm^{-3}, and we conclude that in this range intercept currents can be associated with complete collection.

Discussion

1. Pressure Dependence of W and Autoionization. At electron densities greater than 5×10^{20} electrons cm^{-3} there is a substantial decrease in intercept ion currents N_{ix}/N_{in} (Figure 2). At the same time, these intercepts are

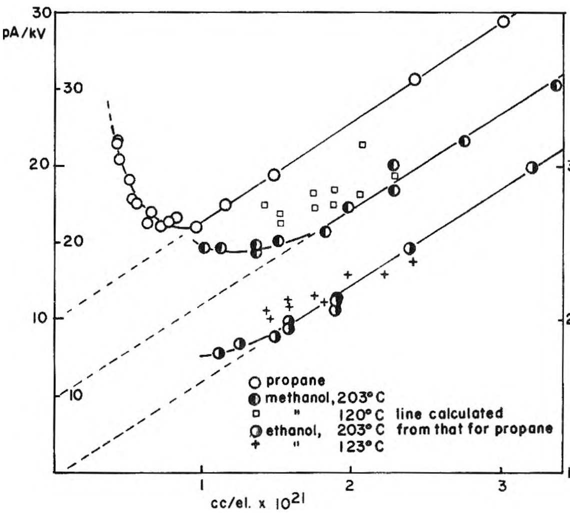

Figure 3. Variation of slope of ion current *vs.* collection potential plots with reciprocal electron density. Lines for methanol and ethanol are those calculated using the empirical constants derived from propane and correction for the difference in *W*. Scales are shifted vertically for clarity of presentation: top, propane; center, methanol, squares at 118°, circles at 204°; bottom, ethanol, crosses at 123°, circles at 203°.

decreased by increases in slope which become density dependent in this range. Equation VII shows that this slope depends most strongly on density as a result of those terms which arise from incomplete collection. At equivalent electron densities, the behavior of different compounds will primarily depend on ionic mobilities. Since mobilities of all ions in strongly polar gases are much smaller than in hydrocarbons, the earlier onset of deviations from the predicted relationship for alcohols is qualitatively consistent with expectations.

The small change in N_{ix}/N_{in} in methanol at 200° at electron densities less than 5×10^{20} cm^{-3} (1.1%) is outside experimental error but it is possible that it is still a result of the same effects. At the same time it must be noted that in this density range the correction for incomplete stopping of the β particle becomes significant (*ca.* 1%).[15] We believe, therefore, that the variation with ρ of extrapolated ionization currents in this range is still a result of incomplete ion collection.

The present measurements have not afforded the precision or reliability necessary to demonstrate unambiguously whether a mechanism such as that suggested in eq 1–4 significantly affects total ionization in alcohol vapors. The small change (*ca.* 1%) in N_{ix}/N_{in} for methanol may be taken as an upper limit for such a contribution. Extension of measurements to higher pressures using different source geometries to improve collection will be required and construction of a cylindrically symmetrical chamber for this purpose has been initiated.

2. W Values for Alcohols. The apparent difficulty in achieving complete ion collection may be a contributor to the divergence of W values for alcohols reported previously.[20-22] In the present study, W values can be obtained from the initial essentially pressure independent

(18) L. B. Leob, "Basic Processes of Gaseous Electronics," University of California Press, Berkeley, Calif., 1960, Chapter 8, p 667.
(19) A. M. Howatson, "An Introduction to Gas Discharges," Pergamon Press, London, 1965, Chapter 3, p 53.
(20) P. Adler and H. K. Bothe, *Z. Naturforsch.*, **20a**, 1700 (1965).
(21) M. LeBlanc and J. A. Herman, *J. Chim. Phys.*, **21**, 1055 (1966).
(22) R. Cooper and R. M. Mooring, *Aust. J. Chem.*, **21**, 2517 (1968).

TABLE I

Compound	W(alcohol), eV per ion pair					$W(alkane)^d$
				This investigation		
	a	b	c	Temp, °C	W	
H_2O^e	29.9	29.9	29.8	240	29.15 ± 0.09^e	28.8^f
CH_3OH	25.5	23.6	26.2	204	25.02 ± 0.09	26.94
C_2H_5OH	25.1	...	22.9	203	24.50 ± 0.09	24.18
n-C_3H_7OH	24.5	...	...	236	23.86 ± 0.08	23.96
i-C_3H_7OH	24.2	...	...	193	24.25 ± 0.09	23.96
n-C_4H_9OH	24.1	...	...	213	23.53 ± 0.12	23.16
$CH_3CHOHC_2H_5$	...	...	...	201	23.53 ± 0.12	23.16
$(CH_3)_2CHCH_2OH$	23.9	...	...	213	23.38 ± 0.11	23.50

[a] P. Adler and H. K. Bothe, *Z. Naturforsch.*, **20a**, 1700 (1965). [b] Water: C. Wingate, W. Gross, and G. Failla, *Radiat. Res.*, **8**, 411 (1958); methanol: M. LeBlanc and J. A. Herman, *J. Chim. Phys.*, **21**, 1055 (1966). [c] R. Cooper and R. M. Mooring, *Aust. J. Chem.*, **21**, 2417 (1968). [d] T. A. Stoneham, D. R. Ethridge, and G. G. Meisels, *J. Chem. Phys.*, **54**, 4054 (1971). [e] Errors are maximum deviations from the mean for water and the butanols and estimated for other compounds. [f] This value is for hydrogen and was taken from J. M. White, *Radiat. Res.*, **18**, 265 (1963).

region of Figure 2 relative to $W(N_2) = 34.6$-eV/ion pair.[23] For methanol, ethanol, 1- and 2-propanol, the values cited correspond to the experimental measurements at the lowest electron densities shown in Figure 2, and the error limit given corresponds to the maximum deviation from the smooth curve drawn through the 200° data. For water and the butanols, W was obtained by averaging all data below an electron density of 7×10^{20} cm^{-3}; the error given corresponds to the maximum deviation from this average and is therefore quite conservative. Also shown in Table I are W values reported by other investigators and the average energy required for ion pair formation in the corresponding alkanes.

Comparison with the earlier data of Adler and Bothe[20] shows our work to yield consistently lower W values; this may be ascribed to the uncertainties in the correction for back-scattering employed by these investigators, as well as to the possibility of incomplete collection; similarly, our $W(H_2O)$ is the smallest reported. The low value reported for methanol by LeBlanc and Herman[21] and that given for ethanol by Cooper and Mooring[22] were both obtained by cavity ionization techniques using ^{60}Co γ rays, where energy deposition must be calculated from Bragg-Gray theory and errors may result when direct radiation interaction with the target gas takes place.

Within the homologous series, W decreases with increasing carbon number but is only little affected by the position of the hydroxyl groups; the three butanols investigated have W values within experimental error of each other. Surprisingly, the change in W brought about by the substitution of a hydroxyl group for a hydrogen atom does not have a consistent effect on W. The tendency is to increase W but the reverse is observed for methanol, 1-propanol, and 2-methyl-1-propanol, although the last two have W values equal to their hydrocarbon counterparts within experimental error.

Conclusions

Experimental evaluations of W for alcohols are subject to error resulting from incomplete ion collection which does not manifest itself in deviations from linearity of the dependence of ion current on collection potential. With appropriate precautions it is possible to assess average energies required for ion pair formation at low pressures with an uncertainty which does not exceed 0.5%. Present data suggest that the contribution of autoionizing states with lifetimes greater than about 10^{-10} sec cannot exceed 1% of total ionization in methanol.

Acknowledgments. This investigation was supported in part by the U. S. Atomic Energy Commission under Contract AT-(40-1)-3606; we are deeply grateful for this assistance. Particularly helpful discussions with Professor G. Freeman and Dr. W. Chupka were much appreciated by the authors.

(23) J. M. White, *Radiat. Res.*, **18**, 265 (1963).

Spectral Shifts of Trapped Electrons in Alkane Glasses at 76°K

N. V. Klassen,* H. A. Gillis, and G. G. Teather

Division of Physics, National Research Council of Canada, Ottawa, Canada K1A OS1 *(Received May 1, 1972)*

Publication costs assisted by the National Research Council of Canada

The spectra of the trapped electron in 3-methylpentane and 3-methylhexane glasses at 76°K as determined by pulse radiolysis have been found to shift toward the blue on a time scale of mseconds, seconds, and minutes. For 3-methylhexane λ_{max} is approximately 2000 and 1700 nm at 3 μsec and 380 sec, respectively. For 3-methylpentane λ_{max} is approximately 1900 at 10 μsec and shifts to about 1700 nm at 380 sec. The spectra at 380 sec are very similar to those determined by others after ^{60}Co irradiation. Geminate recombination occurs simultaneously with the spectral shifts, but an experiment with added biphenyl indicates that the mechanism involved in the spectral shifts is predominantly molecular reorientation rather than detrapping–retrapping.

Introduction

In a recent communication[1] the "immediate" optical absorption spectrum of the trapped electron (e_t^-) in 3-methylhexane (3MH) glass at 77°K, determined 35 nsec after a 40-nsec irradiation pulse, was reported to have $\lambda_{max} \geq 1900$ nm, as contrasted to $\lambda_{max} = 1650$ for the spectrum determined several minutes after ^{60}Co irradiation.[2] These observations strongly imply that the absorption maximum shifts toward the blue with time. Richards and Thomas[3,4] reported that the electron spectrum undergoes a red shift with time in both 3-methylpentane (3MP) and 3MH; for 3MH at 77°K they reported that growth of absorption at λ 1650 nm follows first-order kinetics with $t_{1/2} = 350$ nsec.[3] However, it has been shown that these results are probably due to an instrumental artifact of their Ge photodiode detector.[1]

In the present work we have also measured the immediate spectrum of e_t^- in 3MP glass at 76°K, and confirmed that for both hydrocarbons the spectra do indeed undergo blue shifts so that several minutes after the pulse they closely resemble those determined after ^{60}Co irradiation. The results provide insight into the mechanism responsible for the shifts.

Experimental Section

Phillips pure grade 3MP and Matheson Coleman and Bell practical grade 3MH were used. The 3MH was distilled through a spinning band column. Both hydrocarbons were passed through columns of freshly activated silica gel and molecular sieve 4A and stored over sodium in a vacuum line. Samples were thoroughly degassed before irradiation.

Samples were irradiated in optical cells of 2- or 5-mm light path. The cells were positioned in a dewar with optical windows. All optical windows were Suprasil except for the silica windows in the cell used to determine the immediate spectrum of e_t^- in 3MH.[1] The hydrocarbon glasses were prepared at least 1 hr before an irradiation by pouring liquid nitrogen into the dewar containing the sample. The liquid nitrogen in the light path was prevented from boiling by bubbling helium into the liquid nitrogen at a rate sufficient to cool it to 76°K, as measured by a thermocouple.

Samples were irradiated with 35-MeV electrons from a linear accelerator with pulse widths of 1, 2, or 3 μsec. The dose in a single pulse was 2–30 krads. Any single sample received a total dose of less than 450 krads; it has been shown that at this dose the electron concentration is still linear with dose for both 3MP[5] and 3MH.[2]

The analytical light source was a 500-W projector lamp run at varied voltages. The split light beam method was used in determining the initial spectrum of 3MP. The reference wavelength of 1525 nm was isolated by a wide-band filter, and the reference detector was a Ge photodiode (Philco-Ford L-4521). The variable wavelength was isolated with a Bausch & Lomb high-intensity monochromator. The intensity of the variable beam for $\lambda \geq 950$ nm was measured with a Barnes Engineering InSb A-10 photovoltaic detector, operated at 77°K in a circuit with a rise time of $\sim$7 μsec, and for $\lambda \leq 1050$ nm was measured with an EG&G YAG-100 silicon photodiode in a circuit with a rise time of $\sim$1 μsec. Appropriate filters reduced the amount of light entering the cell at wavelengths shorter than the monochromator setting. Bandwidths at half-height were typically 10–15 nm, and were at the maximum of 25 nm for λ 2240 nm. Measurements could not be made above 2240 nm because of excessive light absorption by the hydrocarbons.

For experiments in which the decay at one wavelength was followed for 380 sec, special precautions were taken to minimize the possibility of optical bleaching. The monochromator, an appropriate filter to remove second-order light, and an electronic shutter were placed between the lamp and the cell. Room lights were extinguished and a shield prevented reflected light from the lamp from reaching the cell. Analyzing light was allowed to pass through the cell for only 17 msec for each measurement, and in a typical experiment measurements were made at 0, 0.5, 1, 2, 3, 4, 5, 8, 11, 14, 17, 63, 126, 189, 252, 315, and 380 sec after the pulse. An appropriate filter was also placed between the cell and the detector to minimize the intensity of Čerenkov light reaching the detector; otherwise the effec-

(1) N. V. Klassen, H. A. Gillis, and D. C. Walker, *J. Chem. Phys.*, **55**, 1979 (1971).
(2) J. Lin, K. Tsuji, and F. Williams, *J. Amer. Chem. Soc.* **90**, 2766 (1968).
(3) J. T. Richards and J. K. Thomas, *J. Chem. Phys.*, **53**, 218 (1970).
(4) J. T. Richards and J. K. Thomas, *Chem. Phys. Lett.* **8**, 13 (1971).
(5) D. P. Lin and L. Kevan, *J. Chem. Phys.*, **55**, 2629 (1971).

tive response time of the detection system was considerably lengthened because of saturation of the detector and/or electronics. The hydrocarbon glass was always bleached with the full light of a projector lamp between pulses. The detector used in the decay experiments was either the InSb photovoltaic detector or the silicon photodiode, as in the spectrum measurements.

Results

3-Methylhexane. Figure 1 shows the spectrum of e_t^- in 3MH glass 35 nsec to 3 μsec after a 40-nsec or 1-μsec pulse. This immediate spectrum was constructed from the averages of the data reported in our earlier communication;[1] corrections have been applied for the absorption in the cell windows to which attention was drawn in the note added in proof of that communication. The temperature of the glass, previously reported as 77°K,[1] has now been more accurately determined as 76 ± 0.3°K. The immediate spectrum was found not to shift or decay significantly for at least 100 μsec after the pulse.

The decay of absorption in 3MH at three wavelengths is shown in Figure 2. The decay curve at 2240 nm remained the same within experimental error when the light intensity was doubled, and also was the same for a sample which had already received a dose of ~250 krads as for a previously unirradiated sample. By combining curves such as those of Figure 2 with the initial spectrum of Figure 1, the spectrum of e_t^- at any time in the interval studied can be calculated. The spectra thus calculated at 8 msec and 380 sec are shown in Figure 1. It is seen that in 380 sec the spectrum has sharpened and the absorption maximum shifted from ~2000 nm, immediately after the pulse, to ~1700 nm. The 380-sec spectrum is very similar to that found in the ^{60}Co radiolysis of 3MH, with λ_{max} reported as 1650 nm.[2]

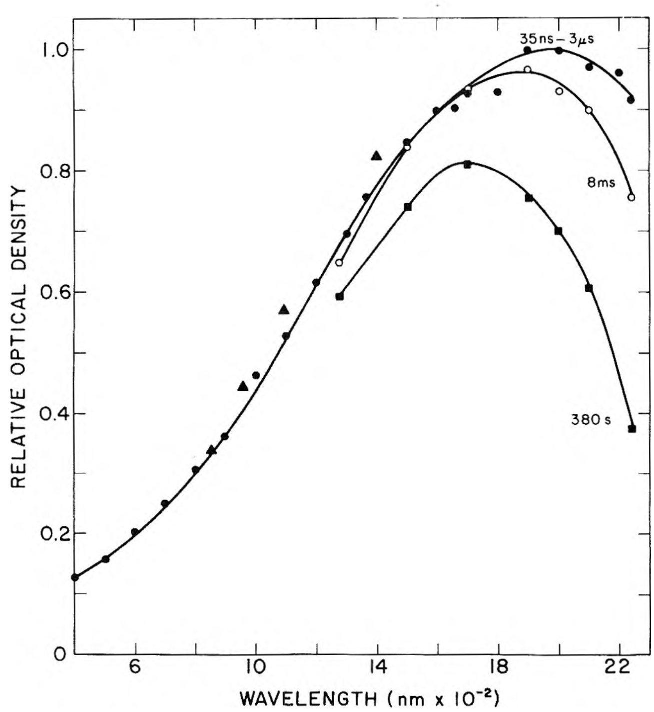

Figure 1. Spectral shift in the optical absorption spectrum of e_t^- in 3MH glass at 76°K. Points ● were obtained with an InAs detector 3 μsec after 40-nsec or 1-μsec pulses and points ▲ were obtained with a Ge photodiode 35 nsec after 40-nsec pulses (see text and ref 1). Points O and ■ were obtained with an InSb detector 8 msec and 380 sec, respectively, after 3-μsec pulses.

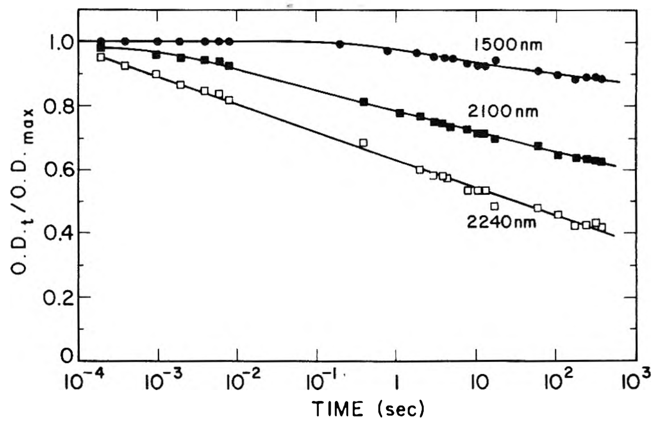

Figure 2. Decay of absorption by e_t^- in 3MH glass at 76°K at three wavelengths. The ordinate represents the ratio of the OD at time *t* to the maximum OD (measured ~10^{-5} sec after 3-μsec pulses).

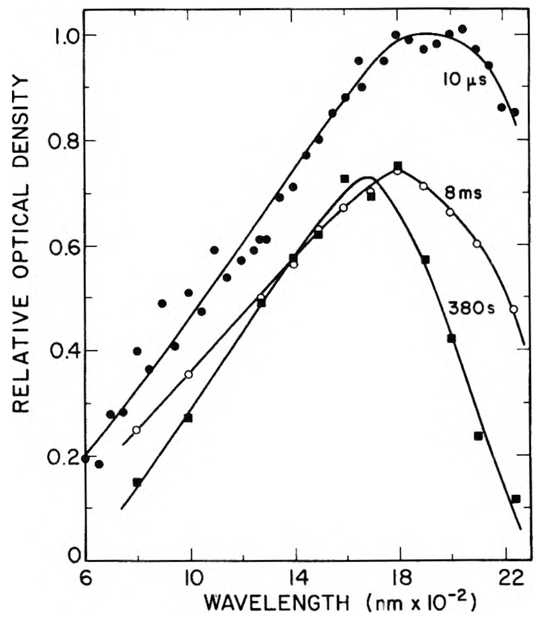

Figure 3. Spectral shift in the optical absorption spectrum of e_t^- in 3MP glass at 76°K. The data points were measured at the times indicated after 1-μsec or 3-μsec pulses.

Decay of e_t^- in 3MH was slightly faster at 86°K than at 76°K. At 86°K OD_t/OD_{max} at 45 msec was 0.62 and 0.97 at 2240 and 1500 nm, respectively. From Figure 2 the corresponding ratios at 76°K are 0.75 and 1.00.

3-Methylpentane. The spectra of e_t^- in 3MP at 76°K at 10 μsec, 8 msec, and 380 sec after the pulse are shown in Figure 3. These have been corrected for the small amount of absorption produced in the windows of the cell and dewar. The spectra at 8 msec and 380 sec were determined in the same way as the spectra at those times for 3MH (Figure 1). The decay of absorption in 3MP in a 5-mm cell at four wavelengths is shown in Figure 4. The 10-μsec spectrum, which by analogy with 3MH is probably the same as a nsec spectrum has $\lambda_{max} \simeq$ 1900 nm. The narrower 380-sec spectrum with $\lambda_{max} \simeq$1700 nm is very similar to the spectrum produced by ^{60}Co γ irradiation with λ_{max} around 1650 nm.[2,6]

(6) J. R. Miller and J. E. Willard, *J. Phys. Chem.*, **76**, 2341 (1972).

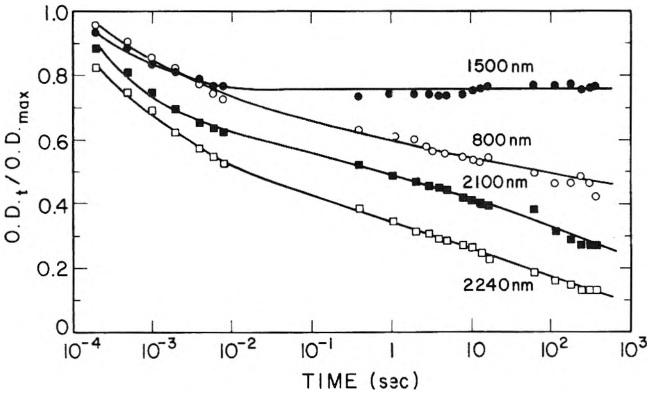

Figure 4. Decay of absorption by e_t^- in 3MP glass at 76°K at four wavelengths. The ordinate represents the ratio of the OD at time t to the maximum OD (measured $\sim 10^{-5}$ sec after 3-μsec pulses).

The following very stringent test for photobleaching at 2240 nm was made. In one experiment the light intensity was doubled and absorption at 2240 nm was followed with the analyzing light on the sample continuously for the first 4 sec after the pulse. The total amount of light incident on the sample in this time was $\sim$100 times greater than for the usual conditions yet the decay curves were the same within experimental error. This is consistent with the low quantum yield for bleaching at 2150 nm reported by Miller and Willard.[6] However for λ 800 nm, OD_t/OD_{max} at 380 sec was $\sim$10% less when the light intensity was increased by a factor of 4 over that used for the experiment of Figure 4 and the usual sequence of analyzing light flashes was maintained. This indicates that under conditions of negligible optical bleaching OD_t/OD_{max} at 380 sec for λ 800 nm would be about 2.5% higher than the value indicated in Figure 4. Similarly for λ 1000 nm, OD_t/OD_{max} at 380 sec was $\sim$5% lower when the light intensity was doubled and the normal sequence of flashes was used. The quantum yield for photobleaching e_t^- in γ-irradiated 3MP was found to be near unity at 950 nm for small extent of photobleaching.[7] If we assume it is also near unity at 800 and 1000 nm in our experiments we can conclude that the contribution of optical bleaching to the decay was unimportant at all wavelengths since the analyzing light intensity was approximately the same at all wavelengths.

The decay curve at 2240 nm was the same for a sample of 3MP which had previously received a total dose of $\sim$200 krads as it was for a previously unirradiated sample.

Electron Scavenging by Biphenyl in 3MP. The decay of e_t^- was also studied in a 3MP glass at 76°K containing 3.4 mM biphenyl. Biphenyl was used to examine the extent to which electrons are detrapped during our observations. At 3.4 mM, biphenyl efficiently scavenges mobile electrons to produce the biphenyl anion (Ph_2^-) with λ_{max} 410 nm.[8] In separate experiments we examined the change after the pulse of OD due to e_t^- at 1500 and 2240 nm and OD due to Ph_2^- at 410 nm (suitably corrected for e_t^- at 410 nm). The results are outlined in Table I. Between 10^{-5} and 8×10^{-3} sec the fraction decay of e_t^- at 1500 and 2240 nm is not noticeably affected by the presence of biphenyl. After 8×10^{-3} sec the decay at 1500 and 2240 nm is more rapid in the presence of biphenyl and this decay is accompanied by an increase in Ph_2^-; for example OD_t/OD_{max} at 1500 nm at 1 and 380 sec is 0.61 and 0.41 with biphenyl, as compared to 0.76 at both these times in pure 3MP. Despite the almost complete decay of OD_{2240} during the period of observation

TABLE I: Effect of 3.4 mM Biphenyl in 3MP on the Decay of e_t^- at 1500 and 2240 nm

	3MP containing 3.4 mM biphenyl				Pure 3MP
Time, sec	OD $e_t^{-\,a}$ (1500 nm)	OD $e_t^{-\,a}$ (2240 nm)	$ODPh_2^{-\,a}$ (410 nm)	OD_{2240}/OD_{1500}	OD_{2240}/OD_{1500}
10^{-5}	0.384	0.390		1.02	1.03
4×10^{-3}	0.290	0.224	0.252	0.77	0.74
10^{-1}	0.256	0.163	0.289	0.64	0.56
1	0.234	0.121	0.315	0.52	0.46
10^2	0.185	0.037	0.374	0.20	0.22
3.8×10^2	0.158	0.013	0.397	0.1[b]	0.17[b]

[a] Normalized to the same dose. [b] Large error possible because of small OD_{2240}.

(10^{-5} to 3.8×10^2 sec) the ratio of OD_{2240}/OD_{1500} remained similar to the ratio in pure 3MP at all times (see Table I). Though we did not obtain data at other wavelengths, we conclude that this indicates that the same spectral shift occurs at the same rate in 3MP containing biphenyl as in pure 3MP.

Discussion

The initial spectra of e_t^- in 3MP and 3MH are broader and have λ_{max} at longer wavelengths than the spectra at 380 sec. This suggests that initially some of the electrons are in shallower traps than at later times. The results do not indicate whether at a given time there is a distribution of trap depths or whether all traps have the same depth.

The area under the absorption curves decreases considerably over our observation time range for both 3MH and 3MP, especially for the latter; in fact we found no definite evidence for growth in absorption at any wavelength over any part of our time range for either hydrocarbon. This implies that during 380 sec there is a considerable decrease in electron concentration, presumably by geminate neutralization, unless the oscillator strength of the initially trapped electrons is somewhat larger than that of the electrons at later times.[9] A somewhat slower rate of electron decay at longer times has previously been reported,[2,7] and the rate of decay at these longer times has been found to be somewhat greater in 3MP than in 3MH.[2] We found the largest change in OD over 380 sec at 2240 nm, but some of the decrease is believed to be due to electron decay. On the other hand, the decrease in OD at 1500 nm could be very approximately proportional to the decrease in the concentration of e_t^- since 1500 nm is in a region of the spectrum in which little spectral change was observed. Therefore the change in the ratio OD_{2240}/OD_{1500} is used here as a very rough measure of the spectral shift.

Gallivan and Hamill[11] noted a very small blue shift in the spectrum of e_t^- in 3MP taken 45 min after a 2-min γ irradiation, as compared to the spectrum they determined initially (time unspecified). This suggests that a further small blue shift may occur after 380 sec.

We have previously shown that the solvated electron (e_s^-) in liquid propane at 88°K has a broad initial spectrum

(7) D. W. Skelly and W. H. Hamill, *J. Chem. Phys.*, **44**, 2891 (1966).
(8) J. B. Gallivan and W. H. Hamill, *J. Chem. Phys.*, **44**, 2378 (1966).
(9) The oscillator strength for e_t^- in 3MP at long times has been estimated as 0.46.[10]
(10) W. H. Hamill in "Radical Ions," E. T. Kaiser and L. Kevan, Ed., Wiley, New York, N. Y., 1968, p 356.
(11) J. B. Gallivan and W. H. Hamill, *J. Chem. Phys.*, **44**, 1279 (1966).

with $\lambda_{max} \geq 2000$ nm.[12] This spectrum was obtained 0.16-2 μsec after the pulse and spectra were not obtained at later times, but the similarity of the initial spectrum of e_s^- to the initial spectra of e_t^- in 3MH and 3MP suggests that spectral shifts might also be observed in liquid hydrocarbons in which e_s^- has a sufficient lifetime. Richards and Thomas[13] reported that the initial spectrum of the solvated electron in liquid 3MH at 193°K has λ_{max} 1500 nm, but we believe this result is due to the same instrumental artifact which accounts[1] for their reported[3] spectral changes in 3MH glass.

Spectral blue shifts for trapped electrons have been observed in aqueous glasses at various temperatures[14] and in various alcohol glasses at 77°K.[3,15] Also when an alcohol glass is γ irradiated at 4°K and then warmed to 77°K an irreversible blue shift occurs.[16] Two possible mechanisms of these shifts have been discussed for electrons initially in shallow traps or in traps with a wide distribution of depths.[3,15] In mechanism I the electric field of the electron promotes reorientation of the surrounding dipoles of the medium to deepen the shallow traps. In mechanism II it is postulated that the electrons are thermally excited out of the shallow traps and redistributed into deeper traps. Kevan[15] finds that in alcohol glasses the time required to achieve the final spectrum increases with decrease in polarity, as indicated by the liquid-phase dielectric constant. For 2-propanol, with the lowest dielectric constant of those studied of 18.3 at 25°, this time of about 100 μsec was the longest. Kevan interprets this as favoring the molecular reorientation mechanism, since the charge-dipole and/or polarization interaction would be stronger in more polar matrices. The results in the present study follow the trend in the alcohols in that the much lower dielectric constant ($\sim$2 at 24°) of the hydrocarbons correlates with a much slower spectral shift than even in 2-propanol. By this argument then, mechanism I is implied in the hydrocarbons also.

It is interesting to attempt to compare the rates of spectral shifts in 3MP and 3MH. A measure of the total spectral shift, by our definition above, is the difference between OD_{2240}/OD_{1500} immediately after the pulse and at 380 sec. The percentage of this change which occurs at 1 msec, 8 msec, and 1 sec is 19, 34 and 64, respectively, for 3MH compared to 22, 37, and 65 for 3MP. The close agreement for the two glasses is probably fortuitous but it does suggest that spectral shifts take place on the same time scale in the two hydrocarbons despite the very different viscosities at 77°K of 2.2×10^{12} P for 3MP and 3.2×10^{18} P for 3MH.[17] The absence of a large effect of viscosity on the spectral shifts in these alkane glasses is similar to the conclusion of Kevan that viscosity is not a factor in the rates of spectral shifts in alcohol glasses.[15] We interpret the lack of correlation between the rates of spectral shift and rates of geminate combination as further evidence that spectral shifts do not occur predominantly by a mechanism which involves detrapping, such as mechanism II.

An important difference between studies on alcohol glasses[3,15] and the present work is that, in the former, decreases in absorption at longer wavelengths were accompanied by increases in absorption at shorter wavelengths. Also in alcohol glasses with added biphenyl or benzyl chloride, there was no growth in intensity of the absorption of the biphenyl anion or the benzyl radical over the time period when the trapped electron spectrum was shifting.[15,18] Kevan interprets this as indicating that electrons are not detrapped in alcohol glasses over the μsecond time scale involved, and as further evidence in support of mechanism I. In hydrocarbon glasses the situation is quite different in that geminate neutralization occurs simultaneously with the spectral shifts. Further, the rate of decrease of absorption due to e_t^- is faster after 8×10^{-3} sec at both 1500 and 2240 nm in the presence of biphenyl than in pure 3MP, and this decrease in electron absorption is accompanied by an increase in absorption due to Ph_2^-. Presumably, in the absence of biphenyl some of the electrons which are detrapped or tunnel[19] are retrapped before meeting a positive ion. If the detrapping-retrapping mechanism, mechanism II above, were very important in bringing about the spectral shifts seen here OD_{2240}/OD_{1500} would be expected to be higher in the presence of biphenyl than in its absence since biphenyl would prevent some of the electrons detrapped from shallow traps from entering deep traps. Table I shows that OD_{2240}/OD_{1500} is very similar in the presence and absence of biphenyl at all times, so again mechanism I is favored. It might be argued that mechanism I should result in higher values of OD_{2240}/OD_{1500} in the absence of scavenger if retrapped electrons have the "initial" spectrum. However this effect would be very small since most of the spectral shift takes place in the first second while only a small percentage of the electrons seem to be detrapped in that time.

In summary, we interpret our experiments as indicating that the most important mechanism involved in the spectral shifts in hydrocarbon glasses is molecular reorientation, but geminate neutralization occurs simultaneously, at least in the absence of electron scavengers. Over the time period studied and at all wavelengths, loss of absorption by geminate neutralization is greater than or equal to any increase from molecular reorientation, so that no growth in absorption is seen.

Acknowledgment. The authors are grateful to Dr. D. C. Walker for interesting and helpful discussions.

(12) H. A. Gillis, N. V. Klassen, G. G. Teather, and K. H. Lokan, *Chem. Phys. Lett.*, **10**, 481 (1971).
(13) J. T. Richards and J. K. Thomas, *Chem. Phys. Lett.*, **10**, 317 (1971).
(14) G. V. Buxton, F. C. R. Cattell, and F. S. Dainton, *Trans. Faraday Soc.*, **67**, 687 (1971).
(15) L. Kevan, *J. Chem. Phys.*, **56**, 838 (1972).
(16) H. Hase, M. Noda, and T. Higashimura, *J. Chem. Phys.*, **54**, 2975 (1971).
(17) A. C. Ling and J. E. Willard, *J. Phys. Chem.*, **72**, 3349 (1968).
(18) L. Kevan, *Chem. Phys. Lett.*, **11**, 140 (1971).
(19) J. R. Miller, *J. Chem. Phys.*, **56**, 5173 (1972).

The Effect of Temperature in the Radiolysis of Paraffins

Tino Gäumann,* Serge Rappoport, and Amanz Ruf

Department of Physical Chemistry, Federal School of Technology, Lausanne, Switzerland *(Received May 2, 1972)*

Publication costs assisted by the Federal School of Technology

The radiolysis of n-paraffins with 5 to 16 carbon atoms is reviewed. The G values of the products, excepting dimers, are approximately the same for all the above paraffins. The temperature dependence is expressed as an apparent activation energy. The material balance shows that the product analysis is not complete and that the missing substances have a molecular weight higher than that of the dimers. The hydrogen production is divided into three processes: unimolecular hydrogen production, abstraction by thermal atoms, and abstraction by "hot" hydrogen atoms.

The radiolysis of liquid n-paraffins has been described in a large number of publications (see, *e.g.*, ref 1-3). In most cases the aim of the work was to study the product distribution or influence of additives in the radiolysis of one particular paraffin. If the number of significant products from n-hexane is say 40, then it is likely to increase well over 100 for n-decane. Since the product formation depends also upon temperature, it is somewhat difficult to draw conclusions concerning the general behavior of n-paraffins. In this work we have attempted to describe a general mechanism which shows the yield of products together with their temperature dependence in the radiolysis of n-paraffins in order to survey the field. Our approach is broad and pragmatic: we will classify the products and try to find average G values for all n-paraffins. The temperature dependence of these values is expressed as apparent activation energies obtained by plotting ln G *vs.* $1/T$. We are well aware of the fact that these energies may have no theoretical significance. Our aim is to try to give the radiation chemist a set of values which allows him to estimate a product distribution at any irradiation temperature. We restrict ourselves to the liquid state and to irradiation intensities lower than about 10 Mrads/hr.

The Product Spectrum

The products may be divided into different groups according the number of carbon atoms and their degree of saturation. Hydrogen is the product with the largest G value. The temperature dependence of its yield can be expressed quite accurately as an activation energy. Table I[4-9] gives G values for some paraffins of the general formula C_nH_{2n+2} at room temperature. It can be deduced that $G(H_2)$ is equal to 5.2 at 25° and its temperature dependence corresponds to E_A = 0.35 kcal/mol, independent of the chain length.

A paraffin, C_nH_{2n+2}, forms a series of n-alkanes with 1 to $n - 1$ carbon atoms, which are usually called low molecular weight products. From Table II,[10-15] an average G value of 1.2 at −50° and an E_A = 0.50 kcal/mol can be taken. In Figure 1 the product distribution for some paraffins is given. It is symmetric about $C_{n/2}$ where n is the carbon number of the starting hydrocarbon, except for some possible deviations due to the formation of methane.

The olefins with 2 to $n - 1$ carbon atoms are formed at −50° with an average total G value of 0.30 and E_A = 0.2 kcal/mol (Table III[16]). The C_nH_{2n} olefins have a temperature-independent G value of about 2.1. The ratio trans/cis is smaller than 3 for a double bond in position 2 and about 3.5 when in position 3. It is larger than 6 for the positions 4 and 5 in the parent paraffin.[8]

TABLE I: Yield of Hydrogen at 25°

Paraffin	$G(H_2)$	E_A, kcal/mol	Ref
C_5H_{12}	5.0; 5.25	0.23	4,5
C_6H_{14}	5.24; 5.25	0.32	1,6
C_7H_{16}	5.7; 4.9; 5.25	0.40	2,7,8
C_8H_{18}	5.10	0.37	8
C_9H_{20}	5.40	0.39	8
$C_{10}H_{22}$	4.90	0.16	8
$C_{12}H_{26}$	5.00		8
$C_{16}H_{34}$	5.10		9
Average	5.17 ± .07	0.35	

The products with more than n but less than $2n$ carbon atoms are called intermediate molecular weight products. They are always saturated. At irradiation temperatures lower than −25°, the sum of their G values is 0.6 and independent of the chain length of the parent paraffin, as can be seen from Table IV.[17] Their yield decreases with temperature with a slope corresponding to E_A = −1.5 kcal/mol.

The yield for the dimeric products of the formula $C_{2n}H_{4n+2}$ depends on the chain length of the parent paraffin, but is independent of the temperature below −25° (Table IV). Above this temperature their yield increases,

(1) T. Gaumann, "Aspects of Hydrocarbons Radiolysis," T. Gaumann and J. Hoigné, Ed., Elsevier, Amsterdam, 1968, p 213.
(2) A. V. Topchiev, "Radiolysis of Hydrocarbons," Elsevier, Amsterdam, 1964.
(3) G. R. Freeman, *Radiat. Res. Rev.*, **1**, 1 (1968).
(4) R. O. Koch, J. P. Houtman, and W. A. Cramer, *J. Amer. Chem. Soc.*, **90**, 3326 (1968).
(5) A. Horowitz and L. A. Rajbenbach, *J. Chem. Phys.*, **48**, 4278 (1968).
(6) L. A. Rajbenbach and U. Kaldor, *J. Chem. Phys.*, **47**, 242 (1967).
(7) M. B. Muratbekov and V. V. Saraeva, *Chem. Abstr.*, **72**, 479 (1970).
(8) S. Rappoport and T. Gaumann, *Helv. Chim. Acta*, in press.
(9) W. E. Falconer and R. Salovey, *J. Chem. Phys.*, **44**, 3151 (1966).
(10) W. P. Bishop and R. F. Firestone, *J. Phys. Chem.*, **74**, 2274 (1970).
(11) H. Widmer and T. Gaumann, *Helv. Chim. Acta*, **46**, 2766 (1963).
(12) A. Menger and T. Gaumann, *Helv. Chim. Acta*, **52**, 2477 (1969).
(13) A. Menger and T. Gaumann, *Helv. Chim. Acta*, **52**, 2129 (1969).
(14) H. Widmer and T. Gaumann, *Helv. Chim. Acta*, **46**, 2766 (1963).
(15) E. Pancini, V. Santoro, and G. Spadaccini, *Int. J. Radiat. Chem.*, **2**, 147 (1970).
(16) L. Kevan and W. F. Libby, *J. Chem. Phys.*, **39**, 1288 (1963).
(17) W. E. Falconer and R. Salovey, *J. Phys. Chem.*, **70**, 3203 (1966).

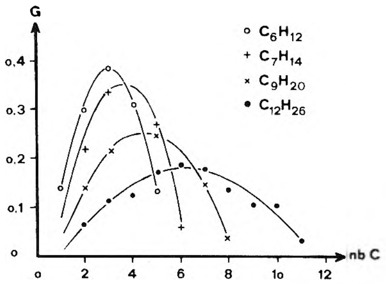

Figure 1. Yield of low molecular weight products, CH_4 + $C_{n-1}H_{2n}$, in the radiolysis of the C_nH_{2n-2} n-paraffin at −50°.

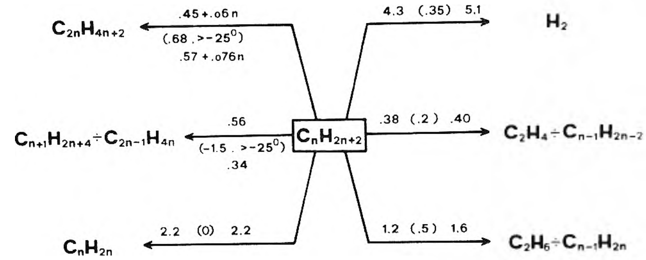

Figure 2. Fragmentation scheme for an n-paraffin. The values given correspond to "G at −70°, (apparent act. energy), G at 25°," respectively.

TABLE II: Yield of Low Molecular Weight Products

	Paraffins			Olefins			
Parent paraffin	$G_{-50°}$	E_A, kcal/mol	Ref	$G_{-25°}$	Ref	$G_{-25°}$	Ref
C_5H_{12}	0.90	0.41	10	0.51; 0.49	10,15	0.33	10
C_6H_{14}	0.76; 1.13	0.30; 0.75	11,12	0.34; 0.51	14,15	0.44; 0.40; 0.47	12–14
C_7H_{16}	1.11	0.53	8	0.44	8	0.38	8
C_8H_{18}	1.51		8	0.30	8	0.34	8
C_9H_{20}	1.19	0.50	8	0.37	8	0.32	8
$C_{10}H_{22}$	1.33[a]		8	0.36	8	0.37	8
$C_{12}H_{26}$	1.10[a]		8	0.24	8		
$C_{16}H_{34}$	0.73[a]	0.61	9				
Average	1.08 ± 0.09	0.05		0.40 ± 0.03			

[a] These values were obtained by extrapolation.

TABLE III: Yield of Olefins with the Same Number of Carbon Atoms as the Parent Paraffin

Paraffin	G(olefin)	Ref
C_5H_{12}	2.44(−78°); 1.94(25°); 2.37(25°); 2.44(25°)	10,15,4,10
C_6H_{14}	2.5(−80°,25°,150°); 1.81(25°); 2.01(25°)	1,15,16
C_7H_{16}	2.27(−60°); 2.12(25°); 2.04(50°)	8
C_8H_{18}	2.11(−50°)	8
C_9H_{20}	2.03(−50°); 2.16(0°); 2.42(50°)	8
$C_{10}H_{22}$	2.10(−25°)	8
Average	2.22 ± 0.06	

corresponding to an apparent activation energy of 0.68 kcal/mol. The values under the heading G_{calcd} are calculated from the regression line: $G_{calcd} = 0.45 + 0.06n$. There is no theoretical reason for a linear dependence and the deviations seem to be large. However, the experimental difficulties in determining the dimer yields for the higher paraffins are great, since there are a maximum of $n(n + 1)/2$ dimeric products formed, of which $m(m + 1)/2$ are diastereomers (where m is the number of secondary radicals, $C_nH\cdot_{n+1}$), and some of their gas chromatographic retention times overlap with those of the intermediate products.[1,18] In Figure 2 we show the product distribution for a C_nH_{2n+2} paraffin.

The Radical Yields

In several publications the existence of radical reactions has been proved.[19-21] The calculation of fragmentation probability for homolytic C–C and C–H bond breaking has been performed for pentane[22] and hexane.[2,11] The authors have, however, not taken into account disproportionation. It should not be neglected in reactions of alkyl radicals, as has been shown by several authors.[23-31] This is especially true at lower temperatures, where the abstraction of hydrogen atoms by primary radicals from the secondary position in the paraffin does not yet come into play. Irradiations of paraffins in the presence of radical scavengers such as O_2[4,32] or I_2[9-11,17] have shown that all of the intermediate molecular weight products, nearly all of the dimers, and part of the other products are formed by radical reactions. In a recent study, we tried to calculate the distribution of the products of radical origin from the radiolysis of n-hexane with as few parameters as possible,[33] as it has been proposed for benzene.[34] For the reaction scheme

$$C_lH_{2l+1}\cdot + C_mH_{2m+1} \begin{cases} \xrightarrow{k_d} C_lH_{2l} + C_mH_{2m+2} \text{ or } C_mH_{2m} + C_lH_{2l+2} \\ \xrightarrow{k_c} C_{l+m}H_{l+m+2} \end{cases}$$

(18) S. Rappoport and T. Gauman, *Helv. Chim. Acta*, in press.
(19) R. W. Fessenden and R. H. Schuler, *J. Chem. Phys.*, **39**, 2147 (1963).
(20) F. Thyrion, J. P. Dodelet, C. Fauquenoit, and P. Claes, *J. Chim. Phys.*, **65**, 227 (1968).
(21) R. A. Holroyd, "Aspects of Hydrocarbons Radiolysis," T. Gaumann and J. Hoigné, Ed., Academic Press, London, 1968, p 1.
(22) C. D. Wagner, *J. Phys. Chem.*, **64**, 231 (1960).
(23) P. S. Dixon, A. P. Stefani, and M. Szwarc, *J. Amer. Chem. Soc.*, **85**, 3344 (1963).
(24) P. S. Dixon, A. P. Stefani, and M. Szwarc, *J. Amer. Chem. Soc.*, **85**, 2551 (1963).
(25) J. O. Terry and J. H. Futrell, *Can. J. Chem.*, **45**, 2327 (1967).
(26) L. I. Bone, L. W. Sieck, and J. H. Futrell, *J. Chem. Phys.*, **44**, 3667 (1966).
(27) R. R. Kuntz and G. J. Mains, *J. Amer. Chem. Soc.*, **85**, 2219 (1963).
(28) R. Barker, *Trans. Faraday Soc.*, **63**, 2640 (1967).
(29) R. R. Kuntz and G. J. Mains, unpublished results.
(30) R. R. Kuntz, *J. Phys. Chem.*, **69**, 4396 (1965).
(31) A. Menger and T. Gaumann, *Helv. Chim. Acta*, **52**, 2477 (1969).
(32) R. D. Koob and L. Kevan, *Trans. Faraday Soc.*, **64**, 422 (1968).
(33) T. Gaumann and B. Reipso, *Advan. Chem. Ser.*, **No. 82**, 445 (1968).
(34) B. Zimmerli and T. Gaumann, *Helv. Chim. Acta*, **52**, 764 (1969).

TABLE IV: *G* **Values for the Formation of Intermediate Molecular Weight and Dimeric Products**

	Intermediate mol wt of product			Dimers			
n-Paraffin	*G* below −25°	e_A above −25°, kcal/mol	Ref	*G* below −25°	G_{calcd}	E_A above −25° kcal/mol	Ref
C_5H_{12}	0.87		2	0.70	0.75	0.68	4
C_6H_{14}	0.60	−1.63	3	0.70	0.81	0.59	11
C_7H_{16}	0.50	−1.61	8	0.75	0.87	0.68	8
C_8H_{18}	0.55		8	0.85	0.93		8
C_9H_{20}	0.60	−1.38	8	0.95	0.99	0.68	8
$C_{10}H_{22}$	0.30		8	1.65	1.05		8
$C_{16}H_{34}$	0.45[a]	−1.22		1.40[a]	1.41	0.59	9
$C_{17}H_{36}$				1.30[a]	1.47		17
Assumed value	0.56 ± 0.06	−1.5				0.68	

[a] These values are obtained by extrapolation.

TABLE V: Some Values of Disproportionation/Combination Ratios

Reaction	*T*, °C	Phase	k_d/k_c	E_A, kcal/mol	Ref
$CH_3\cdot + C_2H_5\cdot$	25	Liquid, isooctane	0.06	0.32	23
		Gas	0.12	0.30	24
$C_2H_5\cdot + C_2H_5\cdot$	25	Liquid, isooctane	0.16	0.32	24
		Liquid	0.34[d]	0.29	*e*
$n\text{-}C_3H_7\cdot + n\text{-}C_3H_7\cdot$	25	Gas	0.154		25
$n\text{-}C_3H_7\cdot + i\text{-}C_3H_7\cdot$	25	Gas	0.41		25
$i\text{-}C_3H_7\cdot + i\text{-}C_3H_7\cdot$	25	Gas	0.69		25
	25	Liquid	1.6[d]	0.26	*e*
$sec\text{-}C_5H_{11}\cdot + sec\text{-}C_5H_{11}\cdot$[a]	25	Liquid	0.67		27
$p\text{-}C_6H_{13}\cdot + p\text{-}C_6H_{13}\cdot$	25	Liquid	0.33,0.73[b]		28,29
$sec\text{-}C_6H_{13}\cdot + sec\text{-}C_6H_{13}\cdot$	25	Liquid	1.00		27
	25	Gas	0.97		30
$C_6H_{13}\cdot + C_6H_{13}\cdot$	−70	Liquid	0.75[c]		31

[a] Radicals with more than four C atoms are derived from n-paraffins, p- and sec- means a primary (position 1) or a secondary radical. [b] This value is too high according to the authors. [c] Corresponds to a mixture of primary and secondary radicals in the ratio 1:3. [d] Value extrapolated to 25°. [e] H. A. Gillis, *Can. J. Chem.*, **49**, 2861 (1971).

we made the following assumptions: $k_d/k_c = 0.8$ for reactions between secondary, 0.53 for primary-secondary, and 0.26 for primary radicals at 25°. Furthermore, we had to assume that the activation energy for the combination is 0.3 kcal/mol higher than that for the disproportionation. These four figures correspond to a weighted average of the data from Table V. Together with the measured product distribution at room temperature, they allow a relatively precise prediction of the results for other temperatures. The calculation of a fragmentation probability for a homolytic bond scission as has been shown for hexane[33] is therefore possible. The calculated figures are given in Table VI. A regular decrease with increasing chain length is seen. The results for *n*-decane do not seem to confirm the calculations, since the results were taken at −25° where abstraction becomes noticeable. The results have not been corrected for this, and consequently the values for primary radicals appear too low and those for the secondary decyl radicals too high. The hydrogen in position 2 is the most labile one, whereas the primary hydrogens are the most stable. The C–C bonds have all nearly identical probabilities, with the exception of C1–C2. The latter figures are not given, for they are small (0.04%) and unreliable and from mass spectrometric decay we have some reasons to believe that other reactions may come into play.[35]

TABLE VI: Probability in % per Bond for Scission as a Function of Position in ***n*****-Paraffins**

	C_6H_{14}	C_7H_{16}	C_8H_{18}	C_9H_{20}	$C_{10}H_{22}$
Temp, °C	−70	−50	−50	−50	−25[a]
C1–H	3.0	2.6	2.2	2.0	0.95
C2–H	9.5	7.4	6.2	5.2	6.5
C2–C3	3.6	3.3	2.2	1.7	0.9
C3–H	8.1	6.95	5.7	4.9	4.7
C3–C4	3.6	3.2	2.3	1.9	0.9
C4–H		6.95	6.8	5.7	6.0
C4–C5			3.0	2.8	1.0
C5–H				6.1	5.8
C5–C6					1.1

[a] The data for $C_{10}H_{22}$ are already influenced by the abstraction reaction.

The Hydrogen Production

Dyne[36] was the first to show that the D_2 yield in diluted solutions of fully deuterated cyclohexane, in nondeuterated hydrocarbons, can be divided into a bimolecular and a unimolecular yield. Later on we were able to subdivide the bimolecular process into two different reaction sequences, one involving hot and the other thermal deuterium atoms.[37] The temperature and scavenger dependence

(35) R. Liardon and T. Gaumann, *Helv. Chim. Acta*, **52**, 528 (1969).
(36) P. J. Dyne and W. M. Jenkinson, *Can. J. Chem.*, **40**, 1746 (1962).
(37) M. Ballenegger, A. Ruf, and T. Gaumann, *Helv. Chim. Acta*, **54**, 1373 (1971).

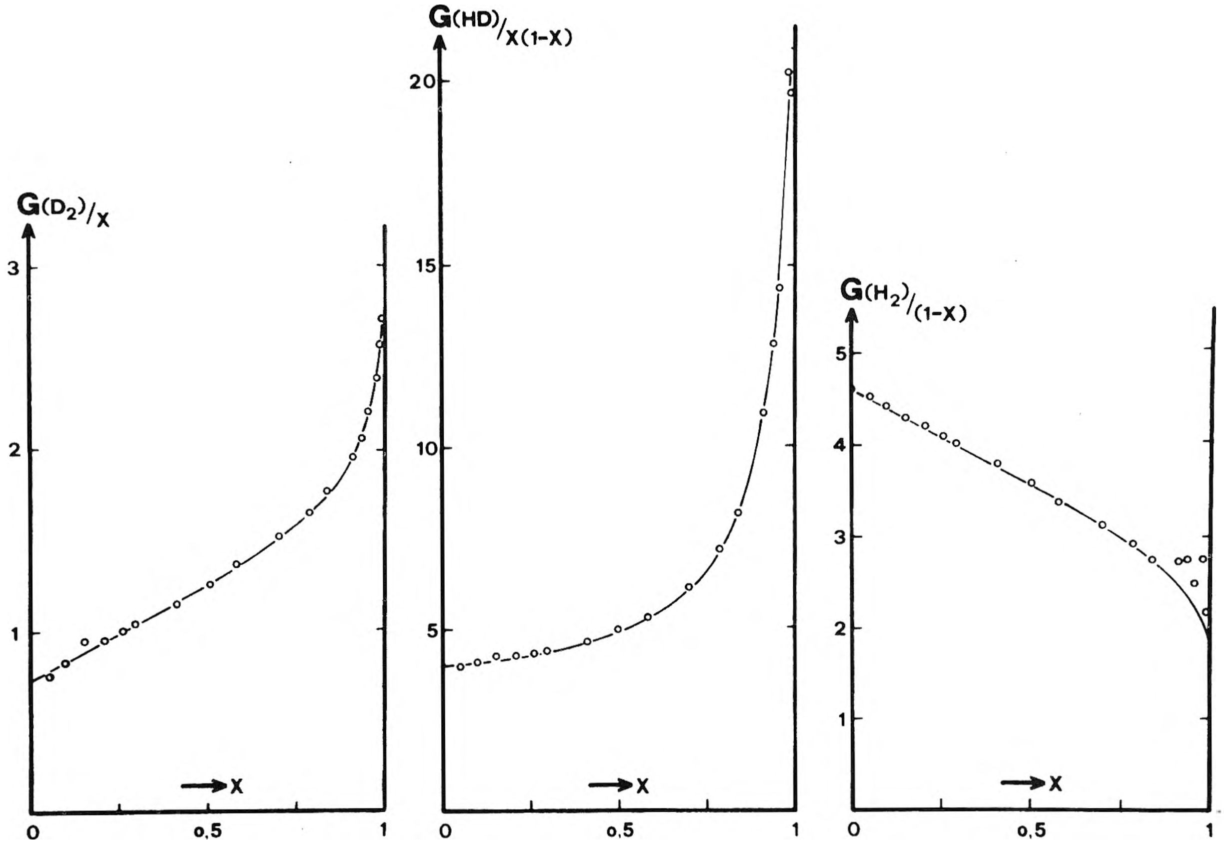

Figure 3. The formation of H_2, HD, and D_2 in *n*-heptane at $-10°$ as a function of the mole fraction of C_7D_{16}.

of these processes in hexane have been measured.[33] There is no difficulty, in principle, in doing analogous measurements with undeuterated paraffins in fully deuterated solvents, in order to obtain information about the production of H_2. Since we developed a continuous deuteration apparatus for paraffins[38] and the necessary measuring equipment for small quantities of H_2, HD, and D_2 mixtures,[39] we were able to measure these processes for a series of deuterated hydrocarbons.[40] Some preliminary results for heptane will be given. The following reaction scheme is postulated.

$$C_7H_{16} \xrightarrow{G_1} H_2 + \text{products}$$
$$C_7H_{16} \xrightarrow{G_2} H' + \text{products}$$
$$C_7H_{16} \xrightarrow{G_3} H + \text{products}$$

$$H(H') + C_7H_{16} \xrightarrow{k_H(k')} H_2 + C_7H_{15}$$
$$H(H') + C_7D_{16} \xrightarrow{k_D(k')} HD + C_7D_{15}$$

H is a thermal hydrogen atom. H′ is a species that abstracts hydrogen without any isotope effect; it may be a hot hydrogen atom or an ion. The following equation can be deduced for the $G(H_2)$ value as a function of the mole fraction, x, of the deuterated heptane

$$G(H_2)/(1-x) = G_1 + G_2(1-x) + G_3(1-x)/(1-\Delta x) \quad (\Delta = 1 - k_D/k_H)$$

Similar equations can be obtained for G(HD) and $G(D_2)$. A total of eight parameters are needed to describe the three curves of $G(H_2)$, G(HD), and $G(D_2)$ *vs.* x. Values of the parameters were chosen to give the best fit to the experimental points, as is shown in Figure 3. The choice of these values is rather critical and the error of a given set of values is probably better than the overall accuracy of the results. The only exception to this is in the determination of the isotope effect for the abstraction reaction by thermal H atoms, because this reaction favors the production of H_2 at small concentrations of C_7H_{18}. In this region, the hydrogen production due to the non-fully deuterated solvent (degree of deuteration, 99.7%) interferes with the measurements. The temperature dependence of these parameters is shown in Figure 4. The results for a wider series of hydrocarbons will be given in a forthcoming publication.[40] Meissner and Henglein[41] determined a G value of 1.5 for thermal hydrogen atom in hexane at 25°. Rajbenbach used scavengers to differentiate between thermal and hot hydrogen atoms and unscavengeable hydrogen. His figures for the two latter processes in pentane (1.0, 2.3, and 1.6)[5] and in hexane (1.36, 2.15, and 1.75)[6] at 25° disagree with our results. This is not unexpected, since his criteria are different from ours. His value of 1.75 for hexane corresponds to an unscavengeable species, whereas our figure of 2.6 corresponds to a unimolecular process. We have shown that N_2O scavenges part of the unimolecular process of deuterated hexane.[33] It might be that every process has several precursors, but we doubt it in this case, since we were able to show that in deuterated cyclohexane the D_2 molecule is either split off from one carbon atom or from two neighboring carbon atoms. It might well be that the scavenger action is not so well defined as is usually believed.

(38) C. Bosshard, O. Piringer, and T. Gaumann, to be published.
(39) D. Stahl, R. Houriet, and T. Gaumann, *Chimia*, **26**, 243 (1972).
(40) T. Gaumann and A. Ruf, *Helv. Chim. Acta*, in press.
(41) G. Meissner and A. Henglein, *Ber. Bunsenges. Phys. Chem.*, **69**, 264 (1965).

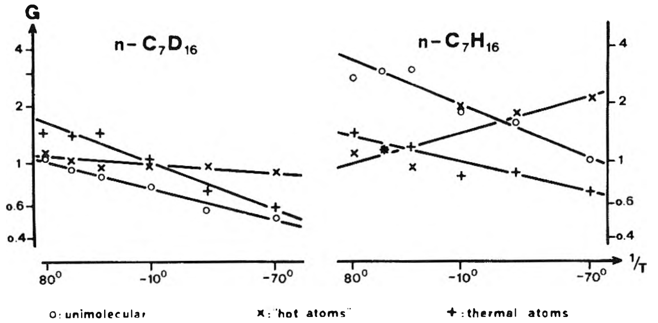

Figure 4. The temperature dependence of the different processes for hydrogen formation in *n*-heptane. The solid lines are the calculated regression lines.

Kuppermann and Betts[42] and Mains and Hong[43] photolyzed HI in the gas phase with different wavelengths. With energies up to 3 eV they found an isotope effect for the abstraction of H and D atoms that depends upon the energy of the abstracting H atom, but that is always larger than 1. Furthermore, there is the probability for thermalizing the hot H atoms which is always much larger than that for an abstraction, whereas our results show that G(H) and G(H′) are comparable. Therefore, it seems improbable that the H′ atoms are "hot" hydrogen atoms with an excess of kinetic energy. Such atoms would, in our parametrical representation, show up in the figure for thermal H atoms but would lower the activation energy; since the observed value is rather lower than what would be expected, it might well be that G(H) also takes into account those hot H atoms that have reacted as such. G(H′) should, in this case, correspond to some species that forms hydrogen by a reaction, that depends on the square of the concentration of the hydrocarbon, and that shows no isotope effect.

Discussion

The question might be raised: does such a unified treatment for all *n*-paraffins make any sense? We see no reason why there should be a difference in the fragmentation scheme for pentane and dodecane, for example; however, we have no proof of the contrary. A short check of Tables I–V shows that the differences between the results of different authors for the radiolysis of the same paraffin are as big as those between different paraffins. This means that our pragmatic approach corresponds at least to a reasonable simplification.

The idea of expressing the temperature dependence as an activation energy is certainly an oversimplification in some cases. The decrease of the yield of intermediate molecular weight products G(i.m.w.p.) is due to an abstraction reaction. Its E_A is of the order of 6–7 kcal/mol. The temperature dependence for the difference

$$\Delta G = G(\text{i.m.w.p.})_{T=-30°} - G(\text{i.m.w.p.})_{T>30°}$$

for heptane gives, for small ΔT, a value for E_a of 7.5 kcal/mol. E_a decreases with increasing ΔT. However, the accuracy of the values does not allow a kinetic calculation.[8]

The G value for the hydrogen, corresponding to the hydrocarbon products formed, is given by the material balance equation $G(H_2)_{calcd} = 0.5[-G(C_2H_4\cdot{-}C_{n-1}H_{2n}) + G(C_2H_4\cdot{-}C_{n-1}H_{2n-2}) + G(\text{i.m.w.p.})] + G(C_nH_{2n}) + G(C_{2n}H_{4n-2})$. We have already shown for hexane that $G(H_2)_{calcd}$ is always smaller than $G(H_2)$.[1] The difference at −78° is about 1 unit of the G value and might be explained by experimental errors. Contrary to $G(H_2)$, $G(H_2)_{calcd}$ changes only very little with temperature. This means that, at least at higher temperatures, some unknown products must be formed with a total G value of at least 1. Since they so far have escaped gas chromatographic analysis, it is reasonable to assume that they have higher molecular weights than the dimers.

Experimental Section

The paraffins irradiated were of Phillips Research grade quality and were subjected to gas chromatographic purification. We were unable to detect any impurity. The samples were degassed by several freezing-thawing cycles using an ultrasonic source and were irradiated in sealed glass ampoules with intensities of either 0.3 or 1.5 Mrads/hr. The products were determined by gas chromatography. The G values for in general eight doses between 1 and 8 Mrads were extrapolated to zero dose where necessary. The full experimental details and the gas chromatographic retention values will be published elsewhere.[8,18]

Acknowledgment. We gratefully acknowledge the financial support of the Swiss National Foundation. We thank Professors A. Kuppermann and G. J. Mains for helpful discussions.

(42) J. Betts, Thesis, California Institute of Technology, 1970; A. Kuppermann and J. Betts, to be published.
(43) K. Hong and G. J. Mains, *J. Phys. Chem.*, to be published.

Picosecond Observations of Some Ionic and Excited-State Processes in Liquids

G. Beck and J. K. Thomas*

Chemistry Department and the Radiation Laboratory,[1] University of Notre Dame, Notre Dame, Indiana 46556
(Received May 5, 1972)

Publication costs assisted by the U. S. Atomic Energy Commission

The design of a pulse radiolysis system for absorption and emission spectroscopy with a response down to 60 psec is described. Events which occur with response times of about 10 psec may also be observed by observing the development of these species during the radiation pulse. The system has been used to investigate the mode of formation of solute excited states in cyclohexane, the benzene excimer in pure benzene, and the rate of formation of solvated electrons in ethanol and 1-propanol. The data show that the excited singlet state of cyclohexane is formed rapidly (<10 psec) in radiolysis, and has a decay constant of 3.6×10^9 sec^{-1}. The state transfers energy to added solutes such as benzene, with $k = 2.2 \times 10^{11}$ M^{-1} sec^{-1}; CCl_4, $k = 2.5 \times 10^{11}$ M^{-1} sec^{-1}; and 9,10-diphenylanthracene, $k = 3.4 \times 10^{11}$ M^{-1} sec^{-1}. No significant yield of the triplet state of the aromatic solutes is observed in pseconds contrary to the large yields of triplets observed in nseconds. The anions and cations of the aromatic solutes are also observed, and exhibit rapid formation but little decay in pseconds. The excimer state of benzene is observed to appear with a delay of 10 psec, and this is considered to be the result of prior formation of the monomer singlet followed by the complexing time which is calculated to be 7 psec. The solvated electron in ethanol is formed rapidly but with a possible delay of 2–5 psec, while the solvated electron in 1-propanol is formed over 50 psec. The data are discussed in terms of current theories of radiation chemistry.

Introduction

Excited states both singlet and triplet are observed in the pulse radiolysis of aromatic solutes in cyclohexane solutions.[2-6] Nanosecond data show that the excited states are produced *via* two distinct processes which are characterized by quite different time dependences. In the concentration range 10^{-3}–10^{-1} M about 80% of the excited states are produced rapidly within 5 nsec while the remaining 20% are produced over about 100 nsec. It has been shown[6] that the development of the excited states over 100 nsec is matched by a decay of the solute anions, which are also observed in these experiments. Typical electron scavengers such as H_2O, SF_6, and alcohols reduce the yield of excited states, the former two scavengers also reducing the yield of anions. These experiments suggest that ion neutralization may lead to the formation of excited states. This is most probably the case for the excited states produced over 100 nsec, and it is suggested that a more rapid ion neutralization event may account for the rapid (<5 nsec) yield also. Schuler[7] and coworkers have suggested that the ion recombination is a geminate event leading to an initially rapid, followed by a slower, recombination. Indeed they can calculate a precise fit to the observed geminate recombination of biphenyl anions in the pulse radiolysis of 0.1 M biphenyl in cyclohexane.[6] This interpretation could certainly explain the faster production of excited states; however, the ion neutralization process could involve the solute cation and the electron, an event which is predicted to be very rapid.

Ion neutralization is very slow in alkane solutions at lower temperatures,[8] and in agreement with the mechanism that ion neutralizations lead to excited states, the excited states of an added solute are observed to grow in slowly while the ions decay.

Recent photochemical experiments by Holroyd[9] and Lipsky and Hirayama[10] show that excited states of cyclohexane and other alkanes can be produced by photochemical excitation at λ <2000 Å. The lifetimes of the excited states are reported to be short (1 nsec), but the states are quenched by typical electron scavengers, *e.g.*, N_2O, CCl_4, and CO_2, and transfer energy to aromatic solutes such as, 2,5-diphenyloxazole and benzene, giving the characteristic fluorescence of these molecules. It is pertinent to inquire into the role of excited singlet states of alkanes in radiolysis.

With the above suggestions and conclusions in mind we have constructed a fast psecond pulse radiolysis apparatus which enables us to investigate events down to ten's of pseconds and hence to directly investigate the initial rapid development of the excited states in the radiolysis of alkanes.

Experimental Section

Our apparatus uses the fine structure of the electron beam of a linear accelerator to initiate the radiolysis, a technique which was first described by Hunt and coworkers.[11] But while they use Čerenkov light flashes to measure the concentration of absorbing species produced, and to perform a time transformation so that a low-frequency

(1) Operated under contract with the U. S. Atomic Energy Commission. This is AEC Document No. COO-38-846.

(2) J. D. McCollum and W. A. Wilson, ASD Technical Report No. 61-170, (1961); and ASD T.D.R. Report No. 62-32, (1962); J. D. McCollum and T. D. Nevitt, ASD T.D.R. Report No. 63-616, (1963).
(3) T. J. Kemp, G. A. Salmon, and P. Wardman in "Pulse Radiolysis," M. Ebert, J. P. Keene, A. J. Swallow, and J. H. Baxendale, Ed., Academic Press, London, 1965, p 294.
(4) E. J. Land and A. J. Swallow, *Trans Faraday Soc.*, **64**, 1221 (1968).
(5) J. W. Hunt and J. K. Thomas, *J. Chem. Phys.*, **46**, 2954 (1967).
(6) J. K. Thomas, K. Johnson, T. Klippert, and R. Lowers, *J. Chem. Phys.*, **48**, 1608 (1968).
(7) S. J. Rzad, P. P. Infelta, J. M. Warman, and R. H. Schuler, *J. Chem. Phys.*, **52**, 3971 (1970).
(8) J. T. Richards and J. K. Thomas, *J. Chem. Phys.*, **53**, 218 (1970).
(9) R. A. Holroyd, *Advan. Chem. Ser.*, **No. 82**, 488 (1968).
(10) F. Hirayama and S. Lipsky, *J. Chem. Phys.*, **51**, 3616 (1969); *Chem. Phys. Lett.*, **5**, 296 (1970).
(11) M. J. Bronskill, W. B. Taylor, R. K. Wolff, and J. W. Hunt, *Rev. Sci. Instrum.*, **41**, 333 (1970).

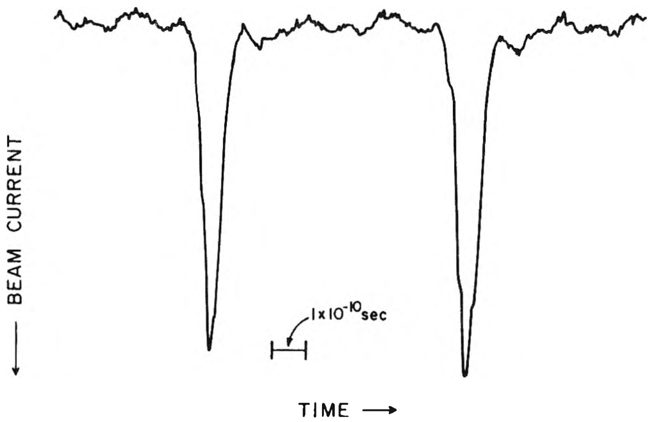

Figure 1. Fine structure pulses from the L-band linear accelerator as observed with a transmission line target.

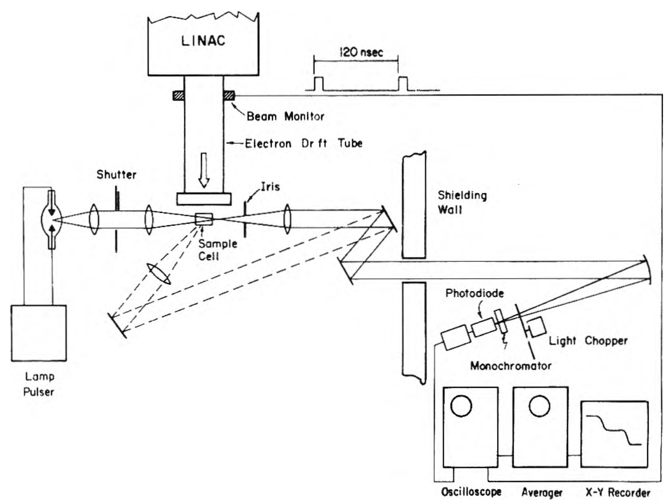

Figure 2. Schematic diagram of the pulse radiolysis system designed for picosecond time resolution.

detection system can be employed, we have developed a detection system with an over-all rise time (10–90%) of 60 psec which enables us to observe emissions as well as absorptions with corresponding time resolution.

The fine structure pulses from the Notre Dame linear accelerator (ARCO, Model LP-7) have an energy of 7 MeV and occur in bursts of 10 nsec total duration. The spacing, determined by the accelerating microwave, is 770 psec. Figure 1 shows typical fine structure pulses observed with a transmission line target[12] having a rise time of 18 psec. These pulses are approximately 45 psec (FWHM) in duration and have a peak current of about 60 A, the width depending very critically on the tuning of the accelerator which operates without a travelling wave prebuncher. The basic pulse radiolysis set-up shown in Figure 2 is conventional except for the light source and the detection system.

As light source we utilize an Osram XBO 450-Watt xenon lamp which is pulsed for 120 μsec to a current of about 600 A with a repetition rate of 10 pps by a specially designed lamp pulser, or a 4-W argon ion laser (Coherent Radiation, Model 52B). The laser has the obvious advantage of single wavelength operation. It should be noted, however, that there is an inherent source of excess photon noise in any laser due to multimode operation. The laser cavity is resonant and hence may have output at all frequencies for which a standing wave can exist between the reflectors. For a 1-m cavity the so-called modes have a frequency separation of 150 MHz, and 10 to 30 of them may oscillate within the fluorescence line width giving rise to mode beating noise[13] which is very significant as the oscillations seem to occur in random sequence with amplitude fluctuations at each frequency. The amplitude of the noise observed is strongly dependent on the conditions in the lasing cavity and increases with increasing detector bandwidth. Using our fast detection system with 6 GHz bandwidth we observed typical values of 20% noise (peak to peak). To overcome this limitation of detectable absorption we have used the laser in single frequency operation by means of a tilted etalon incorporated in the cavity.

The light from the xenon lamp or the laser is focussed through the sample cell (1-cm optical path length) and *via* a lens and mirror system onto the entrance slit of a Bausch & Lomb monochromator (Model 33-86-02). An iris at the exit window of the cell limits the field of view of the detection system and a light chopper decreases the average light intensity falling on the cathode of an ITT F-4014 biplanar photodiode. This is mounted in a high-speed holder[14] which is designed to match the diode to a 50 Ω system and to allow operation of the diode up to 10 kV, as the response to an increase in light level is determined by the flight time of the photoelectrons between cathode and anode. Detailed consideration of the diode performance will be given elsewhere.[14] The linearity of the photocurrent *vs.* light intensity was checked with calibrated neutral density filters and by observing the Čerenkov radiation from cyclohexane with the analyzing light alternately on and off. With complete illumination of the cathode the linearity was better than 3% up to a cathode current of 120 mA. It should be noted, however, that some diodes showed considerable fatigue even at 4 μA mean current.

The output of the diode is fed into a Tektronix S-4 sampling head (rise time 25 psec), stored in a NS-44 digital averager (Northern Scientific), and plotted on an X–Y recorder. An advance trigger for the sampling oscilloscope is provided by operating the linear accelerator in double pulse mode which results in two 10-nsec beam pulses in one rf envelope separated by 120 nsec. These pulses are sensed by a current loop which permits the oscilloscope to be triggered by the first pulse, while the radiolysis events of the second pulse are observed.

Figure 3 shows the response of the detection system to Čerenkov radiation from cyclohexane produced by two fine structure pulses. The diode was operated at 8 kV, corresponding to a flight time of 60 psec. The observed rise and fall times (10–90%) are 75 psec. The rise time in addition to the portion caused by the flight time is due to the pulse shape and trigger jitter.

Results

Water. A typical absorption *vs.* time trace is shown in Figure 4 for the development of the hydrated electron with two fine structure pulses in the radiolysis of a deaerated solution of 10^{-2} *M* $HClO_4$ in water. The wavelength of the observation was 520 nm which was achieved by using an interference filter with a band pass $W_{1/2}$ of 100

(12) G. Beck and D. W. Schutt, *Rev. Sci. Instrum.*, **43**, 341 (1972).
(13) H. Hodara and N. George, *IEEE J. Quantum Electron.*, **2**, 337 (1966).
(14) G. Beck, to be submitted for publication.

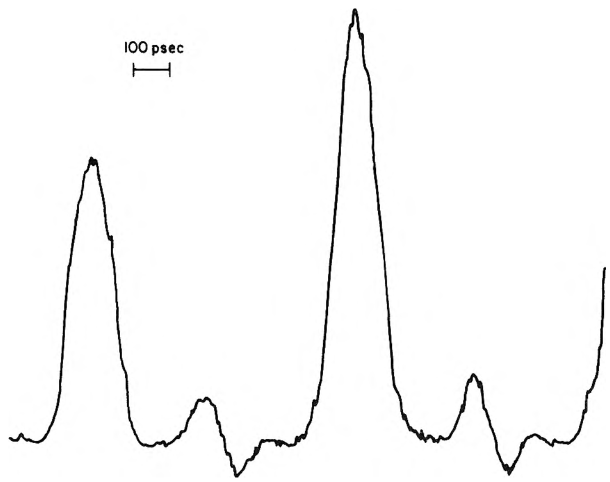

Figure 3. Cerenkov radiation from cyclohexane produced by two fine structure pulses as observed with the picosecond detection system.

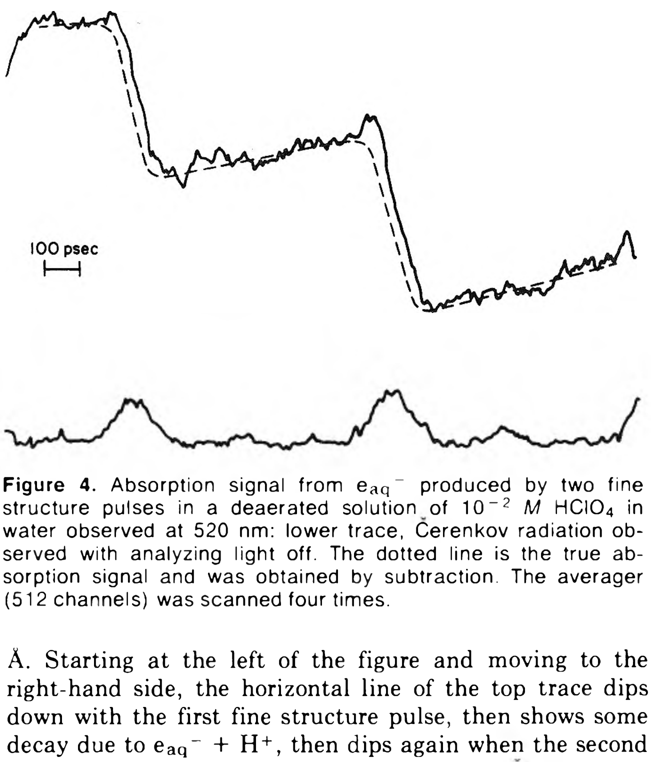

Figure 4. Absorption signal from e_{aq}^- produced by two fine structure pulses in a deaerated solution of 10^{-2} M $HClO_4$ in water observed at 520 nm: lower trace, Čerenkov radiation observed with analyzing light off. The dotted line is the true absorption signal and was obtained by subtraction. The averager (512 channels) was scanned four times.

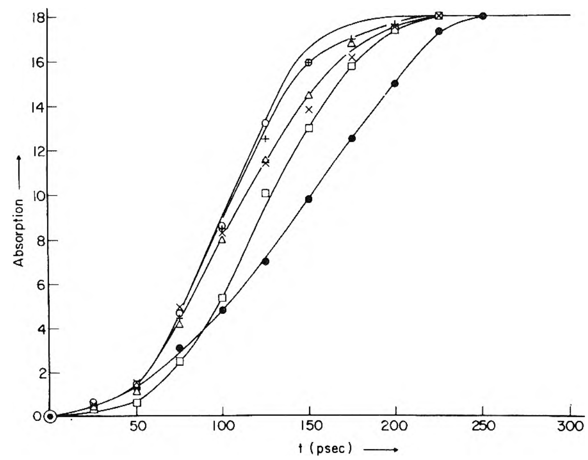

Figure 5. Development of the following species during a fine structure pulse: solid curve to the far left, water; +, ethanol; ●, 1-propanol; □, excimer in pure benzene; Δ, 10^{-2} M biphenyl/C_6H_{12}; ×, 3×10^{-3} M biphenyl in C_6H_{12}; O, 0.1 M biphenyl/C_6H_{12}.

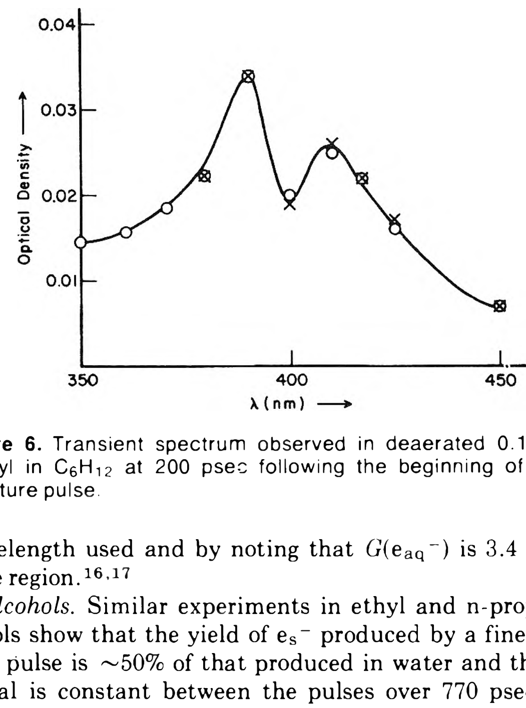

Figure 6. Transient spectrum observed in deaerated 0.1 M biphenyl in C_6H_{12} at 200 psec following the beginning of a fine structure pulse.

Å. Starting at the left of the figure and moving to the right-hand side, the horizontal line of the top trace dips down with the first fine structure pulse, then shows some decay due to $e_{aq}^- + H^+$, then dips again when the second pulse appears. The bottom trace shows the Čerenkov radiation produced in the sample; this was taken with no analyzing light passing through the sample. The true hydrated electron signal is shown as the dotted line which is obtained by subtracting the Čerenkov from the absorption trace. Similar data are observed in pure water, but no decay or growth of e_{aq}^- is observed between the pulses. Usually acid is used in these samples to remove the absorption due to the e_{aq}^- produced in the trigger pulse.

The data from traces such as Figure 4 are plotted as an average e_{aq}^- absorption *vs.* time over the period of the radiation pulse in Figure 5. Hunt and coworkers[15] have shown that e_{aq}^- develops in a time that is short compared to 10 psec so that this trace illustrates the observation of a species that is produced with the radiation pulse, without delay or subsequent growth. These data are also used to measure the radiation dose in the sample by using the appropriate extinction coefficient for e_{aq}^- at the wavelength used and by noting that $G(e_{aq}^-)$ is 3.4 in this time region.[16,17]

Alcohols. Similar experiments in ethyl and n-propyl alcohols show that the yield of e_s^- produced by a fine structure pulse is ~50% of that produced in water and that the signal is constant between the pulses over 770 psec. The absorption produced in these alcohols with the pulse is also shown in Figure 5 and compared to that in water. A slight lag amounting to a few pseconds is observed in ethanol, while a large lag of the e_s^- in alcohol behind e_{aq}^- in water is observed in 1-propanol.

Solutions of Biphenyl and Pyrene in Cyclohexane. Both the biphenyl and pyrene anion were identified in the pulse radiolysis of these solutes in cyclohexane, while the pyrene cation was identified by its absorption at λ 450 nm in the radiolysis of 10^{-2} M pyrene in cyclohexane saturated with SF_6. A typical spectrum for a solution of 0.1 M biphenyl (Ph_2) in cyclohexane (C_6H_{12}) is shown in Figure 6. This spectrum compares favorably with that observed in the radiolysis of Ph_2 in alcohol when Ph_2^- is formed alone.[18]

(15) M. J. Bronskill, R. K. Wolff, and J. W. Hunt, *J. Chem. Phys.*, **53**, 4201 (1970).
(16) R. Bensasson and J. K. Thomas, *J. Chem. Phys.*, **46**, 4147 (1967).
(17) J. W. Hunt, private communication.
(18) S. Arai and L. Dorfman, *J. Chem. Phys.*, **41**, 2190 (1964).

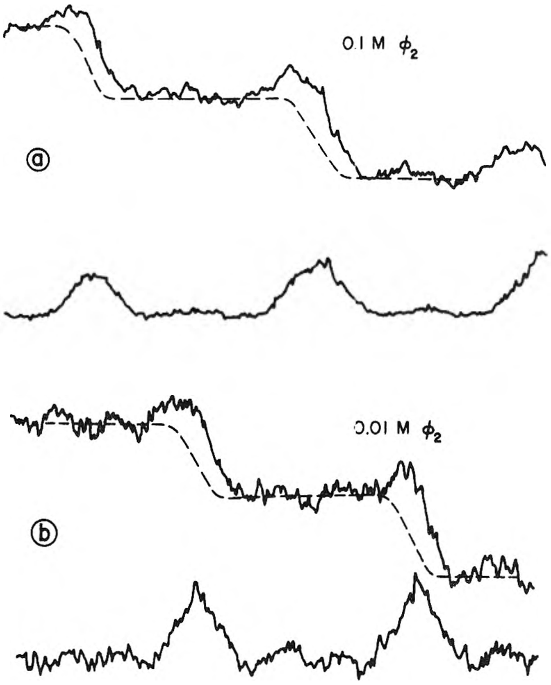

Figure 7. Absorption produced by two fine structure pulses in deaerated solutions of biphenyl (Ph_2) n cyclohexane observed at 404 nm. The dotted line is the true absorption and was obtained by subtraction: a 0.1 M Ph_2; b, 0.01 M Ph_2.

The biphenyl cation has a similar spectrum,[19] and the spectrum in Figure 6 is probably a composite of Ph_2^- and Ph_2^+. It is worthy of note that the absorption decreases toward λ 350 nm, which is contrary to the observation[20,21] at nsecond times where the absorption increases due to the formation of the triplet state Ph_2^T.

Figure 7 shows the development of the Ph_2^- absorption observed at λ 410 nm for 0.1 M and 10^{-2} M biphenyl in C_6H_{12}. The absorptions develop rapidly with the radiation pulse and show no change in the time interval before the next pulse appears. The absorptions during the pulse are compared to water in Figure 5. The 0.1 M Ph_2 in C_6H_{12} shows a development of Ph_2^- *vs.* time that follows the e_s^- in ethanol. The half-life of the electron in the 0.1 M Ph_2-C_6H_{12} solution is 2.7 psec,[22] while the half-life in 10^{-2} M Ph_2-C_6H_{12} is 27 psec. The development of Ph_2^- in the later solution shows a larger lag behind that of e_{aq}^- in water as expected. The G value of Ph_2^- in 0.1 M Ph_2 was measured as 1.1 molecules/100 W.

Similar data were obtained in the pulse radiolysis of pyrene in C_6H_{12} where the pyrene anion was observed with the 488-nm line of the 4-W argon ion laser. This trace is shown as insert B in Figure 8. In the presence of SF_6 the pyrene anion absorption is generally decreased but the absorption at 450 nm is unchanged. This is identified as the pyrene cation[23] and shows a slow growth between the fine structure pulses. In a 3×10^{-2} M pyrene/C_6H_{12} solution saturated with SF_6 the cation shows a faster growth with $t_{1/2} \sim 50$ psec indicating a $k \sim 4 \times 10^{11}$ M^{-1} sec^{-1} for the formation of the pyrene cation.

The singlet excited state of pyrene was observed in the pulse radiolysis of degassed solutions of pyrene in C_6H_{12}. The excited state showed a slow growth between fine structure pulses and will be considered in the next section.

Fluorescence in the Radiolysis of C_6H_{12} Solution. The pulse radiolysis of aromatic solutes in C_6H_{12} leads to fluo-

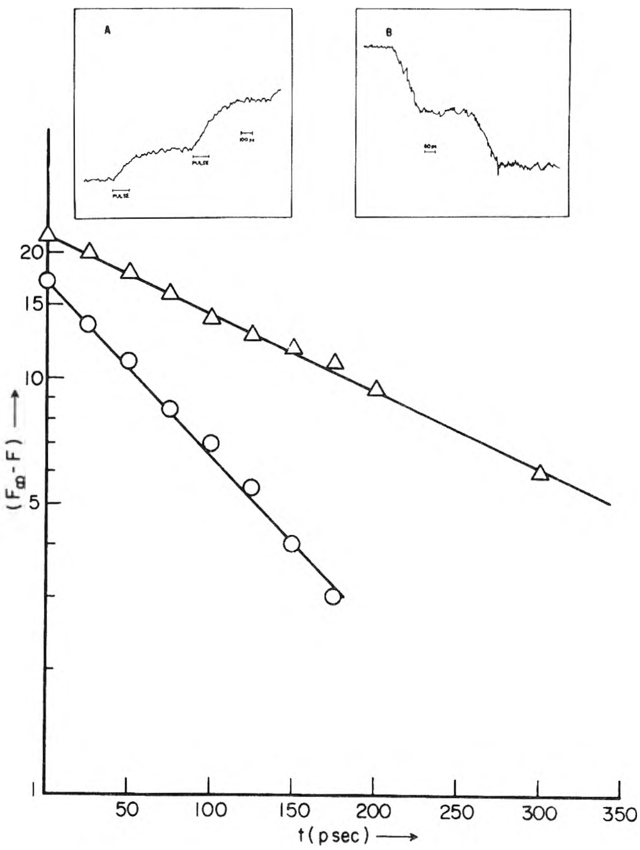

Figure 8. First-order growth of fluorescence in the picosecond pulse radiolysis of 9,10-diphenylanthracene (DPA) in cyclohexane: O, 10^{-2} M DPA; Δ, 10^{-3} M DPA. Insert A shows an oscilloscope trace of the growth of fluorescence of 10^{-2} M DPA monitored at 423 nm. Insert B shows the absorption of the pyrene negative ion produced by two fine structure pulses monitored at 488 nm.

rescence which is characteristic of the added solute. Figure 9 shows the fluorescence from two fine structure pulses in the pulse radiolysis of 10^{-2} M 1,1′-binaphthyl in C_6H_{12}. It can be seen that the fluorescence rises with the pulse and then continues to rise to the next pulse, when the same behavior is repeated. Anthracene, biphenyl, p-terphenyl, 2,5-diphenyloxazole, 1,1′-binaphthyl, and 9,10-diphenylanthracene (DPA) all show this behavior. The most convenient molecule to use is the latter as the quantum yield for fluorescence is unity, the $t_{1/2}$ is 10 nsec[24] which means that little decay of the excited state occurs between pulses, and the fluorescence is situated in the visible part of the spectrum which minimizes the interference from Čerenkov radiation.

The growth of the fluorescence follows first-order kinetics as shown in Figure 8 where $\log(F_\infty - F)$ is plotted *vs.* time, where F_∞ and F refer to the fluorescence at the maximum growth time, *i.e.*, just before the next pulse appears, and F refers to the fluorescence at time t.

The rate of growth of the fluorescence increases with increasing DPA concentration, a plot of the rate constant

(19) J. B. Gallivan and W. H. Hamill, *J. Chem. Phys.*, **44**, 2378 (1966).
(20) L. B. Magnusson, J. T. Richards, and J. K. Thomas, *Int. J. Radiat. Phys. Chem.*, **3**, 295 (1971).
(21) J. H. Baxendale and P. Wardman, *Int. J. Radiat. Phys. Chem.*, **3**, 377 (1971).
(22) G. Beck and J. K. Thomas, *Chem. Phys. Lett.*, **13**, 295 (1972).
(23) J. T. Richards, G. West, and J. K. Thomas, *J. Phys. Chem.*, **74**, 4137 (1970).
(24) I. B. Berlman, "Handbook of Fluorescence Spectra of Aromatic Molecules," Academic Press, New York, N.Y., 1965.

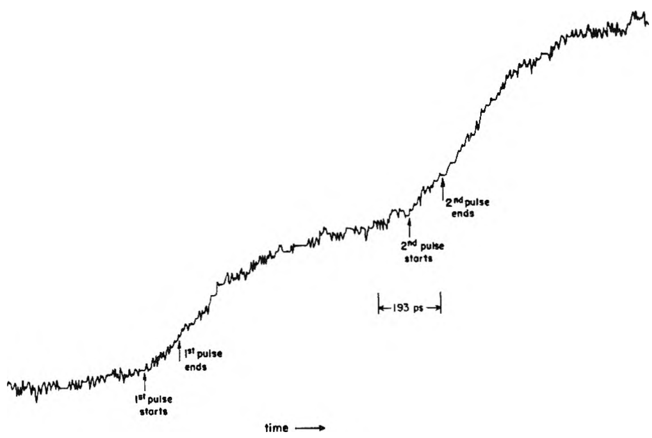

Figure 9. Fluorescence produced by two fine structure pulses in a deaerated solution at 10^{-2} M 1,1-binaphthylincyclohexane.

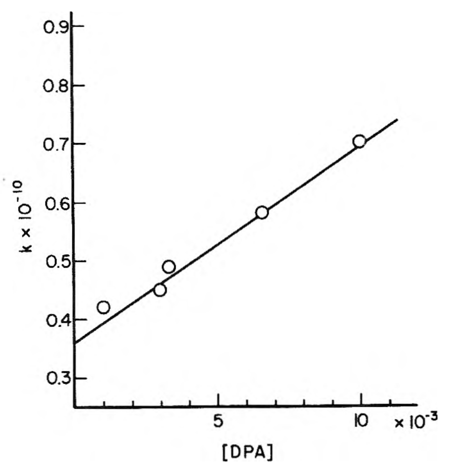

Figure 10. Rate constant for the growth of fluorescence for different concentrations of 9,10-diphenylanthracene (DPA) in cyclohexane.

vs. DPA concentration being linear as shown in Figure 10.

If it is assumed that the following mechanism applies in these experiments

$$C_6H_{12}^* \xrightarrow{\alpha}$$

$$C_6H_{12}^* + DPA \xrightarrow{\beta} DPA^* \longrightarrow h\nu$$

then the observed rate constant $k = \alpha + \beta$[DPA]. The data in Figure 10 then give $\alpha = 3.6 \times 10^9$ sec^{-1} and $\beta = 3.4 \times 10^{11}$ M^{-1} sec^{-1}.

Effect of Additives on the Fluorescence. Many additives such as ethanol, SF_6, CO_2, CCl_4, and benzene reduce the fluorescence of DPA in C_6H_{12}. In all cases the apparent rate of growth or formation of the DPA fluorescence also increases.

Effect of Benzene. At all concentrations of DPA used addition of 10^{-3}–10^{-2} M benzene progressively reduces the fluorescence to a plateau value. Typical data are shown in Figure 11. The plateau yield of fluorescence grows in directly with the radiation pulse and is unaffected by concentrations of CCl_4 up to 5×10^{-2} M. It appears that the DPA fluorescence is derived from at least two different processes, one rapid event and one that grows in between the pulses at a rate which increases with increasing DPA concentration. It is suggested that the slow development of fluorescence is due to an energy transfer to the DPA and that benzene also competes with the DPA

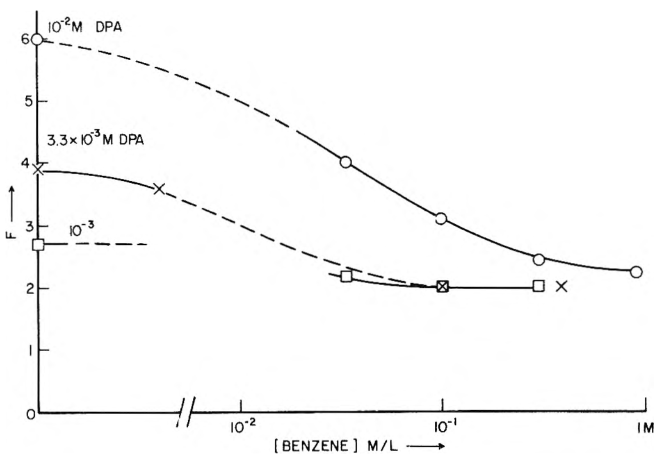

Figure 11. Reduction of fluorescence yield of DPA in C_6H_{12} by benzene: ordinate F = fluorescence yield; O, 10^{-2} M DPA; ×, 3.3×10^{-3} M DPA; □, 10^{-3} M DPA.

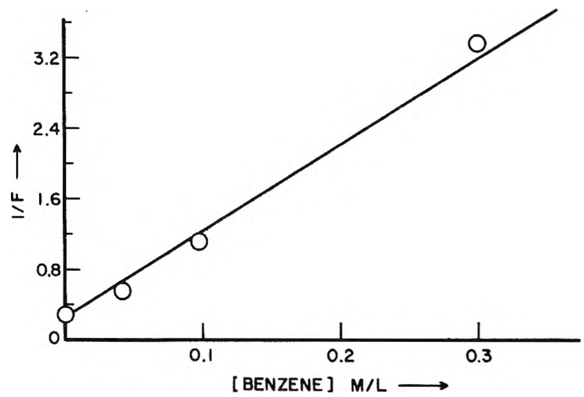

Figure 12. Stern–Volmer plot of the reduction of the fluorescence of 10^{-2} M DPA in C_6H_{12} by benzene.

for the C_6H_{12} singlet energy. The mechanism for the system is as follows

$$C_6H_{12}^* \xrightarrow{\alpha} \tag{1}$$

$$C_6H_{12}^* + DPA \xrightarrow{\beta} DPA^* \longrightarrow h\nu \tag{2}$$

$$C_6H_{12}^* + C_6H_6 \xrightarrow{\gamma} C_6H_6^* \tag{3}$$

and the fluorescence of DPA*, F follows the following relationship

$$\frac{1}{F} = \frac{1}{F_0}\left(1 + \frac{\alpha}{\beta[DPA]} + \frac{\gamma[C_6H_6]}{\beta[DPA]}\right)$$

In this case the fluorescence F is the difference between the measured fluorescence and the fluorescence at high benzene concentrations. The plot $1/F$ *vs.* [C_6H_6] in Figure 12 is linear as demanded by the above equation and gives $\gamma/\beta = 0.65$, *i.e.*, $\gamma = 2.2 \times 10^{11}$ M^{-1} sec^{-1}.

If the resultant DPA fluorescence at high benzene concentration is subtracted from the fluorescence in the absence of benzene then it is possible to investigate the effect of [DPA] in reactions 1 and 2. The expression connecting F and [DPA] is

$$\frac{1}{F} = \frac{1}{F_0}\left(1 + \frac{\alpha}{\beta[DPA]}\right)$$

A plot of $1/F$ *vs.* 1/[DPA] in Figure 13 is linear and gives $\alpha/\beta = 1.05 \times 10^{-2}$, which is in excellent agreement with the direct measure of $\alpha = 3.6 \times 10^9$ sec^{-1} and $\beta = 3.4 \times 10^{11}$ M^{-1} sec^{-1}.

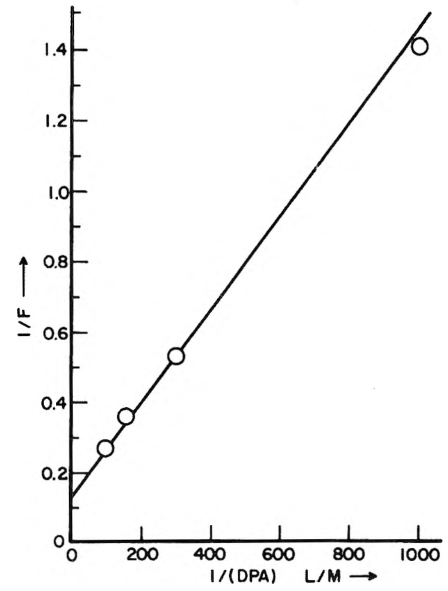

Figure 13. Plot of the inverse of DPA fluorescence *vs.* inverse of DPA competition for DPA in C_6H_{12}.

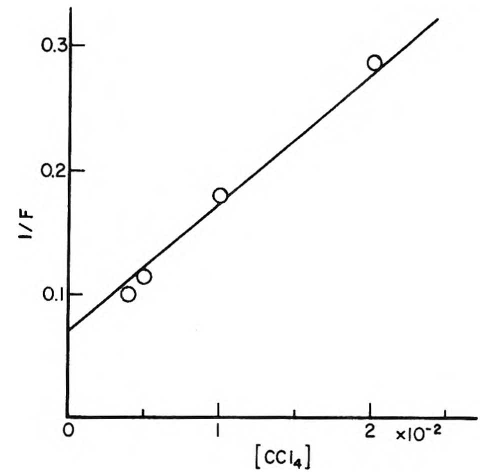

Figure 14. Stern–Volmer plot of the competition of 1,1′-binaphthyl and CCl_4 for the excited state of C_6H_{12}. The ordinate is the inverse of the 1,1′-binaphthyl fluorescence.

Effect of Carbon Tetrachloride. Carbon tetrachloride, CCl_4, reduces the yield of fluorescence of the aromatic solute, *e.g.*, DPA in C_6H_{12}, while the apparent rate of development of the fluorescence increases. On the basis that the CCl_4 and DPA compete for the excitation energy it is possible to measure a rate constant k for the transfer of energy from C_6H_{12} to CCl_4. The direct observation gives k is $3 \pm 1 \times 10^{11}\ M^{-1}\ sec^{-1}$.

With the above mechanism it is also possible to calculate the ratio of two rates of transfer of energy from C_6H_{12} to DPA and CCl_4 from the decrease in the fluorescence yield with increasing CCl_4 concentration. The mechanism is reactions 1 and 2 with 4.

$$C_6H_{12}^* + CCl_4 \xrightarrow{\delta} \qquad (4)$$

This mechanism is similar to that used in the benzene/DPA system and predicts a linear plot of $1/F$ *vs.* $[CCl_4]$, which is observed in Figure 14. The analysis of the data in Figure 14 gives $\delta/\beta = 0.75$, i.e., $\beta = 2.5 \times 10^{11}\ M^{-1}\ sec^{-1}$, which is in agreement with the direct measurement of $\beta = 3 \pm 1 \times 10^{11}\ M^{-1}\ sec^{-1}$.

Benzene. Previously the excimer excited state of benzene B_2^* has been observed in the pulse radiolysis and laser photolysis of pure benzene[25] and benzene in C_6H_{12}.[26] It is not certain how the excited monomer singlet, B^*, is formed, it could be formed by direct excitation to higher excited states followed by a cascade to B^*, or by ion recombination to give B^* directly. The excimer B_2^* is then formed by the process

$$B^* + B \underset{k_2}{\overset{k_1}{\rightleftharpoons}} B_2^*$$

The half-life of this process in benzene is given by

$$t^{1/2} = \frac{0.69}{k_1[B_0] + k_2}$$

and is 7 psec at room temperature if $k_1 = 6 \times 10^9\ M^{-1}\ sec^{-1}$ and $k_2 = 3 \times 10^{10}\ sec^{-1}$.[27]

Figure 15 shows that formation of B_2^* by two fine structure pulses monitored at 520 nm the λ of maximum absorption. The formation of the state *vs.* time during the pulse is shown in Figure 5. It can be seen that the formation of B_2^* lags 10 psec behind the formation of e_{aq}^- in water.

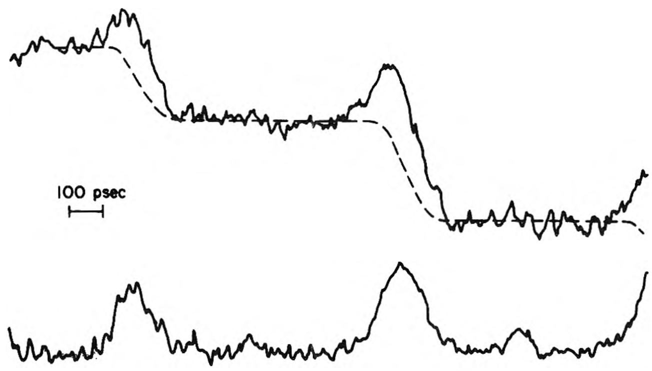

Figure 15. Absorption produced by two fine structure pulses in pure benzene monitored at 520 nm. The Čerenkov radiation shown in the lower trace was subtracted to yield the true emission *vs.* time curve which is shown as dotted line.

Discussion

In previous work[22] the rate constant for reaction of e^- with biphenyl in C_6H_{12} at room temperature was measured as $2.6 \times 10^{12}\ M^{-1}\ sec^{-1}$. This rate parallels the high mobility of electrons in C_6H_{12} measured by electron drift studies. The rate constant predicts that the half-life $t_{1/2}$ of the formation of the biphenyl anion, Ph_2^-, should be 2.7 psec in 0.1 M Ph_2 and 27 psec in $10^{-2}\ M$ Ph_2 in C_6H_{12}. This is too rapid for a direct measurement in the present equipment, however, a reasonable observation of the rate of formation of Ph_2^- in such systems may be achieved by comparing the rate of development of Ph_2^- during the pulse with that of e_{aq}^- in water. The data are shown in Figure 5 for 0.1, 0.01, and 0.03 M Ph_2 in C_6H_{12}, when it can be seen that at 0.1 M Ph_2 the Ph_2^- absorption lags 2 to 4 psec behind the water curve while the data at $10^{-2}\ M$ Ph_2 is identical with that at $3 \times 10^{-3}\ M$ and lag 10 psec behind the water. The absorption curves can be simulated by integrating a triangular voltage pulse

(25) R. Cooper and J. K. Thomas, *J. Chem. Phys.*, **48**, 5097 (1968).
(26) R. Bensasson, J. T. Richards, and J. K. Thomas, *Chem. Phys. Lett.*, **9**, 13 (1971).
(27) J. B. Birks, C. L. Bragia, and M. D. Lumb, *Proc. Roy. Soc., Ser. A*, **283**, 83 (1965).

with base 80 psec with various capacities and displaying the result on an oscilloscope screen. The triangular voltage pulse is equivalent to the actual radiation pulse, and the capacity integration corresponds to equipment distortion and late development of the observed entities. These rather crude computations provide the numbers quoted for the delayed absorptions and approximately conform to the actual radiolysis events. A more extended calculation is underway.

The observed half-life for development of Ph_2^- in 10^{-2} and 3×10^{-3} M Ph_2 solutions is shorter than that calculated from the measured rate constant for e^- plus Ph_2 in C_6H_{12}. We may conclude that the electrons may react prior to thermalization thus distorting the data, or that Ph_2 competes with the geminate recombination of the cation and e^-. This latter event may still play the controlling feature in the lifetime of the e^- in these systems, and will hasten the fate of the electron and effectively the development of Ph_2^-.

At first sight the lack of any significant decay of Ph_2^- between the fine structure pulses, as shown in Figure 7, does not agree with the geminate ion neutralization as described by Schuler and coworkers.[7] Indeed, the $G[Ph_2^-] = 1.1$ in solution at 0.1 M Ph_2 and greater agrees with the estimate of earlier nsec data.[6] This value of 1.1 would be larger however (1.6) if the initial $G(e_{aq}^-)$ in water is 5.0, which is predicted by diffusion theory. It is probably, although calculations have to be made to realize the effect quantitatively, that the initial ion neutralization of the cation and electron is extremely rapid so that at reasonable concentrations of Ph_2 (<1.0 M), it is not possible to capture more than 50% of the electrons. Alternatively, some of the Ph_2^- formed may still react too rapidly for direct observation. The point we wish to make clear for later discussion in relation to excited states is that the electrons all disappear very rapidly in the solutions used, in a time short compared with the observation time of excited states, *i.e.*, ~500 psec, and that the anions do not recombine rapidly in this time domain. We suggest that this is a general phenomenon for polycyclic aromatic solutes in C_6H_{12}, quoting the pyrene and biphenyl data to support it.

The data in solutions of pyrene in C_6H_{12} saturated with SF_6 suggest that the positive ion of the solute may be formed rapidly in the pulse radiolysis of these systems, with a rate constant of 4×10^{11} M^{-1} sec^{-1}. This rate constant is an order of magnitude smaller than the corresponding rate constant for the formation of the anion from electrons, but is in agreement with a ratio of 1/20 for these rates measured in steady-state experiment.[7] This suggests that the positive ion has an abnormally high mobility in alkanes, and is in keeping with the rapid formation of cations in the radiolysis of low-temperature alkane glasses containing aromatic solutes.[19]

The spectrum observed in 0.1 M Ph_2 in C_6H_{12} at 100 psec differs from that observed at 10 nsec in the region of λ 360 mμ. In the nsecond time domain an initial absorption is present a part of which grows in subsequently. This absorption is due to the triplet state of Ph_2 which has an extinction coefficient of 35,400[28] at λ 360 mμ. It is suggested[6,21] and in part observed that the cation–anion neutralization in the 10-nsec time domain leads to a significant yield of triplet excited state, the absence of Ph_2^T at 100 psec being due to the insignificant solute ion neutralization which occurs here.

Singlet excited states are observed to develop rapidly between the fine structure pulses with rates which increase with increasing aromatic solute concentration. The previous arguments and data show that these excited states are not formed by ion neutralization, and it is suggested that they are derived from an energy transfer process from cyclohexane. The observations by Lipsky and Hirayama[10] give concrete support to an excited state of cyclohexane with a lifetime in the nsecond region. The suggested mechanism of singlet energy transfer follows eq 1, 2, and 3 which suggest that the rate constant for the formation of fluorescence should be exponential. This is shown to be true experimentally in Figure 9 where the observed rate constant k is $\alpha + \beta$[solute]. A plot of k *vs.* the solute [DPA] is linear (Figure 10) and gives $\alpha = 3.6 \times 10^9$ sec^{-1} and $\beta = 3.4 \times 10^{11}$ M^{-1} sec^{-1}. The effects of other additives such as benzene and CCl_4 on the yields and rate of growth of the aromatic fluorescence can also be explained in terms of an energy transfer from C_6H_{12} to these solutes. The benzene data also show that a part of the singlet energy is derived by some other rapid process. If the yield of this rapid process is subtracted from the observed yield of fluorescence it is possible to set up Stern–Volmer plots as shown in Figure 12 which give the rate constants for energy transfer from C_6H_{12} to benzene and CCl_4 as 2.5×10^{11} and 2.2×10^{11} M^{-1} sec^{-1}, respectively.

Mechanism 1, 2, and 3 can explain all the experimental data in terms of excited states which have been observed in photochemistry. However, the lifetime of the excited state of C_6H_{12} is measured as 0.28 nsec in the present work, while Lipsky and Hirayama quote 2 nsec. However, they also quote a parameter $\alpha = t_1\beta = 67$ where t_1 is the lifetime of the excited singlet state of C_6H_{12}, and β the transfer constant to a solute. In our experiments we measure a similar parameter for benzene with $\alpha = 71$ in good agreement with the photochemical data. The difference in absolute t_1 must lie in the transfer constant β which Lipsky and Hirayama assumed to be diffusion controlled $\sim 10^{10}$ M^- sec^{-1}. We measure this to be 20-fold faster. The conclusion is that the photochemical data and the psecond radiolysis data are in good agreement.

Our data show that 50% of the excited state of C_6H_{12} is captured in a solution of 10^{-2} M aromatic solute. The singlet yields in such a solution have been measured as 0.5[29] and 0.77.[30] If we take an average of 0.67, subtract the yield of rapid singlet which is 25%, then we may compute a $G(C_6H_{12}{}^*) = 1.0$. The total singlet yield is the 1.17 molecules/100 W. It is emphasized that these numbers are speculative until later precise measurements can be carried out.

The data in C_6H_{12} solution containing DPA and CCl_4 show that the rate of transfer of energy to CCl_4 is $3 \pm 1 \times 10^{11}$ M^{-1} sec^{-1} when measured by the increased rate of development of DPA fluorescence. The competition studies in the yield of fluorescence versus CCl_4 fit a good Stern–Volmer plot (Figure 14) and give a transfer rate constant of 2.5×10^{11} M^{-1} sec^{-1}. We conclude that up to 5×10^{-2} M CCl_4 the quenching of the singlet energy is due to direct reaction with the excited state of C_6H_{12}, and not with a precursor of an earlier reaction such as an electron. This suggests that the excited state of C_6H_{12} may be formed directly, or if formed *via* ion neutralization that this process must occur much faster than 40 psec. As

(28) E. J. Land, *Proc. Roy. Soc., Ser. A*, **305**, 457 (1968).
(29) J. H. Baxendale and P. Wardman, *Trans. Faraday Soc.*, **67**, 2997 (1971).
(30) F. S. Dainton, G. A. Salmon, T. Morrow, and G. F. Thompson, *Chem. Commun.*, 326 (1968).

shown in Figure 5, the development of the absorption of the solvated electron in ethanol and 1-propanol lags behind the production of e_{aq}^- in water. The delayed formations correspond to $t_{1/2}$ = 2–4 and 50 psec respectively for ethanol and 1-propanol. This may be due to a solvation time of the electron in these alcohols. Slower formation times have been observed in low-temperature ethanol glasses,[8] and alcohols at temperatures below −100°.[31] Here the relaxation is observed by a decrease in the spectrum in the infrared which parallels an increase in the yellow→red part of the spectrum, and is associated with the breaking of hydrogen bonding with subsequent orientation of the solvent dipoles to form deeper traps for the solvated electron. The present data may also be explained in this way, although a full spectrum was not observed. Microwave absorption measurements in liquid alcohols[32] show that the relaxation time for the rotation of free monomeric molecules is 21.9 psec in 1-propanol at 20°, which is close to that observed in the present work, while the relaxation time for H bond breakage is 430 psec.

Figure 5 also shows that the formation of the benzene excimer, B_2^*, is delayed 10 psec behind that of the e_{aq}^- in water. This is of the order of the time taken to form the excimer from the ground state and the first excited singlet state. The shape of the curve which shows a large initial delay cannot be calculated by the analog device used for the other curves. It would appear that the formation of the first excited singlet state is delayed with respect to e_{aq}^- in water and that the delay in the excimer formation is the resultant of this process together with the reaction of the excited singlet with ground state benzene. The initial delay in the formation of the excited singlet state could be due to a prior ion neutralization reaction or to the direct formation of a higher excited state with subsequent cascade to the first excited singlet state. These processes are short compared to the excimer formation time of 10 psec.

It is concluded that excited singlet states are formed rapidly in both cyclohexane and benzene in a time that is short compared to 10 psec. Rapid ion neutralization or direct excitation could explain this result. The differing subsequent chemistry in the two liquids lies in the different nature of the two excited states. In cyclohexane the state is short lived, $t_{1/2}$ = 0.2 nsec, has high energy, ~7 V, and transfers energy rapidly, $k = 2\text{–}4 \times 10^{11}\ M^{-1}\ sec^{-1}$. In benzene the first excited singlet state has a $t_{1/2}$ = 20 nsec, an energy of 4.7 V, and a transfer constant $k \sim 2 \times 10^{10}$. Unlike benzene the excited singlet state of cyclohexane is very reactive with conventional electron scavengers such as N_2O, SF_6, and CO_2, a feature which must enter into the treatment of the scavenging data in these systems.

(31) J. H. Baxendale and P. Wardman, *Nature (London)*, **230**, 449 (1971).
(32) S. K. Garg and C. P. Smyth, *J. Phys. Chem.*, **69**, 1294 (1965).

Radiolysis of Aqueous Methane Solutions[1]

G. C. Stevens, Robert M. Clarke, and Edwin J. Hart*

Chemistry Division, Argonne National Laboratory, Argonne, Illinois 60439 *(Received May 8, 1972)*

Publication costs assisted by the Argonne National Laboratory

The γ-ray and electron pulse irradiation of aqueous methane and some ethane solutions is reported. The absorption spectra of the CH_3 and C_2H_5 free radicals have been measured in the wavelength range 210–270 nm. At 210 nm $\epsilon(CH_3) = 850\ M^{-1}\ cm^{-1}$ and $\epsilon(C_2H_5) = 520\ M^{-1}\ cm^{-1}$. The bimolecular recombination rate constants are $1.24 \pm 0.2 \times 10^9$ and $0.96 \pm 0.2 \times 10^9\ M^{-1}\ sec^{-1}$ for CH_3 and C_2H_5, respectively. The rate constant $k(OH + CH_4) = 1.21 \pm 0.4 \times 10^8\ M^{-1}\ sec^{-1}$; $k(CH_3 + H_2O_2) = 3.5 \times 10^7\ M^{-1}\ sec^{-1}$. The yields $G(-CH_4)$, $G(C_2H_6)$, $G(H_2)$, $G(H_2O_2)$, and $G(N_2)$ for N_2O–CH_4 solutions are reported for some acid, neutral, and alkaline solutions. A radiolysis mechanism is also given.

Introduction

Whereas many investigators have studied the radiolysis of gaseous methane as was brought out in a recent review,[2] relatively few papers have appeared on the radiolysis of aqueous methane solutions.[3-7] The results of studies on oxygen-free[4,5] and oxygen-saturated solutions[4,6] demonstrate that only the OH free radical reacts with methane to any appreciable extent. By relative rate constant measurements $k(CH_4 + OH)$ has been established as $1.4 \times 10^8\ M^{-1}\ sec^{-1}$.[7] As expected, CH_3 is the product radical and its re-

(1) Work performed under the auspices of the U.S. Atomic Energy Commission.

(2) G. G. Meisels in "Fundamental Processes in Radiation Chemistry," P. Ausloos, Ed., Interscience, New York, N. Y., 1968, Chapter 6, p 347.
(3) E. J. Hart, J. K. Thomas, and S. Gordon, *Radiat. Res. Suppl.*, **4**, 74 (1964).
(4) G. R. A. Johnson and J. Weiss, *Chem. Ind.*, **13**, 358 (1955).

activity, with O_2,[4] CO_2,[8] CH_3OH,[9] acetone,[10,11] and glycine[12] has been reported. Utilizing pulse radiolysis techniques we measured the absorption spectrum of the CH_3 free radical and its rate of formation and decay in order to establish $k(OH + CH_4)$ and $k(CH_3 + CH_3)$. Product yields have also been determined by γ-ray radiolysis in order to assist in interpreting the mechanism of reaction. Some preliminary results are also reported on the radiolysis of aqueous ethane.

Experimental Section

Matheson research grade CH_4 and C_2H_6 were used without further purification. Research grade N_2O was purified by freezing, thawing, and pumping, followed by refreezing and pumping again. For the N_2O experiments deoxgenated water was saturated with N_2O at 740 mm pressure giving a concentration of 0.025 M. High-pressure methane solutions were prepared by introducing a 1.0 mM N_2O solution into the high-pressure optical cell[13] against a back pressure of CH_4. The cell was then closed, CH_4 admitted to the desired pressure, and the solution equilibrated by shaking for 10–15 min.

Methane solutions of pH 3 and 9 were irradiated by ^{60}Co γ-rays at dose rates between 0.027 and 10 krads/min. The initial rates of C_2H_6 formation were measured at the lower dose rates, whereas $G(CH_3OH)$, $G(-CH_4)$, $G(H_2O_2)$, and $G(H_2)$ were measured at the higher dose rates. In the Linac radiolysis experiments, the pulse length of the 13.5-Mev electron beam was varied between 50 nsec at 5 A and 8 μsec at 0.2 A. Transient spectra were observed down to 220 nm, using an apparatus in which the analyzing light beam was split on a prism after passing through the irradiation cell. This permitted the study of optical changes simultaneously at two wavelengths. A special apparatus designed for work in the short ultraviolet was used at wavelengths below 220 nm.[14] The signal-to-noise ratio was improved by using a pulsed analyzing light source, having a pulse duration of 2–3 msec, a time appreciably longer than the time scale for transient decay. Observations were made with CH_4 solutions saturated at atmospheric pressure and under pressures up to 400 psi in a high-pressure optical cell.[13] For product analysis the electron pulse irradiations were carried out by irradiating 40 ml of solution in a 100-ml syringe. The high-pressure irradiations were carried out in a 30-ml high-pressure cell designed so that solutions could be withdrawn without opening the cell.[15] In all electron pulse irradiations the dose was measured by collection of charge from the cell and Faraday cup in a manner previously described.[16] All ^{60}Co and electron pulse dosimetry was standardized by the Fricke dosimeter using $G(Fe^{3+})$ = 15.6.[17]

The dissolved gases, CH_4, H_2, N_2, and O_2, were separated from the aqueous phase in a Van Slyke apparatus and analyzed on a chromatograph with a molecular sieve column. A residual nongaseous product assumed to be methanol remained in the solution after the removal of gases. For analysis of this water soluble product, the irradiated sample was neutralized, degassed, and forced into a 50-ml syringe to which 500 μM of H_2O_2 was injected. The product was then oxidized to CO_2 by irradiation and the concentration of CO_2 was measured on the Van Slyke apparatus. Clearly this method of analysis is not specific for CH_3OH since HCHO and HCOOH as well as higher molecular weight alcohols, aldehydes, and acids would yield CO_2 on γ-ray irradiation. However, under our conditions where a 100- to 500-fold excess of CH_4 relative to CH_3OH is present, further oxidation of CH_3OH to HCHO or CH_2OH-CH_2OH is unlikely. Therefore we consider CO_2 a reasonably good measure of the CH_3OH present. Figure 1 displays a calibration curve showing CO_2 development in a synthetic solution containing up to 50 μM CH_3OH. The methanol of the irradiated samples fell within this concentration range. Ethane was measured on a 5750 F & M Scientific research chromatograph. An 8-ft column of 80–100 mesh Porapak Q was used to separate the methane, ethane, propane, and butane. The column temperatures used were 24 and 157°. A calibration curve for ethane was prepared by saturating triply distilled water with ethane and measuring the concentration on a Van Slyke apparatus. Then 10-ml samples of 1–10 μM of ethane were prepared and extracted with 10 ml of helium. A 0.5-cc sample of the resulting gas was injected into the chromatograph and the area of the ethane curve was measured. A plot of area (cm^2) *vs.* μM ethane in the aqueous solution provided the calibration curve. The irradiated samples were analyzed for ethane by an identical procedure. The elution times for methane and ethane at room temperature were 1 and 8 min, respectively. Propane and butane eluted in 2.5 and 3 min at 157°. No attempt was made to measure the methane, propane, and butane quantitatively for these runs.

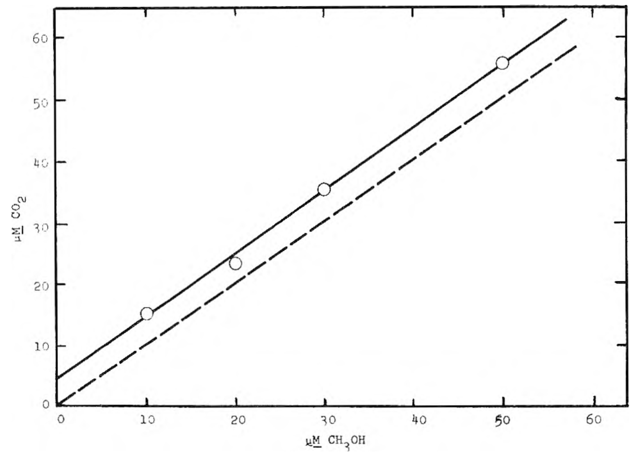

Figure 1. Calibration curve for methanol analysis.

Results and Discussion

A. Transient Spectra. Exploratory experiments demonstrated that under our conditions of electron pulse and γ-ray irradiation only the OH radical reacted directly with CH_4 and no reaction between e_{aq}^- or the H atom and CH_4 was detected. Consequently our goal was to measure the

(5) R. M. Clarke and E. J. Hart, Abstracts of the 160th National Meeting of the American Chemical Society, Chicago, Ill., Sept 1970.
(6) M. Ahmad, *Sci Ind. (Karachi)*, **6**, 57 (1968).
(7) M. Anbar, D. Meyerstein, and P. Neta, *J. Chem. Soc. B*, 742 (1966).
(8) A. Appleby, J. Holian, G. Scholes, M. Simic, and J. J. Weiss, *Int. Congr. Radiat. Res., 2nd*, 65 (1962).
(9) W. V. Sherman, *J. Phys. Chem.*, **71**, 4245 (1967).
(10) D. H. Volman and L. W. Swanson, *J. Amer. Chem. Soc.*, **82**, 4141 (1960).
(11) I. A. I. Taha and R. R. Kuntz, *J. Phys. Chem.*, **73**, 4406 (1969).
(12) G. Moger and O. Dobis, *Magy. Kem. Foly.*, **76**, 4406 (1969).
(13) E. J. Hart and M. Anbar, "The Hydrated Electron," Wiley, New York, N. Y., 1970, p 195.
(14) B. D. Michael and E. J. Hart, manuscript in preparation.
(15) M. H. Studier and E. J. Hart, *J. Amer. Chem. Soc.*, **91**, 4068 (1969).
(16) B. D. Michael, E. J. Hart, and K. H. Schmidt, *J. Phys. Chem.*, **75**, 2798 (1971).
(17) H. Fricke and E. J. Hart, "Radiation Dosimetry, Instrumentation," Vol. 2, F. H. Attix and W. C. Roesch, Ed., Academic Press, New York, N. Y., 1966.

TABLE I: Determination of $\epsilon_{220}(CH_3)$ and $k(CH_3 + CH_3)$ in CH_4–N_2O Solutions[a]

System	No. of expt	λ, nm	Mean $kC_{max} \times 10^{-4}$	Mean OD_{max}	Mean dose (rate)
(1) CH_4–N_2O	7	220	2.34 ± 0.5	0.068 ± 0.005	191 ± 30
(2) N_2O	3	220		0.045	202 ± 4
(3) CH_4–N_2O	4	220		0.053	535
(4) H_2O	4	550		0.275	528

[a] From (1) and (2) $\epsilon(CH_3)_{220}/\epsilon(OH)_{220} = 1.60$ M^{-1} cm^{-1} at a mean dose of 191 rads/pulse. Then $\epsilon(CH_3) = 1.60 \times 520 = 839$ M^{-1} cm^{-1}. From (3) and (4) $[\epsilon(CH_3)_{220}G(CH_3)]/[\epsilon(e_{aq}^-)_{550}G(e_{aq}^-)] = 0.053/0.279$ at a mean dose of 535 rads/pulse. Assuming $G(CH_3)/G(e_{aq}^-) = 2.13$ for these solutions $\epsilon(CH_3)_{220} = 0.089 \times 9.7 \times 10^3 = 865$ M^{-1} cm^{-1}, average $\epsilon(CH_3)_{220} = 852$ M^{-1} cm^{-1}.

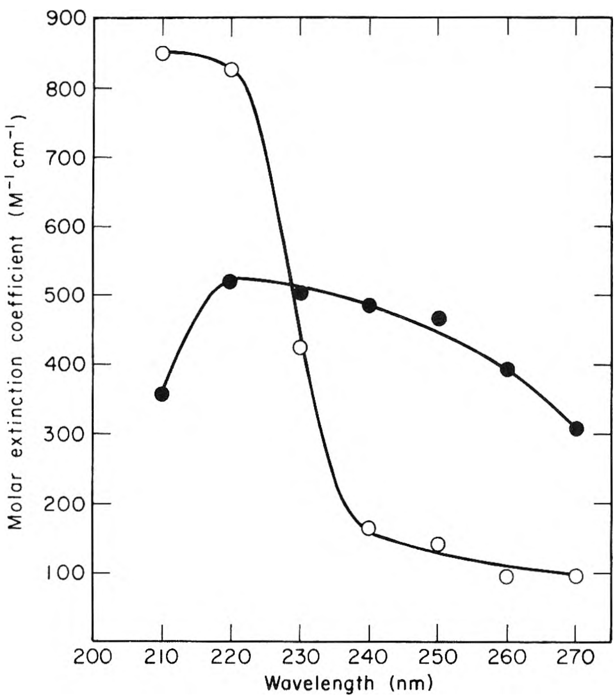

Figure 2. Absorption spectra of the CH_3 and OH radicals in aqueous 0.01–0.02 M CH_4–N_2O solutions at pH 5.5: O, CH_3; ●, OH.

rate constant, $k(OH + CH_4)$, by direct means and to obtain the transient spectrum of the resulting CH_3 radical. In solutions of N_2O and CH_4 two distinct transient species appear on electron irradiation. In 0.02 M CH_4 at pH 5.5 a single species decaying quickly in a few μseconds was found in the 240–270 nm spectral region. At wavelengths down to 210 nm a second species with a half-life of about 20 μsec was also observed. The spectral data on these transients appear in Figure 2, where the optical density for a 8-krad electron pulse is plotted as a function of wavelength for the species existing at the end of a 0.10-μsec pulse and after 1.0 μsec. This short-lived transient decays with a first-order dependence proportional to CH_4 concentration. By comparison of its spectrum with that published for the OH radical Figure 2 demonstrates that the shape of the spectrum, as well as the molar extinction coefficient, agree satisfactorily.

The data on the determination of the molar extinction coefficient $\epsilon(CH_3)$ at 220 nm are assembled in Table I. By comparison with the published value of $\epsilon(OH)$ at 220 and with the published value of $\epsilon(e_{aq}^-)$ at 550 nm a mean $\epsilon(CH_3)$ of 850 M^{-1} cm^{-1} is found at 220 nm. From this reference point the spectrum of Figure 2 has been drawn. We attribute this spectrum to the CH_3 free radical.

TABLE II: Determination of $k(OH + CH_4)$ by Decay of OH Radical Absorption at 250 nm in 1 mM N_2O–CH_4 Solutions at pH

CH_4, mM	$kC \times 10^{-5}$ sec^{-1}	$k(OH + CH_3) \times 10^{-8}$ M^{-1} sec^{-1}
1.17	1.185	1.01 ± 2.5%
1.12	1.481	1.32 ± 1.5
1.08	1.336	1.23 ± 2.4
1.08	1.392	1.29 ± 1.1
Mean	1.273	1.21 ± 0.4

The CH_3 radical decays by second-order kinetics with a mean k_2C_{max} of 2.34 ± 0.5 × 10^4 sec^{-1}. Utilizing the above $\epsilon(CH_3)$ at 220 nm of 850 M^{-1} cm^{-1} we obtain a second-order rate constant of 1.24 + 0.20 × 10^9 M^{-1} sec^{-1} for the reaction

$$CH_3 + CH_3 \rightarrow C_2H_6$$

The rate constant $k(OH + CH_4)$ = 1.21 ± 0.4) × 10^8 M^{-1} sec^{-1} was calculated from the decay of the OH free radical absorption at 250 nm. At this wavelength there is relatively little absorption by the CH_3 free radical (see Table II).

The addition of O_2 to CH_4 solutions produces a characteristic absorption in the 230–250-nm range upon irradiation. The formation at 250 nm is pseudo-first order in oxygen concentration, giving a rate constant of 3.2 ± 0.4 × 10^8 M^{-1} sec^{-1}. The decay was long lived on the msecond scale and this decay could not be analyzed with our pulsed light source. The presence of a small amount of O_2 (about 3 × 10^{-5} M) in 0.046 M CH_4 produces an interesting series of growth and decay curves. A fast initial decay at 250 nm (OH) rapidly forms the CH_3 radical at 210 nm. Its decay is matched by a first-order formation of the long-lived transient again at 250 nm. We attribute this 250-nm absorption to CH_3O_2 radical formation in the sequence

$$OH + CH_4 \rightarrow CH_3 + H_2O$$

$$CH_3 + O_2 \rightarrow CH_3O_2$$

Prolonged electron pulse irradiation of these concentrated CH_4 solutions changes the decay kinetics at 220 nm from second to first order and builds up H_2O_2 in the solution. At a H_2O_2 concentration of 9 × 10^{-4} M this pseudo-first-order decay takes place with a rate constant of 3.2 ± 0.6 × 10^4 sec^{-1}. This corresponds to a second-order rate constant of 3.5 × 10^7 M^{-1} sec^{-1} for the reaction

$$CH_3 + H_2O_2 \rightarrow CH_3OH + OH$$

Similar experiments to those described for CH_4 were carried out with C_2H_6. A spectrum similar to that of the CH_3 radical was observed in the 210–270 nm wavelength range. A plot of the optical density *vs.* wavelength for the C_2H_6

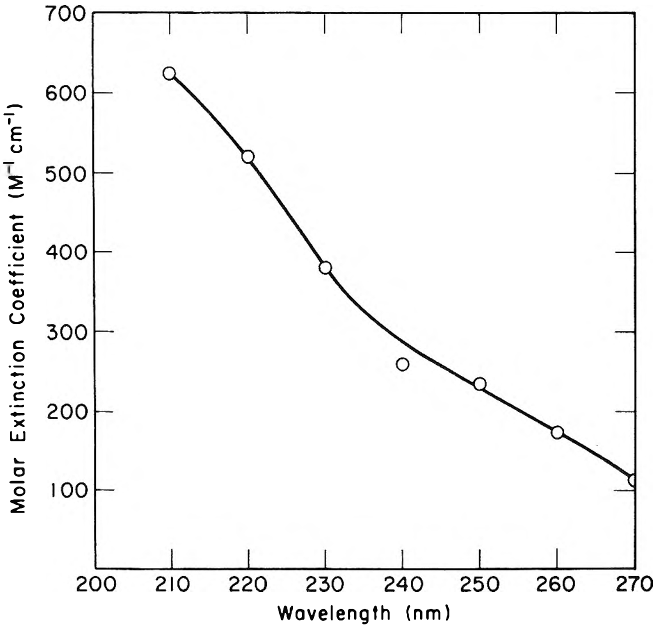

Figure 3. Absorption spectrum of the C_2H_5 radical in aqueous 0.01–0.02 *M* C_2H_6–N_2O solutions at pH 5.5.

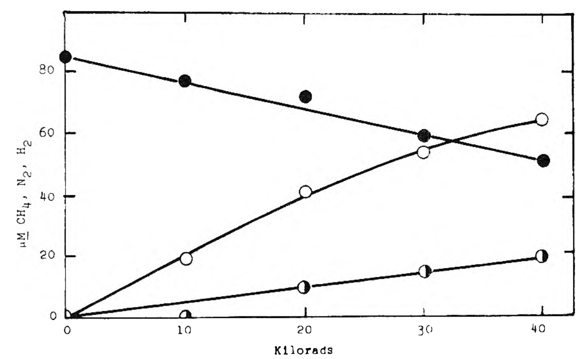

Figure 4. γ-Ray radiolysis of aqueous 85 μM CH_4–80 μM N_2O in neutral solution: ●, CH_4; O, N_2; ◑, H_2.

solutions is shown in Figure 3. By observing the relative molar extinction coefficient of $\epsilon(C_2H_5)$ with $\epsilon(OH)$, $\epsilon(C_2H_5)$ is 520 and 330 M^{-1} cm^{-1} at 220 and 250 nm, respectively. Combined with the second-order decay of C_2H_5 this gives a rate constant of 9.6 ± 2 × 10^8 M^{-1} sec^{-1} for the reaction

$$C_2H_5 + C_2H_5 \rightarrow \text{products}$$

B. ^{60}*Co* γ *Radiolysis.* Methane disappearance and N_2 and H_2 formation are given for the radiolysis of aqueous 85 μM CH_4–80 μM N_2O in neutral solutions in Figure 4. The yields for these irradiations are $G(-CH_4) = 3.0$, $G(H_2) = 0.52$, and $G(N_2) = 2.0$. This irradiation demonstrates that the disappearance of CH_4 is less than the expected G(OH) + $G(e_{aq}^-)$ in these N_2O solutions. $G(H_2)$ being significantly higher than the molecular yield of 0.45 indicates that a small amount of H_2 forms by the H atom reactions. Since $G(N_2)$ is less than the expected 2.8 for the N_2O solutions, some e_{aq}^- reacts with the products of the irradiation, probably H_2O_2.

The formation of molecular H_2O_2 is shown in Figure 5. Here H_2O_2 is plotted as a function of dose for a 1.22 mM CH_4–1.0 mM N_2O solution at pH 9. Note that the initial yield of 0.61 is close to the expected molecular H_2O_2 yield, but upon continued irradiation H_2O_2 reaches a steady state of about 60 μM. Under these conditions where all e_{aq}^- is

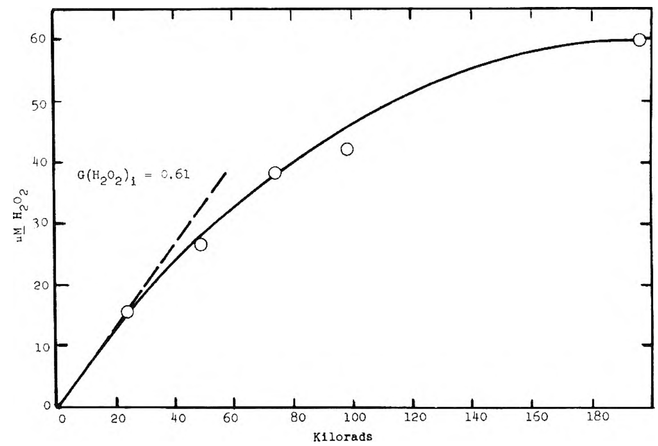

Figure 5. Formation of H_2O_2 in the γ-ray radiolysis of aqueous 1.22 mM CH_4–1.00 mM N_2O at pH 9.2.

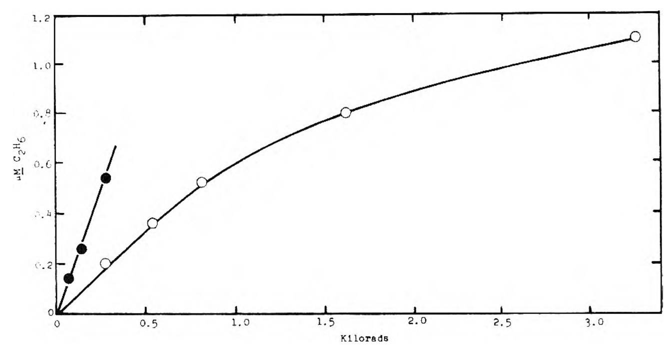

Figure 6. Formation of C_2H_6 in the γ-ray radiolysis of aqueous 120 μM CH_4 in neutral solutions: N_2O [$G(C_2H_6)_i = 1.9$]; no e_{aq}^- scavenger [$G(H_2O_2)_i = 0.74$]; ●, 0.1 mM N_2O; O, no N_2O.

scavenged by N_2O the more likely reaction is that of the CH_3 radical with H_2O_2.

Great difficulty was encountered in measuring the initial yield of C_2H_6 in saturated CH_4 solutions. Micromolar amounts of oxygen impurity caused erratic results. In addition it was found that the steady-state C_2H_6 concentration is only of the order of 1–2 μM. Thus extreme care and very low doses of radiation are required to establish these initial yields. Figure 6 shows the C_2H_6 formation in neutral solutions in the presence and absence of 0.10 mM N_2O. Note that the measurements are carried out with a total C_2H_6 concentration of 1.0 μM or less. The initial yield of $G(C_2H_6) = 1.9$ for N_2O saturated solutions indicates that even under these conditions rather inefficient C_2H_6 formation takes place. The results of these γ-ray irradiations in the presence and absence of N_2O are summarized in Table III where the yields in pure H_2O are also given for com-

TABLE III: Summary of γ-Ray Yields in 0.0012 *M* CH_4

	Without N_2O	With 1.0 mM N_2O	Pure H_2O
pH	3.0	7.0	7.0
$G(C_2H_6)$	0.74[a]	1.88[a]	
$G(H_2)$	0.93	0.49	0.45
$G(-CH_4)$		3.14(0.83)[b]	
$G(CH_3OH)$		0.72	
$G(H_2O_2)$		0.61[a]	0.70

[a] Initial rate. [b] 0.12 mM CH_4.

parison. The yield of methanol, 0.72, corresponds closely with that of $G(H_2O_2)$.

Although quantitative agreement has not yet been achieved, the following mechanism accounts for the general features of our results in saturated CH_4 solutions. Under these conditions all OH radicals may be assumed to react with CH_4.

$$H_2O \longrightarrow H, e_{aq}^-, OH, H_2O_2, H_2 \quad (1)$$

$$e_{aq}^- + N_2O \xrightarrow{H_2O} OH^- + OH + N_2 \quad (2)$$

$$e_{aq}^- + H_2O_2 \longrightarrow OH + OH^- \quad (3)$$

$$H + e_{aq}^- \xrightarrow{H_2O} H_2 + OH^- \quad (4)$$

$$H + H \longrightarrow H_2 \quad (5)$$

$$e_{aq}^- + e_{aq}^- \xrightarrow{2H_2O} H_2 + 2OH^- \quad (6)$$

$$CH_4 + OH \longrightarrow CH_3 + H_2O \quad (7)$$

$$CH_3 + e_{aq}^- \xrightarrow{H_2O} CH_4 + OH^- \quad (8)$$

$$CH_3 + H \longrightarrow CH_4 \quad (9)$$

$$CH_3 + CH_3 \longrightarrow C_2H_6 \quad (10)$$

$$CH_3 + H_2O_2 \longrightarrow CH_3OH + H_2O \quad (11)$$

$$CH_3 + C_2H_6 \longrightarrow CH_4 + C_2H_5 \quad (12)$$

$$H + C_2H_6 \longrightarrow H_2 + C_2H_5 \quad (13)$$

In the absence of N_2O, the main sequence of reactions is 1 and 3-13. Reactions 4-6 and 13 raise $G(H_2)$ yields above 0.45; reactions 7-9, 11, and 12 lower $G(-CH_4)$; reaction 10 forms C_2H_6, whereas reactions 12 and 13 consume it. Methanol forms *via* reaction 11 although its yield is lowered by reaction 3.

In the presence of N_2O all e_{aq}^- reactions are eliminated and the simplified mechanism consisting of reactions 1, 2, 5, 7, and 9-13 dominate.

The low C_2H_6 yield, as well as the rapid establishment of a low steady-state C_2H_6 concentration, indicates an efficient reaction of C_2H_6 with free radicals present during irradiation. Because $k(CH_4 + OH) = 1.2 \times 10^8\ M^{-1}\ sec^{-1}$ and CH_4 is present at the mM level there must be an efficient C_2H_6 scavenging reaction. Therefore we propose reaction 12 although reaction 13 may also contribute to the low steady-state level of C_2H_6. These reactions also account for the low $G(-CH_4)$ yields found in all CH_4 solutions. Support for these reactions has recently been obtained by the observation that extensive methylation readily occurs in these aqueous CH_4 solutions. For example, ethane, propane, isobutane, n-butane, neopentane, isopentane, and n-pentane have been detected in a 5-krad irradiation[18] which corresponds to less than 3% CH_4 reacted. Methyl radicals continuously generated by reaction 6 interact with C_2H_5 radicals from reactions 12 and 13. The higher alkanes then form *via* similar reactions of CH_3 and possibly H with C_3H_8, C_4H_{10}, and so forth.

(18) W. G. Brown and E. J. Hart, unpublished results.

Formation of Excited Singlet States in Irradiated Aromatic Liquids

C. Fuchs, F. Heisel, and R. Voltz*

Laboratoire de Physique des Rayonnements et d'Electronique Nucléaire, Centre de Recherches Nucléaires, 67, Strasbourg 3, France *(Received May 9, 1972)*

Publication costs assisted by Institut National de Physique Nucléaire et de Physique des Particules

Vacuum ultraviolet excited fluorescence and fast electron excited radioluminescence are used to study the mechanisms of formation of the lowest excited singlet states in liquid benzene and alkylbenzenes. From the measurements of fluorescence excitation spectra, it is concluded that the upper singlet levels in these liquids essentially decay by autoionization when their excitation energy is larger than a characteristic critical value, equal to 7 eV in the case of benzene. Efficient recombination fluorescence indicates that charge separation is followed by geminate recombination, without spin relaxation, from the lowest charge-transfer state to the first excited singlet state of the molecules. The scintillation decay laws and absolute yields, measured under electron irradiation, allow one to distinguish the promptly formed singlet states from those resulting from triplet-triplet annihilation in blobs and short tracks. The "prompt" singlet states are found to be produced with G values near unity; the data are interpreted using the general results obtained with vacuum ultraviolet excitation and taking into account the possible track effects.

Introduction

The possible role of excited molecules in the radiolysis of aromatic liquids was discussed by Burton a long time ago[1] and has since been actively studied, using in particular scintillation and pulse-radiolysis techniques.[2,3] However, the sequence of the radiationless processes, leading from the primary highly activated states to the lower excited levels amenable to experimental observation, is still poorly known; the relative importance of molecular bound states

(1) M. Burton, *Actions Chim. Biol. Radiat.*, **3**, 1 (1958).
(2) R. Voltz, *Actions Chim. Biol. Radiat.*, **13**, 1 (1969).
(3) J. K. Thomas, *Ann. Rev. Phys. Chem.*, **21**, 17 (1970).

and of charge-separated states as intermediates in the initial stages of radiation action, for example, is not yet clearly established. The object of the present study was to get more precise information on the early processes responsible for the production of the lowest excited singlet states (^1L_b, denoted by S_1) in liquid benzene and derivatives, under high-energy irradiation.

As a first part of this investigation, it appeared to be useful to reexamine some of the electronic relaxation processes from the highly excited molecular states in the liquids. The experimental method was to measure the variation of fluorescence quantum yield with excitation energies up to the vacuum ultraviolet range. In previous work, the same technique was used to study mainly the behavior of the second (^1L_a, S_2) and third (^1B_b, S_3) excited states in the liquids.[4,5] In this report, attention will be more concentrated on higher vibronic levels, which are those mainly formed after initial activation of the condensed medium by charged particles.

The production of singlet excited molecules in the aromatic liquids under fast electron irradiation is discussed in the second part of this work. The experimental information to be used comes essentially from radioluminescence studies; useful indications on modes and yields of S_1 state formation can indeed be obtained by analyzing the scintillation decay curves and by measuring absolute scintillation yields.[2]

I. Excitation by Vacuum Ultraviolet Light

Valuable information on the radiationless transitions from upper electronic levels of organic molecules in liquids and crystals is obtained from measurements of the fluorescence efficiency as a function of excitation wavelength.[4-6] Since, for the neat aromatic liquids, the fluorescence quantum yield is very low, it is found convenient to introduce small concentrations of a suitable solute, accepting the electronic energy from the aromatic host material and emitting light with a high efficiency. In addition to the electronic relaxation phenomena operative in the pure liquids, the analysis of the results must therefore also consider the solvent–solute energy transfer processes.[7]

Experimental Results

The equipment is illustrated in Figure 1. The exciting system consists of a hydrogen-discharge lamp and a McPherson Model 218 monochromator. The incident light, focused by an LiF lens, enters an irradiation cell where the mirrors N_S and N_M are placed so that a constant intensity ratio is ensured for the beams exciting the sample (C_S) and a sodium salicylate layer (C_M) in identical LiF cells. Two photomultipliers measure the fluorescence intensities I_S and I_M from the sample and from the sodium salicylate monitor preparation (wavelength invariant quantum yield). The setup allowed selective excitation of molecular levels with wavelengths down to 150 nm.

The ratio $I_S(\lambda)/I_M$, obtained for the excitation wavelength λ, provides a relative measurement of the fluorescence quantum yield $\eta(\lambda)$. In the following, we present and discuss the results on the fluorescence excitation spectra, considering the relative fluorescence efficiency $R(\lambda) = \eta(\lambda)/\eta(\lambda_1)$, where $\eta(\lambda_1)$ corresponds to an excitation of the S_1 state.

The experiments were carried out at room temperature with the following degassed and purified liquids containing αNPO (α-naphtyl-2-phenyl-5 oxazole-1,3) as the fluores-

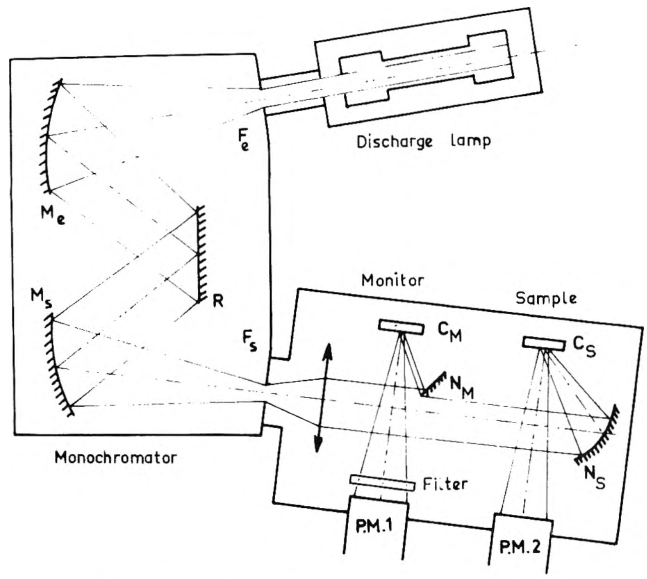

Figure 1. Experimental arrangement.

cent solute: benzene, perdeuterated benzene, toluene, perdeuterated toluene, *p*-xylene, and mesitylene. The results on the variations of the relative fluorescence efficiency R with excitation wavelength and solute concentration, in the case of benzene solutions, are represented in Figure 2.[8] Similar curves were also determined for the other liquids.[9] The action spectra (Figure 2a) have the same general form as those reported by Braun, *et al.*,[4] and by Birks, *et al.*;[5] excitation to the S_2 state leads to a decrease of R with a value approximately constant over the whole second absorption band. A further decrease to a value characteristic for the third excitation band is observed for higher excitation energies E_{exc}. We note, however, that when the latter exceed a critical value W_0 ($\approx$7 eV, for benzene), the efficiency R increases with E_{exc}. In accord with the data of Figure 2b, Laor and Weinreb[10] also observed that $R(\lambda)$ increases with increasing solute concentrations. The data reported in Figure 3 show that chloroform and oxygen act as efficient fluorescence quenchers for excitation energies larger than W_0, but they have a negligible influence if $E_{exc} < W_0$.

Analysis of the Results

The experimental results indicate a drastic change in the behavior of the upper vibronic levels when the excitation energy exceeds the critical quantity W_0; the values characteristic for the various aromatic liquids are reported in Table I. For the reasons to be developed later, energy W_0 is interpreted as a threshold for molecular autoionization in the liquid. We will therefore distinguish between "excited" states ($E_{exc} < W_0$) and "superexcited" states ($E_{exc} \geq W_0$) of the molecules in the condensed phase.

(4) C. L. Braun, S. Kato, and S. Lipsky, *J. Chem. Phys.*, **39**, 1645 (1963).
(5) J. B. Birks, J. C. Conte, and G. Walker, *Proc. Phys. Soc. London, Sect. B*, **1**, 934 (1968).
(6) N. Geacintov, M. Pope, and H. Kallmann *J. Chem. Phys.*, **45**, 2639 (1966).
(7) R. Voltz, *Radiat. Res. Rev.*, **1**, 301 (1968).

(8) By exciting αNPO in aliphatic solutions, we have verified that this solute has a quantum yield constant in the wavelength range used in the present experiments.

(9) C. Fuchs, Thesis, Strasbourg, 1972.
(10) U. Laor and A. Weinreb, *J. Chem. Phys.*, **43**, 1565 (1965); **50**, 94 (1969).

TABLE I: Autoionization and Recombination. Experimentally Determined Parameters

Solvent	W_0, eV	Limits of $\alpha_{150}\,\rho_M$	$\alpha(\lambda)$				$\tau_e k_F$, M^{-1}
			α_{150}	α_{160}	α_{170}	ρ_M	
Benzene	7.0	0.42–0.58	0.7	0.5	0.2	0.7	9
Perdeuterated benzene	7.0	0.22–0.48	0.6	0.4	0.15	0.6	7
Toluene	6.9	0.35–0.65	0.7	0.5	0.4	0.7	20
Perdeuterated toluene	6.9	0.35–0.65	0.7	0.5	0.35	0.7	20
p-Xylene	6.8	0.75–0.92	0.9	0.7	0.4	0.95	
Mesitylene	6.8	0.82–0.95	0.9	0.7	0.4	0.95	

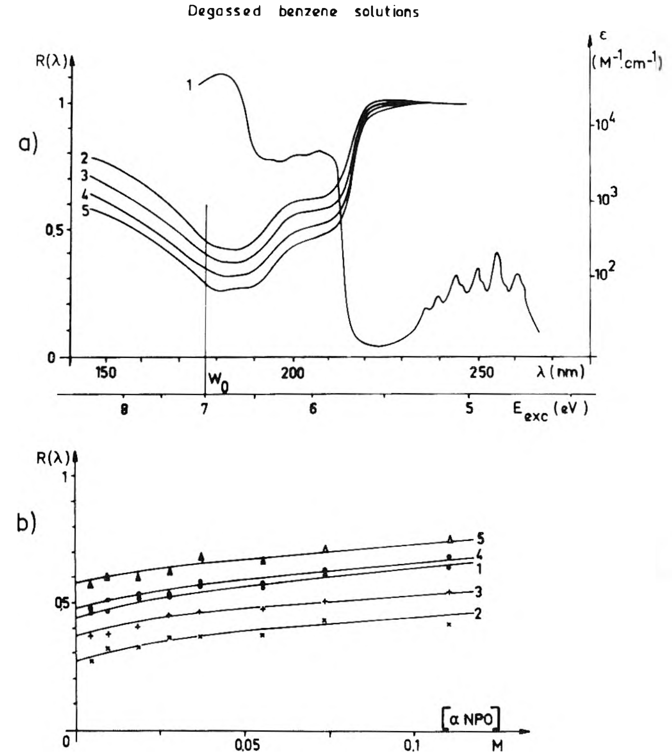

Figure 2. (a) Absorption spectrum of the solvent (1). Fluorescence excitation spectra of the solutions: [αNPO], 10^{-1} *M* (2); 3×10^{-2} *M* (3); 1.5×10^{-2} *M* (4); 5×10^{-3} *M* (5). (b) Variation of $R(\lambda)$ with the solute (αNPO) concentration: λ 205 nm (1); λ 180 nm (2); λ 170 nm (3); λ 160 nm (4); λ 150 nm (5).

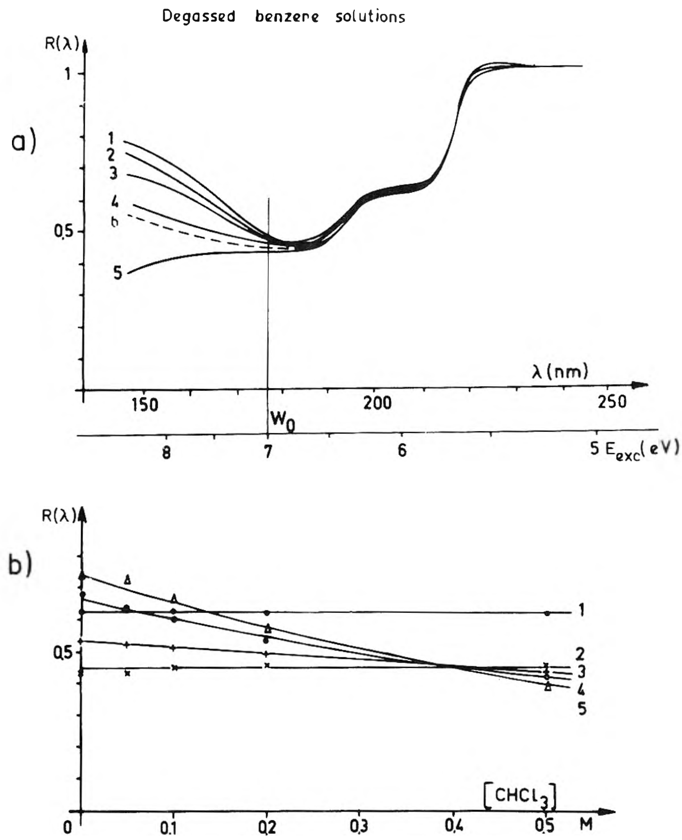

Figure 3. (a) Fluorescence excitation spectra of benzene–αNPO (1.8×10^{-2} *M*) solutions containing chloroform or oxygen: [$CHCl_3$] = 0 (1); 5×10^{-2} *M* (2); 10^{-1} *M* (3); 2×10^{-1} *M* (4); 5×10^{-1} *M* (5); solution under 1 atm of O_2 (6). (b) Variation of $R(\lambda)$ with the chloroform concentration: λ 205 nm (1); λ 180 nm (2); λ 170 nm (3); λ 160 nm (4); λ 150 nm (5).

1. Excited States ($E_{exc} < W_0$). In this energy range, the fluorescence excitation spectra (Figure 2a) illustrate the characteristic deviations from Vavilov's law, already reported for benzene and its derivatives and explained by the existence of photochemical processes in the L_a and B_b states, which reduce the internal conversion efficiency.[11] It is interesting to note that since the relative fluorescence efficiency $R(\lambda)$ is constant over each absorption band, it only depends on the efficiency of the transitions between electronic states (*i.e.*, vibrational relaxation is faster than electronic relaxation). The processes we expect to be of importance for the S_2 and S_3 levels of benzene and its derivatives are indicated in Figure 4 together with the corresponding rate constants. In addition to the well established internal conversion and photochemical processes, we also consider energy transfer from the upper levels of the solvent to the solute, which should not be ignored *a priori*.[7] Denoting by $\tau_3 = (k_{30} + k_{32})^{-1}$, τ_2 and τ_1, the lifetimes of the S_3, S_2, and S_1 levels in the absence of the solute, we can define the following efficiencies: for internal conversion

$$\beta_{32} = \tau_3 k_{32},\ \beta_{21}$$

for energy transfer

$$\epsilon_3 = k_{t3}\tau_3[F]/(1 + k_{t3}\tau_3[F]),\ \epsilon_2,\ \epsilon_1$$

for light emission from S_1

$$\Phi = k\tau_1$$

The fluorescence quantum yield of the solute will be represented by Φ'. In cases like αNPO, where internal conversion of the solute molecule has an efficiency of one ($\beta'_{32} = \beta'_{21} \approx 1$), we easily obtain the fluorescence quantum

(11) J. B. Birks, "Photophysics of Aromatic Molecules," Wiley-Interscience, New York, N. Y., 1970.

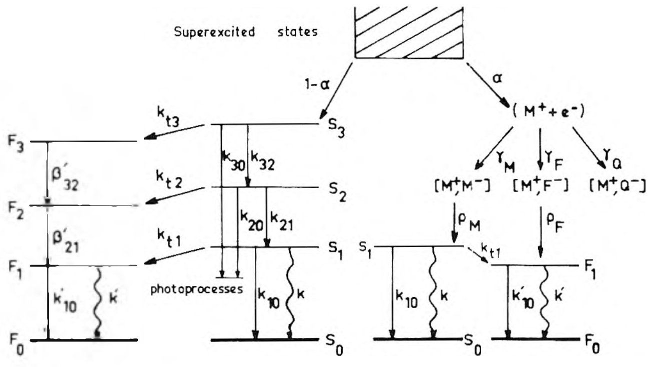

Figure 4. Energy levels and transitions.

yields η_1, η_2, η_3 for excitation in the S_1, S_2, S_3 bands of the solvent. The relative quantities measured in the present study are given by

$$R_2 = \eta_2/\eta_1 = \epsilon_2(\Phi'/\eta_1) + (1 - \epsilon_2)\beta_{21}$$

$$R_3 = \eta_3/\eta_1 = \epsilon_3(\Phi'/\eta_1) + (1 - \epsilon_3)\beta_{32}R_2$$

with $\eta_1 = \epsilon_1\Phi' + (1 - \epsilon_1)\Phi$.

In the limiting cases where $[F] = 0$, we have $R_2 = \beta_{21}$ and $R_3 = \beta_{32}R_2 = \beta_{32}\beta_{21}$. We can evaluate the internal conversion efficiencies from the values obtained by extrapolation to $[F] = 0$ of the experimental curves giving R_2 and R_3 as functions of [F] (*cf.* Figure 2b). The values thus determined are listed in Table II; they agree with the previously published data.[4]

For concentrations [F] high enough so that $\epsilon_1\Phi' \gg (1 - \epsilon_1)\Phi$, the transfer efficiencies can be written as $\epsilon_2 = (R_2 - \beta_{21})/(\epsilon_1^{-1} - \beta_{21})$ and $\epsilon_3 = (R_3 - \beta_{32}R_2)/(\epsilon_1^{-1} - \beta_{32}R_2)$. The experimental values of R_2, β_{21}, β_{32}, and ϵ_1[9] thus allow determination of ϵ_2 and ϵ_3 for the various solute concentrations. If the proposed kinetic scheme is correct, these quantities must agree with Stern–Volmer relations, *i.e.*, $\epsilon^{-1} - 1 = (\tau k_t[F])^{-1}$. This is indeed the case, as illustrated in Figure 5, where the results for the benzene solutions are presented. These Stern–Volmer plots allow determination of the constants $k_{t2}\tau_2$ and $k_{t3}\tau_3$ given in Table II; the values, which may be justified by theoretical arguments,[7] are about three orders of magnitude lower than those of $k_{t1}\tau_1$ characteristic of solvent–solute energy transfer from the S_1 states.[7,11] Similar evidence for energy transfer from the highly excited singlet states in the aromatic liquids was also presented by Laor and Weinreb[10] and by Horrocks.[12]

Following the data in Figure 3, the influence of chloroform and oxygen on the kinetics of the S_2 and S_3 states appears as negligible. This is in accord with the results of Laor and Weinreb,[10] but in disagreement with an analysis of Lawson, *et al.*[13] At variance with our discussion, these authors also ignored solvent–solute energy transfer *via* higher states. They further assumed the direct $S_3 \rightarrow S_1$ transitions to be important; in the present work, we have verified that our results could not be reconciled with a kinetic scheme including such a process. This agrees with the well established "energy gap law"[11] according to which the succession of transitions between neighboring electronic levels should indeed be more probable than a $S_3 \rightarrow S_1$ radiationless transition.

2. *Superexcited States* ($E_{exc} > W_0$). The increase of fluorescence efficiency R with the excitation energy, observed in this energy range (Figure 2a), indicates that the fluorescing lowest singlet states in the liquids have precursors different from the ^1L_a and ^1B_b levels that are sub-

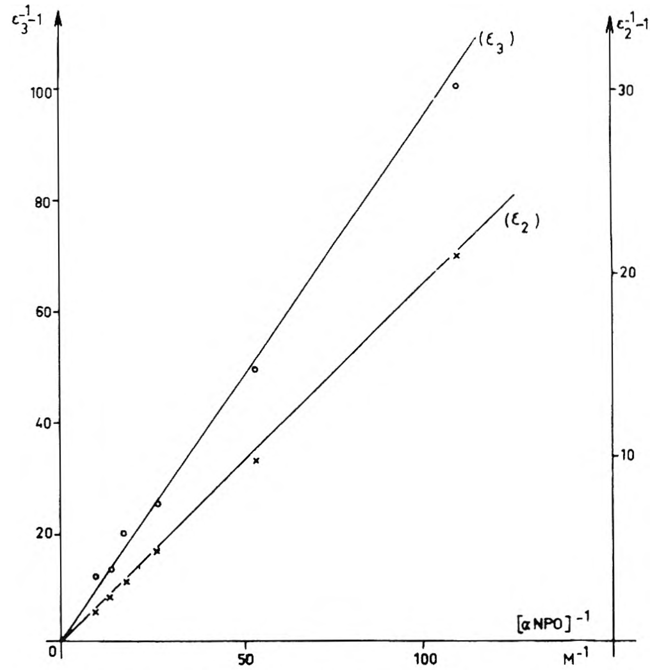

Figure 5. Variations of $\epsilon_2^{-1} - 1$ and $\epsilon_3^{-1} - 1$ with $[F]^{-1}$ (benzene solutions).

TABLE II: Internal Conversion and Energy Transfer from the S_2 and S_3 States. Experimentally Determined Parameters

Solvent	β_{21}	β_{32}	$k_{t2}\tau_2$, M^{-1}	$k_{t3}\tau_3$, M^{-1}
Benzene	0.44	0.61	5.2	1
Perdeuterated benzene	0.55	0.62	4.5	1
Toluene	0.71	0.64	8.5	1
Perdeuterated toluene	0.73	0.66	8.8	1
p-Xylene	0.83	0.82	≈25	1.2
Mesitylene	0.89	0.82	≈25	1.2

mitted to the photochemical processes which strongly reduce the internal conversion efficiencies. The data in Figure 3 further show that, in contrast to the ^1L_a and ^1B_b states, these precursors are severely quenched by chloroform and oxygen known as efficient electron scavengers.[14] These results, together with the evidence from similar studies in crystalline materials,[6] lead to identify the precursors as charge-separated states, and W_0 as a threshold energy where autoionization begins to compete with the fast vibrational relaxation processes from upper vibrational levels of the electronic ^1B_b state.[15]

In the gas phase, superexcited levels have excitation energies larger than the first ionization limit. In the condensed phase, the role of autoionization is not confined to such high activation energies; it must also be considered for lower activated molecular levels.

(12) D. L. Horrocks, *J. Chem. Phys.*, **52**, 519 (1967).

(13) C. W. Lawson, F. Hirayama, and S. Lipsky, "Molecular Luminescence," E. C. Lim, Ed., Benjamin, New York, N. Y., 1969, p 837.

(14) L. G. Christophorou, "Atomic and Molecular Radiation Physics," Wiley, London, 1971.

(15) Direct transitions from the upper molecular states to the S_1 state could in principle be invoked to interpret the increase of R with excitation energy, but such a possibility does not account for the observed influence of chloroform; also, it is difficult to reconcile with the energy gap law for radiationless transitions.[11]

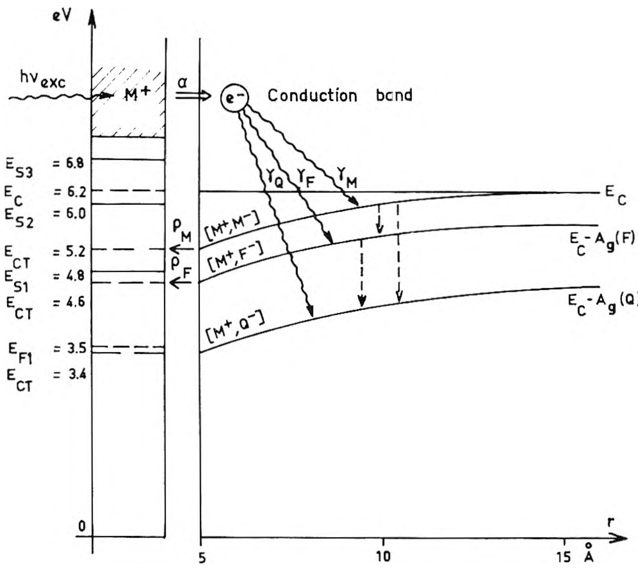

Figure 6. Schematic representation of bound and charge-separated states in liquid benzene. The numerical data used are $I_g = 9.2$ eV and $A_g = 0$ for the solvent. $A_g = 0.6$ eV and 1.75 eV for αNPO and chloroform, respectively, and $P_\pm \approx 2.5$ eV.[9,16]

Information on these charge-separated states essentially comes from the studies with aromatic crystals.[16] A broad conduction band, in which electrons are quasi-free to move and are little localized at any particular molecule, has the bottom edge at an energy $E_c = I_g - P_+ - P_-$, where I_g is the gas-phase ionization energy and P_+, P_- are the polarization energies associated with the holes and electrons, respectively. For liquid aromatics, the onset of these ionization continua may be roughly estimated at $E_c \gtrsim I_g - 3$ eV, assuming $P_+ = P_- \lesssim 1.5$ eV.[16] The charge-separated states below the conducting levels are the charge-transfer (CT) states, in which the positive hole and the electron are located at molecular sites and are correlated by the Coulomb attraction; the excitation energy of these nonconducting states is given by $E_{CT} = I_g - A_g - P_\pm - C(r)$, where I_g and A_g denote the ionization energy and the electron affinity of the gas, $P_\pm$ is the polarization energy associated with the ion pair in the condensed medium, and C is the Coulomb energy dependent on the hole-electron separation distance r. In benzene, the lowest of these CT states, in which the ion pair is situated on neighboring sites ($r \approx 5$ Å), is estimated to be at $E_{CT} \approx 5.2$ eV[9] (*cf.* Figure 6).

The expected sequence of processes initiated by excitation to a molecular superexcited level in the aromatic liquids is schematically pictured in Figure 6. Autoionization is characterized by its efficiency $\alpha(\lambda)$ which should increase with increasing excitation energies E_{exc}. The hot electron in the conduction band is moderated by the mechanisms generally postulated for the subexcitation and subvibrational ranges (excitation of intra- and intermolecular vibrations) and enters the manifold of charge-transfer states before the ion separation reaches the Onsager critical distance.[17] The subsequent ion recombination may be regarded as a succession of radiationless transitions between the charge-transfer states $[M^+, M^-]$ along the energy surface $E_{CT}(r)$, leading finally to the lowest CT level. Ultimate neutralization involves a transition from this state to an isoenergetic neutral molecular state which, following rough numerical estimates like those presented above, should be the S_1 state in all the liquids. From the experimental action spectra it is directly apparent that we cannot invoke recombination in the S_2 or S_3 state, a necessary consequence being that $R(\lambda) \leq R_3 < R_2$, which disagrees with the experimental observations. We denote by ρ_M the efficiency of recombination, in the S_1 state. In the presence of the fluorescent solute F (αNPO) and of the quencher Q (chloroform), electron scavenging by these compounds interferes with the recombination processes. Electron trapping by F is characterized by an efficiency γ_F and leads to one of the localized charge-transfer states $[M^+, F^-]$ which may be subsequently neutralized, yielding an excited solute molecule. Similarly, the efficiencies of formation of the $[M^+, Q^-]$ and the $[M^+, M^-]$-CT states are denoted by γ_Q and γ_M, as indicated in Figure 4. We note that a production of S_1 states from the low $[M^+, Q^-]$ levels is excluded on energetic grounds, which explains the quenching action of chloroform.

Following this analysis, the efficiency of fluorescence upon excitation to superexcited states, in solutions without chloroform, can be expressed as

$$\eta(\lambda) = [1 - \alpha(\lambda)]\eta_3 + \alpha(\lambda)[(1 - \gamma_F)\rho_M\eta_1 + \gamma_F\rho_F\Phi']$$

where the first term represents the production of S_1 states by internal conversion, while the second describes the formation through autoionization followed by recombination; ρ_F denotes the efficiency of the reaction $[M^+, F^-] \rightarrow {}^1F^*$ (lowest excited singlet state of the emitting solute).

For the neat liquids, where $[F] = 0$, the relative fluorescence efficiency is of the form

$$R(\lambda) = \eta(\lambda)/\eta_1 = [1 - \alpha(\lambda)]R_3 + \alpha(\lambda)\rho_M$$

Experimentally, these values can be determined from the curves representing $R(\lambda)$ for various solute concentrations, extrapolated to the axis $[F] = 0$ (Figure 2b). In order to get estimates for the quantities $\alpha(\lambda)$ and ρ_M, we proceed by noting that since $\alpha(\lambda) \leq 1$ and $\rho_M \leq 1$, we have

$$\frac{R(\lambda) - R_3}{1 - R_3} \leq \alpha(\lambda)\rho_M \leq R(\lambda)$$

which leads to upper and lower limits for $\alpha(\lambda)\rho_M$. In the case of benzene solutions, for example, $0.42 \leq \alpha(\lambda)\rho_M \leq 0.58$, at 150 nm. The limits thus obtained, indicated in Table I, allow us to choose a "mean" value (*e.g.*, $\alpha\rho = 0.50$ for benzene) which, inserted in the equation for $R(\lambda)$, allow us to determine ρ_M and $\alpha(\lambda)$, assuming that only the latter quantity depends on the excitation wavelength. For benzene, $\rho_M = 0.7$ and $\alpha(\lambda) = 0.7$, 0.5, and 0.2 at $\lambda = 150$, 160, and 170 nm. All the results are listed in Table I.

In the other limiting case of solutions with high solute concentrations [F], so that $\epsilon_1 \approx 1$, the expression of $R(\lambda)$ becomes

$$R(\lambda) = [1 - \alpha(\lambda)]R_3 + \alpha(\lambda)\rho_M + \alpha(\lambda)\gamma_F(\rho_F - \rho_M)$$

where R_3 and γ_F depend on [F]; since R_3, $\alpha(\lambda)$, and ρ_M are known, the experimental curves for $R(\lambda)$ (Figure 2b) allow us to evaluate the quantities $\gamma_F(\rho_F - \rho_M)$. In all the cases, even for the mesitylene solutions where $\rho_M = 0.95$, positive values were obtained, which means that $\rho_F > \rho_M$. In order to estimate γ_F, we have put $\rho_F = 1$ and found that this electron trapping efficiency increases with the concentration [F] as expected. Figure 7 shows that γ_F can be described

(16) F. Gutmann and L. E. Lyons, "Organic Semiconductors," Wiley, New York, N. Y., 1967.

(17) R. Voltz, "International Discussion on Progress and Problems in Contemporary Radiation Chemistry," Vol. 1, Prague, 1971, p 139.

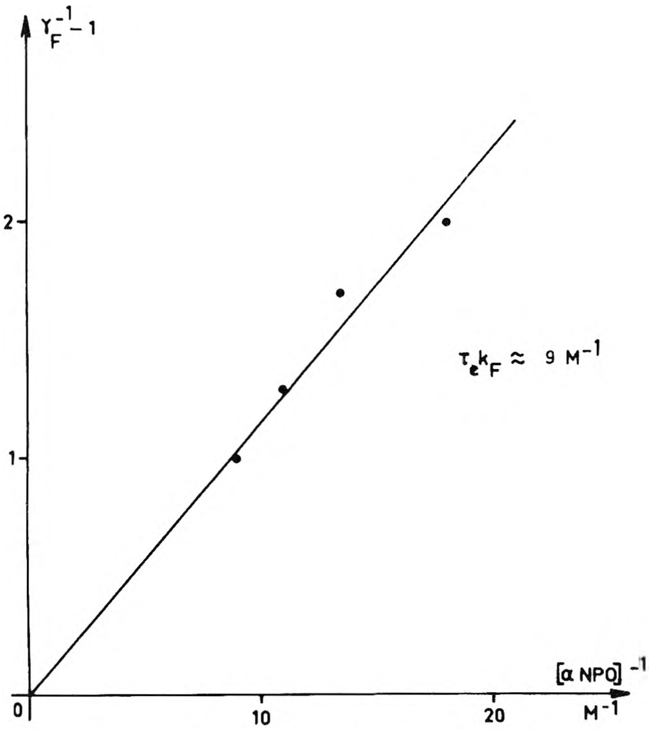

Figure 7. Variation of $\gamma_F^{-1} - 1$ with $[F]^{-1}$ (benzene solutions).

by a Stern–Volmer form, the characteristic constant being $k_F\tau_e \approx 9\ M^{-1}$ for the benzene solutions; k_F must be regarded as the rate constant of electron attachment by αNPO, and τ_e as the mean lifetime of the charge-separated states in the neat solvents. The values derived for the other solutions are indicated in Table I.

In the present context, it does not seem necessary to discuss in detail the data obtained with the solutions containing chloroform (*cf.* Figure 3). As mentioned before, these results are clear evidence for the role of charge-separated precursors of the S_1 states in the liquids excited at energies higher than W_0.

Conclusions

The characteristic increase of fluorescence efficiency with excitation energies exceeding the critical values W_0 indicates that the experimentally observed S_1 states in the aromatic liquids have precursors different from the S_2 and S_3 states which are submitted to the "photochemical" processes that strongly reduce the internal conversion efficiencies. These precursors are identified as charge-separated states which result from autoionization of the singlet excited molecules in the condensed phase.

The energy W_0 is found, for all the liquids, to be approximately equal to $I_g - 2$ eV. It must be considered as the activation energy where autoionization in the broad conduction band begins to compete with the intramolecular vibrational and electronic relaxation processes.

In the explored wavelength range, the ionization efficiency α rapidly increases with excitation energy. This agrees with similar observations on gaseous or crystalline systems.[18]

The high values observed for the efficiency ρ_M of final production of the S_1 state, after excitation in an upper singlet state, imply that geminate recombination without spin relaxation is essentially involved. Also the energy of the lowest CT state must be intermediate between the energies of the S_1 and S_2 states. We note that all these conclusions should be considered in the discussion of the early effects of ionizing particles, which mainly excite molecular levels with $E_{exc} > W_0$ in the aromatic liquids.

II. Excitation by High-Energy Electrons

Among the observable effects of high-energy radiation in aromatic media, luminescence is an experimental tool of particular interest in the present study. The information it provides on the produced singlet states is indeed very direct, rapid (in the nanosecond range), and corresponds to the action of the single incident particles.

Studies of the time dependence of radioluminescence in organic materials led us to distinguish between two different emission components, qualified as "prompt" and "delayed," which have different physical origins.[2] The prompt emission decays as fluorescence and is due to singlet excited molecules produced rapidly, *i.e.*, in a time period notably less than 1 nsec, after the passage of the incident particle. In the case of the liquid solutions with solute concentrations so that $\epsilon_1 \approx 1$, as used in the following experiments, the intensity is of the form

$$I_P(t) = k'\epsilon_1 N_S(0) \exp(-t/\tau_1')$$

where $N_S(0)$ is the initial number of S_1 states, k' is the fluorescence emission rate constant, and τ_1' (= 2.2 nsec for αNPO) is the mean lifetime of the solute lowest excited singlet state. Integrating $I_p(t)$, we obtain the number of photons emitted, per absorbed particle, in the prompt component

$$L_p = \Phi'\epsilon_1 N_S(0)$$

The singlet excited states responsible for the delayed scintillation component are formed through bimolecular reactions of molecules in triplet excited states. In the liquid solutions, the latter were identified as the long-lived solute states, formed by triplet excitation transfer from the solvent.[9,19,20] Denoting the correspondent transfer efficiency by ϵ_T, the intensity of the delayed component is, if $\epsilon_T \approx 1$

$$I_d(t) = k'\alpha_F\epsilon_T N_T(0) \times \int_0^t \frac{\exp[-(t-t')/\tau_1']\,dt'/2t_b}{\left[1 + \frac{t_a}{2t_b}\ln\left(1 + \frac{t'}{t_a}\right)\right]^2\left(1 + \frac{t'}{t_a}\right)}$$

$N_T(0)$ represents the number of excited triplet states initially produced in the zones of high activation density (blobs, short tracks) where the triplet–triplet annihilation processes take place; α_F is defined as the mean number of singlet states produced per triplet state disappearing in such reactions; t_a and t_b are time constants related to the decrease of local triplet-state concentration due, respectively, to the diffusion out of the blobs and short tracks and to the bimolecular annihilation processes.[2] The integrated intensity, *i.e.*, the total number of delayed photons, per incident particle, is

$$L_d = \Phi'\alpha_F\epsilon_T N_T(0)$$

(18) F. I. Vilesov and M. F. Akopyan, "Elementary Photoprocesses in Molecules," B. S. Neporent, Ed., Consultants Bureau, New York, N. Y., 1968, p 22.
(19) F. Spurny, *Collect. Czech. Chem. Commun.*, **35**, 565 (1970).
(20) J. B. Birks, *Chem. Phys. Lett.*, **7**, 293 (1970).

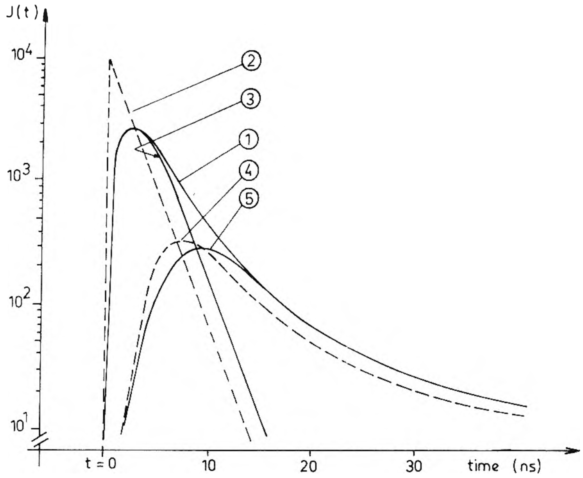

Figure 8. Radioluminescence decay curves (1.8×10^{-2} *M* αNPO in benzene): (1) total luminescence $J(t) = J_p(t) + J_d(t)$ (experimental curve); (2) theoretical prompt luminescence $I_p(t)$; (3) prompt luminescence $J_p(t) = I_p(t) * R(t)$; (4) theoretical delayed luminescence $I_d(t)$; (5) delayed luminescence $J_d(t) = I_d(t) * R(t) = J(t) - J_p(t)$.

TABLE III: S_1 States Formation under Fast Electron Irradiation. Experimentally Determined Parameters

Solvent	L_p/L_d	G_F	G_S	ρ_M	$\beta_{32}\,\beta_{21}$
Benzene	3.5	0.9	0.7	0.7	0.27
Perdeuterated benzene	2.8	1	0.8	0.6	0.34
Toluene	4	1.1	0.9	0.7	0.45
Perdeuterated toluene	3	1.15	0.9	0.7	0.48
p-Xylene	3.5	1.2	0.95	0.95	0.68
Mesitylene	3.5	1.15	0.9	0.95	0.73

While the analysis of the delayed component gives indications on the formation and behavior of triplet states in the blobs and tracks, the prompt component informs us on the direct formation of the S_1 states by the incident particle and its secondaries. For the present purpose, we therefore present, and discuss in some detail, the results on the prompt light emission component, obtained in a systematic study of radioluminescence decay laws and absolute efficiencies in the liquid aromatic solutions.[9,21]

Experimental Results

A first step of the experimental study was to analyze the time dependence of the scintillation intensity $I(t) = I_p(t) + I_d(t)$, and to separate the two components. This allows relative measurements of the quantities L_p and L_d by integrating the intensities and thus determines the ratio L_p/L_d. In order to get the values of L_p (and L_d), we then determined $L_p + L_d$ from the absolute scintillation yields, measured in a second set of experiments. The systems investigated were the same degassed solutions as considered in the previous section, irradiated by the conversion electrons (0.624 MeV) of a ^{137}Cs source.

The device used to analyze the scintillation intensity as a function of time is based on a single-photoelectron technique, and was described in detail before.[22,23] The recorded pulse shape $J(t)$ is the convolution of the actual scintillation intensity $I(t)$ with the impulse response function $R(t)$ of the apparatus: $J(t) = I(t) * R(t)$. $R(t)$ was determined using pulses from Čerenkov emission.[9,21] Knowing the form of $I_p(t)$ from fluorescence decay measurements, we evaluated $J_p(t) = I_p(t) * R(t)$ which was then substracted from $J(t)$ to obtain the shape $J_d(t)$ of the delayed pulse (*cf.* Figure 8). Having thus separated the two scintillation components, we could determine the ratio L_p/L_d by integrating the curves: the values are listed in Table III.

The principle of the method used to measure absolute radioluminescence yield has been described elsewhere.[24] The aromatic solutions are first irradiated by the electrons. The scintillations are observed by a photomultiplier which delivers pulses with a height H such as

$$H = ak\Phi' N_F$$

where a is a constant and k is the photon collection efficiency of the photomultiplier; N_F is the total number of solute molecules excited in the lowest singlet state per incident electron

$$N_F = \epsilon_1 N_S(0) + \alpha_F \epsilon_T N_T(0)$$

In a second step of the experiments, the same solutions are irradiated by short monochromatic pulses, only absorbed by the solute molecules, which are thus excited in their first singlet state. The observed pulse height is here given by

$$H' = ak'\Phi' n$$

where k' is the new photon collection efficiency and n is the mean number of photons absorbed per light pulse; it was measured with a previously calibrated photomultiplier. If we also determine (k'/k) as indicated in ref 24, where the details of the experimental procedures are given, we can evaluate

$$N_F = n(k'/k)(H/H')$$

The results obtained for the various solutions are presented in Table III in terms of the corresponding G values; *i.e.*, $G_F = (100/T_0)N_F$ (T_0 is the incident electron energy in electron volts).

Similarly introducing the 100-eV yields G_S and G_T for $N_S(0)$ and $N_T(0)$, we thus have the values of $G_F = \epsilon_1 G_S + \alpha_F \epsilon_T G_T$, which together with those of $L_p/L_d = \epsilon_1 G_S/\alpha_F \epsilon_T G_T$ are required to determine $\epsilon_1 G_S$ and $\alpha_F \epsilon_T G_T$. The latter of these quantities will not be discussed further. From the data on $\epsilon_1 G_S$, we can derive the values of G_S, indicated in Table III, since the efficiency ϵ_1 of singlet excitation transfer is accurately known from independent experiments.[9] The total yields of excited solute singlet states here obtained are smaller than that, $G_F = 1.55$, determined by Skarstad, *et al.*,[25] for benzene containing *p*-terphenyl as a solute. In their pulse-radiolysis studies with benzene, Cooper and Thomas also measured yields of production of S_1 states, $G_S = 1.66$, which appear as higher than the present values.[26] These differences are not understood. The G values

(21) C. Fuchs, F. Heisel, R. Voltz, and A. Coche, "Organic Scintillators and Liquid Scintillation Counting," D. L. Horrocks and Cheng Tzu Peng, Ed., Academic Press, New York, N. Y., 1971, p 171. In this reference, the function $R(t)$ was, however, taken different from that experimentally determined in the present work; the results reported in ref 21 must therefore be corrected by those in Table III.
(22) G. Pfeffer, Thesis, Strasbourg, 1965.
(23) J. A. Miehe, G. Ambard, J. Zampach, and A. Coche, *IEEE Trans. Nucl. Sci.*, **NS-17**, 115 (1970).
(24) C. Fuchs and G. Laustriat *Rev. Phys. Appl.*, **5**, 617 (1970).
(25) P. Skarstad, R. Ma, and S. Lipsky, *Mol. Cryst.*, **4**, 3 (1968).

reported by Skarstad and Cooper might, however, be suspected as overestimated since they correspond to an absolute scintillation efficiency of 0.042 for the benzene solutions, which is the same as for crystalline anthracene (0.040), known to be the most efficient organic scintillator.[27]

Analysis of the Results

The singlet states, characterized by the G_S values in Table III, are the ultimate results of fast electronic relaxation processes, starting from the very primary activation events. To analyze the results, we should take into account the electron degradation spectrum, the excitation spectrum,[28] and the efficiencies of the radiationless transitions leading the molecules from the initial primary levels to the lowest singlet states, that are observed in the experiments. We thus write

$$G_s = \frac{100}{T_0} N \sum_n \int_{E_1}^{T_0} \eta_n(T)\, \sigma_n(T)\, y(T)\, \mathrm{d}T$$

where N denotes the number of molecules per unit volume. In this expression, $y(T)$ characterizes the degradation spectrum for incident electrons of energy T_0. It may be regarded as the number of electrons with energy T crossing per units of time and energy, a spherical volume presenting a unit cross-sectional area.[29] The lowest integration limit E_1 is the excitation energy of S_1 states. $\sigma_n(T)$ is the excitation cross section of the primary state of energy E_n by an electron of energy T; Σ_n represents the summation over the whole excitation spectrum. The efficiency of formation of an S_1 state from the primary level E_n in the track of an electron with energy T is denoted by $\eta_n(T)$.

From work on the characteristic energy losses of fast electrons in liquids and solids,[30,31] it is known that a large part of the primary collisions excite collective oscillations of the valence electrons (plasmons). In the case of aromatic compounds, the excitation spectra in the condensed phase generally present two major maxima: the first, located around 7 eV in benzene,[32] is attributed to the molecular π electrons; the second, at about 20 eV, is characteristic of all the organic materials and corresponds to an oscillation of the total number of molecular valence electrons. These initially activated plasmons promptly decay to excite isoenergetic states of individual molecules, which thence have excitation energies $E_{\mathrm{exc}} \geq 7$ eV.[17] According to the results of the first section of this study, the molecular states formed after plasmon decay in the aromatic liquids are typically "superexcited."

The following stage of radiation action involves the set of processes converting these highly excited molecular states to the lower S_1 states. Useful information hereupon comes from part I of the present work, but in addition, we must take into account the consequences of spatial correlation for the excited states along the particle tracks in condensed matter.

The significance of bimolecular reactions between excited molecules in condensed aromatic materials under particle irradiation has often been discussed.[2,33,34] According to the recent studies of exciton interaction mechanisms in molecular crystals, the singlet states are submitted to very efficient quenching processes, which appear to be of paramount importance in the present context; the reactions $S_1 + S_1 \rightarrow S_n + S_0$ (S_n: upper singlet states) and $S_1 + T_1 \rightarrow T_n + S_0$ (T_1 and T_n: triplet states), in particular, have high rate constants ($\gamma \approx 10^{-8}$ cm^3 sec^{-1}), meaning that long-range mechanisms are involved.[2,35] In order to describe these effects, we define a critical "quenching distance" R, such that the degradation of electronic energy takes place with certainty if a quenching center (another primary activated molecule) is situated at a distance $d < R$ from the excited molecule; if $d > R$, the probability of quenching is taken as negligible. Considering an electron of energy T, and differential energy loss $\mathrm{d}T/\mathrm{d}x$, in the degradation spectrum, we assume that the quenching species are distributed along the particle path, according to a Poisson law, with a mean free distance given by

$$\lambda(T) = W(\mathrm{d}T/\mathrm{d}x)^{-1}$$

where W is the mean energy required to form a quenching center. The probability of survival of a singlet state in the electron track is then identified with the probability that no quenching center exists within a distance R, *i.e.*

$$P(T) = \exp[-2R/\lambda(T)] = \exp\left[-B\frac{\mathrm{d}T}{\mathrm{d}x}(T)\right]$$

with $B = 2R/W$. Under these conditions, the efficiency $\eta_n(T)$ for the formation, in the electron track, of an S_1 state which can be observed, can be written as

$$\eta_n(T) = \eta_n P(T) = \eta_n \exp\left[-B\frac{\mathrm{d}T}{\mathrm{d}x}(T)\right]$$

where η_n is the conversion efficiency in the absence of track effects, as observed under light irradiation (*cf.* part I). Inserted in the theoretical expression of G_S, we get the obvious simplified form

$$G_s = \frac{100}{T_0} N \sum_n \eta_n \int_{T'}^{T_0} \sigma_n(T)\, y(T)\, \mathrm{d}T$$

with T' such as $\mathrm{d}T(T')/\mathrm{d}x \approx B^{-1}$. Taking $R \approx 10$ Å, $W \approx 50$ eV, we obtain $B^{-1} = W/2R \approx 2.5$ eV/Å or $T' \approx 1$ keV as reasonable orders of magnitude. The integration is then restricted to the high-energy part of the degradation spectrum and yields simply[36]

$$G_s = \frac{100}{Z} \sum_n \eta_n \frac{f_n}{E_n}$$

where Z is the number of valence electrons per molecule and f_n denotes the oscillator strength for the transition to the primary level of energy E_n.

As noted before, most of the primary levels have energies higher than 7 eV in benzene, which is precisely the onset W_0 of superexcitation, as defined in the first part of this study. The efficiencies η_n should then be considered as $\eta_n = \rho_M \alpha_n$, with the autoionization efficiencies α_n increasing rapidly to unity as E_n increases, and with the values determined in

(26) R. Cooper and J. K. Thomas, *J. Chem. Phys.*, **48**, 5097 (1968). These authors do not discriminate between the prompt and delayed singlet states, which explains, at least partially, their higher G_S values.
(27) J. B. Birks, "The Theory and Practice of Scintillation Counting," Pergamon Press, Oxford, 1964.
(28) R. L. Platzman, *Radiat. Res.*, **30**, 20 (1967).
(29) L. V. Spencer and U. Fano, *Phys. Rev.*, **93**, 1172 (1954).
(30) D. Pines, "Elementary Excitations in Solids," Benjamin, New York, N. Y., 1964.
(31) C. J. Powell, *Health Phys.*, **13**, 1265 (1967).
(32) B. L. Sowers, E. T. Arakawa, and R. D. Birkhoff, *J. Chem. Phys.*, **54**, 2319 (1971).
(33) W. G. Burns and R. Barker, *Progr. React. Kinet.*, **3**, 303 (1965).
(34) M. Schott, Proceedings of the 4th Conference on Radiation Research, Evian, 1970, to be published.
(35) V. Ern, J. L. Saint-Clair, M. Schott, and G. Delacote, *Chem. Phys. Lett.*, **10**, 287 (1971).
(36) See, for example, I. Santar and J. Bednář, *Collect. Czech. Chem. Commun.*, **33**, 1 (1968).

Section I for the efficiency ρ_M of recombination in the S_1 state. For relatively higher excitation energies (*e.g.*, $E_n \geq$ 15 eV), geminate neutralization without spin relaxation is expected to become less probable. The kinetic energy of the quasi-free electrons may indeed become sufficient to excite triplet states with concomitant relaxation of initial spin; also C–H and C–C bonding electrons are known to be mainly excited in this energy range for benzene and derivatives.[37] In this case, the excited positive ions do not necessarily convert to their bound ground state, which again might prevent the formation of S_1 molecular states. This suggests that the summation $\Sigma_n(f_n/E_n)$ should be restricted to an energy range limited by an upper value. Introducing an effective number n_{eff} of electrons taking part in transitions to such energy levels, and a corresponding mean excitation energy E_{eff}, we then get the expression

$$G_s = \frac{100}{Z}\,\rho_M(n_{eff}/E_{eff})$$

which may be conveniently compared to the experimental data in Table III.

An inspection of the experimental results on G_S and ρ_M listed together in Table III first allows verification of the expected relationship between these two quantities. This suggests that, in accord with our analysis, the observed relative variations of G_S are related to variations of the recombination efficiency ρ_M. In previous work,[21,25] it has been assumed that the S_1 states mainly result from internal conversion from primary S_3 states; for the sake of comparison, the efficiencies $\beta_{32}\beta_{21}$ of these processes have also been listed in Table III. It is seen that while G_S follows approximately the same ordering as the $\beta_{32}\beta_{21}$ values, the correlation with ρ_M is notably better. The absolute G_S values lead to $(100/Z)(n_{eff}/E_{eff}) \approx 1$. For benzene ($Z = 30$), we may take $E_{eff} \approx 10$ eV and $n_{eff} = 3$, restricting the summation Σ_n over primary states with $E_n \leq 15$ eV, in accord with our preceding arguments.

Conclusions

The description of the very early processes leading to the S_1 states in the aromatic liquids under fast electron irradiation, which has been suggested in part I of this study, does interpret our data on the scintillation yields. Further evidence for the mechanism involving autoionization of the upper primary singlet levels and subsequent geminate ion recombination comes from the observed decrease of G_S with increasing concentrations of chloroform.[9] Similar conclusions have also been drawn from the pulse-radiolysis studies of Cooper and Thomas.[26]

The primary states leading ultimately to the lowest excited singlet levels are mainly activated by the fast electrons of the degradation spectrum, in optical collisions with a relatively small energy transfer ($\leq$ 15 or 20 eV); they thus correspond to only a minor fraction of the "isolated spurs," as defined in ref 38. This, together with the efficient bimolecular quenching reactions of excited molecules in the blobs and short tracks, is considered to account for the low yields of S_1 formation in the condensed aromatic materials under high-energy radiation.[39]

(37) B. O. Jonsson and E. Lindholm, *Ark. Fys.*, **39**, 65 (1969).
(38) I. Santar and J. Bednář, *Int. J. Radiat. Phys. Chem.*, **1**, 133 (1969).
(39) Typical L.E.T. effects in the aromatic materials have been interpreted using similar arguments; *cf.* ref 2.

Temperature Shifts in the Optical Spectra of Solvated Electrons in Methanol and Ethanol[1,2]

K. N. Jha, G. L. Bolton, and G. R. Freeman*

Chemistry Department, University of Alberta, Edmonton, Alberta, Canada T6G 2G2 *(Received May 12, 1972)*

Publications costs assisted by the University of Alberta

At 295 K the e_{solv}^- absorption peak E_{max} and the width of the band at half height $W_{1/2}$ were respectively 1.95 and 1.3 eV in methanol and 1.80 and 1.4 eV in ethanol. At temperatures between 170 and 350 K, $dE_{max}/dT = -2.6 \times 10^{-3}$ eV/deg in methanol and -3.2×10^{-3} eV/deg in ethanol. Increasing T increased $W_{1/2}$ slightly. The shifts in E_{max} caused by changing the temperature or pressure (up to 6000 atm) in a given liquid (alcohol or water) correlate with the product of the dielectric constant and the density, ϵd. Plots of E_{max} *vs.* ϵd overlap for methanol and ethanol, but the curve for water falls at higher values of ϵd for a given E_{max}. Electron–solvent short range interactions appear to be important in determining E_{max}. The e_{solv}^- spectra were not changed in shape by addition of up to 1.4 M KOH. The height of the absorption band increased with increasing base concentration due to scavenging of H_{solv}^+ in the spurs. The molar absorbancy (decadic) coefficient of e_{solv}^- was independent of temperature: $\epsilon(\lambda_{max})$ $(10.2 \pm 0.4) \times 10^3$ M^{-1} cm^{-1} in methanol, $(9.4 \pm 0.4) \times 10^3$ in ethanol and $(18.9 \pm 0.6) \times 10^3$ in water. The oscillator strength of e_{solv}^-, corrected for the refractive index of the solvent, is 0.4 in methanol and ethanol and 0.6 in water and ammonia.

Introduction

The work reported herein was done in parallel with a study of the effects of high pressure on properties of solvated electrons in alcohols and water.[3] Temperature and pressure effects provide complementary information about the properties of species in the liquid phase.[4,5]

A number of temperature[6-11] and pressure[3,10-13] studies of solvated electron optical absorption spectra in ammonia,[7,10,11] water,[3,11-13] and alcohols[3,6,8] have been reported. The spectra shift to higher energies with decreasing temperature and increasing pressure. The present article attempts to correlate the temperature and pressure effects.

New information is also provided about the molar absorbancy (extinction) coefficient and oscillator strength of solvated electrons in alcohols.

Experimental Section

Materials. Absolute methanol, analyzed reagent spectrophotometric grade from Baker Chemical Co., was refluxed for 12 hr after addition of 2 g of 2,4-dinitrophenylhydrazine and 0.5 g of concentrated sulfuric acid to 1 l. of the alcohol. The refluxing system was rinsed with the absolute methanol before filling and was flushed with ultrahigh purity argon (Matheson) before and during refluxing. The alcohol was then distilled and the center 50% was collected. For some experiments the purified methanol was further refluxed with 10 g/l. of sodium borohydride for 5 hr, while bubbling with argon, and distilled.

Absolute reagent quality U.S.P. ethyl alcohol from U. S. Industrial Chemical Co. was usually used as received because of its exceptionally high purity.[14] Some of it was treated with sodium borohydride as above. The borohydride treatment did not affect the measured optical absorption spectra, but it increased the solvated electron half-lives.

For all alcohol distillations the apparatus was rinsed with the initial alcohol just prior to filling, and the receiver was rinsed with the first portions of distillate before collecting the center fraction. The main purpose of the rinsings was to remove water adsorbed on the glass surfaces. The Baker methanol and U. S. I. ethanol reportedly contained 0.01 and 0.005 wt % water, respectively.

Sodium borohydride (Fisher, 98%) and potassium hydroxide (Fisher certified ACS) were used as received. Translucent pellets of the latter, free of carbonate spots on the surface, were selected.

"Singly distilled" water was obtained from a Barnstead still. Two further distillations, one from alkaline permanganate followed by a simple distillation in a Pyrex apparatus, provided "triply distilled" water.

Sample Preparation. Cells and other glassware were cleaned with hot nitric acid, then rinsed several times with singly distilled water, once with dilute sodium bicarbonate solution, then several times with singly, then triply distilled water. The glassware was then dried at 388 K in a clean oven reserved for that purpose. Finally, it was rinsed with the appropriate alcohol or solution just prior to use.

(1) Supported by the National Research Council of Canada.
(2) This work was reported in part in a paper by M. G. Robinson, K. N. Jha, G. L. Bolton, and G. R. Freeman at the C.I.C. Pulse Radiolysis Symposium, Pinawa, Manitoba, Can., Oct 26, 1971.
(3) M. G. Robinson, K. N. Jha, and G. R. Freeman, *J. Chem. Phys.*, **55**, 4933 (1971).
(4) O. E. Weigang, Jr., and W. W. Robertson in "High Pressure Physics and Chemistry" Vol. 1, R. S. Bradley, Ed., Academic Press, London, 1963, Chapter 4.
(5) J. Jortner, *Ber. Bunsenges Phys. Chem.*, **75**, 696 (1971).
(6) (a) M. C. Sauer, Jr., S. Arai, and L. M. Dorfman, *J. Chem. Phys.*, **42**, 708 (1965); (b) S. Arai and M. C. Sauer, Jr., *ibid.*, **44**, 2297 (1966).
(7) R. K. Quinn and J. J. Lagowski, *J. Phys. Chem.*, **73**, 2326 (1969).
(8) J. H. Baxendale and P. Wardman, *Chem. Commun.*, 429 (1971).
(9) R. Vogelsgesang and U. Schindewolf, *Ber. Bunsenges. Phys. Chem.*, **75**, 651 (1971).
(10) R. Olinger, U. Schindewolf, A. Gaathon, and J. Jortner, *Ber. Bunsenges. Phys. Chem.*, **75**, 690 (1971).
(11) B. D. Michael, E. J. Hart, and K. H. Schmidt, *J. Phys. Chem.*, **75**, 2798 (1971).
(12) U. Schindewolf, H. Kohrmann, and G. Lang, *Angew. Chem., Int. Ed. Engl.*, **8**, 512 (1969).
(13) R. R. Hentz, Farhataziz, and E. M. Hansen, *J. Chem. Phys.*, **55**, 4974 (1971).
(14) S. M. S. Akhtar and G. R. Freeman, *J. Phys. Chem.*, **75**, 2756 (1971).

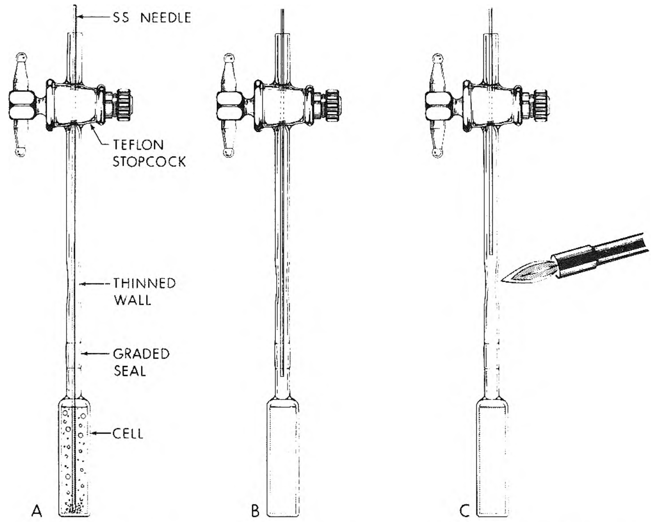

Figure 1. Technique for deaerating and sealing samples (see text).

Samples containing a solute were usually prepared using a microsyringe to transfer the required volume of a stock solution to a cell containing solvent. Stock solutions were made by weighing.

Most samples in the Suprasil optical cells ($1 \times 1 \times 4.5$ cm) were deoxygenated by bubbling for ≥ 20 min with 25 cm^3/min of ultrahigh-purity argon through a stainless steel needle (Figure 1A). The needle was then withdrawn until it was just out of the solution and the argon flow rate was increased somewhat (Figure 1B). The solution was then cooled to 195 K. The tubing was then heated gently with a flame at the place where it was to be sealed, before the needle was withdrawn further. This flushed volatile substances from the heated glass wall. The needle was then withdrawn to just above the point to be sealed (Figure 1C) and the seal was made as quickly as possible.

For some experiments at room and elevated temperatures the argon-flushed sample was simply sealed with a Teflon stopcock. The stopcock leaked at low temperatures. Some samples were degassed on a vacuum line, using freeze-pump-thaw cycles, prior to sealing with a flame. All three techniques resulted in the same electron lifetime for a given type of sample at room temperature.

Temperature Apparatus. The optical cell was held snugly on three sides by a one-piece blackened-brass holder. A steel spring formed the fourth side of the holder. An adjustable slit, usually set at 0.3×2.5 cm, was attached to the side of the holder. Two copper-constantan thermocouples were attached to different points of the holder and another was glued to the side of the optical cell using G.E. RTV silicone rubber adhesive.

The cell holder was fixed in a Styrofoam box of $12 \times 12 \times 27$ cm outside and $7 \times 7 \times 17$ cm inside dimensions. At the place where the electron beam entered the box the Styrofoam was thinned from the outside to 1 cm to minimize spreading of the beam. The analyzing light beam entered and left the box through windows that were evacuated Suprasil cylinders (2×2 cm) press-fitted into the sides of the box. At very low temperatures a stream of dry air was used to keep the windows frost free.

Cold nitrogen or hot air entered the box through the bottom and left through an insulated 30 cm high chimney in the lid. The rate of flow of cold nitrogen was controlled by adjusting the voltage across a 1-kW capacity nichrome coil immersed in a 50-l. dewar of liquid nitrogen. The flow rate and temperature of hot air were controlled by attaching Variacs to the fan motor and heating coil of a heat gun (Master Applicance Corp., Model HG-501L). Temperatures from 130 to 360 K could be maintained within ± 1 K. Temperatures above 370 K caused distortion of the Styrofoam under the cell holder. The sample was assumed to be at the desired temperature when the thermocouple glued to the cell indicated the same temperature as those attached to the holder.

Spectrophotometry. Light from a 450-W xenon arc lamp passed through a quartz lens and an iris and was further focused and transported using spherical and plane front-surfaced (aluminum, coated with silicon monoxide) mirrors. The beam passed through 1.0 cm of sample.

The entrance and exit slits of a Bausch and Lomb Model 33-86-25 monochromator containing a no. 33-86-02 grating were set to give a bandpass of 10 nm at 500 nm. The monochromator wavelength scale was calibrated using a mercury lamp and a helium-neon gas laser (λ 632.8 nm).

The light detector was a SGD-444-2 photodiode from EG & G Inc. (response 20% at 400 nm and 80% at 1000 nm; sensitivity 0.5 $\mu A/\mu W$ at 900 nm; response linear over seven decades of incident power). The absorption signal was amplified and recorded as a voltage on either a Tektronix Type 549 storage oscilloscope or a Tektronix 7704 oscilloscope. Traces were photographed with a Polaroid Model C12 camera using type 47 or 410 Polaroid Land film. Incident light intensity was recorded on a digital voltmeter 20–40 μsec before the electron pulse.

The amplifier had 136-ohm input impedance, a 35-nsec response time and had negative feedback to give linearity and stability. A light shutter was used to protect the sample from photolysis and warming. The rise time of the total measuring system was 70 nsec. The light shutter and monochromator (350–800 nm) were operated by remote control.

Irradiation and Dosimetry. The 1.0- or 0.10-μsec pulses of 1.7-MeV electrons from a van de Graaff generator gave doses of 9×10^{16} or 3×10^{16} eV/g, respectively. The dose delivered in each pulse was monitored by a secondary emission monitor (SEM) or by current collected from the cell holder. These monitors were calibrated against the optical absorption produced in oxygen-saturated 2.0 mM KSCN aqueous solutions. To clarify earlier information[15,16] the $(SCN)_2^-$ absorption spectrum was measured at several temperatures in the range 293 to 332 K (Figure 2): both λ_{max} 478 ± 4 nm and the absorbance per unit dose were independent of temperature. The extinction coefficient[16] ϵ_{475} ($(SCN)_2^-$) 7600 M^{-1} cm^{-1} was used. Assuming that in the bulk solution $G(OH)_{bulk} = G(e_{aq}^-)_{fi} = 2.7$, G(OH) scavenged by 2 mM KSCN is 2.9. This will be shown in a KSCN concentration study to be published.

By comparison with the KSCN dosimeter, oxygen saturated aqueous solutions containing 5, 10, and 50 mM Fe^{2+} gave $G(Fe^{3+}) = 15.5 \pm 1.1$ under the present conditions. The total response time of the 10 mM ferrous dosimeter was 3 sec compared to <1 μsec for the KSCN solution. The latter is the more convenient to use.

Results

λ_{max}, E_{max}, *and* $W_{1/2}$. Spectra were measured in pure methanol and pure ethanol at temperatures from near their

(15) G. E. Adams, J. W. Boag, J. Currant, and B. D. Michael in "Pulse Radiolysis," M. Ebert, J. P. Keene, A. J. Swallow, and J. H. Baxendale, Ed., Academic Press, London, 1965 p 117.
(16) J. H. Baxendale, P. L. T. Bevan, and D. A. Stott, *Trans. Faraday Soc.*, **64**, 2389 (1968).

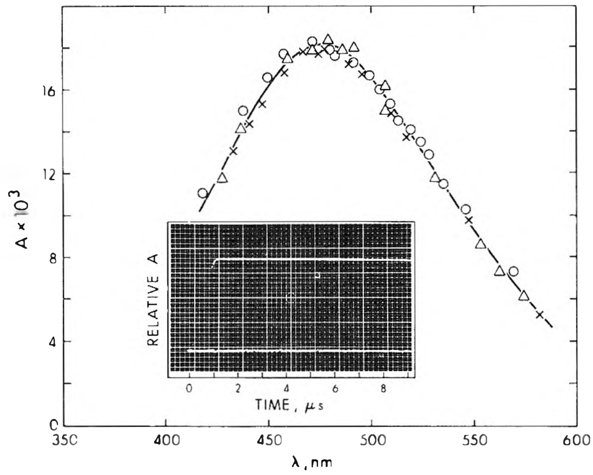

Figure 2. Optical absorption spectrum of $(SCN)_2^-$ after 0.1-μsec pulses of 1.7-MeV electrons in 2 m*M* KSCN solutions in water: A = absorbance/unit dose; temperature: ×, 295 K; Δ, 307 K; O, 332 K. Inset: CRO trace at 478 nm, 295 K.

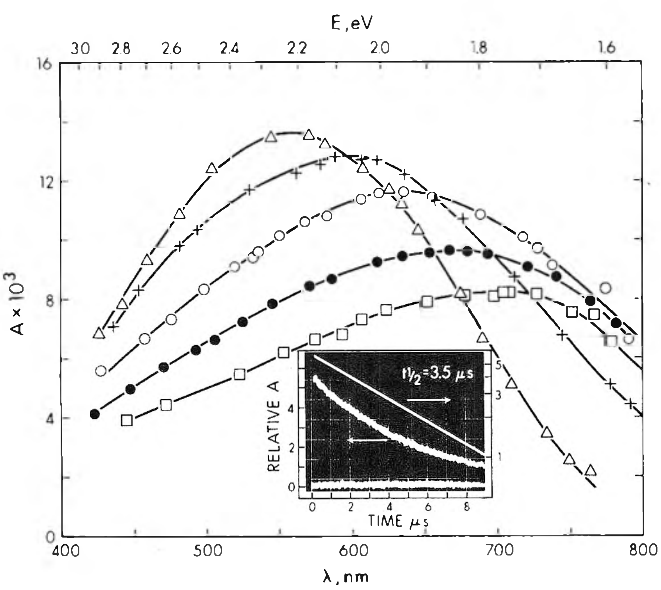

Figure 3. Optical absorption spectra obtained at the end of 1-μsec pulses in methanol: Δ, 183 K; +, 243 K; O, 294 K; ●, 336 K; □, 358 K. Inset: CRO trace at 560 nm, 295 K, 1 m*M* KOH.

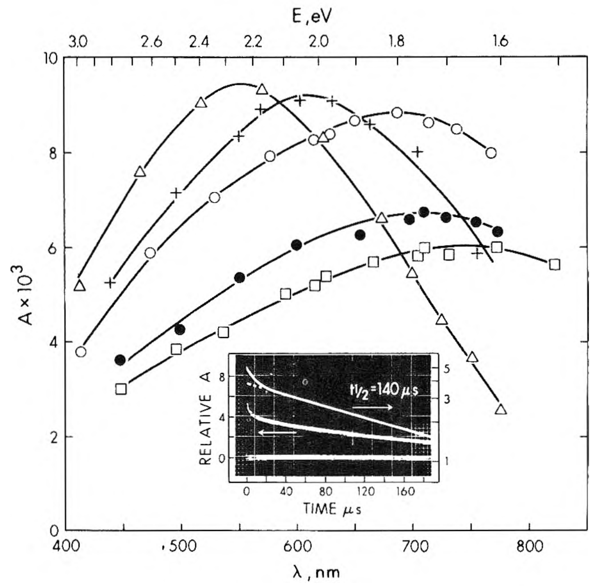

Figure 4. Optical absorption spectra obtained at the end of 1-μsec pulses in ethanol: Δ, 173 K; +, 234 K; O, 296 K; ●, 323 K; □, 343 K. Inset: CRO trace at 605 nm, 167 K, neutral.

melting points to near their boiling points (~170 to 350 K). Representative spectra obtained after 1-μsec pulses are shown in Figures 3 and 4. The spectra obtained after 0.1-μsec pulses at the lower temperatures were identical with those in the figures. At higher temperatures the absorption peak heights per unit pulse dose were greater after the 0.1-μsec than after the 1-μsec pulses because less decay occurred during the shorter pulses.

The values of the wavelength λ_{max} and energy E_{max} at which maximum absorption occurred and the width of the absorption peak at half height $W_{1/2}$ are listed in Table I. Many of the values are averages from several determinations. Increasing the temperature decreased E_{max} but increased $W_{1/2}$ slightly.

The above experiments were repeated with 1.0 m*M* KOH solutions. The absorption peak heights per unit pulse dose were about 20% greater than those in the neutral solutions but the values of E_{max} and $W_{1/2}$ were the same within experimental error. The only exception was that the spectra at the lowest temperatures were slightly broadened toward the blue in the basic solutions. The broadening may be attributed to a small contribution from the low-energy end of the absorption spectrum of $RCHO_{solv}^-$.[17] The latter presumably shifts less with temperature than does the e_{solv}^- spectrum, so the high-energy tail of the e_{solv}^- spectrum overlaps the lower end of the $RCHO_{solv}^-$ spectrum at low temperatures.

The values of E_{max} obtained from the neutral and basic alcohols are plotted against temperature in Figure 5. The

TABLE I: Densities and Dielectric Constants of the Alcohols and Optical Absorption Properties of e_{solv}^-

T, K	*d*, g/cm³ [a]	ε [b]	λ_{max}, nm [c]	E_{max}, eV	$W_{1/2}$, eV [d]
			CH_3OH, Mol Wt 32.04		
183	0.888	69.0	557	2.22	1.1
(195[e])	0.879	63.8	(565[e])	(2.20[e])	(1.26[e])
243	0.836	45.3	600	2.07	1.3
294	0.792	33.5	635	1.95	1.3
(~298[e])	0.788	32.7	(630[e])	(1.97[e])	(1.29[e])
320	0.767	29.0	651	1.90	
336	0.752	26.5	675	1.84	
358	0.729	23.3	710	1.75	
			C_2H_5OH, Mol Wt 46.07		
155	0.908	64.5	545	2.27	~1.3
173	0.892	56.2	555	2.23	1.4
(195[e])	0.871	48.1	(582[e])	(2.13[e])	(1.4[e])
234	0.836	37.0	610	2.03	1.4
296	0.780	24.5	688	1.80	1.4
(~298[e])	0.778	24.2	(700[e])	(1.77[e])	(1.55[e])
323	0.755	20.8	715	1.73	1.5
343	0.737	18.4	745	1.66	1.5

[a] R. W. Gallant, "Physical Properties of Hydrocarbons," Vol. 1, Gulf Publishing Co., Houston, Tex., 1968, Chapter 8. [b] F. Buckley and A. A. Maryott, *Nat. Bur. Stand. U. S. Circ.*, No. 589 (1958); W. Dannhauser and L. W. Bahe, *J. Chem. Phys.*, **40**, 3058 (1964). [c] Wavelength at the absorption maximum; mean deviation ±1%. [d] Width of absorption peak at half height. [e] Reference 6.

(17) M. Simic, P. Neta, and E. Hayon, *J. Phys. Chem.*, **73**, 3794 (1969).

TABLE II: Effects of KOH Concentration on e_{solv}^- Spectra in Alcohols at 295 K

[KOH], M		E_{max}, eV	$10^{-3}G_{fi}\epsilon(\lambda_{max})$, e_s^- l./100 eV mol cm[a]	G_{fi}		$10^{-3}\epsilon(\lambda_{max})$, l./mol cm
			CH_3OH			
0		1.95	19	2.0		9.5
7×10^{-5}		1.92	20	2.0		10.0
0.0010		1.95	23	2.2		10.5
0.029		1.90	27	3.1		8.7
0.34		1.93	33	3.6		9.2
1.0		1.91	38	4.3		8.8
1.4		1.94	41	4.4		9.3
	Av	1.93 ± 0.02			Av	9.4 ± 0.5
			C_2H_5OH			
0		1.80	15	1.7		9.0
0.0005		1.80	19	1.8		10.6
0.0011		1.80	20	1.9		10.5
0.010		1.82	21	2.4		8.8
0.096		1.82	29	3.2		9.1
1.0		1.79	36	4.0		9.0
	Av	1.80 ± 0.01			Av	9.5 ± 0.5

[a] Values based on 2 mM KSCN dosimetry, using $G(OH) = 2.9$ and $\epsilon_{475}((SCN)_2^-) = 7600$ l./mol cm.

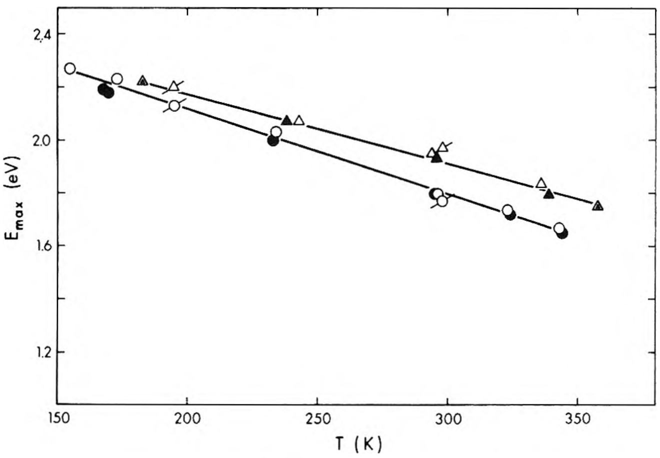

Figure 5. E_{max} for e_{solv}^- in methanol (△) and ethanol (O) at different temperatures. Open points, neutral; filled points, 1 mM KOH; ⧍, Ø, ref 6b.

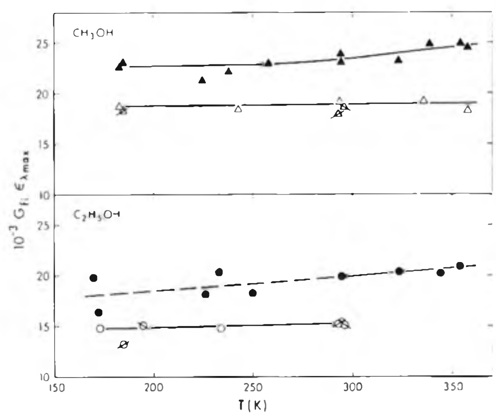

Figure 6. $G_{fi}\epsilon(\lambda_{max})$ for e_{solv}^- in methanol (△) and ethanol (O) at different temperatures. Open points, neutral; filled points, 1.0–1.5 mM KOH. ⧍, Ø, ref 8; ⧍, Ø, ref 6. The units of $G_{fi}\epsilon(\lambda_{max})$ are (electrons l./100 eV mol cm). The fast decay portion observed at low temperatures[8] is not included in these values of $G_{fi}\epsilon(\lambda_{max})$.

relationships are linear with $dE_{max}/dT = -2.6 \times 10^{-3}$ eV/deg in methanol and -3.2×10^{-3} eV/deg in ethanol. The temperature coefficients reported earlier from measurements at 195 and ~298 K were -2.2×10^{-3} and -3.4×10^{-3} eV/deg in methanol and ethanol, respectively.[6]

The addition of up to 1 M KOH did not alter E_{max}, within experimental error (Table II).

$G_{fi}\epsilon(\lambda_{max})$. The height of the absorption maximum per unit pulse dose was used to obtain $G_{fi}\epsilon(\lambda_{max})$, where G_{fi} is the 100-eV yield of e_{solv}^- free ions and $\epsilon(\lambda_{max})$ is the molar absorbancy (extinction) coefficient at the absorption maximum. Values of $G_{fi}\epsilon(\lambda_{max})$ for electron radiolysis of the neutral and basic alcohols are plotted against temperature in Figure 6. Results from ref 6 and 8 are included to show the consistency of the measurements. $G_{fi}\epsilon(\lambda_{max})$ is larger in the basic than in the neutral alcohols. It is independent of temperature in the neutral alcohols but increases slightly with increasing temperature in the basic alcohols. This quantity also increases with increasing base concentration at 295 K (Table II). Densities of the solution, required in the calculation of $G_{fi}\epsilon(\lambda_{max})$, were 0.303 and 0.86 g/cm³ for 0.34 and 1.4 M KOH in methanol, respectively, and 0.842 g/cm³ for 1.0 M KOH in ethanol. Densities of other solutions were interpolated between these and those of the pure alcohols.

$G_{fi}\epsilon(\lambda_{max})$ was measured with pulse doses from 2 to 18 (10^{16} eV/cm³) in methanol containing 1 mM KOH at 185 K. The value obtained was $(2.29 \pm 0.05)10^4$ (e_{solv}^- l./100 eV mol cm), independent of dose. This was a type of confidence test of the measurement and the result agreed with expectation.

Discussion

Effects of Temperature and Pressure on E_{max}. The physical interpretation of optical absorption spectra of electrons solvated in different media has been attempted for several

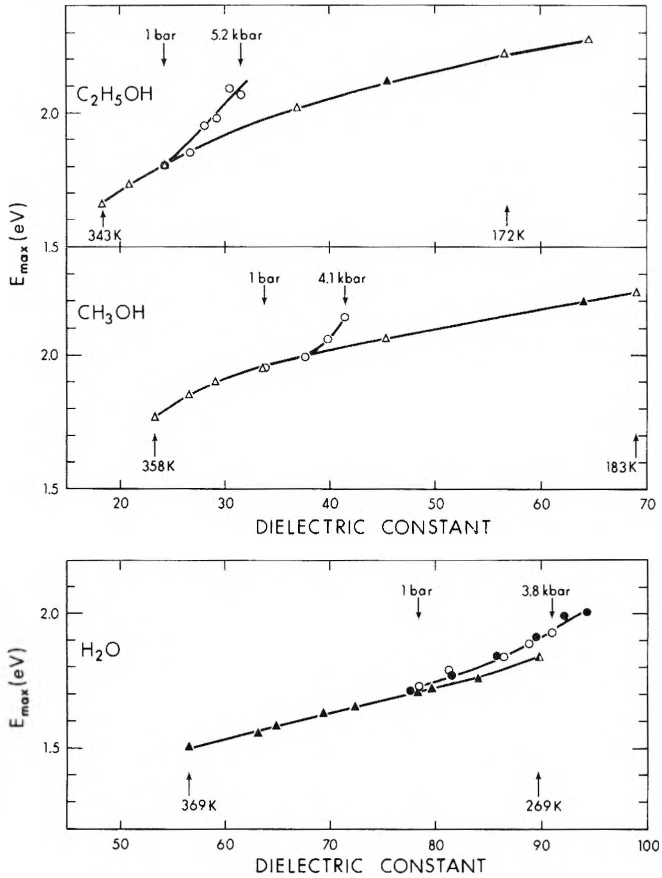

Figure 7. Plot of E_{max} against dielectric constant in ethanol, methanol, and water. Ethanol and methanol: temperature variation at 1 bar, △, present work, ▲, ref 6; pressure variation at 298 K, O, ref 3. Water: temperature variation at 1 bar, ▲, ref 48; ▲, ref 11; pressure variation at 298 K, O, ref 3; ●, ref 13.

decades.[5,6,18-45] Related work has been done with the absorption spectra of solvated halide ions.[46,47] None of the proposed models is entirely satisfactory and it has become increasingly clear that more experimental information is needed. For example, one would like to know more about correlations between the optical excitation energy of the electron and the physical properties of the solvating medium, and particularly of the solvating site in the medium.

The excitation energy E_{max} in a given liquid increases with increasing pressure[3,9,12,13] and decreasing temperature.[6,7,9,11,18] Considering electrons in a number of different liquids, E_{max} tends to increase with the dielectric constant of the liquid,[18] although there is an additional effect of molecular and liquid structure that is not reflected in the bulk dielectric constant.[6,23,43] The dielectric constant ϵ of a given liquid increases with increasing pressure and decreasing temperature, so an initial attempt might be made to correlate the temperature and pressure effects on E_{max} with ϵ.

In Figure 7 are shown the values of E_{max} obtained in ethanol at different temperatures and pressures, plotted against ϵ. Temperature and pressure variations give different results; $dE_{max}/d\epsilon$ from the pressure variation is approximately double that from the temperature variation. Similar behavior is found in methanol and water[3,11,13,48] (Figure 7).

One can partially rationalize the difference between the temperature and pressure effects in these highly polar liquids in terms of a simple physical picture. The potential energy E between the electron and the surrounding dipoles is some function of the distance r between the electron and the dipoles, say r^{-x}. If r is decreased by increasing the pressure then E increases: $r \propto d^{-1/3}$, so $E \propto d^{x/3}$, where d is the density. Decreasing the temperature also decreases r, but it simultaneously decreases the amount of thermal agitation of the dipoles. The smaller amount of thermal agitation allows the dipoles to line up to a greater extent in the electric field of the electron, which causes E to increase more. One would therefore expect a plot of E_{max} against the liquid density to have a greater slope in the temperature study than in the pressure study; *i.e.*, the relative slopes of the temperature and pressure series in the density plots should be in the reverse direction of those in the dielectric constant plots. Such is the case (*cf.* Figure 8 with Figure 7).

The differing effects of temperature and pressure can be discussed in terms of the Kirkwood equation[49]

$$\frac{(2\epsilon + 1)(\epsilon - 1)}{9\epsilon}\frac{M}{d} = \frac{4\pi N}{3}\left(\alpha + \frac{g\mu^2}{3kT}\right) \tag{1}$$

where M is the molecular weight, N is Avogadro's number, α is the optical polarizability of the molecule, g is a correlation parameter, μ is the magnitude of the molecular dipole moment, k is Boltzmann's constant, and T is the absolute temperature. In the three liquids under discussion $\epsilon \gg 1$, so (1) reduces to

$$\epsilon \approx \frac{6\pi N}{M}\left(\alpha + \frac{g\mu^2}{3kT}\right)d \tag{2}$$

Increasing the pressure on water at 298 K from 1 bar to 5 kbars increases ϵ by 20% and d by 15%, so the bracketed term in eq 2 increases by 5%; in the alcohols the respective

(18) J. Jortner, S. A. Rice, and E. G. Wilson in "Metal-Ammonia Solutions," G. Lepoutre and M. J. Sienko, Ed., Benjamin, New York, N. Y., 1964, p 222, and references therein.
(19) I. A. Taub, D. A. Harter, M. C. Sauer, Jr., and L. M. Dorfman, *J. Chem. Phys.*, **41**, 979 (1964).
(20) M. J. Blandamer, R. Catterall, L. Shields, and M. C. R. Symons, *J. Chem. Soc.*, 4357 (1964).
(21) M. J. Blandamer, L. Shields, and M. C. R. Symonds, *J. Chem. Soc.*, 3759 (1965).
(22) K. Fueki, *J. Chem. Phys.*, **44**, 3140 (1966); **45**, 183 (1966).
(23) G. R. Freeman, Gordon Research Conference on Radiation Chemistry, New Hampton, N. H., Aug 1966.
(24) N. F. Mott, *Advan. Phys.*, **16**, 49 (1967).
(25) H. Barzynski and D. Schulte-Frohlinde, *Z. Naturforsch.*, **22a**, 2131 (1967).
(26) J. E. Bennett, B. Mile, and A. Thomas, *J. Chem. Soc., A*, 1393 (1967).
(27) R. H. Land and D. E. O'Reilly, *J. Chem. Phys.*, **46**, 4499 (1967).
(28) O. F. Khodzhaev, B. G. Ershov, and A. K. Pikaev, *Bull. Acad. Sci. USSR, Div. Chem. Sci.*, 244 (1968).
(29) K. Iguchi, *J. Chem. Phys.*, **48**, 1735 (1968); **51**, 3137 (1969).
(30) K. Fueki, *J. Chem. Phys.*, **49**, 765 (1968).
(31) A. Ekstrom and J. E. Willard, *J. Phys. Chem.*, **72**, 4599 (1968).
(32) R. Catterall and N. F. Mott, *Advan. Phys.*, **18**, 665 (1969).
(33) M. Weissmann and N. V. Cohan, *Chem. Phys. Lett.*, **7**, 445 (1970).
(34) K. Fueki, D.-F. Feng, and L. Kevan, *J. Phys. Chem.*, **74**, 1976 (1970).
(35) J. L. Dye, M. G. DeBacker, and L. M. Dorfman, *J. Chem. Phys.*, **52**, 6251 (1970).
(36) W. H. Hamill, *J. Chem. Phys.*, **53**, 473 (1970).
(37) D. A. Copeland, N. R. Kestner, and J. Jortner, *J. Chem. Phys.*, **53**, 1189 (1970).
(38) G. V. Buxton, F. S. Dainton, T. E. Lantz, and F. P. Sargent, *Trans. Faraday Soc.*, **66**, 2962 (1970).
(39) S. Ray, *Chem. Phys. Lett.*, **11**, 573 (1971).
(40) G. V. Buxton, F. C. R. Cattell, and F. S. Dainton, *Trans. Faraday Soc.*, **67**, 687 (1971).
(41) H. Hase and L. Kevan, *J. Chem. Phys.*, **54**, 908 (1971).
(42) H. Hase, M. Noda, and T. Higashimura, *J. Chem. Phys.*, **54**, 2975 (1971).
(43) L. M. Dorfman, F. Y. Jon, and R. Wageman, *Ber. Bunsenges. Phys. Chem.*, **75**, 681 (1971).
(44) R. Catterall, *Nature (Phys. Sci.)*, **229**, 10 (1971).
(45) R. A. Pinkowitz and T. J. Swift, *J. Chem. Phys.*, **54**, 2858 (1971).
(46) J. Franck and R. L. Platzman, *Z. Phys.*, **138**, 411 (1954).
(47) G. Stein, *Advan. Chem. Ser.*, **No. 50**, 230 (1965), and references therein.
(48) W. C. Gottschall and E. J. Hart, *J. Phys. Chem.*, **71**, 2102 (1967).
(49) G. Oster and J. G. Kirkwood, *J. Chem. Phys.*, **11**, 175 (1943).

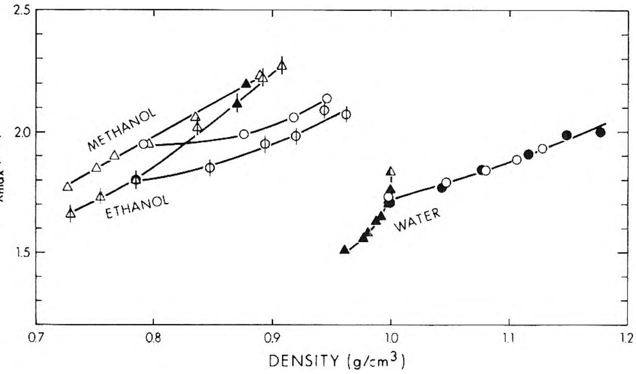

Figure 8. Plot of E_{max} *vs.* density for ethanol (Δ̸, Φ), methanol (Δ, O), and water. Triangles are results from temperature variation at 1 bar, circles from pressure variation at 298 K. References are the same as in Figure 7.

increases are 27%, 21%, and 6%. The effect of pressure on ϵ at constant temperature is therefore mainly due to the change of d, and plots of E_{max} against ϵ and d for the pressure series might be expected to have similar relative slopes. In fact $\partial E_{max}/(\partial d/d_{av}) \approx 2\partial E_{max}/(\partial\epsilon/\epsilon_{av})$ in all three liquids (Figures 7 and 8); d_{av} and ϵ_{av} are the average values of d and ϵ, respectively. The functional dependence of E_{max} on d is greater than that on ϵ in the pressure series. This means that some other liquid property, in addition to ϵ, that depends on the density affects E_{max}.

Increasing T at constant pressure decreases ϵ much more rapidly than d (eq 2, g and μ do not change greatly with T)[49] so in the temperature series, plots of E_{max} *vs.* ϵ have smaller relative slopes than do plots of E_{max} *vs.* d: $\partial E_{max}/(\partial d/d_{av}) \approx 10\,\partial E_{max}/(\partial\epsilon/\epsilon_{av})$ in all three liquids (Figures 7 and 8).

Equations 1 and 2 apply to the bulk liquid, whereas E_{max} is most affected by the solvent molecules immediately surrounding the electron. These molecules are highly polarized by the field of the electron and will be less sensitive to thermal agitation than are those in the bulk solvent. The dielectric constant of the solvation shell of the electron will therefore vary less with temperature than does that of the bulk liquid. The values of ϵ used in Figure 7 should really be those of the solvation shell. In such a plot the curve for the temperature series would have a steeper slope (ϵ would vary over a smaller range), so the temperature and pressure curves would lie closer together.

Plotting E_{max} against the product ϵd brings the temperature and pressure series onto the same curve, for a given compound (Figure 9). The curves for the two alcohols nearly coincide.

One may conclude that solvated electron excitation energies in hydroxylic solvents are determined as much by density, or by some other property of the medium that correlates with the density, as by the dielectric constant. The density effect might be related to the size and compressibility of the "cavity" in and about which the electron wave function is concentrated. The electron-medium short-range interactions appear to be important in this context.

The amount of difference between the temperature and pressure curves in Figure 7 decreases in the order $C_2H_5OH > CH_3OH > H_2O$. It might be significant that the polarizabilities α of the molecules decrease in the same order, being respectively 5.4, 3.9, and 1.5 Å^3.[50] The molecular polarizabilities are anisotropic.

Molar Absorbancy $\epsilon(\lambda_{max})$ *of* e_{solv}^- *in Alcohols.* Values of $G_{fi}\epsilon(\lambda_{max})$ measured under different conditions are shown in Figure 6 and Table II. Free ion yields under the same con-

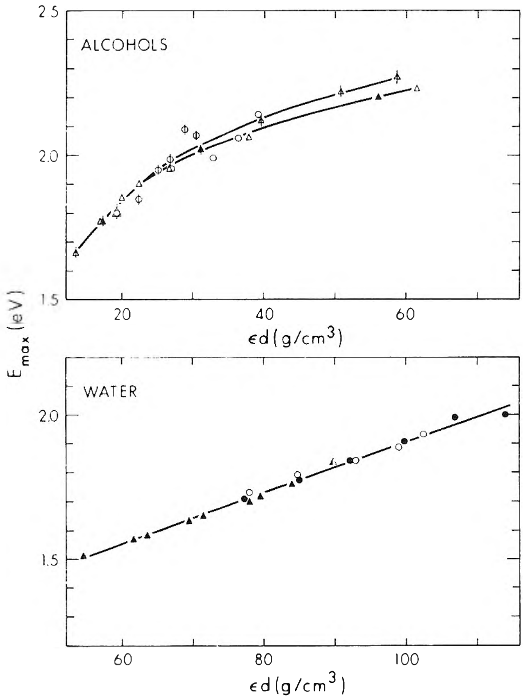

Figure 9. Plot of E_{max} *vs.* the product of the dielectric constant ϵ and the density d for ethanol (Δ̸, Φ), methanol (Δ, O), and water. Triangles are results from temperature variation at 1 bar, circles from pressure variation at 298 K. References are the same as in Figure 7.

ditions have been estimated from earlier studies,[14,51-57] with model calculations of the type reported in ref 14, 52, 58, and 59. The free ions in neutral alcohol are generated by reaction 3 followed by 5.

$$\mathrm{ROH} \longrightarrow [\mathrm{H_{solv}}^+ + \mathrm{e_{solv}}^-] \quad (3)$$

$$[\mathrm{H_{solv}}^+ + \mathrm{e_{solv}}^-] \longrightarrow \text{geminate neutralization} \quad (4)$$

$$[\mathrm{H_{solv}}^+ + \mathrm{e_{solv}}^-] \longrightarrow \mathrm{H_{solv}}^+ + \mathrm{e_{solv}}^- \ \text{(free ions)} \quad (5)$$

$$\mathrm{e_{solv}}^- \longrightarrow \mathrm{RO_{solv}}^- + \mathrm{H} \quad (6)$$

Only the relatively long-lived e_{solv}^- free ions are being discussed, although at the lowest temperatures the tail end of reaction 4 was also observable on the oscilloscope traces; (4) was eliminated from the calculations by extrapolating to zero time the relatively slow signal decay due to (6) observed at longer times (Figure 4).

In the alkaline solutions the free ion yield was increased by scavenging radiolytic cations in the spurs.

$$[\mathrm{H_{solv}}^+ + \mathrm{e_{solv}}^- + \mathrm{K_{solv}}^+ + \mathrm{RO_{solv}}^-] \rightarrow [\mathrm{ROH} + \mathrm{e_{solv}}^- + \mathrm{K_{solv}}^+] \quad (7)$$

where RO^- is either HO^- or an alkoxide ion. The K_{solv}^+ and e_{solv}^- do not react together, so they ultimately become free ions. Thus (7) increases the free ion yield.

$$[\mathrm{K_{solv}}^+ + \mathrm{e_{solv}}^-] \rightarrow \mathrm{K_{solv}}^+ + \mathrm{e_{solv}}^- \ \text{(free ions)} \quad (8)$$

(50) Landolt-Börnstein, "Zahlenwerte und Funktionen," Bd I, Teil 3, 1951, calculated from values of ($P_E + P_A$) on p 514.

(51) H. Seki and M. Imamura, *J. Phys. Chem.*, **71**, 870 (1967).
(52) K. N. Jha and G. R. Freeman, *J. Chem. Phys.*, **48**, 5480 (1968).
(53) H. Ogura, T. Miyagawa, and M. Kondo, *Bull. Chem. Soc. Jap.*, **42**, 1763 (1969).
(54) P. Fowles, *Trans. Faraday Soc.*, **67**, 428 (1971).
(55) J. K. Thomas, K. Johnson, T. Klippert, and R. Lowers, *J. Chem. Phys.*, **48**, 1608 (1968).
(56) J. W. Fletcher, P. J. Richards, and W. A. Seddon, *Can. J. Chem.*, **48**, 1645 (1970).
(57) K. N. Jha and G. R. Freeman, *J. Chem. Phys.*, **57**, 1408 (1972).

TABLE III: Estimation of $\epsilon(\lambda_{max})$ in ROH at Different Temperatures

T, K	$10^{-3}G_{fi}\epsilon(\lambda_{max})$	G_{fi}	$10^{-3}\epsilon(\lambda_{max})$, M^{-1} cm^{-1}	
		C_2H_5OH, neutral		
161	15	1.8	8.3	
298	15	1.7	9.0	
363	15	1.6	9.4	
		C_2H_5OH, 1.5 mM KOH		9.4 ± 0.4
161	≤20	2.0	≤10.0	
298	20	2.0	10.0	
363	21	2.2	9.5	
418	22	2.3	9.6	
		CH_3OH, neutral		
176	19	1.9	10.0	
298	19	2.0	9.5	
423	19	1.9	10.0	
		CH_3OH, 1.0 mM KOH		10.2 ± 0.4
176	23	2.2	10.5	
298	23	2.2	10.5	
423	25	2.3	10.9	
		H_2O, neutral		
292	51 ± 2	2.7[a]	18.9 ± 0.6	

[a] M. Haissinski, *J. Chim. Phys.*, **62**, 1149 (1965); J. C. Russell and G. R. Freeman, *J. Chem. Phys.*, **48**, 90 (1968).

The extent of (7) was estimated by comparison with scavenging yields obtained with nitrous oxide,[52,58,59] using relative scavenging efficiencies equal to the following rate constant ratios.

$$H_{solv}^{+} + RO_{solv}^{-} \rightarrow ROH \quad (9)$$

$$e_{solv}^{-} + H_{solv}^{+} \rightarrow H \quad (10)$$

$$e_{solv}^{-} + N_2O \rightarrow N_2O_{solv}^{-} \rightarrow N_2 + \ldots \quad (11)$$

$k_9 = k_{10}$;[54] $k_{10}/k_{11} = 7.9$ in methanol at zero ionic strength μ and decreases with increasing μ in the manner described;[60] $k_{10}/k_{11} = 4.1$ in ethanol[14] at $\mu = 7 \times 10^{-4}$ and varies with ionic strength in the manner described.[57] The scavenging yields estimated in this way should be near the true values at $\mu < 0.01$, but they become progressively less certain at higher ionic strengths. The effect of ionic strength in the nonhomogeneous reaction kinetics should be similar to that in homogeneous reactions except at the highest concentrations.

The free ion yields in the neutral alcohols at 295 ± 2 K are $G_{fi} = 2.0$ in methanol[51-54] and 1.7 in ethanol,[14,54-57] within 10%. Earlier, lower estimates appear to have been obtained with impure alcohols, as described.[14,51,56,57]

Yields estimated in the above manner for the neutral alcohols and for 1.0 mM KOH in methanol and 1.5 mM KOH in ethanol, at different temperatures, are listed in Table III. Values of $G_{fi}\epsilon(\lambda_{max})$ at the same temperatures were obtained from Figure 6, extrapolating to $T > 360$ K when necessary. The resulting values of $\epsilon(\lambda_{max})$ are given in Table III. Within the experimental uncertainty the values of $\epsilon(\lambda_{max})$ are independent of temperature and of the presence or absence of 1 mM base: $\epsilon(\lambda_{max}) = (10.2 \pm 0.4)10^3$ M^{-1} cm^{-1} in methanol and $(9.4 \pm 0.4)10^3$ M^{-1} cm^{-1} in ethanol.

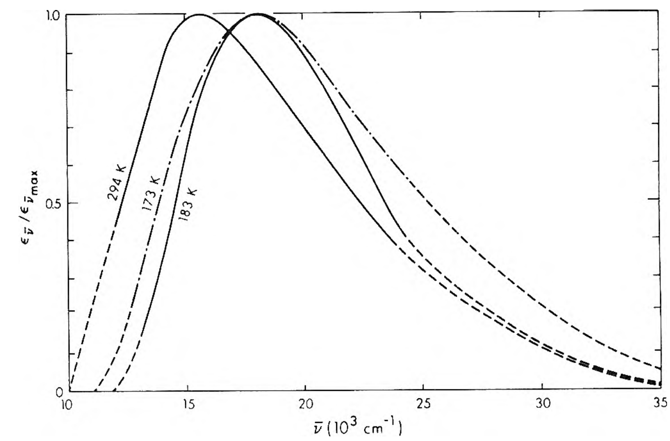

Figure 10. Plots of e_{solv}^{-} spectra to determine oscillator strengths: ——, methanol; —·—·—, ethanol. The dashed portions were estimated by making bell-shaped extrapolations of the appropriate curves in Figures 3 and 4.

The values of $\epsilon(\lambda_{max})$ derived from the other basic solutions are listed in Table II; they are independent of KOH concentration, within experimental error. Because of the uncertain kinetics in the concentrated solutions the values in Table III are preferred to those in Table II. The early estimates of $\epsilon(\lambda_{max})$, 17,000 M^{-1} cm^{-1} in methanol and 15,000 M^{-1} cm^{-1} in ethanol,[6a] were too high because low values of G_{fi} were used.

Measurements were also made with neutral water (Table III): $\epsilon(\lambda_{max}) = (18.9 \pm 0.6)\ 10^3$ M^{-1} cm^{-1}, in agreement with the previously reported 18.4×10^3 M^{-1} cm^{-1},[11] and 18.5×10^3 M^{-1} cm^{-1}.[61]

Oscillator Strength f of e_{solv}^{-}. The oscillator strength of an optical absorption band is given by[62]

$$f = 4.32 \times 10^{-9}[9n_0/(n_0^2 + 2)^2]\int \epsilon_{\bar{\nu}}\, d\bar{\nu} \quad (12)$$

where n_0 is the refractive index of the medium in which the absorber is dissolved and $\epsilon_{\bar{\nu}}$ is the molar absorbancy at wave number $\bar{\nu}$. The term in square brackets is an internal field correction; it equals unity in a low-pressure gas and 0.80 in ethanol at 173 K (Table IV). Values of n_0 were obtained from ref 63.

The e_{solv}^{-} spectra plotted on a wavelength scale are approximately bell-shaped (Figures 3 and 4 and ref 11), so the three most complete curves in Figures 3 and 4 were extrapolated to zero absorbance, then transferred onto a wave number scale (Figure 10). The oscillator strengths estimated by numerical integration under these curves are given in Table IV, along with those for electrons in water[11] and ammonia.[64] The values reported earlier[6a,64,65] were not corrected for the influence of the internal field of the solvent. When this is done and adjustment is made for the change in the values of $\epsilon(\lambda_{max})$, reasonable agreement is obtained between the new and old sets of data. The oscillator strengths appear to be

(58) J. C. Russell and G. R. Freeman, *J. Phys. Chem.*, **72**, 816 (1968).
(59) K. N. Jha and G. R. Freeman, *J. Chem. Phys.* **51**, 2846 (1969).
(60) G. V. Buxton, F. S. Dainton, and M. Hammerli, *Trans. Faraday Soc.*, **63**, 1191 (1967).
(61) E. M. Fielden and E. J. Hart, *Radiat. Res.*, **32**, 564 (1967).
(62) W. Kauzmann, "Quantum Chemistry," Academic Press, New York, N. Y., 1957, p 581.
(63) "International Critical Tables," Vol. 1 and 7, McGraw-Hill, New York, N. Y., 1930.
(64) D. F. Burow and J. J. Lagowski, *Advan. Chem. Ser.*, **No. 50**, 125 (1965).
(65) See summary of f values, uncorrected for n_0, in Table XVI of J. Jortner, *Actions Chim. Biol. Radiat.*, **14**, 7 (1970), p 64.

TABLE IV: Oscillator Strengths for the Visible Absorption Band of e_{solv}^- in ROH

Solvent	T, K	$\tilde{\nu}_{max}$, 10^3 cm^{-1}	$\epsilon(\tilde{\nu}_{max})$ 10^3 M^{-1} cm^{-1}	$\frac{9n_0}{(n_0^2+2)^2}$	f	Literature f	Literature f_{adjust}[a]
C_2H_5OH	173	18.0	9.4	0.80	0.39		
	294	14.5	9.4	0.82		0.87[6a]	0.44
CH_3OH	183	18.0	10.2	0.82	0.36		
	294	15.8	10.2	0.84	0.41	0.78[6a]	0.39
H_2O	292	13.9	18.9	0.84	0.61[b]	0.65[65]	0.65[c]
ND_3[64]	203	7.25	49.5	0.80[d]		0.77	0.62

[a] Value from the literature adjusted to the new $\epsilon(\tilde{\nu}_{max})$ and for the internal field of the solvent. [b] Estimated from the 298 K spectrum in ref 11. [c] The internal field correction (0.84) cancels the revision of $\epsilon(\lambda_{max})$ from 15,800 to 18,900 M^{-1} cm^{-1}. [d] Assuming n_0 = 1.4 at 203 K, by extrapolation from 1.33 at 289 K.[63]

lower than previously thought, especially in methanol and ethanol.

Acknowledgment. We wish to express our appreciation to M. G. Robinson for many useful discussions and for his contributions toward construction of the optical system. We wish to thank the staff of the Radiation Research Center for their aid with the electronic equipment.

Reactive and Elastic Scattering of Ions on Molecules

Arnim Henglein

Hahn-Meitner-Institut für Kernforschung, Sektor Strahlenchemie, Berlin-Wannsee, Germany *(Received May 15, 1972)*

Publication costs assisted by Hahn-Meitner-Institut für Kernforschung

Angular and energy distributions of product ions from simple ion-molecule reactions $X^+ + D_2 \rightarrow XD^+ + D$, where $X^+ = Ar^+, Kr^+$, or O_2^+, were measured. The results were discussed in terms of three collision models; *i.e.*, spectator stripping, impulsive isotropic scattering, and intermediate complex formation. The properties of protonated molecules XH^+ and of possible intermediates XH_2^+ of the ion-molecule reactions were deduced from experiments on the elastic scattering of H^+ and of H_2^+ on X. The potential curves of molecules XH^+ were obtained with high accuracy if rainbow undulations with fine structure could be observed in the differential scattering cross sections. The data from elastic scattering experiments were used to obtain potential energy level diagrams showing the important parts of the potential energy of ion-molecule reactions along the reaction coordinate. In the case of the reaction $Ar^+ + H_2 \rightarrow ArH^+ + H$, 80 to 90% of the heat of reaction is liberated as internal energy of the product ion upon the approach of the reactants, the rest appearing as translational energy upon the separation of the products. Nearly all of the heat of reaction is liberated as translational energy upon the separation of the products in the case of the reaction $Kr^+ + H_2 \rightarrow KrH^+ + H$. This reaction has an activation energy of about 0.7 eV if it is initiated by the $^2P_{3/2}$ ground state of Kr^+. In the case of the reaction $H_2^+ + H_2 \rightarrow H_3^+ + H$, an impulsive scattering mechanism is proposed at low collision energies, since no indication of a potential well for a long-lived H_4^+ intermediate could be obtained from the elastic scattering experiments.

I. Introduction

Studies on reactive and elastic scattering of ions on molecules contribute to our knowledge of the kinematics and dynamics of elementary chemical processes. This research is carried out today under the following two main aspects: (i) the description of ion-molecule reactions in terms of simple collision models which explain the observed angular and velocity distributions and total cross sections, such collision models often are similar to those developed in nuclear physics; and (ii) the *ab initio* and semiempirical calculation of potentials and of trajectories of the colliding particles. It is the purpose of the present paper to review some of the more recent results in reactive and elastic scattering and to show how a combination of both types of studies may be used in order to obtain a deeper insight into the collision mechanism of ion-molecule reactions.

II. Reactive Scattering

(A) Apparatus and Presentation of Data. In the first ex-

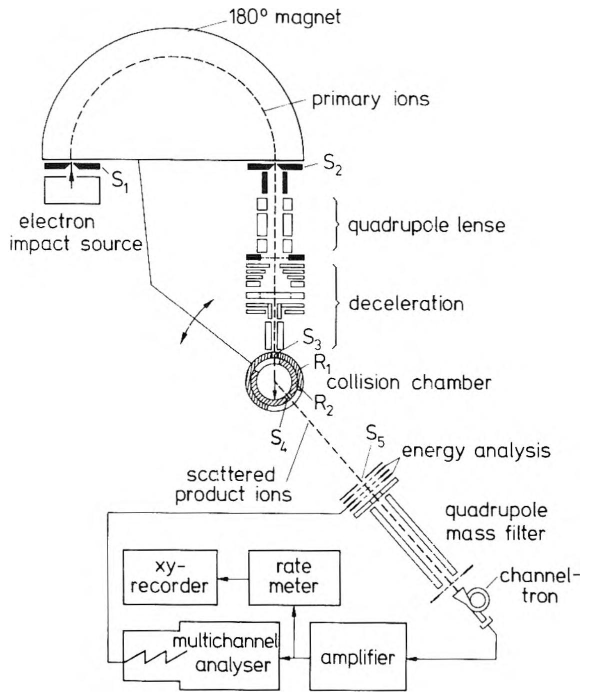

Figure 1. Schematic presentation of an apparatus for measuring energy distributions of scattered ions at different scattering angles.

periments carried out in our laboratory, simple arrangements were used to measure velocity and energy distributions of primary and secondary ions. These experiments permitted recognition of the various types of collisions such as stripping reactions, intermediate complex formation, and transitions between the two.[1] Figure 1 shows schematically a more sophisticated apparatus. The primary ions are produced by electron impact in a commercial ion source, accelerated to 200 eV and mass analyzed in a 180° magnet of 4-cm radius. After passing through the exit slit S_2, they are focussed and decelerated by a system of electrostatic lenses and enter the collision chamber through slit S_3. The collision chamber consists of two concentric tubes R_1 and R_2 each with a small hole S_3 or S_4 and a wide horizontal slit on the opposite side. R_1 is mechanically connected to the primary ion producer. While the analyzer and R_2 are in a fixed position, the ion source together with R_1 can rotate around R_2. The scattered ions enter through slit S_5 into the analyzer. Energy analysis is carried out according to the retarding potential method, mass analysis by a quadrupole mass filter, and detection by a channeltron type secondary emission multiplier. At high ion intensities, the amplified signals are integrated with a ratemeter. At low intensities, the signals are fed into a multichannel analyzer. In order to obtain the integrated energy distribution at a given scattering angle, the potential of the stopping grid of the energy analyzer is periodically modulated with a voltage that is proportional to that of the channel address.[2] The energy resolution amounts to 0.3 eV. Similar apparatuses have been described by other authors.[3-5]

The results of scattering experiments are generally presented in the form of intensity contour diagrams. Figures 2 and 3 show such diagrams. From the scattering center (which in all cases shown lies far to the left and is therefore not included in the drawings) velocity vectors of the product ion emerge in all directions characterized by the

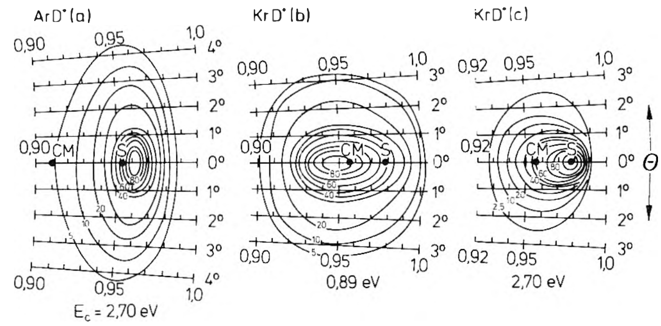

Figure 2. Intensity contour diagrams for the reactions $Ar^+ + D_2 \rightarrow ArD^+ + D$ (a) and $Kr^+ + D_2 \rightarrow KrD^+ + D$ (b and c) (E_c = center of mass collision energy).

scattering angle θ (laboratory system). The velocity of the product ion is expressed in units of v_1, the velocity of the incident ion, and $\theta = 0$ corresponds to the "forward" direction, *i.e.*, the direction of the incident ion. The tip of the velocity vector v_c that characterizes the movement of the center of mass of the system is designated by "CM." M_1 and M_2 are the masses of the incident ion and the molecule, the latter being regarded practically at rest before the collision. At a given angle of observation, product ions of various velocities are detected. Points of equal ion intensity are connected by isointensity lines in the diagrams, whereby the highest intensity is put equal to 100. If isotropic scattering occurs, the isointensity lines show symmetric behavior with respect to a plane perpendicular to v_1 and through point CM. It should also be mentioned that a discussion of center of mass data generally requires the transformation of intensities from the laboratory into the center of mass system.[6] In the following diagrams, laboratory intensities are shown, since in the reactions discussed in this paper (where $M_1 \gg M_2$) the transformation to intensities in a cm-cartesian coordination system does not lead to significant changes in the counter diagrams.

$$\frac{v_c}{v_1} = \frac{M_1}{M_1 + M_2} \tag{1}$$

(B) Examples. Figures 2 and 3 show contour diagrams for the processes $X^+ + D_2 \rightarrow XD^+ + D$ ($X^+ = Ar^+, Kr^+$, and O_2^+). Although these reactions belong to the same type, *i.e.*, D atom transfer, their collision mechanisms are quite different. According to Figure 2a, the intensity distribution of ArD^+ from the reaction

$$Ar^+ + D_2 \rightarrow ArD^+ + D \tag{2}$$

is not symmetric with respect to the CM point. It is peaking close to point "S," which is the calculated location of the tip of the velocity vector v_s, where

$$\frac{v_s}{v_1} = \frac{M_1}{M_1 + m} \tag{3}$$

(1) A. Henglein and G. A. Muccini, *Z. Naturforsch. A*, **17**, 452 (1962); **18**, 753 (1963); A. Henglein, K. Lacmann, and G. Jacobs, *Ber. Bunsenges. Phys. Chem.*, **69**, 279 (1965); A. Ding, A. Henglein, and K. Lacmann, *Z. Naturforsch. A*, **23**, 779 (1968).
(2) G. Bosse, A. Ding, and A. Henglein, *Ber. Bunsenges. Phys. Chem.*, **25**, 413 (1971).
(3) R. L. Champion, L. D. Doverspike, and T. L. Bailey, *J. Chem. Phys.*, **45**, 4377 (1966); L. D. Doverspike, R. L. Champion, and T. L. Bailey, *ibid.*, **45**, 4385 (1966).
(4) W. R. Gentry, E. A. Gislason, Y. T. Lee, B. H. Mahan, and C.-W. Tsao, *Disc. Faraday Soc.*, **44**, 137 (1967).
(5) Z. Herman, J. D. Kerstetter, T. L. Rose, and R. Wolfgang, *Rev. Sci. Instrum.*, **40**, 538 (1969).
(6) R. Wolfgang and R. J. Cross, *J. Phys. Chem.*, **73**, 743 (1969).

m being the mass of the transferred D atom. v_S is the velocity of the product ion formed in a "spectator stripping" process in which Ar^+ collides only with the picked-up D atom while no momentum is transferred to the other D atom (spectator). The lines of equal intensity are rather concentric around point S. This was explained by a small deviation from the spectator stripping model, according to which the spectator D atom receives a small recoil directed at random.[7] Since the peak around point S becomes narrower with increasing collision energy, it was concluded that this recoil is little dependent on the collision energy. This "recoil stripping" model corresponds to the DIPR model (direct interaction with product repulsion) developed by Polanyi and Kuntz.[8]

Reaction 2 is known to have cross sections at low energies which agree with those predicted by the polarization theory of ion–molecule reactions[9]

$$\sigma = \frac{2\pi e}{v_1}\left(\frac{\alpha}{\mu}\right)^{1/2} \tag{4}$$

According to this theory, the potential between the ion and the molecule at distance r is

$$P = -\frac{e^2\alpha}{2r^4} \tag{5}$$

where α is the polarizability of the molecule, e the elementary charge, and μ the reduced mass. The agreement between calculated and observed cross sections must not be taken as a proof for the long-range ion-induced dipole forces being the forces that drive the chemical reaction. These forces are only responsible for the large cross sections of spiraling collisions that lead to a close approach of the particles. The short-range chemical exchange forces that drive the reactions at close approach cannot be described by the potential of eq 5 as will be shown in part IIIB of this paper. At energies above about 5 eV(laboratory system) where eq 4 is no longer applicable and where the trajectories of the colliding particles are little bent, rather large cross sections of reaction 2 are still observed.[10] These large cross sections and the stripping behavior of reaction 2 indicate that collisions with large impact parameters predominantly contribute to the reaction. The products ArD^+ and D are formed in such collisions with rather large initial distances, *i.e.*, only small forces will exist between the products. The small recoil mentioned above may be explained this way.

Mahan and his coworkers[11] have shown that the isointensity lines of lower intensities (which are not shown in Figure 2a) are concentric around the CM point. This fact was interpreted as another contribution to the reaction which they called the "hard-sphere" contribution. It seems plausible to attribute this isotropic intensity distribution to collisions with small impact parameters in which the atoms interact strongly. The isotropic distribution in the cm system indicates that all participating atoms move after the collision with the velocity component v_C in the laboratory system. However, this must not be taken as a proof for the formation of an intermediate complex, that lives longer than the time required for one rotation and decays isotropically. A complex can only be formed if there exists a sufficiently deep potential well for the colliding particles which is not the case for reaction 2 as will be discussed in part IVB. We would rather attribute the isotropic distribution to the scattering of the particles at the steep repulsive branch of the potential which is reached in small-impact parameter collisions. This should result in a similar distribution as in the scattering of hard spheres. In a simplified manner, processes of this kind may be viewed as a collision between the incident ion and the D_2 molecule as a whole followed by the pick up of a D atom: "impulsive isotropic (or "hard-sphere") scattering."

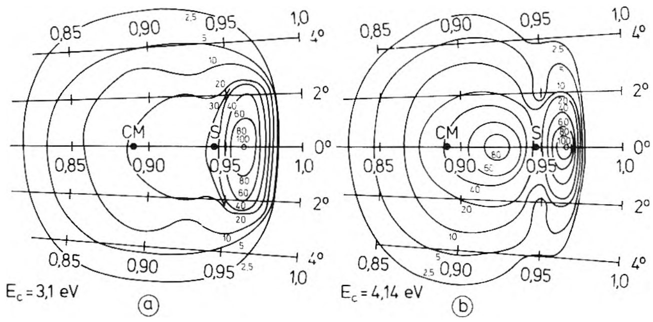

Figure 3. Intensity contour diagrams for the reaction $O_2^+ + D_2 \rightarrow O_2D^+ + D$ at two collision energies (a, 3.1 eV; b, 4.1 eV in cm system).

In an ideal stripping reaction, the translational exoergicity Q which is defined as the difference in the translational energies of the products and reactants is equal to

$$Q = -E_1\frac{m}{M_1 + m} \tag{6}$$

and the product ion carries an amount of vibrational–rotational energy of

$$U = E_1\frac{m}{M_1 + m} + W \tag{7}$$

where E_1 is the energy of the incident ion (laboratory system) and W the heat of reaction.[12] The Q value of reaction 2 was found to become increasingly negative with increasing E_1 as expected from eq 6. Only at low collision energies (<0.1 eV in cm system), were small positive values of Q observed; this indicated that a small fraction of the heat of reaction appears as translational energy of the products.[13,14] Wolfgang and his coworkers[13,15] proposed a "polarization stripping" model for reaction 2 which takes into consideration the strong bending of the trajectories in the long-range potential of eq 5 at low energies. Since most of the trajectories of the D_2 molecule (in the cm system) are bent less than 180° until the reaction occurs at close approach, the product ion receives a preferential forward component of velocity. This explains the very pronounced forward scattering which was observed for ArD^+ at low collision energies.[13-15]

Figure 2b and c show contour diagrams for the reaction

$$Kr^+ + D_2 \rightarrow KrD^+ + D \tag{8}$$

(7) A. Henglein, "Estratto da Rendiconti della Scuola Internazionale di Fisica E. Fermi," XLIV Corso Ch. Schlier, Ed., 1970, p 139.
(8) P. J. Kuntz, M. H. Mok, and J. C. Polanyi, *J. Chem. Phys.*, **50**, 4623 (1969); P. J. Kuntz, *Trans. Faraday Soc.*, **66**, 2980 (1970).
(9) G. Gioumousis and D. P. Stevenson, *J. Chem. Phys.*, **29**, 294 (1958).
(10) D. Hyatt and K. Lacmann, *Z. Naturforsch. A*, **23**, 2080 (1968).
(11) M. Chiang, E. A. Gislason, B. H. Mahan, C.-W. Tsao, and A. S. Werner, *J. Chem. Phys.*, **52**, 2698 (1970).
(12) K. Lacmann and A. Henglein, *Ber. Bunsenges. Phys. Chem.*, **69**, 286 (1965).
(13) Z. Herman, J. Kerstetter, T. Rose, and R. Wolfgang, *Disc. Faraday Soc.*, **44**, 123 (1967).
(14) A. Ding, A. Henglein, D. Hyatt, and K. Lacmann, *Z. Naturforsch. A*, **23**, 2084 (1968).
(15) P. M. Hierl, Z. Herman, and R. Wolfgang, *J. Chem. Phys.*, **53**, 660 (1970).

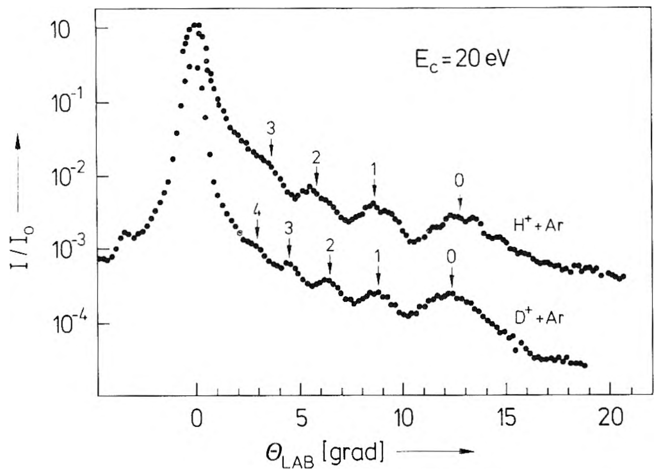

Figure 4. Differential cross section for the scattering of 20-eV protons and 20-eV deuterons on argon *vs.* the laboratory scattering angle.

at two collision energies. Reaction 8 has a cross section about ten times smaller than reaction 2. The intensity is peaking again at point S in Figure 2c which indicates a stripping contribution. However, the "hard-sphere" contribution is of greater importance which can be recognized from the somewhat lower intensity lines which are now concentric around the CM point. At the low collision energy of 0.89 eV (cm system) in Figure 2b, the peak at point S has disappeared and now lies close to the CM point. It is concluded that in reaction 8 collisions with strong repulsion between the products occur much more frequently than in reaction 2. It seems that the krypton reaction has much lower probability at large collision parameters than the argon reaction which also explains the difference in the cross sections.[16] The results from the elastic scattering experiments also point to an impulsive collision mechanism for reaction 8 (see part IVC). The appearance of a stripping contribution at higher energies may be explained by the fact that the D_2 molecule is less stiff here, *i.e.*, interaction with essentially one D atom will become possible.

Figures 3a and b give contour diagrams for the reaction

$$O_2^+ + D_2 \rightarrow O_2D^+ + D \qquad (9)$$

at two collision energies. A steep intensity peak lying beyond point S in the forward direction can be recognized in both diagrams. The low-intensity lines concentric around point CM indicate an isotropic contribution in Figure 3a. A second peak half-way between the points CM and S appears in Figure 3b. Reaction 9 can be initiated by both the ground state $^2\Pi_g$ and the first excited state $^4\Pi_u$ (3.8 eV of excess energy) of the O_2^+ ion. Both states are formed by electron impact on O_2 and therefore the reactions of both states contribute to the isointensity lines of the diagrams. In the first case, the reaction with D_2 is endothermic by 1.8 eV, in the second case exothermic by 2.0 eV.

The sharp intensity peak in the forward direction has been attributed to the reaction of the $^4\Pi_u$ state. The peak occurs, independently of the collision energy, at a point of the contour diagram which corresponds to zero translational exoergicity, *i.e.*, where the internal energy of the product ion is equal to the heat of reaction.[2] The contribution that leads to isotropic scattering in Figure 3a comes from the reaction of the ground state of O_2^+.[2,17] Since the reaction of this state is endothermic, a threshold energy of 17 eV (laboratory system) exists. Below this energy, only the reaction of the excited state occurs. The isotropic scattering has been explained by the formation of an intermediate complex $O_2D_2^+$ that lives longer than the time required for one period of rotation. With increasing collision energy, the internal energy of the complex increases and its lifetime decreases. When its lifetime becomes comparable to the time of a rotation, the dissociation products of the complex are no longer isotropically scattered but preferentially into the forward direction. This effect explains the shift of the second peak in Figure 3b from point CM to point S with increasing collision energy.[2] Such transitions from complex formation to stripping with increasing energy have been observed for many other reactions.[18]

III. Elastic Scattering

(A) Potential Functions. The ion-induced dipole potential of eq 5 can only be valid at distances larger than a few ångströms at which chemical exchange forces become important. At close approach a repulsion arises because of the interaction of the electron shells of the colliding particles. In model calculations of trajectories, the potential of eq 5 (or modifications that take into account the permanent dipole moment of the molecule) has been assumed to be applicable down to a critical distance at which the potential becomes infinitely high.[19] A more realistic 12–6–4 power potential has been proposed by Mason and Vanderslice,[20] this however, has recently been shown to give too narrow potential wells.[21–23] A modified Morse potential has most successfully been used to describe scattering effects. It may be presented in reduced units in the following form

$$U = \exp[2G_1G_2(1 - \rho)] = 2\exp[G_1G_2(1 - \rho)] \qquad (10)$$

with $G_2 = 1$ for $\rho < 1$ and $G_2 \neq 1$ for $\rho \geq 1$. $U = V/\epsilon$ is the absolute potential V divided by the minimum potential ϵ at distance r_m. $\rho = r/r_m$ is the reduced distance of the particles. G_1 and G_1 are parameters that determine the width of the potential well. This potential function has the advantage of varying the attractive part ($\rho > 1$) of the potential without changing the repulsive part and *vice versa*. For example, if the product G_1G_2 is kept constant, the attractive part remains constant while the repulsive part can be varied by using different values of G_1. With increasing G_1 and G_2 the potential well becomes narrower.[21] This potential function is useful for distances below a few ångström where potentials of eq 5 fail. It is the purpose of scattering experiments to determine the parameters ϵ, r_m, G_1, and G_1. High precision in the determina-

(16) G. Bosse, A. Ding, and A. Henglein, *Z. Naturforsch. A*, **26**, 932 (1971).
(17) E. A. Gislason, B. H. Mahan, C.-W. Tsao, and A. S. Werner, *J. Chem. Phys.*, **50**, 142 (1969).
(18) A. Ding, A. Henglein, D. Hyatt, and K. Lacmann, *Z. Naturforsch. A*, **23**, 2090 (1968); A. Henglein, *J. Chem. Phys.*, **53**, 458 (1970); A. Ding, *Z. Naturforsch. A*, **24**, 856 (1969).
(19) J. V. Dugan and J. L. Magee, "Chemical Dynamics," Hirschfelder, Ed., Wiley, New York, N. Y., 1971, p 207.
(20) E. A. Mason and J. T. Vanderslice, *J. Chem. Phys.*, **31**, 594 (1959).
(21) H.-U. Mittmann, H.-P. Weise, A. Ding, and A. Henglein, *Z. Naturforsch. A*, **26**, 1112 (1971).
(22) H.-P. Weise, H.-U. Mittmann, A. Ding, and A. Henglein, *Z. Naturforsch. A*, **26**, 1122 (1971).
(23) H.-U. Mittmann, H.-P. Weise, A. Ding, and A. Henglein, *Z. Naturforsch. A*, **26**, 1282 (1971).

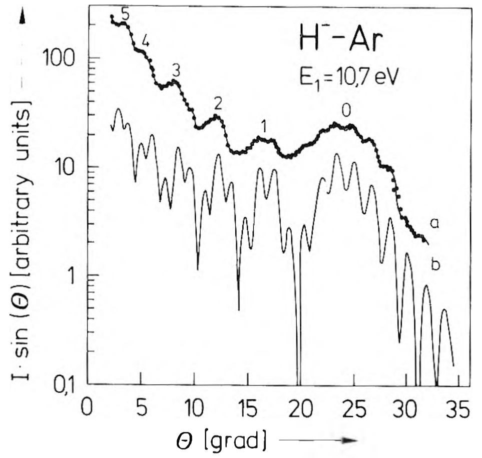

Figure 5. Comparison of measured (a) and calculated (b) differential cross sections for the scattering of 10.7-eV protons on argon.

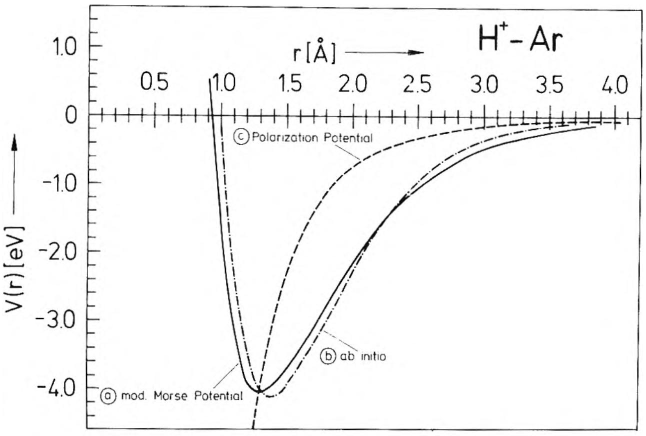

Figure 6. (a) Best potential for H+Ar according to eq 10; (b) potential of *ab initio* calculations,[29] (c) polarization potential according to eq 5.

tion can be reached if wavemechanical effects, the supernumerary rainbows with fine structure, are observed.

(B) Rainbow Effects in Atomic Systems. The apparatus used for elastic scattering experiments had an angular resolution of 0.5 to 1°. The experimental details have already been described. In order to obtain a small scattering center, the neutral target consisted of a beam of gas molecules intersecting the primary ion beam at right angles.[21,24]

Figure 4 shows the measured differential cross section for the elastic scattering of protons and deuterons on argon as function of the scattering angle (laboratory system). Several maxima can be recognized. The arrows pointing downward designate the rainbow maxima, the "primary" rainbow being designated by "O." The figures on the other maxima designate the first, second, and so on "secondary" rainbows. The distance between two secondary rainbows is $\sqrt{2}$ times smaller for D^+ than for H^+, since the wave number of a D^+ ion is correspondingly larger than for an H^+ ion at the same kinetic energy. The arrows pointing upward show the minima of the superimposed fine structure which is best resolved in the surroundings of the primary rainbow. With decreasing energy of the incident ion the rainbows appear at larger angles and additional secondary rainbows appear at small angles. The primary rainbow in the H^+–Ar system had already been detected by Bailey and coworkers.[25] Secondary rainbows have also been found by Champion, *et al.*[26]

Rainbow effects can in principle always be expected if the potential between two particles consists of an attractive portion at long and a repulsive portion at short distances and if the cm-collision energy is sufficiently high (generally more than twice the potential depth ϵ). Under these conditions, particles with different collision parameters and therefore with trajectories that have different values of closest approach during the collision can still experience the same measured scattering angle.[27] Or expressed in terms of wave mechanics, the detector at a given angle records the result of the interference of different "partial waves." According to the partial wave method the differential cross section for scattering into a center of mass angle between θ and $\theta + d\theta$ is equal to

$$I(\theta) = |f(\theta)|^2 \quad (11)$$

where $f(\theta)$ is the scattering amplitude

$$f(\theta) = \frac{1}{2ik}\sum_{l=0}^{\infty}(2l+1)\,\exp(2i\eta_l) - 1)P_l(\cos\theta) \quad (12)$$

k being the wave number of the incident particle and P_l the lth Legendre polynomial. The scattering phase is given by the JWKB approximation as

$$\eta_l = kr_m\left\{\int_{\rho_0}^{\infty}\left(1 - \frac{U(\rho)\epsilon}{E_c} - \frac{\beta_l^2}{\rho^2}\right)^{1/2} d\rho - \int_{\beta_l}^{\infty}\left(1 - \frac{\beta_l^2}{\rho^2}\right)^{1/2} d\rho\right\} \quad (13)$$

$U(\rho)$ being the reduced potential function, E_c the collision energy (cm system), and ρ_0 the distance of closest approach at a reduced collision parameter β_l($\beta = b/r_m$; b = impact parameter). It can readily be shown that angular momentum quantum numbers l up to about 10^3 must practically be taken into account in forming the sum of eq 12. $I(\theta)$ may be obtained by substituting the potential function of eq 10 into eq 13 and solving eq 12 and 13 with a computer. After changing the various parameters that determine the potential function the computation is repeated until the theoretically obtained $I(\theta)$ curve agrees with the experimentally obtained curve within the error of the measurements. A simple procedure has been devised which allows one to change the parameters of the potential function in a systematic way and attain the best values after only a few steps of iteration.[21] Rich, *et al.*,[28] have recently developed an inversion procedure for obtaining the potential function which is not tied to an assumed functional form of the potential. Their results which strongly differ from their earlier ones[26] are in good agreement with our results in all cases where they were able to detect the fine oscillations in the differential cross section.

Figure 5 shows the measured and calculated differential cross sections for the scattering of protons on argon at 10.7 eV. Curve a in Figure 6 shows the potential function used in this calculation. The best parameters were G_1 = 2.50, G_2 = 0.86, ϵ = 4.04 eV, and r_m = 1.31 Å. Curve b in Figure 6 is the potential from *ab initio* calculations by Roach

(24) H.-P. Weise, H.-U. Mittmann, A. Ding, and A. Henglein, *Z. Naturforsch. A*, **25**, 1154 (1970).
(25) F. A. Herrero, E. M. Nemeth, and T. L. Bailey, *J. Chem. Phys.*, **50**, 4591 (1969).
(26) R. L. Champion, L. D. Doverspike, W. G. Rich, and S. M. Bobbio, *Phys. Rev. A*, **2**, 2327 (1970).
(27) K. W. Ford and J. A. Wheeler, *Ann. Phys.*, **7**, 259 (1959).
(28) W. G. Rich, S. M. Bobbio, R. L. Champion, and L. D. Doverspike, *Phys. Rev. A*, **4**, 2253 (1971).

TABLE I: Potential Parameters of Protonated Noble Gases and of He_2^+ as Deduced from Elastic Scattering Experiments

System	ϵ, eV	r_m, A	G_1	G_2	van der Waals radius of noble gas, Å	Isoelectronic molecules	r_m, Å
H^+–He	2.00	0.77	2.20	0.85	1.1	H–H	0.74
H^+–Ne	2.28	0.99	2.68	0.85	1.5	H–F	0.92
H^+–Ar	4.04	1.31	2.50	0.86	1.9	H–Cl	1.27
H^+–Kr	4.45	1.47	2.50	0.80	2.0	H–Br	1.41
H^+–Xe	6.75	1.74	3.80[a]	1.08	2.2	H–I	1.60
He^+–He	2.55	1.05	2.35	0.90			

[a] This rather large G_1 value indicates a distortion probably due to charge exchange between H^+ and Xe.[25]

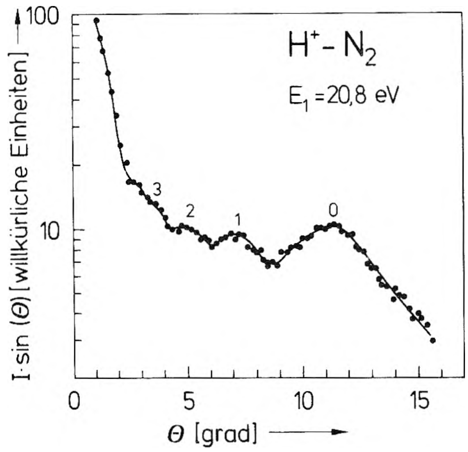

Figure 7. Differential cross section for the scattering of 20.8-eV protons on N_2 *vs.* laboratory scattering angle.

and Kuntz.[29] Finally, curve c shows the polarization potential according to eq 5. It clearly does not describe the interaction between H^+ and Ar at reduced distances $\rho < 2.5$ (at larger distances, rainbow scattering experiments do not yield reliable information).

The potential function of eq 10 was also found to be useful for describing the scattering of protons on other noble gases are slightly higher than those of the isoelectronic molecules. The following relationship between the r_m ters G_1 and G_2. The van der Waals radii r_w of the noble gases and the r_m values of the isoelectronic neutral hydrides are also shown. The r_m values of the protonated noble gases are slightly higher than those of the isoelectronic molecules. The following relationship between the r_m value of protonated noble gases and the van der Waals radius r_w is true to within 10%

$$r_m = 0.72 r_w \qquad (14)$$

This indicates that the proton penetrates rather deeply into the electron shell upon formation of a protonated molecule. The dissociation energy of the protonated molecule is equal to the potential depth ϵ minus the zero point energy $h\nu/2$ which amounts to 0.15–0.20 eV for the cases of Table I. $D(Ar-H^+)$, for example, is calculated as 3.84 eV. Using the known difference in ionization potentials of Ar and H, $D(Ar^+-H)$ is obtained as 6.0 eV. The heat of reaction of the ion–molecule reaction 2 is obtained as 1.5 eV, since the bond strength of hydrogen is 4.5 eV. The heat of the reaction $H_2^+ + Ar \rightarrow ArH^+ + H$ is calculated as 1.2 eV. It can similarly be derived that reaction 8 is exothermic with 0.20 or 0.86 eV depending on whether Kr^+ initiates the reaction in its $^2P_{3/2}$ or $^2P_{1/2}$ ground state.[22,23]

(C) Rainbow Effects in Polyatomic Systems. In the elastic scattering of polyatomic ions such as H_2^+ on atoms or of monoatomic ions such as H^+ on polyatomic targets, rainbow effects can often be observed. However, the anisotropy in the potential that is expected from the different molecular orientations during the collisions as well as inelastic processes that lead to vibrational excitation of the polyatomic collision partner make the rainbow maxima less pronounced. As has been calculated by Cross,[30] the supernumerary rainbows and the fine oscillations are easily quenched by anisotropy in the potential while the primary rainbow is only slightly affected. In those cases, in which secondary rainbows are observed, the anisotropy in the potential may therefore be assumed to be not too large. A number of such cases has been observed.[23] However, the superimposed fine structure has always been found to be completely washed out. Calculation of the potential depth ϵ can still be carried out even if only the primary rainbow is observed, although the result is less accurate than in the atomic cases described above.[23]

Figure 7 shows the differential cross section as function of the scattering angle for the elastic scattering of H^+ on N_2. The primary and three secondary rainbows can be recognized. A proton affinity of the nitrogen molecule of 4.0 eV was calculated from the scattering data. Using this value, the heats of reaction of the well-known ion–molecule reactions $N_2^+ + H_2 \rightarrow N_2H^+ + H$ and $H_2^+ + N_2 \rightarrow N_2H^+ + H$ are obtained as 1.4 and 1.3 eV, respectively. Proton affinities for other molecules have also been reported.[23]

In the scattering of H_2^+ on various gases X, a broad primary rainbow and in some cases additional secondary rainbows were found. Values of $\epsilon(X-H_2^+)$ could be calculated within an accuracy of 10–20%.[23] Table II[31] shows the ϵ values obtained this way as well as calculated dissociation energies $D(X^+-H_2)$. The latter are positive with the exception of $D(Kr^+(^2P_{3/2})-H_2)$. The negative value obtained here means an activation energy for the formation of the KrH_2^+ configuration from $Kr^+(^2P_{3/2})$ and H_2.

IV. Discussion

(A) Potential Energy Levels of Ion–Molecule Reactions. The results from the experiments on the elastic scattering of H^+ and of H_2^+ on various atoms and molecules X are compiled in Figures 8a–d in the form of potential energy level diagrams. Since secondary rainbows are observed in the scattering of H_2^+, it is concluded that the anisotropy of the $X-H_2^+$ potential is not very pronounced and there-

(29) A. C. Roach and P. J. Kuntz, *Chem. Commun.*, 1336 (1970).
(30) R. J. Cross, *J. Chem. Phys.*, **52**, 5703 (1970).
(31) H.-P. Weise and H.-U. Mittmann, private communication.

TABLE II: $\epsilon(X-H_2^+)$ Values from Elastic Scattering Experiments of H_2^+ on Various Gases X and Calculated[a] Dissociation Energies $D(X^+-H_2)$[b]

Molecule X	$\epsilon(X-H_2^+)$, eV	$D(X^+-H_2)$, eV	$\Sigma_i(h\nu_i/2)$, eV
Ar[c]	1.3	1.3	0.3
Kr[c] $^2P_{3/2}$	1.1	−0.7	0.3
Kr[c] $^2P_{1/2}$	1.1	0.1	0.3
N_2[d]	1.1	0.9	0.3
H_2[d]	1.5	0.8	0.7

[a] $D(X^+ - H_2) = \epsilon(X - H_2^+) - \Sigma_i(h\nu_i/2) + I(X) - I(H_2)$ (I = ionization energy). [b] The estimated zero point energies $\Sigma_i(h\nu_i/2)$ of XH_2^+ used in the calculations are also given. [c] Reference 23. [d] Reference 31.

fore $D(X^+-H_2)$ in Table II is rather close to the dissociation energy of the XH_2^+ configuration of lowest potential energy reached during ion–molecule reactions of the types $H_2^+ + X \rightarrow XH^+ + H$ and $X^+ + H_2 \rightarrow XH^+ + H$. The diagrams of Figure 8 contain on the left-hand side the levels of the reactants, on the right-hand side those of the products and in the middle the level of the intermediate XH_2^+ configuration. The levels given by dashed lines were not derived from scattering data but from mass spectroscopic appearance potential measurements or theoretical calculations. The diagrams thus give information about important parts of the potential energy of the reacting systems along the reaction coordinate.

(B) The Reaction $Ar^+ + H_2 \rightarrow ArH^+ + H$. As can be seen from Figure 8a, the potential energy surface of the reaction $Ar^+ + H_2$ is strongly attractive, the energy level of ArH_2^+ lying only a little higher than that of $ArH^+ + H$. ArH_2^+ is therefore unstable with respect to its decay into $ArH^+ + H$. Since there is no potential well for ArH_2^+ and since ArH_2^+ has only a few internal degrees of freedom, its lifetime is probably much shorter than the time required for one rotation, which makes the observed impulsive mechanism of the $Ar^+ + H_2$ reaction understandable. It is expected from the attractive potential of Figure 8a that 80–90% of the heat of reaction is liberated as internal energy of the product ion during the approach of the reactants and that only 10–20% appears as translational energy of the products. This is in good agreement with the experimental findings at low collision energies.[13-15]

A comparison may now be made with the polarization–stripping model proposed by Wolfgang and coworkers.[13,15] According to this model, the long-range ion-induced dipole forces between the reactants and the products control the kinematics of the reaction at low collision energies. It is assumed that the reactants approach until stripping takes place at the distance $r_c = r(ArH^+) + 0.5r(H_2)$ where the r's are the equilibrium distances of the corresponding molecules. The potential energy at this point is $P = -e^2\alpha_{H_2}/2r_c^4$. Immediately afterwards, the ion-induced dipole potential between the products is $P' = -e^2\alpha_H/2r'_c{}^4$ where $r'_c = r(ArH^+) + r(H_2)$. Taking $r(H_2) = 0.74$ Å and $r(ArH^+) = 1.32$ Å, one calculates $r_c = 1.69$ Å and $r'_c = 2.06$ Å. Using $\alpha_{H_2} = 0.93 \times 10^{-24}$ cm^3, P is calculated as -0.84 eV and $P' = -0.2$ eV. Since the potential energy is -1.5 eV with respect to the reactants at large distances between the products, the potential energy according to the polarization–stripping model must suddenly drop from -0.84 to -1.7 eV during stripping. Such a potential jump seems highly unplausible. It apparently arises in the model because of the assumption made that the behavior of the system can correctly be described by the polarization potential of eq 5 even at distances smaller than 2–3 Å where the chemical forces become important. This assumption is by no means justified. We do, however, agree with Wolfgang that the mechanism of collision is still impulsive even at thermal energies and that the strong forward scattering observed here has to be explained by the strong bending of the trajectory of the H_2 molecule as already mentioned in part IIB.

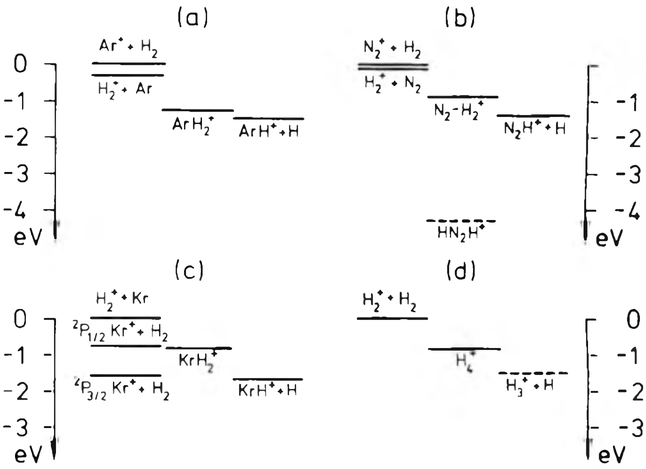

Figure 8. Energy levels from scattering data (solid lines) and other data (dashed lines) for various ion–molecule reactions of the types $X^+ + H_2 \rightarrow XH^+ + H$ and $H_2^+ + X \rightarrow XH^+ + H$.

(C) The Reactions of N_2^+, Kr^+, and H_2^+ with H_2. A similar energy level diagram is shown by Figure 8b for the $N_2^+ + H_2$ reaction. However, a somewhat larger fraction of the heat of reaction might be expected to appear as translational energy of the products than in the $Ar^+ + H_2$ reaction. This is in agreement with the experimental observations according to which the angular and velocity distributions of N_2H^+ are broader than those of ArH^+. $N_2H_2^+ + H_2$ are formed by electron impact on hydrazine at 11.9 eV; $N_2H^+ + H_2 + H$ are produced from hydrazine at 14.8 eV.[32] A configuration of $N_2H_2^+$ must therefore exist which has 2.9-eV less energy than $N_2H^+ + H$. Since stripping was observed for the reaction $N_2^+ + H_2 \rightarrow N_2H^+ + H$ even at small collision energies,[4,13,14,33,34] it is concluded that the reaction does not proceed through that low-energy configuration. Otherwise, the system would go through a deep potential well along the reaction coordinate and the formation of an intermediate long-lived complex that isotropically decays would be probable. The reaction apparently proceeds on a part of the potential hypersurface far away from the potential hole. Probably, the low-energy configuration corresponds to $H-N-N-H^+$ while the reaction goes through $N-N-H_2^+$.

The energy level diagram of Figure 8c for the $Kr^+ + H_2$ reaction looks quite different. Nearly all of the heat of reaction is liberated upon the separation of the products. In the case of the reaction of the lower ground state $^2P_{3/2}$ of Kr^+, a threshold of 0.6 eV exists which is in agreement with calculations of Kuntz.[35] (In a diagram given earlier,

(32) V. H. Dibeler, J. L. Franklin, and R. M. Reese, *J. Amer. Chem. Soc.*, **81**, 68 (1959).
(33) K. Lacmann and A. Henglein, *Ber. Bunsenges. Phys. Chem.*, **69**, 292 (1965).
(34) W. R. Gentry, E. A. Gislason, B. H. Mahan, and C.-W. Tsao, *J. Chem. Phys.*, **49**, 3058 (1968).
(35) P. J. Kuntz and A. C. Roach, *J. Chem. Soc., Faraday Trans. 2*, **68**, 259 (1972).

the zero point energy of KrH_2^+ was not taken into consideration and therefore a lower value of 0.33 eV of the threshold was given.)[23]

The diagram of Figure 8d shows that H_4^+ is unstable with respect to its decay into $H_3^+ + H$. The H_4^+ level lies half-way between the levels of the reactants and products. At high energies, the reaction $H_2^+ + H_2 \rightarrow H_3^+ + H$ shows stripping behavior. At low energies, the H_3^+ intensity is peaking around the CM point in the contour diagram which is explained by intermediate complex formation.[36-38] However, since there is no potential well for H_4^+ according to Figure 8d, we would rather explain the observed symmetry of product intensity around the CM point by the impulsive isotropic scattering model as in the case of the $Kr^+ + H_2$ reaction. (The level of $H_3^+ + H$ in Figure 8d was calculated assuming a proton affinity of H_2 of 4.1 eV, since $\epsilon(H_2\text{-}H^+)$ from *ab initio* calculations is 4.56 eV[39,40] and the zero point energy of H_3^+ is about 0.5 eV.)

(36) J. Durup and M. Durup, *J. Chim. Phys.*, **64**, 386 (1967).
(37) M. T. Bowers, D. D. Elleman, and J. King, *J. Chem. Phys.*, **50**, 4787 (1969).
(38) L. D. Doverspike and R. L. Champion, *J. Chem. Phys.*, **46**, 4718 (1967).
(39) W. Kutzelnigg, R. Ahlrichs, I. Labib-Iskander, and W. A. Bingel, *Chem. Phys. Lett.*, **49**, 4965 (1967).
(40) I. G. Csizmadia, R. E. Kari, J. C. Polanyi, A. C. Roach, and M. A. Robb, *J. Chem. Phys.*, **52**, 6205 (1970).

Hot Electron Injection into Dense Methane, Carbon Monoxide, and Carbon Dioxide[1]

P. Smejtek and M. Silver*

Department of Physics, University of North Carolina, Chapel Hill, North Carolina 27514 *(Received May 19, 1972)*

Publication costs assisted by the University of North Carolina

We have been studying injection currents in order to understand the electronic transport properties in liquids and dense gases. In particular we use tunnel cathodes to inject hot electrons into CH_4, CO, and CO_2 We have measured the current *vs.* voltage characteristics for various densities. In order to analyze our data we use a simple model for injection. From this model we can estimate the cross section for momentum exchange scattering and the energy relaxation time of the hot electrons. The density dependence of these parameters and their implication are discussed.

Introduction

Despite the recent excellent research using drift techniques,[2] the nature of the quasi-free electron in liquids remains obscure. Part of the difficulty is that we do not know the energy of the conducting state nor what cross section to use for momentum exchange scattering. In order to look into these questions we have been injecting electrons into dense gases. As will be seen, from such experiments one can determine the diffusion cross section and the lifetime of the injected hot electrons as a function of density. Since the relevant cross sections are known at low densities, we can see what density dependent changes take place as one approaches liquid densities. Assuming no change in the scattering length, density can be expected to affect the cross sections through multiple scattering[3] and through atom-atom correlation.[4] The problem might be further complicated since the scattering length will likely be altered by the presence of near neighbors.

In this paper we will show some preliminary experimental results which indicate that none of the simple models mentioned above is adequate. Basically, the experiment consists of injecting hot electrons into the media and measuring the current as a function of applied electric field. In order to interpret such experiments one adopts a model. We have chosen a simple model in order to minimize computational difficulty in the analysis of our data. In the absence of more sophisticated theoretical guidance, we believe that this is a viable approach recognizing that this may lead to controversy regarding the approximations and errors (which for our experimental conditions we estimate to be less than 50% from more exact calculations) in our derived parameters.

Figure 1 shows a schematic representation of what may happen to an electron injected into a dense medium from a metallic electrode. The entering electron may be back scattered into the electrode (process 1). In such an event this electron does not contribute to the current. The electron may undergo several momentum exchange scatterings and then give up part of its kinetic energy by exciting vibrations or rotations of a host molecule. This may occur closer or further from the electrode than the position of the maximum in the potential. In the former case the electron has a barrier to overcome in order to be collected by the anode while in the latter the electron has a barrier to overcome in order to be returned to the cathode. These two possibilities are depicted by process 2 and 3 in Figure 1.

Model for Injection

In our model we assume that every electron undergoes many scattering events before it is either collected or ther-

(1) Supported by the Army Research Office.
(2) H. S. W. Massey, E. H. S. Burhop, and H. B. Gilbody, "Electronic and Ionic Impact Phenomena," Oxford University Press, London, 1969; D. E. Golden, N. F. Lane, A. Temkin, and E. Gerjuoy, *Rev. Mod. Phys.*, **43**, 642 (1971).
(3) W. Legler, *Phys. Lett. A.*, **31**, 129 (1970).
(4) M. H. Cohen and J. Lekner, *Phys. Rev.*, **158**, 305 (1967).

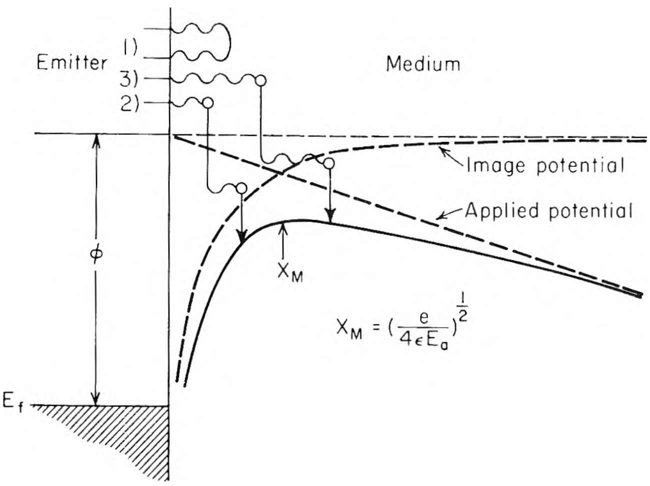

Figure 1. Schematic representation of the injection process.

malized. If the electron is thermalized we assume that it undergoes many scattering events before it is collected either by the anode or cathode as the case may be. In this case the electron motion can be evaluated from the continuity of current equation

$$\nabla j = 0 \tag{1}$$

Because energy relaxation in these systems is expected to be very fast, we make our first approximation and that is that we are dealing with a two-state system; the hot electron state where the total energy of the electrons is essentially constant and is equal to some average energy the electrons have before thermalization, and the thermalized electron state where the electron has a kinetic energy equal to $3kT/2$. The thermalized electrons are produced only through the energy relaxation of the hot electrons. Our second approximation is that the energy relaxation can be characterized with a single characteristic time τ. With these two approximations eq 1 may be written as a system of two coupled equations

$$-\nabla j_h - n_h/\tau = 0 \tag{2}$$

$$-\nabla j_t + n_h/\tau = 0 \tag{3}$$

where the subscript h stands for hot and the subscript t stands for thermalized, and n is the density of carriers. Equations 2 and 3 follow from eq 1 because

$$j = j_h + j_t \tag{4}$$

and

$$\frac{dn_h}{dt} = -\frac{dn_t}{dt} = -\frac{n_h}{\tau} \tag{5}$$

The expressions for the respective currents j_h and j_t are

$$j_h = -D_h\frac{\partial n_h}{\partial x} + n_h\mu_h E(x) \tag{6}$$

$$j_t = -D_t\frac{\partial n_t}{\partial x} + n_t\mu_t E(x) \tag{7}$$

where the D and μ are the diffusion coefficients and the mobilities, respectively, $E(x) = E_a - e/4\epsilon x^2$ is the position-dependent electric field, and E_a is the applied voltage divided by the electrode spacing.

To further simplify the problem we assume that the diffusive motion of the hot electrons starts after the first mean free path, λ, and that λ is large enough so that the contribution of the image potential energy to the total energy of the hot electron may be neglected. This is the case if the energy of the hot electrons is 1 eV or more and if λ is greater than 10 Å (these conditions are generally met in our experiments). We have made more exact calculations and the errors introduced due to our approximations are less than 60% if the energy is 0.3 eV and electron mfp 5 Å. For the case of electrons having an energy of about 1 eV, the field driven motion is small compared with the diffusive motion and further D_h can be considered to be approximately constant, independent of position. The current of hot electrons is

$$j_h \simeq -D_h\partial n_h/\partial x \tag{8}$$

One final set of approximations is made and these are related to the boundary conditions. The boundary conditions for the hot electrons is given in terms of the current balance

$$j_0 = n_h(\lambda)v(\lambda)/4 + \int_\lambda^\infty n_h(x)\mathrm{d}x/\tau \tag{9}$$

where j_0 is the current available from the emitter, $n_h(\lambda)$ is the density of hot electrons at $x = \lambda$, and $v(\lambda) = [(2\epsilon_0/m)[1 + eE_a\lambda/\epsilon_0 + (e^2/4\epsilon\lambda\epsilon_0)]]^{1/2}$, where ϵ_0 is the average kinetic energy of the hot electrons measured above the barrier maximum at $x = x_m$. The boundary condition for the density of thermalized electrons is that n_t is finite everywhere, including at the electrodes.

With these boundary conditions one can solve for the total current j collected by the anode and this is

$$j = \frac{j_0}{1 + v(\lambda)\gamma\tau/4}\,\frac{\int_0^\infty \exp\left\{-\left[Z + \left(\frac{k\rho}{Z + \rho\lambda} + \frac{\gamma Z}{\rho}\right)\right]\right\}\mathrm{d}Z}{\int_0^\infty \exp\left\{-\left[Z + \frac{k\rho}{Z + \rho\lambda}\right]\right\}\mathrm{d}Z} \tag{10}$$

where

$$\gamma = 1/x_0 = (D_h\tau)^{-1/2} \text{ for } x_0 \leq x_m \tag{11}$$

$$\gamma = -\frac{\mu_h E_a}{2D_h} + \left[\frac{\mu_h E_a^2}{2D_h} + \frac{1}{x_0^2}\right]^{1/2} \text{ for } x_0 > x_m \tag{12}$$

The other parameters are $\rho = \mu_t E_a/D_t$ and $\kappa = e\mu_t/4\epsilon D_t$. There are two independent parameters at each density which determine the current and these are the thermalization time τ and momentum exchange scattering cross section σ_p which is defined as $1/N\lambda$ where N is the number density of the medium. They are obtained by comparing the experimental data with the predictions of the model. A typical fit between the experimentally observed current voltage characteristics and that obtained from our theoretical model is shown in Figure 2. A small computer was used to make a least-squares fit to our data to obtain the values for τ and σ_p. Considering the approximations, the fit is good and the low density values for σ_p and τ agree with other experiments.[2]

Experimental Results

As a source of electrons we use a tunnel cathode.[5] We have previously reported[6] results using these electrodes in helium, liquid argon, and cyclohexane as well as other liquids and gases. The gases used were obtained commercially and the impurity level was in CO_2, 50 ppm, in CH_4, 100 ppm, and in CO, 1000 ppm. The electronics and the experimental set up is shown in Figure 3. There are two independent circuits. One of the circuits is used for the operation of the electron emitter. This circuit consists of a power supply with a potentiometer to bias the Al–Al_2O_3–Au diode, a

(5) R. M. Handy, *J. Appl. Phys.*, 37, 4620 (1966).
(6) D. G. Onn and M. Silver, *Phys. Rev. A*, **3**, 1773 (1971); M. Silver, P. Kumbhare, P. Smejtek, and D. G. Onn, *J. Chem. Phys.*, **52**, 5195 (1970); M. Silver, D. G. Onn, and P. Smejtek, *J. Appl. Phys.*, **40**, 2222 (1969); P. Smejtek, M. Silver, and D. G. Onn, *J. Chem. Phys.*, in press.

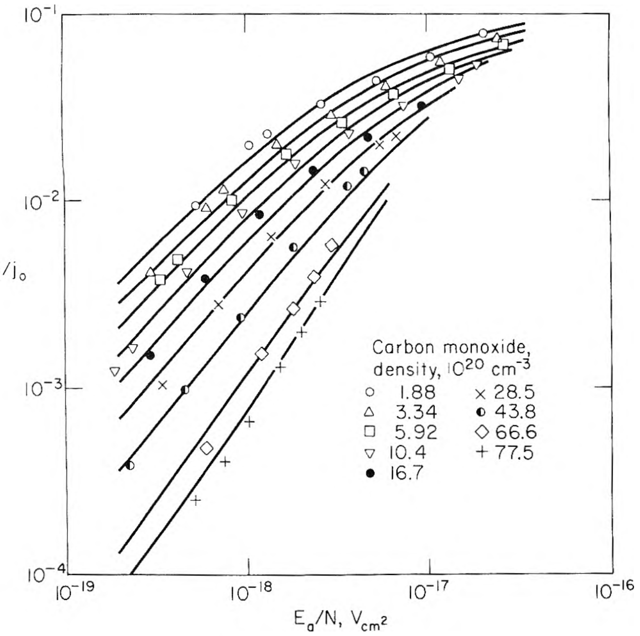

Figure 2. Comparison between theory and experiment for the current *vs.* E_a/N in CO_2. Solid lines are theory and points are the experimental results. In order to obtain the agreement shown, it was necessary to make the thermalization time and the cross section density dependent (these dependences are depicted in Figures 5 and 6).

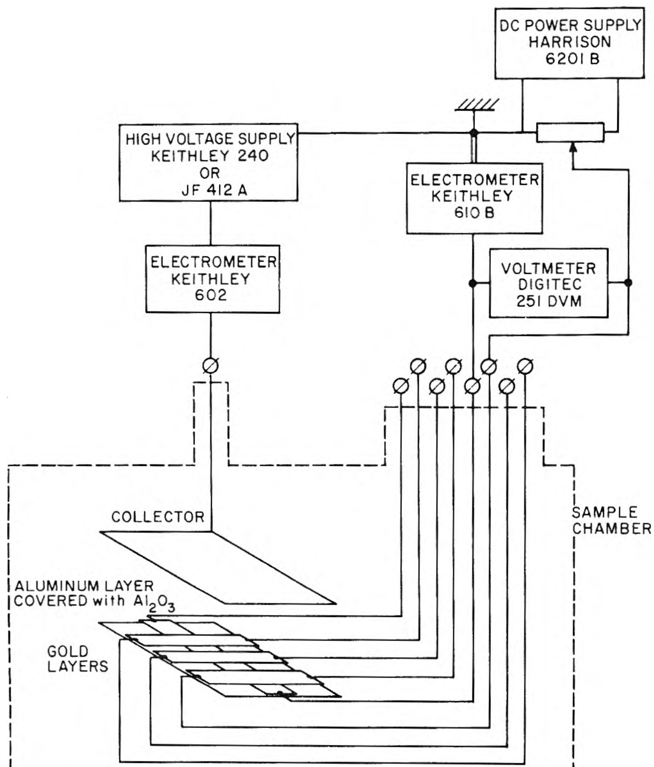

Figure 3. Schematic diagram of the experimental setup and electronics.

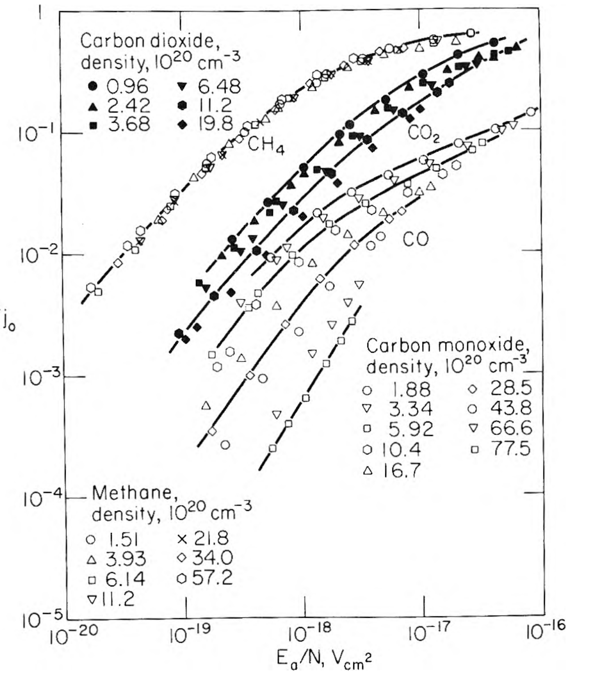

Figure 4. Experimental current-voltage characteristics in methane (T = 200°K), carbon dioxide (T = 318°K), and carbon monoxide (T = 160°K). j is the current collected in gas, j_0 is the emitter current measured in vacuum, and E_a/N is the ratio of the applied electric field and gas density. No theoretical comparison is shown.

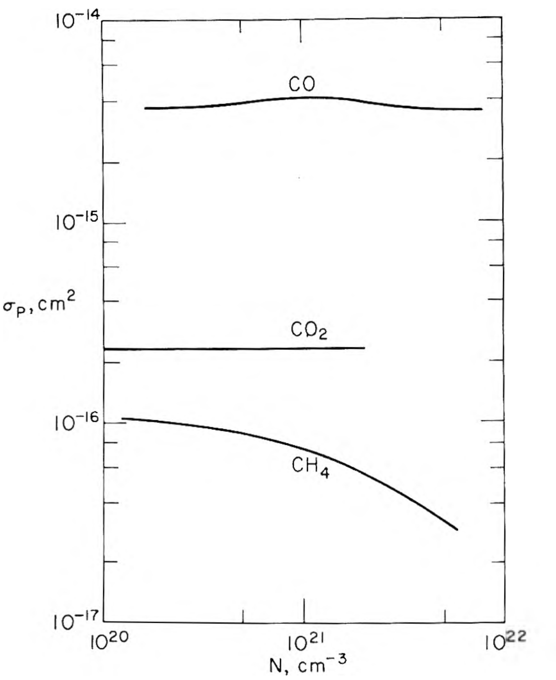

Figure 5. Momentum exchange scattering cross section *vs.* density as derived from theory using the experimental data shown in Figure 4.

Keithley 610B electrometer, and a digital voltmeter to monitor the diode film current and bias voltage. The electron emitter is operated under conditions which ensure a long lifetime and stability of the emitted current.[7] The second circuit is used for the measurement of the injected current (electrometer Keithley 602) as a function of the electric field applied between collector and emitter (gold layer).

The current is plotted *vs.* the ratio of the applied field to the gas density. Our experimental results for the electron injection into methane, carbon dioxide, and carbon monoxide are shown in Figure 4. The drop of the current with density for a given E/N indicates the loss of injected hot electrons due to their thermalization within the range of the image barrier. This decrease of the current with density is

(7) D. G. Onn, P. Smejtek, and M. Silver, to be submitted for publication.

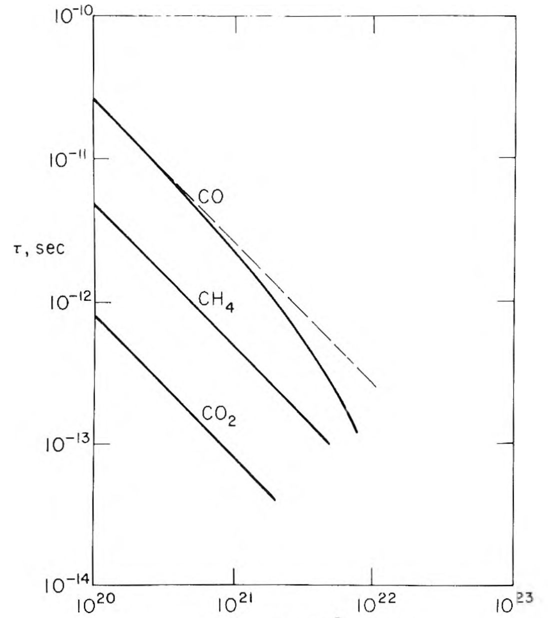

Figure 6. Thermalization time *vs.* density as derived from theory using the experimental data shown in Figure 4. The thermalization distance x_0 can be estimated from eq 11 assuming the average kinetic energy of injected electrons to be 1 eV.

clearly seen in CO and CO_2. In methane, however, we do not find that the current voltage characteristics drop as in CO and CO_2. Rather, the current *vs.* E/N is independent of density. This suggests that the thermalization is occurring well beyond the range of the image potential.

Using these data we have calculated the density dependence of the cross section for the momentum exchange scattering σ_p and the lifetime τ. These are shown in Figure 5 and 6, respectively.

Discussion

The experimental results presented are in accord with our simple model for injection. While the many simplifications used in the model might raise questions regarding how precise the derived scattering cross sections might be, the agreement between the model and the data do indicate that momentum exchange scattering and energy relaxation are very important in determining the current. When energy relaxation is fast the image potential also must be considered. This is generally true at very high density and is expected to be very important in the liquid phase.

The derived scattering cross sections and thermalization times show very interesting density dependences. Density dependences of the relevant cross sections were previously noted from drift experiments[8] and from theory.[9] Comparison between our experimental results and drift show that there is general accord, *i.e.*, the cross section for momentum exchange scattering in CH_4 decreases with increasing pressure.

The theories of Lekner[10] and Davis[11] which are single scattering theories but which include molecule–molecule correlation predict a density dependence of the momentum exchange scattering cross section. Legler[3] has calculated a density dependence from a multiple scattering theory but he does not include molecule–molecule correlation. The predictions of the variation of σ_p with density in CH_4 are shown in Figure 7, and the experimentally derived density dependence from Figure 5 is repeated for clarity.

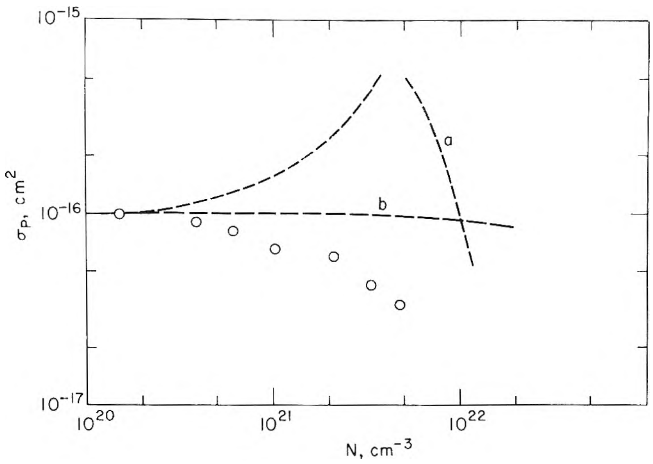

Figure 7. Comparison between the experimentally derived momentum exchange scattering cross section (circles) and that calculated from the theory: (a) Lekner,[10] (b) Legler.[3]

Neither of these theories[3,10] by themselves seem to be satisfactory. A multiple scattering theory including molecule–molecule correlation might work in CH_4. This is presently being tried.

That the momentum exchange cross sections in CO and CO_2 are independent of density is somewhat reassuring. As Davis has pointed out[11] the incoherent scattering might dominate in these anisotropic molecules. Since CH_4 is spherical the incoherent terms might be expected to be small. Incoherent scattering may also mute the effects of multiple scattering and again little or no density dependence might be expected. All of these points require further theoretical investigation.

The density dependence of τ indicates the opening of new inelastic channels or the widening of the present ones. That the hot electron lifetime might vary as the reciprocal of the gas density was expected and is apparent in CO_2 and CH_4. What the extra density dependence in CO is due to is not understood.[12] Two possibilities come to mind. (1) The presence of nearest neighbors affects the selection rules for rotational and vibrational excitations. This would increase the inelastic cross section and thereby decrease τ as the density is increased. (2) Clustering of molecules at these densities provide new rotational and vibrational modes. These new channels of the energy loss would decrease electron lifetime faster than the reciprocal density. Both of these speculations suffer from the fact that they are not found in CH_4 and CO_2. Further investigations including wider density range are in progress to clarify these points.

Many experiments on drift and photoinjection of electrons into liquids of these molecules are being performed. We believe that our experimental results show that at present there is no general rule one can follow regarding the prediction of what mean free paths or lifetime one should use in the liquid phase from data obtained in the gas or from the isolated molecule. Consequently, we urge caution when interpreting data in the liquid phase or when applying models using isolated molecule parameters.

(8) H. Lehning, *Phys. Lett. A*, **29**, 719 (1969); H. Lehning, *ibid.*, **28**, 103 (1968).
(9) B. Kivel, *Phys. Rev.*, **116**, 926 (1959); T. F. O'Malley, *ibid.*, **130**, 1020 (1963).
(10) J. Lekner, *Phys. Rev.*, **158**, 130 (1967).
(11) H. T. Davis, L. D. Schmidt, and R. M. Minday, *Phys. Rev.*, **3**, 1027 (1971).
(12) We have previously observed a similar effect in dense N_2 and H_2; *J. Chem. Phys.*, in press.

On the Negative Species Formed in γ- or Ultraviolet-Irradiated Nonpolar Glasses

T. B. Truong and A. Bernas*

Equipe de Recherches C.N.R.S. no. 98, Laboratoire de Chimie Physique de l' Université, Paris VI, Centre d'Orsay, 91-Orsay, France
(Received May 30, 1972)

Publication costs assisted by the Petroleum Research Fund

As previously shown by several authors, negative species formed in photoionized or γ-irradiated solid solutions can be sensitively characterized by optically stimulating a neutralization luminescence. At least in nonpolar matrices, the neutralization luminescence excitation spectrum closely parallels the negative species absorption spectrum. For TMPD photoionized in 3MP or MCH, and pure γ-irradiated 3MP and MCH, three distinct negative species are thus characterized: (1) the matrix trapped electrons, among which glass relaxation effects permit us to distinguish type a and type b trapped electrons; (2) the TMPD anion, or a negatively charged TMPD photoproduct; and (3) a third species X^- observable only after large uv or γ-ray doses and electron ir bleaching. Since the solute photoionization is accompanied by the solvent sensitized dissociation, the species X^- can very likely be identified with $R\cdot^-_{solv}$, R· deriving from a hydrogen atom abstraction from the solvent molecule. The technique of neutralization luminescence stimulation permits us to differentiate $R\cdot^-_{solv}$ from $R\cdot_{solv}$ which have both an optical absorption in the same uv region.

Introduction

Delayed luminescence in organic glasses associated with γ irradiations or solute photoionization, either spontaneous or optically or thermally induced, has attracted considerable attention in recent years.

It has been noticed in particular that in nonpolar glasses such as 3-methylpentane (3MP) and methylcyclohexane (MCH), the excitation spectrum of the charge recombination luminescence closely parallels the matrix trapped electron and the solute anion absorption bands and may serve to identify the latter.[1]

In the particular case of *N,N,N',N'*-tetramethyl-*p*-phenylenediamine (TMPD), widely used as a solute in photoionization experiments, $TMPD^-$ formation has been assumed[2,3] but not conclusively characterized.[4] In the course of a recent study of TMPD and diphenyl-*p*-phenylenediamine (DPPD) photoionized in a methyltetrahydrofuran (MTHF) glass,[5] some extra bands present for TMPD and absent for DPPD have appeared in the stimulated luminescence spectrum.

The present report deals mostly with TMPD photoionized at 77 K in a MCH glass. Owing to the much higher glass viscosity the trapped electrons (e_t^-) thermal decay is significantly reduced compared to 3MP.[6]

For comparison, a few experiments on uv-irradiated TMPD-3MP systems and γ-irradiated MCH or 3MP glasses are also described.

Experimental Section

Degassed solutions of purified TMPD in MCH (4×10^{-3} *M*) in sealed Suprasil tubes are irradiated under λ 325 ± 50 nm with a high-pressure Hg arc (Osram HBO 500) and uv filter. The stimulated luminescence spectra are recorded with a Jobin Yvon "Bearn" spectrofluorometer equipped with a Sefram recorder and two additional filters. A red one which cuts λ <550 nm is placed at the exit of the excitation monochromator (exit slit 0.3 mm, $(\Delta\lambda/\lambda)_{max}$ = 4% at λ 850 nm). Another filter with a passing band λ 430 ± 80 nm is set in front of the analyzing monochromator (slit width 2 mm, $\Delta\lambda/\lambda$ = 10% at λ_{an} 480 nm). For uv stimulation the red filter is removed and the analyzing monochromator slit is set at 1.0 mm ($\Delta\lambda/\lambda$ = 2% for λ_{an} = 480 nm). Unless otherwise stated, all reported spectra are recorded 30 min after the end of the irradiation, when spontaneous isothermal luminescence has become negligible. The time required for scanning the entire spectrum is about 5 min. The recorded spectra are corrected for the e_t^- consumption under successive bleachings and for the variation with λ of the excitation light flux, the stimulated luminescence I_{SL} being itself linear with the bleaching light intensity.

The I_{SL} spectra viewed either at λ_{an} = 480 or 390 nm corresponding, respectively, to TMPD phosphorescence and fluorescence maximum, are the same. The results are reproducible within 15%.

Results and Discussion

1. Effect of Glass Relaxation. Typical neutralization luminescence excitation spectra for TMPD in MCH glass are presented in Figure 1. For presentation conveniences, we shall divide the spectrum into three regions, as shown.

Increasing the glass relaxation time Δt_1 between vitrification and irradiation is found to decrease the stimulated luminescence intensity I_{SL} in region 1—in agreement with previous observations[7]—and particularly in region 1a. For prolonged annealing at 77 K, the region 1a luminescence vanishes. As is well known, the I_{SL} also decreases when the delay Δt_2 between the irradiation and stimulation is increased due to spontaneous recombination of some of the photoelectrons. Δt_2 is found to affect 1a more than 1b. After taking account for the decrease of 1b which overlaps

(1) A. Déroulède, *J. Lumin.*, **3**, 302 (1971).
(2) J. B. Gallivan and W. H. Hamill, *J. Chem. Phys.*, **44**, 1279 (1966).
(3) A. Bernas, M. Gauthier, D. Grand, and D. Leonardi, *Int. J. Radiat. Phys. Chem.*, **1**, 229 (1969).
(4) A. Bernas and D. Grand, *J. Chim. Phys.*, **67**, 566 (1970).
(5) A. Bernas, D. Grand, and T. B. Truong, *J. Chem. Soc., Chem. Commun.*, 759 (1972).
(6) J. Lin, K. Tsuji, and F. Williams, *J. Amer. Chem. Soc.*, **90**, 2766 (1968).
(7) K. Funabashi, P. J. Herley, and M. Burton, *J. Chem. Phys.*, **43**, 3939 (1965).

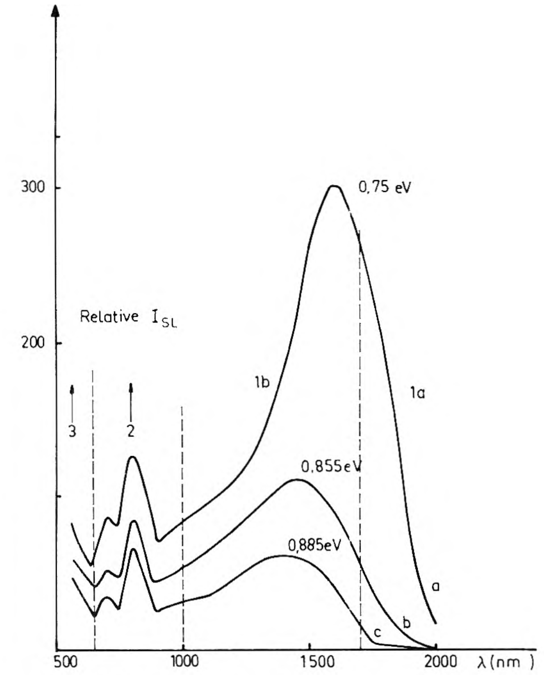

Figure 1. Neutralization luminescence excitation spectrum for photoionized TMPD in MCH; effect of glass relaxation times Δt_1 and Δt_2; [TMPD] = 4×10^{-3} *M*, *T* = 77 K, dose 1.7×10^{20} photons cm^{-2}: curve a, Δt_1 = 5 min, Δt_2 = 4 min; curve b, Δt_1 = 5 min, Δt_2 = 30 min; curve c, Δt_1 = 3 hr, Δt_2 = 30 min.

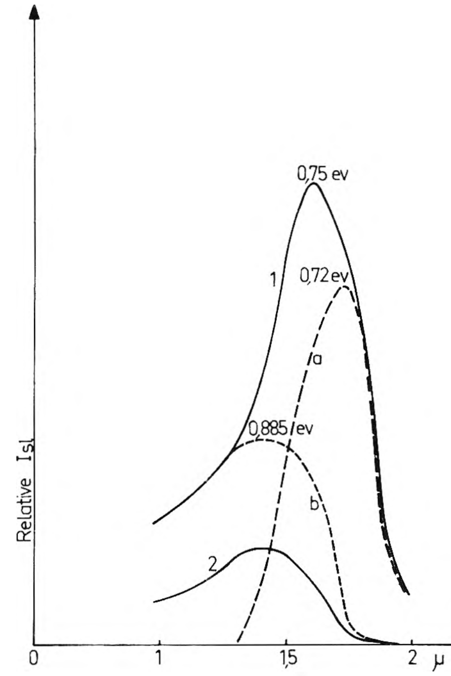

Figure 2. Decomposition of the e_t^- luminescence excitation band into 1a band (shallow traps) and 1b (deeper traps); [TMPD] = 4×10^{-3} *M*, *T* = 77 K; curve 1, Δt_1 = 5 min, Δt_2 = 4 min; curve 2, Δt_1 = 3 hr, Δt_2 = 30 min; curve b, curve 2 normalized at 1300 nm; curve a, difference between 1 and b.

regions 2 and 3, it is found that the latter are not affected by Δt_1 or Δt_2. The influence of Δt_1 and Δt_2 is illustrated by curves c and b of Figure 1. The rate of sample vitrification also intervenes: for slower vitrification the 1a luminescence is weaker.

These observations, along with reported results in the literature[7-9] support the existence in 3MP and MCH glasses of "physical" or "intermolecular" electron traps more or less permanent and deep. The influence of Δt_2 and Δt_1 allows a decomposition of the e_t^- band into 1a and 1b bands with λ_{max} at 0.72 and 0.88 eV, respectively (Figure 2). To our knowledge, the 1a and 1b trapped electrons have not been discriminated before.

The transient traps 1a, created by rapid cooling, progressively disappear as the glass relaxes. Once bleached off, these shallow traps cannot be repopulated by subsequent bleaching in region 2. The more permanent and deeper traps 1b, as we shall see later, can be partially refilled by bleaching in region 2 or 3.

The ν_{max} of the e_t^- band is found to be shifted toward the blue ($\Delta\nu_{max} \simeq$ 0.15 eV) as Δt_2 increases. For TMPD in 3MP, slight differences are observed: the effects of Δt_1 and Δt_2 are more pronounced but, whatever their duration, the shallow traps 1a are always present.

For both matrices, it must be concluded that the trapping centers undergo molecular reorganization not only on a microseconds scale[10] but over periods of hours.

2. Effect of Dose. The areas under the region 1 and 2 bands, respectively, are found to increase and then decrease with increasing uv irradiation time, whereas the luminescence intensity in region 3 is found to increase regularly with dose. The same trends have been reported for the e_t^- absorption band and the optical density in spectral region 3 for γ-irradiated MCH and 3MP glasses.[11,12]

As remarked elsewhere,[5] the ν_{max} of the e_t^- band is shifted towards the blue as the dose increases, for uv or γ irradiations. It may be noted that the ν_{max} shift with increasing dose ($\Delta\nu_{max} \simeq$ 0.15 eV) is the same as the ν_{max} shift following glass relaxation (Figure 2).

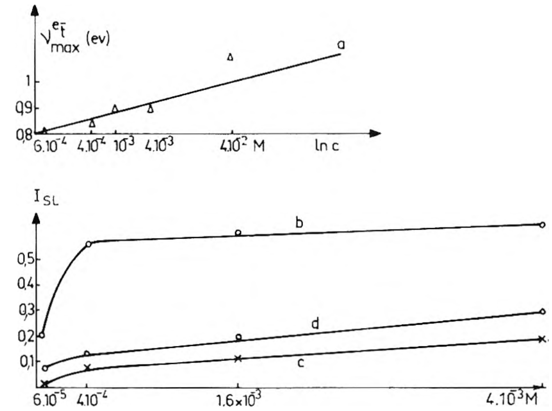

Figure 3. Effect of TMPD concentration c on ν_{max} of the e_t^- band and on the luminescence intensities I_{SL} in region 1 (e_t^-) and in region 2 (A^-), respectively; curve a, $\nu_{max}{}^{e_t^-}$ *vs.* ln c; curve b, area under e_t^- band *vs. c;* curve c, area under A^- bands *vs c;* curve d, ratio A^- bands area/e_t^- band area *vs. c.*

3. Effect of Solute Concentration. The areas of the I_{SL} bands in region 1 (curve b, Figure 3) and in region 2 (curve c, Figure 3) increase with solute concentration *c* from 6×10^{-5} to 4×10^{-3} *M*. For higher concentrations, the glasses become opaque and the experiments become less conclusive.

The ratio of the integrated intensities I_{SL} in region 2 to I_{SL} in region 1 is found to increase with *c* (curve d, Figure 3).

There is also a blue shift of ν_{max} of the e_t^- band with

(8) O. Janssen and K. Funabashi, *J. Chem. Phys.*, **46**, 101 (1967).
(9) B. Wiseall and J. E. Willard, *J. Chem. Phys.*, **46**, 4387 (1967).
(10) J. T. Richards and J. K. Thomas, *Chem. Phys. Lett.*, **8**, 13 (1971).
(11) M. Shirom and J. E. Willard, *J. Amer. Chem. Soc.*, **90**, 2184 (1968).
(12) A. Eckstrom, R. Suenram, and J. E. Willard, *J. Phys. Chem.*, **74**, 1888 (1970).

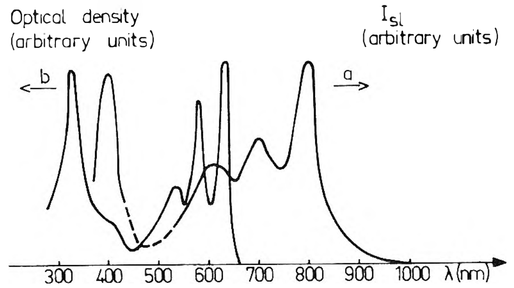

Figure 4. TMPD⁻ luminescence excitation spectrum (a). compared to $TMPD^+$ absorption spectrum (b) in 3MP glass at 77K (in the range ~430–550 nm, luminescence recording is not possible due to bleaching light scattering).

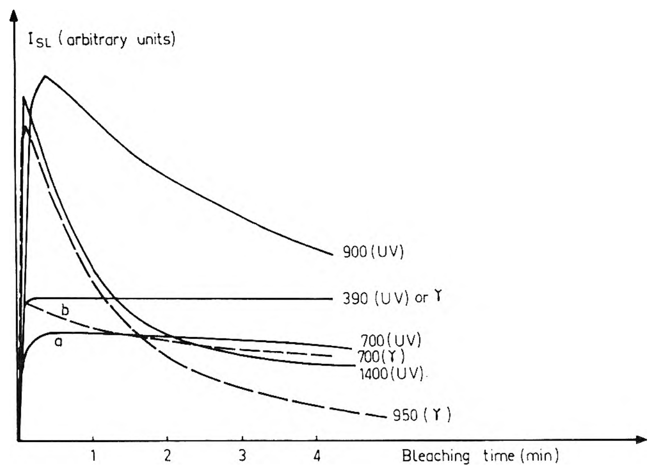

Figure 5. I_{SL} decay curves for photoionized TMPD in MCH or γ-irradiated MCH bleached under various bleaching wavelengths (λ_b).

increasing c: $\nu_{max} = a \log c$ + constant (curve a, Figure 3).

Extrapolation to $c = 0$ gives $\nu_{max} = 0.8$ eV, which is the approximate value we have found for pure γ-irradiated MCH at low doses.[5]

4. Effect of Selective Bleachings. a. When $\lambda_b = 2000$ nm, the 1a band can be removed whereas the 1b band decreases in intensity but cannot be totally suppressed. For $1700 > \lambda_b > 1500$ nm, 1a and 1b can both be removed; band 2 is unchanged in MCH but increases for TMPD–3MP systems; band 3 intensity increases in MCH and 3MP after high uv or γ-ray doses.

b. After a short uv irradiation ($t = 1$ min in our experimental conditions), a sample which has been completely bleached off with ir light, then subsequently excited with λ_b comprised between 950 and 580 nm will partially recover the 1b e_t^- band. The 1a band in MCH, once bleached off, will never be restored. For higher uv doses, band 3 increases in intensity in MCH and 3MP. Analogous regenerating of the ir e_t^- spectrum by excitation in a solute anion band and electron transfer from one type of trap to another have been previously depicted for γ-irradiated systems.[2,12,13] Similar observation has also been made for TMPD photoionized in 3MP bleached first in the ir and then in the near-uv (360 to 400 nm).[14] The possible regeneration of the e_t^- band, together with the increase of I_{SL} in region 2 with increasing solute concentration, the presence of similar stimulated luminescence bands for TMPD photoionized in MTHF, and their absence in DPPD–MTHF system[5] or in pure γ-irradiated MCH and 3MP seem to demonstrate the existence of TMPD⁻ or of a negatively charged TMPD photoproduct. The related luminescence excitation spectrum appears very similar to the well-known $TMPD^+$ absorption spectrum (Figure 4).

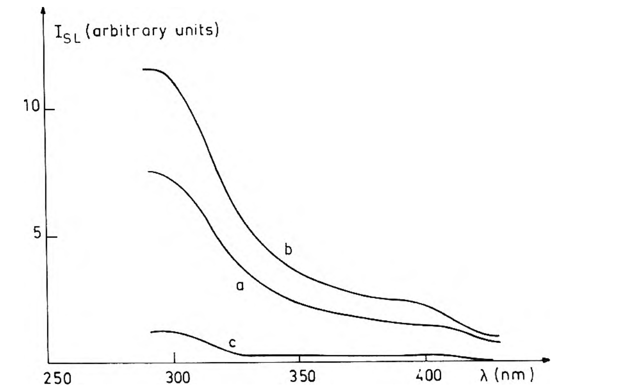

Figure 6. I_{SL} of γ-irradiated 3MP glass in spectral region 3, *i.e.*, X⁻ region: curve a, 2-min ir stimulation, dose 1.1×10^{20} eV g^{-1}; curve b, 30-min ir stimulation, dose 1.1×10^{20} eV g^{-1}; curve c, 30-min ir stimulation, dose 4×10^{20} eV g^{-1}.

The existence of traps of two different natures is also confirmed by the observation of quite different luminescence decay curves accompanying bleachings in regions 1 and 2, respectively (Figure 5). One should particularly notice the dissimilarity between curve a (in which case the 700-nm bleaching affects TMPD⁻) and curve b (in which case the 700-nm bleaching affects e_t^-).] On the time scale used, the number of charges undergoing neutralization per unit time upon visible excitation attain a nearly stationary state. Similar luminescence signals have been recently reported for γ-irradiated 3MP glasses.[15]

c. After large uv doses, for $650 < \lambda_b < 550$ nm, the 1b and 2 bands (which have been optically bleached off) are partially recovered for the photoionized TMPD in MCH or 3MP glass.

d. In region 3 the TMPD⁻ luminescence excitation spectrum overlaps that of another species X⁻. The contribution of the latter increases steadily with dose whereas that of TMPD⁻ first increases and then declines.

For a pure, γ-irradiated (1×10^{20} eV g^{-1}) MCH or 3MP sample, the following preliminary observations have been made. (1) If the stimulation occurs immediately after the irradiation, the excitation spectrum attributable to X⁻ is absent. (2) Following a 1400-nm bleaching, the stimulated luminescence becomes observable in region 3. Its intensity increases with the ir 1400-nm bleaching time (Figure 6) as was observed through absorption measurements.[12] (3) If the 1400-nm bleaching is followed by a 380-nm bleaching, the e_t^- band is partially regenerated, which shows that a 380-nm light can photodetach the electron from X⁻. (4) After a prolonged glass relaxation Δt_2, no X⁻ excitation spectrum is obtained, which is compatible with the generally adopted view that, during Δt_2, the shallowest, that is, the electrons trapped the nearest their parent cations, suffer neutralization; for such e_t^-, attachment to a X species would not compete with neutralization. (5) After high γ-ray doses (4×10^{20} eV g^{-1}) corresponding to a negligible concentration of e_t^-,[11,12] in either MCH or 3MP samples, a weak I_{SL} in re-

(13) A. Déroulède, F. Kieffer, and M. Magat, *Advan. Chem. Ser.*, **No. 82,** 401 (1968).
(14) W. M. McClain and A. C. Albrecht, *J. Chem. Phys.*, **43,** 468 (1965).
(15) K. Funabashi, C. Hebert, and J. L. Magee, *J. Phys. Chem.*, **75,** 3221 (1971).

gion 3 is observed only after an ir stimulation (curve c, Figure 6).

The nature of the uv absorbing species X^- has already been the subject of some debate.[12,15] Previous studies and the present one agree that X^- is observable only after heavy radiation doses and derives from the solvent.

The uv absorption[15] or stimulated emission band cannot be a second e_t^- (β) band since its intensity varies in opposite direction from the ir trapped electron band. It does not seem to be correlated with a dielectron formation which would give rise to an absorption at longer wavelength than e_t^-.[16]

It has been suggested that X is very likely a solvent radical although a decrease in [R·] following an e_t^- bleaching and R·$^-$ formation has not been recorded through epr spectroscopy.[11,17]

For the uv-irradiated systems, it has been repeatedly shown[18-22] that solute photoionization is accompanied by a solvent-sensitized dissociation, leading to R· + H whenever the solvent molecules contain mobile hydrogen atoms. Quantitatively it has been estimated that the ratio solute cation/solvent radical is of the order of one for 3MP.[23]

Hence, our photochemical results seem to support the identification of X^- with R·$^-_{solv}$; R· deriving from a H-atom loss by the solvent molecule. We should also point out that a dissociative electron capture by 3MP or MCH molecules is not feasible on energetic grounds.

The last point which deserves emphasis is that the incoming, thermalized electrons do not seem to attach to R·; it is only after having been trapped and optically (not thermally) released, that mobile electrons appear capable of producing R·$^-$. Similar results have been previously reported for γ-irradiated acetonitrile in glassy MTHF.[24] One may tentatively offer two suggestions. (a) The electron capture would be of a resonant type and the bleaching electron with 0.15–0.12-eV kinetic energy[5] would encounter radicals stabilized in the immediate vicinity of the electron-trapping cavities. (b) The bleaching light would serve not only to release the trapped electrons but also to induce some C–H vibrational excitation in the radical, thereby increasing the electron capture cross section.

Further experiments are in progress to test these tentative interpretations.

(16) A. Eckstrom, *Rad. Res. Rev.*, **2**, 381 (1970).
(17) D. P. Lin and L. Kevan, *J. Chem. Phys.*, **55**, 2629 (1971).
(18) B. Smaller, *Nature (London)*, **195**, 593 (1962).
(19) B. N. Shelimov, N. V. Fok, and V. V. Voevodsky, *Dokl. Akad. Nauk SSSR*, **144**, 596 (1962), V. G. Vinogradova, *et al.*, *ibid.*, **154**, 188 (1964).
(20) Kh. S. Bagdassarian, *et al.*, *Dokl. Akad. Nauk SSSR*, **152**, 349 (1963); **153**, 374 (1963); **160**, 625 (1965).
(21) S. Siegel and K. Eisenthal, *J. Chem. Phys.*, **42**, 2494 (1965).
(22) B. Brocklehurst, *et al.*, *Trans. Faraday Soc.*, **62**, 1793 (1966).
(23) M. C. Peraudeau, Thèse 3ème cycle, Paris, 1970; A. Bernas, *et al.*, 5th International Conference on Photochemistry, New York, N. Y., Sept 1969.
(24) M. A. Bonin, J. Lin, K. Tsuji, and F. Williams, *Advan. Chem. Ser.*, **No. 82**, 269 (1968).

Pulse Radiolysis of Solutions of Stilbene. I. Evidence for Triplet and Singlet Excited State Formation

Sir Frederick Dainton, E. A. Robinson, and G. A. Salmon*

Cookridge High Energy Radiation Research Center, The University of Leeds, Cookridge Hospital, Leeds, LS16 6QB, England

(Received March 20, 1972)

Publication costs assisted by the University of Leeds

The triplet state of *trans*-stilbene has been estimated, both by direct observation and by an energy transfer method, to have a natural first-order decay constant, $k = 1.06 \pm 0.26 \times 10^7$ sec^{-1}, in benzene solution. This species can transfer triplet energy to anthracene with a second-order rate constant, $k = 2.6 \pm 0.5 \times 10^9\ M^{-1}$ sec^{-1}. Other energy transfer processes involving the cis and trans isomers of stilbene have been investigated.

Introduction

Extensive studies of the direct and photosensitized isomerization of stilbene in solution[1-4] have led to the conclusion that the active intermediate is the triplet state of stilbene. The observed photostationary state[3] of isomeric composition [cis]/[trans] = 1.8 agrees with theoretical calculations[5] of the first excited triplet energy surface.

Studies of the radiation-induced isomerization of stilbene in benzene and cyclohexane[6,7] led to the observation of a radiostationary state in dilute solutions similar to that of the photoreaction. This fact combined with the ef-

(1) S. Malkin and E. Fischer, *J. Phys. Chem.*, **66**, 2482 (1962).
(2) R. H. Dyck and D. S. McClure, *J. Phys. Chem.*, **36**, 2326 (1962).
(3) S. Malkin and E. Fischer, *J. Phys. Chem.*, **68**, 1153 (1964).
(4) G. S. Hammond, *et al.*, *J. Amer. Chem. Soc.*, **86**, 3197 (1964).
(5) P. Borrell and H. H. Greenwood, *Proc. Roy. Soc., Ser. A*, **298**, 453 (1967).
(6) E. Fischer, H. P. Lehmann, and G. Stein, *J. Chem. Phys.*, **45**, 3905 (1966).
(7) R. R. Hentz, D. B. Peterson, S. B. Srivastava, H. A. Barzynski, and M. Burton, *J. Phys. Chem.*, **70**, 2362 (1966).

fects of additives of known triplet energy also suggested that the mechanism involved the triplet state as an intermediate.

The yield of cis to trans conversion, $G(c \rightarrow t)$, showed some tendency to be higher than expected on the basis of the photochemical results, especially in more concentrated solutions, and to account for this it was proposed that a free-radical mechanism[6] or an anionic mechanism[7] yielding the thermodynamically more stable[8,9] trans isomer was involved. The yield of trans to cis conversion, $G(t \rightarrow c)$, appeared to be free of such complications and estimates of the total yield of excitation in benzene were made, based on the observed limiting yield for this process.

Several attempts to observe the triplet–triplet absorption spectrum of *trans*-stilbene in solution using flash photolysis have been unsuccessful.[4,10,11] The species was assumed therefore to have a lifetime in solution too short for resolution by this method. Kinetic arguments based on quenching experiments have led to an estimate for the lifetime of the triplet in solution of 77 nsec[4] and the estimate obtained by Ullman[12] is in good agreement with this. The triplet–triplet absorption spectrum with absorption maxima in the near-ultraviolet region has been detected using flash photolysis of rigid solutions of *trans*-stilbene at 77 K.[13,14]

The singlet state of *trans*-stilbene was studied by Andreeshchev and coworkers[15] who found that it possessed a fluorescence spectrum (λ_{max} 360 nm) and a lifetime less than 0.2 nsec. They reported a quantum yield of fluorescence, ϕ_f, of 0.04, to be compared with Malkin and Fischer's[3] value of 0.08 at room temperature. No reports of luminescence from *cis*-stilbene at room temperature have appeared.

An earlier work[16] used pulse radiolysis in an attempt to examine the roles of excitation and ionization in the isomerization reaction. Solutions of the isomers in benzene and cyclohexane were studied and transient absorptions similar to those described below[13,14] were observed in the near-uv region. The absorptions were assigned to the triplet state of stilbene and their decay rates yielded an estimate for the triplet lifetime orders of magnitude longer than earlier estimates. This conclusion was supported by the observation that the triplet state of anthracene is formed in benzene solutions containing this solute as well as *cis*-stilbene and the variation of $G(^3\text{anth}^*)$ with solution composition was consistent with the expected exothermic energy transfer from ^{3}*cis*-stilbene* to anthracene.

In an attempt to resolve this discrepancy and to provide more information on the isomerization mechanism and the radiation chemistry of the solvents used, further work has been carried out using microsecond and nanosecond pulse radiolysis. The results of this work are reported here. A subsequent paper will deal with the role of ionization.[17]

Experimental Section

Details of the apparatus and procedure for microsecond pulse radiolysis have appeared elsewhere[18] and with the exception that an EMI 931A photomultiplier tube was used for some of the earlier work the details remain the same. However, the later experiments used an EMI 9781 photomultiplier operating with anode currents up to 3.5 mA. To avoid fatigue of the dynodes and fluctuations in the dynode voltages due to a large drain on their power supply, the light falling on the photomultiplier cathode was made intermittent with a rotating sector. A series of trapezoidal light flashes were thus produced with a maximum intensity of 5.5 msec duration and the accelerator was triggered so that irradiation of the sample with the electron pulse occurred during the period in which the sample was illuminated with the steady maximum intensity of one of the light flashes. Any transient absorption signals were thus superimposed on the trapezoidal signals from the light flashes and these steady signals were "backed-off" using a synchronous clamp incorporating a reed switch.[19] By suitable synchronization of the opening of this switch the ac coupling time constant of 10 μsec used to back-off the steady light level could be increased to 0.1 sec during the steady light period when the transient signal was displayed. The higher output from the photomultiplier thus achieved permitted the use of less gain on the oscilloscope vertical amplifier and hence reduced the significance of the amplifier noise.

In the nanosecond pulse radiolysis experiments pulses of 10- and 25-nsec duration were used with electron beam currents in excess of 2 A. The analyzing light was produced by using a pulsed xenon lamp. The photomultiplier used was an RCA 1P28 tube operated at fixed gain, and anode currents of the order of 30 mA were used. The output from the photomultiplier was resolved into high-frequency (transient signal) and low-frequency (light pulse) components and the former displayed on a Tektronix 454 oscilloscope for photographing. The anode current was read visually from the light pulse output, displayed on a Tektronix 545 oscilloscope. The overall rise time of the detection equipment using the 454 oscilloscope was about 3 nsec. This apparatus has been described elsewhere.[20a]

Materials. Cyclohexane (Hopkin and Williams, MFC), which had been purified by passage down a column containing silver nitrate on alumina,[20b] was distilled once before use. Benzene (British Drug Houses, Analar) was purified by washing with concentrated sulfuric acid, followed by water. After thorough drying the solvent was refluxed over potassium and collected under nitrogen. *cis*- and *trans*-stilbene were both supplied by Eastman Kodak. The former was used as supplied while *trans*-stilbene was recrystallized three times from ethanol and stored under vacuum for 2 days. Chromium acetylacetonate was synthesized and supplied by Dr. J. Raistrick of this laboratory. Other chemicals used were of the highest purity available and were used as supplied.

(8) R. B. Williams, *J. Amer. Chem. Soc.*, **64**, 1395 (1942).
(9) G. Fischer, K. A. Muszkat, and E. Fischer, *J. Chem. Soc. B*, 156 (1968).
(10) Quoted in D. Schulte-Frohlinde, H. Blume, and H. Gusten, *J. Phys. Chem.*, **66**, 2486 (1962).
(11) W. G. Herkstroeter and G. S. Hammond, *J. Amer. Chem. Soc.*, **88**, 4769 (1966).
(12) E. F. Ullman and W. A. Henderson, *J. Amer. Chem. Soc.*, **89**, 4390 (1967).
(13) W. G. Herkstroeter and D. S. McClure, *J. Amer. Chem. Soc.*, **90**, 4522 (1968).
(14) G. Heinrich, H. Blume, and D. Schulte-Frohlinde, *Tetrahedron Lett.*, 4693 (1968).
(15) E. A. Andreeshchev, V. S. Viktorova, S. F. Kilin, Yu. P. Kushakevich, and I. M. Rozman, *Opt. Spectrosc.*, **24**, 387 (1968).
(16) F. S. Dainton, C. T. Peng, and G. A. Salmon, *J. Phys. Chem.*, **72**, 3801 (1968).
(17) Part II of this series.
(18) T. J. Kemp, J. P. Roberts, G. A. Salmon, and G. F. Thompson, *J. Phys. Chem.*, **72**, 1464 (1968).
(19) This apparatus was designed by Mr. D. H. Ellison of this laboratory.
(20) (a) D. H. Ellison, G. A. Salmon, and F. Wilkinson, *Proc. Roy. Soc., Ser. A*, **328**, 23 (1972); (b) E. C. Murray and R. N. Keller, *J. Org. Chem.*, **34**, 2234 (1969).

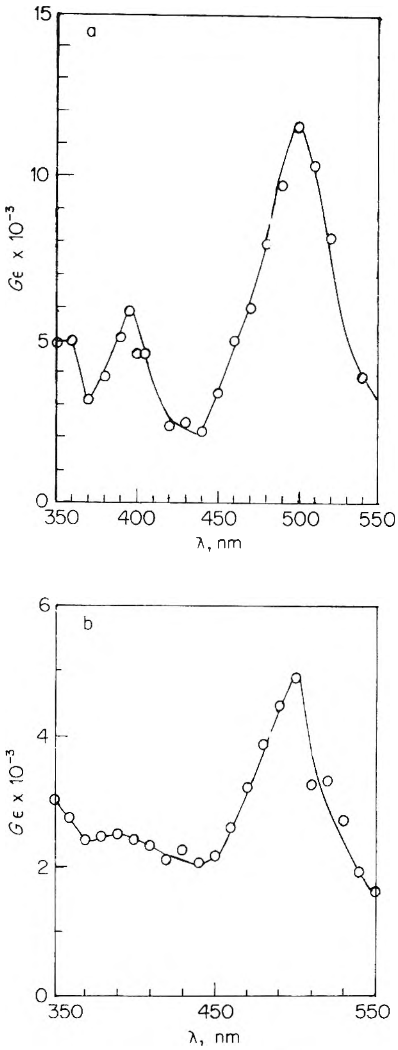

Figure 1. Absorption spectrum of a 10^{-2} *M* solution of (a) *trans*-stilbene and (b) *cis*-stilbene in cyclohexane at the end of a 2.3-μsec pulse.

Results and Discussion

1. Transient Spectra on the Microsecond Time Scale. The end-of-pulse absorption spectra observed on irradiating 10^{-2} *M* solutions of *cis*- and of *trans*-stilbene in cyclohexane with 5-krad pulses of 2.3-μsec duration are shown in Figure 1. That part of the absorption with λ_{max} 500 nm has been attributed[16] to the anion of stilbene because of its similarity with the reported spectrum of this species.[21,22] The absorption in the region 350–450 nm, with maxima at 360 and 395 nm, is less well defined when *cis*-stilbene is the solute. Part of this absorption is very long-lived and in Figure 2 the absorption remaining 100 μsec after the absorption of a 10-krad pulse by a 10^{-2} *M trans*-stilbene solution is compared with the permanent absorption produced by a 3-min γ irradiation to a comparable dose. On correcting the transient signals by subtracting the absorption remaining after 350 μsec, the residual absorption decayed according to a second-order rate law with $k/\epsilon \simeq 10^6$ cm sec^{-1}, which is difficult to reconcile with the previous suggestion[16] that this absorption is due to the triplet state of stilbene. Figure 3 shows the spectrum of the transient absorption in the near-uv region where *trans*-stilbene is the solute. The dependences of the yields of absorbing species at the maxima, 360 and 395 nm, on the concentration of *trans*-stilbene (Figure 4) are similar and this fact together with the similarity in the decay of the absorption at both wavelengths suggests that a single species is responsible for the absorption. Figure 4 also shows the concentration dependence of the yield of permanent product, estimated 250 μsec, after the passage of the pulse.

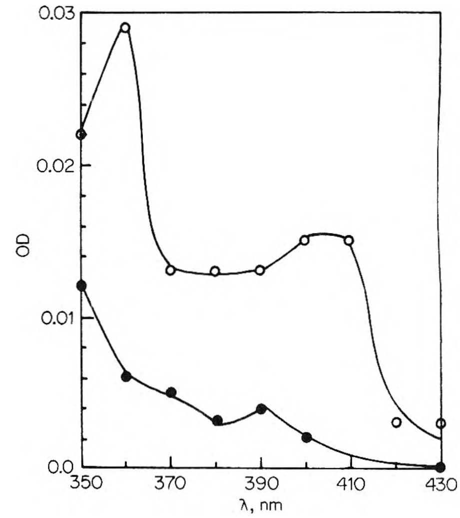

Figure 2. Absorption spectrum (O) remaining 100 μsec after the pulse in 10^{-2} *M trans*-stilbene and (●) after a 3-min γ irradiation of a similar solution to the same dose.

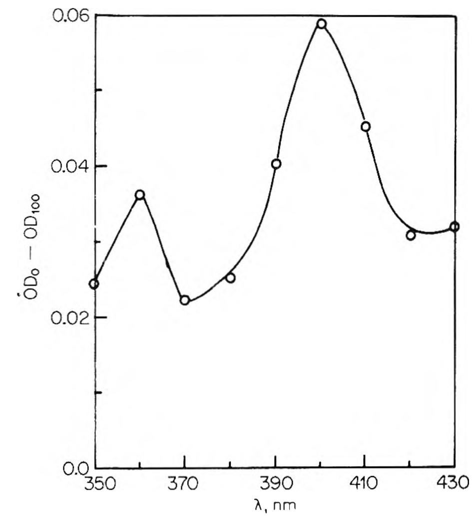

Figure 3. Difference between the spectrum at the end of the pulse (OD_0) and after 100 μsec (OD_{100}) for a 10^{-2} *M trans*-stilbene solution in cyclohexane given a 10-krad 2.3 μsec pulse.

The end-of-pulse spectrum formed on irradiating solutions of *tran*-stilbene in benzene with a 6-krad pulse of 0.6 μsec duration is shown in Figure 5. The absorption maximum in the visible region is associated with ionic species of stilbene.[16] Again, part of the absorption in the near-uv region is very long-lived, and after correction for this (estimated 350 μsec after the pulse) the remaining absorption at 360 nm decayed in a second-order manner with $k/\epsilon = 3 \pm 1 \times 10^6$ cm sec^{-1}. The transient spectrum observed using *cis*-stilbene as the solute in benzene is similar to that of *trans*-stilbene.

(21) F. S. Dainton and G. A. Salmon, *Proc. Roy. Soc., Ser. A*, **285**, 319 (1965).
(22) E. R. Zabolotny and J. F. Garst, *J. Amer. Chem. Soc.*, **86**, 1645 (1964).

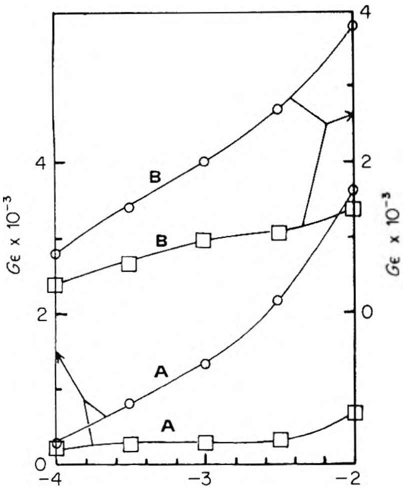

Figure 4. Effect of changing *trans*-stilbene concentration in cyclohexane on $G\epsilon$ at 395 (A) and 360 nm (B) at the end of the pulse (O) and after 250 μsec (□).

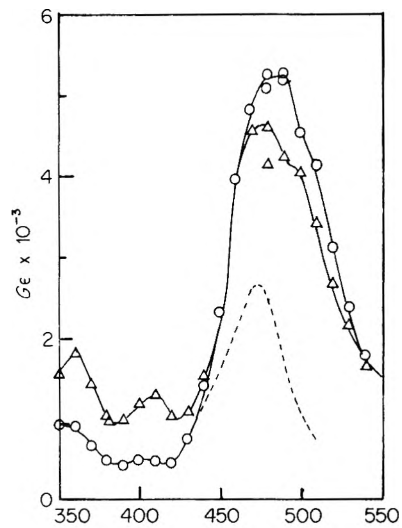

Figure 5. Absorption spectra at the end of a 6-krad, 0.6 μsec pulse for 10^{-2} (O) and 10^{-1} *M* (Δ) *trans*-stilbene solutions in benzene and (- - - -) for a 10^{-2} *M trans*-stilbene solution in benzene saturated with SF_6.

2. Effect of Added Solutes of Known Triplet State Energy. Naphthalene. The yields of triplet excited state of naphthalene (^{3}naph*) in benzene and cyclohexane have been investigated previously.[23a] For a 10^{-1} *M* solution of naphthalene in cyclohexane $G\epsilon$[23b] at 412.5 nm is 46,900, and in benzene $G\epsilon$ at 420 nm is 34,000. Table I shows the effect of various concentrations of stilbene (cis or trans) on this absorption in the two solvents. The observed quenching of ^{3}naph* by stilbene is expected since the energy level of the triplet state of each isomer is appreciably less than that of naphthalene. In addition to reducing the end-of-pulse yields of ^{3}naph*, stilbene also increased the rate of their decay. The first half-life of the decay in the presence of 10^{-4} *M trans*-stilbene in cyclohexane was observed to be about 1 μsec indicating that the second-order rate constant for this energy transfer process is about $10^{10}\ M^{-1}\ sec^{-1}$.

If the absorption in the near-uv region were due to the triplet state of *trans*-stilbene then it would be expected to be enhanced by the presence of naphthalene. Some enhancement of these absorptions was observed in solutions with [*trans*-stilbene] = 10^{-4} *M* and [naphthalene] = 0.1 *M*. The enhancement is however small and its significance is doubtful. The wavelengths of interest are close to those at which the triplet state of the second solute absorbs and large fluorescence signals attributable to the second solute tend to distort the absorption signals because of overload effects in the detection equipment.

TABLE I: Effect of Stibene on $G(^3$naph*) in Benzene and Cyclohexane

Solvent	$[C_{10}H_8]$, *M*	[Stilbene], *M*	λ, nm	$G\epsilon 10^{-3}$
C_6H_{12}	10^{-1}	0	412.5	46.9[a]
	10^{-1}	$5 \times 10^{-5}S_t$	412.5	20.0 ± 10%
	10^{-1}	$10^{-4}S_t$	412.5	7.8 ± 10%
	10^{-1}	$5 \times 10^{-4}S_t$	412.5	0.9 ± 10%
	10^{-1}	$10^{-4}S_c$	412.5	17.7 ± 10%
	0	$10^{-4}S_t$	360	0.8 ± 20%
	10^{-1}	$10^{-4}S_t$	360	2.3 ± 50%
	0	$10^{-4}S_t$	395	0.3 ± 20%
	10^{-1}	$10^{-4}S_t$	395	1.2 ± 50%
C_6H_6	10^{-1}	0	420	34.0[a]
	10^{-1}	$10^{-4}S_t$	420	31.1 ± 10%
	10^{-1}	$6 \times 10^{-4}S_t$	420	4.9 ± 10%

[a] Reference 23a.

TABLE II: Effect of Stilbene on the Yield at the End of the Pulse and Rate of Decay of *p*-Terphenyl Triplet State in Benzene[a]

[Stilbene], *M*	$G\epsilon_{455}10^{-3}$	$10^5\ k$, sec^{-1}
0	100 ± 10%	3.4 ± 10%
10^{-5} trans	115 ± 10%	2.2 ± 10%
3×10^{-5} trans	115 ± 10%	2.2 ± 10%
10^{-4} trans	80 ± 10%	5.4 ± 10%
3×10^{-4} trans	44 ± 5%	12.0 ± 10%
10^{-3} trans	25 ± 5%	
0	113 ± 10%	1.1 ± 10%
10^{-5} cis	111 ± 10%	1.3 ± 10%
3×10^{-5} cis	107 ± 10%	1.6 ± 10%
10^{-4} cis	96 ± 10%	3.5 ± 10%
3×10^{-4} cis	60 ± 5%	8.0 ± 10%
10^{-3} cis	21 ± 5%	20.8 ± 10%

[a] [PTP] = 10^{-2} *M*; pulse length = 0.6 μsec; dose = 5 krads.

p-Terphenyl (PTP). Pulse radiolysis of PTP in benzene produces an intense absorption at 455 nm which has been ascribed to the excited triplet state of the solute.[24] In the presence of *trans*- or *cis*-stilbene this absorption was diminished and its decay was faster (Table II). Simultaneous observation of the absorption at 360 nm was not possible for the reasons already mentioned. The end-of-pulse yields shown in Table II indicate that there is a competition between PTP and stilbene for the precursors of the triplet states. The most likely precursors are the singlet excimer ($^1B_2$*) and the triplet states of benzene (^{3}B*) which have lifetimes of 26.8 and 30 nsec, respectively, in the pure solvent[24,25] and which have energy levels

(23) (a) G. F. Thompson, Ph.D. Thesis, University of Leeds, 1968. (b) The units of ε are $dm^3\ mol\ cm^{-1}$.
(24) F. S. Dainton, T. Morrow, G. A. Salmon, and G. F. Thompson, *Proc. Roy. Soc., Ser. A*, **328**, 481 (1972).
(25) R. Cooper and J. K. Thomas, *J. Phys. Chem.*, **48**, 5097 (1968).

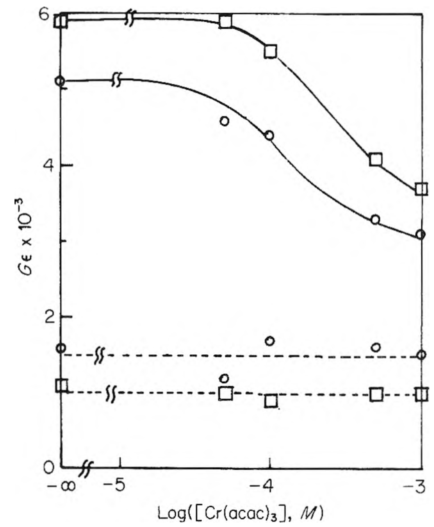

Figure 6. Effects of chromium trisacetylacetonate on the end-of-pulse absorption of 10^{-2} M solution of *trans*-stilbene in cyclohexane at 360 (○) and 395 nm (□) and on the spectrum observed 100 μsec after the pulse at 360 (○, ---) and 395 nm (□, ---).

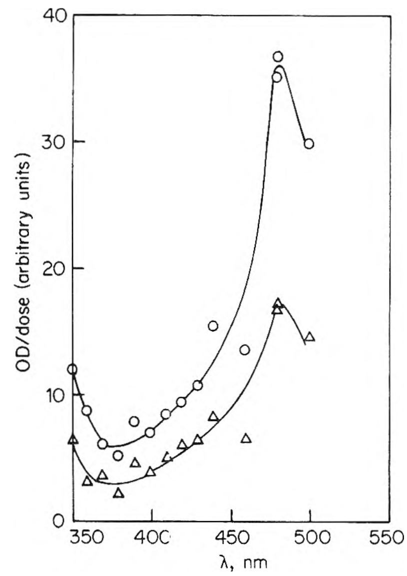

Figure 7. Spectrum immediately after (○) and 550 nsec after (△) a 1-krad, 25 nsec pulse delivered to 10^{-2} M *trans*-stilbene in benzene.

such that singlet and triplet energy transfer to both PTP and stilbene by reactions 1–4 are expected.

$$^1B_2^* + PTP \rightarrow (^1PTP^*) + 2B \quad (1)$$

$$^1B_2^* + S \rightarrow {}^1S^* + 2B \quad (2)$$

$$^3B^* + PTP \rightarrow (^3PTP^*) + B \quad (3)$$

$$^3B^* + S \rightarrow {}^3S^* + B \quad (4)$$

The singlet excited states of PTP (τ = 1.02 nsec)[26] and stilbene ($\tau \sim 0.2$ nsec) formed in reactions 1 and 2 undergo rapid intersystem crossing to their respective triplet states. Consequently the yield of (^{3}PTP*) observed at the end of the pulse should conform to eq I where G_S and G_T represent the yields of the singlet excimer and triplet states of benzene, respectively, and ϕ_T is the fraction of PTP singlet excited states which undergo intersystem crossing to the triplet state.

$$G(^3\text{PTP}^*) = \frac{G_S\phi_T k_1[\text{PTP}]}{(k_1[\text{PTP}] + k_2[\text{S}])} + \frac{G_T k_3[\text{PTP}]}{(k_3[\text{PTP}] + k_4[\text{S}])} \quad (\text{I})$$

Now ϕ_F, the quantum yield for fluorescence, for PTP is approximately unity[27] and ϕ_T is therefore approximately zero. The first term in expression I will therefore be negligible in comparison with the second and the equation will reduce to expression II.

$$1/G(^3\text{PTP}^*) = G_T^{-1}\left[1 + \frac{k_4[\text{S}]}{k_3[\text{PTP}]}\right] \quad (\text{II})$$

The data in Table II when suitably plotted yielded the expected linear graphs of $[G(^3\text{PTP}^*)\epsilon]^{-1}$ *vs.* [stilbene] from which the ratio k_4/k_3 was deduced to be 34 ± 8 for *trans*-stilbene and 55 ± 12 for *cis*-stilbene. The enhancement of the rates of decay of ^{3}PTP* by both stilbene isomers indicate that both isomers can deactivate this species with rate constants of about 10^9 M^{-1} sec^{-1} even though the energy level of the cis isomer lies only 4.2 kJ mol^{-1} below that of *p*-terphenyl.

Chromium Trisacetylacetonate. A number of metal chelate complexes have been shown to deactivate the triplet excited states of aromatic hydrocarbons.[28] In the case of chromium acetylacetonate energy transfer takes place and the chelate undergoes the transition[29] $^4A_{2g} \rightarrow {}^2E_g$ for which the energy change is 155 kJ mol^{-1}. Consequently the *trans*-stilbene triplet state should be deactivated by this solute since its triplet energy level lies significantly above this. Chromium acetylacetonate has the advantage that when it is subject to pulse radiolysis in solution no transient absorptions are produced in the 350–400-nm region. The effect of chromium acetylacetonate on the absorptions at 360 and 395 nm was therefore readily studied for cyclohexane solutions with [stilbene] = 10^{-2} M and the results are shown in Figure 6. Similar reductions of the end-of-pulse absorptions occur at both wavelengths. Measurements made 100 μsec after the pulse indicate that the yield of the permanent product absorbing in this region is unaffected by the presence of the chromium acetylacetonate.

The rate constant for the quenching of the stilbene triplet by the chelate complex is expected to fall within 10^9–10^{10} M^{-1} sec^{-1}. Therefore in the presence of 10^{-4} M chromium trisacetylacetonate the *trans*-stilbene triplet will have a half-life of less than 10 μsec. The decays of the absorptions at 360 and 395 nm were unaffected by the presence of the complex throughout the range of concentrations used and we conclude that these absorptions are probably not those of the *trans*-stilbene triplet state. Presumably the chelate attenuates the absorptions by scavenging precursors of the absorbing species. The near-uv absorptions may well be due to radicals formed by the addition to stilbene of radicals derived from the solvent, and this view is supported by the effect of nitrous oxide on these absorptions and by studies in other solvents which will be described in part II.[17]

3\. *Nanosecond Pulse Radiolysis.* Figure 7 shows the end-of-pulse spectrum induced in a 10^{-2} M solution of

(26) J. B. Birks, "Photophysics of Aromatic Molecules," Wiley-Interscience, New York, N.Y., 1970, p. 123.
(27) E. J. Bowen, *Advan. Photochem.*, **1**, 1 (1963).
(28) A. J. Fry, R. S. Liu, and G. S. Hammond, *J. Amer. Chem. Soc.*, **88**, 478 (1966).
(29) (29) D. J. Binet, E. L. Goldberg, and L. S. Forster, *J. Phys. Chem.*, **72**, 3017 (1968).

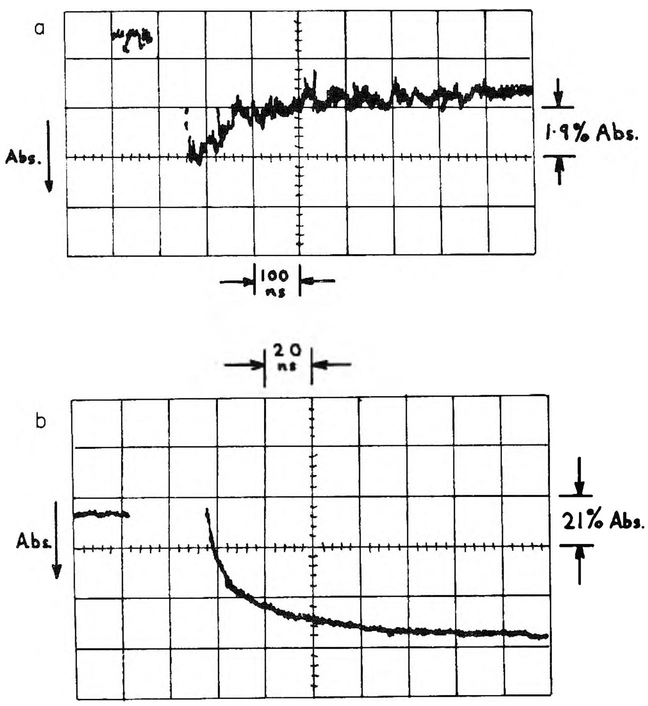

Figure 8. (a) Decay of absorption at 350 nm for a 10^{-2} *M trans*-stilbene solution in benzene following a 6-krad, 25-nsec pulse. (b) Growth of absorption at 427.5 nm for a solution in benzene containing 10^{-1} *M trans*-stilbene and 8×10^{-3} *M* anthracene following a 6-krad, 25-nsec pulse.

trans-stilbene in benzene by a 25-nsec pulse of about 1 krad; the spectrum remaining 550 nsec after the pulse is also shown. An oscilloscope trace of the decay of the absorption observed at λ 350 nm is shown in Figure 8. Throughout the wavelength range studied an initial rapid decay of absorption occurs. Figure 9 illustrates the spectrum of the absorption decaying over the first 500 nsec following the pulse. There are two peaks with λ_{max} 480 and 360 nm which is in marked contrast to cyclohexane solutions where a single peak is observed at 500 nm with a tail stretching into the uv.[17] The long-wavelength absorption in each solvent is assigned to the enhanced yield of ionic species observable on this time scale.

After correction for the absorption remaining after 450 nsec the absorption in the benzene solution with λ 350–360 nm decayed in a first-order manner with a rate constant $k = (0.9 \pm 0.1) \times 10^7$ sec^{-1}. The extent of the ab-

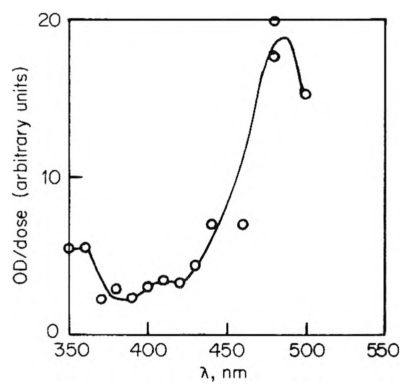

Figure 9. Difference between the spectrum observed for 10^{-2} *M trans*-stilbene in benzene immediately after a 1-krad, 25-nsec pulse and that observed 500 nsec later.

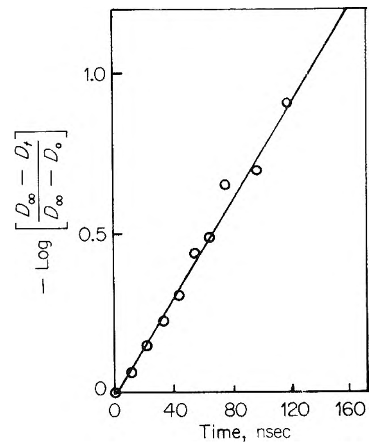

Figure 10. Growth of optical density, *D*, at 427.5 nm after a 1-krad, 25-nsec pulse in a benzene solution containing 0.1 *M trans*-stilbene and 0.004 *M* anthracene.

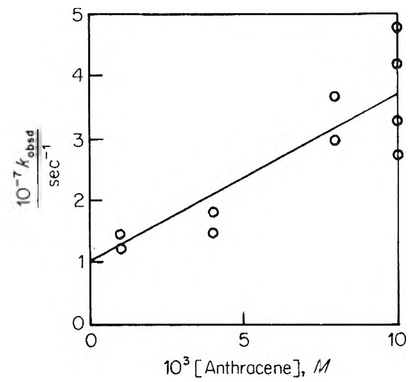

Figure 11. Dependence on anthracene concentration of the first-order rate constant for growth of ^{3}anthracene* in 10^{-1} *M* solutions of *trans*-stilbene in benzene.

sorption decaying in this manner is $\Delta(G\epsilon) = 1800 \pm 180$ at 350 nm and 2300 ± 230 at 360 nm. The lifetime of this species (τ = 111 nsec) is similar to that estimated[4,12] for the triplet state of stilbene and the absorption spectrum is also similar to that reported for the triplet state.[13,14]

The triplet state of anthracene (A) (λ_{max} 427.5 nm in benzene) has been observed in pulse irradiated solutions containing anthracene and stilbene.[16] This was attributed to the transfer of energy from the triplet state of stilbene to anthracene. If the triplet state of stilbene has the lifetime reported above then the occurrence of this energy transfer should be directly observable by the nanosecond pulse radiolysis technique. Accordingly benzene solutions with [*trans*-stilbene] = 0.1 *M* and various concentrations of anthracene were investigated. The triplet state absorption was observed to buildup after the pulse according to a first-order rate law as the typical oscilloscope traces and kinetic plots in Figures 8b and 10 illustrate. The first-order rate constant was found to be linearly dependent on the anthracene concentration (see Figure 11) in accord with the expected mechanism involving reactions 5 and 6, *i.e.*, $k_{obsd} = k_5 + k_6[\mathrm{A}]$.

$$^3\mathrm{S_t}^* \rightarrow \phi_t\mathrm{S_t} + \phi_c\mathrm{S_c} \tag{5}$$

$$^3\mathrm{S_t}^* + \mathrm{A} \rightarrow {}^3\mathrm{A}^* + \mathrm{S_t} \tag{6}$$

Treatment of the data by the method of least squares yielded $k_5 = (1.06 \pm 0.26) \times 10^7$ sec^{-1} and $k_6 = (2.6 \pm 0.5) \times 10^9$ M^{-1} sec^{-1} and the solid line in Figure 11 was

TABLE III: Effect of Anthracene (A) on the Initial and Final Yields of ($^3A^*$) in a 10^{-1} *M* Solution of *trans*-Stilbene in Benzene

10^3[A], *M*	[S_t], *M*	$G\epsilon_{427.5}10^{-3\,a}$	$G\epsilon_{427.5}10^{-3\,b}$
1	10^{-1}	7.9 ± 0.4	13 ± 1
1	0^c		57
4	10^{-1}	18 ± 1	38 ± 2
4	0^c		86
8	10^{-1}	22 ± 6	58 ± 7
8	0^c		114
10	10^{-1}	30 ± 10	90 ± 15
10	0^c		120

^{a} At the end of the pulse. ^{b} At time, $t = \infty$. ^{c} Taken from ref 23a.

computed using these values. Within the experimental error the value of k_5 obtained in this way agrees with the rate constant measured for the decay of the uv absorptions in the absence of anthracene and thus lends support to the suggestion that these absorptions are due to the triplet excited state of *trans*-stilbene.

Table III shows the variation with anthracene concentration of the end-of-pulse and maximum yields of ($^3A^*$). Comparison of the data with those obtained by Thompson[23a] for solutions without stilbene shows that the presence of stilbene lowers $G(^3A^*)$. A similar comparison of the data in ref 16 obtained using *cis*-stilbene shows that *cis*-stilbene has a similar effect.

Concurrent observation of the absorption at 360 nm was not possible in these experiments.

4. Emission Measurements. Solutions of *trans*-stilbene in benzene and cyclohexane were observed to give rise to light emission during the pulse in excess of the Čerenkov levels observed from the pure solvent. In both solvents, the wavelength of maximum emission from the solute was at 360 nm although self-absorption by stilbene led to a rapid falloff in intensity at shorter wavelengths. Within the limits set by the detection equipment (overall rise time in the microsecond mode of operation = 25 nsec) no buildup or decay of the emission was observable. With 10^{-2} *M* solutions of *trans*-stilbene the intensity of the emission was less than ten times that of the Čerenkov emission from the solvent alone, observed under the same conditions. In comparable experiments using naphthalene, Thompson[23a] observed emission levels of the order of 80 times that of the Čerenkov emission. It seems likely therefore that the emission observed in this study was fluorescence from the singlet state of *trans*-stilbene for which ϕ_f is small[3,15] in comparison with that for naphthalene (ϕ_f = 0.28).[30]

Nitromethane can act as a quencher of singlet states.[24] The effect of this additive on the emission from solutions of *trans*-stilbene in cyclohexane was investigated. Since the sensitivity of the detection system is wavelength dependent and since the quantum efficiency of the photomultiplier is unknown the data are presented in Figure 12 as the relative fluorescence yields, R_f, *i.e.*, the ratio of the signal from the photomultiplier observed during the pulse per unit dose to that observed in the absence of nitromethane. A correction for the Čerenkov emission was applied by observing the pure solvent under identical conditions. The fact that the effect of the nitromethane is greater the lower the stilbene concentration suggests that nitromethane is not acting as a quencher of singlet states but prevents their formation by competing with stilbene

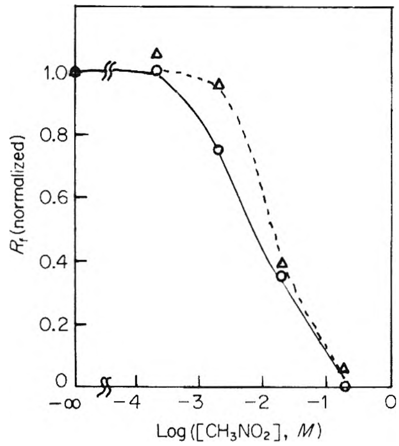

Figure 12. Effect of nitromethane on the normalized relative fluorescence intensity, R_f, at 360 nm during a pulse of radiation absorbed by a 10^{-3} *M* (O) and a 10^{-2} *M* (Δ) solution of *trans*-stilbene in cyclohexane.

for the solvent ions, which when captured by stilbene in the absence of nitromethane give rise to singlet excited states on neutralization.

Conclusions

In cyclohexane containing low concentrations of stilbene, the majority of excited singlet states (formed by an ionic process) apparently undergo intersystem crossing to the lowest triplet state. The natural decay of the latter proceeds with a rate constant of the order of 10^7 sec^{-1} in benzene and this value is probably little different from that applicable in cyclohexane. This rapid process is the final step in the isomerization process and Malkin and Fischer[3] have estimated that the *trans*-stilbene triplet decays with equal probability to the cis and trans ground states.

An absorption observed at 350–360 nm in benzene solutions, which decays rapidly in a first-order manner, is assigned to the triplet state. No absorption in this region which could be so assigned was observable in cyclohexane. In general, the triplet states of aromatic molecules absorb at longer wavelengths in benzene than in cyclohexane and it may be that the triplet state of stilbene in cyclohexane absorbs at wavelengths below 350 nm where measurements are not possible due to the large extinction coefficient of stilbene itself in this region.

Comparison of our observations with the reported absorption spectrum[13,14] suggests that the triplet absorbs at shorter wavelengths in benzene at room temperature than in paraffinic glass at 77 K. A red shift in any triplet–triplet absorption is to be expected on raising the temperature or by changing from paraffinic to an aromatic medium. It is possible that the triplet state responsible for the absorption is twisted about the central double bond to a greater degree in liquid benzene than in the rigid glass. The calculations of Borrell and Greenwood[5] suggest that such twisting would increase the separation of the first and second excited triplet levels. The separation calculated by these authors to apply near the minimum in the first excited triplet energy surface is between 3 and 4 eV. Absorption at 360 nm corresponds to a transition of 3.4 eV.

(30) A. R. Horrocks and F. Wilkinson, *Proc. Roy. Soc., Ser. A*, **306**, 257 (1968).

Fischer, *et al.*,[6] report that $G(\mathrm{t}\rightarrow\mathrm{c})$ is 1.33 for a 10^{-2} M solution of *trans*-stilbene in benzene. The corresponding value obtained by Hentz, *et al.*,[7] is 1.5. On the basis of the accepted mechanism for the isomerization this corresponds to $G(^3\mathrm{S_t}^*) \sim 3$. The yield measured in the present work is $G\epsilon_{360} = 2400$. If the assignment is correct then the extinction coefficient of *trans*-stilbene triplet at 360 nm is about 800 M^{-1} cm^{-1}. This is significantly smaller than the value reported by Herkstroeter and McClure[13] (3×10^4 M^{-1} cm^{-1} at 378 nm). Such a reduction in ϵ may also be due to the molecule being in a twisted form in solution.

The energy transfer phenomena observed in the present work are in accord generally with the reported effect of second solutes on the isomerization process in benzene and cyclohexane. Fischer, *et al.*,[6] report that *p*-terphenyl can enhance the isomerization yields in benzene solutions. They report, however, that the cis to trans conversion was enhanced with less efficiency than the reverse process. They suggest that this is due to the fact that while the triplet level of *trans*-stilbene lies 42 kJ mol^{-1} below that of *p*-terphenyl, the triplet level of *cis*-stilbene is only 4 kJ mol^{-1} lower than that of *p*-terphenyl. However our results suggest that *p*-terphenyl should enhance the isomerization process in both directions to the same degree because both isomers can deactivate the *p*-terphenyl triplet with a rate constant of about 10^9 M^{-1} sec^{-1}. Herkstroeter and Hammond[11] measured the quenching constants for reaction of *cis*- and *trans*-stilbene with a series of sensitizers of different energies. They found that molecules with triplet energies around 230 kJ mol^{-1} (like *p*-terphenyl) are quenched with almost equal efficiency by both isomers. They propose that the efficiency of *cis*-stilbene in these reactions is higher than expected, because this isomer is able to undergo nonvertical excitation during collisional energy transfer.

Acknowledgment. The authors are indebted to the S. R. C. for the provision of the pulse radiolysis equipment and the award to E. A. R. of a Research Studentship during the tenure of which this work was carried out.

Ab Initio Studies of the Interactions of an Electron and Two Water Molecules as a Building Block for a Model of the Hydrated Electron

Conrad A. Naleway and Maurice E. Schwartz*

Department of Chemistry and Radiation Laboratory,[1] University of Notre Dame, Notre Dame, Indiana 46556
(Received April 26, 1972)

Publication costs assisted by the U.S. Atomic Energy Commission

As a first step toward understanding the hydrated electron from a microscopic viewpoint, a simple dimer of H_2O plus an extra electron has been studied by the *ab initio* LCAO-SCF-MO approach with a "double ζ" basis set for numerous geometrical configurations. The energetics of the system show most stability for a configuration with two protons from different H_2O molecules pointing toward one another, much as in the D defects of the Bjerrum model for ice. This gives a natural viewpoint for the discussion of electron trapping. Some indication is given of planned further work using a many water model based on the present studies.

Introduction

In this paper we discuss some first studies directed toward an understanding of the hydrated electron from a fundamental, microscopic viewpoint involving quantum mechanics. Specifically, we examine *ab initio* quantum mechanical calculations on an electron and one or two water molecules, that is, H_2O^- and $(H_2O)_2^-$ for a number of different geometrical configurations. These studies are not designed to constitute a complete model for the hydrated electron, including its "excited state." Rather, the studies have been done to examine the energetics of the interaction of a relatively localized electron with one and two water molecules, which we intend subsequently to use in a "building blocks" approach for a many water plus electron model from which the properties of the hydrated electron may be inferred. That is, energetics from these studies will be used as pair-wise interaction energies in a many water plus electron system, much in the spirit of the recent work[2a] on electrons in hydrocarbons by Funabashi and Maruyama. Thus in a sense our many water studies will be "semiempirical," with interactions and orbitals taken from the present simpler studies. In a somewhat independent project we are also working on a pseudopotential-based model for the many water plus electron problem, and we believe that the results of two such fundamental, but alternate, approaches will be very useful in a rigorous and more nearly correct description of this important problem. A recent experimental paper[2b] has summarized previous theoretical studies, which are so different from our own that they need not be reviewed here.

Although the present studies are by no means complete, some of the results are so suggestive, especially as regards a "trapping" mechanism, that we shall make some speculation about the "true" system.

We have considered five basic kinds of geometrical arrangements for the two water molecules, as shown in Figure 1. The first two are configurations which are energetically favored for the neutral dimer: I is the normal linear hydrogen bond form, the most stable dimeric form of water; II is the so-called bifurcated hydrogen bond form, consisting of two nonlinear hydrogen bonds, and being slightly less stable than I.[3] The last three configurations are energetically unfavorable for the neutral dimer because of H···H repulsions, but turn out to be relatively favorable when an extra electron is present; III, the double H-H bridge, with a C_{2v} geometry having the pairs of protons from the two monomers pointing toward each other; IV, the perpendicular form, a D_{2d} geometry differing from III in that one monomer has been rotated 90° out of the plane; and V, the single H-H bridge, a planar C_2 geometry with a pair of protons from the monomers pointing toward one another while the other pair is in a trans arrangement.

The approach taken has been to consider the energy of the $(H_2O)_2^-$ system as a function of the oxygen-oxygen distance (R_{OO}) for fixed experimental monomer geometries[4] (R_{OH} = 1.80882 bohr, θ_{HOH} = 104.52°). For those geometries showing especial energy lowering effects, a few further studies involving O-H stretching have been done. H_2O^- was studied at the neutral monomer geometry. All calculations are within the *ab initio* LCAO-SCF-MO model,[5] using the "split" gaussian atomic basis set of essentially double ζ quality.[6] To our knowledge these are the most flexible, extended calculations yet done on these systems. We employ the atomic units (au) of length (1 bohr = 0.52917 Å) and energy (1 hartree = 27.21 eV).

Some comments on the basis set used are appropriate. It is a flexible, diffuse, valence-type basis set, with ten orbitals per oxygen and two per hydrogen. Thus a total of 14 MO's per monomer, or 28 per dimer, could be formed (of which five and ten, respectively, would be doubly occupied). Because an isolated water molecule has no affinity for an extra electron (in the sense of a bound state) the lowest energetically preferred states in which the extra electron would be found are plane waves. But since the system considered here (the dimer) is isolated in a vacuum, these very diffuse orbitals are not realistic since they would extend most of their density into regions of space

(1) The Radiation Laboratory is operated under contract with the U. S. Atomic Energy Commission. This is AEC Document No. COO-38-835. Some of this work was presented at the Conference on Elementary Processes in Radiation Chemistry, held at the University of Notre Dame, Apr 4-7, 1972.

(2) (a) K. Funabashi and Y. Maruyama, *J. Chem. Phys.*, **55**, 4494 (1971); (b) G. Kenney-Wallace and D. C. Walker, *ibid.*, **55**, 447 (1971).
(3) P. Kollmann and L. C. Allen, *J. Chem. Phys.*, **51**, 3286 (1969).
(4) G. Herzberg, "Electronic Spectra of Polyatomic Molecules," Van Nostrand, New York, N. Y., 1966.
(5) C. C. J. Roothaan, *Rev. Mod. Phys.*, **23**, 69 (1951); **32**, 179 (1960).
(6) (a) M. E. Schwartz, *Chem. Phys. Lett.*, **6**, 631 (1970); (b) S. Huzinaga, *J. Chem. Phys.*, **42**, 1293 (1965); (c) J. L. Whitten, *ibid.*, **44**, 359 (1966).

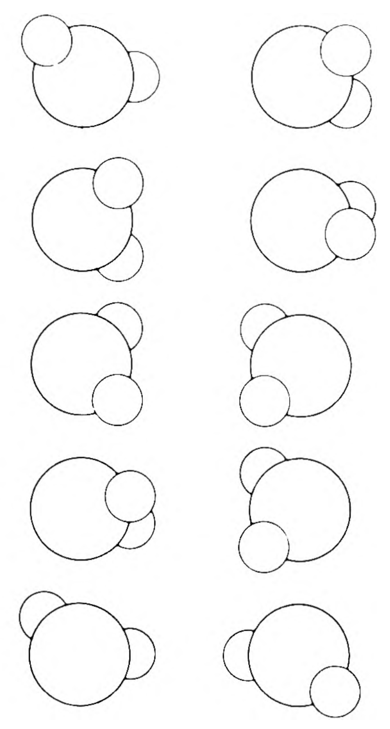

Figure 1. Dimeric forms studied.

where no molecules occur. Since the optimum orbitals could not be determined unambiguously (at least at the present time) they must by requirement have most of their density in the vicinity of the system. The relatively localized basis is in the spirit of our intention to extend these results into a many water model,[2a] in which delocalized, plane-wave-type states could be constructed by linear combinations of the valence basis orbitals from many water molecules.

Previous studies[2b] have all used localized concepts in their entire formulation of models for both ground and excited states of the trapped electron, while the present one and its progeny will only use them to get certain energetic information about *physically* localized regions. Whether the "complete" description will be localized or not remains to be seen, of course. Some support for this approach is evident from an examination of Table I. Here three of the most preferred configurations attained by use of our "valence" basis set (to be discussed later) were studied with two different and more diffuse basis sets. Both a partially "split" plus 3s oxygen atomic basis set as well as a minimum basis set plus atomic 3s's and 3p's on the oxygens and 2s orbitals on the hydrogen were studied. The extra orbitals were two-term gaussian fits from ref 6b. Table I shows that the relative total energy of the dimer plus electron (occupying a very diffuse orbital) is basically determined by the stability of the dimer alone, and has little to do with the presence of the extra electron. Also note that here the eigenvalues of the extra electron in the environment of the dimer is essentially a constant for all of the different configurations studied.

TABLE I: Total Energies for a Few Configurations of Dimer of H_2O Plus an Excess Electron, Using More Diffuse Base Sets[a]

Configuration	$E(H_2O)_2$	$E(H_2O)_2^-$	Eigenvalue (e_{extra}^-)[b]
	Basis Set A[c]		
Double HH bridge R_{OO} = 6.0	−151.9914	−151.9828	0.0086
Single HH bridge R_{OO} = 7.0; $R(OH_I)$ = 2.2	−151.9287	−151.9199	0.0088
Linear H bond R_{OO} = 5.67	−152.0165	−152.0078	0.0087
	Basis Set B[c]		
Double HH bridge R_{OO} = 6.0	−151.9486	−151.9405	0.0081
Single HH bridge R_{OO} = 7.0; $R(OH_I)$ = 2.2	−151.8802	−151.8722	0.0080
Linear H bond R_{OO} = 5.67	−151.9721	−151.9680	0.0041

[a] All in au. [b] Eigenvalue for excess electron in field of dimer potential. [c] Basis set A: "split" + [3s(2) on oxygen]. Basis set B: minimum + [(3s(2) + 3p(s)) on oxygen] + [2s(2) on hydrogen]. (See discussion of basis set in text.)

Results and Discussion

With our double ζ valence basis set, the neutral monomer energy was calculated as −76.0034 au, and that of H_2O^- as −75.7554 au. Table II summarizes the calculated total energies and "stabilization energies" for the dimeric forms; that is, the energy lowerings associated with the dimeric forms relative to separated H_2O and H_2O^-. The definition of stabilization is somewhat arbitrary, of course, and we choose this one with the viewpoint[2a] that the *monomer* negative ion is the basis for the many molecule system. We shall only discuss energetics in the present paper. Orbital coefficients, electron distributions, and the like are to be deferred to a subsequent paper, where they will be considered in the context of the many water system, which will be a more complete and more nearly correct model for the hydrated electron.

Table II shows that the normal hydrogen bonded forms of the dimer[3] are not energetically preferred when the extra electron is present, and that preferred orientations of the molecules place their protons toward one another as an energy lowering mechanism, in agreement with qualitative expectations. From energy *vs.* R_{OO} considerations, it is apparent that there are slight overall expansions of $(H_2O)_2^-$ compared to $(H_2O)_2$ for these stabilized forms; interpolated minimum energy values of R_{OO} are 6.29 for III, 6.11 for IV, and 7.14 for V. The neutral R_{OO} distances are 5.67 for both hydrogen bonded types I and II, and the average values are 5.22 in ice at 0° and 5.52 in liquid water at 27°.[7] Conversely, the minimum energy occurs for smaller R_{OO} values for the H bonded cases, R_{OO} = 5.05 for I and 5.33 for II.

These results are particularly interesting when considered in light of Bjerrum's model for the formation of defects in ice (ref 8; see also pp 115–117 of ref 7), which is schematically given in our Figure 2. The single H–H bridge form V gives the most stabilization energy for an extra electron, with an O–O distance about 1.81 au or 0.96 Å larger than the ice O–O distance. Now this form V has essentially the same type geometry as the so-called D defect in ice, for which simple calculations[9] indicate an increase of about 1 Å in R_{OO}. Furthermore, the increased

(7) D. Eisenberg and W. Kauzmann, "The Structure and Properties of Water," Oxford University Press, New York, N. Y., 1969.
(8) N. Bjerrum, *K. Dan. Vidensk. Slesk., Mat. Fys. Skr.*, **27**, 1 (1951).
(9) D. Eisenberg and C. A. Coulson, *Nature (London)*, **199**, 368 (1963).

TABLE II: Total and "Stabilization" Energies for Dimers of H_2O Plus an Electron

Configuration	$E(H_2O)_2$, au	$E(H_2O)_2^-$, au	ΔE_{stab}, eV
Linear hydrogen bond I			
$R_{OO} = 4.5$	−152.0064	−151.7941	−0.96
$R_{OO} = 5.0$	−152.0178	−151.8009	−1.15
$R_{OO} = 5.0$; $R(OH) = 2.0$	−152.0096	−151.8006	−1.14
$R_{OO} = 5.67$	−152.0186	−151.7974	−1.05
$R_{OO} = 7.0$	−152.0137	−151.7860	−0.74
Bifurcated hydrogen bond II			
$R_{OO} = 5.0$	−152.0147	−151.7951	−0.99
$R_{OO} = 5.67$	−152.0163	−151.7952	−0.99
$R_{OO} = 6.00$	−152.0157	−151.7936	−0.95
Double HH bridge III			
$R_{OO} = 5.00$	−151.9679	−151.8114	−1.43
$R_{OO} = 5.50$	−151.9866	−151.8320	−1.99
$R_{OO} = 6.00$	−151.9947	−151.8415	−2.25
$R_{OO} = 6.00$; $R(OH_I) = 2.00$	−151.9561	−151.8400	−2.21
$R_{OO} = 8.0$	−152.0023	−151.8083	−1.34
Perpendicular IV			
$R_{OO} = 4.21$	−151.9315	−151.7209	+1.03
$R_{OO} = 6.00$	−151.9994	−151.8292	−1.91
$R_{OO} = 8.00$	−152.0030	−151.8027	−1.19
$R_{OO} = 11.00$	−152.0050	−151.7553	+0.08
Single HH bridge V			
$R_{OO} = 5.02$	−151.8977	−151.6909	+1.85
$R_{OO} = 6.00$	−151.9855	−151.8191	−1.64
$R_{OO} = 6.00$; $R(OH_I) = 2.01$	−151.9506	−151.8373	−2.14
$R_{OO} = 6.00$; $R(OH_I) = 2.20$	−151.8862	−151.8329	−2.02
$R_{OO} = 7.00$	−151.9999	−151.8495	−2.47
$R_{OO} = 7.00$; $R(OH_I) = 2.00$	−151.9780	−151.8704	−3.04
$R_{OO} = 7.00$; $R(OH_I) = 2.2$	−151.9319	−151.8748	−3.16
$R_{OO} = 7.00$; $R(OH_I) = 2.4$	−151.8747	−151.8702	−3.03
$R_{OO} = 7.00$; $R(OH_I) = 2.8$	−151.7405	−151.8366	−2.17
$R_{OO} = 8.91$	−152.0046	−151.8187	−1.63
$R_{OO} = 8.91$; $R(OH_I) = 2.01$	−151.9642	−151.8469	−2.40
$R_{OO} = 10.0$	−152.0052	−151.7826	−0.65

R_{OO} in the D defect pair means a slightly shorter R_{OO} between that rotated molecule in the pair whose nearest neighbor has rotated in turn to form an H bond with it, while this neighbor in turn has its lone pairs directed toward its next neighbor's lone pairs to form a so-called L defect (see Figure 2). The electron is stabilized in a linearly H bonded pair by a shorter R_{OO} (Table II), and the L defect forms a "barrier" to the extra electron because it is energetically less favorable (we have done a calculation of such a dimeric form for $R_{OO} = 5.5$ and found an energy just 0.9 eV lower than $H_2O + H_2O^-$). These two effects would complement the D defect stabilization, and we thus conclude that the D defect forms a "natural" trap for the hydration of an electron.

Even further stabilization can occur for the single H–H bridge form V when the inner hydrogens of the pair move toward one another; from Table II we note that about 0.7 eV energy lowering is obtained when each inner O–H bond is stretched by about 0.4 au (0.2 Å). Such stabilization does not occur for O–H stretching in the other forms considered.

The structure of liquid water is of course not so well ordered as ice, but there is probably sufficient local ordering in clusters of molecules to allow for the Bjerrum fault type trapping discussed above.[7] Further, the other forms such as the double H–H bridge III and the perpendicular form IV might have reasonable opportunities for electron trapping in the liquid.

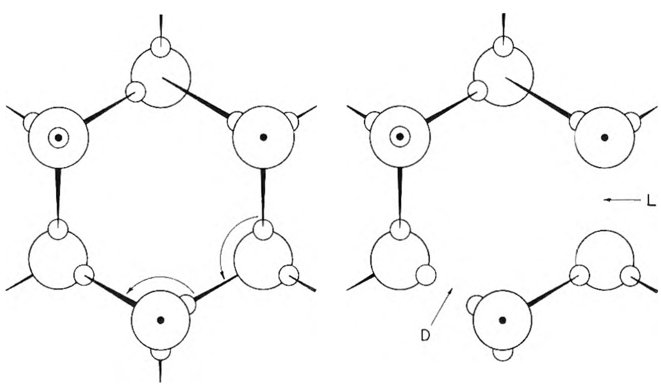

Figure 2. Schematic diagram of formation of D and L defects, looking down the C axis of the ice crystal (*cf.* ref 7).

The possibility of a second D defect participating in the trapping process merits consideration. Further energetic stability might be achieved if a second pair of water molecules would rotate so that two D defects would coexist side by side. The resulting array would enclose one water molecule within four neighboring molecules, all roughly directing the positive ends of their dipoles toward it. Whether or not the true trap is actually a single defect or some collective group of such defects must be weighed on both energetic as well as entropic grounds. Whereas individual D-type defects are probably preexistent in water

TABLE III: Excitation Energies for the Dimeric Models

Configuration	ΔE, eV
Linear hydrogen bond I	
$R_{OO} = 4.5$	2.24
$R_{OO} = 5.0$	2.38
$R_{OO} = 5.0$; $R(OH) = 2.0$	2.38
$R_{OO} = 5.67$	2.21
$R_{OO} = 7.0$	1.48
Bifurcated hydrogen bond II	
$R_{OO} = 5.0$	2.45
$R_{OO} = 5.67$	2.32
$R_{OO} = 6.00$	2.08
Double HH bond III	
$R_{OO} = 5.00$	1.68
$R_{OO} = 5.50$	1.76
$R_{OO} = 6.00$	1.94
$R_{OO} = 6.00$; $R(OH_I) = 2.00$	1.77
$R_{OO} = 8.00$	2.12
Perpendicular IV	
$R_{OO} = 4.21$	2.71
$R_{OO} = 6.00$	3.67
$R_{OO} = 8.00$	1.82
$R_{OO} = 11.00$	0.37
Single HH bridge V	
$R_{OO} = 5.02$	1.83
$R_{OO} = 6.00$	2.59
$R_{OO} = 6.00$; $R(OH_I) = 2.01$	3.76
$R_{OO} = 6.00$; $R(OH_I) = 2.20$	5.20
$R_{OO} = 7.00$	2.48
$R_{OO} = 7.00$; $R(OH_I) = 2.00$	3.91
$R_{OO} = 7.00$; $R(OH_I) = 2.20$	5.10
$R_{OO} = 7.0$; $R(OH_I) = 2.4$	6.40
$R_{OO} = 8.91$	1.93
$R_{OO} = 8.91$; $R(OH_I) = 2.01$	3.14
$R_{OO} = 10.00$	0.82

and ice, the probability of a cluster of such defects being localized with a small neighborhood depends on the degree of order in the system being studied. In highly crystalline materials such as ice I, the probability of any local concentrations of such defects is surely small, and such a trap would need to be created by the electron itself, requiring both a relaxation period (of the order of molecular rotation) and probably some activation energy.

So far we have considered only the ground state of our model systems. Now one of the characteristic features of the hydrated electron is its absorption spectrum, which has been studied under a variety of conditions.[2,10-12] While there is much evidence for the localization of the hydrated electron in its ground state,[10] it is by no means obvious that its absorption spectrum is due to excitation to a localized excited state, an assumption built into previous theoretical models.[2b] Indeed, recent experimental evidence[2b] suggests otherwise. Nevertheless, we have looked at the excitation energies for our model dimer systems, and have summarized them in Table III. Here the energies are differences between SCF energies calculated from the two different states. They all span a region of about 0.5 to 5 eV, which encompasses the experimental peak range of about 1.7 to 2.0 eV.[10] Note that the most stable form V has a "poor" excitation energy of 5.2 eV. This "success" by no means establishes a complete model, in view of the forced localization in both states and the experimental evidence[2b] against excited localization. Also, the excited states of the dimers generally showed some tendency to shift the extra electronic charge outside of the dimer, and in a real environment this might well lead to delocalization. We shall look more realistically at excited states in our many water studies, in which localization or delocalization will emerge as results and not as initial assumptions.

It is worth emphasizing again that all of these systems of dimer plus electron have higher total energies than the neutral dimer plus a free electron, and it is only the *relative* energies we have considered above in discussing "stability." For example, if we consider a perfect crystal of ice, all dimer interactions correspond to linear H bond types, and the introduction of a defect would give relative stability at that localized region.

Of course the above discussion assumes that we can discuss a many water plus electron system as though only dimeric interactions are important. We are carrying out further rigorous calculations on larger clusters of water molecules and an electron to examine this assumption quantitatively.

But in the meantime it must be realized that the dimeric calculations are strongly suggestive of a trapping mechanism, and that they do show what important features one should seek in calculations on larger clusters.

(10) E. J. Hart and M. Anbar, "The Hydrated Electron," Wiley-Interscience, New York, N. Y., 1970.
(11) M. J. Bronskill, R. K. Wolff, and J. W. Hunt, *J. Chem. Phys.*, **53**, 4201 (1970).
(12) B. D. Michael, E. J. Hart, and K. H. Schmidt, *J. Phys. Chem.*, **75**, 2798 (1971).

COMMUNICATIONS TO THE EDITOR

γ Radiolysis of Xenon Trioxide in Aqueous Solution

Publication costs assisted by the U. S. Atomic Energy Commission

Sir: Aqueous solutions of XeO_3 were irradiated with ^{60}C γ rays (1100 Ci) either at pH 6.0 or 1.25 (solutions acidified with H_2SO_4) and saturated with either air or 99.999% argon. Dose rates of 5.6, 0.50, and 0.13 $\times$ 10^{18} eV g^{-1} hr^{-1} were used, and the effect of solute concentration was studied at the highest dose rate. It has been shown in previous work,[1] by gas analysis and iodometry, that XeO_3 is decomposed into Xe and O_2 by γ radiolysis of its aqueous solutions. In the present work, we have measured yields of the disappearance of XeO_3 by iodometry following the method of Appelman and Malm.[2]

At pH 1.25 the initial G, molecules of XeO_3 decomposed per 100 eV absorbed, is the same in aerated and argon-saturated solutions. The amount of decomposition increases linearly with dose up to at least 20% decomposition of the solute. G increases with increase in solute concentration and with decrease in dose rate, I. Results for a 1.2 $\times$ 10^{-2} M solution are presented in Table I. At pH 6 in aerated solutions the initial G is high and increases with increase in solute concentration as shown in Table II for I = 5.6 $\times$ 10^{18} eV g^{-1} hr^{-1}. With decrease in dose rate to aerated solutions at pH 6, G increases; *e.g.*, for an 8.5 $\times$ 10^{-3} M solution, G increases from 10.5 to 44 with decrease in I from 5.6 to 0.13 $\times$ 10^{18} eV g^{-1} hr^{-1}. In solutions saturated with argon at pH 6, G decreases slightly with increase in solute concentration and becomes almost constant at approximately 7.5 for concentrations greater than 10^{-2} M. The $G \approx 7.5$ at high concentrations is independent of the dose rate while G at small concentrations increases with decrease in I.

TABLE I: Effect of Dose Rate, *I*, on $G(-XeO_3)$ for Aerated and Argon-Saturated Solutions of 1.2 $\times$ 10^{-2} *M* XeO_3 at pH 1.25

I^a	0.13	0.50	5.6
G, aerated	6.13	5.2	4.1
G, argon	6.09	5.12	4.1

^{a} Units of 10^{18} eV g^{-1} hr^{-1}.

TABLE II: Dependence of $G(-XeO_3)$ on XeO_3 Concentration in γ Radiolysis of Aerated Solutions at pH 6^a

$[XeO_3]$, 10^{-2} *M*	G	$[XeO_3]$, 10^{-2} *M*	G
0.17	10.0	1.30	12.3
0.38	9.6	1.45	18.7
0.85	10.5	1.60	20.8

^{a} Dose rate of 5.6 $\times$ 10^{18} eV g^{-1} hr^{-1}

It has been noted[3] that more than 1 mol of hydrogen peroxide is consumed for 1 mol of XeO_3 in the thermal reaction; however, the ratio H_2O_2/XeO_3 has not been determined. A systematic study of the thermal reaction has been undertaken; preliminary results indicate that the reaction is rather complex. The ratio for reactants consumed, H_2O_2/XeO_3, varies with pH and with the ratio of initial concentrations of H_2O_2 and XeO_3. Under oxygen and at pH 1.25, H_2O_2/XeO_3 increases from 1 to 3 with increase in H_2O_2 concentration while in neutral solution the ratio increases from 0.5 to 1.

The results for aerated solutions at pH 1.25 are explained with the following reaction scheme.

$$H + O_2 \rightarrow HO_2 \qquad (1)$$

$$XeO_3 + HO_2 \rightarrow XeO_2 + OH + O_2 \qquad (2)$$

$$XeO_2 \rightarrow Xe + O_2 \qquad (3)$$

$$2\,OH \rightarrow H_2O_2 \qquad (4)$$

$$XeO_3 + (1\text{-}3)H_2O_2 \rightarrow XeO_2 + (1\text{-}3)H_2O + (1\text{-}2)O_2 \qquad (5)$$

In argon-saturated solutions, reaction 1 is absent and reaction 6

$$H + XeO_3 \rightarrow XeO_2 + OH \qquad (6)$$

is substituted for reaction 2. With the primary radiolytic yields at pH 1.25 ($G(H)$ = 3.65, $G(OH)$ = 2.95, $G(H_2O_2)$ = 0.8), G = 5.02 for H_2O_2/XeO_3 = 3 and G = 7.75 for H_2O_2/XeO_3 = 1. Thus, in the reaction scheme proposed, the effect of dose rate on G is related to an effect of dose rate on H_2O_2 concentration and, thereby, on the consumption ratio H_2O_2/XeO_3. Experiments have been undertaken for test of the proposal.

The large values of G and dose-rate effect for aerated solutions at pH 6 suggest a chain reaction for which a reaction scheme is proposed that includes reactions 3 and 4 and the following reactions.

$$O_2 + e_{aq}^- \rightarrow O_2^- \qquad (7)$$

$$XeO_3 + O_2^- \rightarrow XeO_2 + O_3^- \qquad (8)$$

$$XeO_3 + O_3^- \rightarrow XeO_2 + O_2 + O_2^- \qquad (9)$$

$$2O_2^- + H_2O \rightarrow HO_2^- + OH^- + O_2 \qquad (10)$$

$$XeO_3 + (0.5\text{-}1)H_2O_2 \rightarrow XeO_2 + (0.5\text{-}1)H_2O + (0.75\text{-}1)O_2 \qquad (11)$$

(1) C. Heitz and F. Simon, *Radiochem. Radioanal. Lett.*, **5**, 341 (1970).
(2) E. H. Appelman and J. G. Malm, *J. Amer. Chem. Soc.*, **86**, 2141 (1964).
(3) J. G. Malm and E. H. Appelman, *Atom. Energy Rev.*, **7**, 3 (1969).

In argon-saturated solutions, reactions 6, 12, and 13 re-

$$XeO_3 + e_{aq}^- \rightarrow XeO_2 + O^- \quad (12)$$

$$O^- + H_2O \rightarrow OH^- + OH \quad (13)$$

place reactions 7-10. With the primary radiolytic yields at pH 6 ($G(e_{aq}^-) = 2.65$, $G(H) = 0.55$, $G(OH) = 2.7$, $G(H_2O_2) = 0.7$), $G = 6.85$ for $H_2O_2/XeO_3 = 1$ and $G = 10.5$ for $H_2O_2/XeO_3 = 0.5$ in the argon solutions. From the absence of a chain reaction in the argon solutions, it is concluded that OH does not react with XeO_3. Again, for small concentrations of XeO_3 in the argon solutions at pH 6, the effect of dose rate on G is explained in terms of its effect on the ratio H_2O_2/XeO_3.

Laboratoire de Chimie Nucleaire **C. Heitz***
Strasbourg-Cronenbourg (67), France
Laboratoire Curie **M. Haissinsky**
Paris, France

Received September 20, 1972